Chemical Biology for Parasitology: Development of Chemical Probes for a Bromodomain in the Parasite *Schistosoma mansoni*



Darius James Benedict McArdle

St Cross College, University of Oxford

Thesis submitted for the degree of:

Doctor of Philosophy in Chemical Biology

Hilary Term 2023

Under the supervision of:

Prof Stuart J. Conway (University of Oxford)

Dr Rosa Cookson (GlaxoSmithKline)

Table of Contents

Abstract i

Acknowledgements ii

Abbreviations iv

Chapter 1: Introduction 1

1.1 Epigenetics 2
1.2 Post translational modifications on histones 3
1.3 Bromodomains 4
1.4 Chemical probes for the human BET bromodomains 6
1.5 Photoaffinity probes for human bromodomians 13
1.6 Schistosomiasis and *S. mansoni* 20
1.7 Epigenetics of *S. mansoni* 22
1.8 Previous work towards a bromodomain of *S. mansoni* 26
1.9 Project aims 34

Chapter 2: Structure-based optimisation of small molecule ligands for SmBRD3(2): targeting the HFF shelf 35

2.1 Introduction and aims 36
2.2 Ligand design and synthesis 37
2.2.1 Ligand design 37
2.2.2 Stereoselective synthesis of a primary amine intermediate 38
2.2.3 C-N coupling reactions for the synthesis of novel I-BET726 analogues 40
2.2.4 Ester hydrolysis for the synthesis of novel I-BET726 analogues 45
2.3 Biological evaluation of I-BET726 derivatives 47
2.3.1 Binding affinity and crystallographic analysis of novel analogues for *Sm*BRD3(2) 47
2.3.2 Phenotypic screening of SmBRD3 ligands on *S. mansoni* 51
2.3.3 Investigation of parasite permeability by LCMS 59
2.4 Conclusions 63

Chapter 3: Structure-based optimisation of small molecule ligands for *Sm*BRD3(2): targeting the ZA channel region 65

3.1 Introduction and aims 66
3.2 Isopropyl carbamate fragments for SAR investigation of the ZA channel region 67
3.2.1 Ligand design 67
3.2.2 Synthesis 70
3.2.3 Binding affinity of isopropyl carbamate fragments to *Sm*BRD3(2) 72
3.3 Quinoline-based analogues for SAR investigation of the ZA channel region 74
3.3.1 Ligand design 74
3.3.2 Synthesis 76
3.3.3 Binding affinity of quinoline-based analogues to *Sm*BRD3(2) 81
3.3.4 *Ex vivo* evaluation of quinoline-based THQ analogues on *S. mansoni* 83
3.4 Investigation of selectivity between human and *S. mansoni* bromodomains 89
3.4 Conclusions 90

Chapter 4 Photoaffinity probes for the evaluation of cellular SmBRD3 engagement 92

4.1 Introduction and aims 93
4.2 Probe design 94
4.2.1 *Sm*BRD3(1) selective photoaffinity probe 94
4.2.2 Photoaffinity probe based on an *Sm*BRD3(2) optimised I-BET726 derivative 96
4.3 Synthesis 99
4.3.1 *Sm*BRD3(1) selective photoaffinity probe, **4.2** 99
4.3.1.1 Synthesis of a diazirine-alkyne functionalised tag intermediate 99
*4.3.1.2. Synthesis of the dimethylisoxazole intermediate OXFBD03 (**1.37**)* 102
*4.3.1.3 Synthesis of the photoaffinity probe **4.2*** 103
4.3.2 I-BET726 derivative-based probes for *Sm*BRD3 105
4.4 *In vitro* biological evaluation on recombinant *Sm*BRD3 108
4.4.1 Binding affinity to *Sm*BRD3(1,2) and *Sm*BRD3(2) 108
4.4.2 Photoactive crosslinking to recombinant *Sm*BRD3 110
*4.4.2.1 Crosslinking of **4.2** to SmBRD3(1,2)* 110
*4.4.2.2 Crosslinking of **4.5** to SmBRD3(1,2) and SmBRD3(2)* 114
4.5 Investigation of *Sm*BRD3 photoaffinity probes within the *S. mansoni* proteome 121
4.5.1 Evaluation of photoaffinity probes for *Sm*BRD3 on *S. mansoni* lysate 121
4.5.2 Evaluation of a polyclonal antibody for *Sm*BRD3 on *S. mansoni* lysate 127

4.5.3 Investigation of the interaction of photoaffinity probes with live *S. mansoni* 130
4.6 Conclusions 134

Chapter 5 Conclusions and future work 136

5.1 Conclusions 137
5.2 Future work 140

Chapter 6 Experimental 144

6.1 General Chemistry Methods 145
6.2 Synthetic procedures and compound data 149
6.2.1 Compounds from Chapter 2 149
6.2.2 Compounds from Chapter 3 184
6.2.3 Compounds from Chapter 4 201
6.2.4 Previously reported BET BRD ligands 220
6.3 General Biology Methods 221
6.3.1 Biological reagents and pH measurements 221
6.3.2. Protein expression and purification 221
6.3.2.1 Fermentation conditions for bromodomain containing proteins 223
6.3.2.2 Purification conditions for Hig-tagged bromodomain containing proteins 223
6.3.2.3 Purification conditions for His-tag cleaved *Sm*BRD3(1,2) 225
6.3.3 Isothermal Titration Calorimetry 227
6.3.4 Protein X-ray crystallography 228
6.3.4.1 Crystallisation of SmBRD3(2) 228
6.3.4.2 Data collection and processing 229
6.3.4.3 Structure solution and refinement 229
6.3.5 Phenotypic screening 232
6.3.5.1 Ethics statement 232
6.3.5.2 Schistosomula drug screen 232
6.3.5.3 Adult worm drug screen 233
6.3.5.4 Miracidia drug screen 233
6.3.6 Determination of compound parasite permeability 234
6.3.7 *In silico* molecular docking 236
6.3.8 *In vitro* diazirine probe crosslinking to recombinant protein 237
6.3.9 Parasite lysate preparation 238
6.3.10 Parasite lysate diazirine probe engagement 239

6.3.11 *Sm*BRD3 antibody production 240
6.3.12 Western blotting 241
6.3.13 Fluorescence-based parasite localisation 242

References 244

Appendices 263

Appendix A: Protein expression and purification 264
Appendix B: Isothermal Titration Calorimetry (ITC) Data 270
Appendix C: *In vitro* crosslinking to recombinant protein 286
Appendix D: EC_{50} curves 292
Appendix E: NMR spectra of novel compounds 294
Appendix F: Image permissions 359

Chemical Biology for Parasitology: Development of Chemical Probes for a Bromodomain in the Parasite *Schistosoma mansoni*

Schistosoma mansoni is a water-born parasite responsible for at least 200,000 deaths a year. This parasite has multiple life cycle stages exhibiting large differences in phenotype. These changes occur without alterations in DNA sequence and therefore are likely mediated by epigenetics. For the aim of developing new therapeutics to combat *S. mansoni*, it is important to understand the biological mechanisms of this parasite. Epigenetic proteins are promising targets, however, the 'readers' of acetyl lysines on histones, the bromodomains (BRDs), have received little attention to date. Our hypothesis is that ligands for the bromodomain and extra terminal (BET) family orthologue, *Sm*BRD3, which has two BRDs in tandem, may disrupt the epigenetic mechanisms, and hence the overall function, of the parasite.

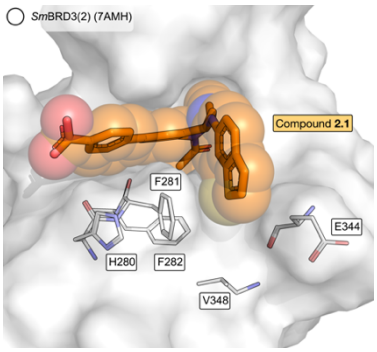


Figure 0.1. Co-crystal structure of compound **2.1** bound to *Sm*BRD3(2).

Building on previous work, this report describes development of novel I-BET726 derivatives with higher affinity for the second domain, *Sm*BRD3(2). Higher affinity was achieved by employing groups to effectively fill the HFF cleft (**Figure 0.1**). The ethyl ester analogues of these compounds affect the schistosomula and adult worm life cycle stages of *S. mansoni*. Furthermore, two of these compounds affected the miracidia to sporocyst transformation, suggesting epigenetics play a role. Based on a pro-drug hypothesis, the effects induced on *S. mansoni* by these compounds implies an importance of *Sm*BRD3 at multiple life cycle stages. To confirm our pro-drug hypothesis, LCMS studies on parasite lysate were carried out, which indicated ethyl ester analogues were more permeable to the parasite than the acid analogues, with some *in situ* release of the acid. Phenotypic screening and LCMS analysis of *Sm*BRD3(1) selective ligands hints at differing functions for the two domains. Finally, the phenotypic screening results prompted the development of photoaffinity probes for *Sm*BRD3, and work is ongoing to identify the cellular targets of these probes.

Acknowledgements

Firstly, I would like to thank my supervisor Stuart for all the support during my time in the Conway group. I've learnt a huge amount over the past four years, and a lot of this is from your guidance. In addition, I would like to thank your support during the COVID-19 pandemic, ensuring the group were able to make progress on our projects in that 'unprecedented time'. I'm pleased you'll be joining me in California, and it would be great to venture from 'NorCal' to 'SoCal' to visit the new lab. I would also like to thank our collaborators Karl and the Hoffmann group. This project has benefitted hugely from your group, and I learnt a lot during my 3-month period in your lab. Thank you, Gilda, for all your work on screening my compounds, and Jo, Ben and Adam for your guidance and work with me in Aberystwyth. Jo, I hope this is the end of my many questions! Maze, although we never met in person, thank you for your initial work on the *Sm*BRD3 project and your help at the beginning of my DPhil. The project has been great to work on and this is largely due to the position you left it in. Thank you Pearse, Manfred, and Mike for your assistance with HPLCs, lysate analysis and crystallography. Finally, thank you to the NMR and MS spectrometry teams for all your advice and assistance, in particular Nader, for also always being a friendly face in the basement NMR room.

Outside of the work relating to this project, there are many more people I wish to thank from the Conway group. To all the G11 and G12 lab members, both past and present, thank you for being such a great bunch of people to work with. Adam, you were the social hub of the Conway group and always made G12 a pleasure to work in, with notable mention of the 'HPLC peephole' and disco Fridays. Also, thank you for your advice in the lab over the years. Thank you to my fellow final year DPhils, Katrina, Jenny and Patrick. Katrina, I've really enjoyed working in the same group with you. It's been great to have a buddy to go for Taylor's lunches and Horsebox coffees, and I'm really glad you'll be ending up in California. Maybe I'll see you there soon! Jenny and Patrick, it's also been great working with you, and

Patrick, I've enjoyed our gigs playing in 'My Chemical Bromance' and The Donuts Kings. To my Part IIs: Lily, Aleksy, and Josh. Thank you for being the best Part II students a DPhil could ask for. Lily, I hope your life in the world of law is less stressful without pink and insoluble compounds. I'm sad I couldn't give you one of those excess 2 L beakers for your leaving present. Aleksy, thank you for doing great on your project, despite the lab shift system, and it was a pleasure to have a fellow ex-Thornden boy in the Conway group. Josh, I was unsure about having a Part II for my final DPhil year, but it turned out to be great and we had some laughs. Your wavy t shirts should have a specific mention. To the post docs, past and present: Debs, Maria, Pascal, Antoine, and Marta, thank you for signing off all those reactions in my lab books, your guidance, and being a pleasure to work with. Maria, thank you for keeping me company during our stint in the AJR lab. Glen, I've enjoyed our overlapped music tastes in the lab, and will always hear "nine coronas" in the song "My Sharona". Antoine, I've enjoyed trying to speak a little French with you and remembering "a plus dans le bus!". Jess, thank you for being so smiley throughout the whole time we shared in the CRL, along with proofreading a chapter of this thesis. Alistair, I've enjoyed our N site rants, and I wish you all the best with your macrocycles!

I have also benefitted hugely from the support of people outside the Conway group. Elliot, it's been great to have you as a close friend during the DPhil, with our coffee and walks, gigs with 'My Chemical Bromance', the California road trip and chilling in JC's pool. To the 'Warzone boys', gaming in the evenings with you all during the pandemic kept me sane, and I look back on those evenings fondly. I want to thank my housemates over these past few years: Dylan, James, Willem, Finlay, Denis, Katerina, and Linda. Thank you for being a pleasure to live with! To Naomi, thank you for all your support, cheering me on in the past year. You've truly helped to prevent me become fully 'unhinged' in the final stages of my DPhil, particularly during laptop death crises, and I'm looking forward on your behalf for a (hopefully) far more chilled out version of me. Finally, to my parents, thank you for the huge amount of support, advice, and guidance you have given me from day 1.

Abbreviations

Ac	acetyl
ACT	2-aryl-5-carboxytetrazole
AUR	auranofin
β-ME	β-mercaptoethanol
BCP	bromodomain containing protein
BD1	N-terminal bromodomain
BD2	C-terminal bromodomain
BET	bromodomain and extra terminal
BINAP	(2,2′-bis(diphenylphosphino)-1,1′-binaphthyl)
Boc	*tert*-butyloxycarbonyl
br	broad
BRD	bromodomain
BrettPhos	2-(dicyclohexylphosphino)3,6-dimethoxy-2′,4′,6′-triisopropyl-1,1′-biphenyl
BrettPhos Pd G3	[(2-di-cyclohexylphosphino-3,6-dimethoxy-2′,4′,6′- triisopropyl-1,1′-biphenyl)-2-(2′-amino-1,1′ -biphenyl)]palladium(II) methanesulfonate methanesulfonate
CAD	Charged Aerosol Detector
CBSS	Chrenin's balanced salt solution
CHI	Chromatographic Hydrophobicity Index
CI	confidence interval
COSY	correlated spectroscopy
CuAAC	copper-catalyzed azide-alkyne cycloaddition
CV	column volume(s)
CyJohnPhos	2-(dicyclohexylphosphino)biphenyl
Da	dalton
DAPI	4′,6-diamidino-2-phenylindole
dba	dibenzylideneacetone
DCC	*N*,*N*'-dicyclohexylcarbodiimide
DEA	diethanolamine
DIPEA	*N*,*N*-diisopropylethylamine
DMAP	*N*,*N*-4-dimethylaminopyridine
DME	dimethoxyethane

DMF	*N*,*N*-dimethylformamide
DMSO	dimethyl sulfoxide
DNA	deoxyribonucleic acid
dppf	1,1′-bis(diphenylphosphino)ferrocene
DSF	differential scanning fluorimetry
EC_{50}	half maximal effective concentration
E. Coli	*Escherichia coli*
EDTA	ethylenediamine tetraacetic acid
ee	enantiomeric excess
ELSIA	enzyme-linked immunosorbent assay
eq.	equivalents
Et	ethyl
FA	formic acid
FDA	Food and Drug Administration
FP	fluorescence polarisation
h	hour(s)
HAT	histone acetyltransferase
HATU	1-[bis(dimethylamino)methylene]-1*H*-1,2,3-triazolo[4,5-b]pyridinium 3-oxid hexafluorophosphate
HDAC	histone deacetylase
HEPES	(4-(2-hydroxyethyl)-1-piperazineethanesulfonic acid)
HMBC	Heteronuclear Multiple Bond Correlation
HPLC	high performance liquid chromatography
HRMS	high resolution mass spectrometry
HSQC	Heteronuclear Single Quantum Coherence
i-Pr	isopropyl
IEDDA	inverse electron-demand Diels–Alder reaction
IMAC	immobilized metal affinity chromatography
IPA	isopropyl alcohol
IPTG	isopropyl β-D-1-thiogalactopyranoside
ITC	isothermal titration calorimetry
KAc	ε-*N*-acetylated lysine
K_d	disossiation constant
LC	liquid chromatography
LCMS	liquid chromatography–mass spectrometry
LDA	lithium diisopropylamide

LDS	lithium dodecyl sulfate
LiHMDS	lithium bis(trimethylsilyl)amide
LRMS	low resolution mass spectrometry
m	medium
Me	methyl
MES	2-(*N*-morpholino)ethanesulfonic acid
min	minute(s)
mp	melting point
MS	mass spectrometry
MWCO	molecular weight cut-off
n-Bu	*n*-butyl
NMR	nuclear magnetic resonance
NOESY	Nuclear Overhauser Effect Spectroscopy
o-NBA	*o*-nitrobenzyl alcohol
OD	optical density
PBS	phosphate-buffered saline
PBSTx	phosphate-buffered saline and TritonX-100 solution
PDB	protein data bank
PEI	polyethylenimine
Ph	phenyl
PMT	post translational modification
PPI	protein-protein interaction
PVDF	polyvinylidene fluoride
PZQ	praziquantel
R_f	retardation factor
rt	room temperature
RuPhos	2-dicyclohexylphosphino-2′,6′-diisopropoxybiphenyl
s	second(s)
S. mansoni	*Schistosoma mansoni*
SAR	structure-activity relationship
satd.	saturated
SDS-PAGE	sodium dodecyl-sulfate polyacrylamide gel electrophoresis
SEC	size exclusion chromatography
s.e.m	standard error of the mean
SPAAC	strain-promoted alkyne-azide cycloadditions
SSC	saline-sodium citrate buffer

TBTA	tris(benzyltriazolylmethyl)amine
^{t}Bu	*tert*-butyl
TCEP-HCl	tris(2-carboxyethyl)phosphine hydrochloride
TfO	trifluoromethanesulfonate
TFA	trifluoroacetic acid
THF	tetrahydrofuran
THQ	tetrahydroquinoline
TIC	total ion chromatogram
TLC	thin-layer chromatography
TMS	trimethylsilane
UV	ultraviolet
w	weak
Xphos	2-Dicyclohexylphosphino-2′,4′,6′-triisopropylbiphenyl

Chapter 1

Introduction

1.1 Epigenetics

An epigenetic trait is defined by Berger *et al.* as "a stably heritable phenotype resulting from changes in a chromosome without alterations in the DNA sequence".[1] Epigenetics in the natural world is exemplified by the metamorphosis of the caterpillar to the butterfly — a transition between two life cycle stages with very different phenotypes, but the same DNA sequence. Examination of another species, the honeybee, *Apis mellifera*, reveals queen and female worker bees of the same colony are genetically identical, however, differ significantly in phenotype due to epigenetic processes.[2] The differentiation between these two phenotypes is influenced by the intake of royal jelly during development, exemplifying the effect of environmental factors on a species' epigenome. Epigenetic processes control gene expression, and within *Homo sapiens* are vital throughout the full lifespan. The influence of the environment can be observed through phenotypic changes throughout a human's life, mediated *via* epigenetics,[3] and misregulation of epigenetic processes can lead to the development of a variety of diseases.[4–6]

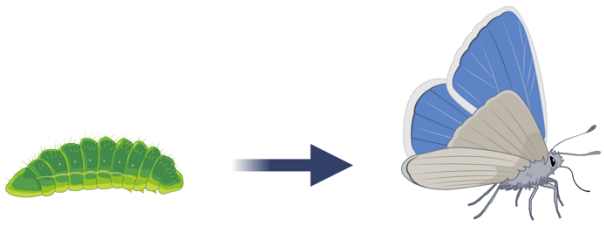


Figure 1.1. Cartoon depicting the metamorphosis of a caterpillar to a butterfly. The metamorphosis results in a large change in phenotype with constant DNA sequence and is therefore mediated by epigenetics. Created with BioRender.com.

At the molecular level, the change in phenotype results from modulation in chromosome structure.[1] A major mechanism for this modulation is through post-translational modifications (PMTs) of histone proteins.

1.2 Post translational modifications on histones

In eukaryotes, DNA, the biological set of instructions for all living things, is tightly coiled around histone proteins when inactive. DNA is wrapped around an octamer of histone proteins, and each octamer comprises of two copies of each of the histones H3, H4 H2A and H2B, which forms the nucleosome, the basic subunit of chromatin (**Figure 1.2**).

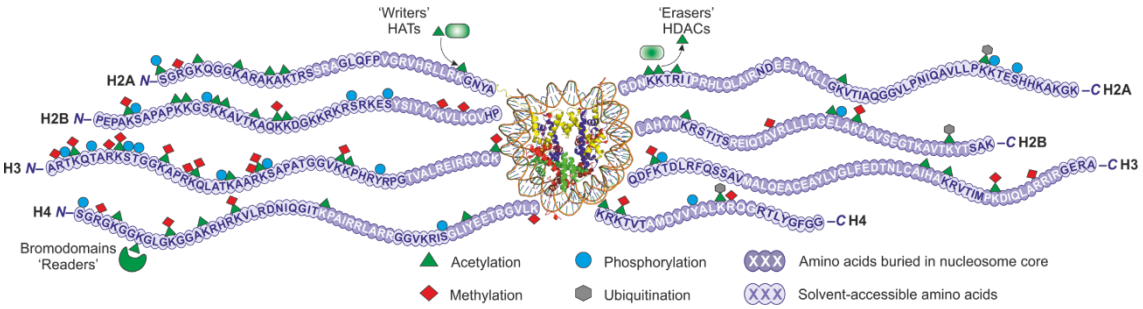


Figure 1.2. Representation of DNA wrapped around histone proteins and post-translational modifications, such as acetylation, methylation, phosphorylation, and ubiquitination, on lysine tails. Acetylation can be added with the histone acetyl transferases (HAT) 'writers', removed with the histone deacetylases (HDAC) 'erasers', and read by the bromodomains (BRD) 'readers'. Reproduced from Jennings *et al.,* Copyright 2014, Future Science Group.[7]

The tight packing of DNA enables these large biomolecules to be contained in the nucleus of cells, however, this arrangement restricts gene expression and transcription. Modifications on histone proteins can change chromosome structure, enabling gene expression, and the major modifications on histones include acetylation, methylation, phosphorylation, adenosine diphosphate (ADP)-ribosylation, glycosylation, sumoylation and ubiquitylaiton.[8] The combination of these marks comprises the histone code, which has been proposed to regulate the expression of the information contained in the genetic code, and to be essential to cell processes and resulting phenotypes.[9] Acetylation can occur on N-termainl lysine residues on histones, and the modification neutralises the charge found on lysine tails, weakening the DNA-histone interaction, resulting in the relaxation of the tightly bound chromatin.[10] This relaxation enables a change in the recruitment of transcription factors, affecting gene expression. The proteins responsible for adding, removing, and reading epigenetic markers on histones are named the 'writers', 'erasers'

and ‘readers’, and in the case of histone acetylation are the histone acetyl transferases (HATs), histone deacetylases (HDACs) and bromodomains (BRDs).

1.3 Bromodomains

Bromodomains (BRDs) were first discovered in 1992 after the identification of a novel protein module while studying the *Drosophilia* gene, *Brahma*.[11,12] These protein modules of approximately 110 amino acids are found as part of bromodomain-containing proteins (BCPs), which includes a variety of multidomain proteins exhibiting other modules such as HATs, histone methyl transferases (HMTs), and E3 ligases. In humans there are 46 BCPs with a total of 61 BRDs, which can be divided into 8 families, classified according to sequence similarity (**Figure 1.3**).

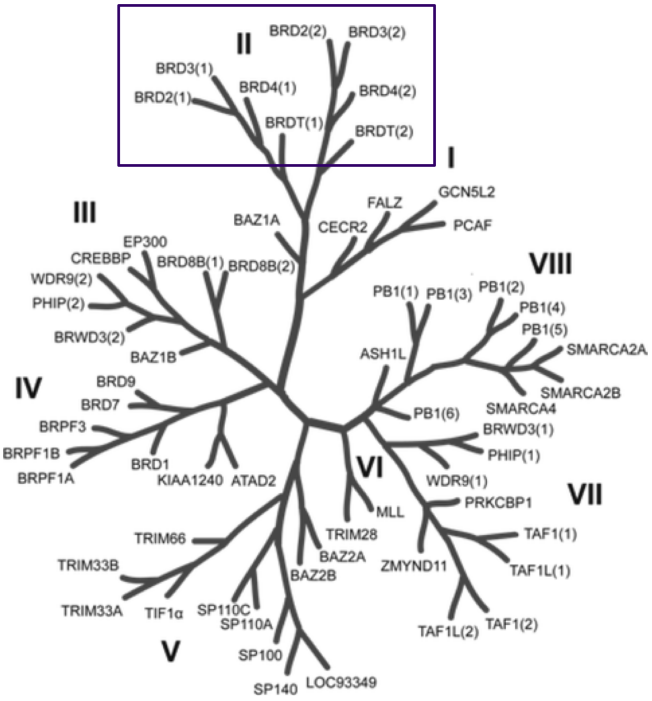


Figure 1.3. Phylogenetic tree depicting the sequence similarity between the 61 bromodomains within the 8 families. The bromodomain and extra-terminal family is highlighted with a box. Adapted with the permission of the Journal of Medicinal Chemistry.[13] Copyright (2013) American Chemical Society.

Within the many protein-protein interactions (PPIs) between BRDs and other proteins, BRDs bind to acetylated lysine (KAc) residues on histone proteins, which influences the recruitment of transcription factors that regulate gene expression. Structurally, these protein

modules are formed of a bundle of four alpha helices (named Z, A, B and C) and a hydrophobic KAc-binding pocket that is formed by a large loop between the αZ and αA (the ZA loop) and a shorted loop between αB and αC (the BC loop) (**Figure 1.4**). Typically, acetyl lysines form a hydrogen bond between the carbonyl oxygen and the NH_2 group of an asparagine residue. However, in some bromodomains a similar interaction is found with other hydrogen-bond donors such as threonine or tyrosine.[13] Despite the hydrophobicity of the KAc binding pocket, most bromodomains exhibit four or five, well-ordered water molecules at the base of the pocket, which also form hydrogen bonds with KAc, the BRD and each other.[13]

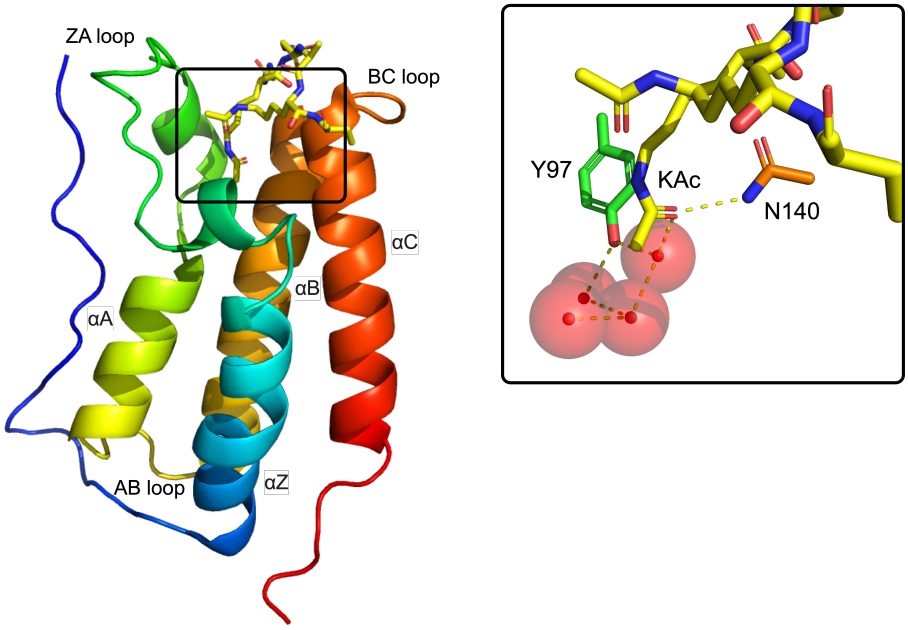


Figure 1.4. X-ray crystal structure of the first domain of BRD4 in complex with diacetylated histone 4 peptide (H4K12AcK16Ac, carbon = yellow) (PDB ID: 3UVX).[14] There is a direct hydrogen bond between the carbonyl oxygen of the KAc and N140, and a water mediated hydrogen bond between the KAc and Y97.

Despite BRDs having been studied since 1992, the overall understanding of the role of BRDs in cellular function and disease is relatively early in development.[15] The exception to this is the bromodomain and extra-terminal (BET) family. The biological roles of the BET family were revealed relatively early, and extensive research has suggested its role in human diseases, notably cancer and immune response.[15–22] The human BCPs in this family

consist of BRD2, BRD3, BRD4, and BRDT. They are characterised by the presence of two BRDs, enabling multiple KAc binding, and an extra terminal domain, involved in recruiting effector proteins.[23] Binding of KAc is enabled by a hydrogen bond between a conserved asparagine residue [N140 in BRD4(1)] and the carbonyl oxygen of the KAc, as well as a water-mediated hydrogen bond between a tyrosine [Y97 in BRD4(1)] and the carbonyl oxygen of KAc (**Figure 1.4**). Binding affinity of KAc to the bromodomains is typically weak, and K_d values for isolated peptides range from approximately 10 μM to low micromolar values.[15] This interaction can therefore be easily disrupted, and elucidation of the biological function of the human BET bromodomains has benefitted from a large array of chemical probes.[13,24,25]

1.4 Chemical probes for the human BET bromodomains

A chemical probe can be defined as "a selective small-molecule modulator of a protein's function, that allows the user to ask mechanistic and phenotypic questions about its molecular target in biochemical, cell-based or animal studies".[26] Chemical probes for the BET bromodomains mimic KAc using a variety of synthetic groups, and the first two of these BET-BRD ligands were reported in 2010. These two compounds, (+)-JQ1 (**1.1**) and I-BET762 (**1.2**) were developed by Filippakopoulos *et al*.[27] and Nicodeme *et al*.[28] respectively, and use a diazepine KAc mimic. The chemical probe I-BET151 (**1.3**), developed by Dawson *et al*.,[29] and two ligands developed in the Conway Group, OXFBD02[30] (**1.4**) and OXFBD04[31] (**1.5**), use a dimethylisoxazole group as a KAc mimic. The BET bromodomain ligand I-BET726[32] (**1.6**), and its more recent analogue I-BET567[33] (**1.7**), mimic KAc using an *N*1-acetyl group. Finally, dual BRD and other protein targeting compounds are present in the literature and one such example, BI2536 (**1.8**), developed as a kinase PLK1 inhibitor,[34] also shows strong binding to human BRD4(1).[35]

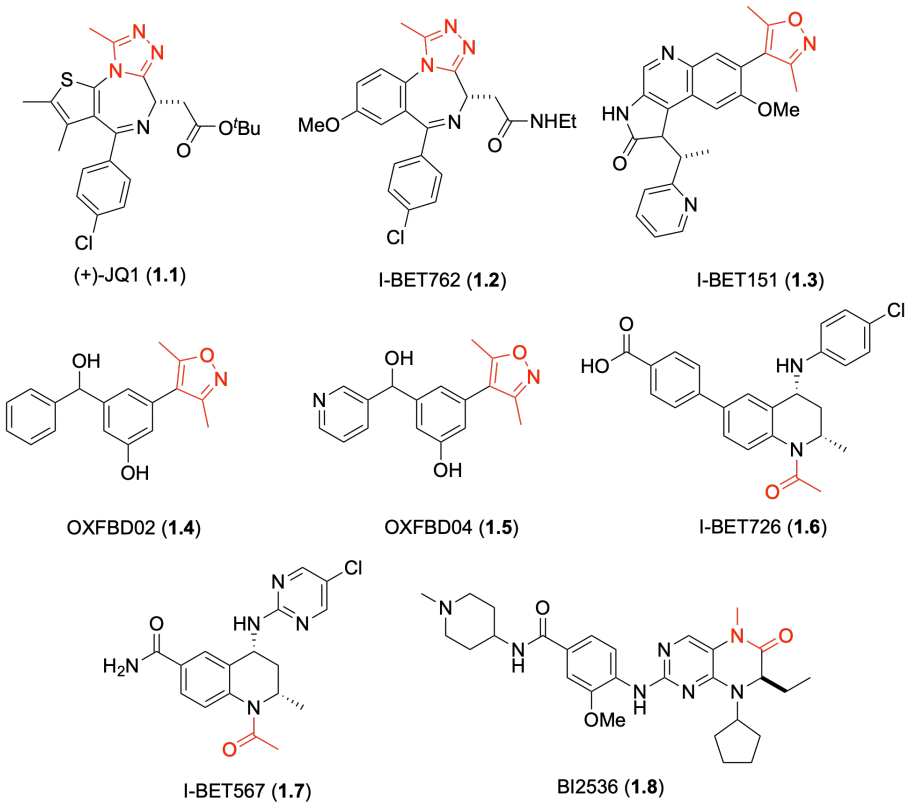


Figure 1.5. Examples of BET bromodomain ligands **1.1**–**1.8**. The acetyl-lysine mimicking component of each compound is highlighted in red.

Examination of the crystal structure of I-BET726 (**1.6**) bound to BRD4(1) (**Figure 1.6**) highlights other conserved motifs which are proposed to be important for ligand binding.[32] Analogous to KAc residues, this compound engages with Y97 with a water-mediated hydrogen bond, and directly with N140 using the oxygen of the *N*1-acetyl group (**Figure 1.6 A**). Another common motif found in the BET bromodomains is the WPF shelf, which comprises of W81, P82 and F83 in BRD4(1) (**Figure 1.6 B**). When bound to BRD4(1), the chlorophenyl ring of I-BET726 (**1.6**) makes a hydrophobic interaction with this moiety, contributing to binding affinity. The phenyl ring of the benzoic acid group of **1.6** also engages in lipophilic interactions with W81, in an edge-to-face arrangement. The carboxylic acid of this group, however, is proposed to project away from the ZA channel to therefore not significantly influence binding.[32] I-BET726 (**1.6**) is a chiral non-racemic ligand, and the (2*S*)-methyl group makes direct contact with L94. A methyl group or larger moiety in the (2*R*)-position would clash with the carbonyl oxygen of N140, and therefore, this compound

requires (2*S*)-stereochemistry for binding.[32] Indeed, an I-BET726 (**1.6**) analogue with the (2*R*)-stereochemistry showed severely reduced binding to BRD4.[32] Initial biological studies showed use of **1.6** on neuroblastoma cell lines reduced cell survival and xenograft growth *via* suppression of the oncogene MYCN expression.[36] Furthermore, I-BET726 (**1.6**) was shown to have anti-inflammatory effects, increasing the survival rate of mice in a mouse septic shock model.[32]

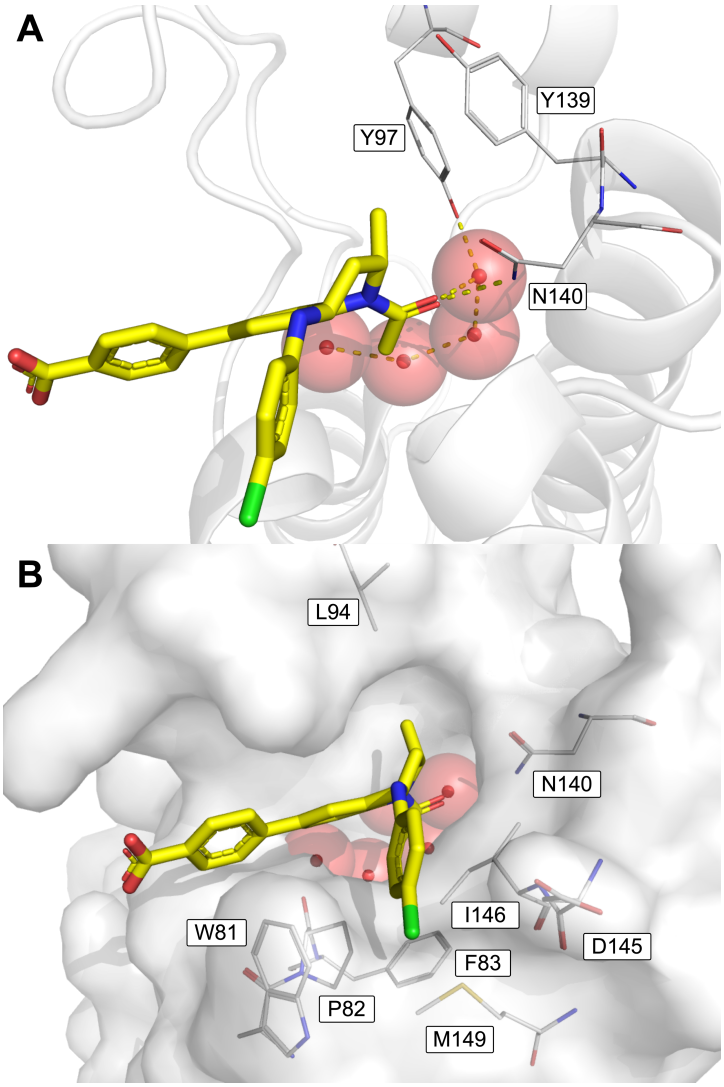


Figure 1.6. X-ray crystal structure of I-BET726 (**1.6**) (carbon = yellow) bound to human BRD4(1) (cartoon and carbon = white) (PDB ID: 4BJX).[32] **A**) I-BET726 (**1.6**) forms a hydrogen bond directly with N140 and with Y97 *via* a water molecule. **B**) The WPF shelf is important for binding of **1.6**, and the chlorophenyl group is positioned near this shelf and the residues M149, I146, and D145.

Examination of the dimethylisoxazole compound OXFBD02 (**1.4**) bound to BRD4(1) highlights the importance of conserved water molecules in the ZA channel region for BET

BRD ligand binding (**Figure 1.7**).[30] As seen with the carbonyl of the *N*1-acetyl of I-BET726 (**1.6**), the oxygen of the dimethylisoxazole OXFBD02 (**1.4**) forms a hydrogen bonding interaction with the conserved asparagine residue, N140, of BRD4(1) (**Figure 1.7 A**). The nitrogen from the dimethylisoxazole forms a water-mediated hydrogen bond with Y97, and the phenyl ring of OXFBD02 (**1.4**) is proposed to form a lipophilic interaction with the WPF shelf.[30] However, in contrast to I-BET726 (**1.6**), this compound engages with conserved water molecules residing in the ZA channel through the phenolic group (**Figure 1.7 B**). The initial report of phenotypic activity of OXFBD02 (**1.4**) showed this compound influenced the proliferation of hematopoietic cancer and adenocarcinoma cell lines.[30]

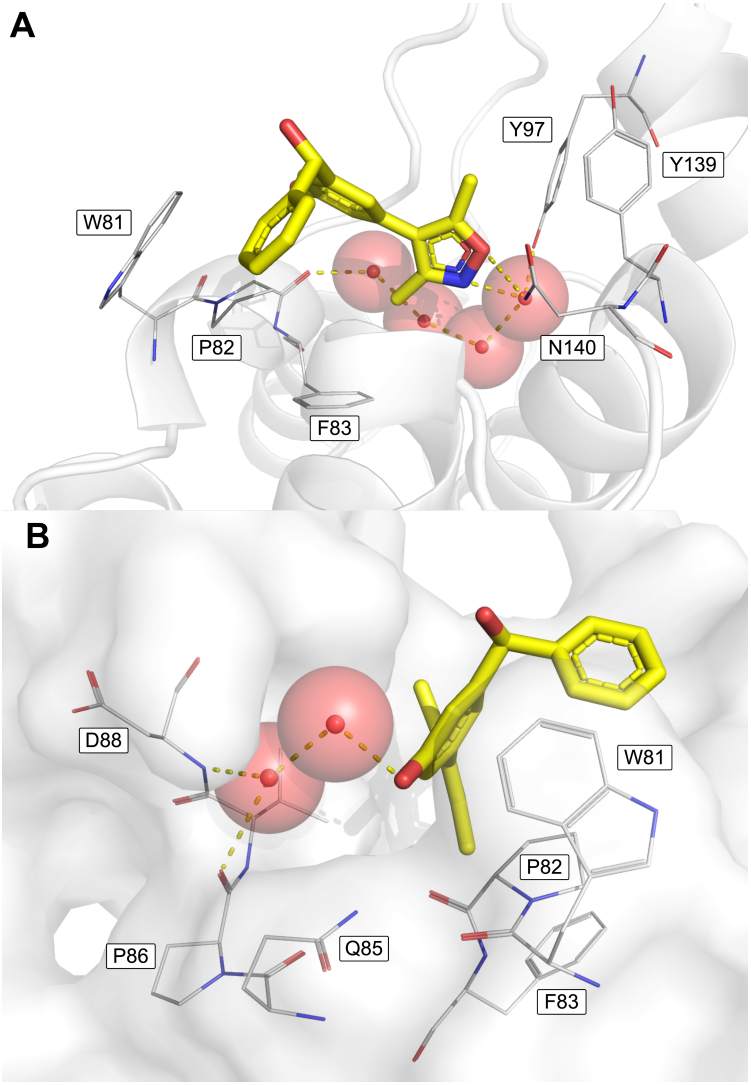


Figure 1.7. Crystal structure of OXFBD02 (**1.4**) in the binding pocket of BRD4(1) (PDB ID: 4J0S).[30] **A**) Binding mode of the KAc mimic of OXFBD02 (**1.4**). **B**) Engagement of the phenolic OH of OXFBD02 (**1.4**) with the ZA channel water molecules.

The first generation of BET inhibitors are classed as pan-BET ligands, as these compounds do not show significant selectivity for the N-terminal BRD (BD1), over the C-terminal BRD (BD2). This lack of selectivity is a result of the high structural similarity between BET BRDs, and the individual roles of the first and second domains of BET BCPs are unable to be investigated using pan-BET ligands. More sequence similarity is seen between the N-terminal domains of each BET BCP [for example BRD2(1) and BRD3(1)], and correspondingly between the C-terminal domains, compared with the N-terminal and C-terminal domains within a BET BCP [for example BRD3(1) and BRD3(2)] (**Figure 1.3**). Differences in amino acid sequence in the binding pockets of N-terminal and C-terminal domains result in polarity differences and comparatively narrower binding region in the C-terminal domain.[24]

Selective inhibitors, exploiting this structural difference between BET BD1 and BD2 domains, have been reported in the literature (**Figure 1.8**).[24,37–39] Work in 2013 by McLure *et al*. developed RVX-208 (**1.9**), a BET BD2 selective ligand, which increases the production of ApoA-1 in hepatocytes *in vitro*.[37] Faivre *et al*. at AbbVie produced ABBV-744 (**1.10**), which shows high selectivity for the second bromodomains of the BET family, with more than 290 fold selectivity over the first domains of BRD2, 3 and 4, and with antiproliferative effects on acute myeloid leukaemia and prostate cancer cell lines.[38] Researchers at GSK developed GSK778 (**1.11**) and GSK046 (**1.12**) as BET BD1- and BD2-selective ligands, respectively.[39] Use of these ligands revealed BD1 inhibition replicated the phenotype of the effect of pan-BET BRD ligands in cancer models, whereas BD2 inhibition predominantly affects inflammatory and autoimmune disease models.[39] It is suggested the higher selectivity shown with these compounds for the BRDs within the BET family can reduce off-target effects and toxicities seen with pan-BET BRD inhibitors.[24] Indeed, BD selective BET ligands have progressed to assessment in clinical trials, for example, RVX-208 (Apabetalone) (**1.9**) has been approved to commence research in Phase II clinical trials for pulmonary arterial hypertension.[40]

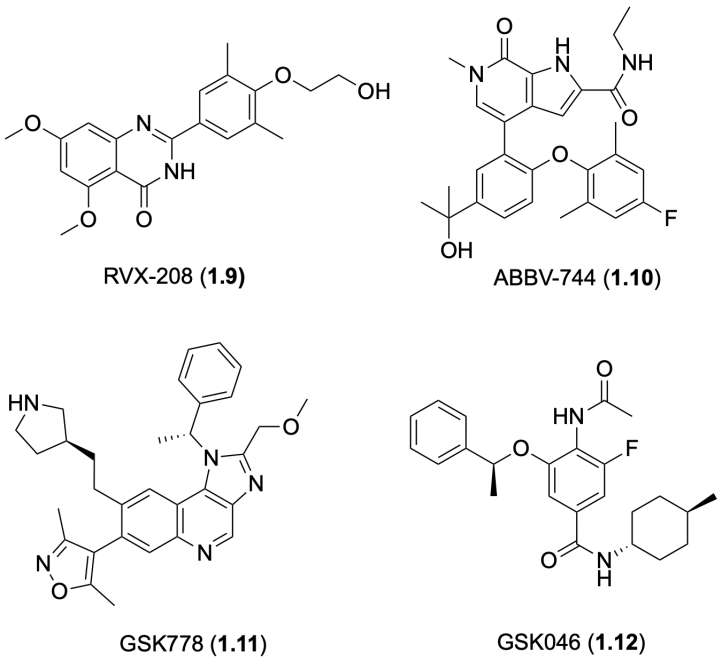


Figure 1.8. Structures of exemplar BET BD1 and BD2 selective compounds **1.9**–**1.12**.[37–39]

BET BD2 selective ligands based upon, or inspired by, the tetrahydroquinoline scaffold, exemplified by I-BET726 (**1.6**) and I-BET567 (**1.7**), have also been developed. Work by Slavish *et al.*, published in 2020, developed a tetrahydroquinoline-based BRD2 ligand, SJ432 (**1.13**) which exhibited 80-fold selectivity for BRD2(2) over BRD2(1), and 152-fold selectivity for BRD4(2) over BRD4(1).[41] Selectivity resulted from the benzonitrile moiety of this compound, which exploits the amino acid difference of D160 in BRD2(1) and H433 in BRD2(2). H433 of BRD2(2) forms a favourable π-π stacking interaction with the phenyl ring of SJ432 (**1.13**), as well as contributing to a water mediated hydrogen bonding interaction with the linker nitrogen atom of this compound and the backbone carbonyl oxygen of L381 (**Figure 1.9. A**).[41] The work by Slavish *et al.* maintained the tetrahydroquinoline core for SAR studies. However, Hirst and co-workers replaced the tetrahydroquinoline with a tetrahydroquinoxaline, containing a cyclo propyl group in the 2-position of the tetrahydroquinoxaline ring, to introduce selectivity for BRD4(2).[42] The result of this work was GSK340 (**1.14**), which has nanomolar affinity to BRD4(2) (pIC_{50} = 7.2) with 50-fold selectivity over BRD4(1). The tetrahydroquinoxaline was suggested to introduce BRD4(2) selectivity

by altering the angle of groups engaging with the WPF shelf and the BRD2(2) specific H433.[42] During this study, co-crystallisation of GSK340 (**1.14**) with BRD2(2) revealed a hydrogen bond between the tetrahydropyridine nitrogen and a water network in the ZA channel exit (**Figure 1.9. B**). The benzylic alcohol forms a hydrogen bond with the BRD2(2) specific H433 and solvent.[42]

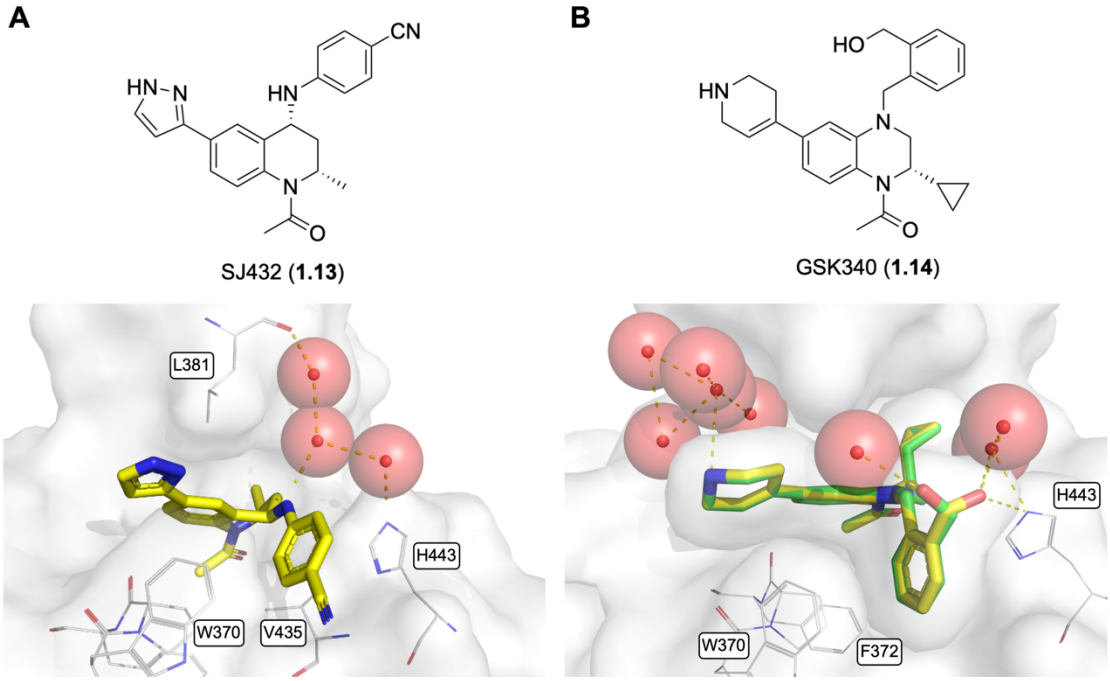


Figure 1.9. A) Co-crystal structure of SJ432 (**1.13**) (carbon = yellow) bound to BRD2(2) (carbon = white) (PDB ID: 6DDJ).[41] **B**) The two binding conformations of the hydroxyl group GSK340 (**1.14**) (carbon = yellow and green) bound to BRD2(2) (carbon = white) (PDB ID: 6FFG).[42] The binding interactions important for domain selectivity are highlighted in both **A**) and **B**).

Despite a wealth of literature on BET BRD ligands, there are, to date, no FDA approved BET inhibitors in the clinic. Often, candidate drug attrition in late-stage clinical trials is a result of inadequate knowledge of off-target activity.[43–45] Chemical biology approaches, for example photoaffinity labelling, can be used to characterise whole proteome protein-ligand interactions, providing valuable information during pre-clinical drug development and potentially reducing attrition.[45,46] A number of studies have used photoaffinity probes to examine the proteome wide interactions of BET BRD ligands.

1.5 Photoaffinity probes for human bromodomains

Photoaffinity probes are useful tools in the fields of chemical biology and drug discovery for identifying cellular targets of biologically active compounds, and the determination of binding site location.[47] They can provide important information on the selectivity and target engagement of a chemical probe in the proteome. These probes consist of photoreactive groups combined with the protein ligand. The ligand interacts non-covalently with its protein targets within a biological system. Upon irradiation, the photoactive group reacts with protein to form a covalent bond. Downstream analysis of the targets using SDS-PAGE or mass spectrometry are enabled using a tag or a ligation handle. The commonly used photoreactive groups are aryl azides, benzophenones, and diazirines (**Figure 1.10**).[48,49]

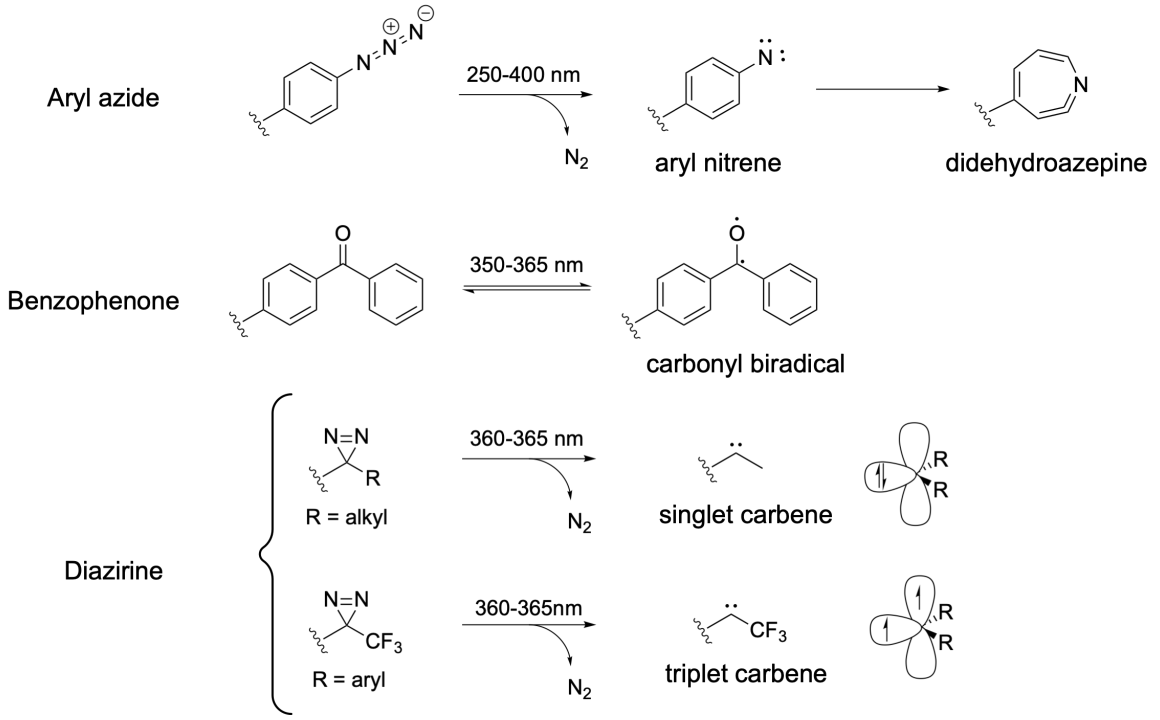


Figure 1.10. Examples of common photoactive groups used in the literature and their corresponding reactive intermediates upon irradiation.[48,49]

Upon irradiation with UV light, with a λ_{max} of approximately 250 nm, aryl azides form an aryl nitrene.[48] The major pathway of photoaffinity labelling by aryl azides occurs by rearrangement of the nitrene to a didehydroazepine, and nucleophilic addition of protein residues to this intermediate to form an azepine.[48] The didehydroazepine intermediate is

very selective in its reactivity to functional groups, such as with amines but not hydrocarbons, reducing the crosslinking ability to proteins, and a further limitation of aryl azides is the required low λ_{max} for activation, introducing the possibility of UV damage to biomolecules.[48,50] Benzophenones are activated at 350–365 nm and form a triplet carbonyl biradical, which can insert into the bonds of protein residues.[48] An advantage of benzophenones over aryl azides is that the longer wavelength required for activation is less damaging to protein primary structure. Drawbacks of this functional group, however, are their large size, which can affect binding of the probe to proteins, and the long irradiation times required for activation, which can increase the possibility of non-specific crosslinking.[48,51] A solution to the limitations described above is the use of diazirines as a photoreactive group. Their small size and efficient activation at longer wavelength UV radiation has led to significant use in the literature.[50] Upon irradiation diazirines are transformed into highly reactive carbenes. The reactive carbenes can crosslink to amino acid residues in proteins. A limitation of the use of these groups is typically low photolabeling yields due to fast quenching of the reactive carbene with water, however, this characteristic has the advantage of decreasing unspecific labelling.[50] Diazirines also isomerise to a diazo intermediate, which can either further convert to the carbene or alternatively react as the diazo intermediate (**Figure 1.11**).

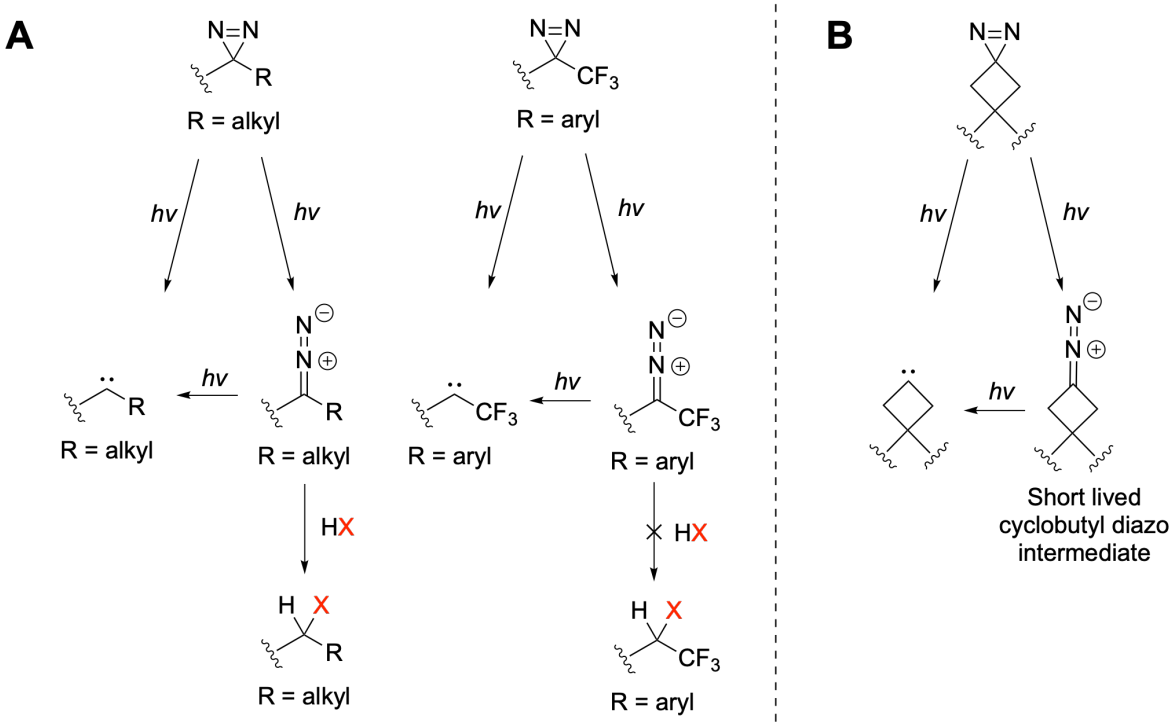


Figure 1.11. A) The carbene and diazo intermediates that result from the UV irradiation of alkyl and aryl-trifluoro diazirines. The diazo intermediate resulting from alkyl diazirines react with acidic residues (HX) in a pH dependent manner, or degrade to the carbene, whereas aryl-trifluoro diazo intermediates are electronically stable and only degrade to the carbene.[52] **B**) The cyclobutene-based 'PALBOX' employs ring strain to reduce the lifetime of the diazo intermediate.[53]

Alkyl diazirines form singlet carbenes, whereas aryl-trifluoro diazirines predominantly form triplet carbenes.[50] This difference can influence the reactivity profile of the group.[48] Furthermore, the aryl-trifluoro group stabilises the diazo isomer to acid, and therefore the labelling capacity from this diazirine arises only from the carbene (**Figure 1.11 A**).[54,55] Work by Woo and co-workers has demonstrated the reactivity difference between the two different diazirines.[52] Alkyl diazirines preferentially react with acidic residues in a pH-dependent manner due to the contribution of the diazo intermediate, whereas aryl-trifluoro diazirines react with all 20 amino acids, consistent with the reactivity profile of the carbene.[52] Woo and co-workers have recently developed a cyclobutene-based diazirine, termed PALBOX, to use ring strain to reduce the lifetime of the diazo intermediate produced from alkyl diazirines (**Figure 1.11 B**).[53] These probes showed pH-independent labelling and reduced background labelling of proteins. In summary, the diazirine reactivity differences are important considerations for the design of these photoaffinity probes.

Other reported examples of photoreactive groups employ ACT (2-aryl-5-carboxytetrazole), and *o*-NBA (*o*-nitrobenzyl alcohol).[56,57] Interestingly, isoxazoles, discussed in **section 1.4** as a KAc binding mimic, have recently been reported to exhibit photoactive properties, which has been applied to chemical proteomics.[58]

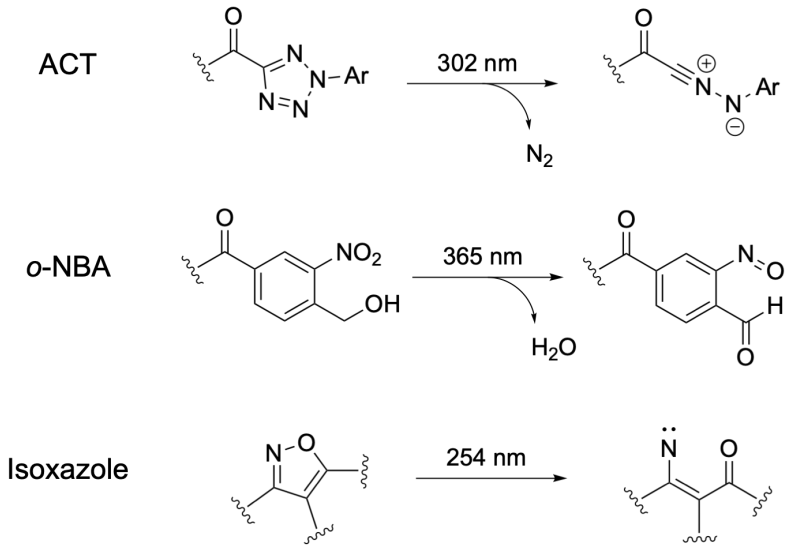


Figure 1.12. Further examples of photoreactive groups.[56–58]

After covalent modification of proteins using photoreactive groups, a tag, for example a fluorophore or biotin, can be employed to assist in analysis. Probes functionalised with tags can be cell impermeable due to their size. To overcome this limitation, smaller probes employing ligation handle, for example an alkyne, allow the addition of later stage functionality, accomplished using click chemistry (**Figure 1.13**). Click chemistry commonly refers to a copper(I)-catalysed 1,3-dipolar cycloaddition between an alkyne and azide, named copper-catalysed alkyne azide cycloaddition (CuAAC), and was first reported separately by Sharpless and Meldal in 2002.[59,60] For use in live biological systems, Cu(I) is unsuitable due to its toxicity and therefore work, notably by the Bertozzi and co-workers, has developed copper-free click reagents. These reactions employ strain-promoted [3+2] azide-alkyne cycloaddition (SPAAC) between azides and strained cyclooctynes.[61,62] A further, copper-free biorthogonal ligation alternative is the inverse-electron-demand Diels-Alder (IEDDA) reaction, which occurs between tetrazines and alkenes, notably trans-

cyclooctene.[63] It should be noted that aryl azide photoreactive groups are incompatible with the use of alkyne reactive handles, due to possible click reactions between the azide photoreactive group and the alkyne.

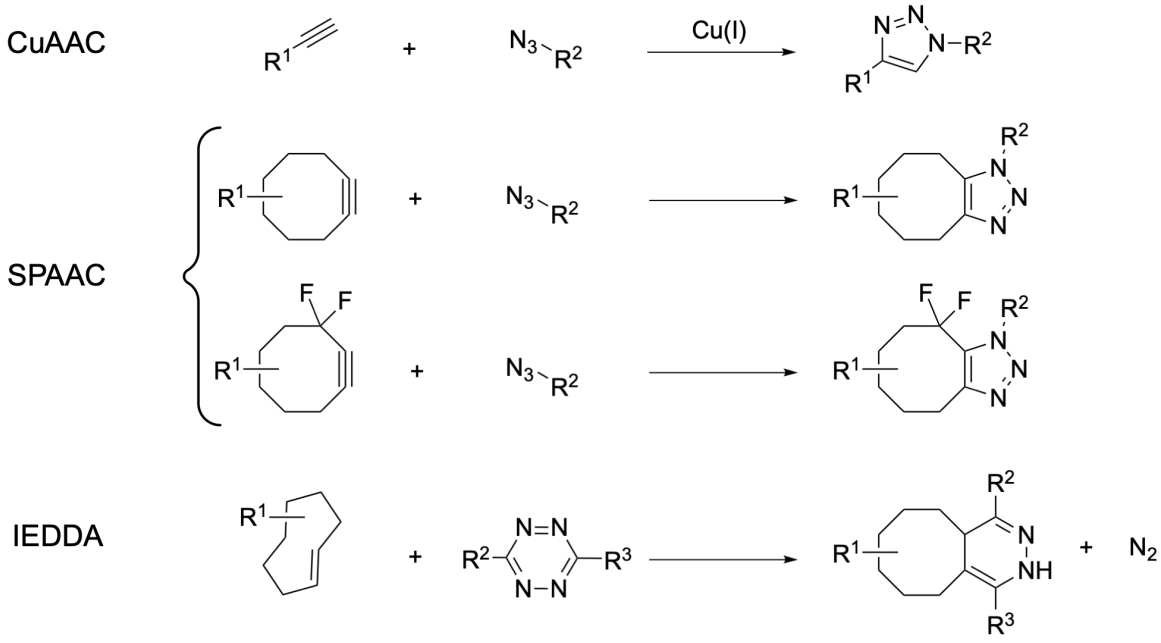


Figure 1.13. Examples of biorthogonal click chemistry reactive handles.[59–63]

The technology described above has been used to develop photoaffinity probes for the BET bromodomains (**Figure 1.14**), revealing information about the whole proteome targets of BET BRD ligands.

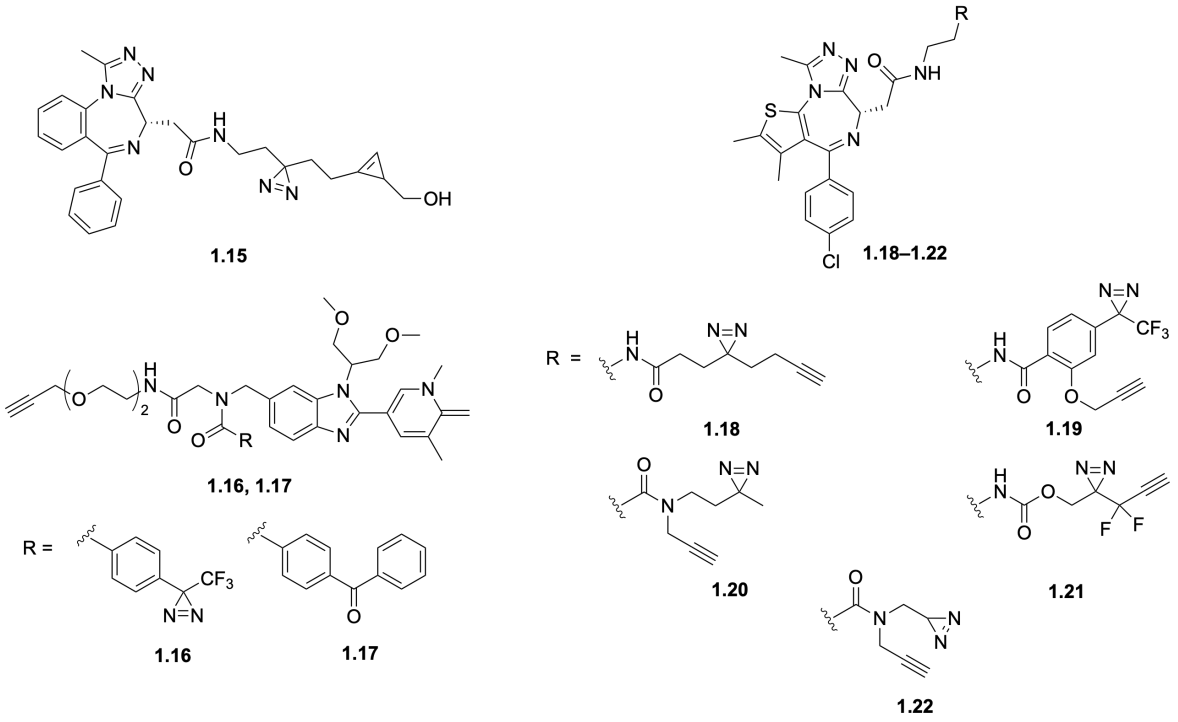


Figure 1.14. Examples from the literature of BET BRD photo affinity probes.[45,64,65]

Li *et al*. developed a photoaffinity probe based on the BRD4 ligand GQ841819X, a close analogue of (+)-JQ1 (**1.1**), employing a diazirine and a copper-free cyclopropene-based ligation handle (**1.15**).[65] This probe crosslinked to BRD4 *in vitro* and was used to image and label BRD4 in live mammalian cells. Use of the probe for *in situ* labelling in HepG2 cells revealed 161 high-confidence protein targets, which were proposed to also be targets of (+)-JQ1.[65] Fallon *et al.* examined a wide variety of photoactive groups with a range of linker lengths appended to a reported pan-BET inhibitor, which were rapidly synthesised using one-pot Ugi reactions.[45] The probes with high photocrosslinking yields with recombinant BRD4(1) and BRD4(2) exhibited an aryl-trifluorodiazirine (**1.16**) and a benzophenone (**1.17**), and these probes were progressed to in-cell proteomic investigation. These probes enriched 135 and 95 proteins, respectively, with an overlap of 66 proteins between the two probes. Competition experiments with the parent ligand revealed that with the diazirine **1.16,** only the BET bromodomains were competed, whereas competition experiments with the benzophenone probe **1.17** revealed competitive engagement with a zinc-finger domain (ZMYM1) and a known BRD4 interactor, SUPT16H.[45] This study highlights that the choice

of photoaffinity group affects the labelling outcome of these probes. Different labelling outcomes from the choice of photoaffinity group was also found in work by Conway *et al*., when evaluating the labelling profile of a selection of different fully functionalised diazirine-based tags.[64] Five different alkyl-diazirine tags exhibiting an alkyne tag were appended to the ligand (+)-JQ1 (**1.18**–**1.22**) and the proteins enriched were identified using MS-based proteomics. A large difference in the number and type of proteins labelled were observed for each diazirine tag. For example, the BET bromodomains BRD3 and BRD4 were enriched by **1.20**, whereas **1.19** and **1.21** enriched very few proteins, and no BRD-containing proteins over corresponding controls.[64]

Traditional photoaffinity probes, such as those above, typically suffer from poor signal-to-noise labelling and low crosslinking yields.[66] Furthermore, as outlined above, the choice of photoaffinity group and the positioning of such group significantly affects the proteins labelled in chemical proteomic experiments. Work from collaboration between the MacMillan group and Merck have recently developed a catalytic diazirine labelling approach, which is proposed to address the issues associated with traditional photoaffinity probes.[66]

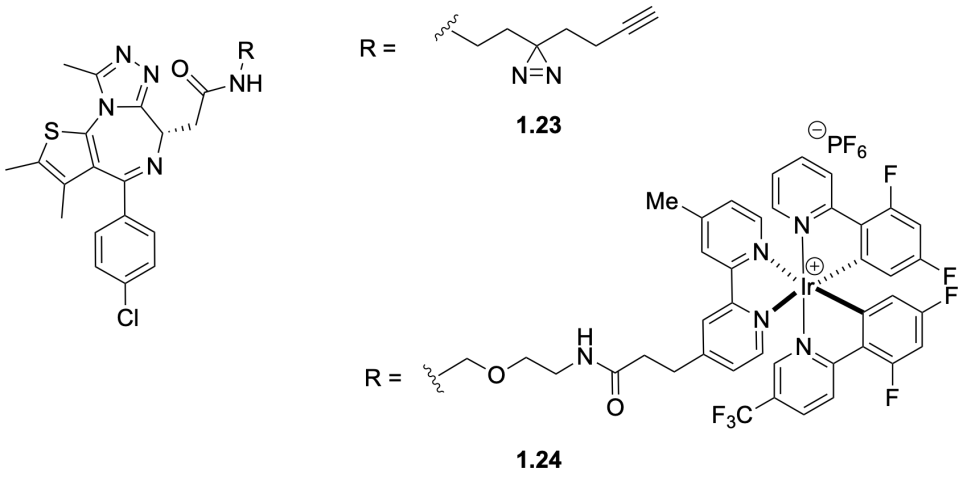


Figure 1.15. Structures of traditional diazirine-based (+)-JQ1 probe (**1.23**) and iridium-based (+)-JQ1 probe (**1.24**).[66]

Upon irradiation with blue light, a Dexter energy transfer occurs from the iridium catalyst component to separate excess diazirine-biotin probe components. This results in spatially

dependent labelling of target proteins, and due to the non-stoichiometric catalytic labelling, results in significant signal enhancement.[66] An iridium-containing probe (**1.24**), based upon (+)-JQ1 (**1.1**), labelled BRD3 and BRD4 in HeLa cells, along with known (+)-JQ1 (**1.1**) off targets HADHA and SRRM2. The transmembrane protein ALCAM was also identified as a putative new off-target of (+)-JQ1. In experiments with the traditional diazirine probe **1.23**, using UV irradiation at 350 nm, enrichment of BRD proteins were not observed using Western blot or chemoproteomics.[66] This iridium catalytic approach could be applied in future chemoproteomic studies and is particularly desirable for the study of proteins with low expression. Furthermore, this method may be useful to study the proteome of other species for which the expression levels of proteins are little characterised or unknown.

1.6 Schistosomiasis and *S. mansoni*

Metazoan parasites are organisms which undergo large changes in phenotype, through multiple life cycle stages, which are essential to its survival and proliferation. Similar to the metamorphosis of the caterpillar to the butterfly, these transformations occur with constant DNA sequence and epigenetic mechanisms likely play a key role in these processes. One group of parasites that show this wide variety of phenotypically distinct life forms during its life cycle are the blood flukes of the *Schistosoma* genus. These are water born parasites that cause the neglected tropical disease schistosomiasis, a disease which affects an estimated 200 million people and contributes to at least 200,000 deaths a year.[67,68] Infection with *Schistosoma* parasites increases the risk of developing certain types of cancers, modulates the immune system leading to reduced efficacy of vaccines, and is responsible for millions of disability adjusted life years lost.[69] Furthermore, the WHO has targeted schistosomiasis for elimination by 2030 in the recent 'Ending the Neglect to Attain the Sustainable Development Goals' roadmap.[70] For this aim, it is important to understand the underlying biology and biochemical machinery of these parasites.

The life cycle of Schistosome parasites (**Figure 1.16**) is largely aquatic and involves infecting snail intermediate hosts and mammal primary host.[71] First, schistosome eggs

hatch into miracidia in fresh water and locate and penetrate the intermediate host, aquatic snails, and develop into sporocysts. These sporocysts then multiply and develop further to the human infective form, cercariae, which penetrate the skin of mammals. The cercariae lose their tails and become schistosomula, which migrate in the venous blood stream to the hepatic portal vein of the liver where they develop into adult male and female worms. These adult worms migrate to the mesenteric veins and pair up for sexual reproduction. Females lay eggs, which are responsible for the majority of initial infections and symptoms, and the eggs exit the hosts body to continue the life cycle.[71]

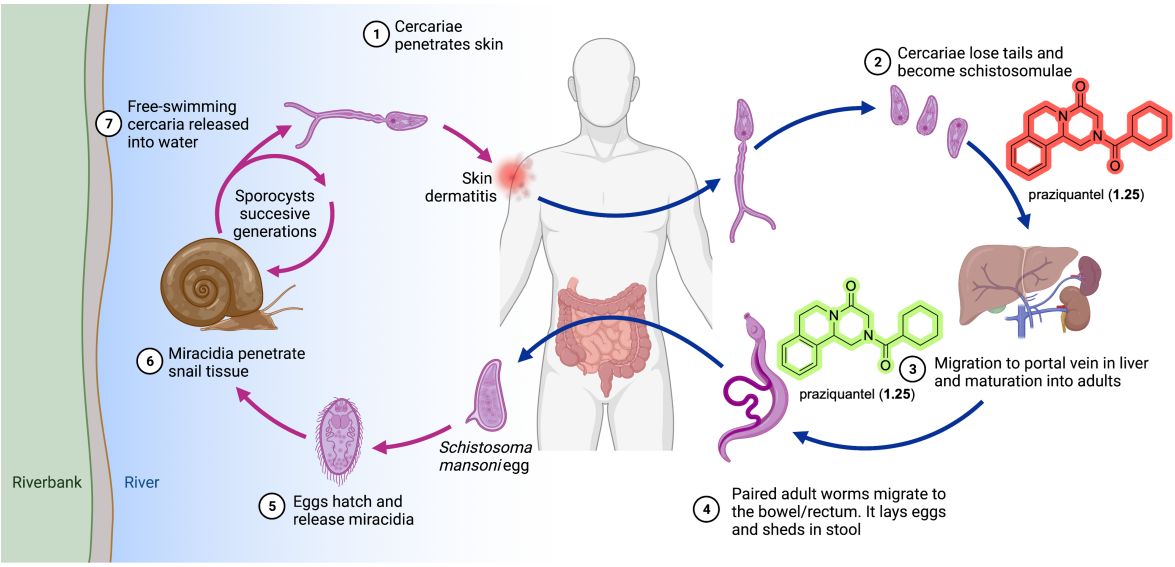


Figure 1.16. A simplified cartoon of the life cycle of *S. mansoni*.[72] Praziquantel (**1.25**) is mostly ineffective against the schistosomula life cycle stage. **Figure 1.16** was reproduced and modified with permission from Prof. Stuart Conway (S.J.C.), using a figure created by S.J.C. with Biorender.com.

The species *Schistosoma mansoni* is one of the *Schistosoma* species responsible for the greatest number of human cases of schistosomiasis, is the most geographically wide spread, and is primarily considered a human rather than zoonotic parasite.[73] The main drug used to combat this parasite is praziquantel (**1.25**), due to its high efficacy on all *Schistosoma* species, its low cost, and low human toxicity.[74,75] However, this drug is mostly ineffective against schistosomula, with an initial effect on schistosomes after administration in the first few days of infection which rapidly drops over time, to a minimum level 28 days post infection.[74] The mechanism of action of this drug is unconfirmed, however, it is

suggested to act by disruption of *S. mansoni* voltage-gated calcium channels.[75–78] Due to its mass administration in schistosomiasis preventative campaigns, along with isolated reports in reduction in efficacy and isolation of resistant strains, there is a concern of resistance to praziquantel developing.[75,77–79] Consequently, there has been a concerted effort towards the discovery of new drugs targeting *S. mansoni*. Due to the likely importance of epigenetics in the parasite life cycle, a number of studies have aimed to understand and target the epigenetic mechanisms of the parasite.

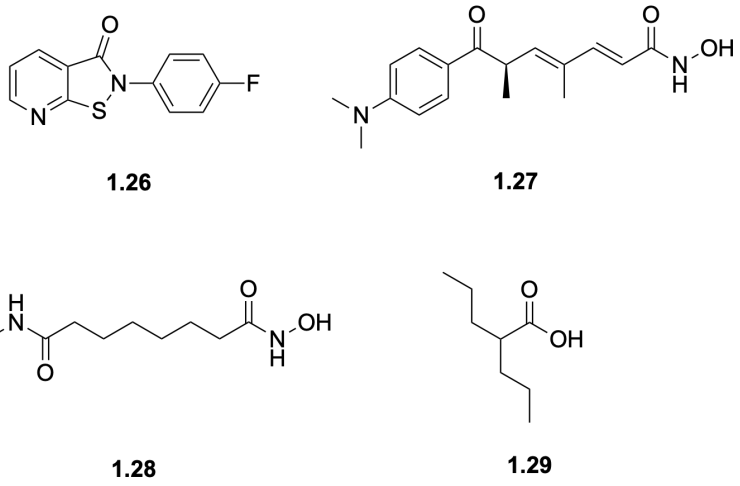
1.7 Epigenetics of *S. mansoni*

In eukaryotes, the nucleosome is formed from two copies of histones H2A, H2B, H3 and H4, assembled as an octamer, and stabilised with a linker histone H1. Work by Anderson *et al*. has detected all five of these histone families in *S. mansoni* at all six life cycle stages by *in silico* analysis, using the *S. mansoni* genome and transcriptome data.[80] This work showed some core *S. mansoni* histone isoforms show high similarity to humans, for example 100% identity to human H4.A, and 79–99% identity to human H3 forms. Post translational modification on these histones are important in schistosome function.

Histone methylation is important for the progression between life forms of *S. mansoni*. A study by Roquis *et al*. showed methylation of histones is present at low levels at the miracidium life stage and progressively increases to the adult stage.[81] In the same study, human histone methyltransferase inhibitors prevented the transition of miracidium to sporocyst life forms. Another investigation showed bivalent H3K4/H3K27 trimethylation on *S. mansoni* cercariae histone H3 is similar to embryonic stem cells of vertebrates, and this modification was suggested to maintain gene transcription in a poised state for rapid differentiation upon infection of the primary host.[82]

Histone acetylation has been shown to be important in mortality and egg production of *S. mansoni*. GCN5 and CBP1 are human HAT proteins, and a study by Carneiro *et al*., aimed at characterising the role of *S. mansoni* orthologues *Sm*GCN5 and *Sm*CBP1, showed

inhibition of these proteins by a human HAT inhibitor PU139[83] (**1.26**) decreased transcription of the gene *Smp14*, a gene for which activation was shown to be dependent on histone acetylation.[84] The study showed this decrease in transcription affected the production and structure of eggs produce by female schistosomes, and this effect was also seen after dsRNAi knockdown of *Sm*GCN5 and *Sm*CBP1. In a work by Dubois *et al*., human HDAC inhibitors Trichostatin A (TSA) (**1.27**),[85] suberoylanilide hydroxamic acicd (SAHA) (**1.28**),[86] and valproic acid (VPA) (**1.29**),[87] were shown to inhibit total HDAC activity at all life cycle stages, with TSA and VPA causing mortality in juvenile schistosomes and adults.[88]



1.26 **1.27**

1.28 **1.29**

Figure 1.17. Structures of known human HAT and HDAC inhibitors **1.26**–**1.29**.[83,85–87]

Work by Lancelot *et al*. investigated the NAD^+-dependent HDACs, the sirtuins.[89] Incubation with known human sirtuin inhibitors Sirtinol (**1.30**),[90] Salermide (**1.31**),[91] and MS3 (**1.32**),[92] (**Figure 1.18**) induced apoptosis and death of schistosomula, the separation of adult worm pairs, and a reduction in egg laying. Comparison of the phenotype from knockdown of *Sm*Sirt1 using RNAi suggested *Sm*Sirt1 was the principal target of the compounds.[89] These studies demonstrated the importance of histone acetylation to the function of *S. mansoni* and the HATs are HDACs were proposed to be potential novel targets for the disease. However, for potential therapeutic use, species selective inhibitors of parasite epigenetic proteins are required.

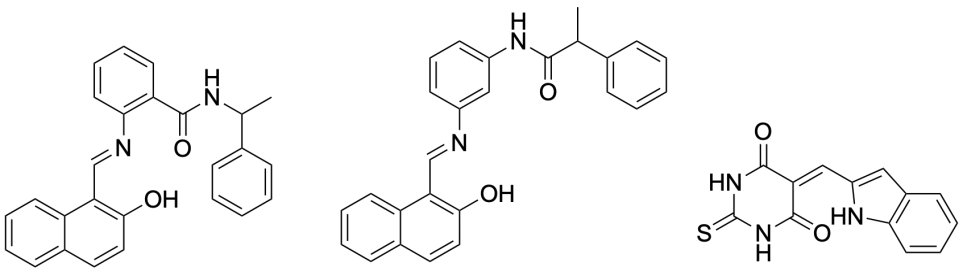


Figure 1.18. Structures of human Sirtuin inhibitors **1.30**–**1.32**.[90–92]

A number of studies for the identification of species selective and novel ligands have focussed on the HDACs of *S. mansoni*. Homogeneous and heterogeneous fluorescence-based deacetylase assays have been developed for the *S. mansoni* sirtuin *Sm*Sirt2.[93] The homogeneous assay was used to identify hits for *Sm*Sirt2, which led to optimisation using structure activity relationship (SAR) studies to produce ligands showing an effect on the phenotype of *S. mansoni*, notably affecting the schistosomula viability, adult worm pairing and egg production.[94] Five *Sm*Sirt2 ligands developed in this study were selective for the parasite isoform of Sirt2 over the human equivalent and were non-toxic to human cancer cells, a promising result of therapeutic value.

Significant attention has been given to *S. mansoni* HDAC, *Sm*HDAC8. The class I *Sm*HDACs (SmHDAC1, 3 and 8) are expressed across all life-cycle stages, and with the exception of the schistosomula stage, *Sm*HDAC8 exhibits the most abundant mRNA transcripts within this class.[95] An investigation by Marek *et al*. used the crystal structure of *Sm*HDAC8 with known, generic HDAC inhibitors to design new *Sm*HDAC inhibitors with reduced affinity for human HDACs.[96] One of these inhibitors, **1.33**, induced apoptosis and mortality in *S. mansoni* schistosomula and unpairing in adult worms. A further study by Heimburg *et al*. employed structure-based design on a benzohydroxamate template.[97] This work identified novel *sm*HDAC8 inhibitors with high species selectivity over human HDAC1 and HDAC6, and the most potent compound (**1.34**), with an EC_{50} of 16.1 μM against schistosomula, killed schistosomula *in vitro* and caused a significant decrease in adult worm pairing and egg laying. In a 2021 study, Ghazy *et al*. chemically optimised

benzohydroxamate-based *Sm*HDAC8 inhibitors, and the result of this work was a further analogue (**1.35**) with potency against schistosomula, with an EC_{50} of 3.5 μM.[98]

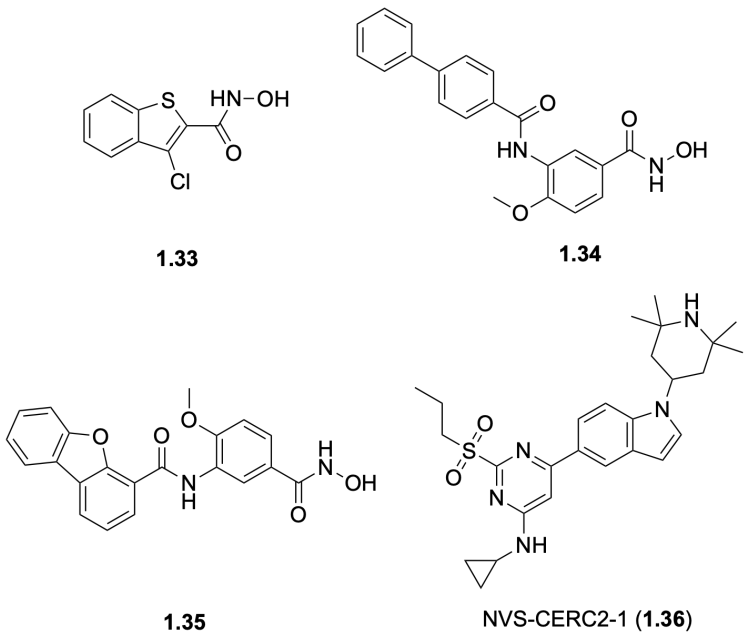


Figure 1.19. Structures of *Sm*HDAC8 inhibitors **1.33**–**1.35** and NVS-CERC2-1 (**1.36**).[96–99]

To date, the role of BRDs in *S. mansoni* is not well understood,[84,100,101] and in broader scope the role of BRDs in parasites is also not well understood.[102] The *S. mansoni* HAT proteins, *Sm*GCN5, and *Sm*CBP1, have been expressed as multidomain constructs containing the bromodomain, or as the sole bromodomain, however, only histone acetyltransferase activity was investigated in these studies, and the bromodomain was little explored.[103,104] *Sm*GCN5 acetylates histones H3 and H2A,[103] whereas *Sm*CBP1 primarily acetylates H4.[104] A study by Whately *et al*. examined the performance of known human epigenetic probes and inhibitors on a high throughput drug discovery assay, aimed at schistosomula.[105] From this probe selection, 16 bromodomain ligands were included and five were determined as hits, which were progressed to testing on adult worms. The BET bromodomain ligand (+)-JQ1 (**1.1**) was included in this collection, which showed activity on the juvenile *S. mansoni*. Of the BRD ligands investigated, the human non-BET BRD ligand NVS-CECR2-1[99] (**1.36**) was the most active against juvenile schistosomula and adult worms, showing 5 to 6 times lower EC_{50} values on adult worms than (+)-JQ1 (**1.1**). NVS-CECR2-1 (**1.36**) binds to the human

BCP CECR2 and a *S. mansoni* orthologue was identified by BLASTp analysis.[105] This study showed, assuming negligible off-target effects, inhibition of the bromodomains can negatively affect the ability of the parasite to function. However, these compounds were not confirmed to bind to the *S. mansoni* bromodomain orthologues *in vitro*. To date, there has been no published study on the rational design of ligands for a bromodomain of *S. mansoni*. However, previous work in the Conway Group (University of Oxford), in collaboration with the Hoffmann Group (University of Aberystwyth), has initiated a comprehensive, targeted study for ligands of an *S. mansoni* bromodomain.

1.8 Previous work towards a bromodomain of *S. mansoni, Sm*BRD3

Although BRDs had been identified in the previously characterised HAT proteins *Sm*GCN5,[103] *Sm*CBP1 and *Sm*CBP2,[104] a comprehensive search for the BRDs of *S. mansoni*, including the had not been published. Bioinformatic analysis using a combination of sequence similarity and domain-based searches has been used to characterise *S. mansoni* histone methyltransferases (HMTs) and histone demethylases (HDMs).[106] The same approach was applied by Dr Gilda Padalino (G.P.) (University of Aberystwyth) to identify 22 bromodomain-containing proteins in *S. mansoni*, featuring 29 distinct BRDs in total (**Figure 1.20 A**). For a selection of these BCPs, a close human homologue was assigned based on sequence similarity, revealing the previously identified *Sm*GCN5, *Sm*CBP1, and *Sm*CBP2. Despite four BCPs featured in the human BET family, only one BET homologue was identified in *S. mansoni* (Smp_147950, UniProt: G4V8V7). This BCP shares highest similarity with human BRD3 (37.5% sequence identity), with two BRDs in tandem, and was therefore denoted *Sm*BRD3.

A heat map (**Figure 1.20 B**) showing the relative expression of the BCPs across the *S. mansoni* life cycle (**Figure 1.20 C**) was generated by G.P., using a published RNA-Seq database.[107] It shows *Sm*BRD3 as one of the more highly expressed BCPs in the

S. mansoni proteome, with highest expression occurring in miracidia and sporocysts. Comparatively high expression, contrasted with the other BCPs, was also shown for the therapeutically relevant life-cycle stages, the schistosomula and adult worms.

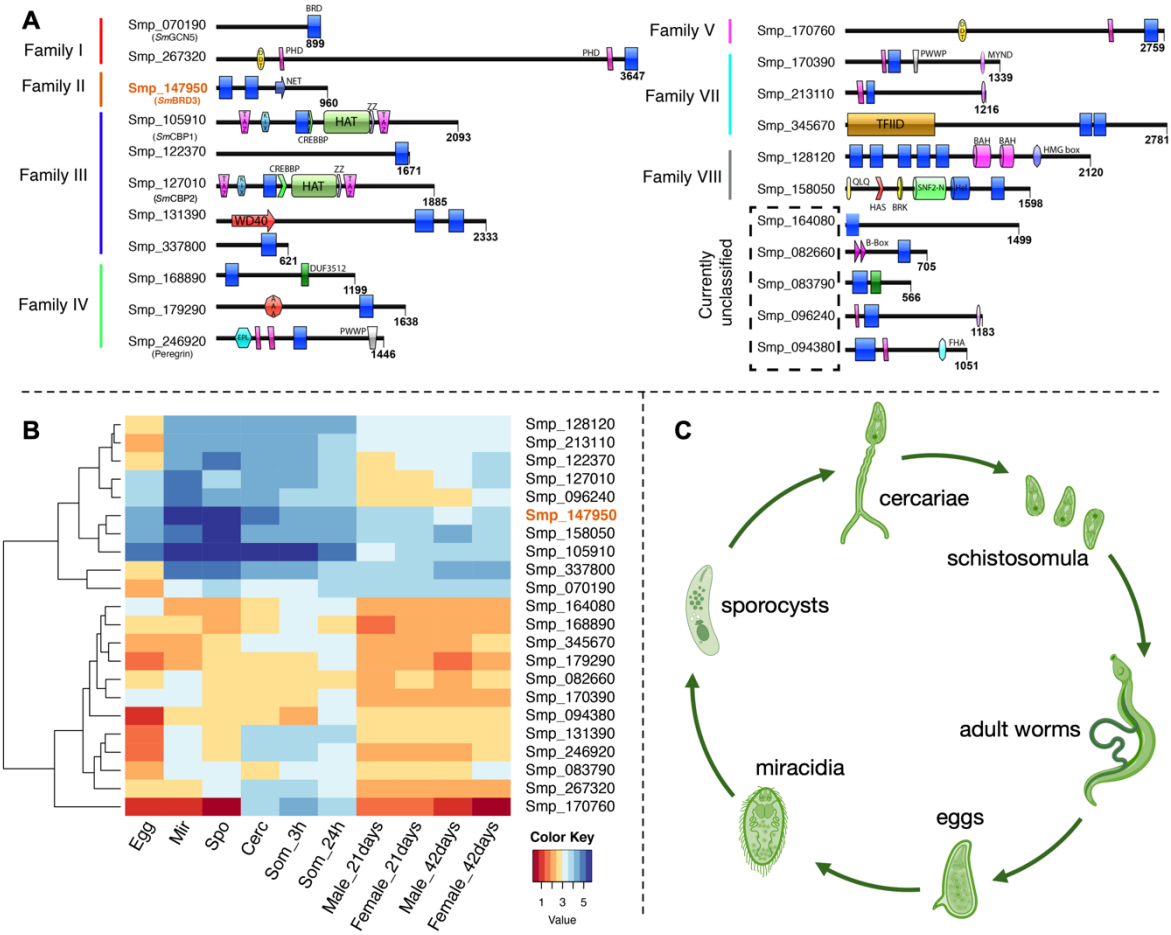


Figure 1.20. A) Domain architecture representation of the 22 putative *S. mansoni* BCPs classified by family.[108] Where no family can be defined, the BCP is labelled 'currently unclassified'. Gene ID (Smp; according to the *S. mansoni* v7 genome annotation), common name (in parentheses) and total protein length (in number of amino acids – aa) are all indicated. **B**) Heat map illustration of BCP gene expression across the *S. mansoni* lifecycle (derived from RNA-Seq meta data); *Sm*BRD3 (Smp_147950) is highlighted in orange. Relative expression levels are indicated as a colour range from blue (high expression) to red (low expression). Abbreviations: Mir: miracidia; Spo: sporocyst; Cerc: cercaria; Som: schistosomula. **C**) A simplified cartoon of the *S. mansoni* lifecycle. **Figure 1.20** was adapted with the permission of Prof. Stuart J. Conway (S.J.C.), consisting of the simplified cartoon of the *S. mansoni* lifecycle prepared by S.J.C. using Biorender.com, and the domain architecture representation and expression heat maps prepared by G.P..

Comparison between the human BET BRD primary amino acid sequences and *Sm*BRD3, by Dr Matthias Schiedel (M.S.) and Prof. Stuart J. Conway (S.J.C.) (University of Oxford), revealed similarities in the conserved motifs and residues important for KAc binding (**Figure 1.21**). Both the first [*Sm*BRD3(1)] and second [*Sm*BRD3(2)] BRDs of *Sm*BRD3 possess the

N and Y residues important for KAc binding [for example Y296 and N339 in *Sm*BRD3(2), analogous to N140 and Y97 in BRD4(1)]. The WPF shelf is found in *Sm*BRD3(1) (W56, P57, F58). In contrast, in *Sm*BRD3(2) the tryptophan and proline residues are replaced with a histidine and phenylalanine, forming an HFF shelf (H280, F281, F282).



Figure 1.21. A multiple sequence alignment of the *Sm*BRD3(1,2) protein construct, *Sm*BRD3, *Hm*BRD3, and *Hm*BRD4. The region identified as the N-terminal BRD is indicated with a green bar and the region identified as the C-terminal BRD is indicated with a white bar. Sequence alignment was carried out by G.P. using MUSCLE[109] and the amino acid sequences of *Sm*BRD3 (Uniprot ID: A0A5K4EQL3), the *Sm*BRD3(1,2) construct, human BRD3 (Uniprot: Q15059) and human BRD4 (Uniprot: O60885). The figure was generated by G.P. using ESPript 3 server[110] to visualise the multiple sequence alignment. Conserved residues are indicated by vertical blue boxes, strict identity is indicated by white letters in red boxes and similarity is indicated by red letters in white boxes. **Figure 1.21** was reproduced with the permission of S.J.C..

To elucidate the function of *Sm*BRD3 in the function and life cycle of *S. mansoni*, previous work in the group, by M.S., focussed on the identification of ligands for this BCP. Constructs of *Sm*BRD3 BRDs, *Sm*BRD3(1), *Sm*BRD3(2) were required to enable the identification of ligands. Recombinant *Sm*BRD3(1), *Sm*BRD3(2), and *Sm*BRD3(1,2) constructs were designed and expressed by M.S. from *E. coli*. Stable constructs of *Sm*BRD3(1,2) and *Sm*BRD3(2) were expressed in good yields, however, this was not possible for *Sm*BRD3(1). Analysis by S.J.C. of the full protein structure, predicted by AlphaFold,[111] (**Figure 1.22 A**)

indicated the helix comprising residues 617-638, and the subsequent disordered residues 639-660, form intra protein interactions in the region between *Sm*BRD3(1) and *Sm*BRD3(2) (**Figure 1.22 B**). It was proposed by S.J.C. that these interactions are required to stabilise *Sm*BRD3(1), which although present in *Sm*BRD3(1,2), rendered the first domain unstable when expressed alone.

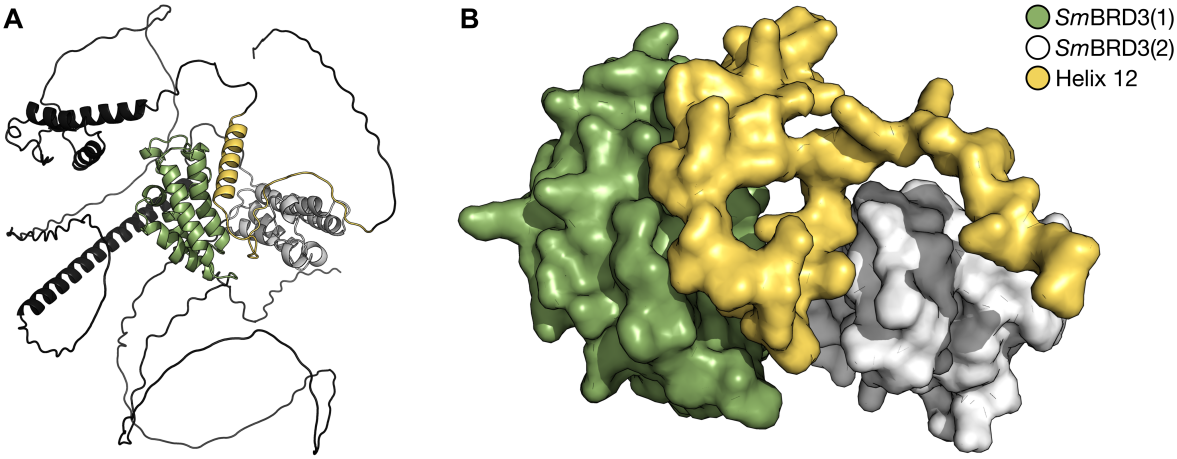


Figure 1.22 A) The structure of the full length *Sm*BRD3 protein (Uniprot ID: A0A5K4EQL3) predicted by AlphaFold.[111] Helix 12 (gold) is located between *Sm*BRD3(1) (green) and *Sm*BRD3(2). **B**) Surface representation of *Sm*BRD3 predicted by AlphaFold. It is proposed hydrophobic intraprotein interactions between *Sm*BRD3(1) (green) and helix 12 (gold) are important in the stabilisation of the *Sm*BRD3(1) bromodomain, which are not present when *Sm*BRD3(1) is expressed alone. As *Sm*BRD3(2) (white) forms fewer hydrophobic interactions with helix 12 (gold), the second BRD can be produced as a stable construct. **Figure 1.22** was reproduced with the permission of S.J.C..

Using the construct of *Sm*BRD3(2), differential scanning fluorimetry (DSF)[112] was used by M.S. to screen 697 compounds, comprising of 153 compounds from the PPI-net library, 160 compounds from the Conway Group in-house library of human and *T. cruzi* BRD ligands, and 384 compounds from the Maybridge Fragment Library against *Sm*BRD3(2).[30,31,113–122] Analysis of the screening data revealed a number of hits, including the known human BET bromodomain ligand, I-BET726 (**1.6**) (**Figure 1.23**). Selected compounds (**Figure 1.23 C**) were then assessed against *Sm*BRD3(1,2) using DSF (**Figure 1.23 B**). The human BET bromodomain ligands OXFBD02 (**1.4**), and (+)-JQ1 (**1.1**) were found to stabilise *Sm*BRD3(1,2) but not *Sm*BRD3(2), implying these compounds bound preferentially to *Sm*BRD3(2). I-BET726 (**1.6**) and BI2536 (**1.8**) stabilised both *Sm*BRD3(2) and *Sm*BRD3(1,2), indicating these compounds bind to either both BRDs or to just *Sm*BRD3(2).

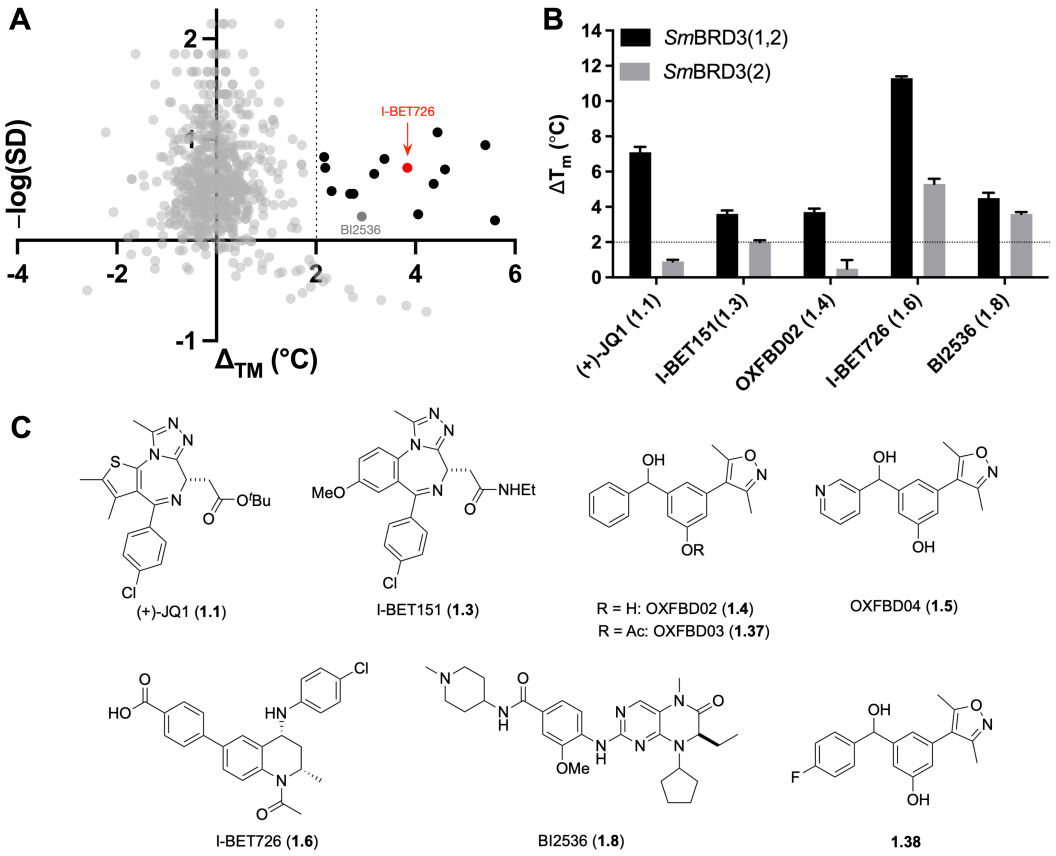


Figure 1.23. A) A scatter plot of ΔT_M (°C) plotted against –log(SD) for 697 screened compounds against *Sm*BRD3(2). Black and red dots represent the compounds with a ΔT_M (°C) greater than 2 °C, with I-BET726 (**1.6**) represented by the red dot. **B**) Bar chart representing the thermal shift values, ΔT_M (°C), for selected hit compounds **1.1** and **1.3**–**1.6** and **1.8** on *Sm*BRD3(1,2) (black bars) and *Sm*BRD3(2) (grey bars). **C.** Structures of selected BRD ligands **1.1**, **1.3**–**1.6**, **1.8**, **1.37** and **1.38**. DSF screening was carried out by M.S. and the results were analysed by M.S. and S.J.C.. **Figure 1.23. A** and **B** were reproduced (**A**) and modified (**B**) with the permission of S.J.C..

To confirm the DSF results and to quantitatively assess the extent of binding, M.S. used isothermal titration calorimetry (ITC) to determine K_d values for compounds **1.1**, **1.3**–**1.6**, **1.8**, **1.37** and **1.38** (**Table 1.1**). The analogues of OXFBD02 (**1.4**), OXFBD03[30] (**1.37**) and **1.38**[31], were later tested on *Sm*BRD3(1,2) and *Sm*BRD3(2) by the author of this dissertation. Complementary to the DSF data, the results showed (+)-JQ1 (**1.1**) and the dimethylisoxazole based ligands (**1.4**, **1.5**, **1.37** and **1.38**) bound to *Sm*BRD3(1,2), whereas no binding was detected for *Sm*BRD3(2), indicating selective binding for the first domain. Compounds **1.1**, **1.4** and **1.37** showed nanomolar affinity for *Sm*BRD3(1,2). Also analogous with the DSF data, I-BET151 (**1.3**), I-BET726 (**1.6**) and BI2536 (**1.8**), bound to *Sm*BRD3(1,2)

however, the affinities were in the micromolar range, with I-BET726 (**1.6**) showing the highest affinity for both constructs out of these three compounds.

Table 1.1. The *Sm*BRD3(1,2) and *Sm*BRD3(2) ITC K_d and pK_d values for compounds **1.1**, **1.3**–**1.6**, **1.8**, **1.37** and **1.38**. Values are n=1 ± error of the curve fit. A heatmap colour scale of green to red is used, with red representing higher affinity and green representing lower affinity.

Compound	*Sm*BRD3(1,2) K_d (nM)	*Sm*BRD3(1,2) pK_d	*Sm*BRD3(2) K_d (nM)	*Sm*BRD3(2) pK_d
(+)-JQ1 (1.1)	445 ± 106	6.4	no binding	-
I-BET151 (1.3)	2830 ± 283	5.5	6160 ± 785	5.2
OXFBD02 (1.4)	683 ± 166	6.2	no binding	-
OXFBD04 (1.5)	2950 ± 261	5.5	no binding	-
I-BET726 (1.6)	1520 ± 520	5.8	1850 ± 361	5.7
BI2536 (1.8)	1990 ± 277	5.7	3810 ± 576	5.4
OXFBD03 (1.37)	675 ± 97.6	6.2	no binding	-
1.38	1750 ± 301	5.8	no binding	-

Given the sequence similarity of *Sm*BRD3 with human BET BRDs, and the binding affinity data, it was expected that I-BET726 (**1.6**) would occupy the KAc binding pocket of *Sm*BRD3(2). To confirm this, M.S., with the help of Dr Michael McDonough (University of Oxford), co-crystallised this compound with *Sm*BRD3(2) (**Figure 1.24**). This was the first X-ray crystal structure of a BRD from *S. mansoni* and showed a very similar overall fold to human BRD4(1). The crystal structure shows the close alignment between Tyr (Y97 and Y139) and Asn (N140) residues in BRD4(1) and the corresponding residues (Y296, Y338 and N339) in *Sm*BRD3(2). It also clearly indicated a hydrogen bond between N339 and the carbonyl oxygen atom of I-BET726 (**1.6**), and a hydrogen bond between Y296 and the same atom mediated by a water molecule (**Figure 1.24 B**). Furthermore, the crystal structure

showed the replacement of the WPF shelf with the residues H280, F281, and F282 in *Sm*BRD3(2) resulted in the formation of a narrow channel, the HFF cleft, defined by F281, E344, V345, and V348. The chlorophenyl group of I-BET726 (**1.6**) was observed to reside in the HFF cleft (**Figure 1.24 D**), and it was apparent that the occupancy of this cleft was sub-optimal. Therefore, it was suggested the WPF-HFF structural difference could be exploited, by the development of novel I-BET726 derivatives, to achieve higher affinity ligands for *Sm*BRD3(2).

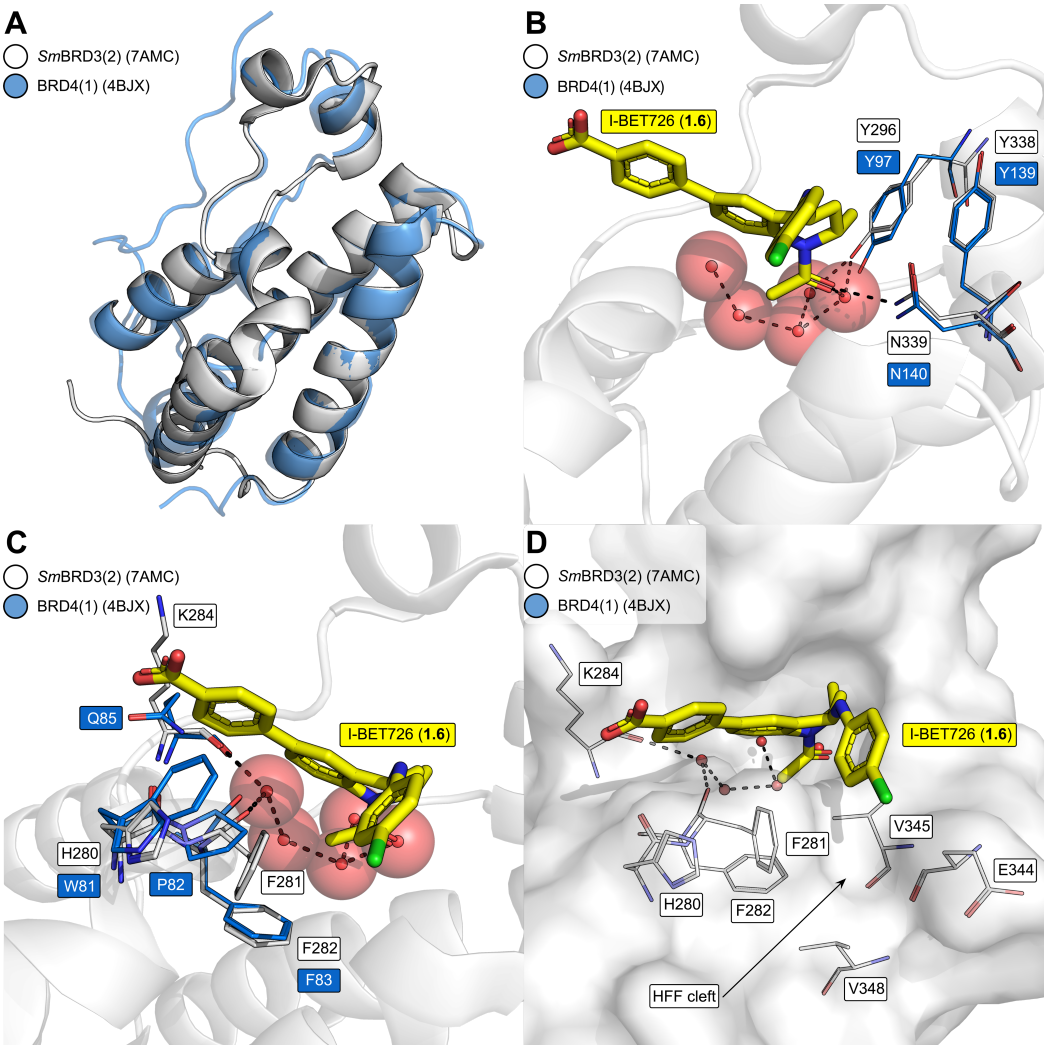


Figure 1.24. The X-ray crystal structure of I-BET726 (**1.6**) bound to *Sm*BRD3(2) (PDB ID: 7AMC). **A**) The overall fold of *Sm*BRD3(2) (white cartoon) is similar to that of human BRD4(1) (blue cartoon; PDB ID: 4BJX). **B**) The X-ray crystal structure of I-BET726 (**1.6**) bound to *Sm*BRD3(2) (cartoon and carbon = white; PDB ID: 7AMC) overlaid with the X-ray crystal structure of *Hm*BRD4(1) (carbon = blue; PDB ID: 4BJX). The N and Y residues important for binding of KAc- and KAc-mimic binding is conserved between the two proteins and this binding is highlighted. **C**) the WPF shelf region of *Hm*BRD4(1) carbon = blue; PDB ID: 4BJX) and HFF motif in *Sm*BRD3(2) (cartoon and carbon = white; PDB ID: 7AMC). **D**) A narrow channel, the HFF cleft, is defined by F281, E344, V345, and V348. The chlorophenyl group of I-BET726 partly occupies the HFF cleft. **Figure 1.24** was produced by S.J.C. and reproduced with permission from S.J.C..

1.9 Project aims

Epigenetics is likely important in directing the large phenotypic changes observed during the life cycle of *S. mansoni*. It has been suggested targeting the epigenetic mechanism of *S. mansoni* could be a novel therapeutic route for the treatment of schistosomiasis, and a number of studies in the literature have examined this hypothesis. The BRDs of *S. mansoni*, however, have received little attention. Previous work in the group has focussed on identifying ligands for the *S. mansoni* BET bromodomain orthologue, *Sm*BRD3. The X-ray crystal structure of the BET BRD ligand I-BET726 (**1.6**), the highest affinity ligand identified for the second domain of *Sm*BRD3, reveals information which could be used for structure guided development of higher affinity ligands for this domain. By further applying chemical biology techniques to the field of parasitology, the aims of the work described in this dissertation are to investigate the *S. mansoni* bromodomain *Sm*BRD3 by:

- The synthesis and evaluation of novel I-BET726 derivatives for the elucidation of the function of *Sm*BRD3 in *S. mansoni* (**Chapter 2** and **Chapter 3**).
- The development of photoaffinity probes based upon *Sm*BRD3 ligands for the investigation of parasite target engagement and selectivity (**Chapter 4**).

Chapter 2

Structure-based optimisation of small molecule ligands for *Sm*BRD3(2): targeting the HFF shelf

2.1 Introduction and aims

Previous work in the Conway Group had identified the human BRD probe, I-BET726 (**1.6**), as a ligand for *Sm*BRD3 (K_d [*Sm*BRD3(1,2)] = 1520 ± 520 nM; K_d [*Sm*BRD3(2)] = 1850 ± 361 nM) (**Chapter 1**). This compound was the highest affinity *Sm*BRD3(2) ligand identified and was co-crystallised with the second domain to elucidate its mode of binding. The binding mode is similar to that observed for human BRD4(1); N339 forms a hydrogen bond with the carbonyl oxygen of I-BET726 and Y296 forms a water-mediated hydrogen bond with the same atom (**Figure 1.24**). However, the co-crystal structure indicated the occupancy of HFF cleft by the chlorophenyl group of I-BET726 (**1.6**) was non-optimal. The affinity of **1.6** is also orders of magnitude lower for *Sm*BRD3(2) than for human BET BRDs (K_d [BRD4] = 4.4 ± 0.9 nM).[32] As the affinity of many BET bromodomains ligands result from the binding of lipophilic groups to the WPF shelf of human bromodomains, it was reasoned that novel I-BET726 derivates, with higher affinity for *Sm*BRD3(2), could be developed. High affinity ligands can be used to study domain function. Therefore, the aims of the work described in this chapter were to:

- Synthesise novel I-BET726 derivatives with varying lipophilic groups for optimised interaction with the HFF shelf.
- Determination of the extent of binding of these compounds to *Sm*BRD3(2) *via* isothermal titration calorimetry (ITC).
- To conduct phenotypic screening of novel I-BET726 derivatives, along with known human BRD ligands, to determine the overall and domain-specific functions of *Sm*BRD3.

2.2 Ligand design and synthesis

2.2.1 Ligand design

The design strategy employed to develop higher affinity ligands for *Sm*BRD3(2) was to replace the chlorophenyl group of I-BET726 (**1.6**) with bicyclic aromatic groups (**Figure 2.1**). It was reasoned these groups would result in more effective HFF cleft occupancy and therefore higher *Sm*BRD3(2) affinity *via* hydrophobic interactions with the HFF shelf. A series of groups were chosen to explore the effect of heteroatom type and position, and the difference between [5,6]- and [6,6]-bicyclic aromatic groups on *Sm*BRD3(2) affinity.

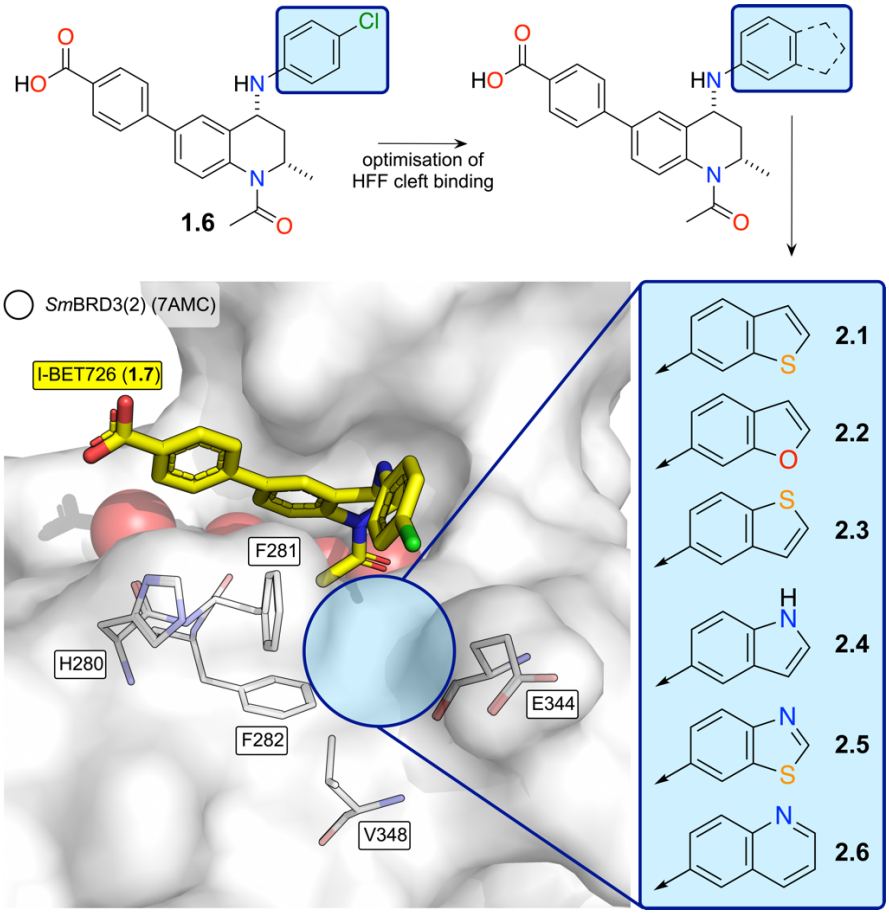
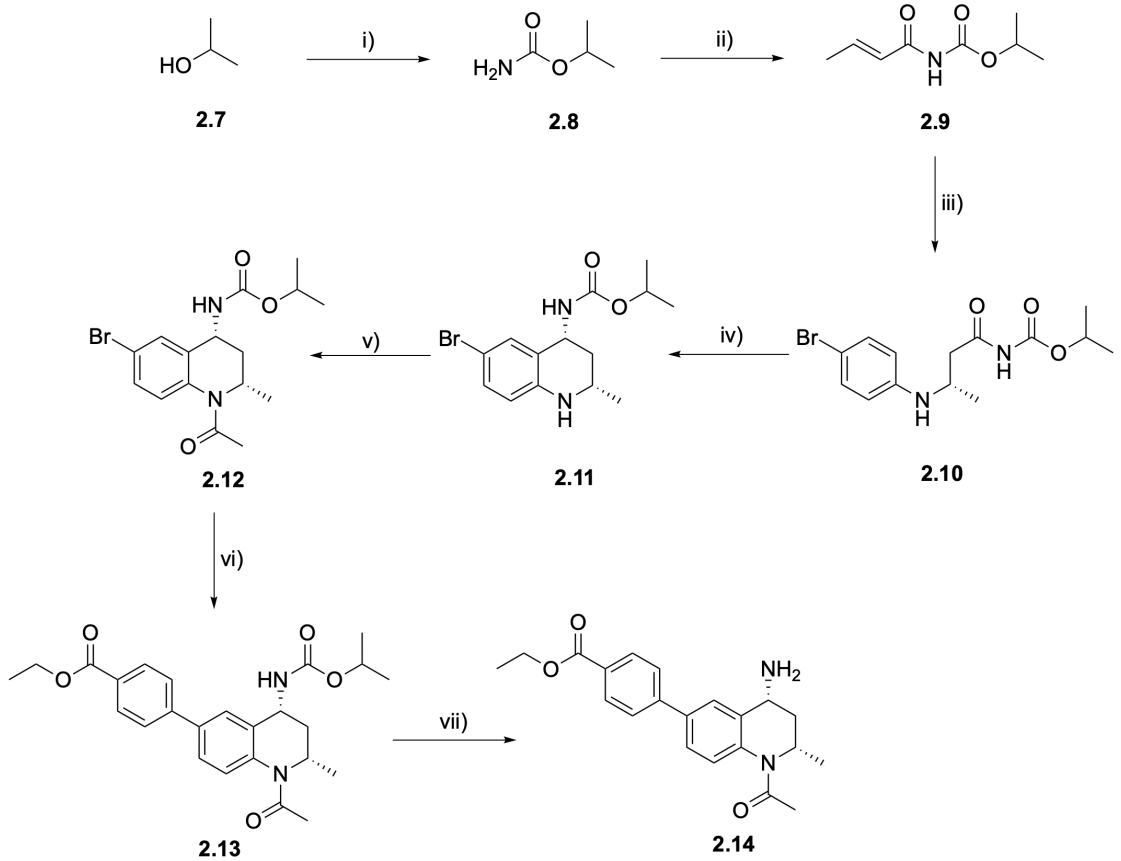


Figure 2.1. Target molecules **2.1**–**2.6** for binding optimisation to *Sm*BRD3(2) and the co-crystal structure of I-BET726 (carbon = yellow) bound to *Sm*BRD3(2) (carbon = white) (PDB ID: 7AMC). The bicyclic aromatic groups of **2.1**–**2.6** were proposed to more effectively occupy the HFF cleft.

2.2.2 Stereoselective synthesis of a primary amine intermediate

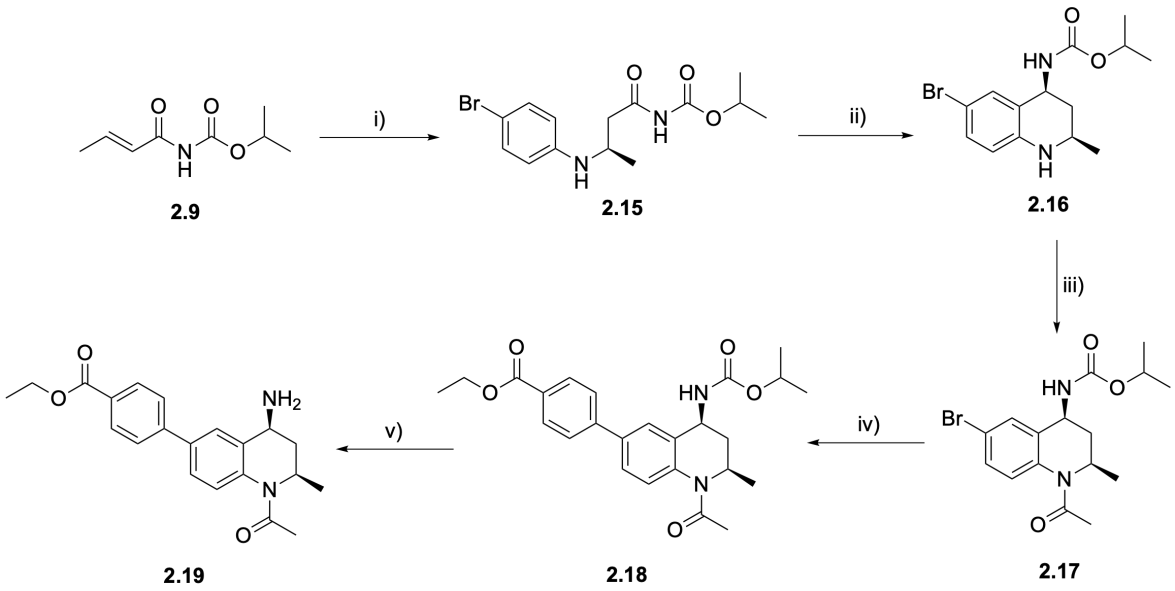
The synthetic strategy proposed was to follow the stereoselective synthesis to a primary amine intermediate (**2.14**) (**Scheme 2.1**), as described by Gosmini *et al.*[32] and using work by Shadrick *et al.*,[123] followed by palladium-catalysed Buchwald-Hartwig coupling of heteroaromatic bromides and a base-mediated ethyl ester hydrolysis.



Scheme 2.1. Synthesis of the primary amine intermediate **2.14.** *Reagents and conditions*: i) TFA, *i*-PrOH, NaOCN, rt, 79%; ii) Crotonoyl chloride, LiHMDS, THF, −78 °C, 61%; iii) (*R*)-BINAP(OTf)$_2$(H$_2$O)$_2$Pd, 4-bromoaniline, toluene, rt, 95%; iv) NaBH$_4$, EtOH, MgCl$_2$·6H$_2$O, H$_2$O, <0°C to rt, 98%; v) Pyridine, AcCl, CH$_2$Cl$_2$, 90%; vi) {4-[(Ethyloxy)carbonyl]-phenyl}boronic acid, Pd(Ph$_3$)$_4$, satd. Na$_2$CO$_{3(aq)}$, DME, 105 °C, 91%; vii) AlCl$_3$, NEt$_3$, MeOH, CH$_2$Cl$_2$, 0 °C, 84%.

Acid mediated addition of *i*-PrOH to NaOCN (**Scheme 2.1**, step i), proceeded in a yield of 79%, followed by strong base-mediated reaction of isopropyl carbamate with crotonoyl chloride (step ii), which occurred in a yield of 61%. The first stereoselective step (step iii) in the synthetic route, an aza-Michael addition of 4-bromoaniline to intermediate **2.10**, occurred in a yield of 95% and in an enantiomeric excess (ee) of 93% (determined by

HPLC), comparable to the reported ee of 92% by Gosmini *et al*.[32] The cyclisation (step iv) proceeded in a yield of 98% and an ee of 89%, indicating the cyclisation largely conserved the stereochemistry introduced in step iii. Acylation of **2.11** to introduce the *N*1-acetyl-based KAc mimic occurred with a 90% yield, and the Suzuki coupling (step vi) occurred with a 91% yield. Finally, removal of the isopropyl carbamate group using $AlCl_3$, MeOH and NEt_3 proceeded in a yield of 84%.



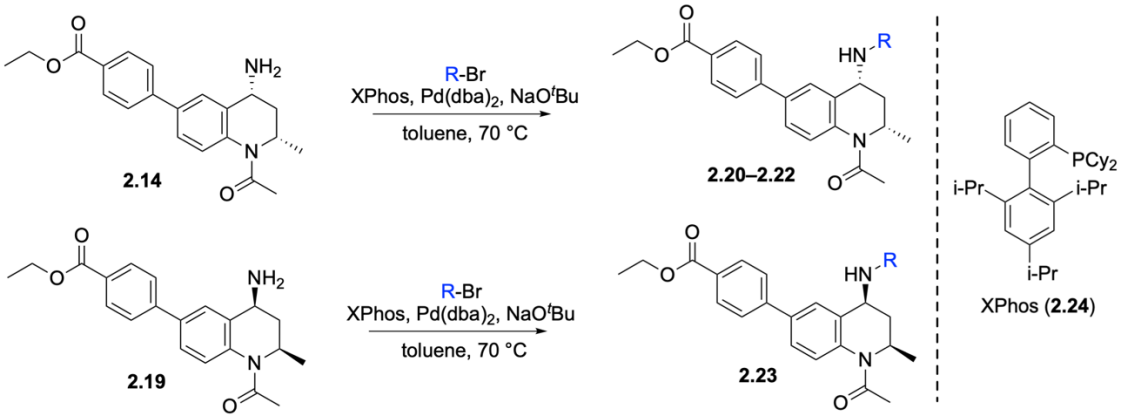
Scheme 2.2. Synthesis of primary amine intermediate **2.19**. *Reagents and conditions*: i) (*S*)-BINAP$(OTf)_2(H_2O)_2$Pd, 4-bromoaniline, toluene, rt, 90%; ii) $NaBH_4$, EtOH, $MgCl_2{\cdot}6H_2O$, H_2O, <−10°C, 93%; iii) Pyridine, AcCl, CH_2Cl_2, 88%; iv) {4-[(ethyloxy)carbonyl]-phenyl}boronic acid, $Pd(Ph_3)_4$, $Na_2CO_{3(aq)}$, DME, 105 °C, 80%; v) $AlCl_3$, NEt_3, MeOH, CH_2Cl_2, 0 °C, 82%.

For reasons discussed in **section 2.3.1**, it was desirable to synthesise the opposite enantiomer of intermediate **2.14**, **2.19** (**Scheme 2.2**). This was achieved using (*S*)-BINAP$(OTf)_2(H_2O)_2$Pd, instead of the *R*-enantiomer, in the aza-Michael addition to give **2.15** in a 90% yield and 85% ee. Cyclisation to **2.16** occurred in a 93% yield and an ee of 80%. Due to approximate retention in ee for the opposite enantiomer **2.11** for the same step, it is expected the reduction in ee is due to experimental variation between intermediate synthesis batches (of reactions iii and iv, **Scheme 2.1**, and i and ii, **Scheme 2.2**) and error associated with the chiral HPLC analysis, instead of direct reduction in ee *via* reaction ii,

Scheme 1.2. Finally, the acetylation, Suzuki coupling and isopropyl carbamate removal in steps iii, iv and v of **Scheme 2.2** proceeded in high yields of >80%.

2.2.3 C-N coupling reactions for the synthesis of novel I-BET726 analogues

Once the primary amines **2.14** and **2.19** were in hand, it was envisaged that novel I-BET726 derivates could be synthesised *via* Buchwald-Hartwig coupling with the appropriate heterocyclic bromides. The target compounds initially chosen to occupy the HFF shelf more effectively were to include benzothiophene and benzofuran groups. At first, the catalyst chosen for coupling between amines **2.14** and **2.19** and the appropriate bromides (**Figure 2.2**) was $Pd(dba)_2$, due to its use in the synthesis of I-BET726.[32] XPhos was chosen as the ligand due to its reported effectiveness and compatibility with close analogues of benzothiophene and bromobenzofuran bromides, benzothiazole and benzoxazole halides,[124] availability in the lab and experimental observation of successful test reactions.



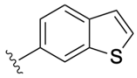
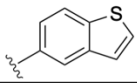
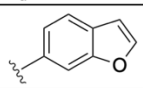
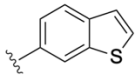
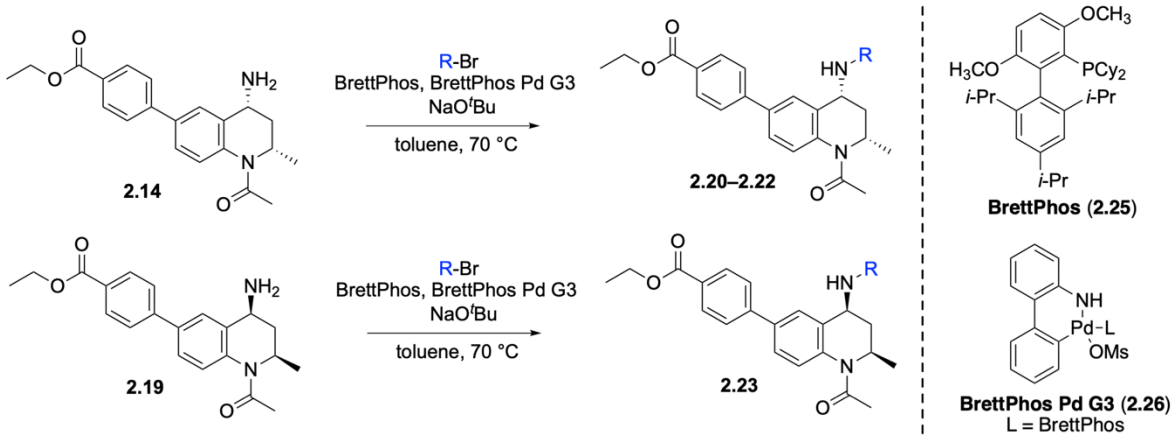
Compound	R-Br	Yield (%)
2.20		**22**
2.21		**20**
2.22		**22**
2.23		**21**

Figure 2.2. Synthesis of compounds **2.20**–**2.23** using $Pd(dba)_2$ and XPhos.

Yields of only 20–22% (**Figure 2.2**) were achieved in the Buchwald-Hartwig couplings, and a number of side products were observed *via* TLC analysis during these reactions. These side products were uncharacterized, however, during TLC analysis, two spots were observed to have close retention times to the product on the TLC plate, and partial isolation of these side products during compound purification indicated a ^{1}H NMR spectra similar to the product. It was proposed these compounds were diastereomers from epimerization at one of the stereogenic centres, and the close retention time to the product resulted in challenging separation from the product during purification. It was suggested these problems could be alleviated with optimised coupling conditions. More recent literature for this class of reaction employs the ligand BrettPhos along with a BrettPhos palladium catalyst, BrettPhos Pd G3, as a selective and higher yielding ligand and palladium catalyst combination for primary amines.[125–128] This combination resulted in higher yields of 66-87% and comparatively undemanding purifications (**Figure 2.3**).



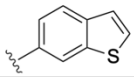
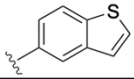
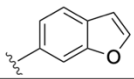
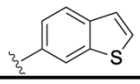
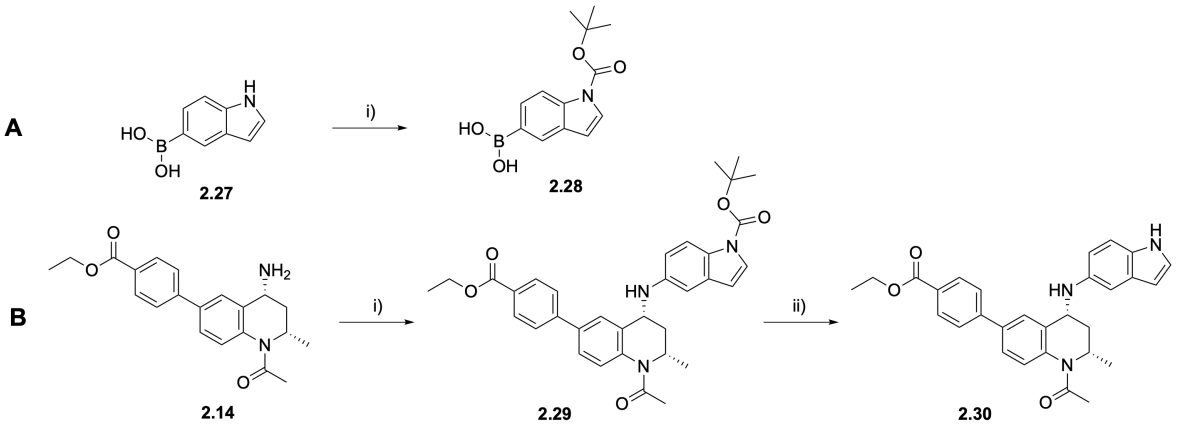
Compound	R-Br	Yield (%)
2.20		**87**
2.21		**66**
2.22		**68**
2.23		**69**

Figure 2.3. Synthesis of compounds **2.20**–**2.23** using BrettPhos and BrettPhos Pd G3.

Once the Buchwald-Hartwig coupling reactions had been optimised for benzothiophene and benzofuran analogues **2.20**–**2.23**, further compounds with bicyclic aromatic head groups were also investigated. The additional groups chosen were indole, benzothiophene, and quinoline.

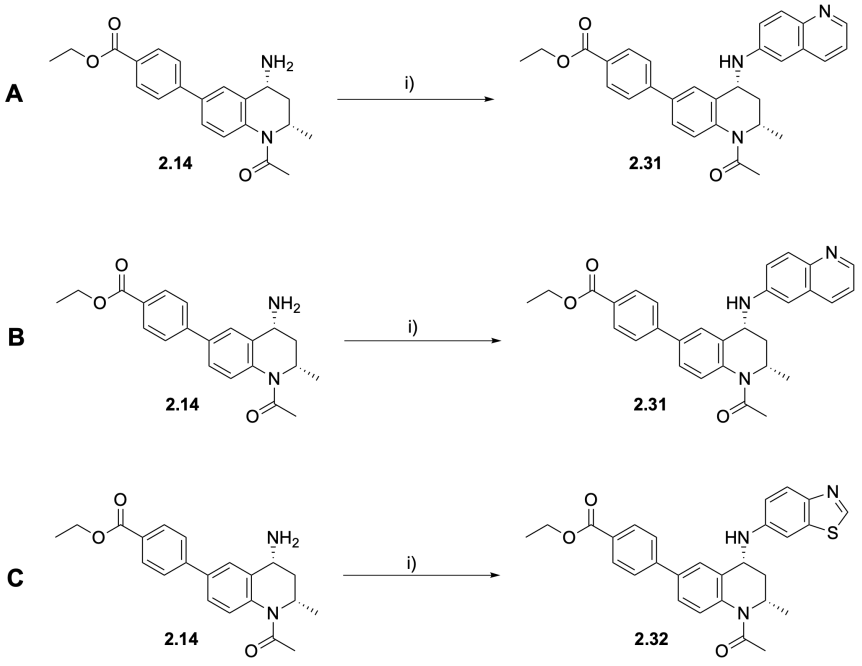
Initial efforts to synthesise an indole derivative using XPhos, $Pd(dba)_2$, and 5-bromoindole resulted in no observed product formation. As suggested by the literature, the 1.2 eq. of NaO^tBu was replaced with 2.2 eq. of LiHMDS.[124,128,129] This modification alleviates the need for N-H protection and avoids undesired C-N coupling. It is suggested this is due to interactions between the deprotonated indole N with Li, preventing interactions with the palladium centre.[129] However, it was observed that amine **2.14** was unstable to LiHMDS. It therefore became clear that use of a protecting group on the indole N-H was required for coupling to primary amine **2.14**. The *tert*-butyloxycarbonyl (Boc) protecting group was chosen due to its ease of removal with strong acid and stability under basic conditions. To avoid further efforts in optimisation of the components of Buchwald type C-N Pd cross-coupling (ligand, catalyst, solvent, base, and temperature), the copper-catalysed C-N coupling Chan-Lam reaction was chosen as a simpler alternative with fewer components for optimisation (**Scheme 1.3**).



Scheme 1.3. The synthetic route to compound **2.30** *via* a Chan-Lam coupling. **A**) Synthesis of intermediate **2.28**. *Reagents and conditions:* i) $(Boc)_2O$, DMAP, MeCN, rt, 1 h, 49%; **B**) Synthesis of compound **2.30**. *Reagents and conditions:* i) Intermediate **2.28**, $Cu(OAc)_2$, NEt_3, CH_2Cl_2, 3 Å molecular sieves, rt, 15 h; 53%. ii) TFA, CH_2Cl_2, rt, 30 min, 46%.

Chan-Lam cross-coupling reactions occur between a boronic acid and an amine, therefore a protected boronic acid indole was required. Direct Boc protection of 5-indoylboronic acid (**2.27**) using catalytic DMAP resulted in a 49% yield (**Scheme 2.3 A**). The Chan-Lam reaction between boronic acid **2.28** and primary amine **2.14** using $Cu(OAc)_2$ and NEt_3 gave compound **2.29** in a 53% yield (**Scheme 2.3 B**). Subsequent Boc deprotection, using TFA, resulted in the production of **2.30** in a 46% yield. The low yield, despite the reaction proceeding to completion, was attributed to product loss in the aqueous work-up and purification. This result indicated that Chan-Lam coupling could be an effective alternative for the synthesis of future analogues, if initial Buchwald-Hartwig coupling reactions were unsuccessful, eliminating the need for extensive Buchwald condition screening.

The final target compounds that were synthesised were to exhibit benzothiazole and quinoline head groups. It was expected that Buchwald-Hartwig coupling reactions to make these compounds would be effective when using the corresponding bromides (**Scheme 2.4.**).



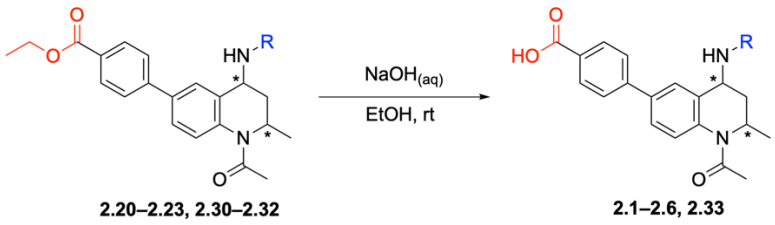
Scheme 2.4. The Buchwald-Hartwig coupling reactions to synthesise compounds **2.31** and **2.32. A**) *Reagents and conditions:* 6-bromoquinoline, CyJohnPhos, $Pd(OAc)_2$, NaO^{t}Bu, toluene, 100 °C, 15 h, 30%; **B**) *Reagents and conditions:* 6-bromoquinoline, BrettPhos, BrettPhos Pd G3, NaO^{t}Bu, toluene, 70 °C, 16 h, 30%; **C**) *Reagents and conditions:* 6-bromobenzothaizole, BrettPhos, BrettPhos Pd G3, NaO^{t}Bu, toluene, 70 °C, 16 h, 48%.

Initially, compound **2.31** was synthesised using the ligand CyJohnPhos and $Pd(OAc)_2$ as the palladium catalyst source, with a 30% yield. These were chosen based on a literature procedure for Buchwald-Hartwig coupling of 2-chloro-6-bromoquinoline, a structurally close quinoline halide.[130] Due to the optimisation of coupling conditions using the BrettPhos ligand and BrettPhos Pd G3 catalyst for compounds **2.20**–**2.23**, the same conditions were employed for the synthesis of compound **2.31**. This resulted in a yield of 23%, however, in this case the product was further purified by semi-preparative HPLC, instead of purification only silica gel flash column chromatography, and it is expected product was lost using non-optimal HPLC purification conditions. Further work is therefore needed to accurately determine the optimised coupling conditions for **2.31**. Compound **2.32** was synthesised using BrettPhos and BrettPhos Pd G3 in a 48% yield.

In all C-N coupling reactions for the synthesis of compounds **2.20**–**2.23** and **2.30**–**2.32** the reaction did not proceed to completion. Hydrolysis of the ethyl ester of intermediate **2.14** was observed in the reported synthesis of I-BET726,[32] despite anhydrous conditions, and although this side product was not isolated in these cases, it is reasonable to suggest formation of this side product could inhibit the Pd and Cu-catalysed C-N cross couplings.

2.2.4 Ester hydrolysis for the synthesis of novel I-BET726 analogues

The final step in the reported synthesis of I-BET726 (**1.6**) uses $NaOH_{(aq)}$ to hydrolyse the ethyl ester, giving the final desired benzoic acid product.[32] For the target novel I-BET726 derivatives, it was envisaged the same strategy could be used.



2.20–2.23, 2.30–2.32 **2.1–2.6, 2.33**

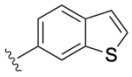
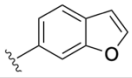
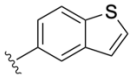
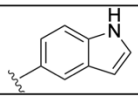
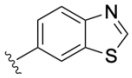
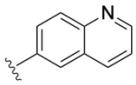
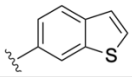
Compound	Stereochemistry at *	R	Yield (%)
2.1	(2*S*,4*R*)		**87**
2.2	(2*S*,4*R*)		**20**
2.3	(2*S*,4*R*)		**41**
2.4	(2*S*,4*R*)		**32**
2.5	(2*S*,4*R*)		**69**
2.6	(2*S*,4*R*)		**36**
2.33	(2*R*,4*S*)		**32**

Figure 2.4. Ethyl ester hydrolysis for the synthesis of compounds **2.1**–**2.6** and **2.33** and the corresponding yields.

The corresponding ethyl ester analogues were dissolved in EtOH and a 2 M solution $NaOH_{(aq)}$ was slowly added. Dropwise addition of the NaOH solution was important. When the addition was performed too fast, precipitation of the ethyl ester starting material occurred, causing prolonged reaction times. The ester hydrolysis for the different analogues showed a variability of yields, ranging from 20 to 87%. This variability is mostly attributed to the purification of the final compounds, particularly as TLC analysis indicated full conversion

to the product and negligible side products in all cases. Lower yields were observed for compounds purified by semi-preparative HPLC, for example compound **2.33**, and for future synthesis of these compounds, care must be given to optimise the semi-preparative HPLC conditions for effective mass recovery.

Chiral HPLC analysis of compounds **2.1**–**2.6** and **2.33** revealed ee values ranging from 79 to 89%. Chirality was introduced with intermediates **2.10** (ee = 90%) and **2.11** (ee = 89%) for compounds exhibiting the (2*S*,4*R*) absolute configuration and intermediates **2.15** (ee = 89%) and **2.16** (ee = 80%) for compounds exhibiting the (2*R*,4*S*) configuration. It was suggested that the variation in ee for compounds **2.1**–**2.6** and **2.33** is therefore due to experimental variation in the stereoselective synthetic steps and error in chiral HPLC analysis, and it was reasoned the C-N coupling and subsequent ester hydrolysis steps had negligible effect on the ee of the final product.

2.3 Biological evaluation of I-BET726 derivatives

2.3.1 Binding affinity and crystallographic analysis of novel analogues for *Sm*BRD3(2)

With novel I-BET726 derivatives **2.1**–**2.6** and **2.33** in hand, the binding affinity of each ligand for *Sm*BRD3(2) was determined using isothermal titration calorimetry (ITC). The first compound synthesised, compound **2.1**, exhibited a benzothiophene head group and has a K_d = 701 ± 127 nM, accounting for approximately a 2.6-fold increase in affinity for *Sm*BRD3(2) compared with I-BET726 (**1.6**). To confirm the hypothesis that the benzothiophene group would more effectively occupy the cleft formed by the HFF shelf, and to aid in the design of further analogues, compound **2.1** was co-crystalised with *Sm*BRD3(2). The work to produce this crystal structure was carried out with the help of Dr Michael McDonough (University of Oxford).

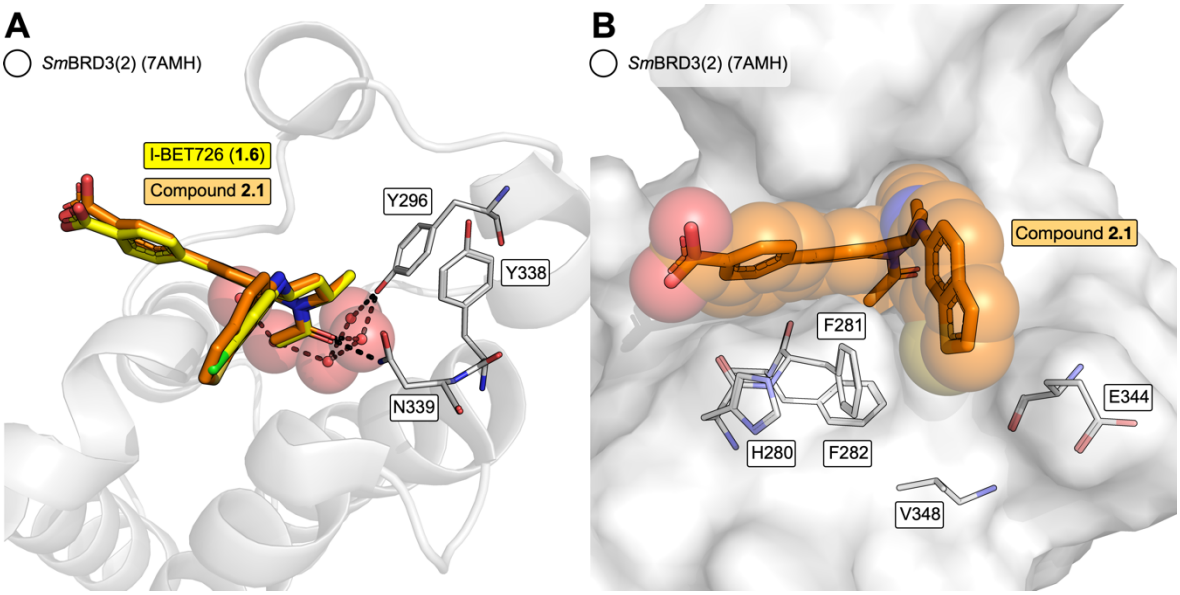
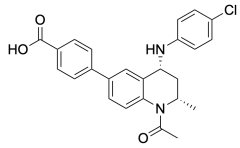
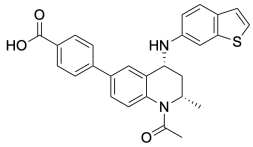
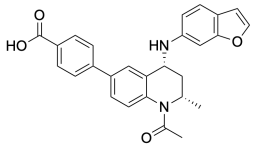
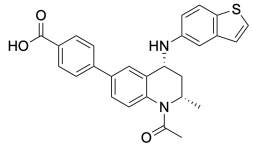
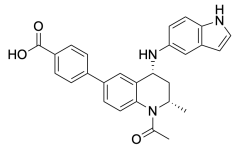
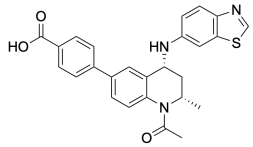
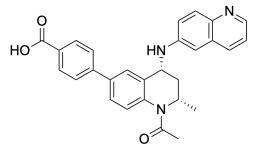
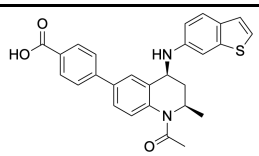


Figure 2.5. A) The X-ray crystal structure of compound **2.1** bound to *Sm*BRD3(2) (cartoon and carbon = white, PDB ID: 7AMH), overlaid with I-BET726 (**1.6**) bound to *Sm*BRD3(2) (PDB ID: 7AMC). **B**) The benzothiophene group of **2.1** occupies the HFF cleft more effectively than the chlorophenyl group of I-BET726 (**1.6**).

The crystal structure shows compound **2.1** binds to *Sm*BRD3(2) in the same orientation as I-BET726 (**1.6**), forming the same interactions with N339 and Y296 (**Figure 2.5**). Notably,

the benzothiophene group is observed to more effectively occupy the HFF cleft, which could explain the increase in affinity for compound **2.1** compared to I-BET726 (**1.6**). The crystal structure inspired the design of further analogues, which were subsequently synthesised and their affinities for *Sm*BRD3(2) were determined using ITC (**Table 2.1**).

Table 2.1. The *Sm*BRD3(2) K_d values of I-BET726 (**1.6**) and compounds **2.1**–**2.6** and **2.33** determined using ITC. A heatmap colour scale of green to red is used, with red representing higher affinity and green representing lower affinity.

Compound Number	Compound Structure	*Sm*BRD3(2) K_d (ITC, nM)	pK_d
I-BET726 (**1.6**)		**1850 ± 361[a]**	**5.7**
2.1		**701 ± 127[b]**	**6.2**
2.2		**1180 ± 235[c]**	**5.9**
2.3		**553 ± 18.6[c]**	**6.3**
2.4		**651 ± 24.9[b]**	**6.2**
2.5		**1183 ± 170[b]**	**5.9**
2.6		**364 ± 51.6[b]**	**6.4**
2.33		**no binding**	**-**

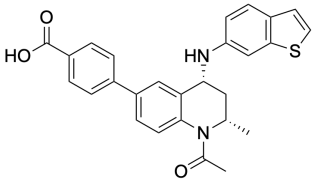
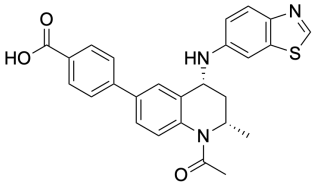
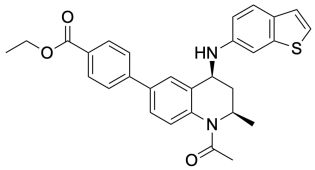
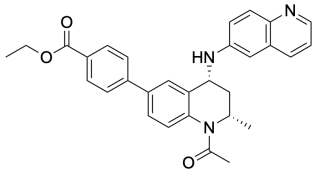
[a] Single value ± error of the curve fit; [b] mean value of 3 repeats ± 95% CI; [c] mean value of 2 repeats ± 95% CI.

The opposite enantiomer of compound **2.1**, **2.33**, was synthesised for possible use as a negative control in phenotypic screening. No binding to both *Sm*BRD3(2) and *Sm*BRD3(1,2) was observed (tested at 20 μM **2.33** and 160 μM protein), which is comparable with data on human bromodomains, where the enantiomer of an I-BET726 derivative showed reduced binding to *Hm*BRD4(1).[32] Replacement of the benzothiophene group with a benzofuran moiety (**2.2**) resulted in a reduction in affinity for *Sm*BRD3(2). Inspired by the crystal structure, compound **2.3** was synthesised to examine the effect of moving the S atom to the more solvent exposed position. This alteration resulted in an increase in *Sm*BRD3(2) affinity. The indole analogue **2.4** showed a similar affinity for SmBRD3(2) as **2.1**, and the benzothiazole derivate (**2.5**) showed a decrease in affinity, with a K_d comparable to benzofuran analogue **2.2**. Finally, use of a [6,6]-bicyclic head group *via* a quinoline showed the largest increase in affinity, and analogue **2.6** is the highest affinity compound for *Sm*BRD3(2) in this series, with a K_d of 364 ± 51.6 nM.

The corresponding ethyl ester analogues **2.20**–**2.23** and **2.30**–**2.32** were also evaluated for binding to *Sm*BRD3(2). However, in all cases no binding was detected by ITC. This contrasts with literature observations that structure-activity relationship (SAR) modifications in the locality of the ethyl ester group in human BRDs is well tolerated, as determined by a peptide-based FRET assay.[32] To determine if this observation was a structure-affinity relationship effect or a problem in compound solubility, compounds **2.1**, **2.5**, **2.23** and **2.31** were tested using a Charged Aerosol Detector (CAD) solubility assay (**Table 2.2**). The solubility assay involves diluting 5 μL of a 10 mM DMSO compound solution to 100 μL using phosphate buffer saline, pH 7.4, and equilibrated for 1 h at rt. The solution is then filtered and quantified using a suitably calibrated Charged Aerosol Detector.[131] For additional physiochemical information, Chrom logD values were determined by least-square fitting of experimental Chromatographic Hydrophobicity Index (CHI) values to calculated CLogP values for over 20,000 research compounds.[132] CHI values were measured using a reverse phase HPLC column with varying mobile phase, as previously reported.[133,134] The CAD

solubility and Chrom logD assays were carried out and analysed by the Physchem Team, Discovery Analytical, NCE Molecular Discovery at GSK.

Table 2.2 Aqueous solubility and Chrom LogD of compounds **2.1**, **2.5**, **2.23** and **2.31**.

Compound	Structure	Aqueous Solubility by CAD (μM)	Chrom LogD (pH 7.4)
2.1		**≥259**	**2.83**
2.5		**≥260**	**1.78**
2.23		**1**	**7.61**
2.31		**13**	**5.95**

The solubility data indicated the benzoic acid analogues **2.1** and **2.5** are more soluble than the ethyl ester analogues **2.23** and **2.31,** by ≥259-fold or ≥20-fold, respectively. Furthermore, the solubility of ethyl esters **2.23** and **2.31** fall below the concentration of 20 μM used to test these compounds by ITC. The affinity of the ethyl ester analogues could therefore not be determined due to poor solubility.

2.3.2 Phenotypic screening of *Sm*BRD3 ligands on *S. mansoni*

After the identification of both known and novel BRD ligands binding to *Sm*BRD3, it was desirable to phenotypically screen these compounds against different life cycle stages of *S. mansoni*, with the aim of elucidating the function of this bromodomain-containing protein in the parasites. The effects of these compounds were evaluated on the sexually immature larval schistosomulae, both male and female sexually mature adult worms, and snail infective miracidia life forms of *S. mansoni* by Dr Gilda Padalino (G.P.). There was a concern that the acid-containing I-BET726 derivatives may not show high permeability into the parasites, as indicated by the Chrom logD values of compounds **2.23** and **2.31**, and the need of these compounds to cross the seven-layered heptalaminate membrane of the *S. mansoni* tegument. Therefore, the ethyl ester precursors were also evaluated, despite not showing any binding to *Sm*BRD3(2), with the reasoning that they may act as pro-drugs to release the *Sm*BRD3(2) binding ligands *in situ*.

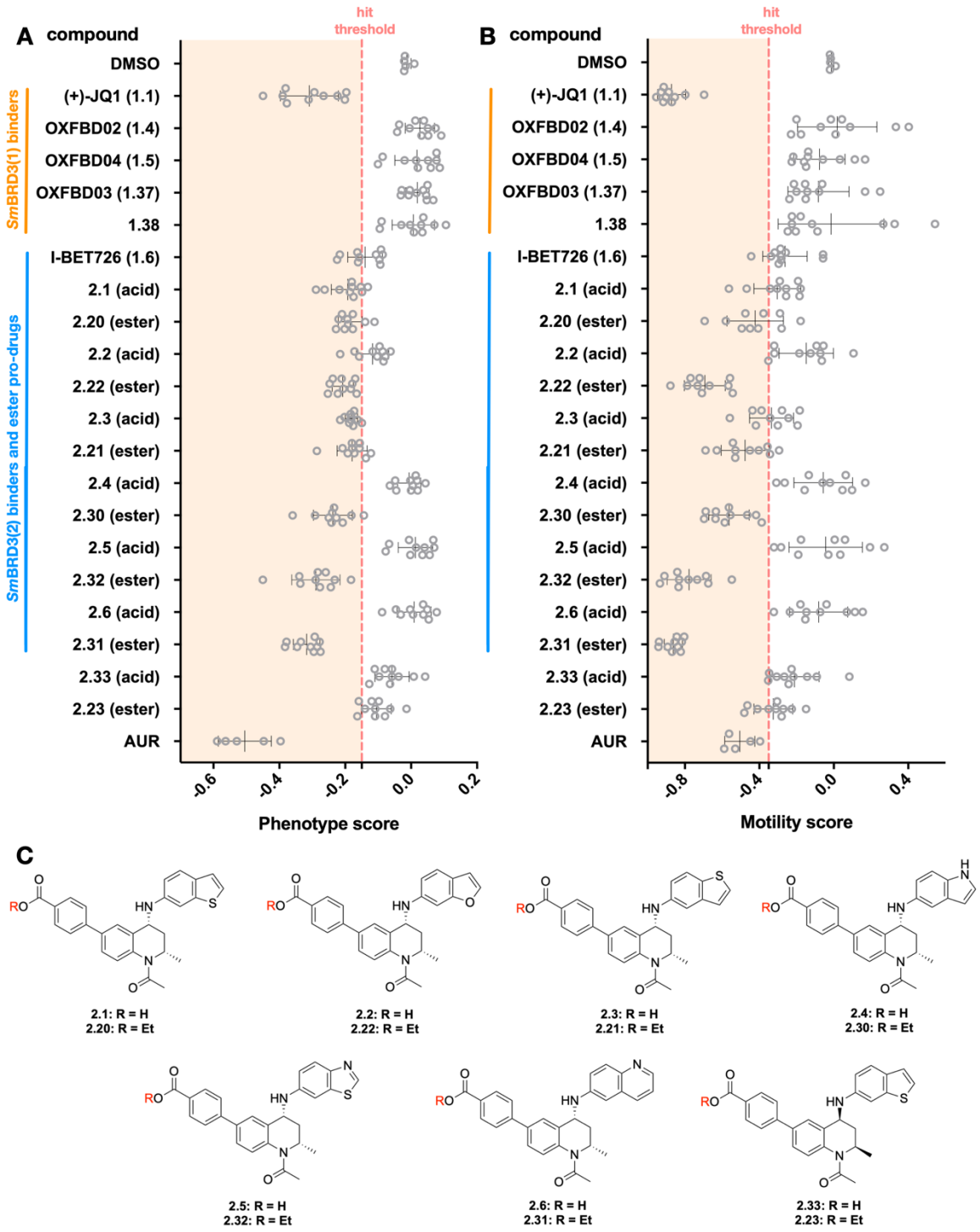


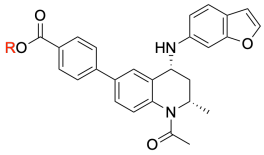
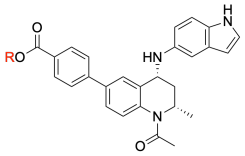
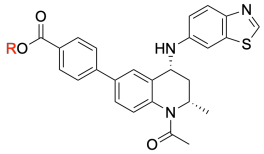
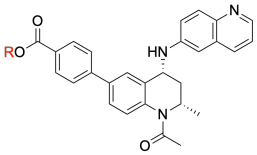
Figure 2.6. The effect of compounds **1.1**, **1.4**–**1.6**, **1.37**, **1.38**, **2.1**–**2.6**, **2.20**–**2.23**, **2.30**–**2.33** on the **(A)** phenotype and (**B**) motility of schistosomula (at 20 µM in 0.6% DMSO, following 72 h incubation). Negative (0.6% DMSO) and positive (10 µM auranofin in 0.6% DMSO) controls were included in each drug screen (4-5 in total, two technical replicates each). The compound score is shown as grey dots and the whiskers represent the average score and standard deviation across the screens. Hit threshold is delineated by the vertical dashed red lines in the graphs; −0.15 and −0.35 for phenotype and motility scores, respectively. **C**) The structures of compounds **2.1**–**2.6**, **2.20**–**2.23**, **2.30**–**2.33**. Schistosomula screening was carried out and analysed by G.P..

A high-throughput, high-content imaging platform known as 'Roboworm' was used to phenotypically screen compounds against the larval stage schistosomula, as described in the literature (**Figure 2.6**).[105,135] Briefly, following 72 h co-incubation of schistosomula and compound within a 384-well plate, parasites were imaged and the images were analysed by a custom built software package, whereby individual parasites were segmented and assigned a score for the independent metrics of 'phenotype' and 'motility'. These metrics are scored according to the procedure reported by Paveley *et al*.[135] In short, the phenotype of individual schistosomula is scored according to a collection of visual phenotype descriptors, for example 'dead', 'granular' and 'enlarged', and schistosomula motility is assigned by the cumulative change in area occupied by single schistosomula between time frames. The data for each well is represented as a mean for these scores from individual parasites in the well, which are normalised relative to the DMSO controls, enabling plate to plate comparisons.[136] Hits were classed as compounds that significantly affected both phenotype (hit threshold of −0.15) and motility (hit threshold of −0.35) of schistosomula, and only plates with Z' scores[136] above 0.35 were included in analysis.

The carboxylic acid analogues of the I-BET726 derivates were not classed as hits in this assay, showing no significant effect on the schistosomula motility. However, four ethyl ester analogues were classed as significant hits: the benzofuran (**2.22**), indole (**2.30**), quinoline (**2.31**), and benzothiazole analogues (**2.32**), with the quinoline and benzothiazole showing the most significant effect. The carboxylic acid counterparts of these compounds all have affinity for *Sm*BRD3(2), and therefore the activity of these ethyl ester analogues could be due to the release of the *Sm*BRD3(2) binding form *in-situ*, *via* the activity of an esterase enzyme. The benzothiophene analogues **2.20** and **2.21** also affected the schistosomula, whereas the opposite enantiomer of **2.20**, **2.23**, was not classed as a hit. All the *Sm*BRD3(1) selective ligands induced no effect with the only exception of (+)-JQ1 (**1.1**), which was classed as a hit, consistent with observations in the literature.[105]

The more active compounds **2.22** and **2.30**–**2.32** were further evaluated using a dose-dependent titration to determine EC_{50} values (**Table 2.3**). These values were in the low micromolar range for both phenotype and motility, however, there is only moderate correlation between the K_d values of their corresponding acid analogues. This is likely due to the number of other characteristics of these compounds that could affect the activity of schistosomula, for example permeability, and metabolic stability.

Table 2.3. The *Sm*BRD3(2) K_d values (ITC) for the carboxylic acids **2.2, 2.4**–**2.6**, and schistosomula phenotype and motility EC_{50} values for the corresponding ethyl esters **2.22**, **2.30, 2.32** and **2.31**. A heatmap colour scale of green to red is used with red representing higher affinity and higher *ex vivo* activity and green representing lower affinity and *ex vivo* activity. EC_{50} values were determined by a dose-dependent titration carried out by G.P., with EC_{50} values calculated by G.P..

Compound Numbers	Compound Structure	*Sm*BRD3(2) K_d (ITC, nM) (R=H)	Schistosomla Phenotype EC_{50} (μM) (R=Et)	Schistosomla Motility EC_{50} (μM) (R=Et)
2.2 (R=H) **2.22** (R=Et)		**1180 ± 235**[c]	**2.43**	**3.92**
2.4 (R=H) **2.30** (R=Et)		**651 ± 24.9**[b]	**2.97**	**1.81**
2.5 (R=H) **2.32** (R=Et)		**1183 ± 170**[b]	**2.14**	**2.85**
2.6 (R=H) **2.31** (R=Et)		**364 ± 51.6**[b]	**1.11**	**3.30**

[a] Single value ± error of the curve fit; [b] mean value of 3 repeats ± 95% CI; [c] mean value of 2 repeats ± 95% CI.

The *Sm*BRD3(1) selective ligands, I-BET726 (**1.6**) and novel I-BET726 derivatives were also assessed for their activity on sexually mature adult *S. mansoni* (**Figure 2.7**). Adult worm motility was quantified as described in the literature using a digital image processing-based system, WormAssayGP2,[137] which is a modified imaging system based upon

WormAssay.[138] The observations of the effect on schistosomula motility was broadly mirrored in adult worms (**Figure 2.7 A**). The ethyl ester I-BET726 derivates showed a significant effect in comparison to their acid counterparts. Analogous to the schistosomula screening data, (+)-JQ1 (**1.1**) induced a significant decrease on motility whereas the other *Sm*BRD3(1) selective ligands showed little effect on worm motility. Despite the effect on worm motility shown for a range of these compounds, none of the compounds were lethal to the parasite.

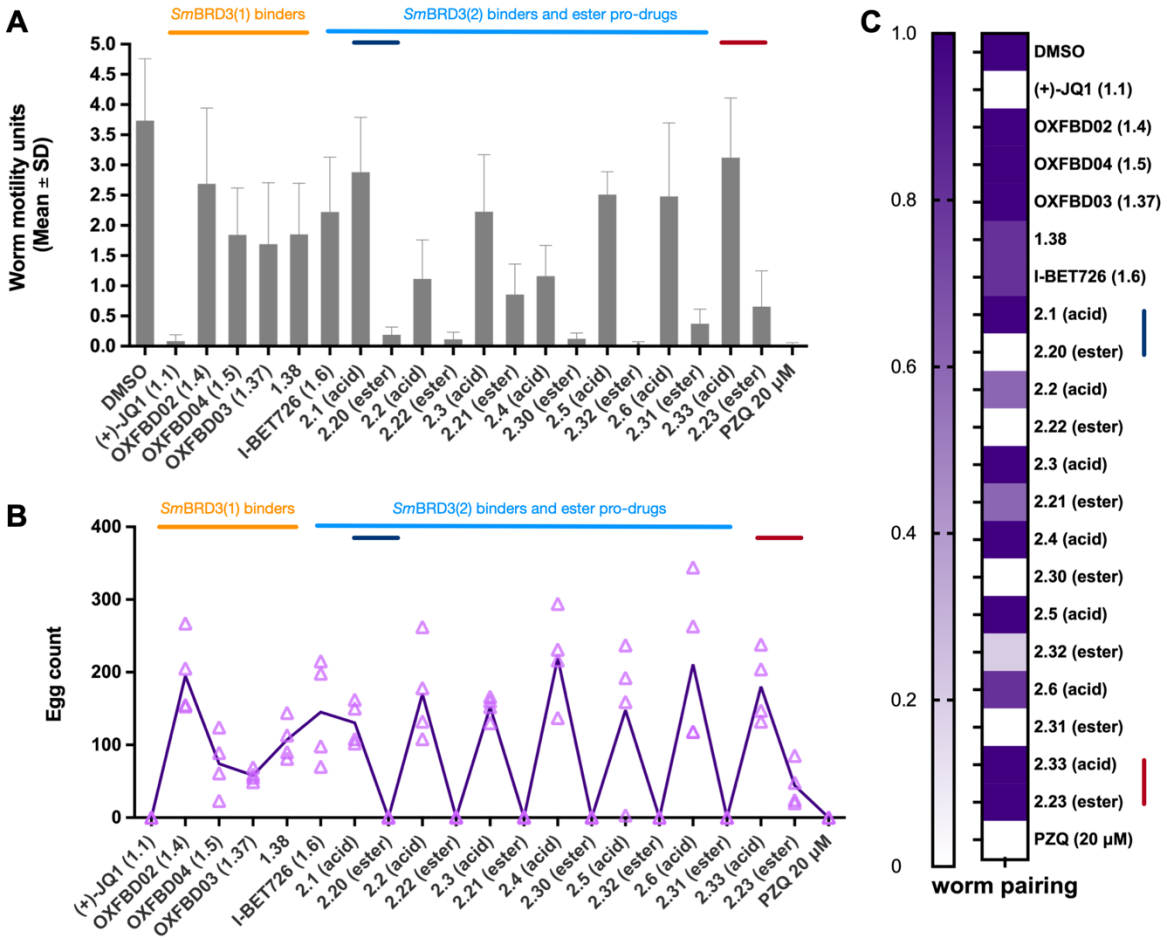


Figure 2.7. The effect of compounds **1.1**, **1.4**–**1.6**, **1.37**, **1.38**, **2.1**–**2.6**, **2.20**–**2.23**, **2.30**–**2.33** on motility, pairing, and egg production of *S. mansoni* adult worms. Compounds **2.1** and **2.20** and their corresponding enantiomers **2.33** and **2.23** are labelled with dark blue and red bars respectively. **A**) Worm motility following 72 h compound-treatment (20 µM in 0.5% DMSO). Negative (0.5% DMSO) and positive (20 µM praziquantel – PZQ in 0.5% DMSO) controls are included in each screen (n = 2 independent compound screens, 2 technical replicate each). The grey bars represent the mean worm motility (+ standard deviation). **B**) *In vitro* laid egg count resulting from 72 h compound incubation after collection and enumeration. For each compound tested, individual egg counts are represented in a scatter plot; the purple line represent the mean trend across the compound treatments. **C**) The effect of compound treatment on worm pairing, with 1 and 0 corresponding to 100% and 0% of parasite pairs following 72 h drug-treatment, respectively, (mean of n = 2 compound screens). The screening and analysis on adult *S. mansoni* worms was carried out by G.P..

Compounds that affect worm motility also can be associated with reduced oviposition and decreased worm pairing. Therefore, egg count and worm pairing were also assessed (**Figure 2.7 A** and **B**). Compounds that significantly affected worm motility were shown to also induce negligible oviposition. These compounds also affected worm pairing, with compounds **2.20**, **2.22**, **2.30**, and **2.31** resulting in complete unpairing of male and female worms.

Compounds **2.33** and **2.23**, the opposite enantiomers of compounds **2.1** and **2.20** respectively, were used as negative controls. Despite also showing an effect on worm motility, **2.23** had a reduced effect compared with its enantiomer **2.20**. Furthermore, this compound had a lower effect on worm oviposition and adult worm paring compared with its enantiomer. *Ex vivo* worm pairing is highly variable metric, however, compound **2.23** showed negligible effect on adult worm pairing, whereas incubation with its enantiomer **2.20** resulted in complete unpairing of adult worms. Assuming the validity of the ethyl ester pro-drug hypothesis (see **section 2.3.3**), these observations suggest that the phenotypic effects are, at least in part, due to inhibition of *Sm*BRD3.

*Sm*BRD3 is most abundant in the miracidia and sporocyst life-cycle stages of the parasite (**Chapter 1, Figure 1.20**). It was therefore desirable to probe the effect of these compounds on these two life-cycle stages. To directly probe the epigenetic mechanisms of these parasite life stages, the effect of *Sm*BRD3 ligands on the miracidia to sporocyst transformation was investigated *ex vivo*. The acid analogue **2.6** showed the highest affinity in ITC experiments for *Sm*BRD3(2), and its corresponding ethyl ester **2.31** showed an effect on schistosomula and adult worm life stages. Therefore, miracidia were incubated as a dose-response titration with ethyl ester **2.31**. This compound induced a concentration-dependent inhibition of the miracidia to sporocyst transformation (**Figure 2.8**). In contrast, incubation with OXFBD02 (**1.4**), which showed negligible effect on the schistosomula and adult worm life stage, did not affect the transformation in a concentration-dependent manner, with only a modest effect at 25 μM.

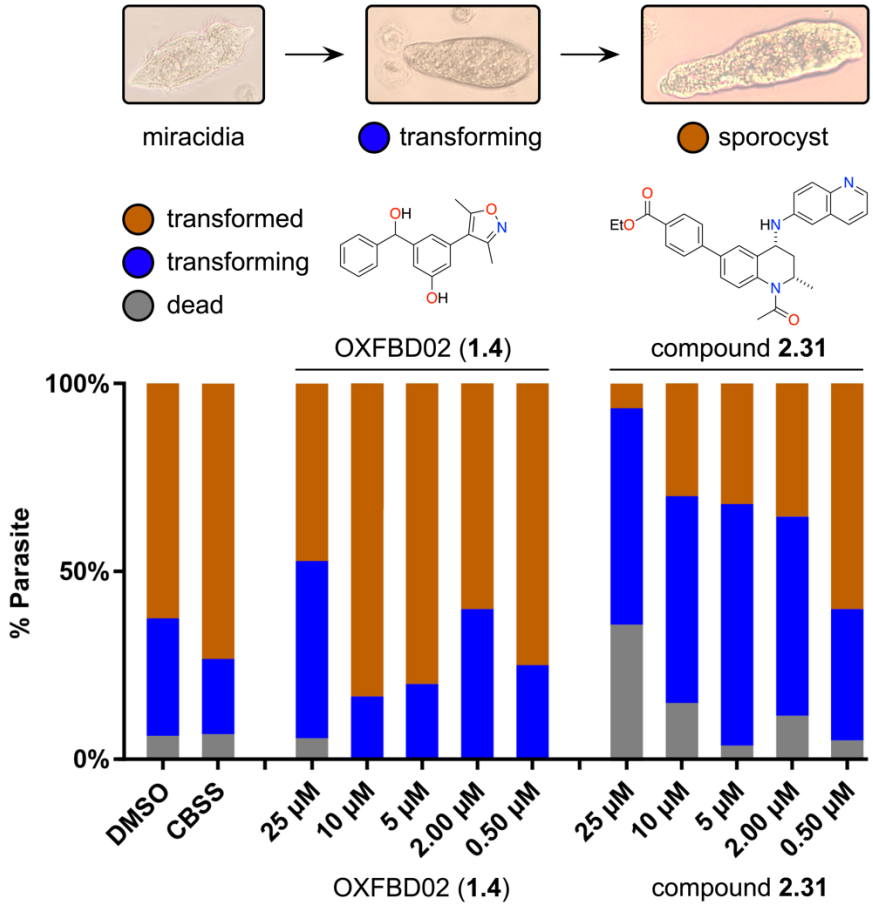


Figure 2.8. Differential activity of compound OXFBD02 (**1.4**) and compound **2.31** on the *ex vivo* miracidia to sporocyst transformation. Miracidia were exposed to the selected compounds in a dose-response titration (CBSS containing 25, 10, 5, 2, or 0.5 µM in 1% DMSO). Dead parasites (in grey), transforming miracidia (in blue) and fully transformed sporocysts (in brown) were enumerated after 48 h (scored as percentage of parasite population - % parasite). Each titration point was measured in triplicate and compared to parasites cultured in CBSS with 1% DMSO (controls) at a constant temperature of 26 °C, in the dark. The screening on miracidia and subsequent analysis was carried out by G.P..

To determine the effect of BRD ligands on this transformation, further compounds were tested (**Figure 2.9**). Similar to the quinoline analogue **2.31**, the benzothiophene derivative **2.20** also showed a concentration-dependent inhibition on the transformation of miracidia to sporocyst. Interestingly, the opposite enantiomer of **2.20, 2.23**, showed significant parasite lethality at 10 µM and 25 µM, indicating these enantiomers may have different protein targets. Of the *Sm*BRD3(1) selective ligands, (+)-JQ1 (**1.1**) was lethal to the parasite at 25 µM, whereas OXFBD04 (**1.5**) only showed a modest effect at the same concentration. In general, the *Sm*BRD3(1) selective ligands did not show a clear concentration-dependent effect on transformation.

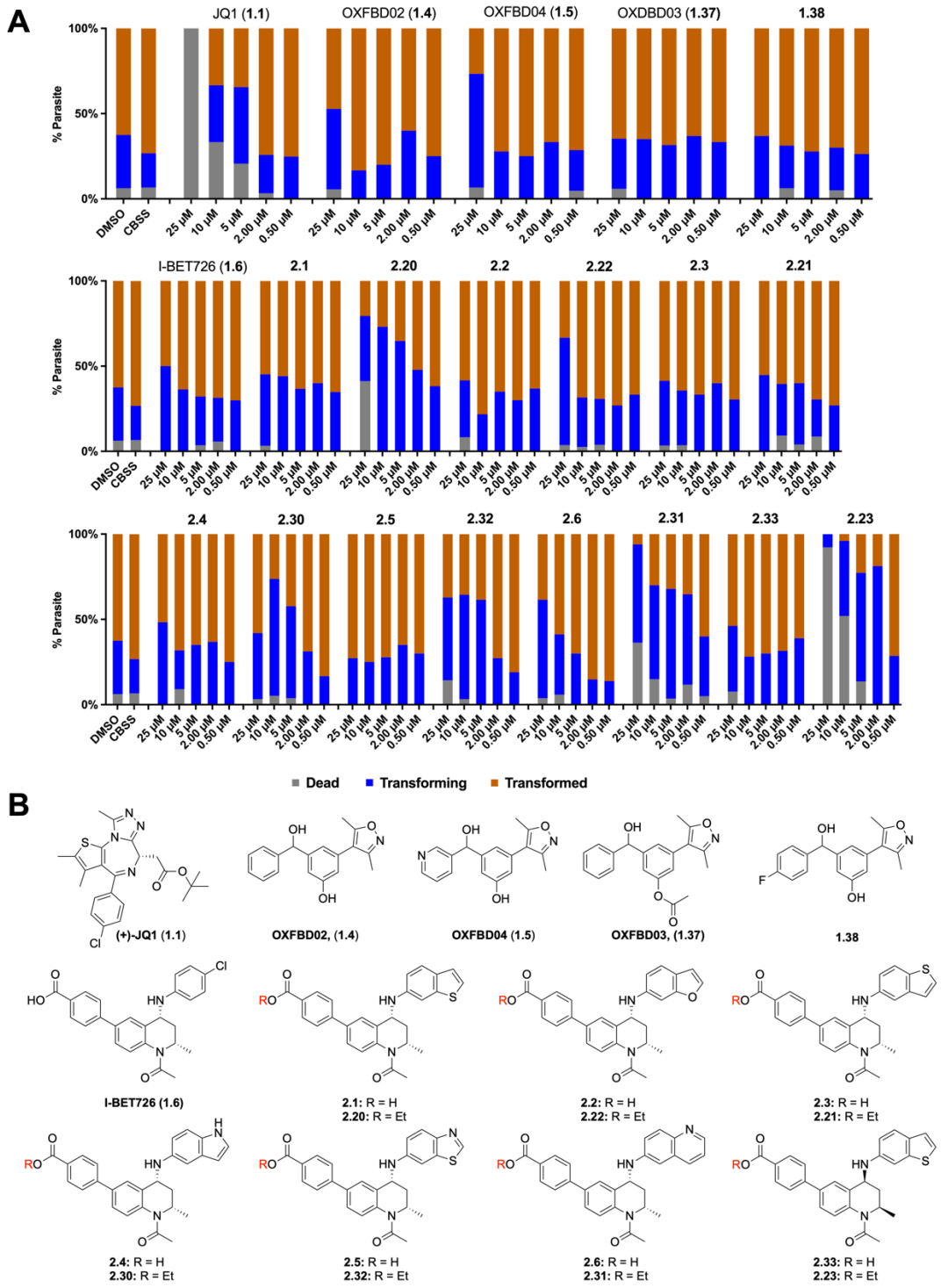


Figure 2.9. **A**) The activity of *Sm*BRD3(1) selective ligands and I-BET726 derivatives on the *ex vivo* miracidia to sporocyst transformation. **B**) The structures of *Sm*BRD3(1) selective and I-BET726 derivatives screened on the miracidia to sporocyst transformation. The screening on miracidia and subsequent analysis was carried out by G.P..

The clear concentration-dependent effects of compounds **2.31** and **2.20** on the transformation of miracidia to sporocyst suggest these compounds could be affecting the epigenetic mechanisms of these life stages of *S. mansoni*, indicating an engagement of

these compounds, albeit the carboxylic acid forms after possible conversion *in-situ*, with *Sm*BRD3. Comparable to data with other *S. mansoni* life stages, the *Sm*BRD3(1) selective ligands showed no clear concentration-dependent effect on transformation and the compound (+)-JQ1 (**1.1**) was lethal to the parasite at 25 μM. This information could be interpretated to indicate the lack of importance of the first domain of *Sm*BRD3(1) for parasite transformation, and also indicate off-target interactions causing the lethality of (+)-JQ1. Alternatively, inhibition of *Sm*BRD3(1) may be lethal to the miracidia life stage.

2.3.3 Investigation of parasite permeability by LCMS

The carboxylic acid analogues of the I-BET726 derivatives were mostly inactive on schistosomula and adult worms, whereas the corresponding ethyl ester analogues showed activity. Binding affinity for *Sm*BRD3 was not detected for the ethyl ester analogues (tested by ITC at 20 μM) due to low solubility, and these compounds could be inhibitors of *Sm*BRD3(2). Alternatively, it was hypothesised the ethyl esters may act as pro-drugs, by crossing the *S. mansoni* tegument, and once inside the parasite releasing the *Sm*BRD3(2)-binding acid. Furthermore, with the exception of (+)-JQ1 (**1.1**), the *Sm*BRD3(1) selective ligands did not induce a significant effect on schistosomula and adult worms. Two possible explanations for this observation could be the lack of importance of *Sm*BRD3(1), compared with *Sm*BRD3(2), or these compounds failed to enter the parasite due to physiochemical properties. To support the pro-drug hypothesis and provide insight into the inactivity of dimethylisoxazole based ligands, the parasite permeability of compounds was assessed by LCMS after compound incubation with adult worms and lysis.

Compounds **1.37**, **2.6** and **2.31**, along with a DMSO control, were incubated with male and female adult worm pairs for 24 hours (20 μM concentration in 0.2% DMSO or 0.2% DMSO only). The worms were then washed three times with media to remove excess compound from the surface of the worm, and frozen. The worms were later lysed using MeOH to extract all possible compound present in the worms, and worm lysate methanol solutions were

examined by LCMS. Approximate compound concentrations in these samples were estimated from the raw TIC area using a two-point calibration curve, generated from compound standard solutions. The samples for compound detection were prepared by Dr Josephine Forde-Thomas (J.F.T.) (University of Aberystwyth) and LCMS experiments were carried out and analysed by Dr Manfred Beckmann (University of Aberystwyth).

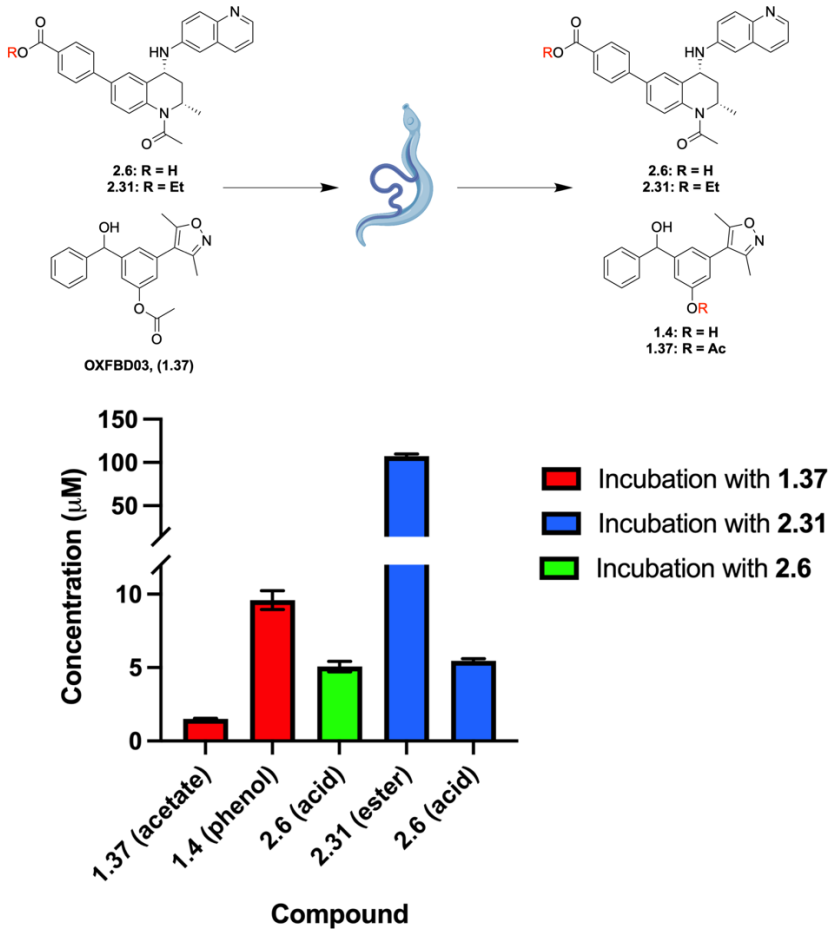


Figure 2.10 Estimation of the concentrations of **1.37, 1.4**, **2.6** and **2.31** in *S. mansoni* lysate following 24 h incubation with compounds **1.37** (red), **2.6** (green) and **2.31** (blue). The concentration estimations were calculated as an average (n = 3) from the analysis of lysate from male adult worms, 5 worms per well, with error bars representing the s.e.m.. Lysate samples were prepared by J.F.T. and analysed by Dr Manfred Beckmann. **Figure 2.10** was created with the use of Biorender.com.

High quantities of the ethyl ester, compound **2.31**, were detected in worm lysate samples compared with its acid counterpart **2.6** and the dimethylisoxazole-based ligand **1.37**, indicating this compound has high permeability across the *S. mansoni* adult worm tegument. This result suggests the ethyl esters do indeed enter the parasite and are significantly more permeable than the corresponding acids. The quantity of the acid **2.6** that was detected in

the lysate after incubation with **2.31** was comparable with the approximate concentration of **2.6** after incubation with **2.6**, indicating the ester can be converted to the acid in the worm. Given the low permeability of the acid **2.6**, it is expected the quantity of this compound detected in lysate, after incubation of *S. mansoni* with **2.6**, is due to presence of the compound in the worm gut, rather than crossing the tegument. A lower quantity of the dimethylisoxazole-based ligand **1.37** was detected in the lysate compared with **2.6**. However, after incubation with **1.37**, a higher approximate concentration of its phenol counterpart, **1.4**, was present compared with **2.6**. This result indicated **1.37** was readily transformed to the hydrolysis product **1.4** in the presence of the worm.

There was a concern that the transformations of **2.31** to **2.6**, and **1.37** to **1.4**, occurred in the media, instead of or as well as inside the worm. Therefore, the media was analysed by LCMS to detect these compounds and possible transformations occurring independent of the adult *S. mansoni* worms. For detection of compounds in media samples, the media was lyophilized and resuspended in MeOH. The suspension was centrifuged (to remove precipitates originating from the media), and the supernatant MeOH solution was analysed using LCMS. Media in both the presence and absence of *S. mansoni* adult worms was analysed.

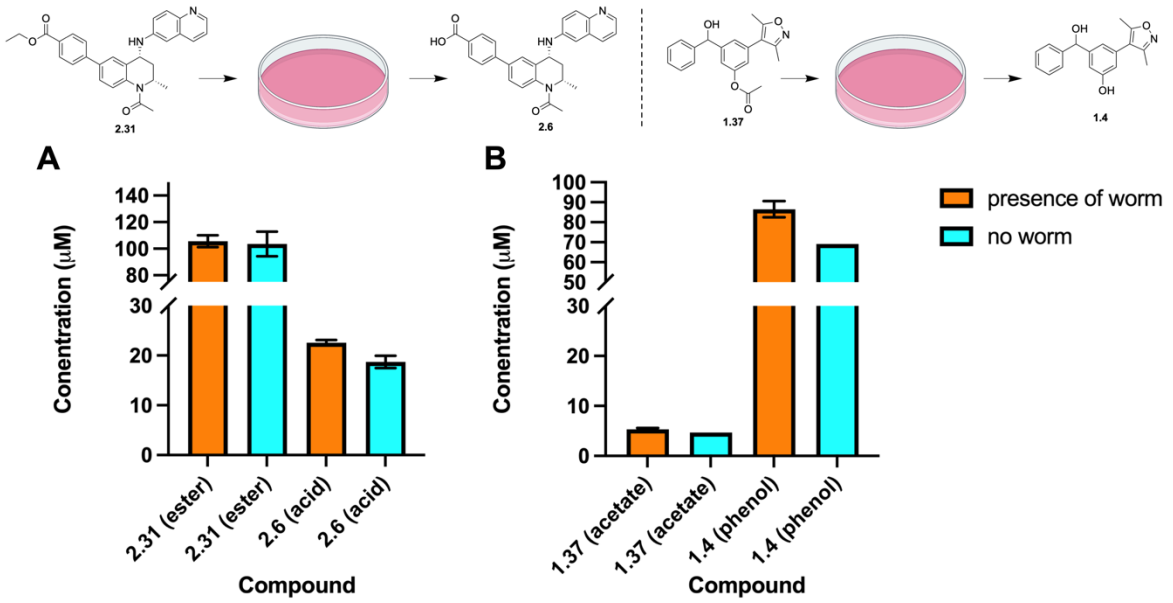


Figure 2.11. A) Estimation of the concentration of **2.6** and **2.31** in media after incubation with **2.31** (20 μM) in the presence and absence of *S. mansoni*. The concentration estimations were calculated as an average (presence of worm n=3, no worm n=2) from the analysis of media in the presence (5 worms per well) or absence of worms, with error bars representing the s.e.m. **B**) Estimation of the concentration of **1.37** and **1.4** in media after incubation with **1.37** (20 μM) in the presence and absence of *S. mansoni*. The concentration estimations were calculated as an average (presence of worm n=2, no worm n=1) from the analysis of media in the presence (5 worms per well) or absence of worms with error bars representing the s.e.m. Media samples were prepared by J.F.T. and analysed by Dr Manfred Beckmann. **Figure 2.11** was created with the use of Biorender.com.

Analysis of the media samples after incubation with **2.31** revealed hydrolysis of **2.31** to **2.6** in the presence and absence of *S. mansoni*, showing this transformation occurred in the media. However, a marginally higher quantity of **2.6** was detected in the presence of the worm. This higher approximate concentration may be due to this transformation occurring in the worm, with transformed **2.31** being released from the worm, in addition to hydrolysis in the media. The media samples after incubation of **1.37** indicated this compound is readily deacetylated to **1.4** in media in the presence and absence of worms. Therefore, the results of the worm lysate analysis after incubation with compound **1.37** could be thought of as incubation of the worms with mostly **1.4**, in combination with **1.37**. Higher quantities of **1.4** were detected in the lysate compared with **2.6**, suggesting this dimethylisoxazole-based probe enters the parasite.

2.4 Conclusions

The aims of this chapter were to design and synthesise novel I-BET726 derivatives for optimised interactions with the HFF shelf of *Sm*BRD3(2), and to determine the extent of binding of these compounds to this domain. These compounds were then to be assessed in phenotypic screening on *S. mansoni*, along with *Sm*BRD3(1) selective ligands, to elucidate the function of *Sm*BRD3. A total of 7 I-BET726 derivates were synthesised with bicyclic heterocyclic head groups, all of which showed enhanced binding to *Sm*BRD3(2) compared with I-BET726 (**1.6**). It can therefore be concluded that more effective occupation of the HFF cleft *via* these head groups is a successful SAR strategy to develop higher affinity ligands. The highest affinity compound for *Sm*BRD3(2) was based on a quinoline head group, compound **2.6**, with a K_d of 364 ± 51.6 nM. The phenotypic screening data showed the ethyl ester analogues of these I-BET726 derivatives influenced the function of *S. mansoni* across three life-cycle stages. In particular, the ethyl ester derivative of compound **2.6**, **2.31**, showed a significant effect on schistosomula motility and phenotype and an effect on adult worm motility, oviposition, and worm pairing. This compound also reduced the transformation of the miracidia to sporocyst life-cycle stages, suggesting this compound may target the epigenetic mechanisms of the parasite, possibly *via Sm*BRD3 inhibition.

It was hypothesised that the ethyl ester analogues were more active due to enhanced parasite permeability relating to more favourable physiochemical properties. Once in the parasite, it was reasoned the *Sm*BRD3(2) binding compound would be released *in situ*. The LCMS experiment supports the idea of greater parasite permeability for the ethyl ester analogues, and the lack of parasite permeability for their acid counterparts. The data also indicated some conversion of **2.31** to compound **2.6** occurs in the parasite. Finally, the LCMS results after incubation with OXFBD03 (**1.37**) suggested some OXFBD02 (**1.4**) entered the parasite, indicating a lack of effect of selective *Sm*BRD3(1) inhibition. Further work is needed to determine the extent of parasite permeability, however, particularly in comparison to (+)-JQ1 (**1.1**), which showed an effect on *S. mansoni*.

The SAR strategy described in this chapter focussed on the HFF cleft, however, affinity could be further enhanced by exploring SAR in other regions of the binding pocket of *Sm*BRD3, notably the ZA channel region (**Chapter 3**). Furthermore, to probe target engagement and determine in-parasite selectivity of *Sm*BRD3 ligands, photo-affinity pull down probes could be designed (**Chapter 4**).

Chapter 3

Structure-based optimisation of small molecule ligands for *Sm*BRD3(2): targeting the ZA channel region

3.1 Introduction and aims

The work described in **Chapter 2** focused on developing ligands with enhanced affinity for *Sm*BRD3(2) by targeting the HFF shelf. This was achieved by replacing the chlorophenyl group of I-BET726 (**1.6**) with bicyclic aromatic groups. The benzoic acid group of **1.6** projects along another vector into the ZA channel region of the KAc binding pocket. This offers an alternative area of *Sm*BRD3(2) in which to enhance interactions and therefore to increase affinity (**Figure 3.1**). An increase in affinity for *Sm*BRD3(2) could lead to a larger effect in phenotype on *S. mansoni*.

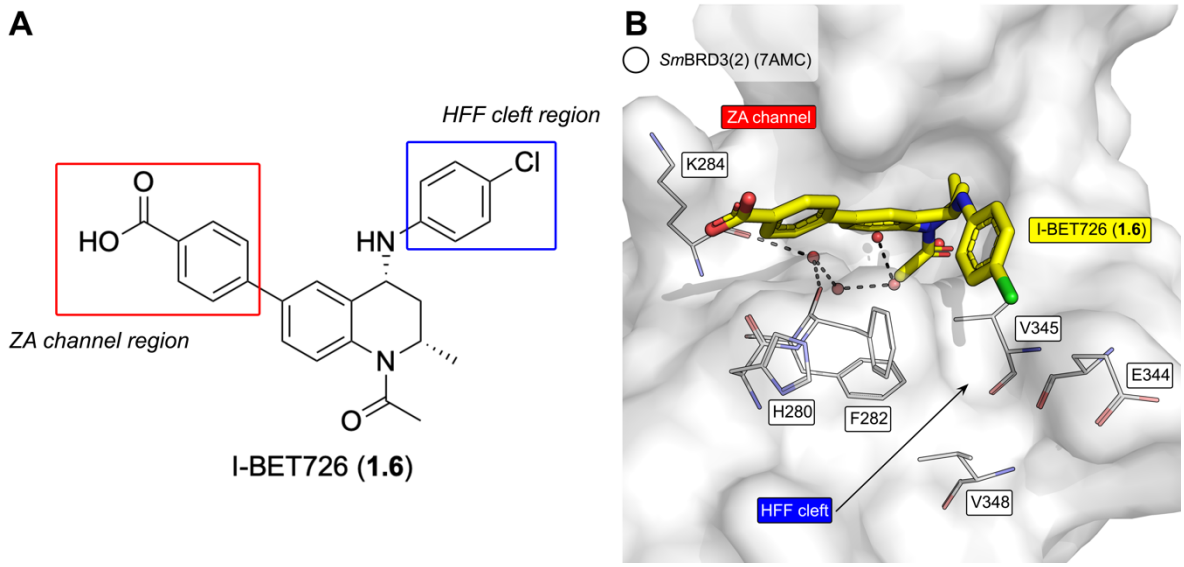


Figure 3.1. A) The structure of I-BET726 (**1.6**) with the benzoic acid (red) and chlorophenyl (blue) groups highlighted. **B**) An X-ray crystal structure of I-BET726 (**1.6**) (carbon = yellow) bound to *Sm*BRD3(2) (carbon = white) (PDB ID: 7AMC) with the ZA Channel and HFF Cleft regions labelled. The benzoic acid of I-BET726 (**1.6**) projects into the ZA channel region.

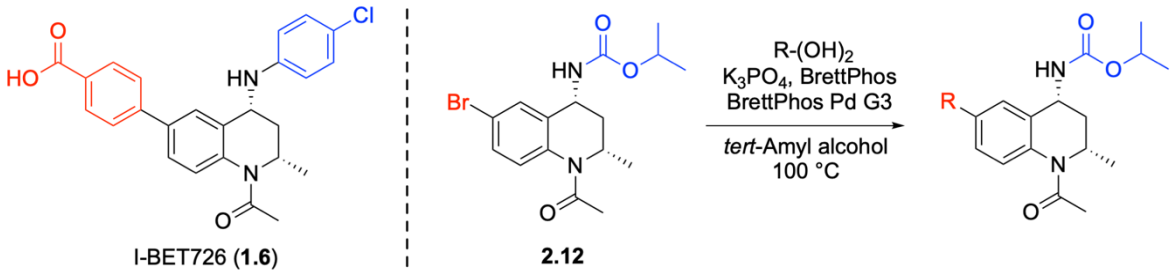
The aims of this chapter are to:

- Develop tetrahydroquinoline ligands for investigation of SAR in the ZA channel region.
- Assess whether SAR for targeting the HFF and ZA channel regions are additive.
- Evaluate the effects in phenotype on *S. mansoni* from compounds developed from this SAR investigation.

3.2 Isopropyl carbamate fragments for SAR investigation of the ZA channel region

3.2.1 Ligand design

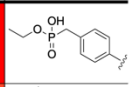
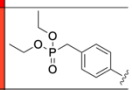
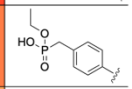
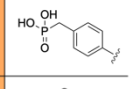
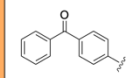
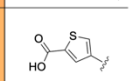
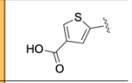
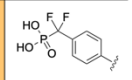
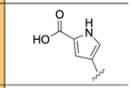
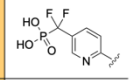
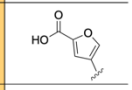
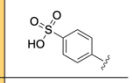
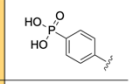
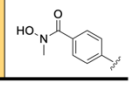
Inspired by the work of *Shadrick et al.*,[123] it was decided that SAR in the ZA channel region could be investigated using a semi-fragment-based approach. By retaining the isopropyl carbamate group which occurs earlier in the synthesis of I-BET726, Shadrick *et al*. used this approach to introduce selectivity between human BRD2(1) and BRD2(2). Selectivity was achieved by the introduction of varying 2- and 3-heteroaryl substituted tetrahydroquinoline based ligands, with the aim of differential engagement with the varying positioned ZA channel water molecules in the different domains. These compounds were synthesised using Suzuki coupling with intermediate **2.12** (**Scheme 3.1**).

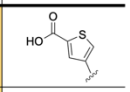
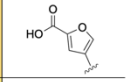
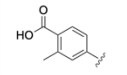
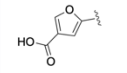
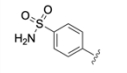
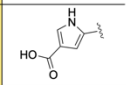
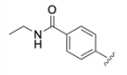
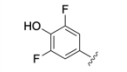
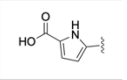
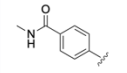
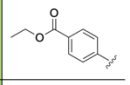
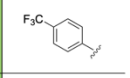
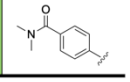


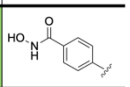
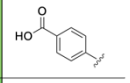
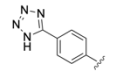
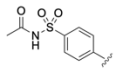
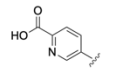
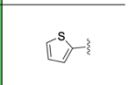
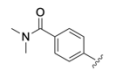
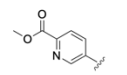
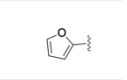
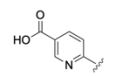
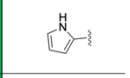
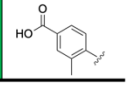
Scheme 3.1. Structure of I-BET726 (**1.6**) and the synthetic route to isopropyl carbamate-based THQ ligands developed by Shadrick *et al*..[123]

To further investigate *Sm*BRD3(2) binding, varying R groups were applied. In contrast to SAR development for the HFF shelf (**Chapter 2**), suggestions for R groups to engage with water molecules and residues in the ZA channel were less clear, and therefore it was decided *in silico* docking would aid in the decision of target molecules. A library of compounds was designed by Aleksy Kwiatkowski (A.K.) and docked using Genetic Optimisation for Ligand Docking (GOLD) software and the crystal structure of **2.1** bound to *Sm*BRD3(2). The compounds were ranked by ChemPLP score (**Table 3.1**).

Table 3.1 Docking ChemPLP scores of varying R groups by *in silico* docking into *Sm*BRD3(2) using GOLD. *In silico* docking was carried out by A. K..[139] A heatmap colour scale of green to red is used with 'hot' colours representing higher ChemPLP score.

Compound	ChemPLP score	R
3.1	116.28	
3.2	113.89	
3.1	112.03	
3.3	110.52	
3.4	110.37	
3.5	110.05	
3.6	109.61	
3.7	109.5	
3.8	109.47	
3.9	109.25	
3.10	109.13	
3.11	109.05	
3.12	108.98	
3.13	108.92	

Compound	ChemPLP score	R
3.14	108.90	
3.15	108.74	
3.16	108.36	
3.17	108.26	
3.18	108.26	
3.19	108.25	
3.20	108.21	
3.21	107.34	
3.22	107.19	
3.23	106.87	
2.13	106.78	
3.24	106.34	
3.25	106.16	

Compound	ChemPLP score	R
3.26	106.16	
3.27	106.09	
3.28	105.75	
3.29	105.71	
3.30	105.46	
3.31	105.11	
3.32	104.93	
3.33	104.92	
3.34	104.76	
3.35	104.62	
3.36	103.38	
3.37	103.31	
3.38	103.27	

The compounds were designed broadly according to the following SAR strategies: carboxylic acid bioisosteres (for example **3.11**, **3.12** and **3.18**), heteroaromatic groups to probe binding to the ZA channel waters (for example **3.5, 3.8** and **3.10**), groups to probe displacing the ZA channel waters (**3.16** and **3.38**), addition of a methylene or CF_2 to position the phosphonate for possible engagement with H280 (**3.1**–**3.3**), bicyclo[1,1,1]pentane as a non-aromatic bioisostere of benzene (**3.38**), and esters and amides of corresponding acid analogues (for example **3.20**, **3.23** and **3.29**).

Compounds **2.13**, **3.1**–**3.3**, **3.24**, **3.27**, **3.28**, **3.30** and **3.33** were selected as target compounds for synthesis and biological evaluation (**Figure 3.2.**). Compounds **2.13** and **3.27**, based on a benzoic acid and ethyl ester, were chosen for a direct SAR comparison (matched pair analysis) with I-BET726 (**1.6**), and the acid and ethyl ester analogues developed in **Chapter 2**. Compounds **3.1**, **3.2**, and **3.3** scored highest during *in silico* docking, and therefore were predicted to result in the highest affinity for *Sm*BRD3(2). For the case of **3.3**, docking by A.K. suggested the methylene group could position a phosphonic acid proton close enough to engage in a hydrogen bonding interaction with H280. The predicted pK_a value for deprotonation of a second proton of this group is 7.67 ± 0.30 (Advanced Chemistry Development: http://ilab.psds.ac.uk/, prediction carried out by A. Kwiatkowski),[139] suggesting this proton is ~50% present and therefore can at least partly form this interaction at physiological pH. Despite its comparatively low docking score, compound **3.28** was chosen for its interesting use of a carboxylic acid bioisostere. Similarly, compounds **3.30** and **3.33** also resulted in low docking scores, however, the resulting docking pose suggested the nitrogen could be close enough to water molecules in the ZA channel for hydrogen bonding.[139] Finally, compound **3.24** was selected from the docked structures to investigate the lipophilicty of C-F bonds.

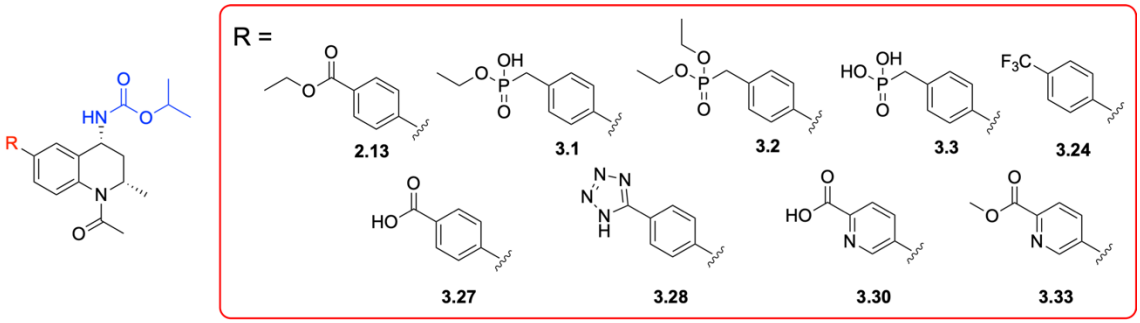
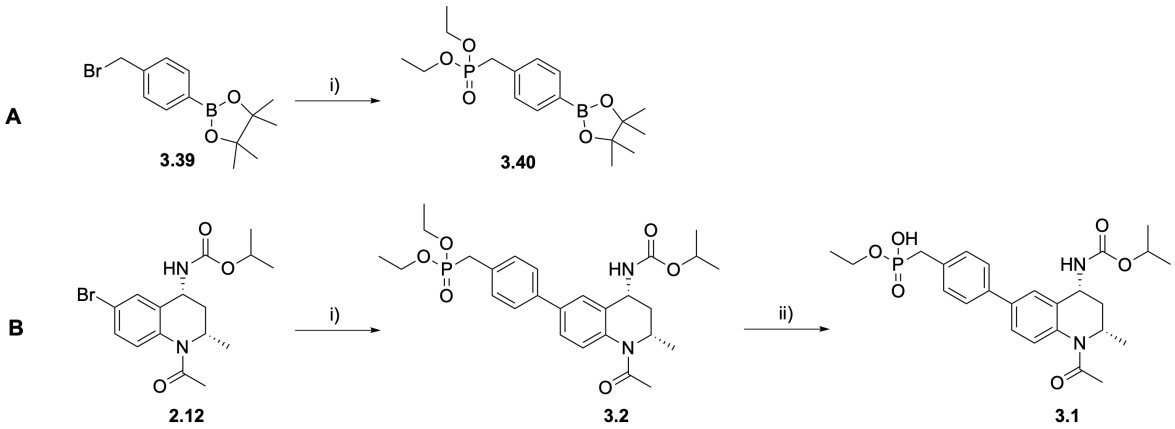


Figure 3.2. Structures of target isopropyl carbamate fragment molecules, chosen by A.K..[139]

3.2.2. Synthesis

Compounds **3.2**, **3.3**, **3.24**, **3.27**, **3.28**, **3.33**, and **3.35** were synthesised by A.K., using intermediate **2.12** and primarily Suzuki coupling of the appropriate boronic acid or boron pinacol ester.[139] Compound **3.1** was synthesised from compound **3.2** *via* NaOH catalysed ester hydrolysis.



Scheme 3.2. **A**) Synthesis of intermediate **3.40**. *Reagents and conditions*: i) $P(OEt)_3$, 140 °C, 1 h, 92%; **B**) Synthesis of compound **3.1**. *Reagents and conditions*: i) **3.40**, $Pd(dppf)Cl_2$, $NaHCO_3$, 1,4-dioxane, 100 °C, microwave irradiation, 63%; ii) $NaOH_{(aq)}$, EtOH, rt – 70 °C, 31%. The synthesis of compound **3.2** was developed by A. Kwiatkowski.[139]

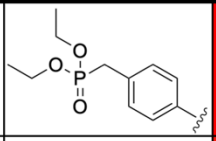
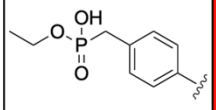
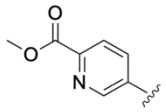
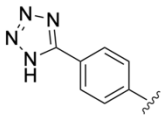
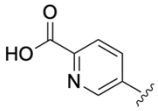
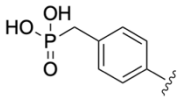
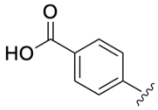
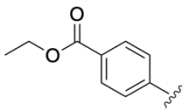
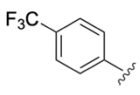
For the synthesis of the monoethyl analogue **3.1**, the synthesis of diethyl analogue developed by A. K., **3.2**, was repeated. An Arbuzov reaction, as described by Garcia-Rodriguez *et al*.,[140] was carried out to yield intermediate **3.40** in a 92% yield. Suzuki coupling (**Scheme 3.2. B**, step i), was then carried out using microwave irradiation to yield compound **3.2** in a 63% yield. Finally, ester hydrolysis of compound **3.2** gave **3.1** in a 31% yield. Hydrolysis of the phosphonate ester was slower than carbonyl esters, with heating to 70 °C, long reaction times and excess NaOH required. Initially the reaction used one equivalent of $NaOH_{(aq)}$ at room temperature, due to concerns of the possibility of hydrolysing the isopropyl carbamate group. However, no reaction was observed after 1 h, therefore, a further 9 equivalents of $NaOH_{(aq)}$ were added and the reaction was left to stir at room temperature overnight. TLC and LCMS analysis indicated no starting material conversion, or product formation, and therefore the reaction mixture was heated to 40 °C. LCMS analysis of the reaction mixture indicated limited

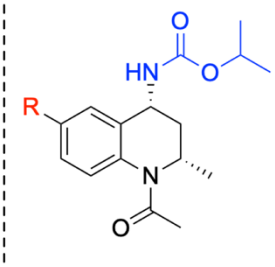
starting material conversion after 6 h, and therefore the reaction was heated to 70 °C and stirred for a further 48 h. A further 10 equivalents of $NaOH_{(aq)}$ was added, after which the mass corresponding to isopropyl carbamate hydrolysis was observed using LCMS. At this point it was decided to work up the reaction, despite the starting material not being fully converted. The low yield can be attributed to incomplete conversion of starting material, side product formation and product loss during purification using semi-preparative HPLC.

3.2.3. Binding affinity of isopropyl carbamate fragments to *Sm*BRD3(2)

Compounds **2.13**, **3.1**, **3.2**, **3.3**, **3.24**, **3.27**, **3.28**, **3.33**, and **3.35** were assessed for their binding affinity for *Sm*BRD3(2) by isothermal titration calorimetry (ITC) (**Table 3.2**).

Table 3.2. K_d and ChemPLP docking score values of compounds **2.13**, **3.1**, **3.2**, **3.3**, **3.24**, **3.27**, **3.28**, **3.30**, and **3.33** binding to *Sm*BRD3(2), as determined by ITC; n = 1, single value ± error of the curve fit. ITC was carried out with the help of A. Kwiatkowski. Predicted cLogD values were determined using Chemicalize, developed by ChemAxon.[141] A heatmap colour scale of green to red is used, with red representing higher measured and predicted affinity, and green representing lower measured and predicted affinity.

Compound	R	K_d (μM)	ChemPLP Score	cLogD (pH 7.4)
3.2		5.21 ± 2.58	113.89	3.92
3.1		6.03 ± 1.73	116.28	0.71
3.33		7.85 ± 4.45	104.92	2.4
3.28		8.12 ± 3.59	105.75	2.3
3.30		12.6 ± 5.77	105.71	−0.71
3.3		26.5 ± 13.5	110.52	−0.24
3.27		33.7 ± 20.6	106.09	−0.03
2.13		> 100	106.78	3.78
3.24		No binding	106.34	4.3



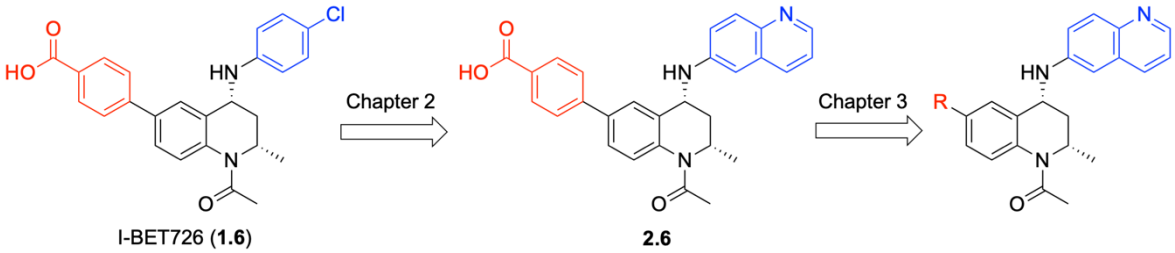
As expected, none of these compounds showed binding affinity for *Sm*BRD3(2) greater than I-BET726 (K_d = 1850 ± 361 nM), or the acid-based derivatives developed in **Chapter 2**. This was predicted due to removal of the hydrophobic interactions enabled by the chlorophenyl and bicyclic aromatic groups with the HFF shelf. In contrast with the observations in **Chapter 2**, the ethyl ester analogue **2.13** showed binding to *Sm*BRD3(2), likely due to greater solubility compared with the ethyl ester analogues in **Chapter 2**, however the binding affinity was too low to accurately determine a K_d by ITC. Furthermore, binding to *Sm*BRD3(2) was detected for the diethyl phosphonate ester **3.2** and the methyl ester **3.33**, also likely resulting from enhanced solubility compared with the ethyl ester analogues in **Chapter 2**. Compounds **3.1**, **3.2**, **3.3**, **3.27**, **3.28**, **3.30**, and **3.33** have K_d values for *Sm*BRD3(2) in the micromolar range and, despite showing large associated error due to the K_d range lying outside the accurate detection ITC detection limit for the concentrations used, these data indicated SAR in the ZA channel region. Compounds **3.1**, **3.2**, **3.28**, **3.30** and **3.33** showed an increase in affinity compared with the benzoic acid analogue **3.27**, and as predicted by *in silico* docking. The monoethyl and diethyl phosphonate analogues **3.1** and **3.2** have the lowest K_d values for *Sm*BRD3(2) in this ligand series. In contrast to the *in silico* docking results, the phosphonic acid analogue **3.3** showed a similar binding affinity to the benzoic acid **3.27**. Finally, compound **3.24** showed no detectable binding to *Sm*BRD3(2), possibly due to insolubility of this analogue in combination with low binding affinity.

Of the compounds synthesised, and despite the magnitude of error associated with K_d measurements of these compounds by ITC, five analogues showed enhancement of affinity compared with the benzoic acid **3.27**. Interestingly, analogues without acidic groups, **3.2** and **3.33**, showed an increase in affinity, indicating acidic groups placed in the ZA channel are not essential for binding, although hydrogen bond acceptor ability in this region is likely important. It was decided these data were indicative of ZA channel SAR to further develop compounds based on these groups.

3.3 Quinoline-based analogues for SAR investigation of the ZA channel region

3.3.1 Ligand design

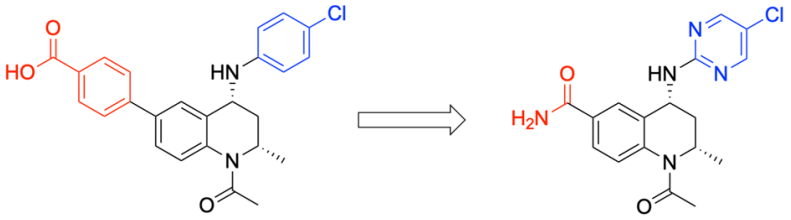
To probe whether the observed ZA channel and HFF cleft SAR are additive, it was decided to replace the isopropyl group of the ligands in **section 3.2** with the quinoline group, producing a ligand series with a quinoline and varying ZA channel targeting R groups (**Figure 3.3**).



I-BET726 (**1.6**) **2.6**

Figure 3.3. Additive SAR novel I-BET726 derivative compound design, with HFF cleft (blue) and ZA channel (red) targeting groups indicated.

After the work on the isopropyl carbamate analogues was completed, Humphreys *et al*. published further SAR work on tetrahydroquinoline derivatives, with the aim of developing an optimised analogue of I-BET726 (**1.6**) for human BET bromodomain targets (**Figure 3.4**).[33]



I-BET726 (**1.6**)

K_d [BRD4] = 4.4 ± 0.9 nM (ITC)
pIC_{50} [BRD4] = 7.0 ± 0.2 (FRET)
pIC_{50} [BRD4(1)] = 8.5 (BROMO*scan*^{SM})
pIC_{50} [BRD4(2)] = 9.4 (BROMO*scan*^{SM})

I-BET567 (**1.7**)

pIC_{50} [BRD4(1)] = 6.9 ± 0.14 (FRET)
pIC_{50} [BRD4(2)] = 7.2 ± 0.16 (FRET)

Figure 3.4 Structures of I-BET726 (**1.6**) and I-BET567 (**1.7**) with corresponding human BRD4 binding affinity data and assays.[32,33]

I-BET567 (**1.7**) was developed with the aim of producing an orally available tetrahydroquinoline (THQ)-based human BET bromodomain inhibitor, and to address issues

with unbound clearance, solubility, permeability and CYP3A4 inhibition, which typically arose during development of other THQ based BRD inhibitors.[33] The 6-position carboxamide was found to reside in the entrance to the ZA channel, engaging in hydrogen bonding with bulk water in the channel.[33] SAR efforts in **Section 3.2** was focused on retaining aromatic groups in the ZA channel region, therefore it was decided an analogue replacing the benzoic acid group with a primary amide would be interesting to determine the effect of this change on binding to *Sm*BRD3(2).

With the above in consideration, the following target molecules were chosen for synthesis (**Figure 3.5**).

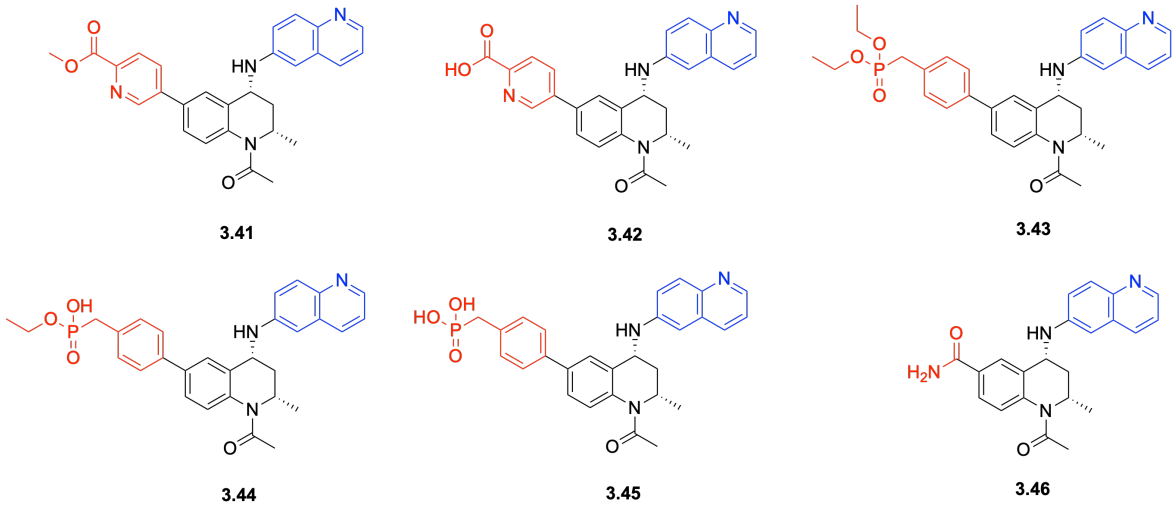


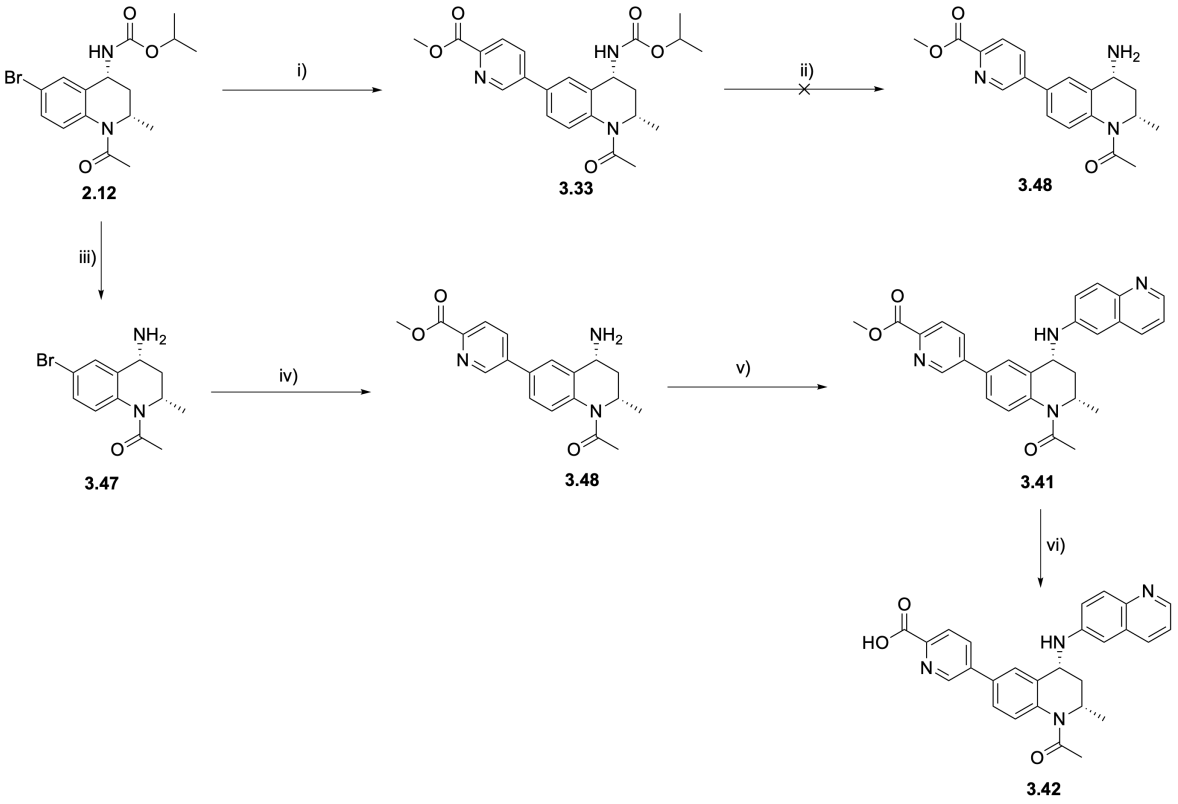
Figure 3.5. The structures of target molecules **3.41**–**3.46** for further ZA channel SAR investigation.

Compounds **3.41**–**3.44** were chosen based on the ITC binding data for compounds **3.1**, **3.2**, **3.30** and **3.33** in **section 3.2.3**. Despite **3.3** not showing significantly improved binding by ITC compared with the benzoic acid **3.27**, the phosphonic acid **3.45** was expected to be available in one step from compound **3.43**, and would be an interesting compound to investigate the effect of a higher polarity group in the ZA channel region. Analogous to the compounds developed in **Chapter 2**, methyl ester and diethyl phosphonate ester compounds **3.41** and **3.43** were beneficial choices for phenotypic screening, with the potential to show enhanced parasite permeability compared with their acid counterparts. Finally, the primary amide

analogue **3.46** was chosen to investigate the removal of an aromatic group in the expected ZA channel region, and for possible engagement of the primary amide with the ZA channel water molecules.

3.3.2 Synthesis

Compounds **3.41** and **3.42** were synthesised *via* a 3/4-step synthesis from intermediate **2.12** (**scheme 3.3**).

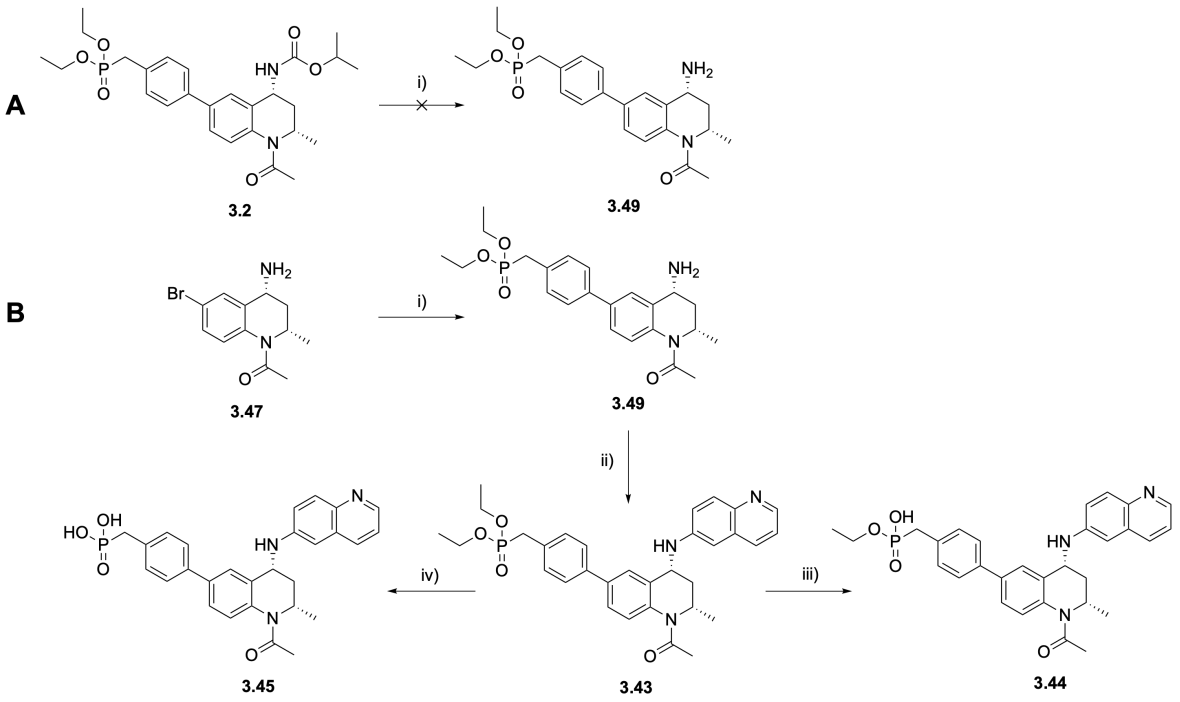


Scheme 3.3. Synthesis of compounds **3.41** and **3.42** from intermediate **2.12**. *Reagents and conditions*: i) [6-(Methyoxycarbonyl)pyridine-3-yl]boronic acid, $Pd(dppf)Cl_2$, NEt_3, MeOH, DME, 120 °C, microwave irradiation, 45 min, 78%, synthesis carried out by A. Kwiatkowskii;[139] ii) $AlCl_3$, NEt_3, MeOH, CH_2Cl_2, 0 °C, 30 min; iii) $AlCl_3$, NEt_3, MeOH, CH_2Cl_2, 0 °C, 30 min, 99%; iv) [6-(Methyoxycarbonyl)pyridine-3-yl]boronic acid, $Pd(dppf)Cl_2$, NEt_3, MeOH, DME, 120 °C, microwave irradiation, 45 min, 54%; v) Quinoline-6-boronic acid, $Cu(OAc)_2$, NEt_3, CH_2Cl_2, rt, 3 Å molecular sieves, 20 h, 18%; vi) $NaOH_{(aq)}$, EtOH, rt, 2 h, 18%.

Initially, the synthesis of **3.41** was intended to follow a similar route to that used previously (**Chapter 2**), with isopropyl carbamate removal, to produce a primary amine **3.48**, occurring after functionalisation of the 6-position of the THQ ring using a Suzuki reaction. The primary

amine intermediate **3.48** would then enable the quinoline head group to be added using a metal catalysed C-N coupling reaction. However, test reaction of isopropyl carbamate removal with $AlCl_3$ on compound **3.33**, previously synthesised by A. K.,[139] resulted in no reaction (**scheme 3.3**). It was suggested this was due to interaction of the pyridine nitrogen atom of compound **3.33** with $AlCl_3$. Previously patented work had reported the synthesis of intermediate **3.48** *via* the primary amine intermediate **3.47**.[142] Therefore, the isopropyl carbamate group was removed first with $AlCl_3$ in a 99% yield, followed by a Suzuki reaction with [6-(methyoxycarbonyl)pyridine-3-yl]boronic acid and $Pd(dppf)Cl_2$ to produce **3.48** in a 54% yield. A trial Buchwald-Hartwig reaction of primary amine **3.48** with 6-bromoquinoline, using BrettPhos, BrettPhos Pd 3 and NaO^tBu, produced a significant number of side products and **3.41** was not isolated under these conditions. It was therefore decided to employ the alternative copper-catalysed Chan-Lam coupling reaction, using $Cu(OAc)_2$, quinoline-6-boronic acid and NEt_3, which after purification by semi-preparative HPLC gave **3.41** in an 18% yield. Ester hydrolysis of **3.41** using NaOH, followed by purification using semi-preparative HPLC, also gave **3.42** in an 18% yield. The low yield, despite a simple functional group transformation, can be attributed to unoptimised semi-preparative HPLC conditions, resulting in product loss during purification.

Compounds **3.43**–**3.45** were synthesised using a similar synthetic route as compounds **3.41** and **3.42** (**scheme 3.4**).

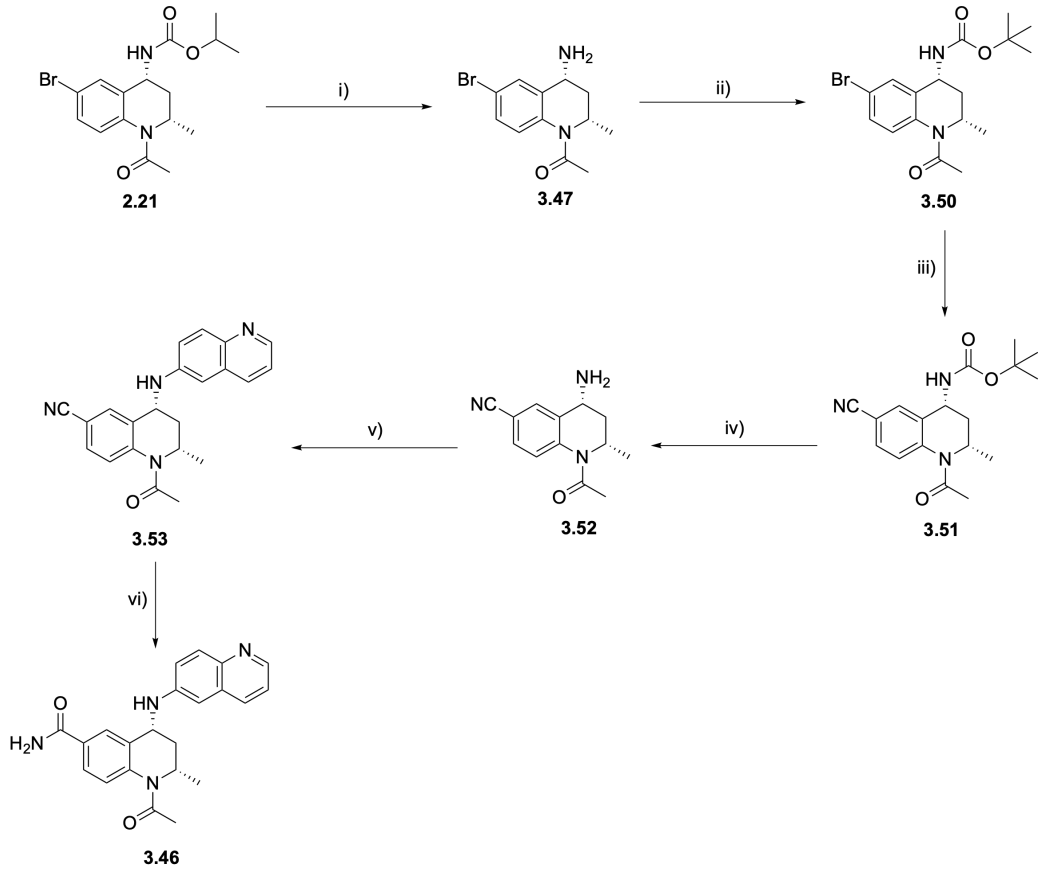


Scheme 3.4. Synthesis of compounds **3.43**–**3.45**. **A**) *Reagents and conditions*: i) $AlCl_3$, NEt_3, MeOH, CH_2Cl_2, 0 °C, 30 min; **B**) *Reagents and conditions*: i) **3.40**, $Pd(dppf)Cl_2$, $NaHCO_{3(aq)}$, 1,4-dioxane, 100 °C, microwave irradiation, 1.5 h, 56%; ii) 6-Bromoquinoline, BrettPhos, BrettPhos Pd G3, NaO^tBu, toluene, 70 °C, 23 h, 31%; iii) $NaOH_{(aq)}$, EtOH, 70–80 °C, 26 h, 29%; iv) Bromotrimethylsilane, CH_2Cl_2, rt, 19 h, 42%.

Analogous to initial approach to the synthesis of **3.41** and **3.42** (**scheme 3.3**), removal of the isopropyl carbamate group of **3.2** to reveal primary amine **3.49** using $AlCl_3$ was attempted. Reaction with $AlCl_3$ resulted in degradation of compound **3.2**, and therefore no product isolation. This is likely due to reactions between the phosphonate ester, $AlCl_3$ and MeOH. As with the synthesis of **3.41** and **3.42**, Suzuki coupling of boron pinacol ester intermediate **3.40** with amine **3.47** was therefore executed, producing intermediate **3.49** in a 56% yield. Buchwald-Hartwig C-N coupling was then carried out on primary amine intermediate **3.49**, using 6-bromoquinoline, BrettPhos, BrettPhos Pd G3 and NaO^tBu, yielding **3.43** in 31%. As with the isopropyl carbamate analogue exhibiting a monoethyl phosphonate, **3.1**, compound **3.44** was synthesised using NaOH and a temperature of 70-80 °C in a 29% yield. This reaction proceeded to completion with no side products observed. The low yield is likely due to

problematic extraction of the product from the aqueous components during work up and a poor mass recovery during semi-preparative HPLC purification. The phosphonic acid analogue **3.45**, was synthesised from **3.43** using bromotrimethylsilane, in a 42% yield, with the reaction proceeding to completion and with no significant side products. As with **3.44**, the low yield can be attributed to difficulties during work up and purification using semi-preparative HPLC.

Compound **3.46** was synthesised partially following a previously reported synthetic route to primary intermediate **3.52** (**scheme 3.5**, steps ii, iii and iv), developed by Humphreys *et al*.[33] Humphreys *et al*. used a synthetic route to intermediate **3.52** using an enantiopure starting material, resulting in a higher ee than routes used by Gosmini *et al*.,[32] and the synthesis of analogues in previous sections. However, it was decided the synthetic route to the final compound **3.46** should occur *via* Boc protection of primary amine **3.47**. This was so the ee of the final compound would be approximately comparable to other analogues synthesised during this work, thereby enabling better comparison of K_d for SAR determinations.



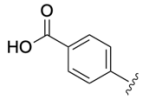
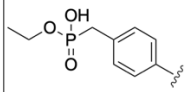
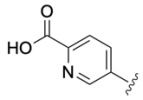
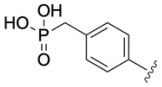
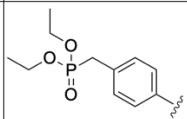
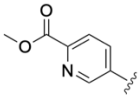
Scheme 3.5. Synthesis of compound **3.46**. *Reagents and conditions:* i) $AlCl_3$, NEt_3, MeOH, CH_2Cl_2, 0 °C, 30 min, 99%; ii) Di-*tert*-butyl dicarbonate, NEt_3, CH_2Cl_2, rt, 4 h, 62%; iii) $Zn(CN)_2$, $Pd(PPh_3)_4$, DMF, 115 °C, 21 h, 44%; iv) TFA, CH_2Cl_2, rt, 1 h; v) 6-Bromoquinoline, BrettPhos, BrettPhos Pd G3, NaO^tBu, toluene, 70 °C, 18 h, 47% (2 steps); vi) HOOH, K_2CO_3, DMSO, H_2O, rt, 4 h, 54%.

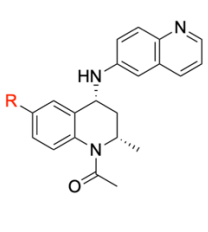
Boc protection of primary amine **3.47** proceeded in a 62% yield, followed by a Negishi cyanation of bromide intermediate **3.50**, which produced **3.51** in a 44% yield. To introduce the quinoline head group, a two-step reaction was employed, first removing the Boc protecting group using TFA to give a primary amine intermediate **3.52**, which was not purified, and subsequently subjected to Buchwald-Hartwig coupling conditions using 6-bromoquinoline, BrettPhos, BrettPhos Pd G3 and NaO^tBu. This gave intermediate **3.53** in a 47% yield over two steps. Finally, base-mediated nitrile hydrolysis yielded **3.46** in 54%. The ee of compound **3.46** was determined as 90% using chiral HPLC, which is comparable to **3.41**, **3.43** and the I-BET726 derivatives developed in **Chapter 2**.

3.3.3 Binding affinity of quinoline-based analogues to *Sm*BRD3(2)

Compounds **3.41**–**3.46** were evaluated using isothermal titration calorimetry (ITC) for binding affinity to *Sm*BRD3(2) (**Table 3.3**).

Table 3.3 K_d values of compounds **2.6** and **3.41**–**3.46** binding to *Sm*BRD3(2), measured using ITC, and predicted cLogD values (pH 7.4). Predicted cLogD values were determined using Chemicalize, developed by ChemAxon.[143] A heatmap colour scale of green to red is used with 'hot' colours representing higher affinity.

Compound	R	K_d (nM)	cLogD (pH 7.4)
2.6		**364 ± 51.6[b]**	**1.05**
3.44		**744 ± 57.8[c]**	**1.77**
3.42		**789 ± 175[c]**	**0.17**
3.45		**841 ± 54.9[c]**	**0.81**
3.43		**1825 ± 402[c]**	**4.97**
3.41		**2410 ± 355[a]**	**3.41**
3.46		**4685 ± 1107[c]**	**1.64**



[a] Single value ± error of the curve fit; [b] mean value of 3 repeats ± 95% CI; [c] mean value of 2 repeats ± 95% CI.

Compounds **3.41**–**3.45**, which were designed based on the binding affinity data for isopropyl carbamate analogues in **section 3.2.3**, have a higher affinity for *Sm*BRD3(2) than the isopropyl carbamate analogues. This observation was to be expected, due to the addition of the HFF cleft targeting quinoline group, and therefore favourable hydrophobic interactions in this region of the binding pocket. In contrast to the isopropyl carbamate analogues **3.1**, **3.2**, **3.30** and **3.33**, replacement of the benzoic acid group did not result in compounds with higher

affinity. It can therefore be concluded that the SAR identified for groups targeting the ZA channel in **section 3.2.3** is not additive with the SAR identified for targeting the HFF cleft (**Chapter 2**).

Replacement of the benzoic acid group with a primary amide (**3.46**) resulted in a large decrease in affinity. This result indicates the phenyl ring is very important for affinity to *Sm*BRD3(2), likely *via* a hydrophobic interaction with the HFF shelf, specifically through edge-to-face interactions with H280 and F281, while residing in the ZA channel. The analogues **3.41** and **3.43** have a low micromolar affinity for *Sm*BRD3(2). These data showed the largest contrast with the data for the isopropyl carbamate ligand series, as isopropyl carbamate-based ligands **3.2** and **3.33** showed an enhancement in affinity comparable with their acidic derivatives **3.1** and **3.30**. The decrease in affinity for **3.41** and **3.43** can either be attributed to the likely decrease in solubility *via* addition of the hydrophilic quinoline head group, or to an unfavourable change in binding conformation compared with the isopropyl carbamate-based analogues. Finally, compounds **3.42**, **3.44** and **3.45** have similar affinity for *Sm*BRD3(2), in the nanomolar range, however, the K_d values are not as low as with compound **2.6**, exhibiting the original benzoic acid group. Comparing these data with the K_d values for **3.41**, **3.42** and the ethyl ester analogues previously developed (**Chapter 2**), indicates, as well as the likely increase in solubility with more polar acidic groups, that charged groups in the ZA channel region may be important for affinity for this ligand series.

In summary, compounds **3.42**, **3.44** and **3.45** have K_d values in the nanomolar range for *Sm*BRD3(2), however, the designed SAR strategies targeting the ZA channel and the HFF cleft are not additive, and therefore these compounds did not show a higher affinity than compound **2.6**. It was proposed the SAR of these groups are not additive due to the comparatively large structural difference between the isopropyl carbamate and quinoline groups. In addition to different solubility properties, the isopropyl carbamate ligand series may likely bind to *Sm*BRD3(2) in a slightly different conformation, thereby resulting in non-translational SAR information to the quinoline ligand series.

3.3.4 *Ex vivo* evaluation of quinoline-based THQ analogues on *S. mansoni*

Despite the observation of non-additive SAR, it was nonetheless desirable to assess the compounds in phenotype against *S. mansoni*. Compounds **3.41**–**3.46** were initially screened by Dr Josephine Forde-Thomas (J.F.T.) at an initial concentration of 10 μM against the *S. mansoni* schistosomula and hits were identified as described in **Chapter 2** (**Figure 3.6**).

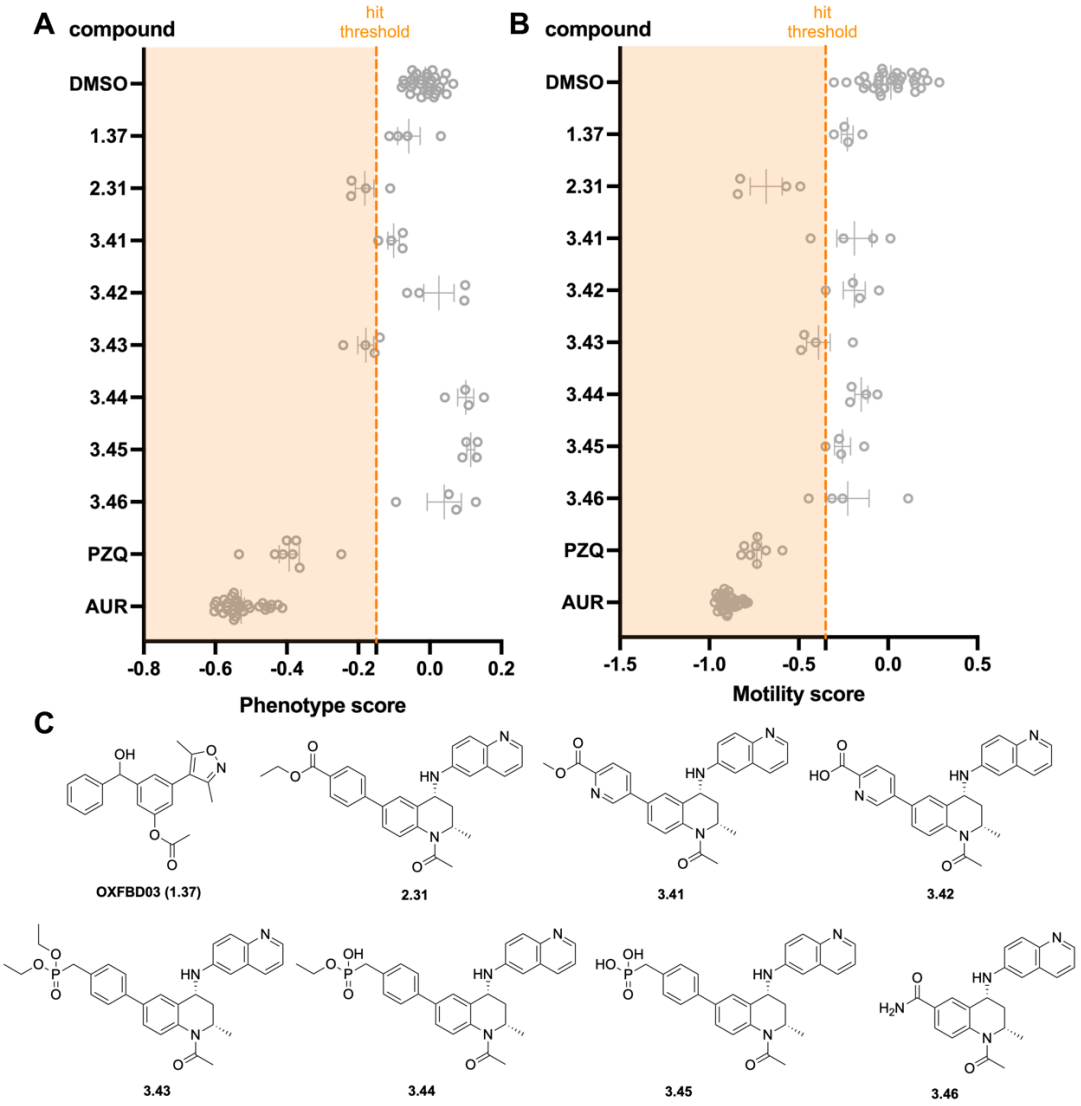


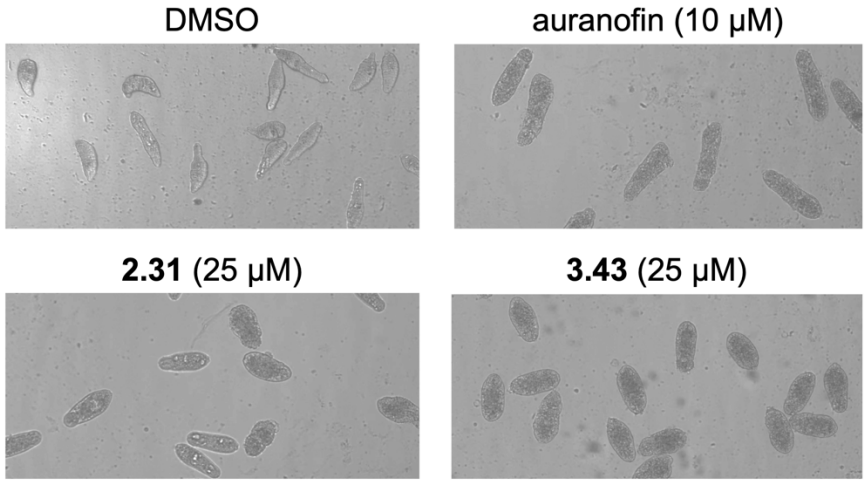
Figure 3.6. The effect of compounds **1.37**, **2.31** and **3.41**–**3.46** on the **(A)** phenotype and (**B**) motility of schistosomula (at 10 μM in 0.6% DMSO, following 72 h incubation). Negative (0.6% DMSO) and positive (10 μM Auranofin (AUR) and 10 μM Praziquantel in 0.6% DMSO) controls were included in each drug screen (4-8 in total, two technical replicates each). The compound score is shown as grey dot and whiskers represent the average score and standard deviation across the screens. Hit threshold is delineated by the vertical dashed red lines in the graphs; −0.15 and −0.35 for phenotype and motility scores, respectively. **C**) The structure of compounds **1.37**, **2.31**, **3.41**–**3.46**. The schistosomula screen was carried out by J.F.T..

Compound **2.31**, developed in **Chapter 2**, was included in the screen as a further positive control, and OXFBD03 (**1.37**) as a further negative control, and out of the compounds tested only compounds **2.31** and **3.43** were classed as hits at 10 μM. However, **3.43** showed a less significant effect on schistosomula motility than **2.31**. Compounds **3.46** and **3.41** have the lowest binding affinity for *Sm*BRD3(2) (K_d = 4685 ± 1107 nM and K_d = 2410 ± 355 nM, respectively), and were not observed to effect schistosomula. However, compounds **3.42**, **3.44** and **3.45** have affinity for *Sm*BRD3(2) in the nanomolar range but were not classified as hits in this assay. This observation may be due to poor parasite permeability. All three have acidic groups, with low predicted cLogD values (**Table 3.3**), and therefore are likely to have poor parasite permeability. In addition, the lack of effect of compound **3.46** on schistosomula could also be due to poor parasite permeability, with a low predicted clogD (clogD (pH 7.4) = 1.64), which is comparable with **3.44** (clogD (pH 7.4) = 1.77).

Based on the data in **Chapter 2**, it was proposed the ethyl ester analogues show higher parasite permeability than the corresponding acid derivatives, which was confirmed by LCMS parasite lysate experiments with compounds **2.6** and **2.31** (**Chapter 2**). The LCMS experiments also indicated some conversion of the ethyl ester (**2.31**) to acid form (**2.6**) in the presence of the adult worms, with the acid form potentially inducing the phenotypic effects. Compound **3.41** has a methyl ester group, and therefore a similar pro-drug hypothesis could have been made for this compound. However, this compound showed no significant activity, despite the acid derivative **3.42** having nanomolar affinity for *Sm*BRD3(2) (K_d = 789 ± 175 nM). Furthermore, and in contrast to the data in **Chapter 2** for the ethyl ester analogues, the methyl ester **3.41** binds to *Sm*BRD3(2) (K_d = 2410 ± 355 nM). Given the binding affinity of both the ester and acid derivatives for *Sm*BRD3(2), the low activity of **3.41** against the schistosomula life-cycle stage could therefore be attributed to poor permeability (predicted logD (pH 7.4) = 3.41) compared with the ethyl ester analogues (**Table 2.2**, **Chapter 2**) and compound **3.43** (predicted logD (pH 7.4) = 4.97). Alternatively, the instability of the compound in media could be an issue, resulting in ester hydrolysis before entering the parasite.

With the identification of **3.43** as a hit, EC_{50} values for **2.31** and **3.43** were then determined (**Figure 3.7 B**) by screening **2.31** and **3.43** against schistosomula using an 8-point titration (50, 25, 10, 5, 2.5, 1.25, 0.625 and 0.313 μM all in 0.6% DMSO), which was conducted by J.F.T..

A



B

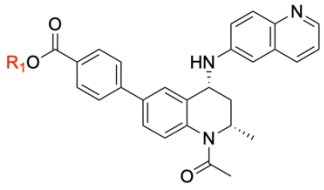
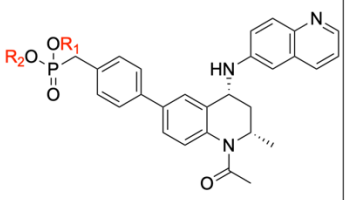
Compound numbers	Compound Structure	*Sm*BRD3(2) K_d (ITC, nM)	Schistosomula Phenotype EC_{50} (μM) (R_1 = Et, R_2 = Et)	Schistosomula Motility EC_{50} (μM) (R_1 = Et, R_2 = Et)
2.6 (R_1 = H) **2.31** (R_1 = Et)		**364 ± 51.6**[b] **n.d.**	**4.81 ± 0.871**	**5.26 ± 0.0205**
3.43 (R_1 = Et, R_2 = Et) **3.44** (R_1 = H, R_2 = Et) **3.45** (R_1 = H, R_2 = H)		**1825 ± 402**[c] **744 ± 57.8**[c] **841 ± 54.9**[c]	**6.33 ± 1.75**	**6.25 ± 0.855**

Figure 3.7. A) Phenotype of schistosomula following 72 h incubation with DMSO, auranofin (10 μM), **2.31** (25 μM) and **3.43** (25 μM). **B**) SmBRD3(2) K_d values (ITC) for compounds **2.6** and **3.43**–**3.45**, and average schistosomula phenotype and motility EC_{50} values (n=2, ± s.e.m.) for corresponding esters **2.31** and **3.43**. [a] Single value ± error of the curve fit; [b] mean value of 3 repeats ± 95% CI; [c] mean value of 2 repeats ± 95% CI; n.d. refers to no detectable binding by ITC. A heat-map colour scale of green to red is used, with red representing higher activity and green representing lower activity.

Compound **3.43** has higher EC_{50} values than **2.31** for both phenotype and motility. **3.43** was expected to show similar parasite permeability to compound **2.31** (Predicted: logD (pH 7.4)

[**3.43**] = 4.97, logD (pH 7.4) [**2.31**] = 4.8; Measured: Chrom LogD (pH 7.4) [**2.31**] = 5.95). The lower activity on schistosomula compared to compound **2.31** could therefore be attributed to the lower affinity for *Sm*BRD3(2) (K_d = 1825 ± 402 nM), than the converted acid derivative of **2.31**, **2.6** (K_d = 364 ± 51.6 nM). However, it is possible **3.43** could be converted to compound **3.44**, which has a higher affinity for *Sm*BRD3(2) (K_d = 744 ± 57.8 nM), *via* the action of an *S. mansoni* esterase enzyme. Work by Serafinowska *et al*. reported conversion of a diethyl phosphonate ester compound to the monoethyl in mice after gastrointestinal absorption and detection by HPLC from blood, indicating this transformation can occur in a mammalian system.[144] Although present at a much lower level compared with the monoethyl, in the same study, Serafinowska *et al*. also identified the phosphonic acid derivative conversion product. It is therefore possible further hydrolysis of monoethyl compound **3.44** to **3.45** may have occurred, however, this transformation is likely to be minimal, due to the monoethyl phosphonate group's chemical stability to hydrolysis. An LCMS experiment, as described in **Chapter 2**, could be used to investigate the occurrence of these transformations on the diethyl phosphonate **3.43** in *S. mansoni*.

Compound **3.43** was then chosen to progress onto testing against adult *S. mansoni* worms to assess the compounds' effect on this life form (**Figure 3.8**).

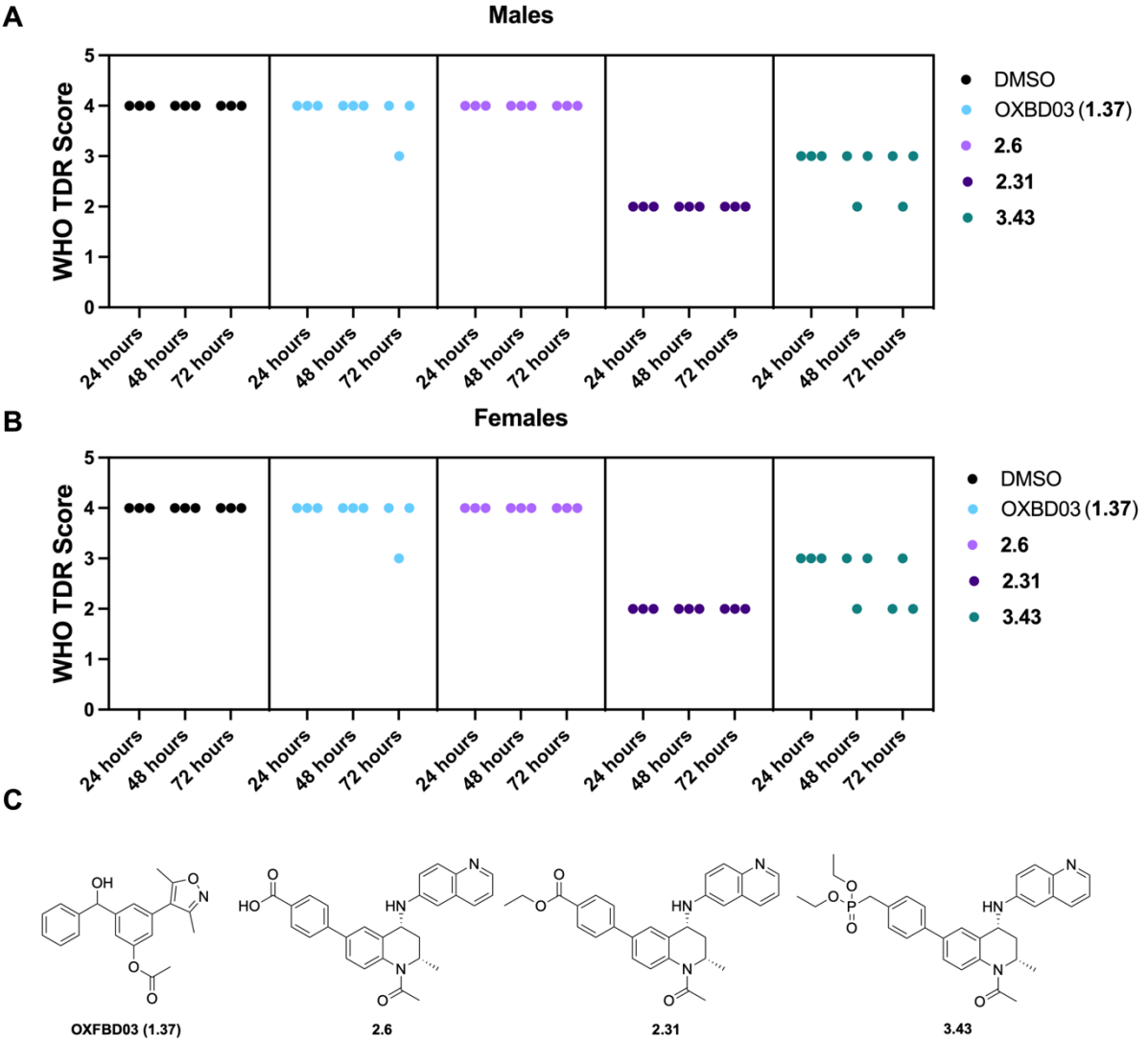


Figure 3.8. The effect of **1.37**, **2.6**, **2.31** and **3.43** on worm motility on Male (**A**) and Female (**B**) *S. mansoni*, as determined by eye using the WHO TDR scoring system after 24, 48 and 72 hour incubation. Compounds were dosed at 20 μM (0.2% DMSO), with DMSO as a negative control (0.2%). Screening on adult worms was carried out by J.F.T..

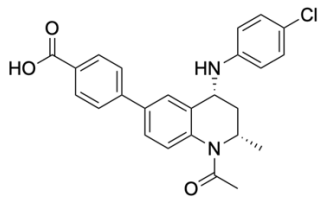
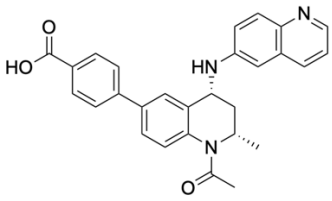
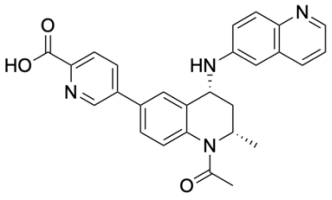
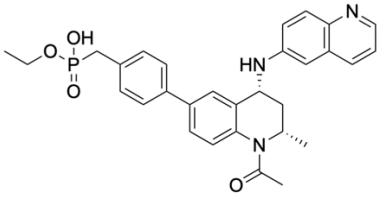
Adult worm motility was assessed using the WHO TDR scoring system, as described by Ramirez *et al*.[145] This was used as an alternative to the digital image processing-based system WormAssay, due to the higher sensitivity offered using this scoring method and the smaller number of compounds tested. Briefly, this motility scoring system is carried out by eye and worm motility is scored accordingly: 4 = normal activity; 3 = slowed activity; 2 = minimal activity with occasional movement of the head or and tail; 1 = no motility with the exception of gut

movements; 0 = worm death.[145] Paired male and female worms are scored as 4. These data showed an almost identical effect of these compounds between male and female adult *S. mansoni*, indicating these compounds do not specifically affect one sex. The data for **1.37**, **2.6** and **2.31** on adult worm motility were largely repeated as seen in **Chapter 2**: **1.37** and **2.6** showed minimal effect, whereas **2.31** affected worm motility. Compound **3.43** affected motility, but not to the same extent as **2.31**. These results were rationalized with the same reasoning as for the schistosomula phenotypic screening data.

3.4 Investigation of selectivity between human and *S. mansoni* bromodomains

Despite novel THQ analogues **3.41**–**3.46** not showing enhanced affinity and activity compared with the novel I-BET726 derivatives developed previously (**Chapter 2**), these compounds represented more significant structural deviations away from I-BET726 (**1.6**), and it was desirable to determine if these changes had introduced selectivity for the parasite *Sm*BRD3(2) over the human BRD4(1). Compounds **2.6**, **3.42** and **3.44**, were therefore tested using ITC to assess their binding affinity to human BRD4(1) (**Table 3.4**).

Table 3.4 The *Sm*BRD3(2) and BRD4(1) K_d values of I-BET726 (**1.6**), **2.6**, **3.42** and **3.44** (ITC). A heat-map colour scale of green to red is used, with red representing higher affinity and green representing lower affinity.

Compound	Structure	K_d [SmBRD3(2)] (nM)	K_d [BRD4(1)] (nM)
I-BET726 (1.6)		**1850 ± 361[a]**	**6.23 ± 1.98[a]**
2.6		**364 ± 51.6[b]**	**13.5 ± 2.47[a]**
3.42		**789 ± 175[c]**	**53.0 ± 4.16[a]**
3.44		**744 ± 57.8[c]**	**17.5 ± 2.89[a]**

[a] Single value ± error of the curve fit; [b] mean value of 3 repeats ± 95% CI; [c] mean value of 2 repeats ± 95% CI.

The measured K_d value for I-BET726 (**1.6**) binding to BRD4(1) was close to the reported value[32] for recombinant BRD exhibiting both domains (K_d [BRD4] = 4.4 ± 0.9 nM). In the case for all novel I-BET726 derivatives tested against BRD4(1), the compounds have significantly higher affinity for the human BRD4(1) over the *Sm*BRD3(2). The compound with the lowest affinity for BRD4(1) is compound **3.42**, however, selectivity for the parasite BRD has not been introduced with these groups. Therefore, these compounds should be considered as tool molecules for studying *Sm*BRD3 function and are inappropriate to be considered as compounds for potential treatment of schistosomiasis.

3.4 Conclusions

Building on the work described in **Chapter 2**, the work in this chapter aimed to develop compounds with further affinity for *Sm*BRD3(2) and higher activity on *Schistosoma mansoni.* To achieve this, an SAR strategy was followed to identify groups that increase affinity by favourable interactions with residues or water molecules in the ZA channel region of the binding pocket of *Sm*BRD3(2). This was first addressed by the design, synthesis, and evaluation of binding using ITC of a semi-fragment based isopropyl carbamate ligand series, which identified groups capable of increasing affinity relative to the benzoic acid group, found in I-BET726 (**1.6**). However, combination of a selection of these groups with a quinoline head group, found to increase affinity by targeting the HFF cleft, did not result in binding affinity greater than the highest affinity compound identified previously, **2.6** (**Chapter 2**). It can therefore be concluded the SAR information identified in this chapter is not additive with SAR strategy from **Chapter 2**. The trend in binding affinity data was also reflected by the phenotypic screening data. None of the compounds **3.41**–**3.46** showed activity greater than **2.31**, developed in **Chapter 2**, on both schistosomula and adult worms. Out of compounds **3.41**–**3.46**, only **3.43** had an effect on schistosomula phenotype and motility and adult worm motility. Despite the lack of affinity increase resulting from the SAR strategy described in this chapter, the data further highlight the importance of physiochemical properties in the development of anti-schistosomal compounds.

After SAR studies to increase the affinity of I-BET726 derivates for *Sm*BRD3(2), it was decided the determination of in-parasite selectivity and demonstration of target engagement of higher activity compounds, particularly **2.31**, (**Chapter 4**) was desirable prior to a continuation of SAR studies on the bromodomain *Sm*BRD3.

Chapter 4

Photoaffinity probes for the evaluation of cellular *Sm*BRD3 engagement

4.1 Introduction and aims

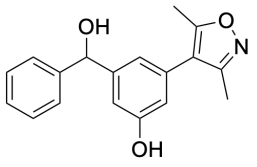
Chapter 2 and **Chapter 3** described SAR studies on novel analogues of I-BET726 aimed at the development of a high affinity ligand for *Sm*BRD3(2). This work resulted in the discovery of compound **2.6**, which displayed the highest affinity for *Sm*BRD3(2) (K_d [*Sm*BRD3(2)] = 364 ± 51.6 nM). The ethyl ester analogue of compound **2.6**, **2.31**, showed an effect on the phenotype of three different life-cycle stages of *S. mansoni*, and LCMS studies indicated this analogue was more permeable to the parasite than the acid form. The data also suggested some ethyl ester was converted to the *Sm*BRD3(2)-binding acid form (**2.6**) *in situ*. *Sm*BRD3(1)-selective BRD ligands were also tested for their phenotypic effects on *S. mansoni*, and despite compounds **1.4** and **1.37** having nano-molar affinity for *Sm*BRD3(1) (K_d [*Sm*BRD3(1,2)] = 683 ± 166 nM and K_d [*Sm*BRD3(1,2)] = 675 ± 97.6 nM), the dimethylisoxazole-based ligands showed little effect in phenotypic screening. Given these results, it was decided photoaffinity probes would be an effective strategy to investigate target engagement and selectivity within the *S. mansoni* proteome. The work in this chapter therefore aimed to:

- Design and synthesise photoaffinity probes based on compounds **2.6** and **2.31** and a dimethylisoxazole-based *Sm*BRD3(1) selective ligand.
- Evaluate photoaffinity probes using binding affinity studies and photoactivated crosslinking to recombinant *Sm*BRD3 constructs.
- Use photoaffinity probes to investigate cellular target engagement and assess proteome wide selectivity in *S. mansoni*.

4.2 Probe design

4.2.1 *Sm*BRD3(1) selective photoaffinity probe

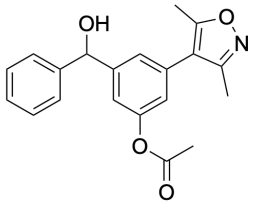
To develop an *Sm*BRD3(1) selective photoaffinity probe, the OXFBD02 (**1.4**) or OXFDB03 (**1.37**) scaffold was chosen, owing to their high affinity for *Sm*BRD3(1) (**Figure 4.1**), and the synthesis of these bromodomain ligand analogues being well established in the group.



OXFBD02 (**1.4**)

K_d [*Sm*BRD3(1,2)] = 683 ± 166 nM

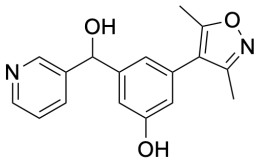
K_d [SmBRD3(2)] = no binding



OXFBD03 (**1.37**)

K_d [*Sm*BRD3(1,2)] = 675 ± 97.6 nM

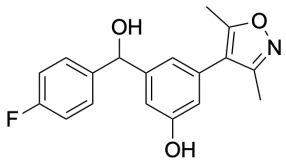
K_d [SmBRD3(2)] = no binding



OXFBD04 (**1.5**)

K_d [*Sm*BRD3(1,2)] = 2950 ± 261 nM

K_d [SmBRD3(2)] = no binding



1.38

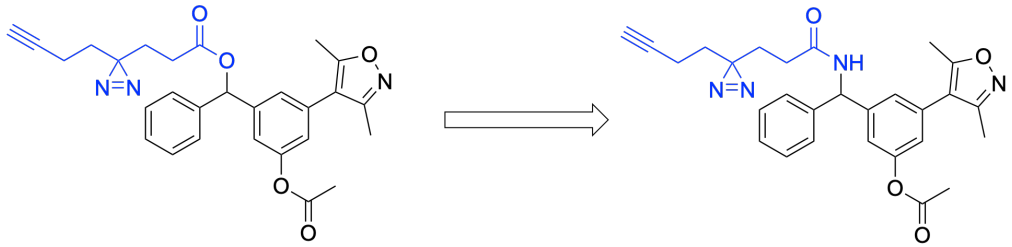
K_d [*Sm*BRD3(1,2)] = 1750 ± 301 nM

K_d [SmBRD3(2)] = no binding

Figure 4.1. The structures of compounds **1.4**, **1.5**, **1.37** and **1.38** and corresponding K_d values for *Sm*BRD3(1,2) and *Sm*BRD3(2).

A diazirine photoreactive group was chosen as the photoaffinity labelling component of the probe. As described in **Chapter 1**, these photoreactive groups are effective for use in photoaffinity probes, due to their small size, which minimizes the effect of this group on protein binding, and efficient irreversible activation at 350–380 nm.[49,50] It was also decided the photoaffinity probe should be functionalised with an alkyne handle, enabling detection of photocrosslinked proteins after UV irradiation using click chemistry. Previous work by Dr Michael Brand (M.B.) had established a diazirine based pull down probe based on **1.37**

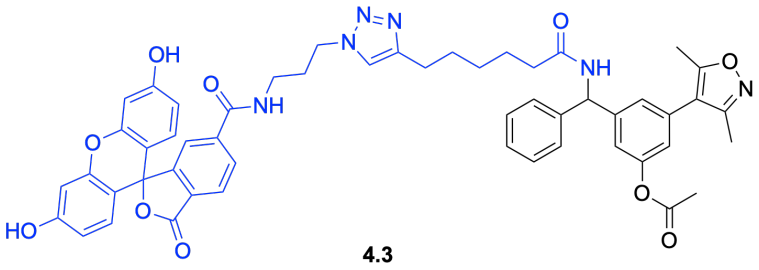
exhibiting an ester linker (**4.1**).[146] Despite an efficient crosslinking yield to recombinant BRD4(1) after UV irradiation (approximately 30% by mass spectrometry), the probe did not display engagement with BRD4 in the human colon cancer cell line, RKO.[146] It was hypothesised that the ester linkage of the compound was unstable in a cellular environment. Work by Dr Giulia Stasi (G.S.) replaced the ester bond of **4.1** with an amide linker, which was proposed to be more stable (**Figure 4.2**). This probe showed approximately 50% maximum crosslinking to recombinant BRD4(1).[147] Both probes employed a terminal alkyne-containing diazirine photocrosslinker, which was developed by Li *et al*.[148]



4.1 **4.2**

Figure 4.2. Dimethylisoxazole based photoaffinity pull down probes designed and synthesised by M.B. (**4.1**) and G.S. (**4.2**).

Work by Dr Matthias Schiedel (M.S.) developed a dimethylisoxazole-based fluorescent probe (**4.3**) (**Figure 4.3**) for FP studies on *Sm*BRD3.[149] The binding affinity FP assay results using **4.3** were inconsistent with the ITC assay results, and therefore this assay was not utilised for this project. However, M.S. showed this compound binds to *Sm*BRD3(1,2) (K_d [SmBRD3(1,2)] = 445 ± 100 nM) by ITC, with no detectable binding to *Sm*BRD3(2), therefore implying this compound is selective for the first domain. This result showed that functionalisation at the biphenyl position of OXFBD03 (**1.37**) with an amide bond and alkyl linker was tolerated for binding to the first domain of *Sm*BRD3(1,2). Therefore, despite the lack of a crystal structure for *Sm*BRD3(1), it was decided the probe developed previously by G.P., compound **4.2**, would likely bind to *Sm*BRD3(1) selectively and was chosen as a suitable photoaffinity probe for this domain.



4.3

Figure 4.3. Structure of the fluorescent probe **4.3**, designed and synthesised by M.S..

4.2.2 Photoaffinity probe based on an *Sm*BRD3(2) optimised I-BET726 derivative

The I-BET726 derivative **2.6** was the highest affinity for *Sm*BRD3(2), and its ethyl ester analogue **2.31** showed activity on *S. mansoni* (**Chapter 2**), therefore, it was decided photoaffinity probes based upon these compounds would be investigated. Analogous to the proposed *Sm*BRD3(1) selective probe, the probes were to employ a diazirine and alkyne click handle. For synthetic tractability, the same terminal alkyne-diazirine photocrosslinking handle exhibited by compound **4.2** was used. However, there was limited SAR information as to where to place the diazirine-alkyne handle on compounds **2.6** and **2.31**. It was assumed additions of the handle to the tetrahydroquinoline core, which resides deep inside the binding pocket of *Sm*BRD3(2), would not be tolerated. Therefore, addition of the tag could have been made on the benzoic acid group, residing in the ZA channel region, or the quinoline, residing in the HFF cleft region. It was decided due to unpredictable ZA channel SAR, and the solubility benefit from retention of the benzoic acid group in the case of **2.6**, the quinoline group should be functionalised with the linker.

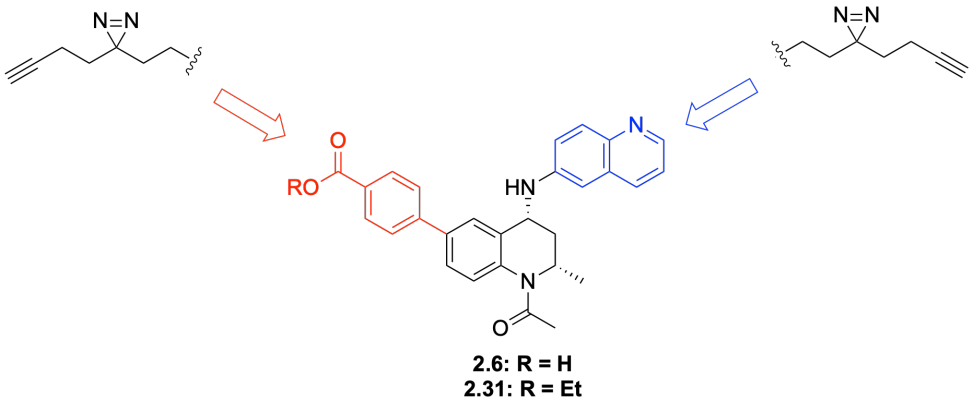


Figure 4.4. Structures of compound **2.6** and **2.31** and suggested diazirine-alkyne linker placement strategies.

It was predicted placement of a linker *via* an amide bond, attached to a methylene group on the 2-position of the quinoline, would be an effective strategy. To aid this prediction, *in silico* docking was carried out using a similar analogue with a simple amide (**4.4**) linker (**Figure 4.5**).

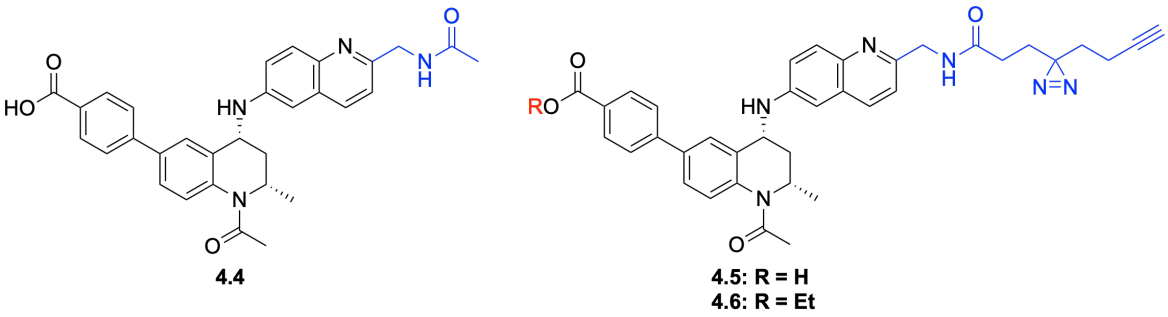


Figure 4.5. Structures of docked simple amide-based compound **4.4** and diazirine containing compounds **4.5** and **4.6**.

Docking was carried out with the help of Patrick Brennan and Romi Aggarwal, using GOLD and the crystal structure of **2.1** bound to *Sm*BRD3(2) (PDB ID: 7AMH) as a template. 50 poses of **4.4** bound to SmBRD3(2) were generated, and the highest rank docking pose was visually inspected using PyMOL (**Figure 4.6.**). The docking results suggested an amide-based linker in the quinoline 2-position would be tolerated, with the amide protruding away from the HFF cleft into a solvent exposed position (**Figure 4.6 A**). Furthermore, the results suggested possible hydrogen bonding between the amide N-H and the glutamic acid residue (**Figure 4.6 B**). This interaction could tether the photoactive handle to amino acid

residues in this region. This result provided confidence in the compound design and it was therefore decided to place the diazirine linker in this position, with desired target molecule **4.5**. The ethyl ester analogue of **4.5**, **4.6**, was also chosen as a target molecule for expected higher parasite permeability, and as a photoaffinity probe based upon the high activity ethyl ester analogue **2.31**.

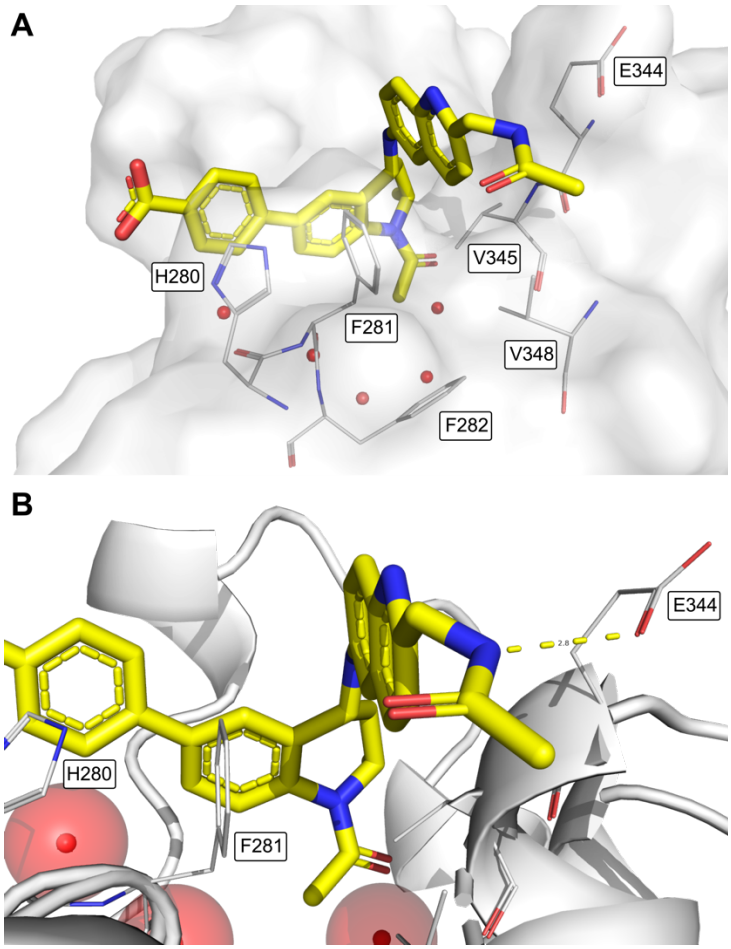


Figure 4.6. A) The highest ranked docking pose of compound **4.4** (carbon = yellow) in the binding pocket of *Sm*BRD3(2) (carbon = white). **B**) The highest ranked docking pose of compound **4.4** in the binding pocket of *Sm*BRD3(2), highlighting a possible hydrogen bond between an N-H of **4.4** and E344.

4.3 Synthesis

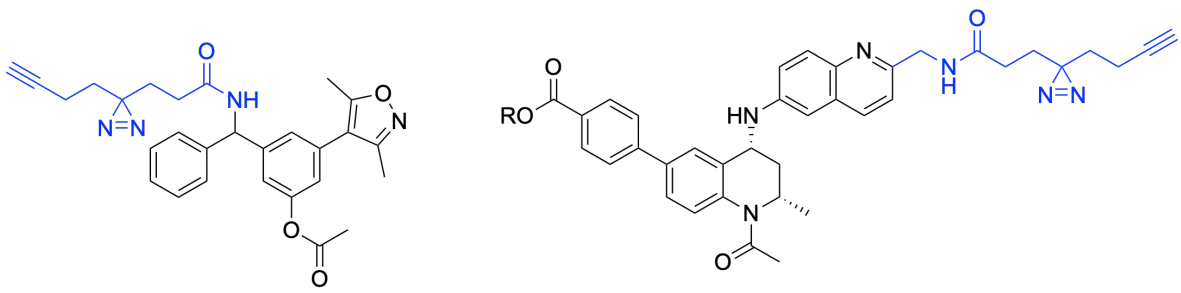


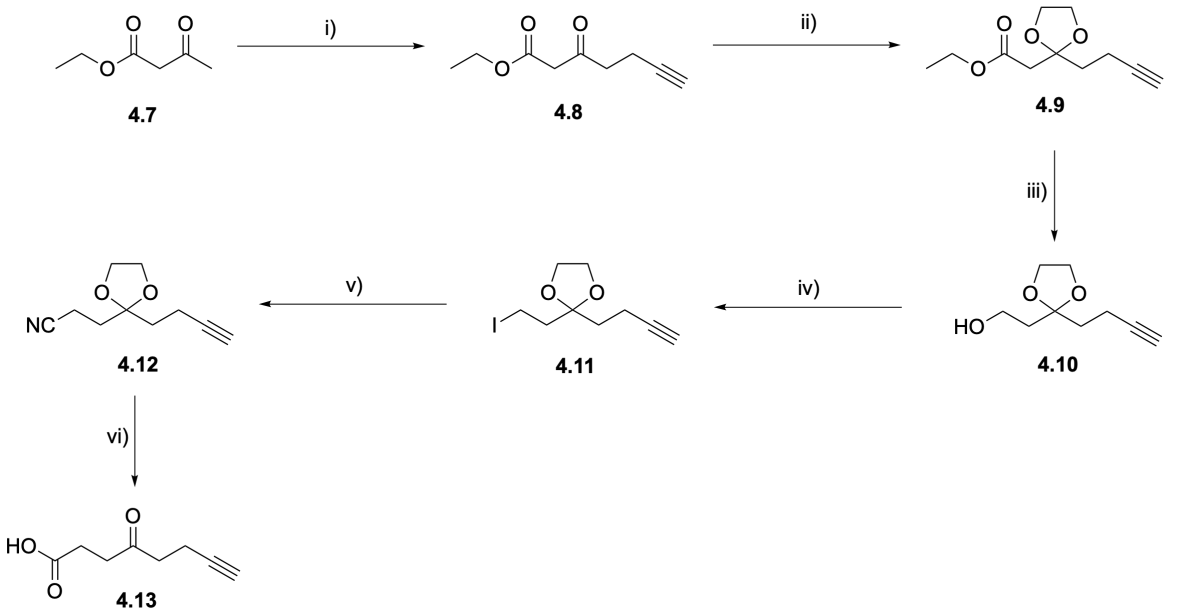
Figure 4.7. Structures of target molecules **4.2**, **4.5** and **4.6**.

With target molecules **4.2**, **4.5** and **4.6** chosen and designed as photoaffinity probes for *Sm*BRD3, a synthetic strategy was devised and executed for **4.2** (**section 4.3.1**), and **4.5** and **4.6** (**section 4.3.2**).

4.3.1 *Sm*BRD3(1) selective photoaffinity probe, 4.2

4.3.1.1 Synthesis of a diazirine-alkyne functionalised tag intermediate

The synthesis of compound **4.2** was based upon previous work by G.S..[147] The strategy employed was to first synthesise a diazirine-alkyne linker intermediate (**4.17**). This was first made *via* intermediate **4.13** by a synthesis devised by M.B. (**Scheme 4.1.**),[146] inspired by work by Li *et al*..[148] Later attempts of the synthesis were conducted using a separate synthetic route to intermediate **4.13** developed by Parker *et al*. (**Scheme 4.2.**).[150]

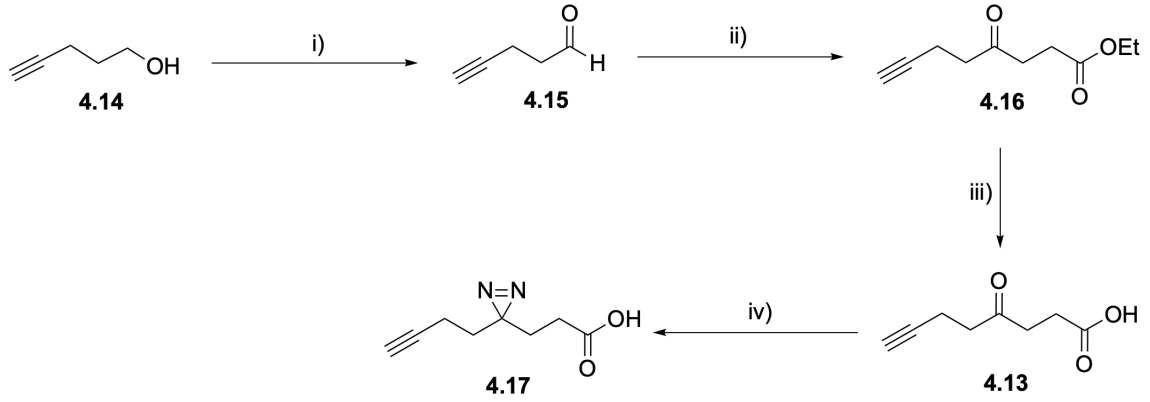


Scheme 4.1. Synthesis of intermediate **4.13**, as developed by M.B.. *Reagents and conditions:* i) *n*-BuLi in hexanes, diisopropylamine, THF, –78 °C to rt, 1 h then ethyl acetoacetate, THF, –78 °C to 0 °C, 1 h, then propargyl bromide, 0 °C to rt, 2 h, 47%; ii) Ethylene glycol, 4-toluenesulfonic acid monohydrate, toluene, 120 °C, 19 h; iii) $LiAlH_4$, THF, 1 h, 54% over 2 steps; iv) Iodine, PPh_3, 1*H*-imidazole, CH_2Cl_2, 70 °C, 3 h; v) KCN, anhydrous DMF, 70 °C, 4 h, 52% over 2 steps; vi) $NaOH_{(aq)}$, reflux, 2 h 15 min, then $HCl_{(aq)}$, rt, 2h, 78%.

The first step in the synthesis of intermediate **4.13** (**Scheme 4.1.** step i), started with alkylation of **4.7** at the position alpha to the ketone with propargyl bromide, using LDA generated *in-situ* from *n*-BuLi and diisopropylamine. Purification using vacuum distillation yielded **4.8** in 47%. It was observed the yield of this step decreased when scaling up the reaction. Using pre-made commercially available LDA did not improve the yield at the larger scales. Protection of the ketone carbonyl using ethylene glycol and a Dean-Stark apparatus proceeded to completion. It was first thought higher yields would be achieved by removing water from ethylene glycol under reflux with Dean-Stark apparatus prior to addition of the starting material, however the reaction proceeded to completion more quickly with all components added from the start of the procedure. There was a concern intermediate **4.9** was volatile under reduced pressure after the observation of lower crude yields with prolonged concentration *in vacuo*, therefore **4.9** was reduced with $LiAlH_4$ (step iii) without further purification, resulting in **4.10** in 54% over two steps. The Appel reaction was executed to produce intermediate **4.11**. This reaction proceeded to completion, however,

there was also a concern compound **4.11** was volatile, and therefore was reacted with KCN without further purification, to yield **4.12** in 52% over two steps. The reaction with KCN proceeded to completion with the use of anhydrous DMF, but not wet DMF. This is likely due to the solvation of cyanide ions by residual water in the latter case, reducing the ability to react with intermediate **4.11**. Finally, two-step nitrile hydrolysis and carbonyl deprotection yielded **4.13** in 78%.

The synthesis of intermediate **4.13** can also be carried out using a shorter, three step synthesis, and **4.13** was subsequently used to synthesise the diazirine containing intermediate, **4.17**, as reported by Parker *et al*. (**Scheme 4.2**).[150]



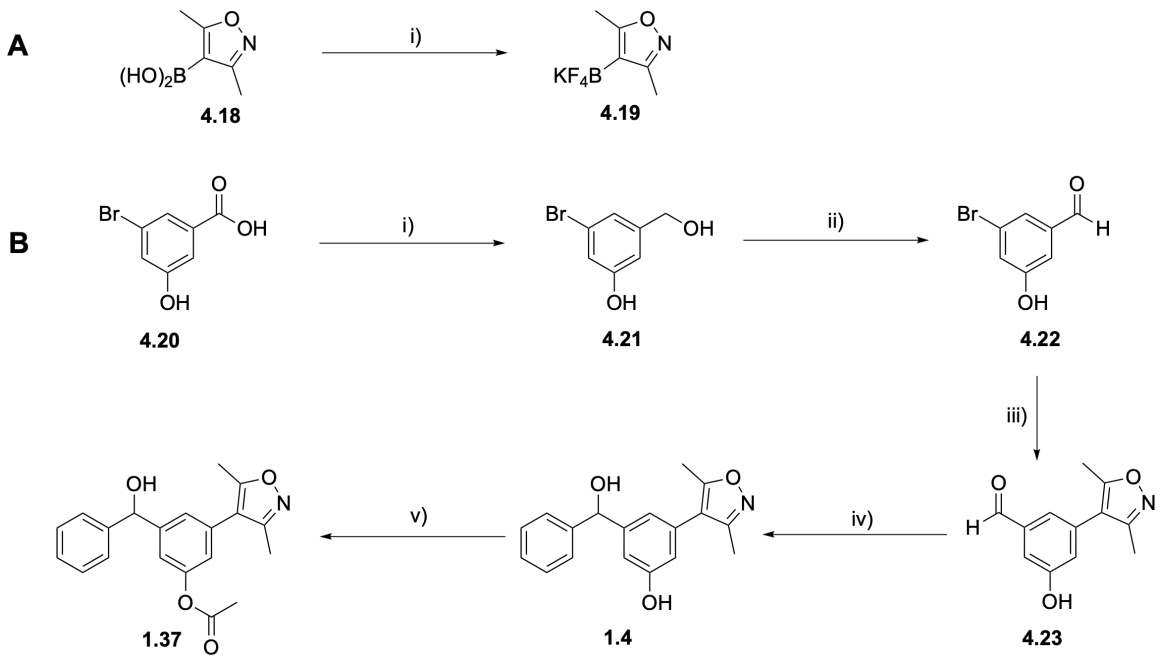
Scheme 4.2. Synthesis of intermediates **4.13** and **4.17**, as described by Parker *et al*.[150] *Reagents and conditions*: i) Oxalyl chloride, DMSO, NEt_3, CH_2Cl_2, –78 °C to rt, 3.5 h, 98%; ii) Ethyl acrylate, 3-benzyl-5-(hydroxyethyl)-4-methylthiazonium chloride, NEt_3, 1,4-dioxane, 80 °C, 54 h, 11%; iii) LiOH, H_2O, MeOH, rt, 6 h, 59%; iv) NH_3, MeOH, 0 °C, 3 h 20 min, then hydroxylamine-*O*-sulfonic acid, MeOH, 0 °C to rt, 16 h, then DIPEA, I_2, rt, 30 min, 48%.

First, a Swern oxidation of 4-pentyn-1-ol (**4.14**) occurred with a yield of 98% and **4.15** was deemed pure enough to proceed to the next reaction. The Stetter reaction of intermediate **4.15** using ethyl acrylate and 3-benzyl-5-(hydroxyethyl)-4-methylthiazonium chloride yielded **4.16** in 11%. The reported literature yield of this reaction is 28%,[150] and it was proposed the reduced yield was due to adding pent-4-ynal too quickly (30 min) compared with the literature (4 h). A significant side product was observed, which during TLC analysis in 20% EtOAc/pentane was present at a lower R_f than the product. This could have resulted from the benzoin condensation of the aldehyde starting material, over the desired Stetter

1,4-addition to ethyl acrylate, which is a known limitation of Stetter reactions involving aliphatic aldehydes.[151] This side product, however, was uncharacterized and therefore this theory is unconfirmed. Hydrolysis of **4.16** using LiOH gave **4.13** in a 59% yield. Finally, using the carboxylic acid intermediate **4.13**, formation of the diazirine containing intermediate **4.17** was carried out as described by Parker *et al*.,[150] giving this compound in a 48% yield.

4.3.1.2 Synthesis of the dimethylisoxazole intermediate OXFBD03 (**1.37**)

Based upon work by M.B. and G.S.,[146,147] the route to probe **4.2** used OXFBD03 (**1.37**) as an intermediate. This was synthesised using work reported by Jennings *et al.* (**Scheme 4.3**).[31]



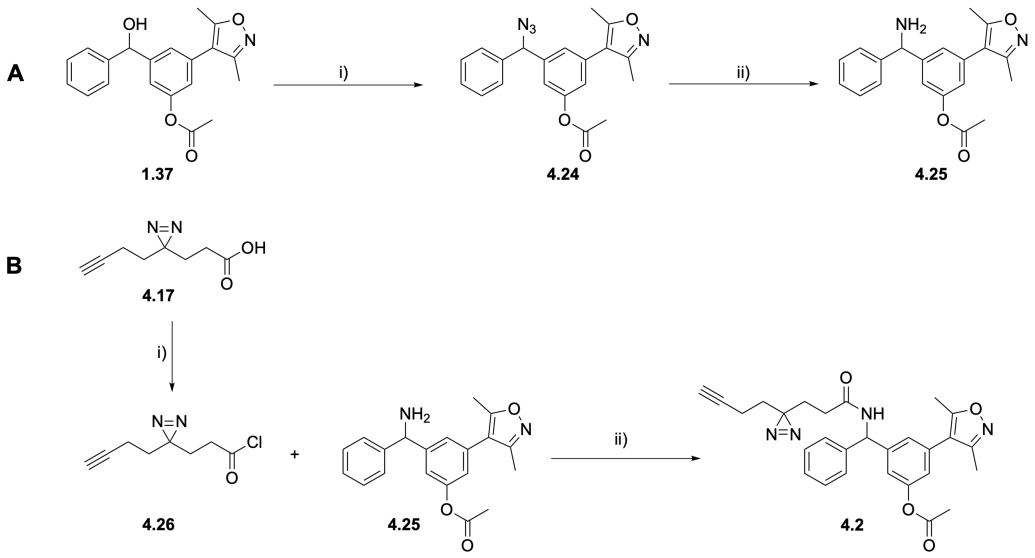
Scheme 4.3. A. Synthesis of intermediate **4.19**. *Reagents and conditions*: i) $KF_{(aq)}$, L-(+)-tartaric acid, THF, MeCN, rt, 1 h, 81%. **B.** Synthesis of OXFBD03 (**1.37**). *Reagents and conditions*: i) BH_3·THF, THF, 0 °C to rt, 24 h, > 99%; ii) MnO_2, $CHCl_3$, EtOAc, 70 °C, 2.5 h, > 99%; iii) Intermediate **4.19**, $Pd(OAc)_2$, RuPhos, Na_2CO_3, EtOH, 80 °C, 15 h, 30%; iv) Phenyl magnesium bromide, THF, 0 °C to rt, 2 h, 76%; v) $NaOH_{(aq)}$, acetic anhydride, rt, 1 h, 99%. Steps iv) and v) were carried out by Lily Latimer-Smith. As previously reported, **1.4** and **1.37** were synthesised as racemic mixtures.[30,31]

Transformation of boronic acid **4.18** to tetrafluoroborate intermediate **4.19**, proceeded in an 81% yield (**Scheme 4.3**). This intermediate was required to minimize protodeborylation during a Suzuki reaction (step iii), with work by Lennox *et al*. showing aryl boronic acids are slowly released from corresponding trifluoroborates during these reactions, reducing the

occurrence of protodeborylation.[152] Reduction of **4.20** with BH_3·THF proceeded well in over 99% yield. Oxidation using MnO_2 to give the aldehyde **4.22** was also carried out in a high yield (over 99%). The Suzuki coupling between **4.22** and **4.19** occurred in a yield of 30%, significantly lower than reported in the literature (85%).[31] It was suggested this was affected by the quality of commercially acquired RuPhos, as LCMS analysis of the commercially available RuPhos indicated oxidation, likely at phosphorus. However, the reaction was not repeated with fresh commercial RuPhos. Steps iv) and v) were executed by Lily Latimer-Smith to give OXFBD03 (**1.37**).

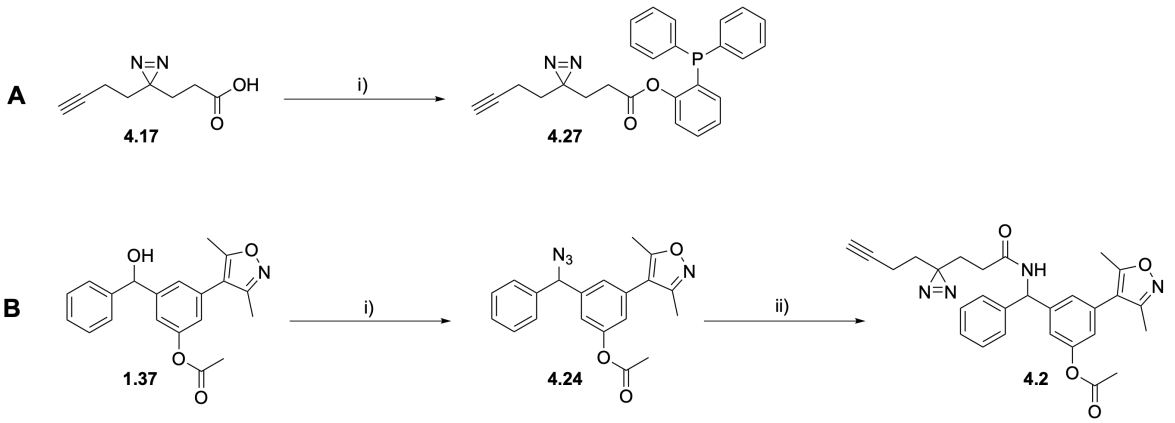
4.3.1.3 Synthesis of the photoaffinity probe **4.2**

The synthesis of **4.2** by G.S. was carried out by conversion of OXFBD03 (**1.37**) to an azide intermediate, followed by Staudinger reduction to the primary amine **4.25** (**Scheme 4.4**).[147] The carboxylic acid **4.17** was converted to the acid chloride **4.26** and then reacted with the amine to give **4.2**. The primary amine intermediate was, however, observed to be unstable during this study. It was therefore suggested by G.S. that isolation of the primary amine could be avoided by using a traceless Staudinger reaction with **4.24**. However initial attempts at this reaction using a phosphine intermediate (**4.27**) were unsuccessful.



Scheme 4.4. Previous synthesis of **4.2** by G.S..[147] **A**) Synthesis of amine intermediate **4.25**. *Reagents and conditions*: i) $(CH_3)_3SiN_3$, $Cu(CF_3SO_3)_2$, CH_2Cl_2, 0 °C to 40 °C, overnight, 70 %; ii) Ph_3P, THF/H_2O, 40 °C, overnight. **B**) Synthesis of probe **4.2**. *Reagents and conditions:* i) $SOCl_2$, 40 °C, 30 min; ii) NEt_3, CH_2Cl_2, 0 °C to rt, 1 h, 38 % over 2 steps.

It was decided to reattempt the traceless Staudinger reaction, which required phosphine intermediate (**4.27**) and the azide (**4.24**) (**Scheme 4.5**).



Scheme 4.5. A) Synthesis of intermediate **4.27**. *Reagents and conditions:* i) (2-Hydroxyphenyl)diphenylphosphine, DMAP, DCC, DIPEA, CH_2Cl_2, rt, 18 h, 58%; **B**) Synthesis of **4.2**. *Reagents and conditions:* i) Trimethylsilyl azide, copper (II) triflate, CH_2Cl_2, 0 °C to 40 °C, 33%; ii) **4.27**, THF, H_2O, 86%.

The phosphine was synthesised in a 58% yield using (2-hydroxyphenyl)diphenylphosphine and DCC. The azide was synthesised using the procedure developed by G.S., which proceeded in a 33% yield. A traceless Staudinger reaction was then carried out between azide **4.24** and phosphine **4.27**, resulting in the desired probe **4.2** in an 86% yield. This result validated the idea that a traceless Staudinger reaction could avoid the use of the unstable intermediate **4.25**.

4.3.2 I-BET726 derivative-based probes for *Sm*BRD3

After synthesis of **4.2**, attention was turned to the synthesis of target molecules **4.5** and **4.6**. Retrosynthetic analysis of **4.5** and **4.6** suggested these compounds could be made first by the coupling of a protected amine functionalised quinoline bromide, followed by deprotection and amide coupling with the diazirine containing acid intermediate **4.17** (**Figure 4.8**).

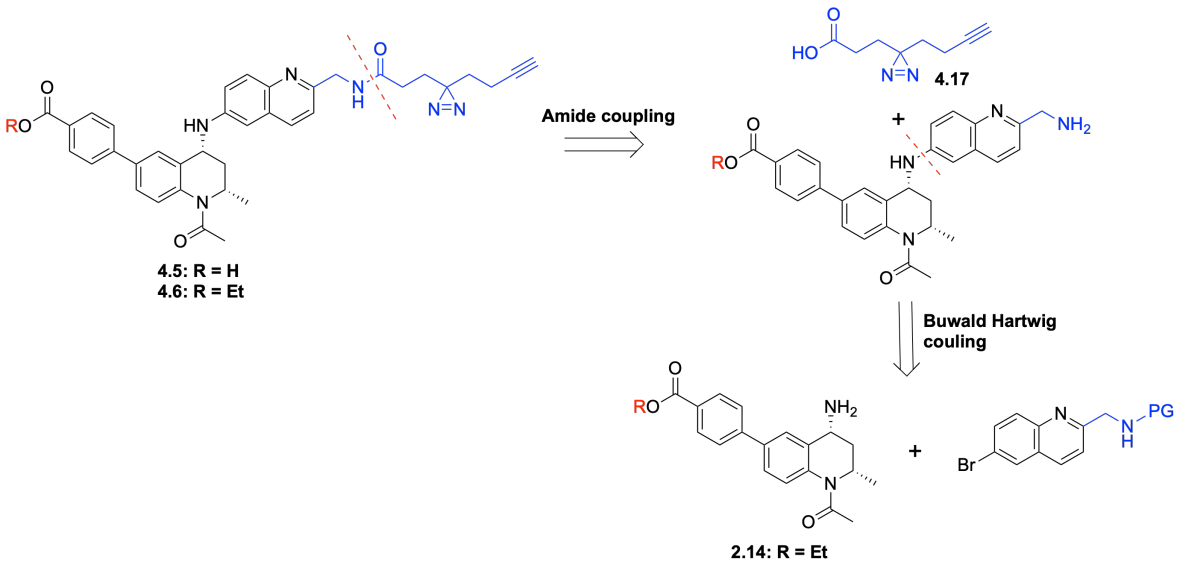
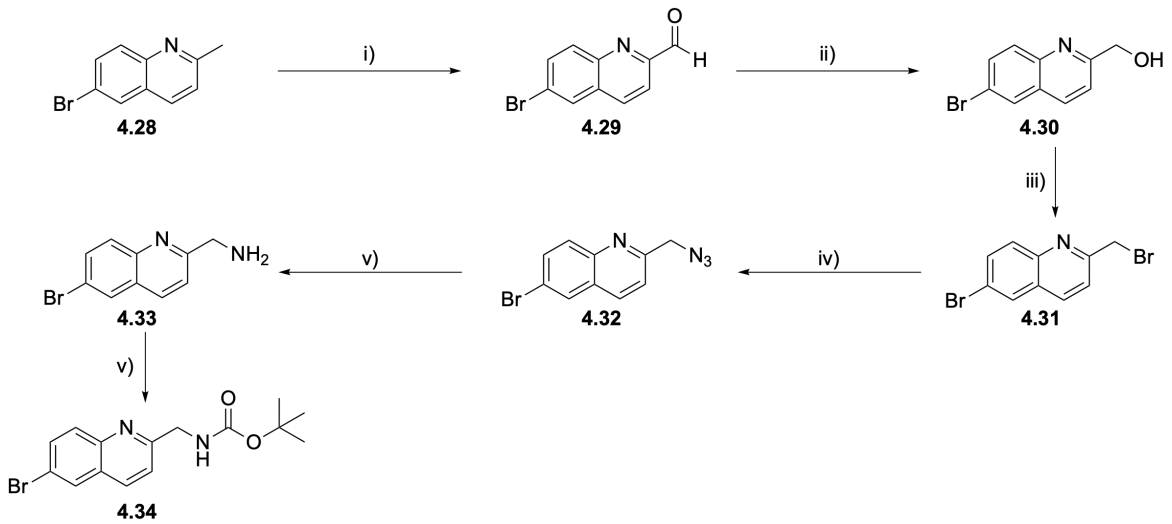


Figure 4.8. Retrosynthetic disconnections of compounds **4.5** and **4.6**. PG = protecting group.

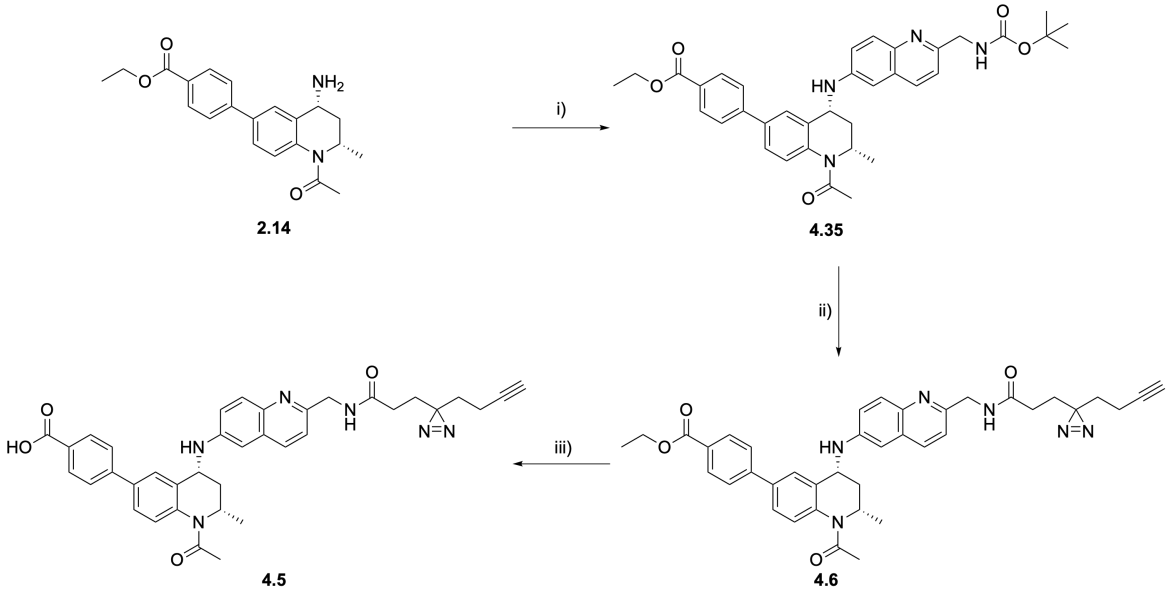
To synthesise a protected quinoline intermediate, a 5-step synthesis developed by Wang *et al*.[153] was used to give amine **4.33**, which was followed by Boc protection (**Scheme 4.6**). A Boc protecting group was the most suitable, due to its relative ease of addition and removal, and stability to the basic Buchwald-Hartwig coupling conditions.



Scheme 4.6. Synthesis of intermediate **4.34**. *Reagents and conditions:* i) SeO_2, 1,4-dixoane, 110 °C, 6 h; ii) $NaBH_4$, MeOH, 0 °C to rt, 30 min, 78% over two steps; iii) PBr_3, Net_3, CH_2Cl_2, 0 °C to rt, 18 h; iv) NaN_3, DMF, rt, 15 h, 55%; v) PPh_3, THF, H_2O, rt, 3 h; v) Boc_2O, CH_2Cl_2, 0 °C to rt, 3 h, 33% over two steps.

A Riley oxidation of 6-bromo-2-methylquinoline (**4.28**), followed by reduction using $NaBH_4$ resulted in **4.30** in a 78% yield over two steps (**Scheme 4.6**). Bromination using PBr_3 followed by displacement with sodium azide gave **4.32** in a 55% yield over two steps. Finally, Staudinger reduction of **4.32** using PPh_3, followed by Boc protection using Boc_2O gave the desired Boc protected quinoline intermediate **4.34** in 33% over two steps.

With intermediate **4.34** in hand, diazirine probes **4.5** and **4.6** were synthesised *via* a Buchwald-Hartwig coupling step of intermediates **2.14** and **4.34** to yield intermediate **4.35** (**Scheme 4.7**).



Scheme 4.7. Synthesis of photoaffinity probes **4.5** and **4.6**. *Reagents and conditions:* i) **4.34**, BrettPhos, BrettPhos Pd G3, NaO^{t}Bu, toluene, 40 °C, 24 h, 36%; ii) HCl in dioxane solution, CH_2Cl_2, rt, 5 h, then **4.17**, HATU, DIPEA, DMF, rt, 24 h, 15%; iii) $NaOH_{(aq)}$, EtOH, rt, 2.5 h, 28%.

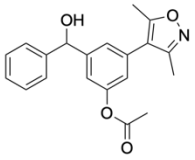
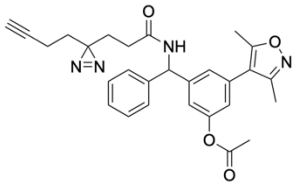
Buchwald-Hartwig coupling of intermediates **2.14** and **4.34** was executed to produce **4.35** in a 36% yield (**Scheme 4.7**). A two-step reaction, consisting of Boc deprotection using HCl, followed by amide coupling of the resulting primary amine intermediate and carboxylic acid intermediate **4.17**, proceeded in a 15% yield to produce **4.6**. Complete consumption of the starting material was observed for both the Boc deprotection and amide coupling steps during TLC analysis, and therefore the low yield is mostly attributed to product loss during the work-up and purification using two flash column chromatography columns (normal and reverse phase silica), isolating only the purest fractions for use in biological studies. Ester hydrolysis of compound **4.6** using $NaOH_{(aq)}$ gave **4.5** in a 28% yield. The reaction proceeded to completion, as indicated by TLC analysis, therefore as with **4.6**, the low yield can be attributed to product loss in the work-up and purification steps.

4.4 *In vitro* biological evaluation on recombinant *Sm*BRD3

4.4.1 Binding affinity to *Sm*BRD3(1,2) and *Sm*BRD3(2)

With photoaffinity probes **4.2, 4.5** and **4.6** in hand, it was desirable to determine the binding affinity of these probes to protein constructs of *Sm*BRD3. First, compound **4.2** was tested by isothermal titration calorimetry (ITC) to determine the K_d for binding to *Sm*BRD3(1,2) and *Sm*BRD3(2) (**Table 4.1**).

Table 4.1. *Sm*BRD3(1,2) and *Sm*BRD3(2) K_d values of compounds **1.37** and **4.2** determined by ITC. A heat map colour scale of green to red is used, with higher affinity indicated by red and lower affinity indicated by green.

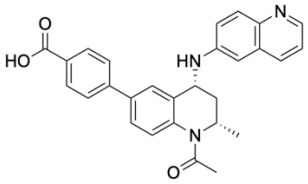
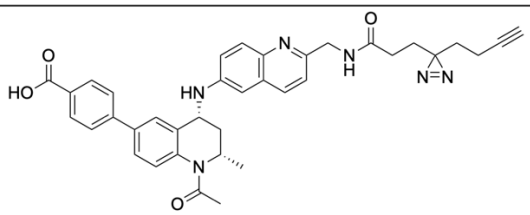
Compound	Structure	*Sm*BRD3(1,2) K_d (nM)	*Sm*BRD3(2) K_d (nM)
OXFBD03 (1.37)		**675 ± 97.6[a]**	**no binding**
4.2		**2835 ± 1088[b]**	**no binding**

[a] Single value ± error of the curve fit; [b] mean value of 2 repeats ± 95% CI.

Compared with the K_d value for OXFBD03 (**1.37**) binding to *Sm*BRD3(1,2), **4.2** showed a significant decrease in affinity, with a K_d = 2835 ± 1088 nM. As for OXFBD03 (**1.37**), no binding of **4.2** to *Sm*BRD3(2) was detected (tested at 20 μM, with 160 μM *Sm*BRD3(2)), indicating this probe is also selective for *Sm*BRD3(1). The average stoichiometry N value of **4.2** binding to *Sm*BRD3(1,2) was determined as 5.89 ± 0.085, however given no binding to *Sm*BRD3(2) was detected, this can be reasoned by possible poor aqueous solubility of **4.2**. Therefore, the ITC results indicated photocrosslinking of this probe to *Sm*BRD3 was expected to occur in, or proximity to, the *Sm*BRD3(1) binding site, and not *Sm*BRD3(2).

The K_d values of compounds **2.6** and **4.5** for *Sm*BRD3(2) were then assessed by ITC (**Table 4.2**).

Table 4.2. *Sm*BRD3(2) K_d values of compounds **2.6** and **4.5** determined by ITC. Red is used to show higher affinity for *Sm*BRD3(2).

Compound	Structure	*Sm*BRD3(2) K_d (nM)
2.6		**364 ± 51.6[a]**
4.5		**263 ± 38.2[b]**

[a] mean value of 3 repeats ± 95% CI; [b] mean value of 2 repeats ± 95% CI.

From work described in **Chapter 2**, **2.6** was identified as the highest affinity compound for *Sm*BRD3(2). When tested by ITC, and in contrast to the ITC results for **4.2**, addition of the diazirine-alkyne handle was favourable for binding to *Sm*BRD3(2) compared with the parent ligand **2.6**. Compound **4.5** binds to *Sm*BRD3(2) with a K_d value of 263 ± 38.2 nM. This result confirmed the *in silico* docking prediction that placement of the reactive handle in this position would be tolerated in terms of binding to *Sm*BRD3(2). The docking pose of **4.4** in the binding pocket of *Sm*BRD3(2) suggested a possible hydrogen bond interaction between the amide N-H and E344 (**Figure 4.6**), and a similar interaction with the amide N-H of **4.5** may contribute to the increase in affinity. This result indicates a further SAR strategy for developing *Sm*BRD3(2) ligands with enhanced affinity. The ethyl ester derivative of **4.5**, probe **4.6**, was also tested by ITC, and analogous with the ethyl ester analogue **2.31**, **4.6** showed no detectable binding to *Sm*BRD3(2). **2.31** has poor solubility compared to I-BET726 benzoic acid-based derivatives (**Chapter 2**), and therefore it was likely the ITC result for the ethyl ester-based compound **4.6** was also due to this reason, however, the solubility was not measured to confirm this hypothesis.

4.4.2 Photoactive crosslinking to recombinant *Sm*BRD3

*4.4.2.1 Crosslinking of **4.2** to SmBRD3(1,2)*

Having shown that compounds **4.2** and **4.5** bind to *Sm*BRD3(1,2) and *Sm*BRD3(2), respectively, their crosslinking efficiencies to recombinant *Sm*BRD3 constructs were determined by mass spectrometry (MS).

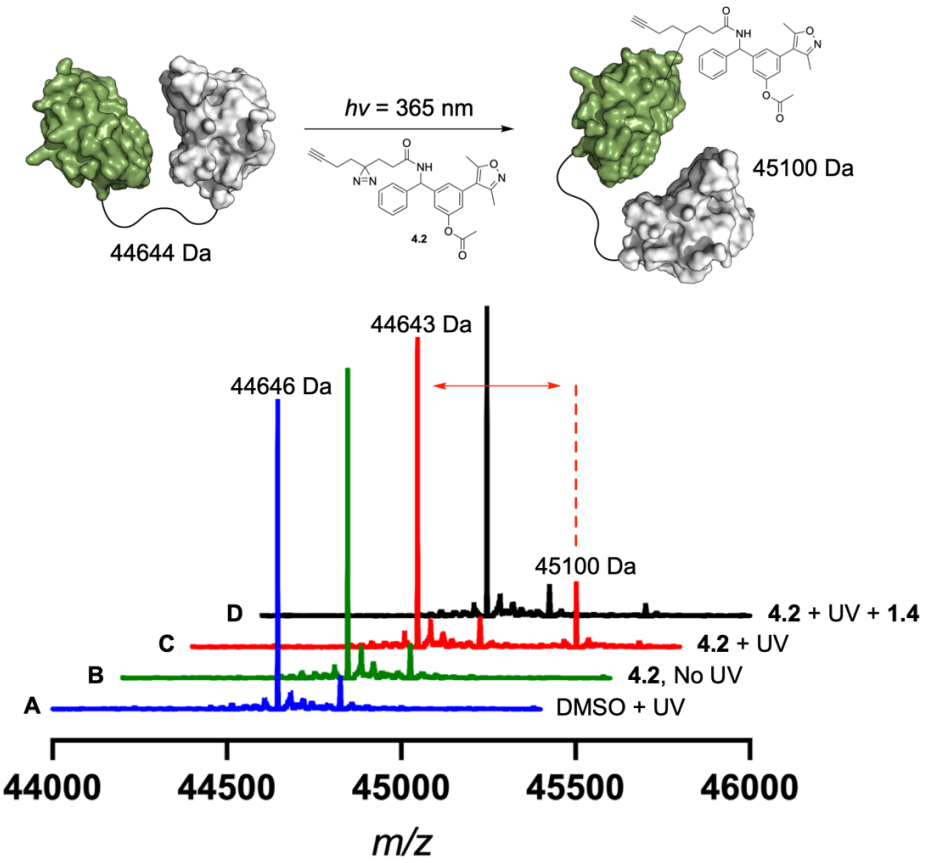


Figure 4.9. Deconvoluted mass spectra of *Sm*BRD3(1,2) after 50 min incubation with DMSO or **4.2** at 4 °C, followed by 10 min irradiation with UV light (where indicated) at 365 nm at 4 °C. **A**) Incubation of *Sm*BRD3(1,2) (10 μM) with DMSO (0.5% *v/v*) followed by UV irradiation. **B**) Incubation of *Sm*BRD3(1,2) (10 μM) with **4.2** (20 μM) and no UV irradiation. **C**) Incubation of *Sm*BRD3(1,2) (10 μM) with **4.2** (20 μM) and UV irradiation. **D**) Incubation of *Sm*BRD3(1,2) (10 μM) with **4.2** (20 μM) and OXFBD02 (**1.4**) (200 μM) and UV irradiation. SmBRD3(1,2) (expected MW = 44644 Da) is represented by the Alphafold[111] predicted structures of *Sm*BRD3(1) (green) and *Sm*BRD3(2) (white) linked by a tether. The expected MW of the *Sm*BRD3(1,2) and **4.2** adduct is 45100 Da.

Incubation of **4.2** (20 μM) with *Sm*BRD3(2) (10 μM), followed by UV irradiation (364 nm) for 10 min resulted in a mass peak at 45100 Da, corresponding to a mass shift of 456 Da from the expected *Sm*BRD3(1,2) molecular weight, consistent with the addition of **4.2** minus N_2 (**Figure 4.9 C**). The peak indicated a crosslinking yield of approximately 19% (calculated

using **Equation 4.1**). The observation of only one mass shift corresponding to crosslinking of one molecule of **4.2** is consistent with ITC results showing **4.2** binds to *Sm*BRD3(1,2), but not to *Sm*BRD3(2), therefore indicating selectivity for the first domain. Co-incubation of **4.2** with 10 equivalents of OXFBD02 (**1.4**) (K_d [*Sm*BRD3(1,2)] = 683 ± 166 nM) resulted in the near total removal of this mass peak, with a crosslinking yield of approximately 5% observed. This result further supports the proposition that the photocrosslinking of **4.2** to *Sm*BRD3(1,2) occurs through specific engagement with the first domain of *Sm*BRD3.

$$Crosslinking\ yield\ (\%) = \frac{Crosslinked\ Protein\ Intensity}{Crosslinked\ Protein\ Intensity + Unmodified\ Protein\ Intensity} \times 100$$

Equation 4.1. Equation used to determine the crosslinking yield of photoaffinity probes.

An uncertainty arising from the work described in **Chapter 2** was the extent to which the I-BET726 derivatives, which were optimised for binding to *Sm*BRD3(2), bind to the first domain of *Sm*BRD3. With a compound capable of selective photocrosslinking in hand, it was decided this question could be qualitatively addressed by using the I-BET726 derivatives as competitors for **4.2** by co-incubation. This study focused on using **2.6** as a competitor, due to being the highest affinity ligand for *Sm*BRD3(2) developed in **Chapter 2**. If the peak corresponding to crosslinking of **4.2** to *Sm*BRD3(1,2) significantly diminished after co-incubation, it would suggest the diazirine probe had been displaced from the first domain binding pocket, indicating **2.6** bound to the first domain.

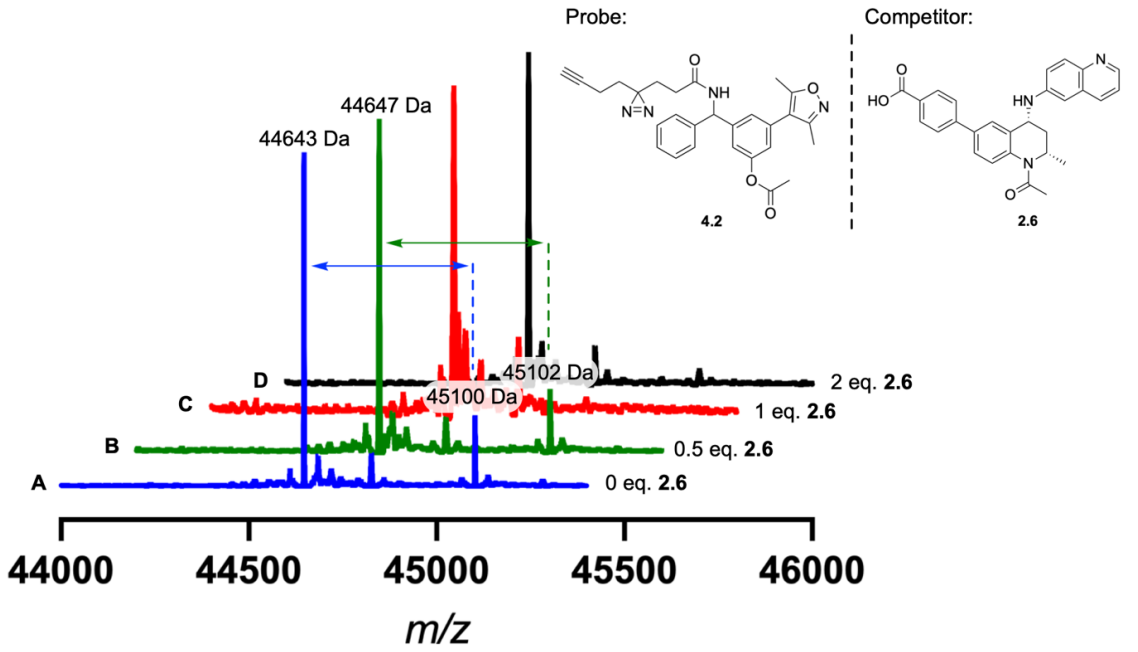


Figure 4.10 Deconvoluted mass spectra of *Sm*BRD3(1,2) after 50 min incubation of *Sm*BRD3(1,2) (10 μM) with **4.2** (20 μM) and **2.6** (where indicated) at 4 °C, followed by 10 min irradiation with UV light at 365 nm at 4 °C. **A**) No incubation with **2.6**; **B**) Incubation with **2.6** (10 μM); **C**) Incubation with **2.6** (20 μM). **D.** Incubation with **2.6** (40 μM).

4.2 was co-incubated with 0.5 (**Figure 4.10 B**), 1 (**Figure 4.10 C**) and 2 (**Figure 4.10 D**) equivalents of **2.6**, relative to the diazirine probe **4.2**. Co-incubation with 0.5 equivalents reduced the crosslinking yield from approximately 19% (**Figure 4.10 A.**) to 15%. Co-incubation with 1 and 2 equivalents reduced the crosslinking yield to a negligible level (0% and 5%, respectively). These data strongly suggest that **2.6** displaced the diazirine probe from the first domain binding pocket and therefore binds to the first domain of *Sm*BRD3(1,2).

With the demonstration that diazirine probe **4.2** crosslinks to *Sm*BRD3(1,2), it was then desirable to determine if the crosslinked adduct of **4.2** with *Sm*BRD3(1,2) was capable of undergoing a CuAAC reaction with an azide bearing a fluorophore, and whether the information contained in the MS data (**Figure 4.9** and **Figure 4.10**) was able to be displayed by in-gel fluorescence after SDS-PAGE. The samples described above were subject to conditions for CuAAC using copper sulfate, the reducing agent TCEP and the Cu(I) ligand TBTA, and incubated with the fluorophore azide **4.36**. The results of these reactions were

then analysed using SDS-PAGE and visualised by Coomassie stain (using visible light) and in-gel fluorescence (using a 605/50 nm filter, UV trans illumination) (**Figure 4.11**).

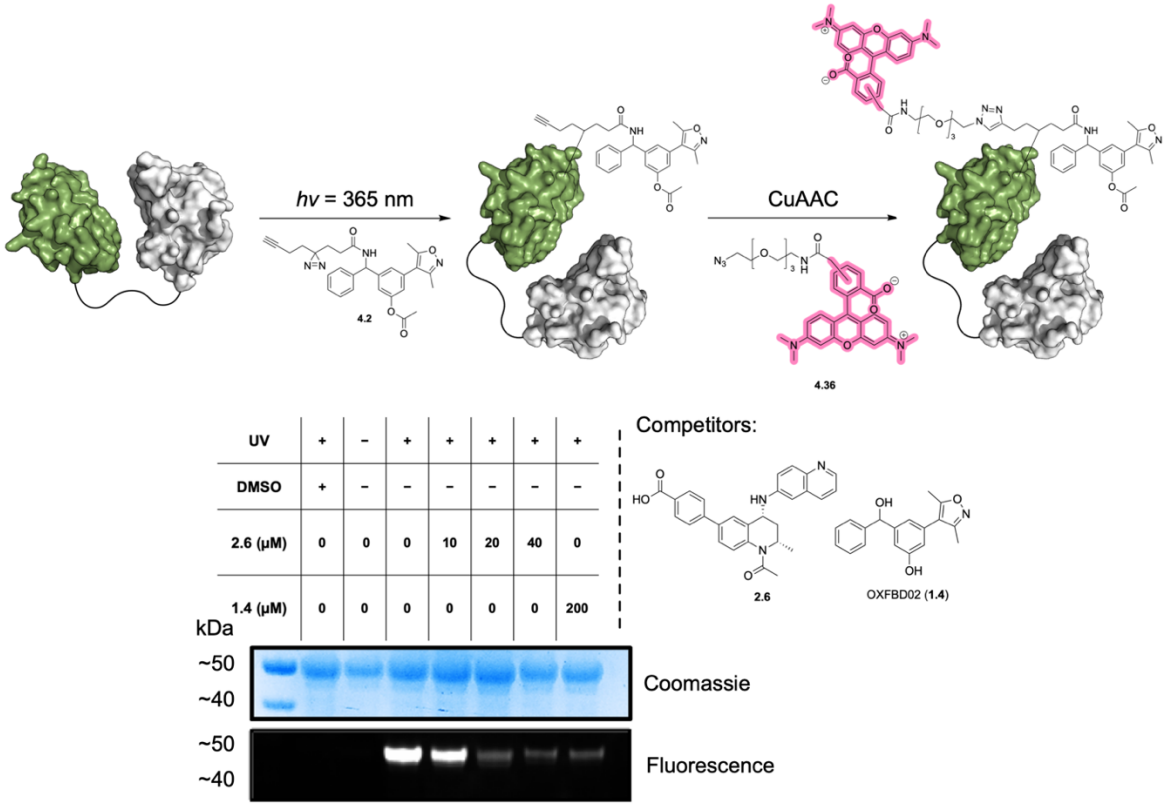


Figure 4.11. Coomassie and in-gel fluorescence analysis of *Sm*BRD3(1,2) separated by SDS-PAGE after 50 min incubation at 4 °C with DMSO or **4.2** (20 μM), with or without a competitor (**1.4** or **2.6**), followed by 10 min irradiation with UV light (where indicated) at 365 nm at 4 °C, and copper catalysed click reaction with Azide fluor-545 (**4.36**).

The sample corresponding to crosslinking of **4.2** with *Sm*BRD3(2) with no competitor, with crosslinking yield of approximately 19%, resulted in a bright fluorescent band corresponding to the approximate molecular weight of *Sm*BRD3(1,2), indicating the occurrence of a click reaction with the fluorophore azide (**Figure 4.11**). The negative controls resulted in no fluorescence on the SDS-PAGE gel. The MS data from co-incubation with the competitor, **2.6**, was reflected on the gel, with a reduction in fluorescence observed for 0.5 equivalents and negligible fluorescence for 1 and 2 equivalents of **2.6**. Finally, the in-gel fluorescence indicated the same result after competition with 10 equivalents of OXFBD02 (**1.4**) as with 2 equivalents of **2.6**.

*4.4.2.2 Crosslinking of **4.5** to SmBRD3(1,2) and SmBRD3(2)*

As with **4.2**, it was then desirable to determine the crosslinking yield of photoaffinity probe **4.5** to *Sm*BRD3(2).

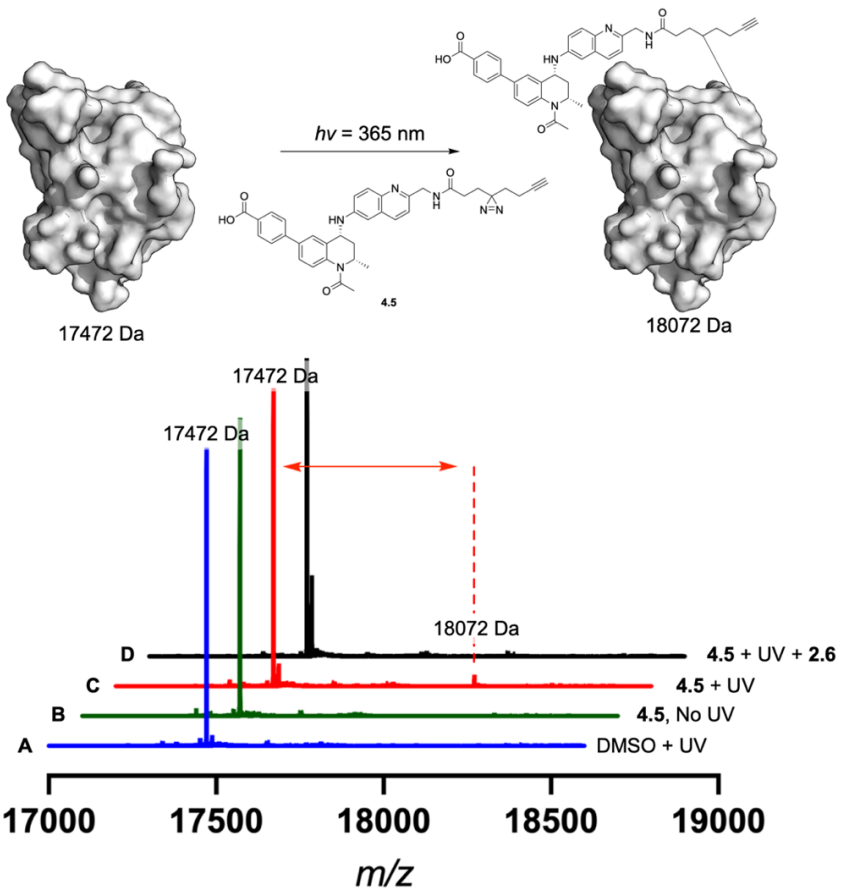


Figure 4.12. Deconvoluted mass spectra of *Sm*BRD3(2) after 50 min incubation at 4 °C followed by 10 min irradiation with UV light (where indicated) at 365 nm at 4 °C. **A**) Incubation of *Sm*BRD3(2) (10 μM) with DMSO (0.5% *v/v*) followed by UV irradiation; **B**) Incubation of *Sm*BRD3(2) (10 μM) with **4.5** (20 μM) and no UV irradiation; **C**) Incubation of *Sm*BRD3(2) (10 μM) with **4.5** (20 μM) and UV irradiation; **D**) Incubation of *Sm*BRD3(2) (10 μM) with **4.5** (20 μM) and **2.6** (200 μM) and UV irradiation; The expected molecular weights of *Sm*BRD3(2) and the **4.5** *Sm*BRD3(2) adduct are 17472 Da and 18072 Da respectively.

*Sm*BRD3(2) was incubated with **4.5** and then irradiated with UV light (365 nm) for 10 min. A small peak corresponding to a mass shift of **4.5** minus N_2 (600 Da), with a crosslinking yield of approximately 5% was observed (**Figure 4.12 C**). Co-incubation with excess parent ligand **2.6** resulted in approximately 2% crosslinking (**Figure 4.12 D**). These data indicated that, despite the nanomolar affinity for *Sm*BRD3(2), **4.5** was unable to photocrosslink the target protein with a high crosslinking yield. This highlights the fact that high affinity for a

target protein does not guarantee high crosslinking yield, and it was likely that the diazirine group was poorly placed to undergo crosslinking with a residue of *Sm*BRD3(2) once activated with UV light. It was therefore attempted to increase the percentage crosslinking by increasing the concentration of **4.5** from 20 µM to 100 µM (**Figure 4.13**).

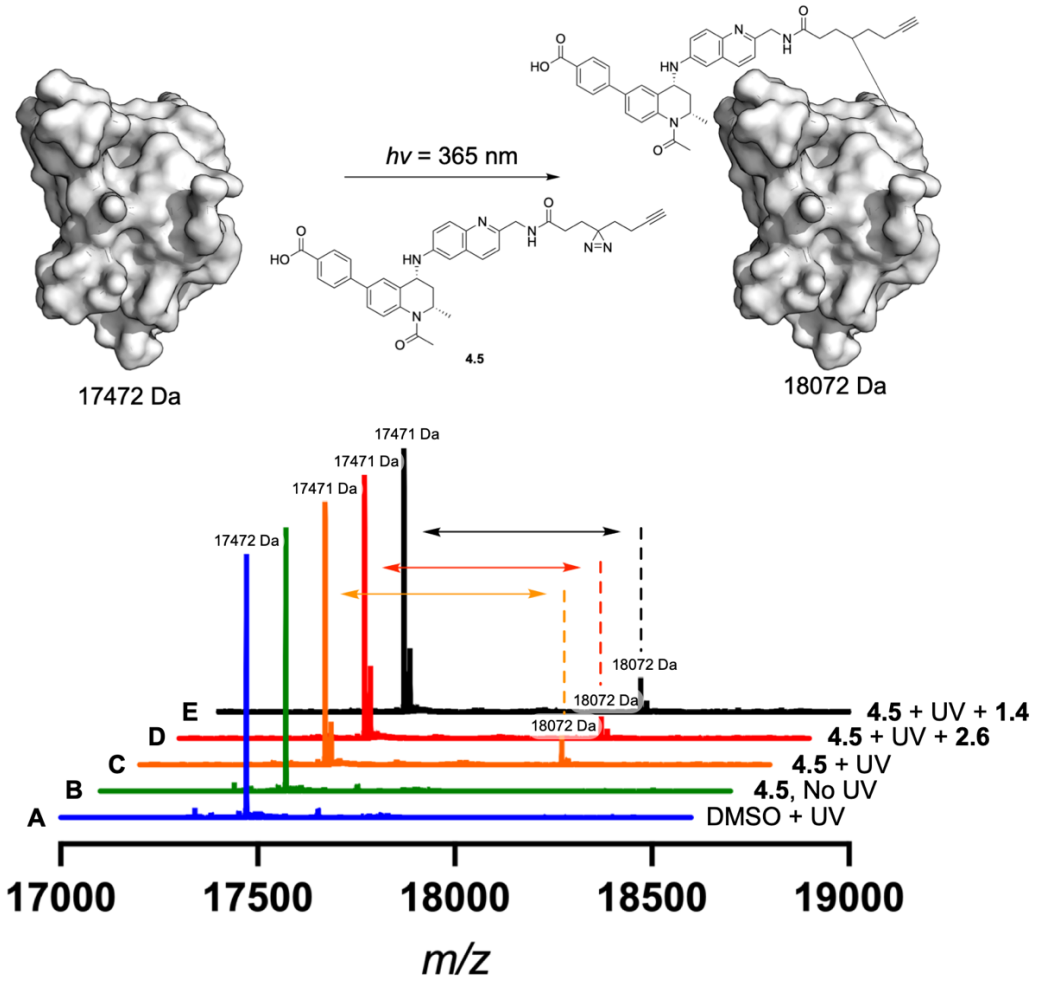


Figure 4.13. Deconvoluted mass spectra of *Sm*BRD3(2) after 50 min incubation at 4 °C followed by 10 min irradiation with UV light (where indicated) at 365 nm at 4 °C. **A**) Incubation of *Sm*BRD3(2) (10 µM) with DMSO (0.5% *v/v*) followed by UV irradiation; **B**) Incubation of *Sm*BRD3(2) (10 µM) with **4.5** (100 µM) and no UV irradiation; **C**) Incubation of *Sm*BRD3(2) (10 µM) with **4.5** (100 µM) and UV irradiation; **D**) Incubation of *Sm*BRD3(2) (10 µM) with **4.5** (20 µM) and **2.6** (150 µM) and UV irradiation. **E**) Incubation of *Sm*BRD3(2) (10 µM) with **4.5** (20 µM) and OXFBD02 (**1.4**) (150 µM) and UV irradiation.

The increase in concentration resulted in only a marginal increase in percentage crosslinking to approximately 10% (**Figure 4.13 C**). This further highlights the likely poor positioning of the diazirine group to undergo efficient crosslinking with *Sm*BRD3(2). Co-incubation of *Sm*BRD3(2) with 1.5 equivalents of **2.6** resulted in a percentage

crosslinking of approximately 8%. The inability to significantly reduce the percentage crosslinking using this competitor could be explained by the higher affinity of the diazirine probe for the protein than the competitor or, be due to unspecific crosslinking independent of binding to the KAc binding pocket of *Sm*BRD3(2). Finally, co-incubation with 1.5 equivalents of OXFBD02 (**1.4**), a *Sm*BRD3(1) selective ligand, did not result in a decrease in percentage crosslinking (12% percentage crosslinking), showing the *Sm*BRD3(1) selective ligand did not displace the photoaffinity probe, as expected.

Crosslinking of **4.5** to *Sm*BRD3(1,2) was also attempted, however, the mass spectra from these samples could not be deconvoluted. Only samples resulting from incubation with **4.5** and subsequent UV irradiation could not be deconvoluted, and it is therefore possible that the crosslinked adduct of **4.5** and *Sm*BRD3(2) was unstable to the MS detection conditions.

With the demonstration of crosslinking to *Sm*BRD3(2), albeit at a low percentage, it was desirable to demonstrate the capability of the crosslinked adducts of **4.5** and *Sm*BRD3(2) to undergo a CuAAC reaction with the azide fluorophore **4.36**. As with **4.2**, it was expected the MS data would be reflected by in-gel fluorescence after click reaction with Azide fluor-545 (**4.36**) and separation by SDS-PAGE (**Figure 4.14**).

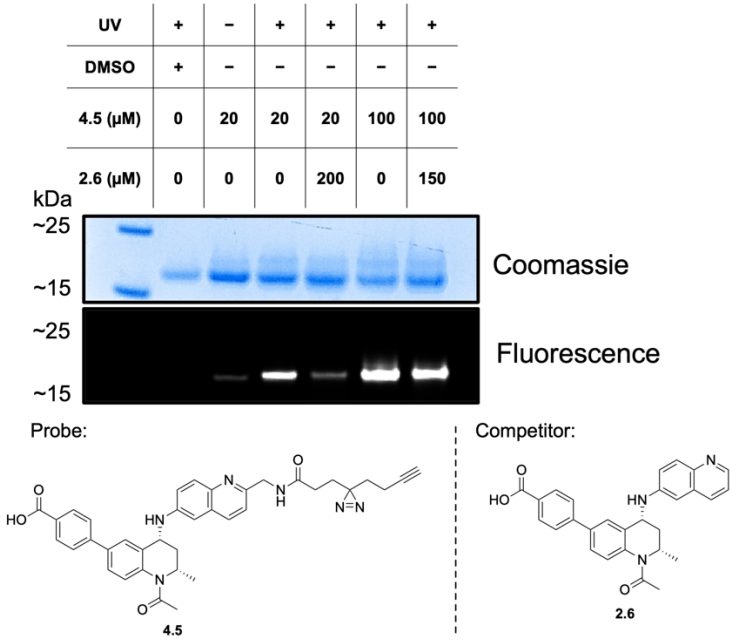


Figure 4.14 Coomassie and in-gel fluorescence analysis of *Sm*BRD3(2) after 50 min incubation at 4 °C with DMSO or **4.5**, with a competitor (**2.6**) where stated, followed by 10 min irradiation with UV light (where indicated) at 365 nm at 4 °C, and a CuAAC click reaction with Azide fluor-545 (**4.36**).

Despite a low percentage crosslinking to *Sm*BRD3(2) (~6%), a bright fluorescent band corresponding to the approximate molecular weight of *Sm*BRD3(2) was observed by in-gel fluorescence after incubation of SmBRD3(2) with **4.5** (20 μM), UV irradiation and click reaction with **4.36**. A brighter fluorescent band was observed from incubation with 100 μM **4.5**. The DMSO and 'No UV' negative controls resulted in negligible fluorescence and pleasingly, incubation of 20 μM of **4.5** with 10 equivalents of parent ligand **2.6** also resulted in greatly reduced in-gel fluorescence, indicating effective competition of the diazirine probe by the parent compound. Finally, co-incubation of **4.5** (100 μM) with 1.5 of equivalents competitor **2.6** resulted in bright, in-gel fluorescence. This corresponds to the MS result that co-incubation with 1.5 equivalents of competitor did not significantly reduce the percentage crosslinking.

Despite unsuccessful attempts at the determination of the crosslinking yield of **4.5** to *Sm*BRD3(1,2), it was hoped that analysis by in-gel fluorescence would alleviate the problems encountered in MS detection and elucidate information on crosslinking of this probe to *Sm*BRD3(1,2) (**Figure 4.15**). The intra-domain selectivity of this probe for

*Sm*BRD3(1,2) could also be investigated by in-gel fluorescence using competition experiments.

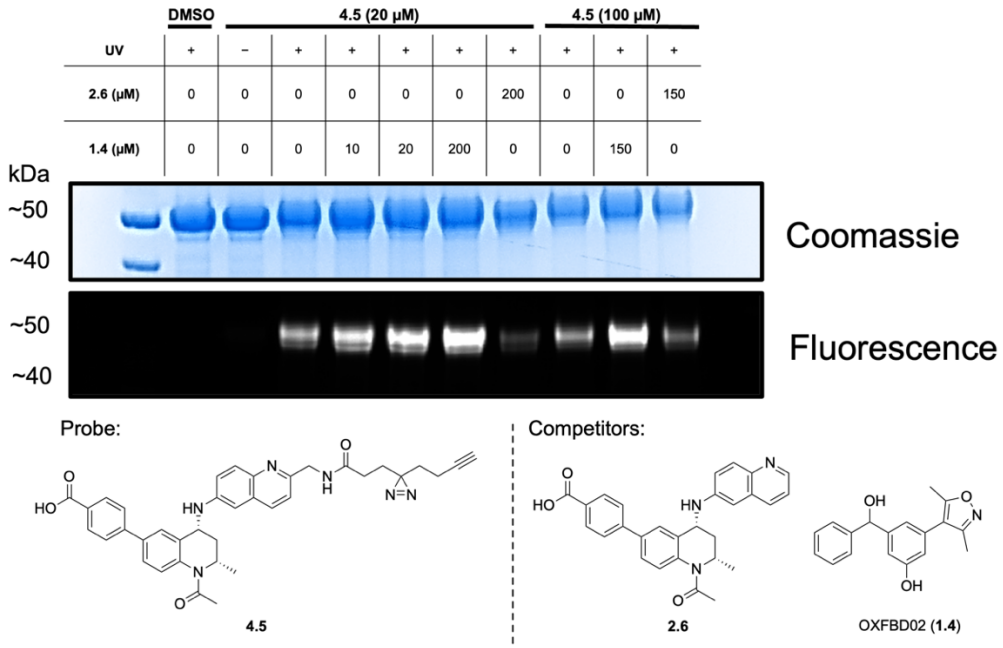


Figure 4.15. Coomassie and in-gel fluorescence analysis of *Sm*BRD3(1,2) after 50 min incubation at 4 °C with DMSO or **4.5**, with a competitor (**1.4** or **2.6**), followed by 10 min irradiation with UV light (where indicated) at 365 nm at 4 °C, and CuAAC reaction with Azide fluor-545 (**4.36**).

The in-gel fluorescence intensity demonstrated crosslinking of **4.5** to *Sm*BRD3(1,2) and subsequent click reaction with **4.36** (**Figure 4.15**). In contrast to the result with *Sm*BRD3(2), increasing the concentration of probe **4.5** from 20 μM to 100 μM did not result in a noticeable increase in fluorescence intensity. Co-incubation of **4.5** (20 μM) with **2.6** (200 μM) resulted in reduced in-gel fluorescence, suggesting crosslinking to *Sm*BRD3(1,2) mostly occurred from binding interactions similar to those between **2.6** and *Sm*BRD3(1,2). To further investigate the engagement of **4.5** with the two domains of *Sm*BRD3(1,2), the first domain selective ligand OXFBD02 (**1.4**) was used a competitor at varying equivalents of 0.5, 1 and 10. It was expected that if **4.5** bound to the first domain in addition to the second, and therefore engaged in photocrosslinking *via* binding to this domain, then competition with OXFBD02 (**1.4**) would decrease the in-gel fluorescence intensity. Surprisingly, increasing equivalents of OXFBD02 (**1.4**) enhanced the observed fluorescence. This result, in combination with the similar appearance in fluorescence for two different concentrations of

4.5, could be explained by crosslinking primarily occurring *via* the second domain of *Sm*BRD3(1,2). Co-incubation with OXFBD02 (**1.4**) could have blocked the binding of **4.5** to the first domain and therefore increased the effective concentration of this probe for binding to the second domain of *Sm*BRD3(1,2). This would then increase crosslinking to *Sm*BRD3(1,2) *via* the binding pocket more favourable to photocrosslinking. Alternatively, binding of OXFBD02 (**1.4**) to the first domain of *Sm*BRD3(1,2) may increase the affinity of **4.5** to the second domain by a cooperative binding effect, resulting in an enhancement of crosslinking to the second domain.

The MS data for **4.5** binding to *Sm*BRD3(2) suggested only a marginal increase in percentage crosslinking when the concentration was increased from 20 μM to 100 μM. A change in fluorescence intensity was seen between these two *Sm*BRD3(2) samples by in gel fluorescence (**Figure 4.14**), however, this difference between the two analyses could be attributed to maximum fluorescence exposure being set to the most intense band, which in the case of *Sm*BRD3(1,2) (**Figure 4.15**) resulted from co-incubation with 10 equivalents of OXFBD02 (**1.4**). Therefore, any difference in fluorescence intensity between different concentrations of **4.5** crosslinking to *Sm*BRD3(1,2) may not have been detected.

The SDS-PAGE gels to assess crosslinking of **4.2** and **4.5** to *Sm*BRD3(1,2) and *Sm*BRD3(2) by in-gel fluorescence showed multiple protein bands, which likely resulted from degradation of the protein constructs during the experiments described above (**Appendix C, Figures S33–S35**). SDS-PAGE analysis of a control experiment examining these constructs after UV irradiation with and without CuAAC crosslinking conditions indicated these constructs were partially unstable to the CuAAC conditions (**Appendix C, Figure S36**).

The work described above demonstrated probes **4.2** and **4.5** crosslinked to recombinant *Sm*BRD3 constructs and underwent CuAAC reactions with a fluorophore azide, enabling detection of crosslinked proteins by in-gel fluorescence. These results indicated probes **4.2**

and **4.5** were effective photoaffinity probes for *Sm*BRD3, and experiments were progressed to examine the engagement of these probes with *Sm*BRD3 in *S. mansoni* lysate.

4.5 Investigation of *Sm*BRD3 photoaffinity probes within the *S. mansoni* proteome

4.5.1 Evaluation of photoaffinity probes for *Sm*BRD3 on *S. mansoni* lysate

To investigate the proteome-wide interactions of photoaffinity probes **4.2** and **4.5**, and therefore to elucidate the cellular interactions of OXFBD03 (**1.37**) and **2.6**, it was initially decided to carry out photoaffinity crosslinking experiments in *S. mansoni* lysate. This was due to concerns of the permeability of UV light through a multicellular parasite. To maintain the most cellularly relevant environment, including native protein folds and interactions, soft lysis conditions were chosen. The buffer choice of PBS with a protease inhibitor was inspired by work from Li *et al*.,[148] which also examined diazirine probes in cell lysate. Adult worm lysis consisted of multiple rounds of flash freeze-thawing and bead beating followed by mechanical lysis using a Dounce homogenizer. Lysate was prepared from the adult worm and schistosomula life stages. The probes **4.2** and **4.5** were then incubated with the lysate for 30 min, followed by UV irradiation for 10 min (365 nm) and a CuAAC click reaction with Azide fluor-545 (**4.36**). The lysate was then separated using SDS-PAGE and analysed by in-gel fluorescence. First, it was desirable to determine the optimum concentration of **4.2** and **4.5** for visualisation of in-gel fluorescence (**Figure 4.16**). Adult worm lysate was chosen for optimisation experiments due to its greater availability over the schistosomula material.

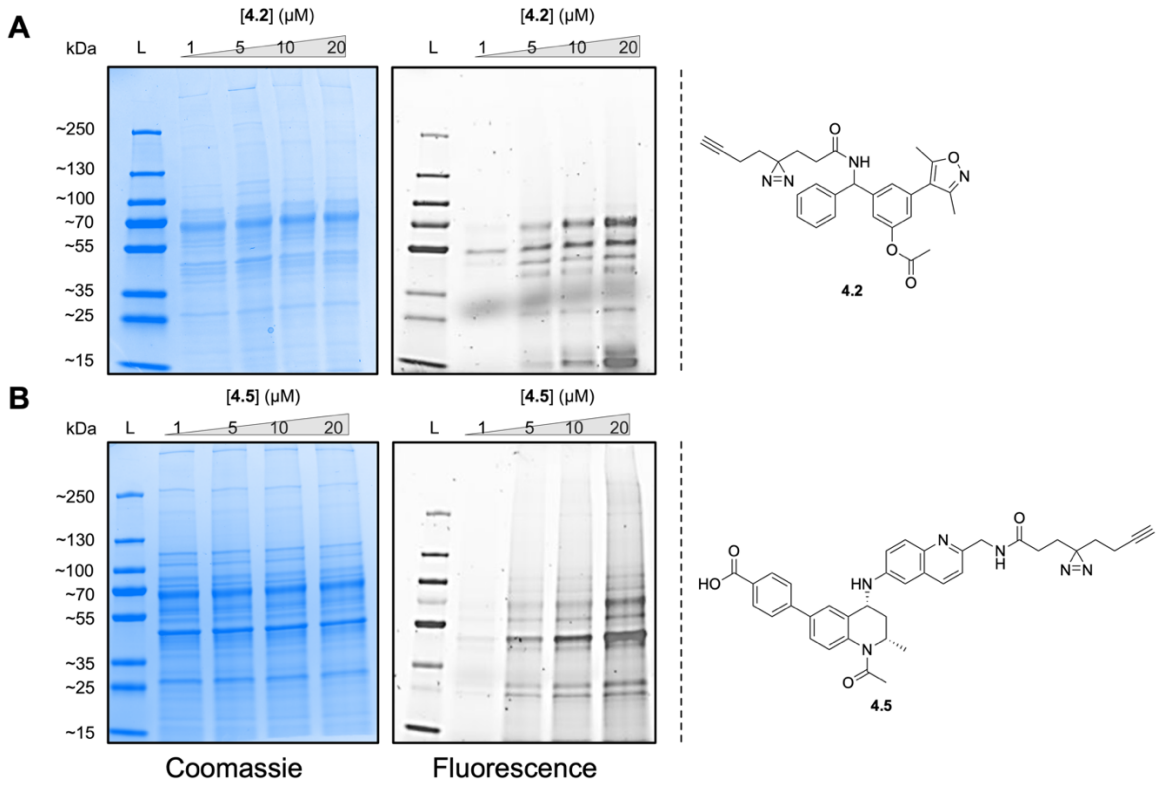


Figure 4.16. Optimisation of probe concentration of **4.2** (**A**) and **4.5** (**B**) for crosslinking to *S. mansoni* adult worm lysate. Photoaffinity probes were incubated with adult worm lysate (1.4 mg/mL) for 30 min, followed by 10 min UV irradiation (365 nm). A click reaction was then carried out with Azide-fluor 545 (**4.36**) and the results were viewed by SDS-PAGE. L = Ladder.

Analysis using in-gel fluorescence revealed a number of cellular targets, demonstrated by fluorescent protein bands after incubation of lysate with **4.2** (**Figure 4.16 A**) and **4.5** (**Figure 4.16 B**) and subsequent UV irradiation and CuAAC click reaction. Increasing concentrations of probe was found to lead to a greater number of engaged cellular targets, as shown by newly visible fluorescent bands. Concentrations of 5 μM and 10 μM were chosen as optimum, due to the occurrence of multiple clear fluorescent bands, while minimising band fluorescence oversaturation and smearing.

With the optimum concentrations determined, it was decided to confirm that UV light was essential to the covalent fluorescent labelling of engaged proteins, and to directly compare the fluorescence in lysate between the two probes (**Figure 4.17**).

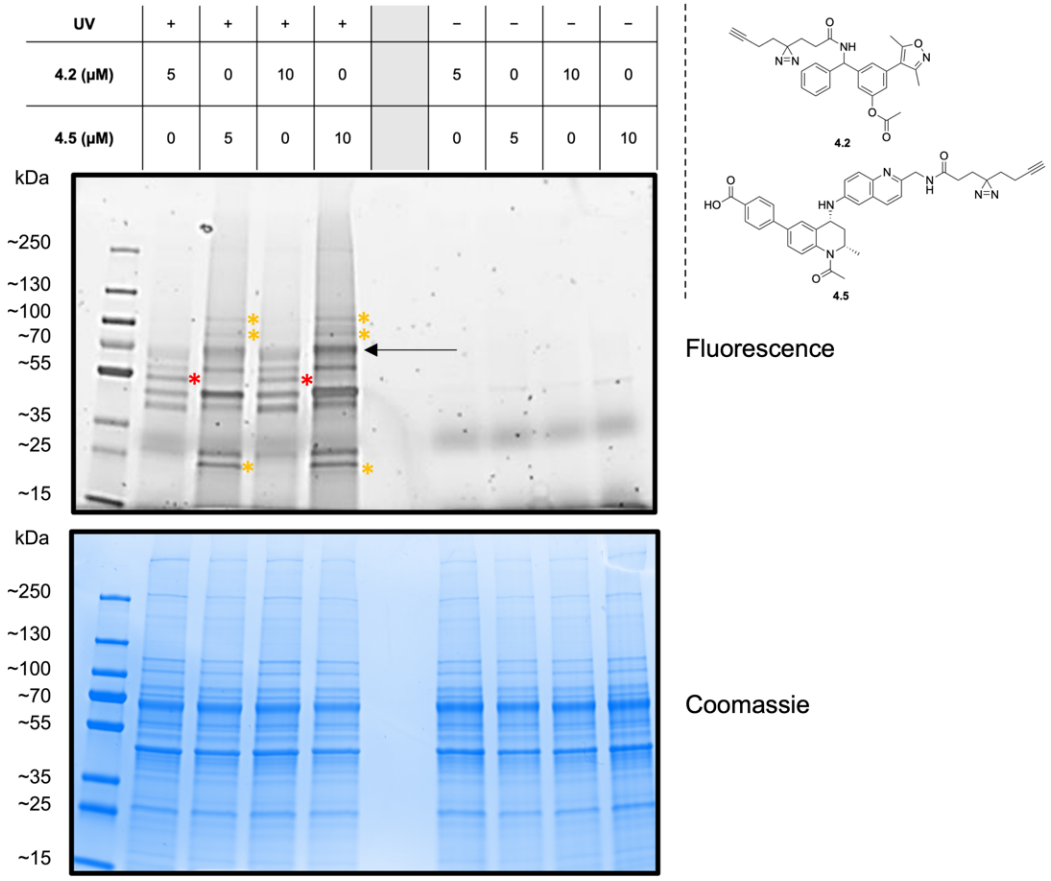


Figure 4.17 SDS-PAGE showing the comparison of probes **4.2** and **4.5** at 5 μM and 10 μM crosslinking to adult worm lysate (1.4 mg/mL) with either UV or no UV irradiation. Putative targets clearly specific to **4.2** are marked with red asterisks, whereas putative targets clearly specific to **4.5** are marked with a gold asterisk. The band of interest is marked with an arrow.

The observation of minimal fluorescence in the absence of UV irradiation strongly suggested engagement of probes **4.2** and **4.5** with the *S. mansoni* proteome was due to activation of the diazirine group of the two probes. Comparative analysis of the proteome-wide selectivity for **4.2** and **4.5** revealed a selection of targets uniquely engaged by each probe, as well as a number of common targets. One of the predicted native isoforms of *Sm*BRD3 has a molecular weight of 76,907 Da (Uniprot ID: A0A5K4EQL3), and so a promising result was the occurrence of in-gel fluorescence at approximately 70 KDa for both probes (marked with an arrow, **Figure 4.17**). It was hoped this band corresponded to crosslinking to the protein of interest, *Sm*BRD3. The in-gel fluorescence indicated probe **4.5** engaged with this target more than probe **4.2**. To test the hypothesis that this target was *Sm*BRD3, a competition experiment was attempted, using the parent ligands of probes **4.2**

and **4.5** to eliminate, or reduce the intensity of this fluorescent band, thereby indicating the observed fluorescence resulted from specific crosslinking to a protein the parent compounds interact with (**Figure 4.18**).

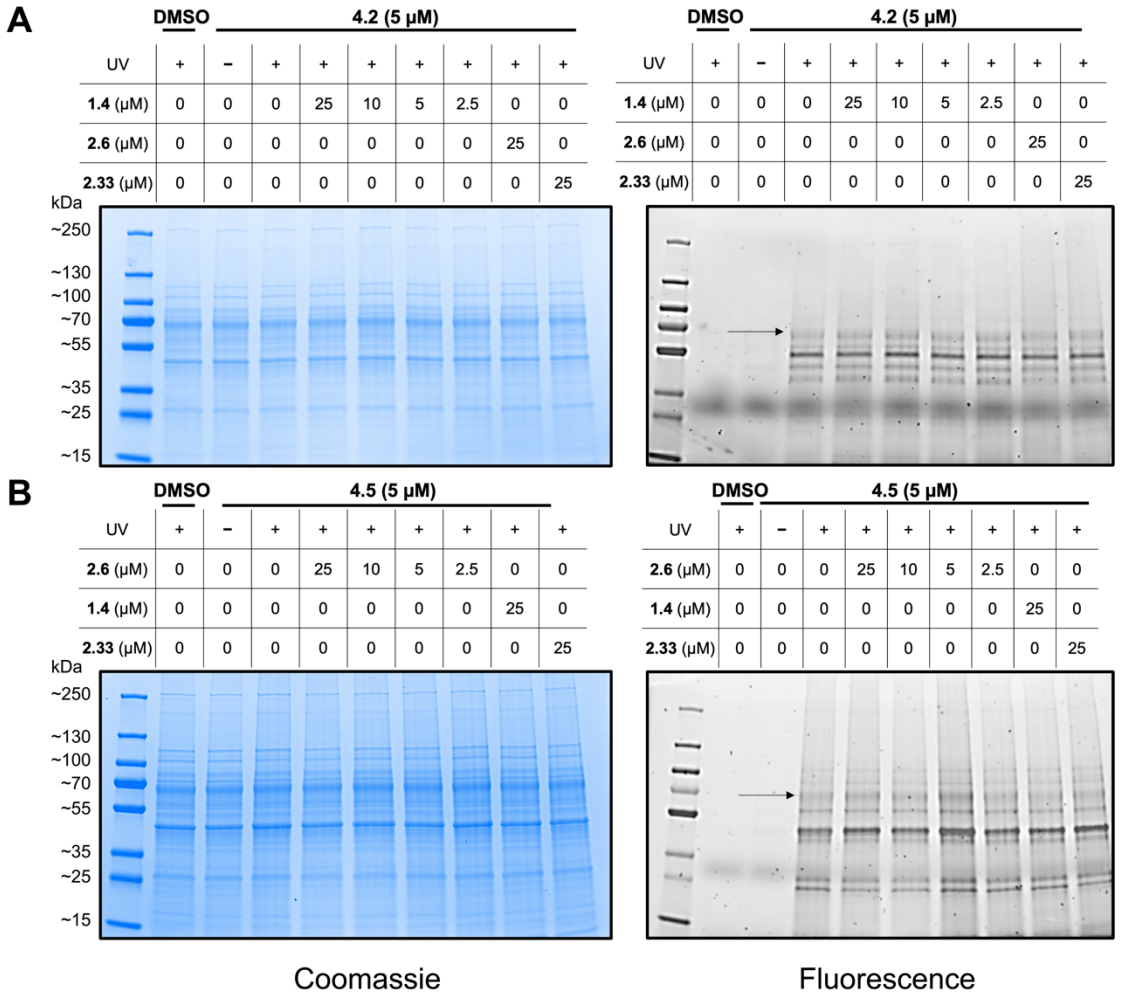


Figure 4.18. SDS-PAGE of competition experiments from co-incubation of competitors and probes **4.2** and **4.5** with adult worm lysate (1.4 mg/mL). **A**) Incubation of **4.2**, plus DMSO and no UV controls, and co-incubations with competitors **1.4, 2.6** and **2.33**, with adult worm lysate. **B**) Incubation of **4.5**, plus DMSO and no UV controls, and co-incubations with competitors **1.4**, **2.6** and **2.33**, with adult worm lysate. The band of interest for displacement with competitors is marked with an arrow.

Probes **4.2** and **4.5** were incubated with adult worm lysate, along with the inclusion of competitor ligands. A concentration gradient was used for the parent ligands of the diazirine probes, to observe possible concentration dependent decrease in fluorescent intensity resulting from competition. Co-incubation with the excess competitor of the 'opposite' parent ligand was also included, for example co-incubation of **4.2** and **2.6** to gain a deeper understanding of the specificity of these probes within the *S. mansoni* proteome. Finally,

co-incubation with the negative control enantiomer **2.33**, shown not to bind to *Sm*BRD3(1,2) in **Chapter 2**, was included to determine if the interactions were stereospecific, along with the inclusion of DMSO and no UV negative controls. An indistinct fluorescence band was observed between approximately 25 and 35 kD for the DMSO and no UV negative controls. This was likely due to an unspecific interaction of the fluorophore azide **4.36** with a component of the adult worm lysate. Co-incubation with all competitor ligands failed to displace the engagement of probes **4.2** and **4.5** with *S. mansoni* lysate. This suggested the fluorescence observed was due to unspecific background crosslinking of the diazirine probes to proteins which were unrelated to the protein targets of parent ligands **1.4** and **2.6**.

As described in **Chapter 1**, it is predicted that *Sm*BRD3 is expressed to a higher extent in schistosomula, compared to the adult worms. The failure of the competitors to eliminate or reduce the intensity of fluorescent bands, implying the failure to identify an interaction with *Sm*BRD3, may be due to low expression of this bromodomain containing protein in the adult worms. Therefore, crosslinking experiments were carried out on schistosomula lysate, which due to higher expression may lead to identification of an interaction with *Sm*BRD3 *via* this experiment by in-gel fluorescence (**Figure 4.19**).

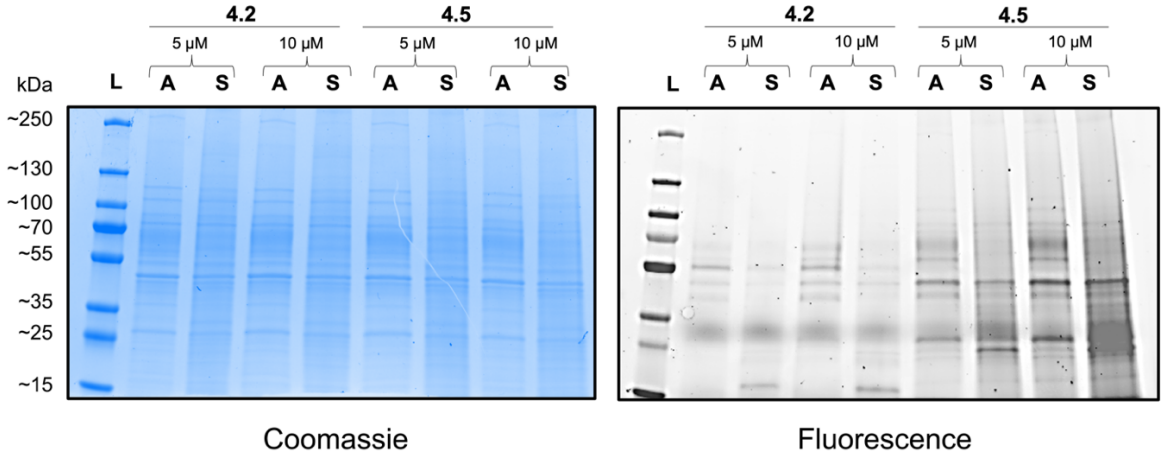


Figure 4.19. Crosslinking of probes **4.2** and **4.5** to adult worm (A) (1.4 mg/mL) and schistosomula (S) (1.3 mg/mL) lysate.

Comparison of the samples between the life-cycle stages revealed a difference in the interaction of these probes. Fewer targets were observed for the interaction of both probes

4.2 and **4.5** with the schistosomula lysate compared with the adult worm lysate. For a given probe, at least one significant fluorescent band was present in the schistosomula lysate which was not observed in the adult worm lysate. However, for the case of both probes, the band in the approximate mass range of 70 kDa observed in adult worm lysate was absent in the schistosomula lysate, contrasting to the prediction this would be more intense if arising from *Sm*BRD3. Human BET bromodomains are primarily located in the nucleus,[154,155] and it is likely this is also the case for *Sm*BRD3 in *S. mansoni* cells. It was therefore hypothesised that the failure to identify a possible band corresponding to *Sm*BRD3 could be due to ineffective extraction of the nuclear proteins during lysis, and in-gel fluorescence occurred from engagement of **4.2** and **4.5** with only the cytosolic *S. mansoni* proteome.

4.5.2 Evaluation of a polyclonal antibody for *Sm*BRD3 on *S. mansoni* lysate

To aid in the determination of the presence of *Sm*BRD3 in parasite lysate, along with possible use in future photoaffinity pull down experiments, a polyclonal antibody capable of detecting *Sm*BRD3 was raised in rabbits. This was produced using His-tag cleaved *Sm*BRD3(1,2), for which details of its expression and purification, along with the details of antibody production from this construct, can be found in **Chapter 6**. A western blot was carried out using the two antibody isolates (arising from two different rabbits) on adult worm and schistosomula lysate samples (**Figure 4.20**). The lysates were prepared as described in **section 4.5.1**.

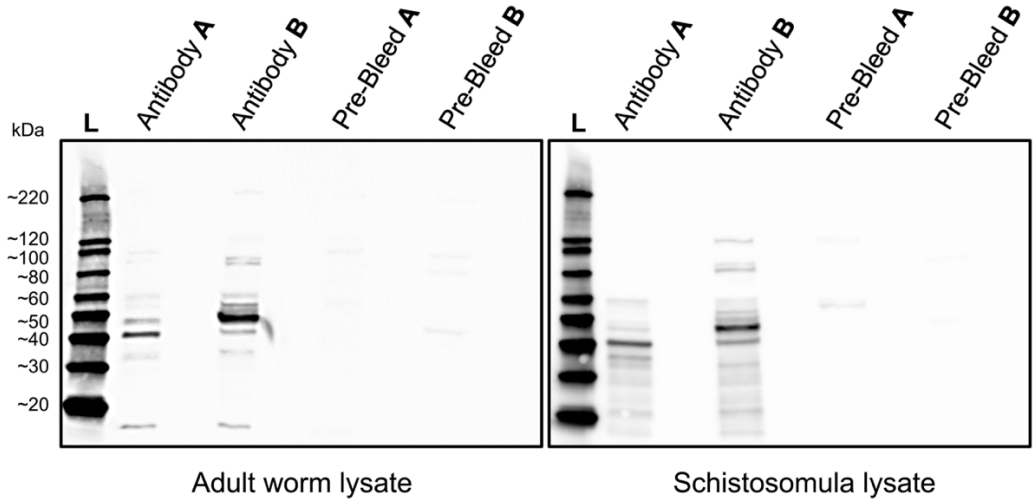


Figure 4.20. Western blot analysis of the interaction of two polyclonal antibody samples **A** and **B** with adult worm (left) (1.4 mg/mL) and schistosomula (right) lysate (1.4 mg/mL), along with antibody production pre-bleeds of antibodies A and B.

Western blot analysis indicated a similarity in the major protein interaction with the antibodies between the adult worm and schistosomula lysate. However, there were more interactions indicated in the schistosomula lysate, as determined by the observation of more intense chemiluminescent bands for this lysate sample. The pre-bleed isolates for both antibodies showed very little interaction with proteins, giving confidence that the chemiluminescent bands arising from incubation with the antibody were mostly interactions

specific to the purified antibody. However, the major chemiluminescent band observed for antibody **A** occurred at a different molecular weight to antibody **B**. Furthermore, the major chemiluminescent bands did not correlate with the approximate molecular weights of the native isoforms of *Sm*BRD3 (76,907 Da [Uniprot ID: A0A5K4EQL3] and 107,553 Da [Uniprot ID: A0A5K4ESD7]).

The inconsistency between the antibody samples and the molecular weight of the major band could be further evidence of ineffective extraction of the nuclear proteins, and therefore of *Sm*BRD3, using the lysis conditions described in **section 4.5.1**. It was decided to produce parasite lysate using denaturing and highly solubilising UTB lysis buffer (9 M Urea, 75 mM Tris-HCl, and 0.15 M β-mercaptoethanol, pH 7.5), which has been used in the literature for western blot analysis of a nuclear protein.[156] A preliminary western blot was carried out on cerceriae, schistosomula, and adult worm lysates, prepared using UTB buffer (**Figure 4.21**).

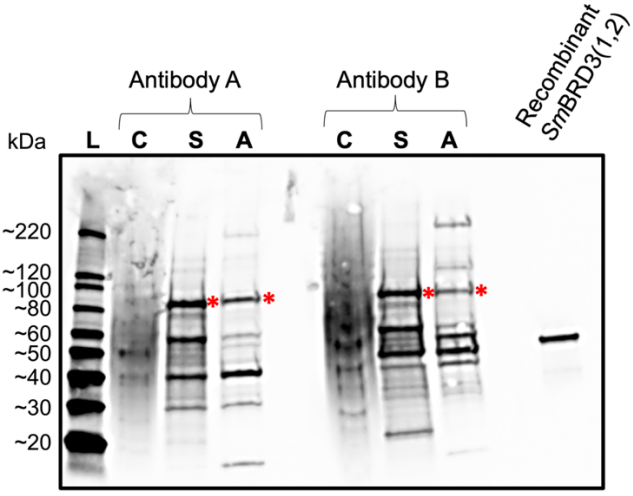


Figure 4.21. Preliminary western blot analysis of cerceriae (C), schistosomula (S) and adult worm (A) lysates, along with recombinant *Sm*BRD3(1,2) as a reference. The protein suspected to be native *Sm*BRD3 is marked with a red asterisk. The lysate samples were prepared by Dr Josephine Forde-Thomas (J.F.T.) and the total protein concentration of the samples were undetermined.

The preliminary western blot analysis of these lysate samples indicated a closer agreement between antibodies A and B. Furthermore, a greater number of significant chemiluminescent bands were observed. Promisingly, a bright chemiluminescent band was

observed in the approximate molecular weight range for a native isoform of *Sm*BRD3 (76,907 Da) (marked with a red asterisk, **Figure 4.21**). The poor separation of cercariae proteins was attributed to the carbohydrate rich component of the tegument, the glycocalyx, which is specific to the cercariae life-cycle stage.[157] Although preliminary, this result suggested UTB buffer was a more effective lysis buffer for extraction of the proteins for which these antibodies interact with, implying the antibodies interact with nuclear proteins. One of these proteins could be *Sm*BRD3. Use of UTB buffer for parasite lysate is a highly denaturing condition, and therefore the lysate generated *via* this strategy would be unsuitable for crosslinking experiments, and later pull-down experiments, with probes **4.2** and **4.5**.

4.5.3 Investigation of the interaction of photoaffinity probes with live *S. mansoni*

To alleviate the need for optimisation of lysis conditions suitable for photocrosslinking in parasite lysate, it was decided to investigate whether compounds **4.2**, **4.5** and **4.6** enter the parasite. Entry of the compound in the parasite could enable an 'in-parasite' crosslinking approach, by incubation of a probe with live parasites followed by UV irradiation. Subsequent lysis and CuAAC click reaction with a tag azide would enable analysis by in-gel fluorescence (*via* a fluorophore azide and SDS-PAGE) or mass spectrometry (*via* biotin azide and streptavidin pull-down).

Compounds **4.2**, **4.5** and **4.6** were tested for activity in phenotype on *S. mansoni*. Activity on parasite phenotype would imply entry of the compound into the parasite, as well as provide information on whether introduction of the diazirine-alkyne handle changes the phenotypic effect on the parasite relative to the parent ligand. Compounds **4.2**, **4.5** and **4.6** were tested on adult worms and the motility was assessed by the WHO-TDR scoring system, as described by Ramirez *et al*.[145] (**Figure 4.22**).

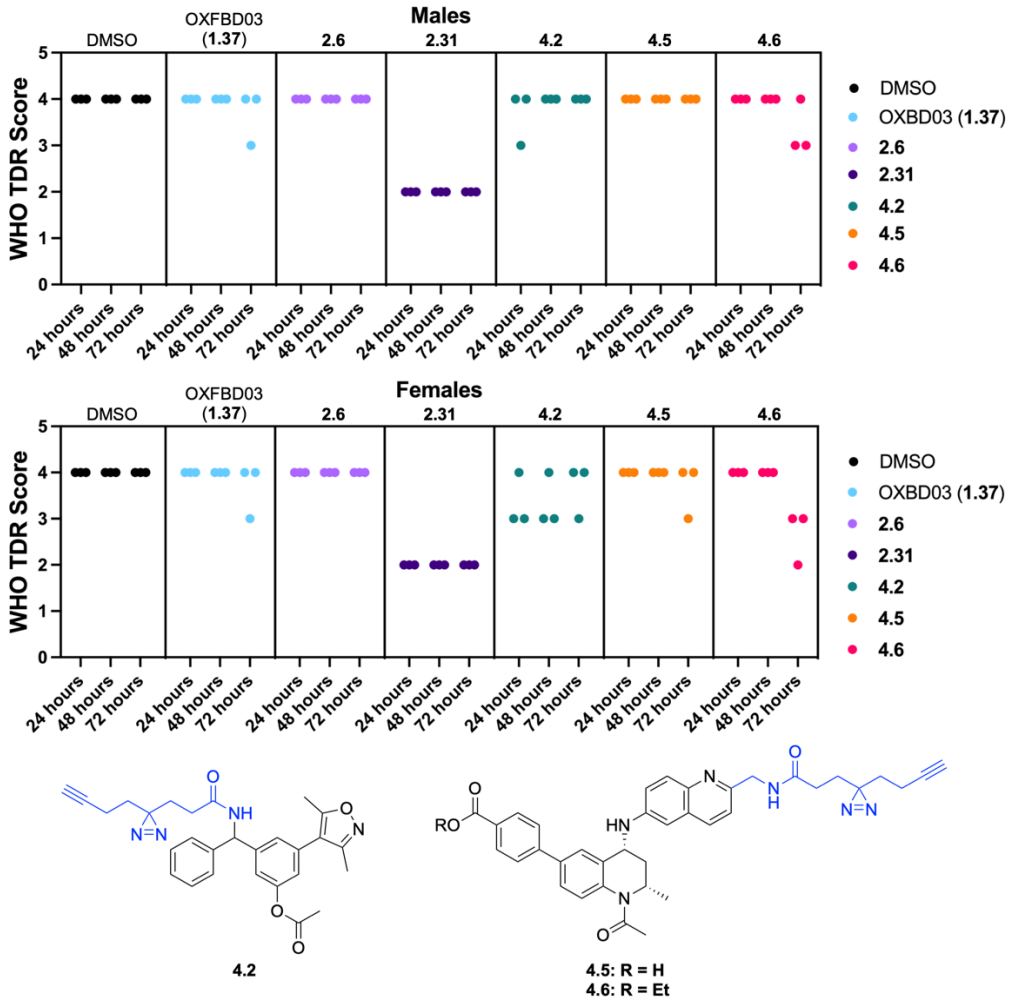


Figure 4.22 The effect of photoaffinity probes **4.2**, **4.5** and **4.6**, compared with their parent compounds **1.37**, **2.6** and **2.31**, on the motility of male and female adult *S. mansoni* after 24, 48 and 72 h incubation, as determined by the WHO TDR scoring system. Phenotypic screening was carried out by J.F.T..

The results indicated that the photoaffinity probes **4.2**, **4.5** and **4.6** affected female worm motility to a higher extent than male worms, however, in all cases the effect difference was minimal. **4.6** showed the largest effect on worm motility out of the photoaffinity probes, however, the effect was not as significant as the 'parent' compound **2.31**. The photoaffinity probe that showed the least effect on worm motility was **4.5**. This result was analogous to the parent ligand **2.6**, which showed no effect on worm motility. Work in **Chapter 2** showed this compound exhibited very poor parasite permeability, likely due to poor physiochemical properties, and therefore it is expected the result observed for **4.5** is also due to poor permeability.

The observation of effects on adult worm motility for compounds **4.2** and **4.6** gave a degree of confidence of parasite permeability and therefore encouraged the pursuit of an in-parasite crosslinking approach. To provide further information of the parasite permeability, a fluorescence-based probe localisation experiment was carried out, using a modified procedure reported by Collins *et al*. for EdU labelling of *S. mansoni*.[158] Male adult *S. mansoni* worms were incubated with probes **4.2**, **4.5** and **4.6** for 24 h and then irradiated under UV light (365 nm) for 10 min. They were then killed, fixed with a formaldehyde solution, and then bleached with formamide bleaching solution and treated with Protinase K to permeabilise the parasites. The parasites were then fixed with formaldehyde solution and washed twice. An in-parasite CuAAC reaction was then carried out using the fluorophore azide AlexaFluor® 488, ascorbic acid and $CuSO_4$, and finally the worms were washed to remove excess fluorophore. The worms were then mounted in medium containing DAPI, to aid in the determination of compound localisation by staining the *S. mansoni* nuclei and visualised using a BioTek Cytation 7 cell imager (**Figure 4.23**). Fluorescence observed for excitation of the AlexaFluor® 488 fluorophore would indicate click reaction between the azide and alkyne of the probe, and therefore would indicate the diazirine probe entered the cell. These experiments were carried out by J.F.T..

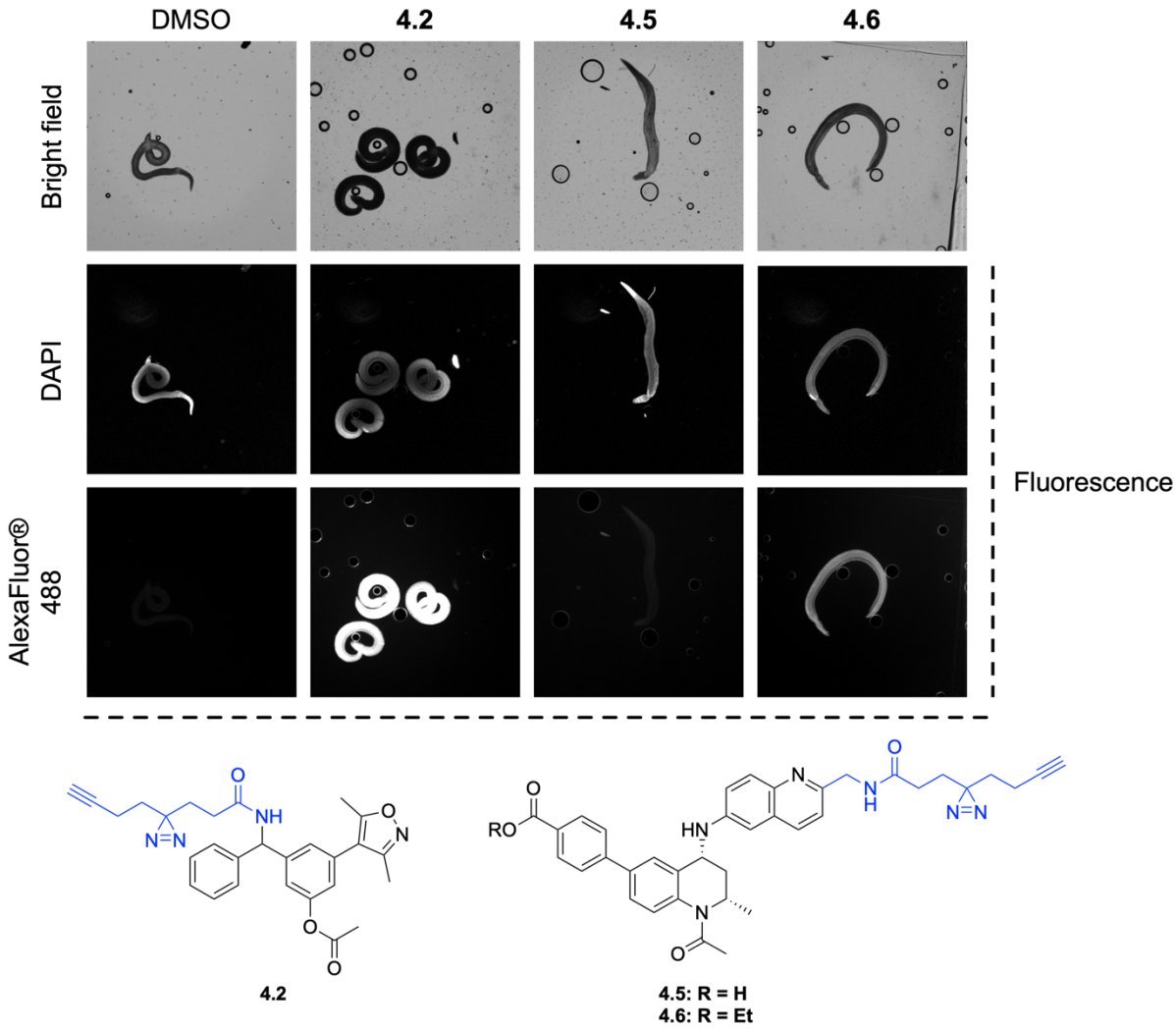


Figure 4.23. Male adult *S. mansoni* worms viewed for visualisation of brightfield (No filter cube, transmitted light), DAPI staining (DAPI filter cube; excitation: 377/50 nm, emission: 447/60 nm) and fluorescence from AlexaFluor® 488 (GFP filter cube; excitation: 469/35 nm, emission 525/39 nm). The worms were prepared and visualised by J.F.T..

Negligible fluorescence was observed for worms incubated with probe **4.5** when excited at 469/35 nm. This strongly suggests the compound does not enter the parasite. The inactivity of **4.5** on adult worm schistosomula can therefore be attributed to negligible parasite permeability. However, worms incubated with **4.2** and **4.6** showed fluorescence when excited at 469/35 nm, indicating both these probes entered the parasite and engaged in a click reaction with the fluorophore azide. The images indicated probes **4.2** and **4.6** were present in the parasite with no specific localisation.

Paraformaldehyde promotes crosslinking between cellular components, and therefore it is likely the fluorescence observed is due to crosslinking of the photoaffinity probes to proteins *via* paraformaldehyde, in addition to possible crosslinking from UV irradiation. Currently, these results only indicate the parasite permeability of these probes, however, a no UV irradiation control could investigate a contribution from UV crosslinking to the observed fluorescence.

With confirmation of probes **4.2** and **4.6** entering the parasite, further work will include the lysis of worms after probe incubation and UV irradiation, using UTB buffer lysis conditions, and analysis of the lysate using SDS-PAGE gel. The observation of in-gel fluorescence would indicate photocrosslinking arising from an in-parasite approach. These experiments could then progress to pull-down studies using a biotin azide and analysis using mass spectrometry.

4.6 Conclusion

The aims of this chapter were to develop photoaffinity probes for the investigation of target engagement and selectivity of *Sm*BRD3 bromodomain ligands. A previously developed photoaffinity probe, **4.2**, was resynthesised using an optimised synthetic route employing a traceless Staudinger reaction. Photoaffinity probes based on the ligands **2.6** and **2.31**, developed in **Chapter 2**, were designed using information from *in silico* docking and synthesised. Probes **4.2**, **4.5** and **4.6** were then evaluated on recombinant *Sm*BRD3(1,2) and *Sm*BRD3(2). **4.2** showed moderate crosslinking to *Sm*BRD3(1,2), and the ITC data indicated this occurred *via* binding to the first domain. This probe was used to show the I-BET726 derivative **2.6** binds to the first domain of *Sm*BRD3(1,2). **4.5** showed a low crosslinking yield to *Sm*BRD3(2) *via* MS analysis, however, CuAAC reaction with an azide fluorophore and in-gel fluorescence analysis using SDS-PAGE showed this was sufficient to observe engagement with *Sm*BRD3(2), *Sm*BRD3(1,2) and the influence of competitor

ligands. Despite low crosslinking yield of **4.5** to *Sm*BRD3(2), it can be concluded from the *in vitro* crosslinking data that probes **4.2** and **4.5** function as photoaffinity probes for *Sm*BRD3, with the capability of CuAAC reactions using the alkyne click handle. In-gel fluorescence indicated engagement of **4.2** and **4.5** with the *S. mansoni* proteome, however, western blot analysis indicated ineffective extraction of the nuclear proteins, and therefore in-gel fluorescence likely arose from unspecific background crosslinking with cytosolic proteins. For the development of an in-parasite crosslinking approach, the permeability of probes **4.2**, **4.5** and **4.6** was investigated, and fluorescence visualisation after an in-parasite click reaction with a fluorophore azide revealed **4.2** and **4.6** entered the parasite. Future work will include continuation of the in-parasite crosslinking approach, with profiling of crosslinked proteins *via* in-gel fluorescence SDS-PAGE and biotin-streptavidin pull-down, enabling identification of interacting proteins using mass spectrometry.

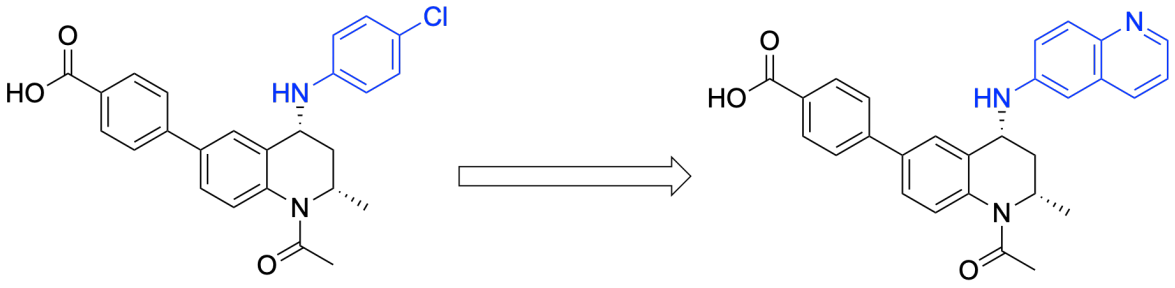
Chapter 5

Conclusions and future work

5.1 Conclusions

The parasite *S. mansoni* undergoes significant phenotypic changes throughout its life cycle, which occur without changes in its genetic code, suggesting a role for epigenetic mechanisms in these processes. At the start of this work, our hypothesis was that ligands for the *S. mansoni* bromodomain containing protein, *Sm*BRD3, could disrupt some epigenetic processes and consequently affect parasite survival and proliferation. The main aims of the work described in this dissertation were to employ a structure-guided approach to develop novel ligands with increased affinity for the *Sm*BRD3 bromodomains, and to use these ligands to elucidate the role of *Sm*BRD3 in *S. mansoni*. If phenotypic effects were observed, we aimed to investigate their cellular targets within *S. mansoni*.

Using the X-ray crystal structure of the human BET-BRD ligand I-BET726 (**1.6**) bound to *Sm*BRD3(2), a small library of compounds was designed with the aim of optimising HFF cleft occupancy. Compounds **2.1**–**2.6** all showed increased affinity for *Sm*BRD3(2), compared with I-BET726 (**1.6**), and the crystal structure of **2.1** bound to *Sm*BRD3(2) confirmed the hypothesis that bicyclic aromatic groups could more effectively occupy the HFF cleft. The result of this work was a quinoline based derivate with a K_d value for *Sm*BRD3(2) of 364 nM, an increase in affinity of approximately 5-fold compared to I-BET726 (**1.6**) (**Figure 5.1**). It can therefore be concluded that targeting the HFF cleft was an effective SAR strategy for increasing *Sm*BRD3(2) affinity.



I-BET726 (**1.6**)

K_d [SmBRD3(2)] = 1850 ± 361 nM

2.6

K_d [SmBRD3(2)] = 364 ± 51.6 nM

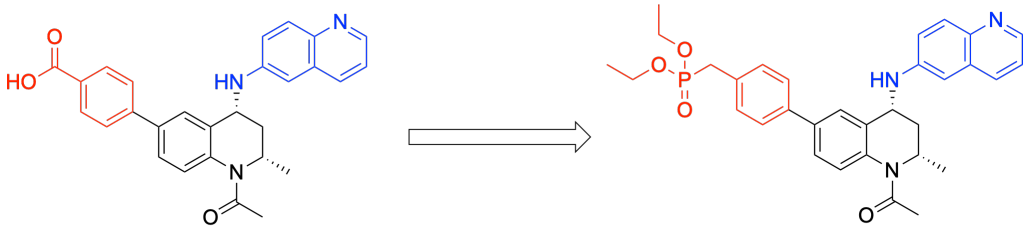
Figure 5.1. The structures of I-BET726 (**1.6**) and **2.6** and their K_d values for *Sm*BRD3(2).

These ligands, and their ethyl ester analogues, were tested in phenotypic screens on *S. mansoni* schistosomula and adult worms. The ethyl ester analogues of the I-BET726 derivatives affected the motility, worm pairing, and oviposition of the adult worms and affected the phenotype and motility of the schistosomula. Interestingly, the ethyl ester derivatives **2.20** and **2.31** affect the transformation of miracidia to sporocysts, a process that involves changes in phenotype without changes in genotype, indicating an effect on epigenetic mechanisms. The enantiomers **2.20** and **2.23** also induced different effects on the schistosomula, adult worm and miracidia life-cycle stages.

It was proposed the ethyl esters of the I-BET726 derivatives, which are not soluble enough for their *Sm*BRD3(2) affinity to be determined using ITC, were acting as prodrugs, and releasing the free acid in the parasite. Treatment of the adult worms with the ethyl ester **2.31** and acid **2.6**, followed by LCMS analysis of the parasite lysate, showed that **2.31** is significantly more permeable than the corresponding acid **2.6**. There was also some evidence the ethyl ester could be converted to the corresponding acid **2.6**, in the presence of the parasite, consistent with the idea that **2.31** can function as a prodrug for **2.6**. Of the human BRD ligands that show high affinity for *Sm*BRD3(1), only (+)-JQ1 (**1.1**) exerted a phenotypic effect. LCMS studies indicated that OXFBD02 (**1.4**), which binds selectively to *Sm*BRD3(1), had a higher worm permeability than the I-BET726 analogue **2.6**. This result indicates that OXFBD02 (**1.4**) can enter the parasite and engage with *Sm*BRD3(1), suggesting that inhibition of *Sm*BRD3(1) alone is insufficient to cause a phenotypic effect, and that (+)-JQ1 (**1.1**) is a promiscuous compound that interacts with multiple *S. mansoni* cellular targets.

To further increase binding affinity to *Sm*BRD3(2), quinoline-based THQ ligands **3.41**–**3.46**, aimed at exploring SAR in the ZA channel region, were designed based on the *in silico* docking and ITC results of an isopropyl carbamate-based THQ library. The ITC results showed the SAR information identified in the isopropyl carbamate ligand series is not additive with SAR revealed in **Chapter 2**, however, new *Sm*BRD3(2) ligands with

nano-molar affinity were identified. Phenotypic screening of these ligands on schistosomula and adult worms showed these compounds were less active than the quinoline based compound **2.31**, however a diethyl phosphonate-based compound, **3.43**, showed the highest activity in the ZA channel targeting compound library. The difference in activity between compound **3.43** and **3.41**, **3.42**, **3.44**–**3.46** was likely, in part, due to parasite permeability. This is influenced by physiochemical properties of these compounds, notably LogD, which is an important consideration for the design of future *Sm*BRD3 chemical probes for *ex vivo* evaluation.



2.31

EC_{50} (μM) [Phenotype] = 4.81 ± 0.0205
EC_{50} (μM) [Motility] = 5.26 ± 0.871

3.43

EC_{50} (μM) [Phenotype] = 6.33 ± 0.856
EC_{50} (μM) [Motility] = 6.25 ± 1.75

Figure 5.2. Structures of **2.31** and **3.43** and corresponding average EC_{50} values (n=2, ± s.e.m) for the phenotype and motility effects on schistosomula.

To assess cellular target engagement with *Sm*BRD3 and investigate other potential targets in the *S. mansoni* proteome, diazirine based photoaffinity pull-down probes were developed (**Figure 5.3**). The ITC results indicated the diazirine probe **4.2**, based on OXFBD03 (**1.37**), binds only to the first domain of *Sm*BRD3(1,2), and this probe was shown to crosslink to *Sm*BRD3(1,2) using mass spectrometry and in-gel fluorescence. Competition experiments using **4.2** qualitatively indicated that the *Sm*BRD3(2) ligand, **2.6**, also binds to *Sm*BRD3(1). A photoaffinity probe based upon **2.6**, **4.5**, was shown to photocrosslink to *Sm*BRD3(2) using mass spectrometry and in-gel fluorescence, and to *Sm*BRD3(1,2) using in-gel fluorescence. Despite a low crosslinking yield of **4.5** to *Sm*BRD3(2), it was concluded probes **4.2** and **4.5** were useful photoaffinity probes for *Sm*BRD3 and were progressed to studies on *S. mansoni* lysate. Probes **4.2** and **4.5** showed target engagement with proteins from the *S. mansoni* proteome *via* in-gel fluorescence, however, competition studies

indicated this resulted from unspecific background photoaffinity labelling, and not engagement with *Sm*BRD3 and other putative off-targets of *Sm*BRD3 ligands. Western blot analysis indicated the parasite lysate primarily contained the cytosolic proteome, and that the nuclear proteins had not been effectively extracted. To provide information for the feasibility of an in-parasite crosslinking approach, the permeability of probes **4.2**, **4.5** and **4.6** was investigated. A fluorescence-based compound localisation experiment demonstrated probes **4.2** and **4.6** entered the parasite, whereas the acid analogue **4.5** did not. This result provides encouragement for future in-parasite crosslinking experiments using **4.2** and **4.6**, which would enable chemoproteomic studies on the *S. mansoni* proteome. For the case of **4.2**, this also gave further evidence that dimethylisoxazole based probes enter adult worms, further suggesting the importance of inhibition of *Sm*BRD3(2), or both domains of *Sm*BRD3, for an effect in phenotype.

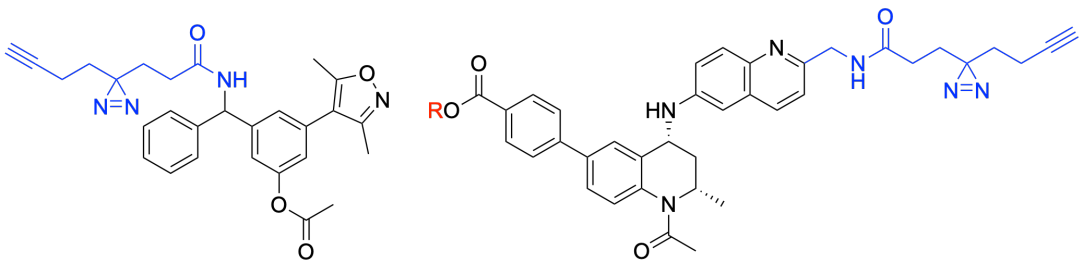


Figure 5.3. Structures of photoaffinity probes **4.2**, **4.5** and **4.6.**

5.2 Future work

Future work could explore further SAR of ligands for *Sm*BRD3(2) with the aim of further increasing affinity, and later with the aim of identifying *Sm*BRD3(2) ligands that have selectivity over the human BET BCPs. A further SAR strategy could be to target the E344 residue, which was proposed to form a hydrogen bond with an amide N-H of photoaffinity probe **4.5**, resulting in approximately 100 nM increase in affinity for *Sm*BRD3(2) compared with its parent ligand **2.6**. Further *Sm*BRD3(2) ligands could exploit this interaction. A similar hydrogen bond was predicted by *in silico* docking of compound **4.4** in the binding pocket of

*Sm*BRD3(2). However, this compound was not synthesised, and therefore the first target molecule for synthesis and binding affinity evaluation for this investigation should be **4.4**.

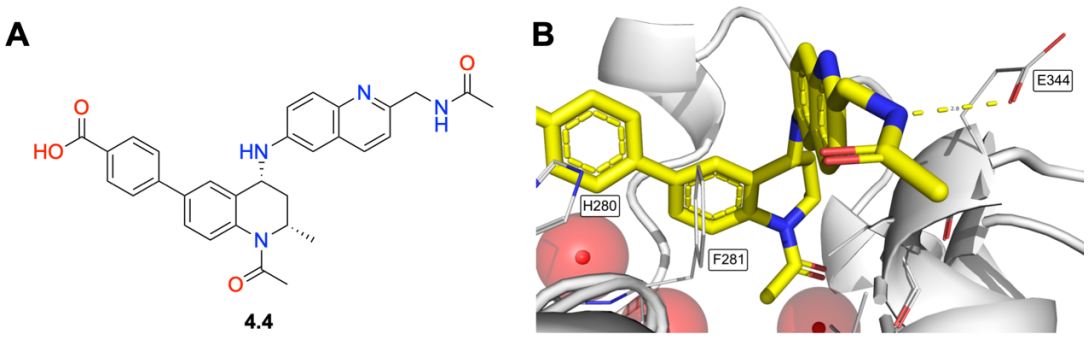


Figure 5.4. A) Structure of amide-based derivative **4.4**. **B**) Highest ranked docking pose of **4.4** bound to SmBRD3(2), indicating a hydrogen bond with E344.

The work described in **Chapter 4** showed qualitatively that the I-BET726 derivative **2.6** bound to the first domain of *Sm*BRD3(1,2). To determine if phenotypic effects of the I-BET726 derivatives are due to primarily *Sm*BRD3(2) inhibition, or inhibition of both *Sm*BRD3(1) and *Sm*BRD3(2), future work could include quantitative measurement of the affinity of the I-BET726 derivatives for *Sm*BRD3(1). In previous work, Dr Matthias Schiedel expressed an *Sm*BRD3(1) construct in *E. coli*, but the protein yield was low, and it was suggested this construct was unstable (**Chapter 1**). To overcome this limitation, mutation of the N339 residue of second domain in the *Sm*BRD3(1,2) to F339 would block binding of ligands the second domain, giving a 'pseudo-*Sm*BRD3(1)'. It is expected biophysical assays of BRD ligands with this construct would provide a quantitative determination of the extent of binding to *Sm*BRD3(1).

To provide more evidence of the pro-drug hypothsis of I-BET726 ethyl ester derivatives, a series of different ester analogues could be synthesised and screened against *S. mansoni* (**Figure 5.5**).

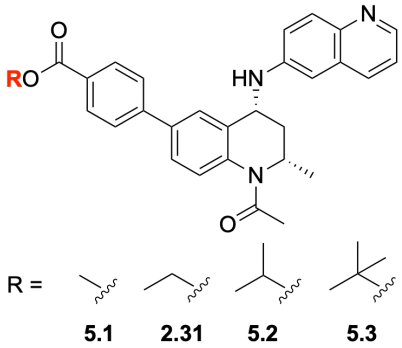


Figure 5.5. Structures of the proposed varying ester-based library.

It is expected increasing the steric bulk of the ester will decrease putative carboxylesterase mediated hydrolysis of these ligands.[159] Further evidence that phenotypic effects are driven by acid analogue **2.6** would be provided if the activity on *S. mansoni* decreases, or the observation of total inactivity, for the *i*-Pr (**5.2**) and ^{t}Bu (**5.3**) esters compared with **2.31** and a methyl ester (**5.1**) analogue.

Immediate future work on diazirine probes for *Sm*BRD3 should involve the pursuit of identifying target engagement of **4.2** and **4.5**/**4.6** with *Sm*BRD3, and the identification of putative off-targets, by an in-parasite crosslinking approach. Further diazirine probes for *Sm*BRD3 can also be developed. It was assumed the activity of (+)-JQ1 (**1.1**) on *S. mansoni* compared with the other *Sm*BRD3(1) ligands was due to off-target effects. This was based on the data from LCMS experiments indicating that OXFBD02 (**1.4**) enters the parasite (**Chapter 2**), and evidence provided in the literature of a number of cellular off targets of (+)-JQ1 (**1.1**) in humans.[64–66] This assumption, however, could be confirmed using a photoaffinity probe based on (+)-JQ1 (**1.1**) to determine the cellular targets of this compound in *S. mansoni*. (+)-JQ1 affected *S. mansoni* in phenotypic screening, so identification of these targets could be beneficial for the development of future chemical probes for *S. mansoni* and antischistosomal compounds.

Compound **4.5** has a low crosslinking yield for *Sm*BRD3(2) (**Chapter 4**) and therefore further probes, based on compounds **2.6** and **2.31**, should also be made with the aim of increasing crosslinking yield to *Sm*BRD3(2), which could aid in showing target engagement with *Sm*BRD3, and identification of off targets for **2.6** and **2.31**. Finally, use of photoaffinity probes based on **2.6**, **2.31** and (+)-JQ1 (**1.1**) with the opposite stereochemistry would be useful to determine stereoselective targets in chemoproteomic studies.

Chapter 6

Experimental

6.1 General Chemistry Methods

Reagents and solvents used were of commercially available reagent grade quality from Sigma-Aldrich, Fluorochem or Alfa Aesar, and used without purification unless otherwise stated. All non-aqueous reactions requiring anhydrous conditions were carried out under an inert atmosphere of argon or nitrogen, unless otherwise stated. Anhydrous solvents were obtained from an MBRAUN MB5 Solvent Purification System and stored over 3 Å molecular sieves under an inert argon atmosphere. Concentration *in vacuo* refers to removal of solvent on a Buchi™ rotary evaporator under reduced pressure in a water bath at 40 °C. Celite® refers to Celite® 545 filter aid, treated with sodium carbonate, flux-calcined (Sigma Aldrich). Brine refers to a saturated aqueous solution of sodium chloride. Petroleum Ether refers to the fraction in the boiling point range 40–60 °C.

^{1}H NMR spectra were measured on a Bruker AVIII HD 400 (400 MHz), AVII 500 (500 MHz), AVIIIHD 600 (600 MHz) or NEO 600 (600 mHz) spectrometer in the stated solvents as a reference for the internal deuterium lock. The chemical shift data for each signal are given as δ in units of parts per million (ppm) relative to tetramethylsilane (TMS) where δ(TMS) = 0.00. The spectra are calibrated using the solvent peak with the data provided by Fulmer *et al*..[160] The multiplicity of each signal is indicated by: s (singlet); d (doublet); t (triplet); q (quartet); m (multiplet); sp (septet) or combinations thereof. The number of protons (n) for a given resonance signal is indicated by nH. Where appropriate, coupling constants (*J*) are quoted in Hz, recorded to the nearest 0.1 Hz. Spectra were assigned using COSY, HSQC and HMBC experiments as necessary. H_aH_b-X refers to diastereotopic protons at position X, where the specific proton is unassigned. Relative stereochemistry was assigned *via* NOESY experiments.

^{13}C NMR spectra were measured on a Bruker AVII 500 (126 MHz), AVIIIHD 600 (151 MHz) or NEO 600 (151 MHz) spectrometer in the stated solvents as a reference for the internal deuterium lock. The chemical shift data for each signal are given as δ in units of parts per

million (ppm) relative to tetramethylsilane (TMS) where δ(TMS) = 0.00. The spectra are calibrated using the solvent peak with the data provided by Fulmer *et al.*[160] The chemical shift is quoted to 1 decimal places, unless two different shifts are indistinguishable, where the shifts are then quoted to 2 decimal places. Spectra were assigned using HSQC and HMBC as necessary.

^{11}B NMR spectra were measured on a Bruker AVIII HD 400 (128 MHz) spectrometer in the stated solvents as a reference for the internal deuterium lock. The chemical shift data for each signal are given as δ in units of parts per million (ppm). The spectra are uncalibrated. Coupling constants (*J*) are quoted in Hz, recorded to the nearest 0.1 Hz.

^{19}F NMR spectra were measured on a Bruker AVIII HD 400 (376 MHz) spectrometer in the stated solvents as a reference for the internal deuterium lock. The chemical shift data for each signal are given as δ in units of parts per million (ppm). The multiplicity of each signal is indicated by: s (singlet); d (doublet); t (triplet); q (quartet); m (multiplet); sp (septet) or combinations thereof. The number of fluorines (n) for a given resonance signal is indicated by nF. The spectra are uncalibrated. Coupling constants (*J*) are quoted in Hz, recorded to the nearest 0.1 Hz.

^{31}P NMR spectra were measured on a Bruker AVIII HD 400 (162 MHz) or NEO 600 (243 MHz) spectrometer in the stated solvents as a reference for the internal deuterium lock. The chemical shift data for each signal are given as δ in units of parts per million (ppm). The spectra are uncalibrated. Coupling constants (*J*) are quoted in Hz, recorded to the nearest 0.1 Hz

Mass spectra were acquired on either an Agilent 6120 (low resolution), Waters LCT Premier XE bench-top, Waters LCT Premier bench-top orthogonal acceleration time-of-flight LC-MS system (low resolution) or Bruker microToF spectrometer (high resolution) using electrospray ionisation (ESI) from solutions of methanol or acetonitrile. *m/z* values are reported in Daltons and followed by their percentage abundance in parentheses.

Melting points were determined using a Griffin capillary tube melting point apparatus or Leica Galen III hot stage microscope and are uncorrected. The solvent(s) from which the sample was crystallised is given in parentheses.

Specific optical rotations were measured using a Schmidt Haensch Unipol polarimeter, using a sodium lamp at 589 nm and a path length of 1.0 dm. The concentration (c) is expressed in g/100 mL (equivalent to g/0.1 dm^3). Specific rotations are denoted $[\alpha]_D^T$ and are given in implied units of 10−1 deg cm^2g^{-1} (where T = ambient temperature in °C).

Analytical high performance liquid chromatography (HPLC): *Method 1* was carried out on a PerkinElmer Flexar system with a Binary LC Pump and UV/vis LC Detector, with detection at 254 nm, using a Dionex Acclaim reverse phase 120 column (C18, 5 µm, 120 Å, 4.6 × 150 mm); [95:5 H_2O: MeCN → 5:95 H_2O: MeCN: H_2O with 0.1% TFA modifier, 10 min; 5 min hold; 1.5 mL min^{-1}]. *Method 2* was carried out on an Agilent 1260 Infinity II® system, with detection at 254 nm, using a Poroshell 120 EC-C18 column [4 µM, 4.6 × 100 mm]; [95:5 H_2O: MeCN → 5:95 H_2O: MeCN with 0.1% formic acid (FA) modifier, 10 min; 5 min hold; 1 mL min^{-1}].

Semi-preparative high performance liquid chromatography (HPLC) was carried out on an Agilent 1260 Infinity II® with an Agilent 5 Prep C18 column [5 µM, 21.2 × 50 mm]; [95:5 H_2O:MeCN with 0.1% FA modifier (1 min), 95:5 H_2O:MeCN → 5:95 H_2O: MeCN with 0.1% FA modifier (10 min), 5 min hold; 20 mL min^{-1}].

Chiral high performance liquid chromatography (HPLC): *Method 1* was carried out on a PerkinElmer Flexar system with a Binary LC Pump and UV/vis LC Detector. *Method 2* was carried out on a Thermofisher/Dionex Ultimate 3000 system comprising of a LPG-3400SD pump, WPS-3000SL autosampler, TCC-3000SD column compartment fitted with the appropriate Daicel Chiralpak column (dimensions: 0.46 cm ø × 25 cm) and corresponding guard column (0.4 cm ø × 1 cm), and a DAD3000 diode array detector, both at 1 $mLmin^{-1}$. The solvent systems and columns used for the chiral separation of each compound are

stated where appropriate, and UV absorbance for both methods was measured at 254 nm. The analysis of samples using *Method 2* was conducted by Pearse Solon (University of Oxford).

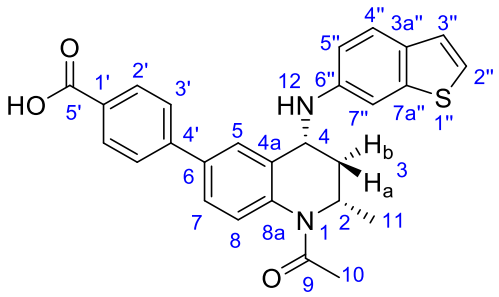
Charged Aerosol Detector (CAD) Solubility assay was carried out by Physchem Team, Discovery Analytical, NCE Molecular Discovery at GSK. 5 µL of 10 mM DMSO stock solution was diluted to 100 µL with pH 7.4 phosphate buffered saline, equilibrated for 1 hour at room temperature and filtered through Millipore Multiscreen$_{HTS}$-PCF filter plates (MSSL BPC). The filtrate was quantified using a suitably calibrated CAD.[131]

Lipophilicity: Chrom logD assay was carried out by Physchem Team, Discovery Analytical, NCE Molecular Discovery at GSK. The Chromatographic Hydrophobicity Index (CHI)[133,134] values were measured using reversed phase HPLC column (50 × 2 mm 3 µM Gemini NX C18, Phenomenex, UK) with fast acetonitrile gradient at starting mobile phase of pHs 2, 7.4 or 10.5. CHI values were derived directly from the gradient retention times using calibration parameters for standard compounds. The CHI value approximates to the volume % organic concentration when the compound elutes. CHI was linearly transformed into a Chrom logD value by least-square fitting of experimental CHI values to calculated ClogP values for over 20,000 research compounds.[132]

6.2 Synthetic procedures and compound data

6.2.1 Compounds from Chapter 2

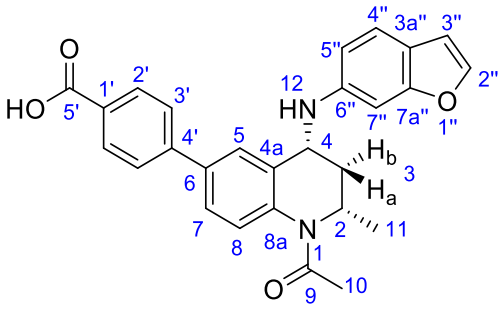
4-{(2*S*,4*R*)-1-Acetyl-4-[(1-benzothiophen-6-yl)amino]-2-methyl-1,2,3,4-tetrahydroquinolin-6-yl}benzoic acid (2.1)



Compound **2.20** (55 mg, 0.113 mmol, 1 eq.) was dissolved in EtOH (0.71 mL). $NaOH_{(aq)}$ (2 M, 565 µL, 1.13 mmol, 10 eq.) was added over 1 h and the resulting solution was left to stir at rt for 3 h. The solution was then acidified to ~ pH 3 with 1 M $HCl_{(aq)}$ and diluted with H_2O (5 mL) and EtOAc (10 mL). The aqueous components were then extracted with EtOAc (3 × 10 mL). The combined organic components were dried over Na_2SO_4, filtered, and concentrated *in vacuo* to give **2.1** as a yellow solid (45 mg, 87%, 94.7% purity by HPLC). To achieve higher purity, **2.1** was purified using semi-preparative HPLC and lyophilised to give **2.1** as an off-white solid: R_f 0.29 (50% EtOAc/petroleum ether, 1% acetic acid); $[\alpha]_D^{25}$ = +308.8 (*c* 0.66, $CHCl_3$); m.p. 115–120 °C (from $CHCl_3$); $\overline{\nu}_{max}$ (thin film)/cm^{-1} 3362 (N-H, w), 3034 (O-H, w), 1704 (C=O, m), 1606 (s), 1488 (m); ^{1}H NMR (400 MHz, CD_3CN) δ_H 8.02–7.94 (2H, m, H-2'), 7.66–7.58 (4H, m, H-7, H-3', H-4''), 7.55 (1H, d, *J* 1.4, H-5), 7.38 (1H, d, *J* 8.2, H-8), 7.19 (1H, dd, *J* 5.5, 0.7, H-3''), 7.16–7.11 (2H, m, H-2'', H-7''), 6.92 (1H, dd, *J* 8.6, 2.2, H-5''), 4.86–4.73 (1H, m, H-2), 4.41 (1H, dd, *J* 12.1, 4.1, H-4), 2.71 (1H, ddd, *J* 12.5, 8.6, 4.1, H_a-3), 2.18 (3H, s, H-10), 1.36–1.24 (1H, m, H_b-3), 1.14 (3H, d, *J* 6.3, H-11); ^{13}C NMR (151 MHz, CD_3CN) δ_C 170.1 (C-9), 167.6 (C-5'), 146.8 (C-6''), 145.8 (C-4'), 142.8 (C-7a''), 139.6 (C-4a), 138.3 (C-8a), 137.6 (C-6), 132.5 (C-3a''), 131.2 (C-2'), 130.0 (C-1'), 127.9 (C-8), 127.7 (C-3'), 126.6 (C-4''), 125.1 (C-7), 124.6 (C-3''), 123.3 (C-5), 122.5 (C-2''),

114.7 (C-5''), 104.6 (C-7''), 50.7 (C-4), 48.7 (C-2), 41.6 (C-3), 23.4 (C-10), 21.7 (C-11); LRMS *m/z* (ESI^-) 455 ($[M–H]^-$, 100%); HRMS *m/z* (ESI^+) [Found: 457.15808, $C_{27}H_{25}O_3N_2{}^{32}S$, requires $[M+H]^+$ 457.15804]; HPLC (Method 2) Retention time = 9.18 min, 99.0%; Chiral HPLC (Method 1), Chiral AD-H column (50:50 hexane/IPA, 1.0 $mLmin^{-1}$) Retention time = 7.3 min (**2.1**, 91.2% UV), Retention time = 11.0 min (opposite enantiomer (**2.33**), 8.8% UV); 82% e.e.

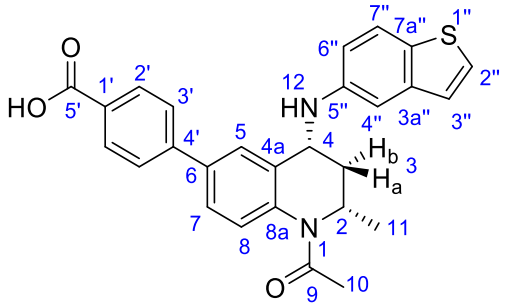
4-((2*S*,4*R*)-1-Acetyl-4-[(1-benzofuran-6-yl)amino]-2-methyl-1,2,3,4-tetrahydroquinolin-6-yl)benzoic acid (2.2)



Compound **2.22** (48 mg, 0.102 mmol, 1.0 eq.) was dissolved in EtOH (0.63 mL). $NaOH_{(aq)}$ (2 M, 0.512 mL, 1.02 mmol, 10 eq.) was added portion-wise over 30 min, and the resulting solution was stirred for 1 h. The solution was then acidified to ~ pH 5 using $HCl_{(aq)}$ (1 M), upon which a precipitate formed, and then extracted with EtOAc (3 × 10 mL). The organic components were dried over Na_2SO_4, filtered, and concentrated *in vacuo*. The crude material was purified using semi-preparative HPLC and the fractions containing **2.2** combined and lyophilised to give **2.2** as a colourless solid (9 mg, 20%): R_f 0.54 (10% MeOH/CH_2Cl_2); $[\alpha]_D^{25}$ = + 177.8 (*c* 0.5, MeOH); m.p. 170–173 °C (from MeOH); $\overline{\nu}_{max}$ (thin film)/cm^{-1} 3404 (N-H, m), 1700 (C=O, m), 1628 (N-H, m); ^{1}H NMR (600 MHz, MeOD) δ_H 8.06–7.95 (2H, m, H-2'), 7.68–7.62 (2H, m, H-5, H-7), 7.59 (2H, d, *J* 8.4 , H-3'), 7.47 (1H, d, *J* 2.2, H-2''), 7.40 (1H, d, *J* 8.1, H-7), 7.36 (1H, d, *J* 9.1, H-4''), 6.83–6.72 (2H, m, H-7'', H-5''), 6.65 (1H, d, *J* 2.1, H-3''), 4.93–4.81 (partially hidden by H_2O peak) (1H, m, H-2), 4.33 (1H, dd, *J* 12.3, 4.1, H-4), 2.74 (1H, ddd, *J* 12.6, 8.6, 4.2, H_a-3), 2.26 (3H, s, H-10), 1.41–1.33 (1H, m, H_b-3), 1.20 (3H, d, *J* 6.4, H-11); ^{13}C NMR (151 MHz, MeOD) δ_C 172.2 (C-9),

170.4 (C-5'), 158.3 (C-7a''), 147.8 (C-6''), 145.9 (C-4'), 143.8 (C-2''), 140.5 (C-4a), 139.3 (C-6), 137.5 (C-8a), 131.7 (C-1'), 131.3 (C-2'), 127.9 (C-8), 127.7 (C-3'), 126.8 (C-5/C-7), 124.1 (C-5/C-7), 122.3 (C-4''), 119.6 (C-3a''), 112.3 (C-5''/C-7''), 107.3 (C-3''), 95.7 (C-5''/C-7''), 51.3 (C-4), 49.6 (C-2), 41.7 (C-3), 23.0 (C-10), 21.5 (C-11); LRMS *m/z* (ESI^-) 439 ($[M-H]^-$, 77%); HRMS *m/z* (ESI^+) [Found: 441.1812, $C_{27}H_{25}O_4N_2$, requires $[M+H]^+$ 441.1809]; HPLC (Method 1) Retention time = 9.7 min, 98.9%; Chiral HPLC (Method 2), Chiral IG-3 column (70:30 hexane/IPA, 0.1% TFA, 1.0 $mLmin^{-1}$) Retention time = 13.8 min (**2.2**, 92.5% UV), Retention time = 18.4 min (opposite enantiomer, 7.5% UV); 85% e.e.

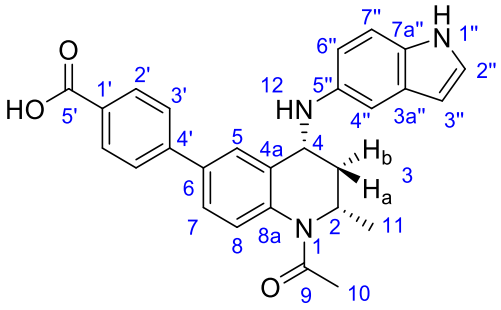
4-((2*S*,4*R*)-1-Acetyl-4-[(1-benzothiophen-5-yl)amino]-2-methyl-1,2,3,4-tetrahydroquinolin-6-yl)benzoic acid (2.3)



Compound **2.21** (36 mg, 0.0742 mmol, 1 eq.) was dissolved in EtOH (0.46 mL). NaOH(aq) (2 M, 0.371 mL, 0.742 mmol, 10 eq.) was added over the course of 30 min and the resulting solution was left to stir for 3 h at rt. After this time the solution was acidified to ~ pH 5, upon which a precipitate formed. EtOAc (10 mL) was added, upon which the precipitate redissolved, and the aqueous and organic components were separated. The aqueous components were extracted with EtOAc (3 × 10 mL) and the combined organic components were dried over Na_2SO_4, filtered, and concentrated *in vacuo*. The crude material was purified using semi-preparative HPLC to give **2.3** as an off-white solid (14 mg, 41%): R_f 0.61 (50% EtOAc/petroleum ether, 1% acetic acid); $[\alpha]_D^{25} =$ +170.1 (*c* 0.37, $CHCl_3$); m.p. 137–143 °C (from $CHCl_3$); $\overline{\nu}_{max}$ (thin film)/cm^{-1} 3352 (N-H, w), 1710 (C=O, m), 1638 (m), 1605 (s), 1513 (m); ^1H NMR (400 MHz, CD_3CN) δ_H 8.03–7.95 (2H, m, H-2'), 7.68 (1H, d, *J* 8.7, H-7''), 7.64–7.59 (3H, m, H-7, H-3'), 7.59–7.57 (1H, m, H-5), 7.44 (1H, d, *J* 5.4, H-2''), 7.39

(1H, d, *J* 8.1, H-8), 7.14 (1H, dd, *J* 5.4, 0.8, H-3''), 7.10–7.08 (1H, m, H-4''), 6.94 (1H, dd, *J* 8.7, 2.3, H-6''), 4.88–4.73 (1H, m, H-2), 4.40 (1H, dd, *J* 12.1, 4.1, H-4), 2.72 (1H, ddd, *J* 12.5, 8.5, 4.1, H_a-3), 2.18 (3H, s, H-10), 1.35–1.24 (1H, m, H_b-3), 1.15 (3H, d, *J* 6.3, H-11); ^{13}C NMR (151 MHz, CD_3CN) δ_C 170.1 (C-9), 167.7 (C-5'), 146.7 (C-5''), 145.7 (C-4'), 142.2 (C-3a''), 139.2 (C-4a), 138.2 (C-8a), 137.7 (C-6), 131.2 (C-2'), 130.2 (C-1'), 130.0 (C-7a''), 128.1 (C-2''), 127.9 (C-8), 127.7 (C-3'), 126.5 (C-7), 124.4 (C-3''), 123.8 (C-7''), 123.4 (C-5), 115.1 (C-6''), 106.1 (C-4''), 50.8 (C-4), 48.7 (C-2), 41.6 (C-3), 23.4 (C-10), 21.7 (C-11); LRMS: *m/z* (ESI$^+$) 457 ([M+H]$^+$, 100%); HRMS *m/z* (ESI$^-$) [Found: 455.14422, $C_{27}H_{23}O_3N_2{}^{32}S$, requires [M–H]$^-$ 455.14349]; HPLC (Method 1) Retention time = 9.97 min, >99.9%; Chiral HPLC (Method 2), Chiral IG-3 column (70:30 hexane/IPA, 0.1% TFA, 1.0 mLmin^{-1}) Retention time = 15.0 min (**2.3**, 92.4% UV), Retention time = 18.5 min (opposite enantiomer, 7.6% UV); 85% e.e.

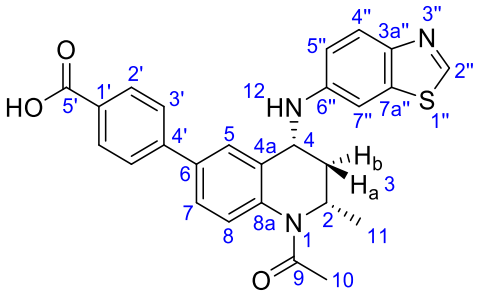
4-{(2*S*,4*R*)-1-Acetyl-4-[(1*H*-indol-5-yl)amino]-2-methyl-1,2,3,4-tetrahydroquinolin-6-yl}benzoic acid (2.4)



Compound **2.30** (27 mg, 0.0577 mmol, 1.00 eq.) was dissolved in EtOH (0.36 mL). $NaOH_{(aq)}$ (2 M, 289 µL, 0.577 mmol, 10.0 eq.) was added portion wise. A precipitate developed, which was redissolved with addition of further EtOH (0.76 mL), and the resulting solution was stirred for 3 h. Further $NaOH_{(aq)}$ (2 M, 578 µL, 1.16 mmol, 20.0 eq.) was added over a period of 1.5 h, after which time the reaction solution was diluted with CH_2Cl_2 (5 mL) and H_2O (5 mL), and the aqueous and organic layers were separated. The aqueous components were acidified to approximately pH 3, then and extracted with EtOAc (3 × 10 mL). The organic components were dried over Na_2SO_4, filtered, and concentrated *in vacuo*. The crude

material was purified using silica gel flash column chromatography (reverse phase, 5–40% MeCN/H_2O) and the pure fractions lyophilized to give **2.4** as a yellow solid (8.2 mg, 32%): R_f 0.24 (50% MeCN/H_2O; reverse phase); $[\alpha]_D^{25}$ = +197.0 (*c* 0.29, MeOH); mp 176–179 °C (lyophilised from MeCN/H_2O); $\overline{\nu}_{max}$ (thin film)/cm^{-1} 3401 (N-H, br, m), 2924 (C-H, w), 1703 (C=O, s), 1631 (C=O, s);^{1}H NMR (400 MHz, MeOD) δ_H 8.45 (1H, s, H-1''), 8.01–7.96 (2H, m, H-2'), 7.77–7.75 (1H, m, H-5), 7.63 (1H, dd, *J* 8.2, 2.2, H-7), 7.61–7.57 (2H, m, H-3'), 7.38 (1H, d, *J* 8.2, H-8), 7.25 (1H, d, *J* 8.6, H-7''), 7.11 (1H, d, *J* 3.1, H-2''), 6.90–6.88 (1H, m, H-4''), 6.79 (1H, dd, *J* 8.6, 2.2, H--6''), 6.25 (1H, dd, *J* 3.1, 0.9, H-3''), 4.90–4.78 (1H, hidden by H_2O peak, H-2), 4.30 (1H, dd, *J* 12.2, 4.1, H-4), 2.74 (1H, ddd, *J* 12.5, 8.6, 4.1, H_a-3), 2.25 (3H, s, H-10), 1.37–1.25 (1H, m, H_b-3), 1.19 (3H, d, *J* 6.3, H-11); ^{13}C NMR (151 MHz, MeOD) δ_C 172.2 (C-9), 170.7 (C-5'), 145.8 (C-4'), 142.3 (C-5''), 141.1 (C-4a), 139.2 (C-1'), 137.5 (C-8a), 132.4 (C-7a''), 131.9 (C-6), 131.3 (C-2'), 130.3 (C-3a''), 127.7 (C-3'), 126.5 (C-7), 125.8 (C-2''), 124.3 (C-5), 113.2 (C-6''), 112.8 (C-7''), 104.5 (C-4''), 101.5 (C-3''), 52.3 (C-4), 49.6 (C-2), 41.8 (C-3), 23.0 (C-10), 21.5 (C-11); LRMS *m/z* (ESI^-) 438 ([M–H]$^-$, 8%); HRMS *m/z* (ESI^-) [Found: 438.1832, $C_{27}H_{24}0_3N_3$ requires [M–H]$^-$ 438.1823]; HPLC (Method 1) Retention time = 6.9 min, 97.9%; Chiral HPLC (Method 2), Chiral IG-3 column (70:30 hexane/IPA, 0.1% TFA, 1.0 $mLmin^{-1}$) Retention time = 15.4 min (**2.4**, 89.6% UV), Retention time = 19.8 (opposite enantiomer, 10.4% UV); 79% e.e.

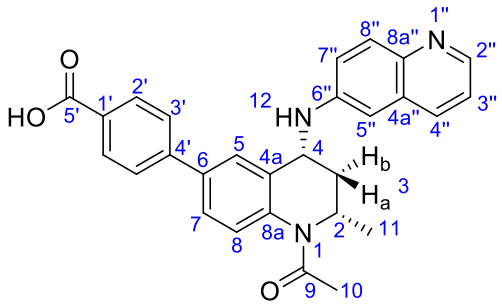
4-{(2*S*,4*R*)-1-Acetyl-4-[(1,3-benzothiazol-6-yl)amino]-2-methyl-1,2,3,4-tetrahydroquinolin-6-yl}benzoic acid (2.5)



Compound **2.32** (61 mg, 0.126 mmol, 1 eq.) was dissolved in EtOH (0.79 mL) and to this solution, $NaOH_{(aq)}$ (2 M, 0.63 mL, 1.26 mmol, 10 eq.) was added portion wise. The solution

was stirred for 1 h 20 min, after which time, $HCl_{(aq)}$ (1 M) was added until a red precipitate formed. The precipitate was redissolved in EtOAc (10 mL) and the solution diluted with H_2O (5 mL). The aqueous and organic components were separated, and the aqueous component was extracted with EtOAc (3 × 10 mL). The combined organic components were dried over Na_2SO_4, filtered, and concentrated *in vacuo*. The crude material was purified using silica gel flash column chromatography (reverse phase, 5–31% MeCN/H_2O) and lyophilised to give **2.5** as an orange-brown powder (40 mg, 69%): R_f 0.23 (50% MeCN/H_2O); $[\alpha]_D^{25}$ = +318.2 (*c* 1.0, MeOH); m.p. 168–172 °C (lyophilised from MeCN/H_2O); $\overline{\nu}_{max}$ (thin film)/cm^{-1} 3358 (N-H, br, w), 3074 (O-H, br, w), 1702 (C=O, m), 1636 (N-H, m); ^{1}H NMR (400 MHz, MeOD) δ_H 8.82 (1H, s, H-2''), 8.01–7.98 (2H, m, H-2'), 7.83 (1H, d, *J* 8.9, H-4''), 7.65 (1H, dd, *J* 8.2, 2.2, H-7), 7.61–7.57 (3H, m, H-5, H-3'), 7.42 (1H, d, *J* 8.2, H-8), 7.22 (1H, d, *J* 2.3, H-7''), 7.07 (1H, dd, *J* 8.9, 2.3, H-5''), 4.96–4.83 (1H, m, H-2) (partially hidden by H_2O peak), 4.41 (1H, dd, *J* 12.2, 4.2, H-4), 2.75 (1H, ddd, *J* 12.5, 8.5, 4.2, H_a-3), 2.27 (3H, s, H-10), 1.44–1.36 (1H, m, H_b-3), 1.20 (3H, d, *J* 6.3, H-11); ^{13}C NMR (151 MHz, MeOD) δ_C 172.2 (C-10), 169.8 (C-5'), 151.7 (C-2''), 148.4 (C-6''), 146.4 (C-3a''), 146.1 (C-4'), 139.9 (C-4a), 139.2 (C-6), 137.7 (C-8a), 137.1 (C-7a''), 131.4 (C-2'), 131.1 (C-1'), 128.0 (C-8), 127.8 (C-3'), 126.9 (C-7), 124.1 (C-4''), 123.8 (C-5), 116.2 (C-5''), 103.4 (C-7''), 50.9 (C-4), 49.6 (C-2), 41.7 (C-3), 23.0 (C-10), 21.5 (C-11); LRMS *m/z* (ESI^+) 458 ($[M+H]^+$, 42%); HRMS *m/z* (ESI^-) [Found: 456.1386, $C_{26}H_{23}N_3O_3S$, requires $[M-H]^-$ 456.1387]; HPLC (Method 1) Retention time = 8.2 min, 99.1%; Chiral HPLC (Method 1), Chiral AD-H column (40:60 hexane/IPA, 1.0 $mLmin^{-1}$) Retention time = 5.9 min (opposite enantiomer, 7.8% UV), Retention time = 7.8 min (**2.5**, 92.2% UV); 84% e.e.

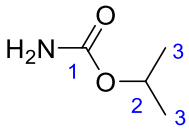
4-{(2*S*,4*R*)-1-Acetyl-2-methyl-4-[(quinolin-6-yl)amino]-1,2,3,4-tetrahydroquinolin-6-yl}benzoic acid (2.6)



Compound **2.31** (51 mg, 0.106 mmol, 1 eq.) was dissolved in EtOH (0.66 mL), $NaOH_{(aq)}$ (2 M, 0.53 mL, 1.06 mmol, 10 eq.) was added dropwise, and the resulting solution was left to stir for 2.5 h. After this time, the solution was acidified to approximately pH 5 using $HCl_{(aq)}$ (1 M), and the aqueous solution was extracted with EtOAc (5 × 10 mL). The combined organic components were dried over Na_2SO_4, filtered, and concentrated *in vacuo*. The crude material was purified using silica gel flash column chromatography (reverse phase, 5–36% MeCN/H_2O) and lyophilised to give **2.6** as a yellow-green solid (17 mg, 36%, 94.7% purity by HPLC). To achieve a higher purity, **2.6** was further purified by semi-preparative HPLC and lyophilised (>99.9% by HPLC). R_f 0.38 (50% MeCN/H_2O; reverse phase); $[\alpha]_D^{25}$ = +369.7 (*c* 0.12, MeOH); mp 194–197 °C (from MeOH); $\overline{\nu}_{max}$ (thin film)/cm^{-1} 3342 (N-H, br, w), 2970 (O-H, br, w), 1703 (C=O, m), 1625 (N-H, s); ^{1}H NMR (600 MHz, MeOD) δ_H 8.47 (1H, dd, *J* 4.3, 1.6, H-2''), 8.07–8.02 (1H, m, H-4''), 7.98 (2H, d, *J* 8.1, H-2'), 7.83 (1H, d, *J* 9.1, H-8''), 7.66 (1H, dd, *J* 8.2, 2.2, H-7), 7.60–7.58 (1H, m, H-5), 7.57 (2H, d, *J* 8.1, H-3'), 7.47–7.40 (2H, m, H-8, H-7''), 7.32 (1H, dd, *J* 8.3, 4.3, H-3''), 6.86 (1H, d, *J* 2.6, H-5''), 4.97–4.87 (1H, m, H-2), 4.49 (1H, dd, *J* 12.1, 4.2, H-4), 2.79 (1H, ddd, *J* 12.5, 8.5, 4.2, H_a-3), 2.29 (3H, s, H-10), 1.49–1.39 (1H, m, H_b-3), 1.22 (3H, d, *J* 6.3, H-11); ^{13}C NMR (151 MHz, MeOD) δ_C 172.2 (C-9), 169.7 (C-5'), 148.3 (C-6''), 146.0 (C-4'), 145.5 (C-2''), 142.2 (C-8a''), 139.4 (C-4a), 139.2 (C-6), 137.7 (C-8a), 137.1 (C-4''), 132.2 (C-4a''), 131.4 (C-2'), 131.0 (C-1'), 128.9 (C-8''), 128.1 (C-5''), 127.8 (C-3'), 127.0 (C-7), 123.8 (C-7''), 123.7 (C-5), 122.7 (C-3''), 104.2 (C-5''), 50.6 (C-4), 49.6 (C-2), 41.6 (C-3), 23.1 (C-10), 21.5 (C-11); LRMS *m/z*

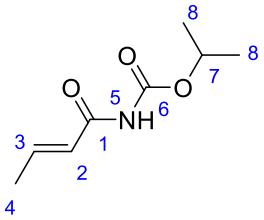
452 (ESI^+) ($[M+H]^+$, 100%) ; HRMS *m/z* (ESI^+) [Found: 452.1972, $C_{28}H_{26}N_3O_3$, requires $[M+H]^+$ 452.1969]; HPLC (Method 1) Retention time = 6.8 min, >99.9%; Chiral HPLC (Method 2), Chiral IG-3 column (70:30 hexane/IPA, 1.0 $mLmin^{-1}$) Retention time = 17.2 min (**2.6**, 91.3% UV), Retention time = 23.9 (opposite enantiomer, 8.7% UV); 83% e.e.

Isopropyl carbamate (2.8) [120,161,162]



Using a modified version of the procedure reported by Laurin *et al.*,[120] trifluoroacetic acid (TFA) (17.0 mL, 222 mmol, 1.7 eq.) was added to a solution of isopropyl alcohol (10.0 mL, 131 mmol, 1.0 eq.) and NaOCN (12.6 g, 195 mmol, 1.5 eq.) in toluene (40 mL) cooled to 0 °C. The resulting suspension was warmed to rt and stirred for 4 h. After this time, H_2O (100 mL) was added and the mixture was extracted with EtOAc (2 × 150 mL). The combined organic components were washed with brine (150 mL), dried over $MgSO_4$, filtered, and concentrated *in vacuo* to yield colourless crystals of isopropyl carbamate (**2.8**) (10.7 g, 79%), which was used without further purification: R_f 0.31 (20% EtOAc/petroleum ether); m.p. 82–84 °C (from EtOAc) [lit.[161] 88–90 °C, lit .[162] 89–93 °C, lit.[120] 90–92 °C]; ^1H NMR (400 MHz, $CDCl_3$) δ_H 4.89 (1H, sp, *J* 6.3, H-2), 4.58 (2H, br s, H-1), 1.24 (6H, d, *J* 6.3, H-3); LRMS *m/z* (ESI^+) 126 ($[M+Na]^+$, 20%). These data are in good agreement with the literature values.[120,161,162]

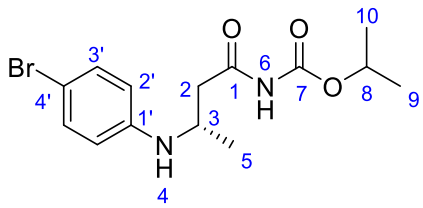
Isopropyl (*E*)-but-2-enoylcarbamate (2.9) [32,120,123]



Using a procedure reported by Shadrick *et al.*,[123] crotonoyl chloride (4.8 mL, 50 mmol, 1.1 eq.) was added to a solution of compound **2.8** (4.6 g, 45 mmol, 1.0 eq.) in anhydrous

THF (43 mL) at −78 °C, followed by LiHMDS (1 M in THF, 90 mL, 90 mmol, 2.0 eq.). The reaction mixture was warmed to rt and was stirred for 16 h. After this time, the reaction was quenched by the addition of chilled saturated $NH_4Cl_{(aq)}$ (50 mL). The resulting solution was extracted with EtOAc (3 × 50 mL). The combined organic components were washed with brine (50 mL), dried over $MgSO_4$, filtered, and concentrated *in vacuo*. The crude material was purified using flash column chromatography (0–20% EtOAc/petroleum ether) to give compound **2.9** as a colourless solid (4.7 g, 61%): R_f 0.39 (17% EtOAc/petroleum ether); m.p. 75–78 °C (from EtOAc) [lit.[123] 91 °C, lit.[120] 72–74 °C]; $\overline{\nu}_{max}$ (neat)/cm^{-1} 3285 (N-H, w), 2980 (C-H, s), 1765 (C=O, s), 1682 (C=O, w), 1647 (C=C, s); ^{1}H NMR (400 MHz, $CDCl_3$) δ_H 7.23 (1H, s, H-5), 7.13 (1H, dq, *J* 15.3, 6.9, H3); 6.87 (1H, dq, *J* 15.3, 1.7, H-2), 4.99 (1H, sp, *J* 6.3, H-7), 1.94 (3H, dd, *J* 6.9, 1.7, H-4), 1.29 (6H, d, *J* 6.3, H-8); ^{13}C NMR (151 MHz, $CDCl_3$) δ_C 166.1 (C-1), 151.5 (C-6), 146.4 (C-3), 123.1 (H-2), 70.4 (C-7), 21.9 (C-8), 18.5 (C-4); LRMS *m/z* (ESI$^+$) 194 ([M+Na]$^+$, 100%); HRMS *m/z* (ESI$^+$) [Found: 194.0786, $C_8H_{13}O_3NNa$, requires [M+Na]$^+$ 194.0788]. These data are in good agreement with the literature values.[32,120,123]

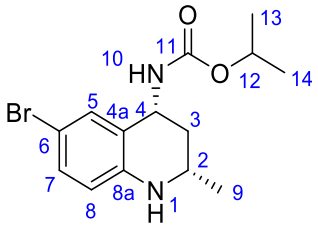
Isopropyl (*S*)-(3-(4'-bromoanilinyl)butanoyl)carbamate (2.10) [32,120,123]



(*R*)-BINAP(OTf)$_2$(H$_2$O)$_2$Pd (728 mg, 0.685 mmol, 0.06 eq.) was added to a solution of compound **2.9** (2.00 g, 11.7 mmol, 1.0 eq.) in anhydrous, de-gassed, toluene (36 mL) and the resulting suspension was stirred at rt for 20 min. 4-Bromoaniline (3.54 g, 20.6 mmol, 1.8 eq.) was then added and the reaction mixture was stirred for a further 21 h. After this time, the reaction mixture was concentrated *in vacuo* and purified using flash column chromatography (0–20% EtOAc/petroleum ether) to give **2.10** as a colourless solid (3.82 g, 95%): R_f 0.16 (20% EtOAc/petroleum ether); $[\alpha]_D^{25}$ = −6.7 (*c* 1.0, MeOH); m.p. 62–68 °C

(from EtOAc) [lit.[123] 131 °C, lit.[120] 128–130 °C]; $\overline{\nu}_{max}$ (neat)/cm^{-1} 3266 (N-H, w), 1748 (C=O, s), 1178 (C-O, m); ^{1}H NMR (400 MHz, $CDCl_3$) δ_H 7.36 (1H, br s, H-6), 7.26–7.21 (2H, m, H-3'), 6.52–6.48 (2H, m, H-2'), 5.02–4.92 (1H, m, H-8), 4.04–3.94 (1H, m, H-3), 3.94–3.84 (1H, m, H-4), 3.09 (1H, dd, *J* 16.0, 5.9, H_aH_b-2), 2.89 (1H, dd, *J* 16.0, 5.9, H_aH_b-2), 1.30–1.26 (9H, m, H-5, H-9, H-10); ^{13}C NMR (151 MHz, $CDCl_3$) δ_C 172.8 (C-1), 151.4 (C-7), 145.9 (C-1'), 132.2 (C-3'), 115.5 (C-2'), 109.5 (C-4'), 70.7 (C-8), 46.2 (C-3), 42.0 (C-2), 21.9 (C-9/10), 20.8 (C-5); LRMS *m/z* (ESI$^-$) 341 ([M^{79}Br−H$^+$]$^-$, 100%), 343 ([M^{81}Br−H$^+$]$^-$, 81%); HRMS *m/z* (ESI$^+$) [Found: 343.0647, $C_{14}H_{20}O_3N_2{}^{79}Br$, requires [M+H]$^+$ 343.0652]; Chiral HPLC (Method 1), Chiral AD-H column (80:20 heptane/ethanol, 0.1% DEA, 1.0 mLmin^{-1}) Retention time = 11.0 min (**2.10**, 96.7% UV), Retention time = 16.3 min (opposite enantiomer (**2.15**), 3.3% UV); 93% e.e. These data are in good agreement with the literature values.[32,120,123]

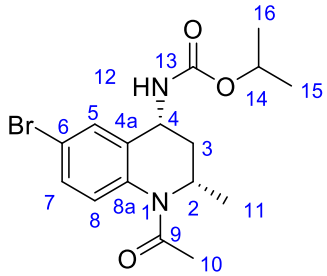
Isopropyl ((2*S*,4*R*)-6-bromo-2-methyl-1,2,3,4-tetrahydroquinolin-4-yl)carbamate (2.11) [32,120,123]



Sodium borohydride (229 mg, 6.05 mmol, 0.75 eq.) was added to a solution of compound **2.10** (2.77 g, 8.07 mmol, 1.0 eq.) in EtOH (143 mL), cooled to a temperature below −10 °C, followed by addition of $MgCl_2{\cdot}6H_2O$ (1.81 g, 8.89 mmol, 1.1 eq.) in water (14.3 mL). The reaction mixture was stirred at a temperature below 0 °C for 2 h and then warmed to rt and stirred for 1 h. The resulting suspension was poured into a mixture of citric acid (60 mL, 0.5 M in water), $HCl_{(aq)}$ (205 mL, 1 M) and CH_2Cl_2 (200 mL) and left to stir for 1 h. After this time, the layers were separated, the aqueous layer extracted with CH_2Cl_2 (3 × 150 mL), and the combined organic components dried over $MgSO_4$, filtered, and concentrated *in vacuo* to give compound **2.11** as a colourless solid (2.60 g, 98%): R_f 0.68 (30% EtOAc/toluene);

$[\alpha]_D^{25}$ = +12.9 (*c* 1.0, MeOH), m.p. 130–136 °C (from toluene) [lit.[123] 167°C, lit.[120] 148–150 °C]; $\overline{\nu}_{max}$ (neat)/cm^{-1} 3309 (N-H, m), 2980 (C-H, s), 1684 (C=O, s); ^{1}H NMR (400 MHz, D_6-DMSO) δ_H 7.38 (1H, d, *J* 9.1, H-10), 7.02 (1H, dd, *J* 8.6, 2.4, H-7), 6.95–6.92 (1H, m, H-5), 6.41 (1H, d, *J* 8.6, H-8), 5.89 (1H, br s, H-1), 4.87–4.79 (1H, m, H-12), 4.77–4.67 (1H, m, H-4), 3.48–3.39 (1H, m, H-2), 1.95–1.85 (1H, m, H_aH_b-3), 1.49–1.40 (1H, m, H_aH_b-3), 1.23 (3H, d, *J* 6.2, H-13/14), 1.20 (3H, d, *J* 6.2, H-13/14), 1.11 (3H, d, *J* 6.2, H-9); ^{13}C NMR (151 MHz, D_6-DMSO) δ_C 156.4 (C-11), 144.2 (C-8a), 129.9 (C-7), 128.6 (C-5), 124.5 (C-4a), 115.6 (C-8), 106.7 (C-6), 66.1 (C-12), 46.2 (C-4), 40.1 (C-2), 36.5 (C-3), 22.0 (C-13/14), 21.5 (C-9); LRMS *m/z* (ESI$^+$) 327 ([M^{79}Br+H$^+$]$^+$, 73%)**;** HRMS *m/z* (ESI$^+$) [Found: 327.0703, $C_{14}H_{20}O_2N_2{}^{79}Br$, requires [M+H]$^+$ 327.0703]; Chiral HPLC (Method 1), Chiral AD-H column (90:10 heptane/ethanol, 0.1% DEA, 1.0 mLmin^{-1}) Retention time = 8.1 min (**2.11**, 94.3% UV), Retention time = 11.5 min (opposite enantiomer (**2.16**), 5.7% UV); 89% e.e. These data are in good agreement with the literature values.[32,120,123]

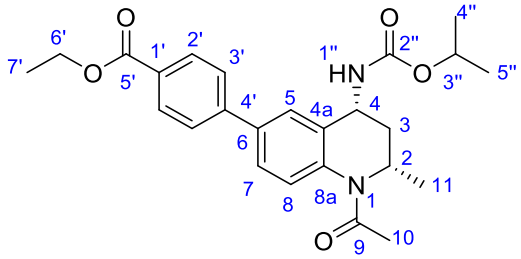
Isopropyl ((2*S*,4*R*)-1-acetyl-6-bromo-2-methyl-1,2,3,4-tetrahydroquinolin-4-yl)carbamate (2.12) [32,120,123]



Compound **2.11** (2.18 g, 6.36 mmol, 1.0 eq.), was dissolved in CH_2Cl_2 (60 mL) under N_2 at room temperature. Pyridine (1.66 mL, 20.5 mmol, 3.2 eq.) was added followed by dropwise addition of acetyl chloride (0.75 mL, 10.5 mmol, 1.7 eq.). The reaction mixture was stirred for 40 min. The reaction mixture was partitioned between EtOAc (250 mL) and saturated $NaHCO_{3(aq)}$ (250 mL). The aqueous layer was extracted with EtOAc (3 × 200 mL), and the combined organic components washed with water and brine, dried over Na_2SO_4, filtered then concentrated *in vacuo* to give compound **2.12** as a brown solid, which was judged to

be pure enough to use in the next step without further purification (2.10 g, 90%). R_f 0.27 (50% EtOAc/petroleum ether); $[\alpha]_D^{25}$ = +209.9 (*c* 1.0, MeOH); m.p. 105–106 °C (from EtOAc) [lit.[123] 163 °C, lit.[120] 141–143 °C]; $\overline{\nu}_{max}$ (neat)/cm^{-1} 3334 (N-H, w), 1688 (C=O, s), 1660 (C=O, s); ^{1}H NMR (400 MHz, D_6-DMSO) δ_H 7.63 (1H, d, *J* 8.6, H-12), 7.47 (1H, dd, *J* 8.4, 2.3, H-7), 7.30 (1H, d, *J* 8.4, H-8), 7.21 (1H, d, *J* 2.3, H-5), 4.87–4.79 (1H, m, H-14), 4.67–4.56 (1H, m, H-2), 4.40–4.31 (1H, m, H-4), 2.44 (1H, ddd, *J* 12.7, 8.6, 4.3, H_aH_b-3), 2.05 (3H, s, H-10), 1.25 (3H, d, *J* 6.3, H-15/16), 1.22 (3H, d, *J* 6.3, H15/16), 1.20–1.14 (1H, m, H_aH_b-3), 1.01 (3H, d, *J* 6.3, H-11); ^{13}C NMR (151 MHz, D_6-DMSO) δ_C 168.4 (C-9), 155.7 (C-13), 139.2 (C-4a), 135.5 (C-8a), 129.6 (C-7), 128.2 (C-8), 125.6 (C-5), 117.9 (C-6), 67.3 (C-14), 47.0 (C-2), 46.7 (C-4), 39.8 (C-3, hidden by D_6-DMSO multiplet, assigned *via* HSQC), 22.6 (C-10), 22.0 (C-15/16), 21.3 (C-11); LRMS *m/z* (ESI)$^+$ 391 ([M^{79}Br+Na]$^+$, 100%); HRMS *m/z* (ESI$^+$) [Found: 369.0803, $C_{16}H_{22}O_3N_2{}^{79}Br$, requires [M+H]$^+$ 369.0808]. These data are in good agreement with the literature values.[32,120,123]

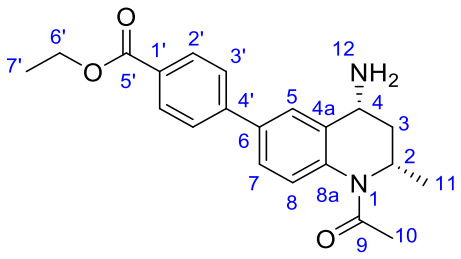
Ethyl 4-((2*S*,4*R*)-1-acetyl-4-((isopropoxycarbonyl)amino)-2-methyl-1,2,3,4-tetrahydroquinolin-6-yl)benzoate (2.13) [32]



A solution of compound **2.12** (1.10 g, 2.98 mmol, 1.0 eq.), {4-[(ethyloxy)carbonyl]-phenyl}boronic acid (0.609 g, 3.14 mmol, 1.05 eq.) and $Pd(Ph_3)_4$ (57 mg, 0.0493 mmol, 0.017 eq.) in DME (11.7 mL) was treated with an aqueous solution of Na_2CO_3 (2 M, 5.87 mL, 11.7 mmol, 3.9 eq.). The mixture was degassed and heated at 105 °C under argon for 2.5 h. After this time the mixture was cooled to rt and partitioned between EtOAc and water. The layers were separated, and the aqueous layer extracted with EtOAc (3 × 100 mL). The combined organic components were washed with water, brine, dried over Na_2SO_4, filtered,

and concentrated *in vacuo* to give a grey-brown solid. This solid was re-dissolved in EtOAc and filtered through a silica plug eluting with a 1:1 EtOAc/petroleum ether mixture. The eluents containing the product were concentrated *in vacuo* to give **2.13** as a colourless solid (1.19 g, 91%). R_f 0.31 (25% acetone/petroleum ether); $[\alpha]_D^{25}$ = +272.6 (*c* 1.0, MeOH); m.p. 73–75 °C (from acetone); $\overline{\nu}_{max}$ (neat)/cm^{-1} 3324 (N-H, w), 1718 (C=O, s), 1695 (C=O, s), 1659 (C=O, s), 1609 (N-H, m); ^{1}H NMR (400 MHz, D_6-DMSO) δ_H 8.08–8.04 (2H, m, H-2'), 7.83–7.78 (2H, m, H 3'), 7.70 (1H, d, *J* 8.7, H-1''), 7.65 (1H, dd, *J* 8.3, 2.1, H-7), 7.48–7.44 (2H, m, H-5, H-8), 4.89–4.81 (1H, m, H-3''), 4.70–4.61 (1H, m, H-2), 4.48–4.40 (1H, m, H-4), 4.34 (2H, q, *J* 7.1, H-6'), 2.48–2.44 (1H, m, H_aH_b-3) (partially hidden by DMSO peak), 2.10 (3H, s, H-10), 1.34 (3H, t, *J* 7.1, H-7'), 1.28–1.21 (6H, m, H-4''/5''), 1.21–1.16 (1H, m, H_aH_b-3), 1.06 (3H, d, *J* 6.3, H-11); ^{13}C NMR (151 MHz, D_6-DMSO) δ_C 168.5 (C-9), 165.5 (C-5'), 155.9 (C-2''), 144.3 (C-4'), 137.1 (C-4a), 136.4 (C-8a), 135.7 (C-6), 129.9 (C-2'), 128.7 (C-1'), 126.7 (C-3'), 126.6 (C-8), 125.5 (C-7), 121.3 (C-5), 67.2 (C-3''), 60.7 (C-6'), 47.1 (C-2), 46.9 (C-4), 40.1 (C-3), 22.7 (C-10), 22.04 (C-4''/5''), 22.01 (C-4''/5''), 21.4 (C-11), 14.2 (C-7'); LRMS *m/z* (ESI$^+$) 461 ([M+Na^{23}]$^+$, 100%); HRMS *m/z* (ESI$^+$) [Found: 439.2220, $C_{25}H_{31}O_5N_2$, requires [M+H]$^+$ 439.2227]; HPLC (Method 1) Retention time = 10.69, 94.6%. The LRMS and ^{1}H NMR data are in good agreement with the literature.[32]

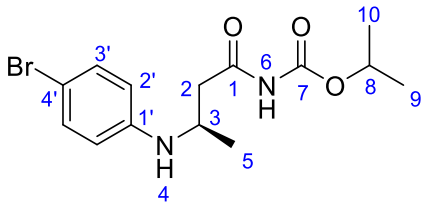
Ethyl 4-((2*S*,4*R*)-1-acetyl-4-amino-2-methyl-1,2,3,4-tetrahydroquinolin-6-yl)benzoate (2.14) [32]



Compound **2.13** (500 mg, 1.14 mmol, 1.0 eq.) was added to a suspension of $AlCl_3$ (760 mg, 5.70 mmol, 5.0 eq.) in anhydrous CH_2Cl_2 (9 mL) and the resulting solution stirred for 20 mins at 0 °C. A solution of anhydrous NEt_3 (1.9 mL, 13.7 mmol, 12 eq.) and anhydrous

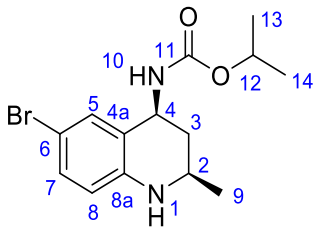
MeOH (2 mL) was added dropwise. The mixture was stirred for 20 min at 0 °C then diluted with EtOAc (20 mL) and saturated Rochelle salt solution (40 mL) and stirred for 30 min. After this time, the solution was filtered through Celite®, eluting with EtOAc, saturated aqueous $NaHCO_3$, acetone and MeOH. The organic components were removed from the filtrate *in vacuo*. The resulting solution was then diluted with EtOAc (50 mL) and the organic and aqueous components were partitioned. The aqueous components were extracted with EtOAc (3 × 50 mL). The organic components were the dried with Na_2SO_4, and concentrated *in vacuo*. The crude material was purified using silica gel flash column chromatography (0–10% MeOH/CH_2Cl_2) to give **2.14** as a colourless solid (339 mg, 84%). R_f 0.69 (10% MeOH/CH_2Cl_2); $[\alpha]_D^{25}$ = +315.0 (*c* 1.0, $CHCl_3$); m.p. 38–45 °C (from EtOAc); $\overline{\nu}_{max}$ (thin film)/cm^{-1} 2978 (C-H, w), 1711 (C=O, s), 1645 (N-H, s); ^{1}H NMR (400 MHz, $CDCl_3$) δ_H 8.14–8.09 (2H, m, H-2'), 7.77–7.75 (1H, m, H-5), 7.72–7.67 (2H, m, H-3'), 7.53 (1H, dd, *J* 8.2, 1.8, H-7), 7.20 (1H, d, *J* 8.2, H-8), 4.91–4.78 (1H, m, H-2), 4.41 (2H, q, *J* 7.1, H-6'), 3.80 (1H, dd, *J* 12.1, 4.4, H-4), 2.56 (1H, ddd, *J* 12.7, 8.6, 4.4, H_aH_b-3), 2.16 (3H, s, H-10), 1.65 (2H, br s, H-12), 1.42 (3H, t, *J* 7.1, H-7'), 1.20–1.11 (1H, m, H_aH_b-3), 1.16 (3H, d, *J* 6.3, H-11); ^{13}C NMR (151 MHz, $CDCl_3$) δ_C 169.6 (C-9), 166.6 (C-5'), 145.0 (C-4'), 140.7 (C-4a), 137.9 (C-6), 136.5 (C-8a), 130.3 (C-2'), 129.5 (C-1'), 127.0 (C-3'), 126.3 (C-8), 125.7 (C-7), 121.6 (C-5), 61.2 (C-6'), 47.8 (C-2), 47.7 (C-4), 44.7 (C-3), 23.1 (C-10), 21.6 (C-11), 14.5 (C-7'); LRMS *m/z* (ESI$^+$) 337 ([M−NH_2+H]$^+$, 25%); HRMS *m/z* (ESI$^+$) [Found: 353.1861, $C_{21}H_{25}O_3N_2$, requires [M+H]$^+$ 353.1860]. The LRMS data are in good agreement with the literature.[32]

Isopropyl (*R*)-(3-(4'-bromoanilinyl)butanoyl)carbamate (2.15)



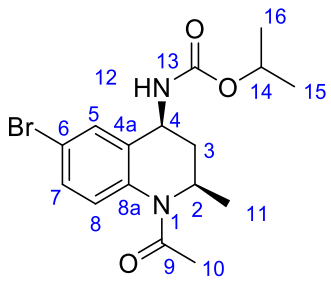
The preparation of **2.15** was based upon a previously reported procedure.[32,120,123] Compound **2.9** (161 mg, 0.940 mmol, 1.0 eq.) was dissolved in anhydrous, degassed toluene (3 mL). (*S*)-BINAP(OTf)$_2$(H$_2$O)$_2$Pd (50 mg, 0.0470 mmol, 0.050 eq.) was added and the resulting mixture was stirred for 20 min. 4-Bromoaniline (240 mg, 1.40 mmol, 1.5 eq.) was added and the resulting solution was stirred for 6 h 25 min. After this time the solution was concentrated *in vacuo* and purified using flash column chromatography (0–50% EtOAc/petroleum ether) to give **2.15** as a colourless solid (291 mg, 90%): R_f 0.13 (20% EtOAc/petroleum ether); $[\alpha]_D^{25}$ = +7.45 (*c* 1.0, MeOH); m.p. 72–88 °C (from EtOAc) [lit.[123] 131 °C, lit.[120] 128–130 °C, (opposite enantiomer)]; ^{1}H NMR (400 MHz, D$_6$-DMSO) δ_H 10.47 (1H, s, H-6), 7.21–7.16 (2H, m, H-3'/2'), 6.54–6.48 (2H, m, H-3'/2'), 5.66 (1H, d, *J* 8.7, H-4), 4.84 (1H, sp, *J* 6.3, H-8), 3.85–3.71 (1H, m, H-3), 2.68 (1H, dd, *J* 15.7, 5.6, H$_a$H$_b$-2), 2.45 (1H, dd, *J* 15.7, 7.5, H$_a$H$_b$-2), 1.22 (6H, d, *J* 6.3, H-9, H-10), 1.12 (3H, d, *J* 6.4, H-5); LRMS *m/z* (ESI$^+$) 365 ([M^{79}Br+Na]$^+$, 64%); Chiral HPLC (Method 1), Chiral AD-H column (80:20 heptane/ethanol, 0.1% DEA, 1.0 mLmin^{-1}) Retention time = 11.0 min (opposite enantiomer (**2.10**), 7.7% UV), Retention time = 16.3 min (**2.15**, 92.3% UV); 85% e.e. These data are in good agreement with the non-stereospecific spectroscopic data of **2.10**.[32,120,123]

Isopropyl ((2*R*,4*S*)-6-bromo-2-methyl-1,2,3,4-tetrahydroquinolin-4-yl)carbamate (2.16)



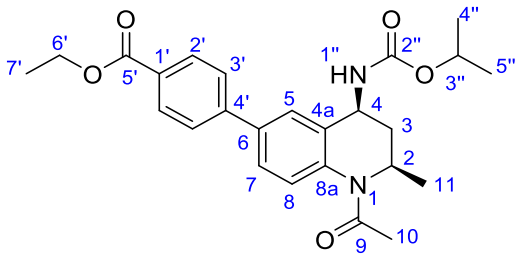
The preparation of **2.16** was based upon a previously reported procedure.[32,120,123] Compound **2.15** (252 mg, 0.734 mmol, 1.00 eq.) was dissolved in EtOH (13 mL) and the resulting solution was cooled to below –10 °C. Sodium borohydride (21 mg, 0.555 mmol, 0.76 eq.) was added to the solution followed by a solution of $MgCl_2{\cdot}6H_2O$ (164 mg, 0.807 mmol, 1.1 eq.) in water (1.3 mL). The resulting suspension was poured into a mixture of citric acid (5.3 mL, 0.5 M), $HCl_{(aq)}$ (1 M, 18 mL) and CH_2Cl_2 (18 mL). The layers were separated and the aqueous components were extracted with CH_2Cl_2 (3 × 30 mL), dried over $NaSO_4$, filtered, and concentrated *in vacuo* to give **2.16** as a colourless solid (224 mg, 93%): R_f 0.68 (30% EtOAc/petroleum ether); m.p. 140–143 °C (from CH_2Cl_2) [lit.[123] 167 °C lit.[120]148–150 °C, (opposite enantiomer)]; $[\alpha]_D^{25}$ = –7.8 (*c* 1.0, MeOH); ^{1}H NMR (400 MHz, D_6-DMSO) δ_H 7.38 (1H, d, *J* 9.1, H-10), 7.02 (1H, dd, *J* 8.6, 2.4, H-7), 6.96–6.93 (1H, m, H-5), 6.42 (1H, d, *J* 8.6, H-8), 4.87–4.79 (1H, m, H-12), 4.77–4.66 (1H, m, H-4), 3.44–3.39 (1H, m, H-2), 1.91 (1H, ddd, *J* 12.4, 5.8, 2.6, H_aH_b-3), 1.49–1.37 (1H, m, H_aH_b-3), 1.23 (3H, d, *J* 6.2, H-13/14), 1.20 (3H, d, *J* 6.2, H-13/14), 1.12 (3H, d, *J* 6.3, H-9); LRMS *m/z* (ESI^+) 349 ($[M^{79}Br+Na]^+$, 8%); Chiral HPLC (Method 1), Chiral AD-H column (85:15 heptane/ethanol, 0.1% DEA, 1.0 $mLmin^{-1}$) Retention time = 6.0 min (opposite enantiomer (**2.11**), 9.9% UV), Retention time = 7.9 min (**2.16**, 90.1% UV); 80% e.e. These data are in good agreement with the non-stereospecific spectroscopic data of **2.11**.[32,120,123]

Isopropyl ((2*R*,4*S*)-1-acetyl-6-bromo-2-methyl-1,2,3,4-tetrahydroquinolin-4-yl)carbamate (2.17)



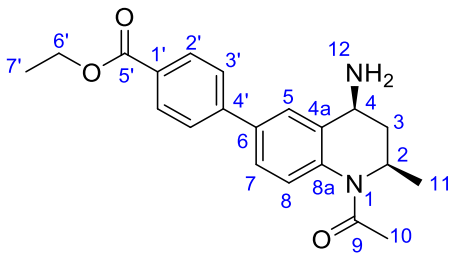
The preparation of compound **2.17** was based upon a previously reported procedure.[32,120,123] Pyridine (0.114 mL, 1.41 mmol, 3.0 eq.) was added to a solution of compound **2.16** (154 mg, 0.471 mmol, 1.0 eq.) dissolved in anhydrous CH_2Cl_2 (4.5 mL) under argon at rt. Acetyl chloride (537 µL, 0.753 mmol, 1.6 eq.) was added dropwise and the reaction mixture was left to stir for 1 h 10 min. After this time the mixture was partitioned with EtOAc (30 mL) and $NaHCO_{3(aq)}$ (30 mL). The aqueous layer was extracted with EtOAc (3 × 30 mL) and the combined organic components washed with H_2O and brine, dried over $NaSO_4$, filtered, and concentrated *in vacuo*. The crude residue was purified using flash column chromatography (50–100% EtOAc/petroleum ether) to give **2.17** as a brown solid (152 mg, 88%): R_f 0.27 (50% EtOAc/petroleum ether); m.p. 127–129 °C (from EtOAc) [lit.[123] 163 °C, lit.[120] 141–143 °C, (opposite enantiomer)]; $[\alpha]_D^{25}$ = –214.1 (*c* 1.0, MeOH); ^{1}H NMR (400 MHz, D_6-DMSO) δ_H 7.63 (1H, d, *J* 8.6, H-12), 7.47 (1H, dd, *J* 8.4, 2.2, H-7), 7.30 (1H, d, *J* 8.4, H-8), 7.21 (1H, d, *J* 2.2, H-5), 4.91–4.75 (1H, m, H-14), 4.67–4.55 (1H, m, H-2), 4.40–4.30 (1H, m, H-4), 2.48–2.40 (1H, m, H_aH_b-3), 2.05 (3H, s, H-10), 1.25 (3H, d, *J* 6.3, H-15/16), 1.22 (3H, d, *J* 6.3, H-15/16), 1.19–1.13 (1H, m, H_aH_b-3), 1.01 (3H, d, *J* 6.3, H-11); LRMS *m/z* (ESI$^+$) 391 ([M^{79}Br+Na]$^+$, 100%). These data are in good agreement with the non-stereospecific spectroscopic data of **2.12**.[32,120,123]

Ethyl 4-((2*R*,4*S*)-1-acetyl-4-((isopropoxycarbonyl)amino)-2-methyl-1,2,3,4-tetrahydroquinolin-6-yl)benzoate (2.18)



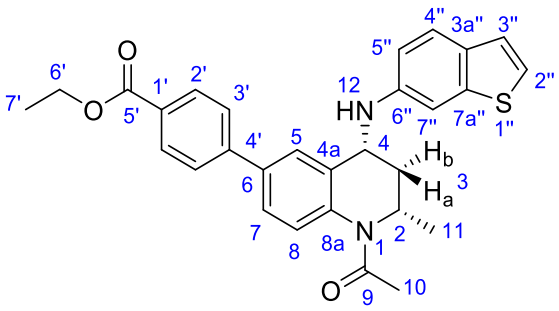
The preparation of compound **2.18** was based upon a previously reported procedure.[32] Degassed $Na_2SO_{4(aq)}$ (2 M, 4.7 mL, 9.40 mmol, 3.93 eq.) was added to a solution of compound **2.17** (879 mg, 2.39 mmol, 1.00 eq.) {4-[(ethyloxy)carbonyl]phenyl}boronic acid (485 mg, 2.50 mmol, 1.05 eq.) and $Pd(Ph_3)_4$ (41 mg, 0.0355 mmol, 0.015 eq.) in degassed DME (9.6 mL). The resulting solution was stirred at 105 °C for 17 h 15 min. After this time, the reaction mixture was cooled to rt and partitioned between EtOAc (20 mL) and water (20 mL). The layers were separated, and the aqueous layer extracted with EtOAc (3 × 50 mL). The combined organic components were washed with water (50 mL) and brine (50 mL), dried over Na_2SO_4, and concentrated *in vacuo*. The grey-brown crude solid was re-dissolved in EtOAc and filtered through a plug of silica. The silica was washed with EtOAc and the filtrate concentrated *in vacuo* to give **2.18** as a brown solid (843 mg, 80%): R_f 0.31 (acetone:petroleum ether 1:3); mp 146–148 °C (from EtOAc) [Opposite enantiomer: 73–75 °C (from acetone)]; $[\alpha]_D^{25}$ = –260.9 (*c* 1.0, MeOH) ^{1}H NMR (400 MHz, D_6-DMSO) δ_H 8.08–8.04 (2H, m, H-2'), 7.83–7.77 (2H, m, H-3'), 7.69 (1H, d, *J* 8.8, H-1''), 7.65 (1H, dd, *J* 8.2, 2.2, H-7), 7.48–7.43 (2H, m, H-5, H-8), 4.90–4.80 (1H, m, H-3''), 4.72–4.60 (1H, m, H-2), 4.49–4.39 (1H, m, H-4), 4.34 (2H, q, *J* 7.1, H-6'), 2.48–2.44 (partially hidden by D_6-DMSO peak) (1H, m, H_aH_b-3), 2.10 (3H, s, H-10), 1.34 (3H, t, *J* 7.1, H-7'), 1.27–1.22 (6H, m, H-4''/5''), 1.24–1.15 (1H, m, H_aH_b-3), 1.06 (3H, d, *J* 6.4, H-11); LRMS *m/z* (ESI^+) 461 ($[M+Na]^+$, 100%). The LRMS and ^{1}H NMR data are in good agreement with the literature values for **2.13**.[32]

Ethyl 4-((2*R*,4*S*)-1-acetyl-4-amino-2-methyl-1,2,3,4-tetrahydroquinolin-6-yl)benzoate (2.19)



The preparation of compound **2.19** was based upon a previously reported procedure.[32] $AlCl_3$ (76 mg, 0.570 mmol, 5.0 eq.) was added to a solution of compound **2.18** (50 mg, 0.114 mmol, 1.0 eq.) dissolved in anhydrous CH_2Cl_2 (0.9 mL) at 0 °C and the resulting suspension was stirred for 20 min. After this time, a solution of anhydrous NEt_3 (0.2 mL, 1.4 mmol, 12 eq.) in dry MeOH (0.2 mL) was added dropwise and the resulting suspension was stirred for a further 1 h 30 min. The reaction mixture was then diluted with EtOAc (5 mL) and saturated Rochelle salt solution (10 mL), and the solution left to stir for 30 min. The suspension was then filtered through Celite®, eluting with EtOAc, saturated $NaHCO_{3(aq)}$, acetone, and MeOH. The organic components were removed *in vacuo* and the aqueous components partitioned between saturated $NaHCO_{3(aq)}$ (10 mL) and EtOAc (10 mL). The aqueous layer was washed with EtOAc (3 × 10 mL) and the combined organic components were dried over Na_2SO_4, filtered, and concentrated *in vacuo*. The crude residue was purified using flash column chromatography (0–10% MeOH/CH_2Cl_2) to give **2.19** as a colourless solid (33 mg, 82%). R_f 0.69 (10% MeOH/CH_2Cl_2); $[\alpha]_D^{25}$ = –264.3 (*c* 1.0, $CHCl_3$); m.p. 120–125 °C (from toluene) [opposite enantiomer: 38–45 °C (from EtOAc)]; ^{1}H NMR (400 MHz, $CDCl_3$) δ_H 8.14–8.09 (2H, m, H-2'), 7.78–7.76 (1H, m, H-5), 7.71–7.67 (2H, m, H-3'), 7.53 (1H, dd, *J* 8.2, 1.9, H-7), 7.20 (1H, d, *J* 8.2, H-8), 4.91–4.78 (1H, m, H-2), 4.41 (2H, q, *J* 7.1, H-6'), 3.81 (1H, dd, *J* 12.0, 4.4, H-4), 2.57 (1H, ddd, *J* 12.8, 8.7, 4.4, H_aH_b-3), 2.16 (3H, s, H-10), 1.65 (2H, br s, H-12), 1.42 (3H, t, *J* 7.1, H-7'), 1.23–1.18 (1H, m, H_aH_b-3), 1.17 (3H, d, *J* 6.4, H-11); LRMS *m/z* (ESI$^+$) 375 ([M+Na]$^+$, 25%). The LRMS data are in good agreement with the literature value for **2.14**.[32]

Ethyl 4-{(2*S*,4*R*)-1-acetyl-4-[(1-benzothiophen-6-yl)amino]-2-methyl-1,2,3,4-tetrahydroquinolin-6-yl}benzoate (2.20)



Method 1:

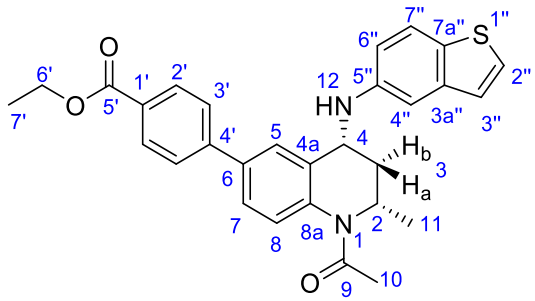
Compound **2.14** (81 mg, 0.230 mmol, 1.0 eq.), 6-bromo[b]benzothiophene (99 mg, 0.465 mmol, 2.0 eq.), $Pd(dba)_2$ (11 mg, 0.0191 mmol, 0.083 eq.), XPhos (36 mg, 0.0755 mmol, 0.33 eq.) and NaO^{t}Bu (27 mg, 0.281 mmol, 1.2 eq.) were dissolved in anhydrous, degassed toluene in a dry microwave vial under argon, and stirred for 24 h at 70 °C. The reaction mixture was then cooled and filtered through Celite®. The residue was washed with toluene and Et_2O and filtrate was partially concentrated *in vacuo* to remove the Et_2O. The subsequent organic solution was washed with H_2O (15 mL) and HCl(aq) (2 M, 15 mL) and the aqueous components were extracted with EtOAc (3 × 20 mL). The combined organic components were washed with H_2O (50 mL) and brine (50 mL), dried over $MgSO_4$ and concentrated *in vacuo*. The crude material was purified by three flash column chromatography columns, (0–60% EtOAc/petroleum ether, 0–15% EtOAc/CH_2Cl_2 and 0–30% EtOAc/toluene, to give compound **2.20** as a yellow solid (25 mg, 22%).

Method 2:

Compound **2.14** (100 mg, 0.284 mmol, 1.0 eq), 6-bromobenzothiophene (121 mg, 0.568 mmol, 2 eq.), BrettPhos (49 mg, 0.0913 mmol, 0.32 eq), BrettPhos Pd G3 (21 mg, 0.0232 mmol, 0.08 eq) and NaO^{t}Bu (33 mg, 0.343 mmol, 1.2 eq) were added to a dry microwave vial and the vial was purged with argon. Degassed anhydrous toluene (1.7 mL) was added and the resulting suspension was stirred for 15 h at 70 °C. After this time the

suspension was filtered through Celite®, eluting with toluene and Et_2O, and the filtrate was concentrated *in vacuo*. The resulting residue was redissolved in EtOAc (50 mL) and washed with H_2O (40 mL) and brine (40 mL). The organic components were dried over Na_2SO_4, and concentrated *in vacuo*. The crude was purified by flash column chromatography (0–60% EtOAc/petroleum ether) to give **2.20** as a yellow solid (120 mg, 87%, 94.8% purity by HPLC). To achieve a higher purity, 50 mg of **2.20** was further purified by semi-preparative HPLC and lyophilised to give **2.20** as an off-white solid (> 99.9% purity by HPLC)**:** R_f 0.43 (10% EtOAc/CH_2Cl_2); $[\alpha]_D^{25}$ = +338.1 (*c* 1.0, $CHCl_3$); m.p. 78–84 °C (from $CHCl_3$); $\overline{\nu}_{max}$ (thin film)/cm^{-1} 3350 (N-H, w), 1711 (C=O, s), 1646 (C=O, s), 1606 (s), 1487 (s), 1277 (s); ^{1}H NMR (400 MHz, CD_3CN) δ_H 8.09–7.89 (2H, m, H-2'), 7.66–7.57 (4H, m, H-7, H-3'. H-4''), 7.56–7.54 (1H, m, H-5), 7.37 (1H, d, *J* 8.2, H-8), 7.18 (1H, dd, *J* 5.4, 0.8, H-3''), 7.16–7.12 (2H, m, H-2'', H-7''), 6.91 (1H, dd, *J* 8.7, 2.2, H-5''), 4.97 (1H, d, *J* 8.0, H-12), 4.86–4.73 (1H, m, H-2), 4.40 (1H, ddd, *J* 12.2, 8.0, 4.2, H-4), 4.31 (2H, q, *J* 7.1, H-6'), 2.71 (1H, ddd, *J* 12.6, 8.5, 4.2, H_a-3), 2.17 (3H, s, H-10), 1.33 (3H, t, *J* 7.1, H-7'), 1.35–1.24 (1H, m, H_b-3), 1.14 (3H, d, *J* 6.3, H-11); ^{13}C NMR (151 MHz, CD_3CN) δ_C 170.0 (C-9), 166.9 (C-5'), 146.8 (C-6''), 145.7 (C-4'), 142.8 (C-7a''), 139.5 (C-4a), 138.2 (C-8a), 137.6 (C-6), 132.5 (C-3a''), 130.8 (C-2'), 130.4 (C-1'), 127.9 (C-8), 127.7 (C-3'), 126.5 (C-4''), 125.1 (C-7), 124.6 (C-3''), 123.3 (C-5), 122.5 (C-2''), 114.7 (C-5''), 104.6 (C-7''), 61.8 (C-6'), 50.7 (C-4), 48.6 (C-2), 41.6 (C-3), 23.4 (C-10), 21.7 (C-11), 14.6 (C-7'); LRMS *m/z* (ESI^+) 485 ($[M+H]^+$, 2.6%); HRMS *m/z* (ESI^+) [Found: 485.1898, $C_{29}H_{29}O_3N_2{}^{32}S$, requires $[M+H]^+$ 485.1893]; HPLC (Method 1) Retention time = 12.4 min, > 99.9%; Chiral HPLC, (Method 1) Chiral AD-H column (40:60 hexane/IPA, 1.0 $mLmin^{-1}$) Retention time = 7.7 min (**2.20**, 91.4% UV), Retention time = 10.1 min (opposite enantiomer (**2.23**), 8.6% UV); 83% e.e.

Ethyl 4-{(2*S*,4*R*)-1-acetyl-4-[(1-benzothiophen-5-ylamino]-2-methyl-1,2,3,4-tetrahydroquinolin-6-yl}benzoate (2.21)



Method 1:

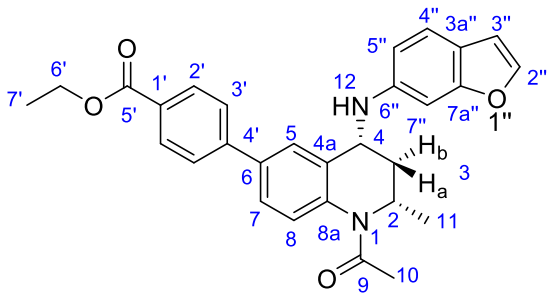
Compound **2.14** (111 mg, 0.315 mmol, 1.0 eq.), 5-bromobenzo[b]thiophene (134 mg, 0.630 mmol, 2.0 eq.), XPhos (48 mg, 0.101 mmol, 0.32 eq.), $Pd(dba)_2$ (15 mg, 0.0260 mmol, 0.083 eq.), NaO^tBu (36 mg, 0.375 mmol, 1.2 eq.) were added to a dry microwave vial and the vial was purged with argon. Anhydrous, degassed toluene (2.2 mL) was added, and the resulting solution was stirred at 70 °C for 27 h at rt. The solution was cooled and filtered through Celite® and the residue was washed with toluene and Et_2O. The filtrate was concentrated *in vacuo* to remove Et_2O and then the remaining organic components were washed with H_2O (10 mL) and $HCl_{(aq)}$ (1 M, 10 mL). The aqueous components were extracted with EtOAc (3 × 30 mL) and the combined organic components were washed with H_2O (20 mL) and brine (20 mL). The combined organic components were dried over $MgSO_4$ and concentrated *in vacuo*. The crude material was purified by flash column chromatography (0–30% EtOAc/toluene) to yield compound **2.21** as a yellow solid (31 mg, 20 %).

Method 2:

Compound **2.14** (100 mg, 0.284 mmol, 1.0 eq), 5-bromobenzothiophene (121 mg, 0.568 mmol, 2.0 eq.), BrettPhos (49 mg, 0.0913 mmol, 0.32 eq), BrettPhos Pd G3 (21 mg, 0.0232 mmol, 0.082 eq) and NaO^tBu (33 mg, 0.343 mmol, 1.2 eq) were added to a dry microwave vial and the vial was purged with argon. Degassed anhydrous toluene (1.7 mL)

was added and the resulting suspension was stirred for 15 h at 70 °C. After this time the suspension was filtered through Celite®, eluting with toluene and Et_2O, and the filtrate was concentrated *in vacuo*. The resulting residue was redissolved in EtOAc (50 mL) and washed with H_2O (40 mL) and brine (40 mL). The organic components were dried over Na_2SO_4, filtered, and concentrated *in vacuo*. The crude was purified using flash column chromatography (0–60% EtOAc/petroleum ether) to give **2.21** as a yellow solid (88 mg, 66%, 94.7% purity by HPLC). To achieve a higher purity, 44 mg of **2.21** was further purified using semi-preparative HPLC and the fractions containing **2.21** lyophilised to give **2.21** as an off-white solid**:** R_f0.34 (50% EtOAc/petroleum ether); $[\alpha]_D^{25} = +324.5$ (*c* 1.0, $CHCl_3$); m.p. 95–99 °C (from $CHCl_3$); $\overline{\nu}_{max}$ (thin film)/cm^{-1} 3360 (N-H, w), 1713 (C=O, s), 1647 (N-H, s), 1606 (s), 1488 (s), 1278 (s); ^{1}H NMR (400 MHz, CD_3CN) δ_H 8.04–7.91 (2H, m, H-2'), 7.68 (1H, d, *J* 8.7, H-7''), 7.63–7.54 (4H, m, H-5, H-7, H-3'), 7.43 (1H, d, *J* 5.4, H-2''), 7.38 (1H, d, *J* 8.0, H-8), 7.13 (1H, d, *J* 5.5, 0.8, H-3''), 7.10–7.08 (1H, m, H-4''), 6.93 (1H, dd, *J* 8.7, 2.3, H-6''), 4.87 (1H, d, *J* 8.0, H-12), 4.83–4.74 (1H, m, H-2), 4.40 (1H, ddd, *J* 12.1, 8.0, 4.1, H-4), 4.31 (2H, q, *J* 7.1, H-6'), 2.72 (1H, ddd, *J* 12.5, 8.6, 4.1, H_a-3), 2.18 (3H, s, H-10), 1.34 (3H, t, *J* 7.1, H-7'), 1.35–1.2 (1H, m, H_b-3), 1.14 (3H, d, *J* 6.3, H-11); ^{13}C NMR (151 MHz, CD_3CN) δ_C 170.0 (C-9), 167.0 (C-5'), 146.7 (C-5''), 145.7 (C-4'), 142.2 (C-3a''), 139.7 (C-4a), 138.2 (C-8a), 137.6 (C-6), 130.9 (C-2'), 130.4 (C-1'), 130.0 (C-7a''), 128.1 (C-2''), 127.9 (C-8), 127.7 (C-3'), 126.5 (C-7), 124.4 (C-3''), 123.8 (C-7''), 123.4 (C-5), 115.1 (C-6''), 106.1 (C-4''), 61.8 (C-6'), 50.8 (C-4), 48.7 (C-2), 41.6 (C-3), 23.4 (C-10), 21.7 (C-11), 14.6 (C-7'); LRMS *m/z* (ESI^+) 485 ($[M+H]^+$, 2.6%); HRMS *m/z* (ESI^+) [Found: 485.18976, $C_{29}H_{29}O_3N_2{}^{32}S$, requires $[M+H]^+$ 485.18934]; HPLC (Method 1) Retention time = 12.3 min, >99.9%; Chiral HPLC (Method 1), Chiral AD-H column (50:50 hexane/EtOH, 1.0 $mLmin^{-1}$) Retention time = 10.9 min (opposite enantiomer, 6.7% UV), Retention time = 13.9 min (**2.21**, 93.3% UV); 87% e.e.

Ethyl 4-{(2*S*,4*R*)-1-acetyl-4-[(1-benzofuran-6-yl)amino]-2-methyl-1,2,3,4-tetrahydroquinolin-6-yl}benzoate (2.22)



Method 1:

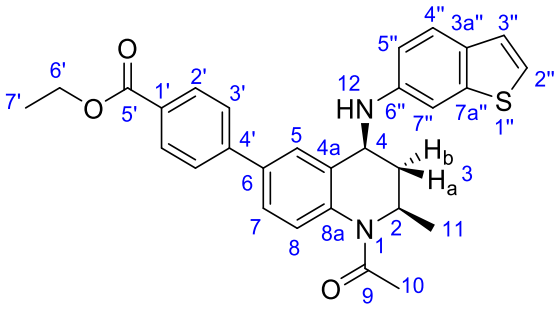
Compound **2.14** (36 mg, 0.10 mmol, 1.2 eq.), 6-bromobenzofuran (17 mg, 0.086 mmol, 1.0 eq.), $Pd(dba)_2$ (5 mg, 0.0087 mmol, 0.10 eq.), XPhos (16 mg, 0.034 mmol, 0.40 eq.) and NaO^tBu (12 mg, 0.12 mmol, 1.2 eq.) were dissolved together in anhydrous, degassed toluene under argon and stirred for 24 h at 70 °C. The reaction mixture was cooled and filtered through Celite®. The residue was washed with toluene and Et_2O, and the Et_2O was subsequently removed *in vacuo*. The resulting organic solution was washed with H_2O (15 mL) and $HCl_{(aq)}$ (2 M, 15 mL). The aqueous components were extracted with EtOAc (3 × 30 mL) and the combined organic components were washed with H_2O (50 mL) and brine (50 mL), dried over $MgSO_4$ and concentrated *in vacuo*. The crude was purified by two flash column chromatography columns (0–80% EtOAc/petroleum ether then 0–30% EtOAc/toluene) to give compound **2.22** as a colourless solid (9 mg, 22%).

Method 2:

Compound **2.14** (133 mg, 0.377 mmol, 1.0 eq.), 6-bromobenzofuran (149 mg, 0.756 mmol, 2.0 eq), BrettPhos (65 mg, 0.121 mmol, 0.32 eq.), BrettPhos Pd G3 (27 mg, 0.0298 mmol, 0.079 eq.) and NaO^tBu (44 mg, 0.458 mmol, 1.2 eq.) were added to a dry microwave vial which was subsequently purged with argon. Degassed, anhydrous toluene (2.2 mL) was added, and the resulting suspension was stirred for 15 h at 70 °C. After this time the suspension was filtered through Celite®, eluting with toluene and Et_2O, and the filtrate

concentrated *in vacuo*. The resulting residue was redissolved in EtOAc (50 mL) and washed with H_2O (40 mL) and brine (40 mL). The organic components were dried over Na_2SO_4, filtered, and concentrated *in vacuo*. The crude material was purified using silica gel flash column chromatography (0–50% EtOAc/petroleum ether) to give **2.22** as a yellow solid (120 mg, 68%, 94.6% purity by HPLC). To achieve a higher purity, 60 mg of **2.22** was purified using semi-preparative HPLC and lyophilised to give **2.22** as a light-green solid: R_f 0.17 (30% EtOAc/petroleum ether); $[\alpha]_D^{25}$ = +258.7 (*c* 1.0, $CHCl_3$); m.p. 84–87 °C (from $CHCl_3$); $\overline{\nu}_{max}$ (thin film)/cm^{-1} 3358 (N-H, w), 1713 (C=O, s), 1629 (s), 1608 (s), 1488 (s); ^{1}H NMR (400 MHz, CD_3CN) δ_H 8.04–7.89 (2H, m, H-2'), 7.65–7.58 (3H, m, H-7, H-3'), 7.57–7.55 (1H, m, H-5), 7.48 (1H, d, *J* 2.2, H-2''), 7.40–7.34 (2H, m, H-8, H-4''), 6.82–6.80 (1H, m, H-7''), 6.78 (1H, dd, *J* 8.3, 2.1, H-5''), 6.68 (1H, dd, *J* 2.2, 1.0, H-3''), 4.93 (1H, d, *J* 8.1, H-12), 4.84–4.74 (1H, m, H-2), 4.43–4.35 (1H, dd, *J* 9.1, 4.4, H-4), 4.32 (2H, q, *J* 7.1, H-6'), 2.71 (1H, ddd, *J* 12.5, 8.5, 4.1, H_b-3), 2.17 (3H, s, H-10), 1.34 (3H, t, *J* 7.1, H-7'), 1.34–1.24 (1H, m, H_a-3), 1.14 (3H, d, *J* 6.3 Hz, H-11); ^{13}C NMR (151 MHz, CD_3CN) δ_C 170.0 (C-9), 167.0 (C-5'), 157.7 (C-7a''), 147.5 (C-6''), 145.7 (C-4'), 143.9 (C-2''), 139.6 (C-4a), 138.2 (C-8a), 137.6 (C-6), 130.9 (C-2'), 130.4 (C-1'), 127.8 (C-8), 127.7 (C-3'), 126.5 (C-7), 123.4 (C-5), 122.5 (C-4''), 119.1 (C-3a''), 112.4 (C-5''), 107.4 (C-3''), 95.4 (C-7''), 61.8 (C-6'), 50.8 (C-4), 48.7 (C-2), 41.6 (C-3), 23.4 (C-10), 21.7 (C-11), 14.6 (C-7'); LRMS *m/z* (ESI^+) 469 ($[M+H]^+$, 11%) HRMS *m/z* (ESI^+) [Found: 469.21239, $C_{29}H_{29}O_4N_2$, requires $[M+H]^+$ 469.21218]; HPLC (Method 1) Retention time = 11.9 min, 99.7%; Chiral HPLC (Method 1), Chiral AD-H column (80:20 hexane/IPA, 1.0 $mLmin^{-1}$) Retention time = 19.7 min (**2.22**, 91.7% UV), Retention time = 28.0 min (opposite enantiomer, 8.3% UV); 83% e.e.

Ethyl 4-{(2*R*,4*S*)-1-acetyl-4-[(1-benzothiophen-6-yl)amino]-2-methyl-1,2,3,4-tetrahydroquinolin-6-yl}benzoate (2.23)



Method 1:

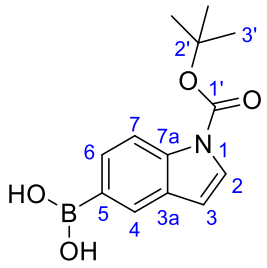
Compound **2.19** (110 mg, 0.31 mmol, 1.0 eq.), XPhos (48 mg, 0.10 mmol, 0.32 eq.), NaO^{t}Bu (36 mg, 0.38 mmol, 1.2 eq.), 6-bromobenzo[b]thiophene (130 mg, 0.61 mmol, 2.0 eq.) and $Pd(dba)_2$ (14 mg, 0.024 mmol, 0.079 eq.) were dissolved in anhydrous, degassed toluene (2.2 mL) in a dry microwave vial under argon. The resulting solution was stirred for 23 h at 70 °C. The reaction mixture was then cooled and filtered through Celite®. The residue was washed with toluene and Et_2O, and the filtrate was concentrated *in vacuo* and subsequently redissolved in toluene (30 mL). The resulting solution was washed with H_2O (30 mL) and $HCl_{(aq)}$ (2 M, 30 mL). The combined organic components were washed with H_2O (20 mL) and brine (20 mL), dried over $MgSO_4$ and concentrated *in vacuo*. The crude residue was purified by flash column chromatography (0–30% EtOAc/toluene) to give compound **2.23** as a yellow solid (31 mg, 21 %).

Method 2:

Compound **2.19** (140 mg, 0.397 mmol, 1.0 eq.), 6-bromobenzo[b]thiophene (169 mg, 0.793 mmol, 2.0 eq.), BrettPhos (68 mg, 0.127 mmol, 0.32 eq.), BrettPhos Pd G3 (29 mg, 0.032 mmol, 0.080 eq.), and NaO^{t}Bu (46 mg, 0.479 mmol, 1.2 eq.) were added to a dry microwave vial which was subsequently purged with argon. Anhydrous, degassed toluene (2.4 mL) was added, and the resulting suspension was stirred for 15 h at 70 °C. After this time the suspension was filtered through Celite®, eluting with toluene and Et_2O, and the filtrate was concentrated *in vacuo*. The resulting residue was redissolved in EtOAc (50 mL)

and washed with H_2O (40 mL) and brine (40 mL). The organic components were dried over Na_2SO_4, filtered, and concentrated *in vacuo*. The crude material was purified using silica gel flash column chromatography (0–60% EtOAc/petroleum ether) to give **2.23** as a yellow solid (132 mg, 69%, 96.2% purity by HPLC). To achieve higher purity, 66 mg of compound **2.23** was further purified using semi-preparative HPLC and lyophilised to give **2.23** as an off-white solid (>99.9%purity by HPLC): R_f 0.43 (10% EtOAc/CH_2Cl_2); $[\alpha]_D^{25}$ = –285.9 (*c* 1.0, $CHCl_3$); m.p. 102–105 °C (from $CHCl_3$) [opposite enantiomer: 78–84 °C (from $CHCl_3$)]; ^{1}H NMR (400 MHz, CD_3CN) δ_H 8.03–7.94 (2H, d, *J* 8.0, H-2'), 7.65–7.57 (4H, m, H-7, H-3', H-4''), 7.57–7.54 (1H, m, H-5), 7.38 (1H, d, *J* 8.2, H-8), 7.19 (1H, dd, *J* 5.4, 0.7, H-3''), 7.16–7.13 (2H, m, H-2'', H-7''), 6.91 (1H, dd, *J* 8.6, 2.2, H-5''), 4.97 (1H, d, *J* 8.0, H-12), 4.87–4.73 (1H, m, H-2), 4.41 (1H, ddd, *J* 12.1, 8.0, 4.1, H-4), 4.31 (2H, q, *J* 7.1, H-6'), 2.71 (1H, ddd, *J* 12.5, 8.6, 4.1, H_b-3), 2.18 (3H, s, H-10), 1.34 (3H, t, *J* 7.1, H-7'), 1.35–1.25 (1H, m, H_a-3), 1.14 (3H, d, *J* 6.3, H-11); ^{13}C NMR (151 MHz, CD_3CN) δ_C 170.0 (C-9), 167.0 (C-5'), 146.8 (C-6''), 145.7 (C-4'), 142.8 (C-7a''), 139.5 (C-4a), 138.3 (C-8a), 137.6 (C-6), 132.5 (C-3a''), 130.9 (C-2'), 130.4 (C-1'), 127.9 (C-8), 127.7 (C-3'), 126.5 (C-4''), 125.1 (C-7), 124.6 (C-3''), 123.3 (C-5), 122.5 (C-2''), 114.7 (C-5''), 104.6 (C-7''), 61.8 (C-6'), 50.7 (C-4), 48.7 (C-2), 41.6 (C-3), 23.4 (C-10), 21.7 (C-11), 14.6 (C-7'); LRMS: *m/z* (ESI$^+$) 507 ([M+Na]$^+$, 28%); HPLC (Method 1) Retention time = 12.4 min, >99.9%; Chiral HPLC (Method 1), Chiral AD-H column (40:60 hexane/IPA, 1.0 mLmin^{-1}) Retention time = 7.2 min (opposite enantiomer (**2.20**), 5.6% UV), Retention time = 10.1 min (**2.23**, 94.4% UV); 89% e.e.

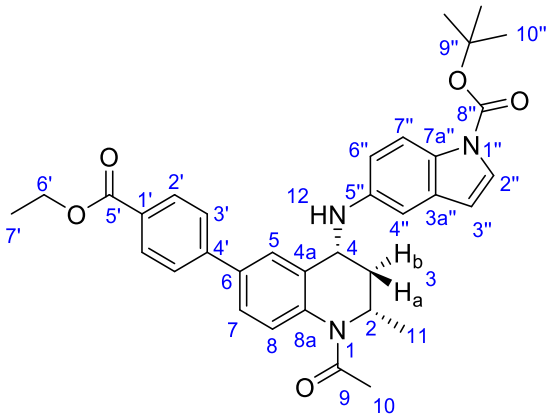
(1-(*tert*-Butoxycarbonyl)-1*H*-indol-5-yl)boronic acid (2.28)[163]



Di-*tert*-butyl dicarbonate (542 mg, 2.48 mmol, 4.0 eq.) and DMAP (15 mg, 0.123 mmol, 0.2 eq.) were added to a solution of 5-indoylboronic acid (100 mg, 0.621 mmol, 1.0 eq.) in

MeCN (2.8 mL). The resulting solution was stirred at rt for 1 h, after which time a solution of aqueous citric acid (0.5 M, 50 mL) was added, and the aqueous components were extracted with EtOAc (3 × 50 mL). The organic components were washed with brine (100 mL), dried over Na_2SO_4, filtered, and concentrated *in vacuo*. The crude material was purified using silica gel flash column chromatography (0–50% EtOAc/petroleum ether) to give **2.28** as an off-white solid (80 mg, 49%). R_f 0.48 (50% EtOAc/petroleum ether); m.p. 82–85 °C (from EtOAc); $\overline{\nu}_{max}$ (thin film)/cm^{-1} 2979 (C-H, w), 1734 (C=O, m), 1331 (m); ^{1}H NMR (600 MHz, $CDCl_3$) δ_H 8.55–8.54 (1H, m, H-4), 8.32–8.26 (1H, m, H-6), 8.26–8.23 (1H, m, H-7), 7.67 (1H, d, *J* 3.7, H-2), 6.74 (1H, d, *J* 3.7, H-3), 1.72 (9H, s, H-3'); ^{13}C NMR (151 MHz, $CDCl_3$) δ_C 149.9 (C-1'), 138.2 (C-7a), 131.5 (C-7), 130.6 (C-3a), 129.6 (C-4), 126.4 (C-2), 124.5 (C-5), 114.9 (C-6), 107.9 (C-3), 84.1 (C-2'), 28.4 (C-3'); ^{11}B NMR (128 MHz, $CDCl_3$) δ_B 4.31; LRMS *m/z* (ESI$^+$) 284 ([M+Na]$^+$, 87%). The R_f, ^{1}H and ^{13}C data are in agreement with the literature.[163]

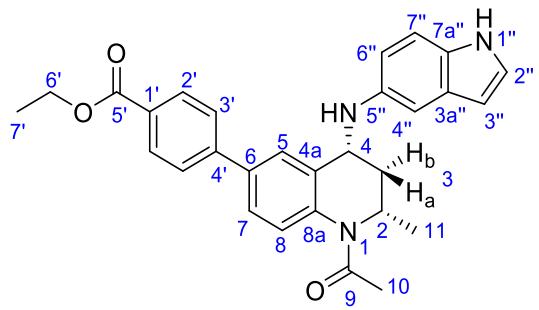
tert-Butyl 5-{(2*S*,4*R*)-(1-acetyl-6-[4-(ethoxycarbonyl)phenyl]-2-methyl-1,2,3,4-tetrahydroquinolin-4-yl)amino}-1*H*-indole-1-carboxylate (2.29)



Compound **2.14** (47 mg, 0.133 mmol, 1 eq.) and boronic acid **2.28** (69 mg, 0.264 mmol, 2 eq.) were dissolved in anhydrous CH_2Cl_2 (1.0 mL) in a round bottom flask containing activated 3 Å molecular sieves, connected to a drying tube containing P_2O_5, open to the atmosphere. NEt_3 (55 µL, 0.395 mmol, 3 eq.) was added and the resulting solution was left to stir at rt for 15 h. The molecular sieves were removed using filtration and the filtrate was

concentrated *in vacuo*. The resulting residue was purified using silica gel flash column chromatography column (0–15% EtOAc/CH_2Cl_2) to give **2.29** as a colourless solid (40 mg, 53%): R_f 0.20 (10% EtOAc/CH_2Cl_2); $[\alpha]_D^{25}$ = +244.3 (*c* 1.0, $CHCl_3$); m.p. 117–121 °C (from CH_2Cl_2); $\overline{\nu}_{max}$ (thin film)/cm^{-1} 3347 (N-H, w), 2978 (C-H, w), 1720 (C=O, s), 1653 (N-H, m); ^{1}H NMR (400 MHz, $CDCl_3$) δ_H 8.06–8.01 (2H, m, H-2'), 8.00–7.91 (1H, m, H-7''), 7.68–7.64 (1H, m, H-5), 7.58–7.49 (4H, m, H-7, H-2'', H-3'), 7.28–7.21 (1H, m, H-8), 6.80–6.79 (1H, m, H-4''), 6.79–6.73 (1H, m, H-6''), 6.40 (1H, d, *J* 3.6, H-3''), 4.99–4.82 (1H, m, H-2), 4.37 (2H, q, *J* 7.1, H-6'), 4.31 (1H, dd, *J* 12.0, 4.2, H-4), 3.84 (1H, br s, H-12), 2.72 (1H, ddd, *J* 12.5, 8.6, 4.2, H_a-3), 2.26 (3H, s, H-10), 1.65 (9H, s, H-10''), 1.38 (3H, t, *J* 7.1, H-7'), 1.36–1.27 (1H, m, H_b-3), 1.21 (3H, d, *J* 6.3, H-11);^{13}C NMR (126 MHz, $CDCl_3$) δ_C 169.6 (C-9), 166.5 (C-5'), 149.9 (C-8''), 144.7 (C-4'), 143.2 (C-5''), 138.8 (C-4a), 137.9 (C-6), 136.6 (C-8a), 131.9 (C-7a''), 130.2 (C-2'), 129.4 (C-1'), 129.1 (C-3a''), 127.0 (C-3'), 126.5 (C-7, C-2''), 126.0 (C-7), 123.0 (C-5), 116.1 (C-7''), 112.7 (C-6''), 107.0 (C-3''), 103.7 (C-4''), 83.4 (C-9''), 61.1 (C-6'), 51.0 (C-4), 47.8 (C-2), 41.4 (C-3), 28.4 (C-10''), 23.3 (C-10), 21.5 (C-11), 14.5 (C-7'); LRMS *m/z* (ESI^+) 568 ($[M+H]^+$, 37%); HRMS *m/z* (ESI^+) [Found: 568.2803, $C_{34}H_{38}O_5N_3$, requires $[M+H]^+$ 568.2806]; HPLC (Method 1) Retention time = 13.1 min, 98.1%; Chiral HPLC (Method 2), Chiral IG-3 column (50:50 hexane/IPA, 1.0 $mLmin^{-1}$) Retention time = 11.2 min (**2.29**, 92.0% UV), Retention time = 17.0 (opposite enantiomer, 8.0% UV); 84% e.e.

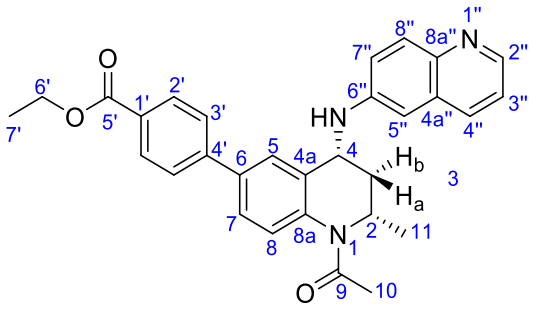
Ethyl 4-{(2*S*,4*R*)-1-acetyl-4-[(1*H*-indol-5-yl)amino]-2-methyl-1,2,3,4-tetrahydroquinolin-6-yl}benzoate (2.30)



TFA (0.8 mL) was added dropwise to a solution of **2.29** (85 mg, 0.150 mmol, 1 eq.) in CH_2Cl_2 (0.8 mL) and the resulting solution was stirred at room temperature for 30 min. After this time, the solution was diluted with EtOAc (15 mL) and neutralised with saturated $NaHCO_{3(aq)}$ (10 mL). The organic and aqueous components were separated, and the aqueous components were extracted with EtOAc (3 × 10 mL). The organic components were combined, dried over $NaSO_4$, filtered, and concentrated *in vacuo*. The crude material was purified using silica gel flash column chromatography (0–50% EtOAc/petroleum ether) to give **2.30** as a yellow solid (32 mg, 46%): R_f 0.28 (50% EtOAc/pentane); $[\alpha]_D^{25}$ = +280.4 (*c* 1.0, $CHCl_3$); mp 104–108 °C (from EtOAc); $\overline{\nu}_{max}$ (thin film)/cm^{-1} 2975 (C-H, m), 1709 (C=O, m), 1647 (N-H, m); ^{1}H NMR (600 MHz, CD_3CN) δ_H 9.00 (1H, s, H-1''), 8.00 (2H, d, *J* 8.2, H-2'), 7.67–7.66 (1H, m, H-5), 7.63 (2H, d, *J* 8.2, H-3'), 7.60 (1H, dd, *J* 8.2, 2.2, H-7), 7.37 (1H, d, *J* 8.2, H-8), 7.26 (1H, d, *J* 8.6, H-7''), 7.13–7.10 (1H, m, H-2''), 6.85–6.82 (1H, m, H-4''), 6.75 (1H, dd, *J* 8.6, 2.3, H-6''), 6.23–6.21 (1H, m, H-3''), 4.81–4.74 (1H, m, H-2), 4.38–4.29 (3H, m, H-4, H-6'), 2.71 (1H, ddd, *J* 12.4, 8.5, 4.0, H_a-3), 2.17 (3H, s, H-10), 1.34 (3H, t, *J* 7.1, H-7'), 1.30 – 1.22 (1H, m, H_b-3), 1.14 (3H, d, *J* 6.3, H-11); ^{13}C NMR (151 MHz, CD_3CN) δ_C 170.0 (C-9), 167.0 (C-5'), 145.8 (C-4'), 142.4 (C-5''), 140.5 (C-4a), 138.2 (C-8a), 137.5 (C-6), 131.4 (C-7a''), 130.9 (C-2'), 130.4 (C-1'), 130.0 (C-3a''), 127.7 (C-3'), 126.3 (C-7), 125.9 (C-2''), 123.7 (C-5), 112.9 (C-6''/7''), 112.9 (C-6''/7''), 103.4 (C-4''), 101.6 (C-3''), 61.8 (C-6'), 51.6 (C-4), 48.8 (C-2), 41.7 (C-3), 23.3 (C-10), 21.8 (C-11), 14.6 (C-7'); LRMS *m/z* (ESI$^+$) 468 ([M+H]$^+$, 13%); HRMS *m/z* (ESI$^+$) [Found: 468.2281, $C_{29}H_{30}O_3N_3$ requires

$[M+H]^+$ 468.2282]; HPLC (Method 1) Retention time = 8.8 min, 97.5%; Chiral HPLC, Chiral IF-3 column (70:30 hexane/IPA, 1.0 $mLmin^{-1}$) Retention time = 14.0 min (**2.30**, 95.4% UV), Retention time = 16.7 (opposite enantiomer, 4.6% UV); 91% e.e.

Ethyl 4-{(2*S*,4*R*)-1-acetyl-2-methyl-4-[(quinolin-6-yl)amino]-1,2,3,4-tetrahydroquinolin-6-yl}benzoate (2.31)



Method 1:

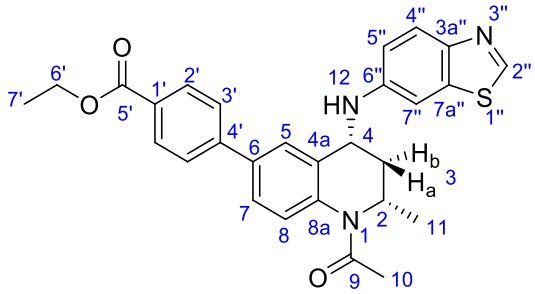
Compound **2.14** (56 mg, 0.159 mmol, 1.2 eq.), 6-bromoquinoline (18 µL, 0.133 mmol, 1.0 eq.), CyJohnPhos (5 mg, 0.0143 mmol, 0.11 eq.), $Pd(OAc)_2$ (2 mg, 0.00891 mmol, 0.067 eq.), and NaO^tBu (15 mg, 0.156 mmol, 1.2 eq.) were added to a dry microwave vial, and the vial was purged with Ar. Anhydrous, degassed toluene (0.32 mL) was added to the vial, and the resulting suspension was stirred at 100 °C for 15 h. After this time the solution was cooled to rt and filtered through Celite®, eluting with toluene, Et_2O, and EtOAc. The washings were partially concentrated *in vacuo* to remove the Et_2O, diluted with EtOAc (10 mL), and washed with H_2O (20 mL) and then $HCl_{(aq)}$ (1 M, 20 mL). The aqueous components were extracted with EtOAc (3 × 20 mL). The aqueous components were then neutralised with saturated $NaHCO_{3(aq)}$ and further extracted with EtOAc (3 × 40 mL). The combined organic components were washed with brine, dried over Na_2SO_4, filtered, and concentrated *in vacuo*. The crude material was purified using silica gel flash column chromatography (0–80% EtOAc/petroleum ether, 1% NEt_3) to give compound **2.31** as a yellow solid (19 mg, 30%).

Method 2:

Compound **2.14** (38 mg, 0.108 mmol, 1.0 eq.), 6-bromoquinoline (29 µL, 0.216 mmol, 2.0 eq.), BrettPhos (19 mg, 0.0346 mmol, 0.32 eq.), BrettPhos Pd G3 (8 mg, 0.00864 mmol, 0.080 eq.), and NaO^{t}Bu (13 mg, 0.130 mmol, 1.2 eq.) were added to a dry microwave vial, and the vial was purged with Ar. Anhydrous, degassed toluene (0.64 mL) was added and the resulting suspension was stirred at 70 °C for 17 h. The solution was then concentrated *in vacuo* and the residue was then redissolved in EtOAc (20 mL) and saturated $NaHCO_{3(aq)}$. The organic and aqueous components were separated and the aqueous components were extracted with EtOAc (3 × 30 mL). The combined organic components were then dried over Na_2SO_4, filtered, and concentrated *in vacuo*. The crude material was purified using silica gel flash column chromatography (0–60% EtOAc/petroleum ether, 1% NEt_3), followed by semi-preparative HPLC to give compound **2.31** as a yellow solid (12 mg, 23%): R_f 0.16 (60% EtOAc/petroleum ether, 1% NEt_3); $[\alpha]_D^{25}$ = +405.8 (*c* 1.0, $CHCl_3$); m.p. 82–86°C (from $CHCl_3$); $\overline{\nu}_{max}$ (thin film)/cm^{-1} 3324 (N-H, m), 2981 (C-H, m), 1712 (C=O, s), 1626 (s), 1608 (s); ^{1}H NMR (400 MHz, CD_3CN) δ_H 8.53 (1H, dd, *J* 4.2, 1.7, H-2''), 7.98–7.92 (2H, m, H-2'), 7.89 (1H, dd, *J* 8.4, 1.7, H-4''), 7.84 (1H, d, *J* 9.1, H-8''), 7.65–7.57 (3H, m, H-7, H-3'), 7.57–7.53 (1H, m, H-5), 7.39 (1H, d, *J* 8.2, H-8), 7.35 (1H, dd, *J* 9.1, 2.6, H-7''), 7.24 (1H, dd, *J* 8.4, 4.2, H-3''), 6.85 (1H, d, *J* 2.6, H-5''), 5.26 (1H, d, *J* 7.9, H-12), 4.90–4.76 (1H, m, H-2), 4.49 (1H, ddd, *J* 12.1, 7.9, 4.1, H-4), 4.30 (2H, q, *J* 7.1, H-6'), 2.74 (1H, ddd, *J* 12.5, 8.5, 4.1, H_a-3), 2.19 (3H, s, H-10), 1.41–1.29 (1H, m, H_b-3), 1.32 (3H, t, *J* 7.1, H-7'), 1.16 (3H, d, *J* 6.3, H-11); ^{13}C NMR (151 MHz, CD_3CN) δ_C 170.1 (C-9), 166.9 (C-5'), 147.1 (C-2''), 147.0 (C-6''), 145.6 (C-4'), 144.1 (C-8a''), 139.1 (C-4a), 138.3 (C-8a), 137.6 (C-6), 134.5 (C-4''), 131.15 (C-4a''), 131.12 (C-8''), 130.8 (C-2'), 130.4 (C-1'), 127.9 (C-8), 127.7 (C-3'), 126.6 (C-7), 123.2 (C-5), 122.5 (C-3''), 122.4 (C-7''), 104.5 (C-5''), 61.8 (C-6'), 50.5 (C-4), 48.6 (C-2), 41.4 (C-3), 23.4 (C-10), 21.7 (C-11), 14.6 (C-7'); LRMS *m/z* (ESI$^+$) 480 ([M+H$^+$]$^+$, 100%); HRMS *m/z* (ESI$^+$) [Found: 480.2278, requires [M+H]$^+$ 480.2282)]; HPLC (Method 1) Retention time = 8.6 min, 95.7%; Chiral HPLC (Method 2), Chiral IG-3 column (40:60

hexane/IPA, 1.0 mLmin^{-1}) Retention time = 9.8 min (**2.31**, 93.1% UV), Retention time = 18.4 min (opposite enantiomer, 6.9% UV); 86% e.e.

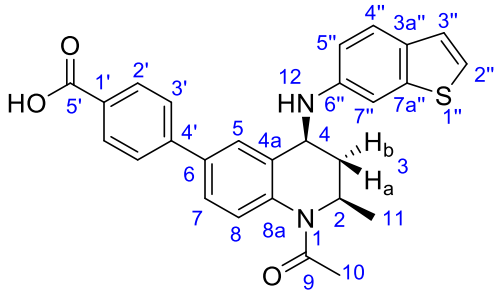
Ethyl 4-{(2*S*,4*R*)1-acetyl-4-[(1,3-benzothiazol-6-yl)amino]-2-methyl-1,2,3,4-tetrahydroquinolin-6-yl}benzoate (2.32)



Compound **2.14** (60 mg, 0.170 mmol, 1.0 eq.), 6-bromobenzothiazole (72 mg, 0.340 mmol, 2.0 eq.), BrettPhos (29 mg, 0.0540 mmol, 0.32 eq.), NaO^{t}Bu (20 mg, 0.208 mmol, 1.2 eq.) and BrettPhos Pd G3 (12 mg, 0.0132 mmol, 0.078 eq.) were added to a dry microwave vial under Ar. Degassed, anhydrous toluene (1 mL) was added and the resulting suspension was stirred at 70 °C for 16 h. After this time, the reaction mixture was cooled to rt, and filtered through Celite®, eluting with toluene, Et_2O, and EtOAc. The filtrate was concentrated *in vacuo*, and then redissolved in EtOAc and satd. $NaHCO_{3(aq)}$. The layers were separated, and the aqueous components were extracted with EtOAc (3 × 10 mL). The combined organic components were dried over Na_2SO_4, filtered, and concentrated *in vacuo*. The crude material was purified using silica gel flash column chromatography (0–70% EtOAc/pentane) to give **2.32** as a yellow solid (40 mg, 48%). R_f 0.15 (50% EtOAc/pentane); $[\alpha]_D^{25}$ = +263.8 (*c* 1.0, $CHCl_3$); m.p. 114–117 °C (from MeCN); $\overline{\nu}_{max}$ (thin film)/cm^{-1} 3341 (N-H, w), 2980 (C-H, w), 1711 (C=O, m), 1642 (C=O, m); ^{1}H NMR (500 MHz, CD_3CN) δ_H 8.70 (1H, s, H-2''), 8.00–7.96 (2H, m, H-2'), 7.83 (1H, d, *J* 8.9, H-4''), 7.63–7.59 (3H, m, H-3', H-7), 7.56–7.53 (1H, m, H-5), 7.38 (1H, d, *J* 8.1, H-8), 7.22 (1H, d, *J* 2.4, H-7''), 7.02 (1H, dd, *J* 8.9, 2.4, H-5''), 5.13 (1H, d, *J* 8.0, H-12), 4.86–4.74 (1H, m, H-2), 4.41 (1H, ddd, *J* 12.2, 8.0, 4.2, H-4), 4.31 (2H, q, *J* 7.1, H-6'), 2.72 (1H, ddd, *J* 12.5, 8.5, 4.2, H_a-3), 2.17 (3H, s, H-10), 1.37–1.25 (4H, m, H-7', H_b-3), 1.14 (3H, d, *J* 6.3, H-11); ^{13}C NMR (126 MHz, CD_3CN) δ_C

170.0 (C-9), 166.9 (C-5'), 150.6 (C-2''), 147.5 (C-6''), 147.0 (C-3a''), 145.6 (C-4'), 139.3 (C-6), 138.2 (C-8a), 137.6 (C-4a), 136.9 (C-7a''), 130.8 (C-2'), 130.4 (C-1'), 127.9 (C-8), 127.7 (C-3'), 126.6 (C-7), 124.5 (C-4''), 123.2 (C-5), 115.8 (C-5''), 103.6 (C-7''), 61.8 (C-6'), 50.7 (C-4), 48.6 (C-2), 41.5 (C-3), 23.4 (C-10), 21.7 (C-11), 14.6 (C-7'); LRMS *m/z* (ESI^+) 486 [$M+H^+$, 100%); HRMS *m/z* (ESI^+) [Found: 486.1844, $C_{28}H_{28}O_3N_3S$, requires $[M+H]^+$ 486.1846]; HPLC (Method 1) Retention time = 10.7 min, 96.0%. Chiral HPLC (Method 1), Chiral AD-H column (50:50 hexane/IPA, 1.0 $mLmin^{-1}$) Retention time = 8.0 min (opposite enantiomer, 7.5% UV), Retention time = 10.6 min (**2.32**, 92.5% UV); 85% e.e.

4-{(2*R*,4*S*)-1-Acetyl-4-[(1-benzothiophen-6-yl)amino]-2-methyl-1,2,3,4-tetrahydroquinolin-6-yl}benzoic acid (2.33)

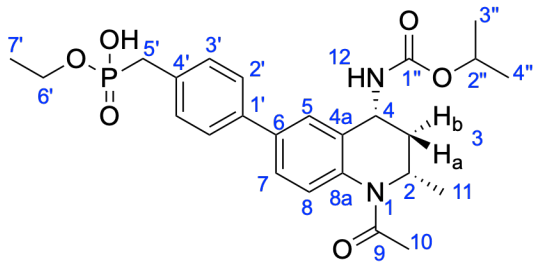


Compound **2.23** (67 mg, 0.138 mmol, 1 eq.) was dissolved in EtOH (0.86 mL), $NaOH_{(aq)}$ (2 M, 695 µL, 1.39 mmol, 10 eq.) was added over 1 h, and the resulting solution was left to stir at rt for 3 h. After this time, the solution was acidified to approximately pH 3 with 1 M $HCl_{(aq)}$, and diluted with H_2O (5 mL) and EtOAc (10 mL). The aqueous components were then extracted with EtOAc (3 × 10 mL). The combined organic components were dried over Na_2SO_4, filtered, and concentrated *in vacuo*. The crude material was purified using semi-preparative HPLC and lyophilised to give **2.33** as an off-white solid (20 mg, 32%): R_f 0.63 (50% EtOAc/petroleum ether, 1% acetic acid); $[\alpha]_D^{25}$ = –247.7 (*c* 0.47, $CHCl_3$); m.p. 118–123 °C (from CH_2Cl_2) [opposite enantiomer: 115–120 °C]; ^1H NMR (400 MHz, CD_3CN) δ_H 8.02 – 7.95 (2H, m, H-2'), 7.66 – 7.58 (4H, m, H-7, H-3', H-4''), 7.55 (1H, d, *J* 1.4, H-5), 7.38 (1H, d, *J* 8.2, H-8), 7.19 (1H, d, *J* 5.5, 0.7, H-3''), 7.16 – 7.13 (2H, m, H2'', H-7''), 6.92 (1H, dd, *J* 8.6, 2.2, H-5''), 4.86 – 4.73 (1H, m, H-2), 4.41 (1H, dd, *J* 12.1, 4.1, H-4), 2.71 (1H, ddd,

J 12.5, 8.6, 4.1, H_b-3), 2.18 (3H, s, H-10), 1.30 (1H, m, H_a-3), 1.15 (3H, d, *J* 6.3, H-11); ^{13}C NMR (151 MHz, CD_3CN) δ_C 170.1 (C-9), 167.6 (C-5'), 146.8 (C-6''), 145.8 (C4'), 142.8 (C-7a''), 139.6 (C4a), 138.2 (C-8a), 137.7 (C-6), 132.5 (C-3a''), 131.2 (C-2'), 130.0 (C-1'), 127.9 (C-8), 127.7 (C-3'), 126.6 (C-4''), 125.1 (C-7), 124.6 (C-3''), 123.3 (C-5), 122.5 (C-2''), 114.7 (C-5''), 104.6 (C7''), 50.7 (C-4), 48.7 (C-2), 41.6 (C-3), 23.4 (C-10), 21.7 (C-11); LRMS *m/z* (ESI^+) 479 ($[M+Na]^+$, 25%); HPLC (Method 1) Retention time = 10.1 min, 99.8%; Chiral HPLC, Chiral AD-H column (hexane/IPA, 1.0 $mLmin^{-1}$) Retention time = 6.7 min (opposite enantiomer (**2.1**), 5.5% UV), Retention time = 9.8 min (**2.33**, 94.5% UV); 89% e.e.

6.2.2 Compounds from Chapter 3

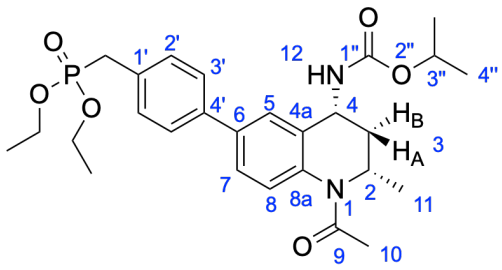
Isopropyl ((2*S*,4*R*)-1-acetyl-6-(4-((ethoxy(hydroxy)phosphoryl)methyl)phenyl)-2-methyl-1,2,3,4-tetrahydroquinolin-4-yl)carbamate (3.1)



Compound **3.2** (54 mg, 0.105 mmol, 1 eq.) was dissolved in EtOH (0.65 mL). $NaOH_{(aq)}$ (2 M, 52 µL, 0.105 mmol, 1 eq.) was added to the solution and the reaction was stirred for 1 h at rt, after which further $NaOH_{(aq)}$ (2 M, 208 µL, 0.416 mmol, 4 eq.) and the solution was stirred for 30 min. Further $NaOH_{(aq)}$ (2 M, 262 µL, 0.524 mmol, 5 eq.) was added and the solution was stirred for 19 h at rt. The solution was then heated to 40 °C for 5 h, and then heated to 70 °C for 48 h. The solution was concentrated *in vacuo*, redissolved in EtOH (0.65 mL) and further $NaOH_{(aq)}$ (2 M, 525 µL, 1.05 mmol, 10 eq.) was added. The resulting solution was stirred at 70 °C for 4 h. The solution was concentrated *in vacuo* and then redissolved in EtOAc (10 mL), and H_2O (10 mL), and the organic and aqueous components were separated. The aqueous components were then extracted with a 9:1 $CHCl_3$/IPA solution (1 × 30 mL) and EtOAc (1 × 30 mL). The organic components were dried over Na_2SO_4, filtered and concentrated *in vacuo*. The crude material was purified by semi-preparative HPLC and lyophilised to give as a colourless solid **3.1** (16 mg, 31%). R_f 0.74 (50% MeCN/H_2O, Reverse phase); $[\alpha]_D^{25}$ = +209.4 (*c* 1.0, MeOH); m.p. 118–122 °C (lyophilised from MeCN/H_2O); $\overline{\nu}_{max}$ (thin film)/cm^{-1} 3301 (N-H, w), 2986 (C-H, w), 1693 (C=O, s), 1632 (C=O, s), 1492 (s); ^1H NMR (400 MHz, D_6-DMSO) δ_H 7.67 (1H, d, *J* 8.8, H-12), 7.58–7.51 (3H, m, H-5, H-2'), 7.40–7.32 (4H, m, H-7, H-8, H-3'), 4.90–4.79 (1H, m, H-2''), 4.72–4.59 (1H, m, H-2), 4.47–4.37 (1H, m, H-4), 3.93–3.82 (2H, m, H-6'), 3.08 (2H, d, *J* 21.3, H-5'), 2.52–2.42 (1H, m, H_a-3), 2.08 (3H, s, H-10), 1.28–1.19 (7H, m, H_b-3, H-3'',H-4''), 1.15 (3H, t, *J* 7.1, H-7'), 1.05 (3H,

d, *J* 6.3, H-11); ^{13}C NMR (151 MHz, D_6-DMSO) δ_C 168.5 (C-9), 155.9 (C-1'') 137.7 (d, *J* 3.6, C-1'), 137.0 (C-6), 136.9 (C-4a), 135.4 (C-8a), 132.8 (d, *J* 8.8, C-4'), 130.4 (d, *J* 6.5, C-3'), 126.5 (C-8), 126.2 (d, *J* 2.8, C-2'), 124.9 (C-5), 120.8 (C-7), 67.2 (C-2''), 60.5 (d, *J* 6.1, C-6'), 47.0 (C-2, C-4), 40.1 (C-3), 33.2 (d, *J* 133.0, C-5'), 22.7 (C-10), 22.05 (C-3''/C-4''), 22.01 (C-3''/C-4''), 21.3 (C-11), 16.3 (d, *J* 6.0, C-7'); ^{31}P NMR (243 MHz, DMSO) δ_P 23.2; LRMS *m/z* (ESI$^+$) 489 ([M+H]$^+$, 100%); HRMS *m/z* (ESI$^-$) [Found: 487.1995, $C_{25}H_{32}O_6N_2P$, requires 487.1992 [M-H]$^-$]; HPLC (Method 2) Retention time = 7.0 min, 96.8%; The enantiomers were unable to be separated by Normal Phase Chiral HPLC for ee determination.

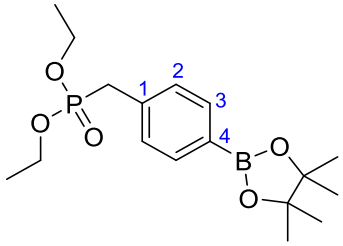
Diethyl ({4'-[(2*S*,4*R*)-1-acetyl-2-methyl-4-({[(propan-2''-yl)oxy]carbonyl}amino)-1,2,3,4-tetrahydroquinolin-6-yl]phenyl}methyl)phosphonate (3.2)[139]



Compound **3.40** (202 mg, 0.570 mmol, 1.05 eq.), compound **2.12** (200 mg, 0.542 mmol, 1.00 eq.), and Pd(dppf)Cl_2 (40 mg, 0.0547 mmol, 0.100 eq.) were added to a microwave vial which was subsequently sealed and flushed with Ar. Degassed 1,4-dioxane (4.0 mL) and degassed saturated $NaHCO_{3(aq)}$ (0.84 mL) were added and the resulting suspension was stirred at 100 °C with microwave irradiation for 2.5 h. The reaction mixture was then filtered through Celite®, eluting with EtOAc and MeOH, and the filtrate concentrated *in vacuo*. The residue was redissolved in EtOAc (40 mL) and H_2O (40 mL) and the aqueous components extracted with EtOAc (3 × 30 mL). The combined organic components were concentrated in vacuo and then purified by flash column chromatography (0–5% EtOH/EtOAc) to give **3.2** as a brown oil (177 mg, 63%); R_f 0.62 (5% EtOH/EtOAc); $[\alpha]_D^{25}$ = +180.1 (*c* 1.0, $CHCl_3$); ^{1}H NMR (400 MHz, MeOD) δ_H 7.64–7.57 (3H, m, H-7, H-3'), 7.52–7.49 (1H, m, H-5), 7.43 (2H, dd, *J* 8.3, 2.6, H-2'), 7.36 (1H, d, *J* 8.1, H-8), 4.97 (1H, h, *J* 6.3, H-3''), 4.89–4.79 (1H, m, H-2), 4.56 (1H, dd, *J* 12.6, 4.4, H-4), 4.16–4.03 (4H, m,

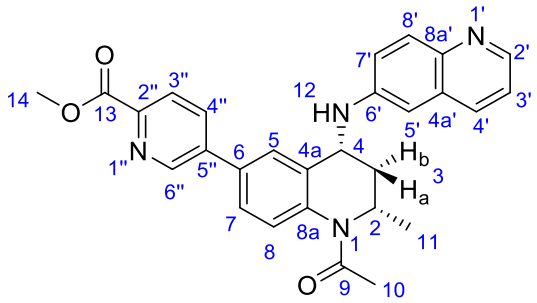
CH_3CH_2OP), 3.32 (2H, d, *J* 21.6, $PCH_2C(1')$), 2.58 (1H, ddd, *J* 12.8, 8.6, 4.4, H_A-3), 2.19 (3H, s, H-10), 1.39 – 1.22 (13H, m, H_A-3, H-4'', CH_3CH_2OP), 1.17 (3H, d, *J* 6.3, H-11); ^{31}P NMR (162 MHz, MeOD) δ_P 27.45; LRMS *m/z* (ESI^+) 539 ($[M+Na]^+$, 100%). The spectroscropic data are in good agreement with the previously reported values.[139]

Diethyl (4-(4,4,5,5-tetramethyl-1,3,2-dioxaborolan-2-yl)benzyl)phosphonate (3.40)[164,165]



Using a procedure as described by Garcia-Rodriguez *et al*,[164] $P(OEt)_3$ (1.59 mL, 9.27 mmol, 5.5 eq.) was added to 4-bromophenylboronic acid pinacol ester (500 mg, 1.68 mmol, 1.0 eq.) and stirred at 140 °C for 1 h. The mixture was purified by vacuum distillation (Kugelrohr) to give **3.40** as a colourless oil (545 mg, 92%): R_f 0.65 (5% EtOH/EtOAc); ^1H NMR (400 MHz, $CDCl_3$) δ_H 7.76–7.72 (2H, m, H-3), 7.32–7.27 (2H, m, H-2), 4.06–3.92 (4H, m, OCH_2CH_3), 3.16 (2H, d, *J* 21.9, $PCH_2C(1)$), 1.33 (12H, s, $OC(CH_3)_4$), 1.23 (6H, t, *J* 7.0, OCH_2CH_3); ^{13}C NMR (101 MHz, $CDCl_3$) δ_C 135.1 (d, *J* 3.0, C-3), 135.0 (C-4), 129.3 (d, *J* 6.5, C2), 83.9 ($BOC(CH_3)_2$), 62.3 (d, *J* 6.8, OCH_2)), 34.2 (d, *J* 137.4, $PCH_2C(1)$), 25.0 ($OC(CH_3)_4$), 16.5 (d, *J* 6.0, OCH_2CH_3), C-4 signal hidden by C-2 peak; ^{31}P NMR (162 MHz, $CDCl_3$) δ_P 25.93; ^{11}B NMR (128 MHz, $CDCl_3$) δ_B 30.67; LRMS *m/z* (ESI^+) 377 ($[M+Na]^+$, 100%); HRMS *m/z* (ESI^+) [Found: 355.1852, $C_{17}H_{28}BO_5P$, requires $[M+H]^+$ 355.1840]. The LRMS, ^1H, ^{13}C and ^{31}P NMR data are in good agreement with the literature.[164,165]

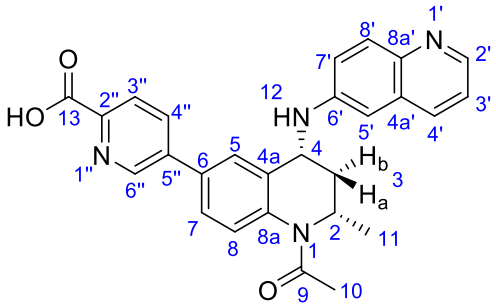
Methyl 5-((2*S*,4*R*)-1-acetyl-2-methyl-4-(quinolin-6-ylamino)-1,2,3,4-tetrahydroquinolin-6-yl)picolinate (3.41)



Compound **3.48** (132 mg, 0.389 mmol, 1.0 eq.) and quinoline-6-boronic acid (135 mg, 0.780 mmol, 2.0 eq.) were dissolved in anhydrous CH_2Cl_2 (2.1 mL) over 3 Å molecular sieves in a dry rbf with a drying tube containing P_2O_5 attached, open to atmosphere. $Cu(OAc)_2$ (106 mg, 0.584 mmol, 1.5 eq.) was added, followed by NEt_3 (162 µL, 1.16 mmol, 3.0 eq.) and the resulting suspension was stirred at rt for 20 h. The mixture was diluted with EtOAc (10 mL) and MeOH (10 mL) and filtered to remove the molecular sieves. The filtrate was concentrated *in vacuo* and the resulting residue partially purified by flash column chromatography (0–10% MeOH/CH_2Cl_2). The fractions containing the product were then concentrated *in vacuo*, further purified by semi-preparative HPLC and lyophilized to give **3.41** as a yellow solid (32 mg, 18%); R_f 0.47 (10% MeOH/CH_2Cl_2); $[\alpha]_D^{25}$ = + 507.3 (*c* 0.5, MeOH); m.p. 133–136 °C (lyophilised from MeCN/H_2O); $\overline{\nu}_{max}$ (thin film)/cm^{-1} 3332 (N-H, m), 2923 (C-H, m), 1727 (C=O, s), 1626 (N-H, m); ^{1}H NMR (600 MHz, CD_3CN) δ_H 8.84–8.83 (1H, m, H-6''), 8.54 (1H, dd, *J* 4.2, 1.7, H-2'), 8.04–8.01 (1H, m, H-3''), 7.80–7.97 (1H, m, H-4''), 7.90 (1H, d, *J* 8.1, H-4'), 7.84 (1H, d, *J* 9.1, H-8'), 7.66 (1H, dd, *J* 8.2, 2.2, H-7), 7.61–7.59 (1H, m, H-5), 7.45 (1H, d, *J* 8.2, H-8), 7.36 (1H, dd, *J* 9.1, 2.6, H-7'), 7.25 (1H, dd, *J* 8.3, 4.2, H-3'), 6.86 (1H, d, *J* 2.6, H-5'), 5.24 (1H, d, *J* 7.9, H-12), 4.87–4.78(1H, m, *J* 7.7, H-2), 4.52 (1H, ddd, *J* 12.1, 7.9, 4.2, H-4), 3.89 (3H, s, H-14), 2.76 (1H, ddd, *J* 12.5, 8.5, 4.2, H_a-3), 2.20 (3H, s, H-10), 1.41–1.31 (1H, m, H_b-3), 1.17 (3H, d, *J* 6.3, H-11); ^{13}C NMR (151 MHz, CD_3CN) δ_C 170.1 (C-9), 166.4 (C-13), 148.8 (C-6''), 147.6 (C-2''), 147.1 (C-2'), 147.0 (C-6'), 144.2 (C-8a'), 139.8 (C-5''), 139.4 (C-4a), 138.9 (C-6), 135.7 (C-4''), 134.6 (C—8a), 134.4 (C-4'), 131.14 (C-8'), 131.12 (C-4a'), 128.1 (C-8), 126.8 (C-7), 126.0 (C-3''),

123.5 (C-5), 122.5 (C-3'/C-7'), 122.4 (C-3'/C-7'), 104.6 (C-5'), 53.0 (C-14), 50.4 (C-4), 48.7 (C-2), 41.4 (C-3), 23.4 (C-10), 21.7 (C-11); LRMS *m/z* (ESI^+) 467 [$M+H^+$, 100%); HRMS *m/z* (ESI^+) [Found: 467.2090, $C_{28}H_{27}N_4O_3$, requires $[M+H]^+$ 467.2078]; HPLC (Method 2) Retention time = 6.1 min, 99.6%; Chiral HPLC (Method 2), Chiral IA column (70:30 hexane/IPA, 1.0 $mLmin^{-1}$) Retention time = 12.3 min (**3.41**, 93.28% UV), Retention time = 22.0 min (opposite enantiomer, 6.72% UV); 87% e.e.

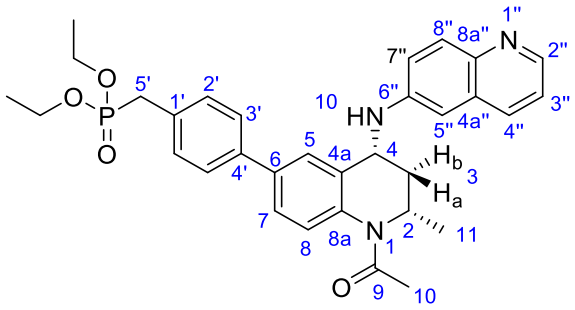
5-((2*S*,4*R*)-1-Acetyl-2-methyl-4-(quinolin-6-ylamino)-1,2,3,4-tetrahydroquinolin-6-yl)picolinic acid (3.42)



3.41 (23 mg, 0.0493 mmol, 1.0 eq.) was dissolved in EtOH (305 µL) and $NaOH_{(aq)}$ (2 M, 247 µL, 0.493 mmol, 10 eq.) was added dropwise to the resulting solution. The reaction mixture was stirred for 2 h, after which the reaction mixture was diluted with EtOAc (5 mL), and H_2O (10 mL), and the aqueous and organic components were separated. The aqueous components were acidified to pH 5 using $HCl_{(aq)}$ (2 M) and extracted with a 9:1 $CHCl_3$/IPA solution (3 × 20 mL). The combined organic components were dried over Na_2SO_4, concentrated *in vacuo*. The crude material was purified by semi-preparative HPLC (and the fractions containing the product lyophilised to give **3.42** as a yellow powder (4 mg, 18%): R_f 0.23 (50% MeCN/H_2O, Reverse phase); $[\alpha]_D^{25}$ = +209.2 (*c* 0.2, MeOH); m.p. 195–198 °C (from MeOH); $\overline{\nu}_{max}$ (thin film)/cm^{-1} 3368 (w), 2926 (C-H, w), 1624 (s), 1387 (m); ^1H NMR (400 MHz, MeOD) δ_H 8.78–8.70 (1H, br. s, H-6''), 8.56 (1H, dd, *J* 4.8, 1.5, H-2'), 8.33 (1H, d, *J* 8.5, H-4'), 8.17–8.09 (2H, m, H-3'', H-4''), 7.91 (1H, d, *J* 9.2, H-8'), 7.72 (1H, d, *J* 8.1, H-8), 7.62–7.56 (2H, m, H-5, H-7'), 7.56–7.47 (2H, m, H-7, H-3'), 6.99 (1H, d, *J* 2.6, H-5'), 4.98–4.87 (partially hidden by H_2O peak) (1H, m, H-2), 4.56 (1H, dd, *J* 12.1, 4.3, H-4), 2.81

(1H, ddd, *J* 12.6, 8.6, 4.3, H_a-3), 2.30 (3H, s, H-10), 1.54 – 1.42 (1H, m, H_b-3), 1.23 (3H, d, *J* 6.3, H-11); ^{13}C NMR (151 MHz, MeOD) δ_C 172.2 (C-9), 167.4 (C-13), 149.1 (C-6'), 148.1 (C-6''), 143.4 (C-2'), 140.6 (C-5''), 139.7 (C-4'), 139.5 (C-8a'), 139.3 (C-4a), 138.7 (C-8a), 137.0 (C-3''), 135.5 (C-6, C-2''), 132.7 (C-4a'), 128.6 (C-7), 127.4 (C-8), 126.7 (C-8'), 126.3 (C-4''), 125.3 (C-7'), 123.7 (C-5), 122.8 (C-3'), 104.1 (C-5'), 50.5 (C-4), 49.6 (C-2), 41.5 (C-3), 23.1 (C-10), 21.5 (C-11); LRMS *m/z* (ESI^+) 453 ([M+H]$^+$, 100%); HRMS *m/z* (ESI^+) [Found: 453.1923, $C_{27}H_{25}O_3N_4$, requires 453.1921 [M+H]$^+$]; HPLC (Method 2) Retention time = 5.2 min, > 99.9%; The enantiomers were unable to be separated by Normal Phase Chiral HPLC for ee determination.

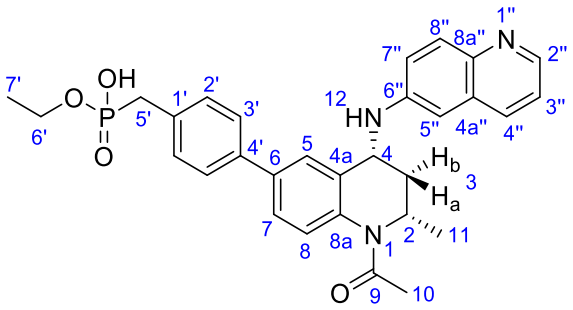
Diethyl (4'-((2*S*,4*R*)-1-acetyl-2-methyl-4-(quinolin-6''-ylamino)-1,2,3,4-tetrahydroquinolin-6-yl)benzyl)phosphonate (3.43)



Compound **3.49** (58 mg, 0.135 mmol. 1.0 eq.), NaO^{t}Bu (16 mg, 0.166 mmol, 1.2 eq.), BrettPhos (23 mg, 0.0428 mmol, 0.32 eq.), BrettPhos Pd G3 (9.8 mg, 0.0108 mmol, 0.080), 6-bromoquinoline (37 µL, 0.274 mmol, 2.0 eq.) were added to a dry microwave vial and the vial was sealed and purged with Ar. Anhydrous, degassed toluene (0.8 mL) was added and the resulting suspension was stirred at 70 °C for 23 h. The reaction was then cooled and diluted with EtOAc and MeOH and filtered through Celite®, eluting with EtOAc and MeOH. The filtrate was concentrated *in vacuo* and the redissolved in EtOAc (20 mL). The organic components were washed with H_2O (20 mL) and brine (20 mL), dried over Na_2SO_4, and concentrated *in vacuo*. The crude material was partially purified by flash column chromatography (0–10% MeOH/CH_2Cl_2) and then further purified by semi-preparative HPLC and lyophilized to give **3.43** as a yellow powder (23 mg, 31%): R_f 0.55 (10%

MeOH/CH_2Cl_2); $[\alpha]_D^{25}$ = +378.9 (*c* 0.4, MeOH); m.p. 98–101 °C (from MeOH); $\overline{\nu}_{max}$ (thin film)/cm^{-1} 3306 (N-H, w), 1626 (s, C=O), 1489 (m), 1383 (m), 1238 (m), 1027 (s); ^{1}H NMR (400 MHz, MeOD) δ_H 8.46 (1H, dd, *J* 4.4, 1.6, H-2''), 8.01 (1H, dd, *J* 8.3, 1.6,H-4''), 7.82 (1H, d, *J* 9.1, H-8''), 7.58 (1H, dd, *J* 8.2, 2.2, H-7), 7.54–7.50 (1H, m, H-5), 7.44–7.37 (4H, m, H-8, H-2', H-7''), 7.33–7.25 (3H, m, H-3',H-3''), 6.82 (1H, d, *J* 2.6, H-5''), 5.00–4.86 (1H, m, H-2), 4.46 (1H, dd, *J* 12.1, 4.1, H-4), 4.05–3.94 (4H, m, CH_2OP), 3.20 (2H, d, *J* 21.7, H-5'), 2.77 (1H, ddd, *J* 12.5, 8.6, 4.2, H_a-3), 2.28 (3H, s, H-10), 1.43 (1H, m, H_b-3), 1.24–1.17 (9H, m, H-11, C$H_3$$CH_2$OP); ^{13}C NMR (151 MHz, MeOD) δ_C 172.2 (C-9), 148.1 (C-6''), 146.3 (C-2''), 143.4 (C-8a''), 140.5 (d, *J* 4.1, C-4'), 140.0 (C-6), 139.4 (C-4a), 136.9 (C-8a), 136.0 (C-4''), 132.03 (C-4a''), 132.02 (d, *J* 9.2, C-1'), 131.5 (d, *J* 6.7, C-2'), 129.8 (C-8'') 127.94 (C-8), 127.86 (d, *J* 2.9, C-3'), 126.5 (C-7), 123.5 (C-5), 123.2 (C-7''), 122.6 (C-3''), 104.3 (C-5''), 63.7 (d, *J* 6.9, CH_2OP), 50.6 (C-4), 49.6 (C-2), 41.6 (C-3), 33.3 (d, *J* 137.9, C-5'), 23.0 (C-10), 21.5 (C-11), 16.6 (dd, *J* 6.0, 1.6); ^{31}P NMR (162 MHz, MeOD) δ_P 27.45; LRMS 558 ([M+H]$^+$, 100%); HRMS *m/z* (ESI$^+$) [Found: 558.2509, $C_{32}H_{37}O_4N_3P$, requires [M+H]$^+$ 558.2516]; HPLC (Method 2) Retention time = 7.0 min, 98.7%; Chiral HPLC (Method 2), Chiral IA column (60:40 hexane/IPA, 1.0 mLmin^{-1}) Retention time = 6.5 min (**3.43**, 93.9% UV), Retention time = 12.1 min (opposite enantiomer, 6.07% UV); 88% e.e.

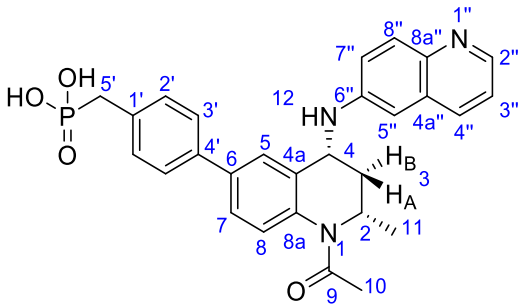
Ethyl hydrogen (4-((2*S*,4*R*)-1-acetyl-2-methyl-4-(quinolin-6-ylamino)-1,2,3,4-tetrahydroquinolin-6-yl)benzyl)phosphonate (3.44)



$NaOH_{(aq)}$ (2 M, 198 µL, 0.395 mmol, 10 eq.) was added to a solution of compound **3.43** (22 mg, 0.0395 mmol, 1 eq.) dissolved in EtOH (244 µL) and the resulting solution was stirred at 70 °C for 5 h 30 min, after which the temperature was increased to 80 °C and left

to stir for a further 20 h. The solution was then left to cool, diluted with H_2O (15 mL), and then acidified to ~ pH 1 using 1 M $HCl_{(aq)}$. The solution was extracted with EtOAc (2 × 15 mL) after which the aqueous components were basified to ~pH 5 using $NaHCO_{3(aq)}$. The aqueous components were then further extracted with a 9:1 $CHCl_3$/IPA solution (6 × 30 mL). The aqueous components were then acidified to ~pH 3 using 1 M $HCl_{(aq)}$ and extracted with 9:1 $CHCl_3$/IPA solution (2 × 30 mL). The combined organic components were dried over Na_2SO_4, filtered, and concentrated *in vacuo*. The crude material was purified by semi-preparative HPLC and lyophilised to give **3.44** as a bright yellow solid (6 mg, 29%): R_f 0.41 (50% MeCN/H_2O, Reverse phase); $[\alpha]_D^{25}$ = +366.2 (*c* 1.0, MeOH); m.p. 156–159 °C (from MeOH); $\overline{\nu}_{max}$ (thin film)/cm^{-1} 3398 (O-H, m), 2926 (C-H, w), 1624 (C=O, s), 1489 (s); ^{1}H NMR (400 MHz, D_6-DMSO) δ_H 8.49 (1H, dd, *J* 4.2, 1.7, H-2''), 7.97 (1H, dd, *J* 8.4, 1.7, H-4''), 7.78 (1H, d, *J* 9.1, H-8''), 7.55 (1H, dd, *J* 8.2, 2.2, H-7), 7.51–7.38 (5H, m, H-5, H-8, H-3', H-7''), 7.31–7.20 (3H, m, H-2', H-3''), 6.87 (1H, d, *J* 2.6, H-5''), 6.63 (1H, d, *J* 8.2, H-12), 4.83–4.69 (1H, m, H-2), 4.48 (1H, ddd, *J* 12.2, 8.2, 4.0, H-4), 3.89–3.78 (2H, m, H-6'), 3.00 (2H, d, *J* 21.3, H-5'), 2.70 (1H, ddd, *J* 12.1, 8.3, 4.0, H_a-3), 2.18 (3H, s, H-10), 1.36–1.21 (1H, m H_b-3), 1.18–0.96 (5H, m, H-11, H-7'); ^{13}C NMR (151 MHz, D_6-DMSO) δ_C 168.9 (C-9), 146.3 (C-6''), 145.4 (C-2''), 142.4 (C-8a''), 137.68 (C-4a/C-4'), 137.67 (C-4a/C-4'), 137.0 (C-8a), 135.9 (C-6), 133.5 (C-4''), 133.1 (d, *J* 9.0, C-1'), 130.4 (d, *J* 6.2, C-2'), 130.0 (C-4a''), 129.6 (C-8''), 126.7 (C-8), 126.1 (d, *J* 2.8, C-3'), 124.9 (C-7), 121.7 (C-7''), 121.6 (C-5), 121.5 (C-3''), 102.6 (C-5''), 60.4 (d, *J* 6.0, C-6'), 48.8 (C-4), 47.3 (C-2), 40.3 (C-3), 33.41 (d, *J* 132.5, C-5'), 23.1 (C-10), 21.4 (C-11), 16.4 (d, *J* 6.0, C-7'); ^{31}P NMR (243 MHz, DMSO) δ_P 23.25; LRMS *m/z* (ESI^+) 530 ($[M+H]^+$, 100%); HRMS *m/z* (ESI^+) [Found: 530.2198, $C_{30}H_{33}O_4N_3P$, requires 530.2203 $[M+H]^+$]; HPLC (Method 2) Retention time = 5.9 min, 98.6%; The enantiomers were unable to be separated by Normal Phase Chiral HPLC for ee determination.

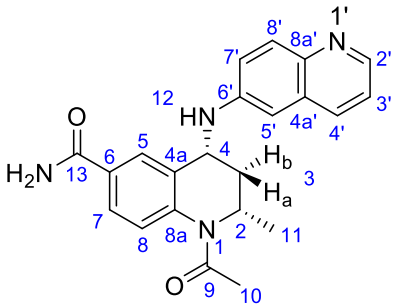
(4-((2*S*,4*R*)-1-Acetyl-2-methyl-4-(quinolin-6-ylamino)-1,2,3,4-tetrahydroquinolin-6-yl)benzyl)phosphonic acid (3.45)



Compound **3.43** (85 mg, 0.152 mmol, 1.0 eq.) was dissolved in anhydrous CH_2Cl_2 (1.9 mL) at rt. Bromotrimethylsilane (81 µL, 0.614 mmol, 4.0 eq.) was added to the resulting solution dropwise. The solution was stirred for 19 h, after which the solution was diluted with CH_2Cl_2 (5 mL) and MeOH (5 mL) and then concentrated *in vacuo*. The crude material was partially purified by flash column chromatography (reverse phase, 5–95% MeCN/H_2O) and the fractions containing the product were lyophilised. The product was then further purified by semi-preparative HPLC, and the fractions containing the pure product lyophilised to give **3.45** as a yellow solid (32 mg, 42%): R_f 0.46 (50% MeCN/H_2O, Reverse phase); $[\alpha]_D^{25}$ = +440.9 (*c* 0.18, MeOH); m.p. 198–202 °C (lyophilised from MeCN/H_2O); $\overline{\nu}_{max}$ (thin film)/cm^{-1} 3310 (N-H, w), 2926 (C-H, w), 1624 (C=O, s), 1489 (s); ^{1}H NMR (400 MHz, D_6-DMSO) δ_H 8.48 (1H, dd, *J* 4.2, 1.7, H-2''), 7.95 (1H, dd, *J* 8.4, 1.7, H-4''), 7.77 (1H, d, *J* 9.1, H-8''), 7.48 (1H, dd, *J* 8.2, 2.1, H-7), 7.45–7.37 (3H, m, H-5, H-7, H-7''), 7.36–7.30 (2H, m, H-3'), 7.25 (1H, dd, *J* 8.4, 4.2, H-3''), 7.22–7.16 (2H, m, H-2'), 6.86 (1H, d, *J* 2.6, H-5''), 6.61 (1H, d, *J* 8.2, H-12), 4.82–4.68 (1H, m, H-2), 4.50–4.40 (1H, m, H-4), 2.77 (2H, d, *J* 21.1, H-5'), 2.72–2.62 (1H, m, H_A-3), 2.16 (3H, s, H-10), 1.36–1.20 (1H, m, H_B-3), 1.11 (3H, d, *J* 6.3, H-11);^{13}C NMR (151 MHz, D_6-DMSO) δ_C 168.7 (C-9), 146.2 (C-6''), 145.3 (C-2''), 142.2 (C-8a), 137.59 (C-4a/C-4'), 137.57 (C-4a/C-4'), 137.0 (C-6), 135.9 (C-8a), 133.6 (d, *J* 8.7, C-1'), 133.4 (C-4''),130.3 (d, *J* 6.0, C-2'), 130.0 (C-4a''), 129.5 (C-8''), 126.6 (C-7''),126.1 (d, *J* 2.8, C-3'), 124.9 (C-7), 121.7 (C-8), 121.6 (C-5), 121.4 (C-3''), 102.4 (C-5''), 48.7 (C-4), 47.2 (C-2), 40.2 (C-3), 35.1 (d, *J* 131.3, C-5'), 23.1 (C-10), 21.3 (C-11); ^{31}P NMR (243 MHz, D_6-DMSO)

δ_P 20.7. LRMS *m/z* (ESI$^+$) 502 ([M+H]$^+$, 100%]; HRMS *m/z* (ESI$^+$) [Found: 502.1887, $C_{28}H_{29}O_4N_3P$, requires 502.1890 [M+H]$^+$]; HPLC (Method 2) Retention time = 5.5 min, 96.2%; The enantiomers were unable to be separated by Normal Phase Chiral HPLC for ee determination.

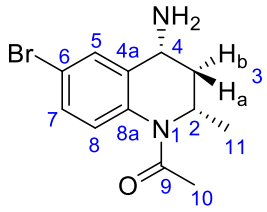
(2*S*,4*R*)-1-Acetyl-2-methyl-4-(quinolin-6-ylamino)-1,2,3,4-tetrahydroquinoline-6-carboxamide (3.46)



Compound **3.53** (30 mg, 0.0842 mmol, 1 eq.) was dissolved in DMSO (0.60 mL) and hydrogen peroxide solution (35% *w/v* in H_2O) (16 µL, 0.165 mmol, 2 eq.) and K_2CO_3 (47 mg, 0.337 mmol, 4 eq.) were added to the resulting solution. The resulting suspension was then stirred at rt for 3 h, after which further hydrogen peroxide solution (35% *w/v* in H_2O) (16 µL, 0.165 mmol, 2 eq.) was added and the suspension stirred for a further 1 h. The suspension was then diluted with EtOAc (5 mL) and H_2O (5 mL) and the organic and aqueous components were separated. The aqueous components were extracted with EtOAc (3 × 10 mL) and the combined organic components were dried over Na_2SO_4, filtered and concentrated *in vacuo*. The crude material was purified by semi-preparative HPLC to give **3.46** as a colourless solid (17 mg, 54%): R_f 0.49 (10% MeOH/CH_2Cl_2); $[\alpha]_D^{25}$ = +236.1 (*c* 0.7, MeOH); m.p 127–131 °C (from MeOH); $\overline{\nu}_{max}$ (thin film)/cm^{-1} 3343 (N-H, m), 1659 (C=O, s), 1626 (C=O, s), 1384 (m); ^{1}H NMR (400 MHz, MeOD) δ_H 8.46 (1H, dd, *J* 4.3, 1.6, H-2'), 8.04–7.99 (1H, m, H-4'), 7.88–7.86 (1H, m, H-7), 7.85–7.79 (2H, m, H-7, H-8'), 7.46–7.38 (2H, m, H-8, H-7'), 7.32 (1H, dd, *J* 8.3, 4.3, H-3'), 6.80 (1H, d, *J* 2.6, H-5'), 4.94–4.80 (1H, m, H-2, partially hidden by H_2O peak), 4.47 (1H, dd, *J* 12.0, 4.2, H-4), 2.77 (1H, ddd, *J* 12.6, 8.6, 4.2, H_a-3), 2.27 (3H, s, H-10), 1.48 – 1.36 (1H, m, H_b-3), 1.21 (3H, d, *J* 6.4, H-11); ^{13}C

NMR (151 MHz, MeOD) δ_C 172.2 (C-9), 171.7 (C-13), 147.9 (C-8a), 146.0 (C-2'), 143.0 (C-8a'), 140.9 (C-6), 139.2 (C-4a), 136.4 (C-4'), 132.7 (C-6'), 132.1 (C-4a'), 129.4 (C-8'), 127.5 (C-7), 127.4 (C-8), 124.8 (C-5), 123.5 (C-7'), 122.6 (C-3'), 104.1 (C-5'), 50.5 (C-4), 49.4 (C-2), 41.5 (C-3), 23.1 (C-10), 21.5 (C-11); LRMS *m/z* (ESI^+) 375 ($[M+H]^+$, 100%); HRMS *m/z* (ESI^+) [Found: 375.1814, $C_{22}H_{23}O_2N_4$, requires 375.1816 $[M+H]^+$]; HPLC (Method 2) Retention time = 4.9 min, 98.5%; Chiral HPLC, Chiral IB N-3 column (40:60 hexane/IPA, 1.0 $mLmin^{-1}$) Retention time = 7.9 min (opposite enantiomer, 5% UV), Retention time = 18.0 (**3.46**, 95% UV); 90% e.e.

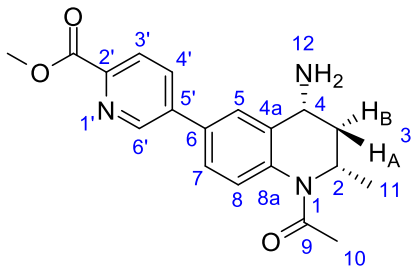
1-((2*S*,4*R*)-4-Amino-6-bromo-2-methyl-3,4-dihydroquinolin-1(2H)-yl)ethan-1-one (3.47) [32,166]



Compound **2.12** (300 mg, 0.812 mmol, 1 eq.) was dissolved in anhydrous CH_2Cl_2 (6.4 mL) and the resulting solution cooled to 0 °C. $AlCl_3$ (541 mg, 4.06 mmol, 5 eq.) was added and the resulting suspension was stirred for 20 min at 0 °C. A mixture of anhydrous MeOH (1.8 mL) and anhydrous NEt_3 (1.4 mL, 10.0 mmol, 12 eq.) was added, after which a white precipitate formed. The suspension was stirred for 10 min and then diluted with EtOAc (30 mL) and satd. Rochelle salt (30 mL). The suspension was then stirred at rt for 30 min, after which the precipitate dissolved. The solution was diluted with satd. $NaHCO_3$ (60 mL) and the organic and aqueous components were separated. The aqueous components were washed with EtOAc (3 × 50 mL) and the combined organic components were then dried over Na_2SO_4 and concentrated in vacuo to give **3.47** as a yellow-brown oil (228 mg, 99%): R_f 0.52 (10% MeOH/CH_2Cl_2); $[\alpha]_D^{25}$ = + 246.7 (*c* 1.0, $CHCl_3$); $\overline{\nu}_{max}$ (thin film)/cm^{-1} 3364 (N-H, w), 2925 (C-H, w), 1648 (C=O, s), 1479.02 (m), 1386.21 (m); ^{1}H NMR (400 MHz, $CDCl_3$) δ_H 7.64 (1H, dd, *J* 2.4, 1.1, H-5), 7.39 (1H, dd, *J* 8.4, 2.4, H-7), 6.97 (1H, d, *J* 8.4, H-8), 4.87–4.72 (1H, m, H-2), 3.74–3.66 (1H, m, H-4), 2.52 (1H, ddd, *J* 12.8, 8.7, 4.4, H_a-3), 2.08 (3H,

s, H-10), 1.16–1.04 (1H, m, H_b-3), 1.11 (3H, d, *J* 6.4, H-11); ^{13}C NMR (151 MHz, $CDCl_3$) δ_C 169.3 (C-9), 142.3 (C-4a), 135.5 (C-8a), 129.9 (C-7), 127.4 (C-8), 126.2 (C-5), 119.9 (C-6), 47.7 (C-2), 47.5 (C-4), 44.4 (C-3), 22.9 (C-10), 21.5 (C-11); LRMS *m/z* (ESI^+) 283 ($[M^{79}Br+H]^+$, 62%); HRMS *m/z* (ESI^+) [Found: 283.0449, $C_{12}H_{16}{}^{79}BrN_2O$, requires 283.0441 $[M+H]^+$]. The LRMS and ^{1}H NMR data are in good agreement with the literature values.[166]

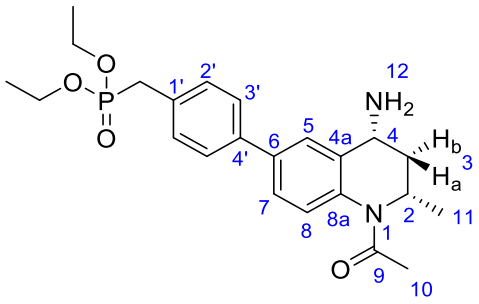
Methyl 5-((2*S*,4*R*)-1-acetyl-4-amino-2-methyl-1,2,3,4-tetrahydroquinolin-6-yl)picolinate (3.48)[142]



Compound **3.47** (160 mg, 0.565 mmol, 1.0 eq.), $Pd(dppf)Cl_2$ (62 mg, 0.0847 mmol, 0.15 eq.) and [6-(methyoxycarbonyl)pyridine-3-yl]boronic acid (123 mg, 0.680 mmol, 1.2 eq.) were added to a dry microwave vial which was then sealed and purged with Ar. Degassed anhydrous MeOH (3.2 mL), NEt_3 (0.16 mL) and DME (0.63 mL) were added to the microwave vial and the resulting solution stirred with microwave irradiation at 110 °C for 45 min. The solution was concentrated *in vacuo* and then purified by flash column chromatography (0–10% MeOH/CH_2Cl_2, 0.1% NEt_3). The fractions containing the product were concentrated *in vacuo*, redissolved in EtOAc (30 mL) and then washed with $HCl_{(aq)}$ (1 M, 30 mL). The aqueous components were then neutralised with satd. $NaHCO_{3(aq)}$ and extracted with EtOAc (3 × 60 mL) and then a 9:1 (*v/v*) $CHCl_3$/IPA solution (3 × 60 mL). The organic components were then dried over Na_2SO_4 to give **3.48** as a brown solid (103 mg, 54%). R_f 0.42 (10% MeOH/CH_2Cl_2); $[\alpha]_D^{25}$ = +275.0 (*c* 1.0, $CHCl_3$); $\overline{\nu}_{max}$ (thin film)/cm^{-1} 2985 (C-H, w), 1726 (C=O, s), 1647 (C=O, s); m.p. 34–36 °C (from CH_2Cl_2); ^{1}H NMR (600 MHz, $CDCl_3$) δ_H 8.99 (1H, d, *J* 2.3, H-6'), 8.21 (1H, d, *J* 8.1, H-3'), 8.06 (1H, dd, *J* 8.1, 2.3, H-4'), 7.79–7.76 (1H, m, H-5), 7.54 (1H, dd, *J* 8.1, 2.1, H-7), 7.24 (1H, d, 8.1, H-8), 4.90–4.78 (1H,

m, H-2), 4.04 (3H, s, C*H*$_3$OC(O)), 3.81 (1H, dd, *J* 12.1, 4.4, H-4), 2.57 (1H, ddd, *J* 12.8, 8.7, 4.4, H$_A$-3), 2.16 (3H, s, H-10), 1.27–1.14 (1H, m, H$_B$-3), 1.17 (3H, d, *J* 6.4, H-11); ^{13}C NMR (151 MHz, $CDCl_3$) δ_C 169.5 (C-9), 165.7 (CH_3OC(O)), 148.3 (C-6'), 146.7 (C-2'), 141.1 (C-4a), 139.5 (C-5'), 137.3 (C-8a), 135.2 (C-4'), 134.4 (C-6), 126.6 (C-8), 125.9 (C-7), 125.4 (C-3'), 121.8 (C-5), 53.1 (CH_3OC(O)), 48.0 (C-2), 47.6 (C-4), 44.7 (C-3), 23.1 (C-10), 21.6 (C-11); LRMS *m/z* (ESI$^+$) 340 ([M+H]$^+$, 100%); HRMS *m/z* (ESI$^+$) [Found: 340.1672, $C_{19}H_{22}N_3O_3$, requires [M+H]$^+$ 340.1656]. The LRMS data is in good agreement with the literature.[142]

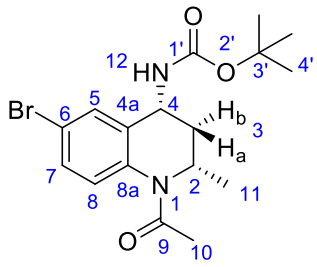
Diethyl (4'-((2*S*,4*R*)-1-acetyl-4-amino-2-methyl-1,2,3,4-tetrahydroquinolin-6-yl)benzyl)phosphonate (3.49)



Compound **3.47** (72 mg, 0.254 mmol, 1.00 eq.), compound **3.40** (95 mg, 0.268 mmol, 1.06 eq.) and Pd(dppf)Cl_2 (19 mg, 0.0260 mmol, 0.102 eq.) were added to a microwave vial and flushed with Ar. Degassed 1,4-dioxane (1.4 mL) and satd $NaHCO_3$ (0.30 mL) were added and the resulting suspension was stirred at 100 °C with microwave irradiation for 1.5 h. The suspension was then filtered through Celite® and concentrated *in vacuo*. The residue was redissolved in EtOAc (20 mL) and washed with $HCl_{(aq)}$ (2 M, 30 mL). The aqueous components were neutralised with satd. $NaHCO_3$ and extracted with EtOAc (1 × 30 mL) and a 9:1 CHCl3/IPA solution (3 × 40 mL). The combined organic components were dried over Na_2SO_4, filtered, and concentrated *in vacuo*. The crude material was purified by flash column chromatography (0–10% MeOH/CH_2Cl_2, 1% NEt_3) to give **3.49** as a brown oil (58 mg, 56%): R_f 0.53 (10% MeOH/CH_2Cl_2); $[\alpha]_D^{25}$ = +130.0 (*c* 1.0, $CHCl_3$); $\overline{\nu}_{max}$ (thin film)/cm^{-1} 3431 (N-H, w), 2984 (C-H, w), 1641 (C=O, s), 1491 (s), 1391 (m); ^{1}H NMR

(400 MHz, $CDCl_3$) δ_H 7.71–7.68 (1H, m, H-5), 7.61–7.54 (2H, m, H-3'), 7.48 (1H, dd, *J* 8.1, 2.1, H-7), 7.42–7.34 (1H, m, H-2'), 7.16 (1H, d, *J* 8.2, H-8), 4.92–4.76 (1H, m, H-2), 4.12–3.96 (4H, m, CH_3CH_2OP), 3.78 (1H, dd, *J* 12.1, 4.3, H-4), 3.19 (2H, d, *J* 21.7, PCH_2), 2.55 (1H, ddd, *J* 12.7, 8.7, 4.3, H_a-3), 2.14 (3H, s, H-10), 1.26 (6H, t, *J* 7.0, CH_3CH_2OP), 1.20–1.09 (4H, m, H_b-3, H-11); ^{13}C NMR (151 MHz, $CDCl_3$) δ_C 169.6 (C-9), 140.5 (C-4a), 139.3 (d, *J* 3.9, C-4'), 138.7 (C-6), 135.7 (C-8a), 131.0 (d, *J* 9.2, C-1'), 130.4 (d, *J* 6.6, C-2'), 127.3 (d, *J* 3.2, C-3'), 126.2 (C-8), 125.3 (C-7), 121.1 (C-5), 62.3 (d, *J* 6.8, CH_3CH_2OP), 47.74 (C-21), 47.70 (C-4), 44.7 (C-3), 33.6 (d, *J* 138.1, PCH_2), 23.1 (C-10), 21.5 (C-11), 16.5 (d, *J* 6.0, CH_3CH_2OP); ^{31}P NMR (162 MHz, $CDCl_3$) δ_P 26.29; LRMS *m/z* (ESI^+) 431 ($[M+H]^+$, 30%); HRMS *m/z* (ESI^+) [Found: 431.2110, $C_{23}H_{32}N_2O_4P$, requires $[M+H]^+$ 431.2094]; HPLC (Method 2) Retention time = 6.18 min, 94.4%

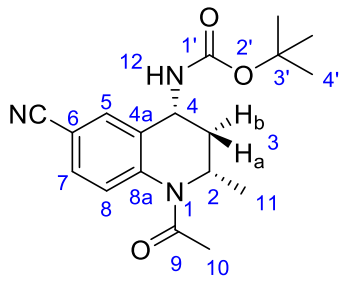
tert-Butyl ((2*S*,4*R*)-1-acetyl-6-bromo-2-methyl-1,2,3,4-tetrahydroquinolin-4-yl)carbamate (3.50)[33,167]



Using a modified previously reported procedure,[167] compound **3.47** (316 mg, 1.12 mmol, 1.0 eq.) was dissolved in CH_2Cl_2 (6 mL). NEt_3 (0.47 mL, 3.37 mmol, 3.0 eq.) and di-*tert*-butyl dicarbonate (268 mg, 1.23 mmol, 1.1 eq.) were added and the resulting solution was stirred at rt for 4 h. The solution was then diluted with CH_2Cl_2 (30 mL), washed with H_2O (30 mL) and the organic and aqueous components were separated. The aqueous components were then extracted with CH_2Cl_2 (3 × 30 mL) and the combined organic components were dried over Na_2SO_4, filtered, and concentrated *in vacuo*. The crude material was purified by flash column chromatography (30–60% EtOAc/petroleum ether) to give **3.50** as a colourless solid (266 mg, 62%): R_f 0.36 (50% EtOAc/Petroleum ether); $[\alpha]_D^{25}$ = +140.5 (*c* 1.0, $CHCl_3$); m.p. 153 – 156 °C (from $CHCl_3$); $\overline{\nu}_{max}$ (thin film)/cm^{-1} 1713 (C=O, s), 1648 (C=O, s), 1527(m),

1482 (m); ^{1}H NMR (400 MHz, $CDCl_3$) δ_H 7.45–7.34 (2H, m, H-5, H-7), 6.98 (1H, d, *J* 8.2, H-8), 4.90–4.77 (1H, m, H-2), 4.74–4.65 (1H, m, H-12), 4.62–4.49 (1H, m, H-4), 2.56 (1H, ddd, *J* 12.7, 8.6, 4.5, H_a-3), 2.08 (3H, s, H-10), 1.50 (9H, s, H-4'), 1.23 – 1.13 (1H, m, H_b-3), 1.11 (3H, d, *J* 6.4, H-11); ^{13}C NMR (151 MHz, $CDCl_3$) δ_C 169.3 (C-9), 155.5 (C-1'), 139.1 (C-4a), 135.6 (C-8a), 130.4 (C-5/C-7), 127.6 (C-8), 126.3 (C-5/C-7), 119.7 (C-6), 80.6 (C-3'), 47.2 (C-2), 46.9 (C-4), 40.9 (C-3), 28.5 (C-4'), 22.9 (C-10), 21.4 (C-11); LRMS *m/z* (ESI^+) 383 ($[M^{79}Br+H]^+$, 13%); HRMS *m/z* (ESI^+) [Found: 383.0983, $C_{17}H_{24}{}^{79}BrN_2O_3$, requires 383.0965 $[M+H]^+$].

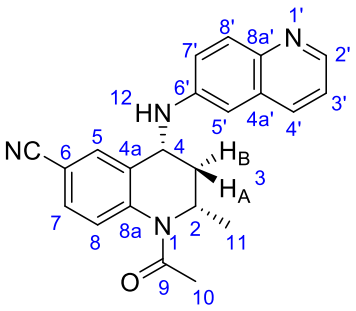
tert-Butyl ((2*S*,4*R*)-1-acetyl-6-cyano-2-methyl-1,2,3,4-tetrahydroquinolin-4-yl)carbamate (3.51)[33]



Anhydrous, degassed DMF (1 mL) was added to a mixture of compound **3.50** (99 mg, 0.258 mmol, 1.0 eq.), $Zn(CN)_2$ (38 mg, 0.324 mmol, 1.3 eq.) and $Pd(PPh_3)_4$ (42 mg, 0.0363 mmol, 0.14 eq.) and the resulting suspension was stirred at 115 °C for 21 h. The suspension was cooled to rt and filtered through Celite®, eluting with EtOAc. The filtrate was then concentrated *in vacuo*. The resulting residue was redissolved in EtOAc (20 mL) and washed with 0.5 M $LiCl_{(aq)}$ (40 mL), H_2O (40 mL) and brine (40 mL). The organic components were dried over Na_2SO_4, filtered, and concentrated *in vacuo*. The crude was purified by flash column chromatography (0–40% EtOAc/Petroleum ether) to give **3.51** as a yellow solid (37 mg, 44%): R_f 0.32 (50% EtOAc/Petroleum ether); $[\alpha]_D^{25}$ = +295.8 (*c* 1.0, $CHCl_3$); m.p 165 – 167 °C (from EtOAc); $\overline{\nu}_{max}$ (thin film)/cm^{-1} 2977 (C-H, w), 2229 (C≡N, w), 1710 (C=O, s), 1656 (C=O, s); ^{1}H NMR (400 MHz, $CDCl_3$) δ_H 7.61–7.53 (2H, m, H-5, H-7), 7.23 (1H, d, *J* 8.1, H-8), 4.88–4.70 (2H, m, H-2, H-12), 4.65–4.52 (1H, m, H-4), 2.60 (1H, ddd, *J* 12.8,

8.6, 4.5, H_a-3), 2.13 (3H, s, H-10), 1.51 (9H, s, H-4'), 1.31–1.21 (1H, m, H_b-3), 1.15 (3H, d, *J* 6.4, H-11); ^{13}C NMR (151 MHz, $CDCl_3$) δ_C 169.1 (C-9), 155.2 (C-1'), 140.6 (C-8a), 138.0 (C-4a), 131.3 (C-7), 127.1 (C-5), 126.4 (C-8), 118.6 (C(6)*C*N), 109.4 (C-6), 80.8 (C-3'), 47.8 (C-2), 46.7 (C-4), 40.5 (C-3), 28.4 (C-4'), 22.9 (C-10), 21.5 (C-11); LRMS *m/z* (ESI^+) 330 ($[M+H]^+$, 14%); HRMS *m/z* (ESI^+) [Found: 330.1827, $C_{18}H_{24}N_3O_3$, requires 330.1812 $[M+H]^+$]. The LRMS data is in agreement with the literature.[33]

(2*S*,4*R*)-1-Acetyl-2-methyl-4-(quinolin-6-ylamino)-1,2,3,4-tetrahydroquinoline-6-carbonitrile (3.53)



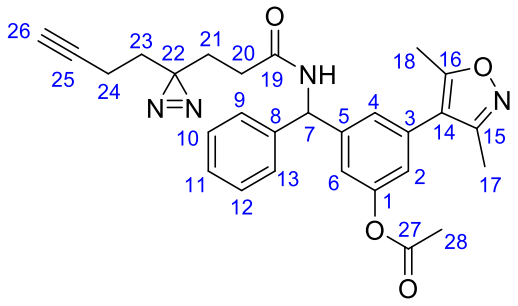
Step 1: Compound **3.51** was dissolved in CH_2Cl_2 (1.0 mL) and TFA (1.0 mL) and the solution was stirred at rt for 1 h. The solution was the concentrated *in vacuo*, the residue redissolved in EtOAc (10 mL) and then washed with saturated $NaHCO_3$ (2 × 20 mL). The aqueous components were then extracted with a 9:1 $CHCl_3$/IPA solution (6 × 20 mL). The combined organic components were then dried over Na_2SO_4, filtered, and concentrated *in vacuo* to give a yellow oil (48 mg) which was continued to Step 2 without purification.

Step 2: The crude material from Step 1 was added to a dry microwave vial with 6-bromoquinoline (57 µL, 0.421 mmol, 2.0 eq.), BrettPhos (36 mg, 0.0671 mmol, 0.32 eq.), BrettPhos Pd G3 (15 mg, 0.0165 mmol, 0.080 eq.) and NaO^{t}Bu (24 mg, 0.250 mmol, 1.2 eq.). The vial was purged with Ar after which anhydrous, degassed toluene (1.7 mL) was added. The resulting suspension was stirred at 70 °C for 18 h. The suspension was cooled to rt, diluted with EtOAc (10 mL) and H_2O (10 mL) and the organic and aqueous components were separated. The aqueous components were extracted with EtOAc (3 × 10 mL) and the combined organic components were dried over $NaSO_4$, filtered and

concentrated *in vacuo*. The crude material was purified by flash column chromatography (0–99% EtOAc/petroleum ether, 1% NEt_3) to give **3.53** as a pale yellow solid (37 mg, 47% over two steps): R_f 0.46 (10% MeOH/CH_2Cl_2); $[\alpha]_D^{25}$ = +221.9 (*c* 1.0, DMSO); m.p 128–132 °C (from EtOAc); $\overline{\nu}_{max}$ (neat)/cm^{-1} 2934 (C-H, w), 2223 (C≡N, w), 1646 (C=O, s), 1525 (m), 1496 (m); ^{1}H NMR (400 MHz, D_6-DMSO) δ_H 8.52 (1H, dd, *J* 4.2, 1.7, H-2'), 8.00–7.94 (1H, m, H-5'), 7.83–7.74 (2H, m, H-7, H-7'), 7.62 (1H, d, *J* 8.2, H-8), 7.49–7.45 (1H, m, H-5), 7.39 (1H, dd, *J* 9.1, 2.6, H-7'), 7.30 (1H, dd, *J* 8.3, 4.2, H-3'), 6.84 (1H, d, *J* 2.6, H-5'), 6.66 (1H, d, *J* 7.9, H-12), 4.76–4.64 (1H, m, H-2), 4.53–4.43 (1H, m, H-4), 2.69 (1H, ddd, *J* 12.4, 8.3, 4.1, H_A-3), 2.19 (3H, s, H-10), 1.37–1.23 (1H, m, H_B-3), 1.13 (3H, d, *J* 6.3, H-11); ^{13}C NMR (151 MHz, D_6-DMSO) δ_C 168.9 (C-9), 145.8 (C-6'), 145.6 (C-2'), 142.5 (C-8a'), 141.2 (C-8a), 138.5 (C-4a), 133.3 (C-4'), 131.0 (C-7), 129.9 (C-4a'), 129.8 (C-8'), 127.17 (C-5/C-6), 127.15 (C-5/C-6), 121.5 (C-7'),121.4 (C-3'), 118.9 (C(6)*C*N), 107.3 (C-6), 102.5 (C-5'), 48.3 (C-4), 47.9 (C-2), 40.1 (C-3), 23.1 (C-10), 21.4 (C-11); LRMS 357 ($[M+H]^+$, 100%); HRMS *m/z* (ESI^+) [Found: 379.1548, $C_{22}H_{20}N_4ONa$, requires 379.1529 $[M+Na]^+$]; HPLC (Method 2) Retention time = 5.9 min, 93.5%.

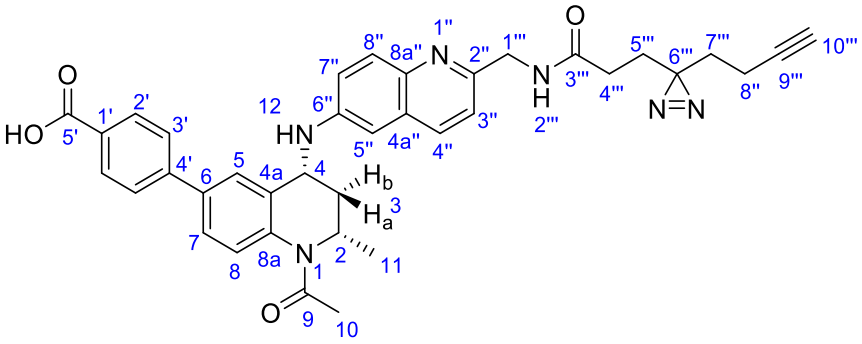
6.2.3 Compounds from Chapter 4

3-((3-(3-(But-3-yn-1-yl)-3*H*-diazirin-3-yl)propanamido)(phenyl)methyl)-5-(3,5-dimethylisoxazol-4-yl)phenyl acetate (4.2)



A solution of compound **4.24** (13 mg, 0.0359 mmol, 1.0 eq.) in THF (0.4 mL) was added to compound **4.27** (28 mg, 0.0657 mmol, 1.8 eq.) and the resulting solution was stirred for 1 h. H_2O (65 µL) was added, and the reaction was stirred for 18 h. The suspension was filtered through Celite®, eluting with THF, and the filtrate was concentrated *in vacuo*. The crude was purified by flash column chromatography (0–40% EtOAc/petroleum ether) to give compound **4.2** as a colourless solid and as a racemic mixture (15 mg, 86%): R_f 0.35 (40% EtOAc/petroleum ether); m.p. 34–38 °C (from EtOAc); $\overline{\nu}_{max}$ (thin film)/cm^{-1} 3293 (C≡*C-H*, m), 1767 (C=O, s), 1650 (s), 1204 (s); ^{1}H NMR (500 MHz, $CDCl_3$) δ_H 7.39–7.34 (2H, m, H-10, H-12), 7.33–7.28 (1H, m, H-11), 7.26–7.24 (2H, m, H-9, H-13), 7.00–6.97 (1H, m, H-6), 6.93–6.90 (2H, m, H-2, H-4), 6.26 (1H, d, *J* 7.9, H-7), 6.09 (1H, d, *J* 7.9, N-*H)*, 2.35 (3H, s, H-17), 2.29 (3H, s, H-28), 2.20 (3H, s, H-18), 2.05–1.97 (4H, m, H-20, H-24), 1.95 (1H, t, *J* 2.6, H-26), 1.92–1.87 (2H, m, H-21), 1.62 (2H, t, *J* 7.4, H-23); ^{13}C NMR (126 MHz, $CDCl_3$) δ_C 170.5 (C-19), 169.4 (C-27), 165.8 (C-15), 158.5 (C-16), 151.4 (C-1), 143.8 (C-5), 140.6 (C-8), 132.2 (C-3), 129.1 (C10, C12), 128.2 (C-11), 127.6 (C-9, C-13), 125.7 (C-4), 121.4 (C-2), 119.6 (C-6), 115.8 (C-14), 82.8 (C-25), 69.4 (C-26), 56.8 (C-7), 32.6 (C-23), 30.4 (C-20), 28.3 (C-21), 28.0 (C-22), 21.3 (C-28), 13.4 (C-24), 11.8 (C-17), 10.9 (C-18); LRMS (ESI$^-$) 483 ([M–H$^+$]$^-$, 40%); HRMS *m/z* (ESI$^-$) [Found: 483.2038, requires $C_{28}H_{27}O_4N_4$ [M–H]$^-$ 483.2038)]; HPLC (Method 1) Retention time = 10.7 min, 98%.

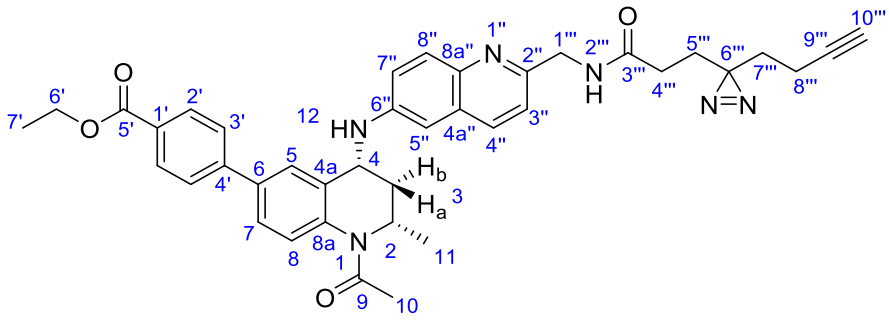
4-((2*S*,4*R*)-1-acetyl-4-((2-((3-(3-(but-3-yn-1-yl)-3*H*-diazirin-3-yl)propanamido)methyl)quinolin-6-yl)amino)-2-methyl-1,2,3,4-tetrahydroquinolin-6-yl)benzoic acid (4.5)



Compound **4.6** (19 mg, 0.029 mmol, 1 eq.) was dissolved in EtOH (0.5 mL) and to the resulting solution NaOH(aq) (2 M, 148 µL, 0.296 mmol, 10 eq.) was added dropwise. The solution was stirred for 2.5 h after which the solution was diluted with H_2O (3 mL). The solution was neutralised to pH 7 and partially concentrated *in vacuo* to remove EtOH. The solution was then diluted with EtOAc (10 mL), and H_2O (7 mL) and the aqueous and organic components were separated. The aqueous components were extracted with EtOAc (10 mL), after which, the aqueous components were acidified to pH 5 and further extracted with EtOAc (3 × 10 mL). The combined organic components were dried over Na_2SO_4, filtered, and concentrated *in vacuo*. The crude material was purified by flash column chromatography (reverse phase, 5–60% MeCN/H_2O) to give **4.5** as a green solid (5 mg, 28%): R_f 0.43 (10% MeOH/CH_2Cl_2); $[\alpha]_D^{25}$ = +283.0 (*c* 0.4, MeOH); m.p. 125–128 °C (from MeOH); $\overline{\nu}_{max}$ (thin film)/cm^{-1} 3303 (C≡*C-H*, w), 2928 (C-H, w), 1626 (C=O, s), 1607 (N-H, m) 1489 (m), 1385 (m); ^{1}H NMR (400 MHz, MeOD) δ_H 8.06 (1H, d, *J* 8.6, H-4''), 8.00–7.96 (2H, m, H-2'), 7.84 (1H, d, *J* 9.2, H-8''), 7.65 (1H, dd, *J* 8.3, 2.2, H-7), 7.59–7.53 (3H, m, H-5, H-3'), 4.47–7.42 (2H, m, H-8, H-3'), 7.37 (1H, d, *J* 8.6, H-3''), 6.86 (1H, d, *J* 2.6, H-5''), 4.98–4.84 (partially hidden by H_2O peak) (1H, m, H-2), 4.58 (2H, s, H-1''), 4.48 (1H, dd, *J* 12.2, 4.1, H-4), 2.78 (1H, ddd, *J* 12.5, 8.6, 4.1, H_a-3), 2.29 (3H, s, H-10), 2.24 (1H, t, *J* 2.7, H-10'''), 2.13 (2H, dd, *J* 8.4, 6.9, H-4'''), 2.00 (2H, td, *J* 7.5, 2.7, H-8'''), 1.79 (2H, dd, *J* 8.4, 6.9, H-5'''), 1.60 (2H, t, *J* 7.5, H-7'''), 1.50–1.37 (1H, m, H_b-3), 1.22 (3H, d, *J* 6.3, H-11); ^{13}C

NMR (151 MHz, MeOD) δ_C 174.7 (C-3''), 172.2 (C-9), 169.6 (C-5'), 154.4 (C-2''), 148.3 (C-6''), 146.1 (C-4'), 143.0 (C-6), 141.3 (C-8a''), 139.2 (C-4a), 138.0 (C-4''), 137.7 (C-8a), 131.4 (C-2'), 131.1 (C-4a''), 130.8 (C-1'), 128.4 (C-8''), 128.1 (C-8), 127.8 (C-3'), 127.0 (C-7), 123.8 (C-7''), 123.7 (C-5), 121.3 (C-3''), 104.4 (C-5''), 83.6 (C-9'''), 70.3 (C-10'''), 50.7 (C-4), 49.6 (C-2), 45.4 (C-1'''), 41.6 (C-3), 33.4 (C-7'''), 30.9 (C-4'''), 29.7 (C-5'''), 28.9 (C-6'''), 23.0 (C-10), 21.5 (C-11), 13.8 (C-8''); LRMS *m/z* (ESI^+) 629 ($[M+H^+]^+$, 47%); HRMS *m/z* (ESI^+) [Found: 629.2868, $C_{37}H_{37}O_4N_6$, requires $[M+H]^+$ 629.2871]; HPLC (Method 2) Retention time = 7.3 min, 99.0 %; Chiral HPLC (Method 2), Chiral IB N-3 column (50:50 hexane/EtOH, 1.0 $mLmin^{-1}$) Retention time = 7.7 min (opposite enantiomer, 5.6% UV), Retention time = 17.5 min (**4.5**, 94.4% UV); 89% e.e.

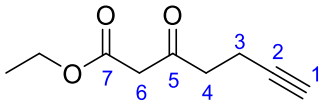
Ethyl 4-((2*S*,4*R*)-1-acetyl-4-((2-((3-(3-(but-3-yn-1-yl)-3H-diazirin-3-yl)propanamido)methyl)quinolin-6-yl)amino)-2-methyl-1,2,3,4-tetrahydroquinolin-6-yl)benzoate (4.6)



Compound **4.35** (57 mg, 0.094 mmol, 1.0 eq.) was dissolved in CH_2Cl_2 (1 mL) and the solution was cooled to 0 °C. HCl in dioxane solution (4 M, 0.12 mL, 0.48 mmol, 5.1 eq.) was added, the resulting solution was allowed to warm to rt and stirred for 2 h. The solution was diluted with further CH_2Cl_2 (0.6 mL) and further HCl in dioxane solution (4 M, 0.24 mL, 0.96 mmol, 10 eq.) and the solution was stirred for 35 min. Further HCl in dioxane solution (4 M, 0.12 mL, 0.48 mmol, 5.1 eq.) was added and the solution was left to stir for 25 min, after which the solution was concentrated *in vacuo*. The residue was then redissolved in CH_2Cl_2 (1 mL) and HCl in dioxane solution (4 M, 0.12 mL, 0.48 mmol, 5.1 eq.) was added. The solution was left to stir for 2 h after which TLC analysis indicated complete consumption

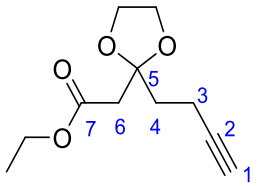
of the starting material and the solution was concentrated *in vacuo*. Compound **4.17** (19 mg, 0.114 mmol, 1.2 eq.) was added to the rbf and the two compounds were dissolved in anhydrous DMF (0.5 mL). HATU (71 mg, 0.187 mmol, 2.0 eq.) and DIPEA (0.08 mL, 0.459 mmol, 4.9 eq.) were added and the solution was left to stir at rt for 24 h. The solution was then diluted with EtOAc (10 mL) and washed with 0.5 M $LiCl_{(aq)}$ (2 × 10 mL) and brine (10 mL). The crude was purified by two flash chromatography columns (50–100% EtOAc/CH_2Cl_2 with 1% NEt_3 [Normal phase silica] then 5–90% MeCN/H_2O [Reverse phase silica]) to give **4.6** as a pale green solid (9 mg, 15%): R_f 0.19 (50% EtOAc/CH_2Cl_2); $[\alpha]_D^{25}$ = +344.2 (*c* 0.2, MeOH); mp 92–95 °C (from MeCN); $\overline{\nu}_{max}$ (neat)/cm^{-1} 3304 (C≡*C*-*H*, s), 1712 (C=O, s), 1626 (N-H, m), 1489 (m); ^{1}H NMR (400 MHz, CD_3CN) δ_H 8.03–7.93 (2H, m, H-2'), 7.88 (1H, d, *J* 8.5, H-4''), 7.79 (1H, d, *J* 9.1, H-8''), 7.67–7.58 (3H, m, H-7, H-3'), 7.57–7.54 (1H, m, H-5), 7.40 (1H, d, *J* 8.2, H-8), 7.34 (1H, dd, *J* 9.1, 2.6, H-7''), 7.23 (1H, d, *J* 8.5, H-3''), 7.14–7.05 (1H, m, H-2'''), 6.85 (1H, d, *J* 2.6, H-5''), 5.21 (1H, d, *J* 7.9, H-12), 4.89–4.76 (1H, m, H-2), 4.52–4.44 (1H, m, H-4), 4.49 (2H, d, *J* 5.5, H-1'''), 4.31 (2H, q, *J* 7.1, H-6'), 2.75 (1H, ddd, *J* 12.5, 8.5, 4.1, H_a-3), 2.20 (3H, s, H-10), 2.18 (1H, t, *J* 2.7, H-10'''), 2.11–2.05 (2H, m, H-4'''), 2.01 (2H, td, *J* 7.5, 2.7, H-8'''), 1.78–1.71 (2H, m, H-5'''), 1.62 (2H, t, *J* 7.5, H-7''), 1.34–1.30 (1H, m, H_b-3), 1.33 (3H, t, *J* 7.1, H-7'), 1.16 (3H. d, *J* 6.3, H-11); ^{13}C NMR (151 MHz, CD_3CN) δ_C 172.2 (C-3''), 170.0 (C-9), 166.9 (C-5'), 154.7 (C-2''), 146.9 (C-6''), 145.6 (C-4'), 143.1 (C-8a''), 139.1 (C-4a), 138.3 (C-8a), 137.6 (C-6), 135.4 (C-4''), 130.8 (C-2'), 130.6 (C-8''), 130.4 (C-1'), 130.1 (C-4a''), 128.0 (C-8), 127.7 (C-3'), 126.6 (C-7), 123.2 (C-5), 122.3 (C-7''), 121.0 (C-3''), 104.7 (C-5''), 84.1 (C-9'''), 70.3 (C-10'''), 61.8 (C-6'), 50.5 (C-4), 48.6 (C-2), 45.8 (C-1'''), 41.5 (C-3), 32.9 (C-7'''), 30.7 (C-4'''), 29.3 (C-5'''), 29.1 (C-6'''), 23.4 (C-10), 21.7 (C-11), 14.6 (C-7'), 13.7 (C-8'''); LRMS *m/z* (ESI^+) 657 ($[M+H^+]^+$, 51%); HRMS *m/z* (ESI^+) [Found: 657.3180, $C_{39}H_{41}O_4N_6$, requires $[M+H]^+$ 657.3184]; HPLC (Method 2) Retention time = 8.56 min, 94.9%; Chiral HPLC (Method 2), Chiral IF-3 column (40:60 hexane/IPA, 1.0 $mLmin^{-1}$) Retention time = 9.0 min (opposite enantiomer, 7.1% UV), Retention time = 15.2 (**4.6**, 92.9% UV); 86% e.e.

Ethyl 3-oxohept-6-ynoate (4.8) [146,168]



n-BuLi in hexanes (2.5 M, 3.1 mL, 7.75 mmol, 2.0 eq.) was added over 5 min to a solution of diisopropylamine (1.1 mL, 7.85 mmol, 2.0 eq.) in anhydrous THF (7.6 mL) at –78°C. The resulting solution was allowed to warm to rt and stir for 1 h. The solution was then cooled to –78 °C, after which a solution of ethyl acetoacetate (0.49 mL, 3.84 mmol, 1.0 mmol) in anhydrous THF (1.5 mL) was added. The solution was warmed to 0 °C and stirred for 1 h, after which propargyl bromide (80% w/v solution in toluene, 457 mg, 3.84 mmol, 1.0 eq.) was added and the resulting solution was stirred for 1 h at 0 °C, then warmed to rt and left to stir for 2 h. The reaction was cooled to 0 °C and quenched *via* slow addition of acetic acid (0.5 mL). The resulting suspension was concentrated *in vacuo* and then redissolved in EtOAc (20 mL) and H_2O (20 mL). The aqueous components were washed with EtOAc (3 × 30 mL), and the combined organic components washed with brine (2 × 40 mL), dried over $MgSO_4$, filtered, and concentrated *in vacuo*. The crude was purified by vacuum distillation (110 °C, 15 mbar) to give compound **4.8** as a yellow oil (303 mg, 47%): R_f 0.59 (20 % EtOAc/petroleum ether); ^{1}H NMR (400 MHz, $CDCl_3$) δ_H 4.20 (2H, q, *J* 7.1, OC*H*$_2$CH$_3$), 3.46 (2H, s, H-6), 2.81 (2H, t, *J* 7.2, H-4), 2.48 (2H, td, *J* 7.2, 2.8, H-3), 1.95 (1H, t, *J* 2.8, H-1), 1.28 (3H, t, *J* 7.1, OCH$_2$C*H*$_3$); LRMS *m/z* (ESI$^-$) 167 ([M–H$^+$]$^-$, 100%). These data are in agreement with the previously reported values.[146,168]

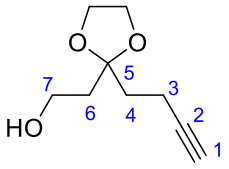
Ethyl 2-(2-(but-3-yn-1-yl)-1,3-dioxolan-2-yl)acetate (4.9) [146,168]



A solution of compound **4.8** (2.31 g, 13.7 mmol, 1.0 eq.), ethylene glycol (0.85 mL, 15.2 mmol, 1.1 eq.) and 4-toluenesulfonic acid monohydrate (0.130 g, 0.683 mmol, 0.050 eq.) in toluene (100 mL) was stirred at 120 °C for 19 h with a Dean—Stark apparatus.

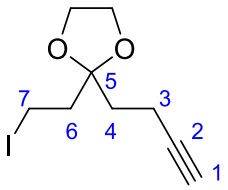
The reaction was cooled to rt, diluted with EtOAc (200 mL) and washed with $Na_2CO_{3(aq)}$ (1 M, 200 mL). The organic components were washed with brine (200 mL), dried over $MgSO_4$, filtered, and concentrated *in vacuo* to give a yellow oil (3.07 g). The crude product **4.9** was used in the next reaction without further purification: R_f 0.46 (20 % EtOAc/petroleum ether); ^{1}H NMR (400 MHz, $CDCl_3$) δ_H 4.15 (2H, q, *J* 7.1, OCH_2CH$_3$), 4.04–3.93 (4H, m, O(CH_2)$_2$O), 2.65 (2H, s, H-6), 2.34–2.26 (2H, m, H-3), 2.15 – 2.08 (2H, m, H-4), 1.92 (1H, t, *J* 2.7, H-1), 1.26 (3H, t, *J* 7.1, OCH$_2$CH_3); LRMS *m/z* (ESI$^+$) 235 ([M+Na]$^+$, 19%). The spectroscopic data are in agreement with the previously reported values.[146,168]

2-(2-(But-3-yn-1-yl)-1,3-dioxolan-2-yl)ethan-1-ol (4.10)[146,168]



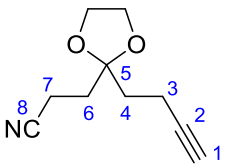
The crude product **4.9** (2.92 g, 13.8 mmol, 1.0 eq.) was dissolved in anhydrous Et_2O (68 mL) and cooled to 0 °C. $LiAlH_4$ in THF solution (1 M, 20.6 mL, 20.6 mmol, 1.5 eq.) was added dropwise and stirred for 1 h. Further $LiAlH_4$ in THF solution (1 M, 5.00 mL, 5.00 mmol, 0.36 eq.) was added and stirred for 15 min, after which a further $LiAlH_4$ in THF (1 M, 8.00 mL, 8.00 mmol, 0.58 eq.) was added and the reaction stirred for 1 h. The reaction was quenched with dropwise addition of EtOAc (10 mL) followed by H_2O (2 mL). Saturated Rochelle salt solution (50 mL) was added and allowed to stir until the precipitate became uniform, after which the organic and aqueous components were separated. The aqueous components were washed with EtOAc (3 × 60 mL) and the combined organic components were washed with brine (40 mL), dried over Na_2SO_4, filtered and concentrated *in vacuo* to give compound **4.10** as a yellow oil (1.26 g, 54% over two steps): R_f 0.13 (20% EtOAc/petroleum ether); ^{1}H NMR (400 MHz, $CDCl_3$) δ_H 4.05 – 3.95 (4H, m, O(CH_2)$_2$O), 3.78–3.74 (2H, m, H-7), 2.30–2.24 (2H, m, H-3), 1.97–1.90 (5H, m, H-1, H-4, H-6); LRMS *m/z* (ESI$^+$) 193 ([M+Na]$^+$, 21%). These data are in agreement with the previously reported values.[146,168]

2-(But-3-yn-1-yl)-2-(2-iodoethyl)-1,3-dioxolane (4.11) [146]



Iodine (2.25 g, 8.86 mmol, 1.2 eq.) was added to a solution of PPh_3 (2.13 g, 8.12 mmol, 1.1 eq.) and 1*H*-imidazole (1.51 g, 22.2 mmol, 3.0 eq.) in anhydrous CH_2Cl_2 (50 mL) and the resulting solution was stirred for 15 min. A solution of compound **4.10** (1.26 g, 7.40 mmol, 1.0 eq.) in anhydrous CH_2Cl_2 (13 mL) was added over 15 min. The reaction was stirred at 70 °C for 3 h, after which the reaction was cooled to rt and quenched with 10% w/v $Na_2S_2O_3$ (40 mL) and then diluted with H_2O (30 mL). The aqueous components were washed with CH_2Cl_2 (3 × 60 mL) and the combined organic components washed with brine (100 mL), dried over Na_2SO_4, filtered and concentrated *in vacuo*. The residue was redissolved in petroleum ether (37 mL) and Et_2O (5 mL) and stirred for 5 min. The suspension was filtered, and the solid residue washed with a solution of petroleum ether (18 mL) and Et_2O (2.5 mL). The filtrate was concentrated *in vacuo* to give compound **4.11** as a colourless oil (1.80 g). The crude product was used in the next step without further purification: R_f 0.68 (10% EtOAc/petroleum ether) ^{1}H NMR (400 MHz, $CDCl_3$) δ_H 3.95 (4H, s, O(C*H*$_2$)$_2$O), 3.19–3.10 (2H, m, H-7), 2.32–2.22 (4H, m, H-4, H-6), 1.95 (1H, t, *J* 2.7, H-1), 1.90 – 1.84 (2H, m, H-3); LRMS *m/z* (ESI$^+$) 281 ([M+H]$^+$, 2.25%). These data are in agreement with the previously reported values.[146]

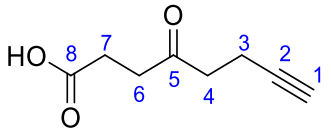
3-(2-(But-3-yn-1-yl)-1,3-dioxolan-2-yl)propanenitrile (**4.12**)[146]



Crude compound **4.11** (1.80 g, 6.43 mmol, 1.00 eq.) was dissolved in anhydrous DMF (11.7 mL). KCN (439 mg, 6.74 mmol, 1.05 eq.) was added and the reaction was stirred at 70 °C for 4 h. The reaction was cooled to rt and diluted to satd. $NaHCO_{3(aq)}$ (23 mL) and

EtOAc (80 mL). The organic components were washed with $LiCl_{(aq)}$ (0.5 M, 2 × 48 mL), brine (40 mL) and dried over $MgSO_4$, filtered and concentrated *in vacuo*. The crude was purified by flash column chromatography (0–30% EtOAc/petroleum ether) to give **4.12** as a colourless oil (696 mg, 52% over 2 steps): R_f 0.22 (20% EtOAc/petroleum ether); ^{1}H NMR (400 MHz, $CDCl_3$) δ_H 3.98 (4H, s, O(CH_2)$_2$O), 2.41 (2H, t, *J* 7.9, H-7), 2.26 (2H, td, *J* 7.9, 2.6, H-3), 2.04 (2H, t, *J* 7.9, H-6), 1.96 (1H, t, *J* 2.6, H-1), 1.86 (2H, t, *J* 7.9, H-4); LRMS *m/z* (ESI$^+$) 180 ([M+H]$^+$, 100%). These data are in agreement with the previously reported values.[146]

4-Oxooct-7-ynoic acid (4.13) [146,150]



Method 1:

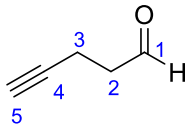
Following a previously reported procedure,[146] a solution of compound **4.12** (0.696 g, 3.88 mmol, 1.0 eq.) in 10% w/v NaOH (7 mL) was stirred under reflux for 2 h 15 min. The solution was cooled and washed with Et_2O. The aqueous components were acidified to pH 1 with 5 M $HCl_{(aq)}$ and the solution stirred at rt for 2 h. The solution was extracted with CH_2Cl_2 (4 x 20 mL) and the combined organic components were dried over $MgSO_4$, filtered, and concentrated *in vacuo* to give compound **4.13** as a brown solid (469 mg, 78%).

Method 2:

Following a procedure described by Parker *et al.*,[150] LiOH (395 mg, 16.5 mmol, 5 eq.) and H_2O (0.30 mL) was added to a solution of **4.16** (601 mg, 3.30 mmol, 1 eq.) in MeOH (25 mL) and the resulting solution was stirred at rt for 4 h. The solution was then diluted with H_2O (20 mL) and acidified to approximately pH 3 using 6 M $HCl_{(aq)}$. The solution was then concentrated *in vacuo* to remove the MeOH and the resulting aqueous components were extracted with CH_2Cl_2 (3 × 30 mL). The combined organic components were dried over Na_2SO_4 and concentrated *in vacuo*. The resulting crude material was then redissolved in

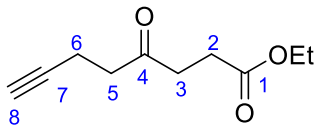
EtOAc (30 mL) and washed with $NaOH_{(aq)}$ (2 M, 20 mL). The organic and aqueous components were separated, and the aqueous components were reacidified using 2 M $HCl_{(aq)}$. The aqueous components were extracted with EtOAc (3 × 30 mL), dried over Na_2SO_4 and concentrated *in vacuo* to give **4.13** as a brown solid (302 mg, 59%): R_f 0.08 (20% EtOAc/Petroleum ether); m.p. 50–53 °C; ^{1}H NMR (400 MHz, $CDCl_3$) δ_H 2.78–2.63 (6H, m, H-4, H-6, H-7), 2.47 (2H, td, *J* 6.9, 2.7, H-3), 1.95 (1H, t, *J* 2.7, H-1); LRMS *m/z* (ESI^-) 153 ($[M–H]^-$, 100%). These data are in agreement with the previously reported values.[146,150]

Pent-4-ynal (4.15) [169–171]



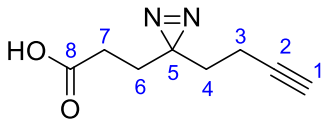
Oxalyl chloride (3.00 mL, 35.0 mmol, 1.1 eq.) was dissolved in anhydrous CH_2Cl_2 (68 mL) and the resulting solution was cooled to −78 °C. A solution of anhydrous DMSO (5.00 mL, 70.4 mmol, 2.2 eq.) in CH_2Cl_2 (14 mL) was then added over 20 mins. The resulting solution was left to stir at −78 °C for 30 mins. A solution of 4-pentyn-1-ol (3.0 mL, 32.2 mmol, 1.0 eq.) in CH_2Cl_2 (27 mL) was added over 10 mins and the resulting solution was stirred for 60 min at –78 °C, after which a white precipitate formed. NEt_3 (22.4 mL, 161 mmol, 5.0 eq.) was then added and the resulting suspension was stirred at –78 °C for 60 mins, and then left to warm to rt and stirred for an additional 2.5 h. H_2O (100 mL) was added and the organic and aqueous components were separated. The aqueous components were acidified with 1% (*v/v*) $HCl_{(aq)}$ and extracted with CH_2Cl_2 (3 × 100 mL). The combined organic components were then washed with satd. $NaHCO_{3(aq)}$ (200 mL) and the aqueous components were extracted with CH_2Cl_2 (3 × 100 mL). The combined organic components were washed with brine (300 mL), dried over Na_2SO_4 and concentrated *in vacuo* to give **4.15** as a yellow oil (2.59 g, 98%): R_f 0.34 (20% EtOAc/petroleum ether); ^{1}H NMR (400 MHz, $CDCl_3$) δ_H 9.79 (1H, t, *J* 1.1, H-1), 2.72 – 2.65 (2H, m, H-2), 2.50 (2H, tdd, *J* 7.1, 2.7, 0.7, H-3), 1.98 (1H, t, *J* 2.7, H-5). The ^{1}H NMR data are in agreement with the literature.[171]

Ethyl 4-oxooct-7-ynoate (4.16) [150]



A solution of crude **4.15** (2.59 g, 31.5 mmol, 1.0 eq.) and ethyl acrylate (6.9 mL, 63.3 mmol, 2.0 eq.) in anhydrous dioxane (38 mL) was added dropwise to a suspension of 3-benzyl-5-(hydroxyethyl)-4-methylthiazonium chloride (1.19 g, 4.41 mmol, 0.14 eq.), NEt_3 (3.08 mL, 22.10 mmol, 0.70 eq.) and ethyl acrylate (6.9 mL, 63.3 mmol, 2.0 eq.) in anhydrous 1,4-dioxane (45 mL) over 30 mins and the resulting suspension was left to stir for 54 h at 80°C. The reaction mixture was concentrated *in vacuo* and the residue then resuspended in CH_2Cl_2 (150 mL). The organic components were washed with $H_2SO_{4(aq)}$ (1 M, 100 mL), satd. $NaHCO_3$ (100 mL) and brine (100 mL). The organic components were then dried over Na_2SO_4 and concentrated *in vacuo*. The crude was purified by flash column chromatography (0–20% EtOAc/pentane) to give **4.16** as a yellow oil (611 mg, 11%): R_f 0.32 (20 % EtOAc/Pentane); ^{1}H NMR (400 MHz, $CDCl_3$) δ_H 4.12 (2H, q, *J* 7.2, OCH_2CH_3), 2.76–2.69 (4H, m, H-3, H-5), 2.63–2.57 (2H, m, H-2), 2.46 (2H, td, *J* 7.3, 2.6, H-6), 1.94 (1H, t, *J* 2.6, H-8), 1.25 (3H, t, *J* 7.2, OCH_2CH_3); LRMS *m/z* (ESI$^+$) 205 ([M+Na]$^+$, 100%). The spectroscopic data are in agreement with the literature.[150]

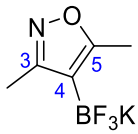
3-(3-(But-3-yn-1-yl)-3*H*-diazirin-3-yl)propanoic acid (4.17) [146,148,150]



Following a procedure from Parker *et al.*,[150] NH_3 in MeOH (7 M, 9.6 mL) was added to a flame-dried sealed tube under argon, containing compound **4.13** (152 mg, 0.986 mmol, 1.0 eq.) at 0 °C. The solution was stirred for 3 h 20 min at 0 °C, after which a solution of hydroxylamine-*O*-sulfonic acid (156 mg, 1.38 mmol, 1.4 eq.) in anhydrous MeOH (1.2 mL) was added dropwise. The reaction was stirred for 1 h at 0 °C then allowed to warm to rt and stir for 15 h. The solution was filtered, and the remaining residue was washed several times with MeOH. The combined filtrate was then concentrated *in vacuo*. The resulting residue

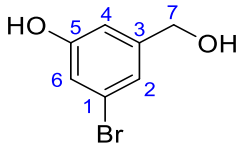
was resuspended in anhydrous MeOH (9 mL) and cooled to 0 °C. Under light sensitive conditions, DIPEA (0.38 mL, 2.18 mmol, 2.2 eq.) was added, followed by I_2 (250 mg, 0.985 mmol, 1.0 eq.) portion-wise until a dark brown colour persisted for more than 30 min. The reaction was diluted with EtOAc (10 mL) and washed with $HCl_{(aq)}$ (1 M, 10 mL), saturated $Na_2SO_{3(aq)}$ (2 × 10 mL) and brine (10 mL). The combined organic layers were dried over Na_2SO_4 and concentrated *in vacuo*. The crude was purified by flash column chromatography (0–50% EtOAc/petroleum ether, 1% acetic acid) to give **4.17** as a colourless oil (79 mg, 48%): R_f 0.34 (40% EtOAc/petroleum ether, 1% acetic acid); ^{1}H NMR (400 MHz, DMSO) δ_H 9.89 (1H, br. s, COO*H*), 2.15 (2H, t, *J* 7.9, H-7), 2.02–1.96 (3H, m, H-1, H-6), 1.78 (2H, t, *J* 7.4, H-4), 1.66–1.59 (2H, m, H-3); LRMS *m/z* (ESI$^-$) 165 ([M–H]$^-$, 100%). These data are in agreement with the previously reported values.[146,148,150]

Potassium (3,5-dimethylisoxazol-4-yl)trifluoroborate[31,172] **(4.19)**



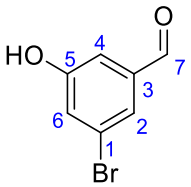
To a suspension of 3-5-dimethylisoaxzole-4-yl boronic acid (3.00 g, 21.3 mmol, 1 eq.) in MeCN (72 mL) was added $KF_{(aq)}$ (10 M, 8.52 mL, 85.2 mmol, 4 eq.) and the solution was left to stir until the 3-5-dimethylisoaxzole-4-yl boronic acid dissolved. A suspension of L-(+)-tartaric acid (6.55 g, 43.6 mmol, 2 eq.) in THF (45 mL) was added to the solution dropwise and the resulting solution stirred at rt for 1 h. The reaction mixture was filtered, and the residue washed with MeCN. The filtrate was concentrated *in vacuo* to give compound **4.19** as a colourless solid (3.51 g, 81 %): R_f 0.01 (50 % Et_2O/petroleum ether); m.p. >200 °C (from MeCN) [Lit[31,172] >200 °C]; ^{1}H NMR (400 MHz, DMSO) δ_H 2.19 (3H, s, C(3)CH_3), 2.04 (3H, s, C(5)CH_3);^{19}F NMR (377 MHz, DMSO) δ_F −134.1 – −34.9 (3F, m, C(4)BF_3K); LRMS *m/z* (ESI$^-$) 164 ([M–K]$^-$, 100%). These data are in agreement with the literature.[31]

3-Bromo-5-(hydroxymethyl)phenol (4.21) [30,31]



3-Bromo-5-hydroxybenzoic acid (5.00 g, 23.0 mmol, 1.0 eq.) was dissolved in anhydrous THF (100 mL) under Ar at 0 °C. BH_3.THF solution (1 M, 69.1 mL, 69.1 mmol, 3.0 eq.) was added dropwise and the reaction was allowed to warm to rt and stirred for 24 h. The reaction was cooled to 0 °C and diluted with MeOH (150 mL) and $HCl_{(aq)}$ (1 M, 50.0 mL). The volatile components were removed *in vacuo* and the residue diluted with H_2O (80 mL), which was extracted with EtOAc (3 × 100 mL). The combined organic components were washed with satd. $NaHCO_3$ (100 mL) and brine (100 mL), dried over Na_2SO_4, filtered and concentrated *in vacuo* to give **4.21** as a colourless solid (4.67 g, >99 %): R_f 0.15 (30% EtOAc/petroleum ether); m.p. 70–74 °C (from EtOAc); ^{1}H NMR (400 MHz, D_6-DMSO) δ_H 9.80 (1H, br. s, C(5)O*H*), 6.91–6.89 (1H, m, H-2), 6.79 (1H, t, *J* 2.1, H-6), 6.73–6.70 (1H, m, H-5), 5.28–5.18 (1H, m, C(7)O*H*), 4.43–4.37 (2H, m, H-7); LRMS *m/z* (ESI^-) 201 ([M(^{79}Br)–H^+]$^-$, 100%). These data are in agreement with the literature.[30,31]

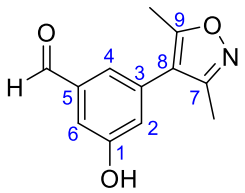
3-Bromo-5-hydroxybenzaldehyde (4.22) [30,31]



Compound **4.21** (4.469 g, 22.01 mmol, 1.0 eq.) was dissolved in anhydrous $CHCl_3$ (39 mL) and anhydrous ethyl acetate (7.4 mL). Activated MnO_2 (13.40 g, 154.1 mmol, 7.0 eq.) was added and the resulting solution was stirred for 2.5 h at 70 °C under light sensitive conditions. The solution was cooled to rt and filtered through Celite®. The residue was rinsed with $CHCl_3$ and the eluant was concentrated *in vacuo* to give **4.22** as a colourless solid (4.424 g, >99 %): R_f 0.51 (30% EtOAc/petroleum ether); m.p. 131–135 °C (from $CHCl_3$) [Lit[31] 137–139 °C; Lit[30] 137–140 °C]; ^{1}H NMR (400 MHz, D_6-DMSO) δ_H 10.47 (1H, br. s, C(5)O*H*),

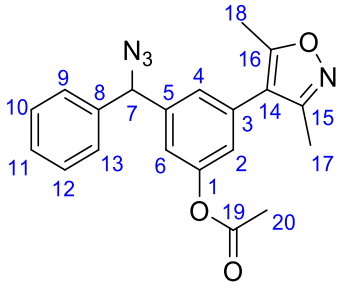
9.88 (1H, s, H-7), 7.51 (1H, t, *J* 1.6, $C_{Ar}H$), 7.30–7.21 (2H, m, 2 × $C_{Ar}H$); LRMS *m/z* (ESI^-) 199 ([M(^{79}Br) – H]$^-$, 100%). These data are in agreement with the literature.[30,31]

3-(3,5-Dimethylisoxazol-4-yl)-5-hydroxybenzaldehyde (4.23) [31]



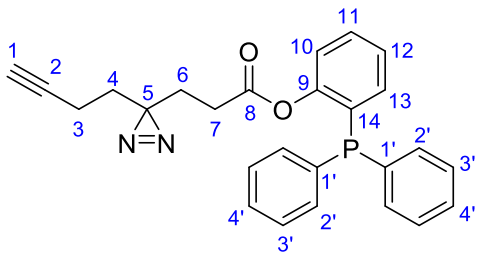
Na_2CO_3 (0.435 g, 4.10 mmol, 3.0 equiv.) was ground to a fine powder and added to a microwave vial with compound **4.22** (0.275 g, 1.37 mmol, 1.0 eq.) and compound **4.19** (0.417 g, 2.05 mmol, 1.5 eq.). The microwave vial was purged with Ar and degassed EtOH (0.28 mL) was added. The resulting solution was stirred at 80 °C for 30 min. $Pd(OAc)_2$ (37 mg, 0.165 mmol, 0.12 eq.) and RuPhos (76 mg, 0.163 mmol, 0.12 eq.) was added to a separate microwave vial and this vial was subsequently purged with Ar. Degassed EtOH (0.14 mL) was added and the solution was stirred. Once this solution turned brick red, it was transferred to the vial containing compounds **4.19, 4.22** and Na_2CO_3. The vial was rinsed with EtOH (0.14 mL) and the resulting solution was transferred to the vial containing compounds **4.19, 4.22** and Na_2CO_3. The resulting solution was stirred for 15 h at 80 °C. The solution was cooled to rt, diluted with EtOAc (5 mL) and filtered through Celite®. The volatile components were filtered, concentrated *in vacuo* and the resulting residue redissolved in EtOAc (20 mL). This was washed with H_2O (3 × 30 mL) and the combined organic components concentrated *in vacuo*. The crude was purified by flash column chromatography (0–50% EtOAc/petroleum ether) to give compound **4.23** as a yellow solid (90 mg, 30%): R_f 0.11 (20 % EtOAc/petroleum ether); m.p 169–173 °C (from EtOAc) [Lit[30] 184–187 °C; Lit[31] 184–186 °C]; ^1H NMR (400 MHz, Acetone-d_6) δ_H 10.02 (1H, s, C(O)*H*), 7.43–7.41 (1H, m, H-4), 7.36 (1H, dd, *J* 2.5, 1.4, H-2), 7.16 (1H, dd, *J* 2.5, 1.6, H-6), 2.44 (3H, s, C(7)CH_3), 2.26 (3H, s, C(9)CH_3); LRMS *m/z* (ESI^-) 216 ([M–H]$^-$, 62%). These data are in agreement with the literature.[31]

3-(Azido(phenyl)methyl)-5-(3,5-dimethylisoxazol-4-yl)phenyl acetate[173] (4.24)



OXFBD03 (**1.37**) (synthesised by Lily Latimer Smith) (140 mg, 0.415 mmol, 1.0 eq.) was dissolved in anhydrous CH_2Cl_2 (0.8 mL) at 0 °C. Trimethylsilyl azide (0.27 mL, 2.03 mmol, 4.9 eq.) was added, followed by copper (II) triflate (15 mg, 0.0415 mmol, 0.10 eq.). The reaction was allowed to warm to rt and stir for 2 h, and then heated to 40 °C and stirred for 16 h. The reaction was then cooled to 0 °C and quenched with satd. $EDTA_{(aq)}$ (0.31 mL), diluted with H_2O (5 mL) and then extracted with CH_2Cl_2 (3 × 10 mL). The combined organic components were dried over Na_2SO_4, filtered and concentrated *in vacuo*. The crude was purified by flash column chromatography (0–20% EtOAc in petroleum ether) to give **4.24** as a colourless oil (50 mg, 33%): R_f 0.68 (30% EtOAc in petroleum ether); ^{1}H NMR (400 MHz, CDCl3) δ_H 7.43–7.30 (5H, m, H-9, H-10, H-11, H-12, H-13), 7.07–7.06 (1H, m, H-6), 7.04–7.03 (1H, m, H-4), 6.96–6.94 (1H, m, H-2), 5.74 (1H, s, H-7), 2.38 (3H, s, H-18), 2.30 (3H, s, H-20), 2.24 (3H, s, H-17); LRMS *m/z* (ESI$^+$) 363 ([M+H]$^+$, 61%). These data are in agreement with the previously reported values.[173]

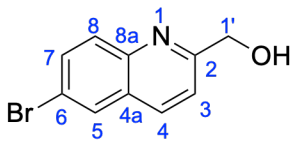
2-(Diphenylphosphaneyl)phenyl 3-(3-(but-3-yn-1-yl)-3*H*-diazirin-3-yl)propanoate (4.27)



Compound **4.17** (40 mg, 0.241 mmol, 1.2 eq.) and (2-hydroxyphenyl)diphenylphosphine (56 mg, 0.201 mmol, 1.0 eq.) were dissolved in anhydrous CH_2Cl_2 (3.4 mL). DMAP (3 mg,

0.0246 mmol, 0.12 eq.), DCC (58 mg, 0.281 mmol, 1.4 eq.) and DIPEA (0.0489 mL, 0.281 mmol, 1.4 eq.) were added and the reaction was stirred at rt for 18 h. The reaction was then cooled to 0 °C, diluted with CH_2Cl_2 (20 mL) and filtered. The organic solution was washed with $HCl_{(aq)}$ (1 M, 10 mL), satd. $NaHCO_3$ (10 mL) and brine (10 mL). The combined organic components were dried over Na_2SO_4 and concentrated *in vacuo*. The crude material was purified by flash column chromatography (0–30% EtOAc/petroleum ether) to give **4.27** as a colourless solid (50 mg, 58%): R_f 0.43 (10% EtOAc/petroleum ether); m.p. 60–63 °C (from $CHCl_3$); $\overline{\nu}_{max}$ (thin film)/cm^{-1} 3299 (C≡C-H, m), 2917 (C-H, m), 1761 (C=O, s), 1587 (m), 1466 (m), 1435 (s); ^{1}H NMR (500 MHz, $CDCl_3$) δ_H 7.41–7.28 (11H, m, H-10, H-2', H-3', H-4'), 7.18–7.11 (2H, m, H-11, H-12), 6.81 (1H, ddd, *J* 7.6, 4.4, 1.7, H-13), 2.08–2.02 (2H, m, H-7), 2.00–1.95 (3H, m, H-1, H-3), 1.62–1.55 (4H, m, H-4, H-6); ^{13}C NMR (126 MHz, $CDCl_3$) δ_C 170.2 (C-8), 152.6 (d, *J* 16.8, C-9), 135.6 (d, *J* 10.0, C-14/C-1'), 134.1 (d, *J* 20.5, C-3'), 133.8 (d, *J* 2.3, C-13), 130.3 (d, *J* 14.8, C-14/C-1'), 130.1 (C-10), 129.3 (C-4'), 128.8 (d, *J* 7.2, C-2'), 126.4 (C-11/C-12), 122.6 (C-11/C-12), 82.7 (C-2), 69.4 (C-1), 32.3 (C-6), 28.4 (C-7), 27.9 (C-4), 27.5 (C-5), 13.4 (C-3); ^{31}P NMR (162 MHz, $CDCl_3$) δ_P −15.87; LRMS (ESI^+) 427 ($[M+H]^+$, 100%); HRMS m/z (ESI^+) [Found: 427.1566, requires $C_{26}H_{24}O_2N_2P$ $[M+H]^+$ 427.1570]; HPLC (Method 1) Retention time = 13.5 min, 98.1%.

(6-Bromoquinolin-2-yl)methanol (4.30) [174,175]

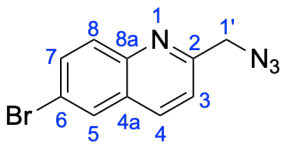


Step 1: 6-Bromo-2-methylquinoline (1.00 g, 4.50 mmol, 1.0 eq.) was dissolved in 1,4-dioxane (90 mL). SO_2 (600 mg, 5.40 mmol, 1.2 eq.) was added to the solution and the resulting suspension was stirred at 110 °C for 6 hours. The solution was then cooled to rt and concentrated *in vacuo*. The resulting suspension was then redissolved in CH_2Cl_2 (100 mL) and the organic components were washed with saturated $Na_2CO_{3(aq)}$ (70 mL) and

brine (70 mL). The organic components were then dried over Na_2SO_4 and concentrated *in vacuo*.

Step 2: The crude material from step 1 was dissolved in MeOH (17 mL) and cooled to 0 °C. $NaBH_4$ (77 mg, 2.04 mmol, 0.45 eq.) was added portion-wise and the resulting solution was allowed to warm to rt and left to stir for 30 min. The solution was concentrated *in vacuo* and then redissolved in CH_2Cl_2 (100 mL), washed with $NaHCO_3$ (100 mL) and brine (100 mL) and dried over Na_2SO_4. The organic components were then filtered and concentrated *in vacuo*. The crude was purified by flash column chromatography (0–50% EtOAc/Petroleum ether) to give **4.30** as a brown solid (835 mg, 78% over 2 steps): R_f 0.19 (50% EtOAc/Petroleum ether); m.p. 136–140 °C (from EtOAc); $\overline{\nu}_{max}$ (neat)/cm^{-1} 3315 (w), 2981 (O-H, w), 1596 (w), 1492 (w); ^{1}H NMR (400 MHz, $CDCl_3$) δ_H 8.05 (1H, d, *J* 8.5, H-8), 7.98 (1H, d, *J* 2.2, H-5), 7.94 (1H, d, *J* 8.9, H-8), 7.78 (1H, dd, *J* 9.0, 2.2, H-7), 7.32 (1H, d, *J* 8.5, H-4), 4.91 (2H, d, *J* 4.6, H-1'), 4.28 (1H, t, *J* 4.6, C(1')O*H*); ^{13}C NMR (151 MHz, $CDCl_3$) δ 159.7 (C-2), 145.6 (C-8a), 135.9 (C-4), 133.4 (C-7), 130.5 (C-8), 129.9 (C-5), 128.8 (C-4a), 120.3 (C-6), 119.4 (C-3), 64.3 (C-1'); LRMS *m/z* (ESI$^+$) 238 ([M^{79}Br+H]$^+$, 74%) & 240 ([M^{81}Br+H]$^+$, 69%]. The NMR and LRMS data are in good agreement with the literature.[174]

2-(Azidomethyl)-6-bromoquinoline (4.32) [176]

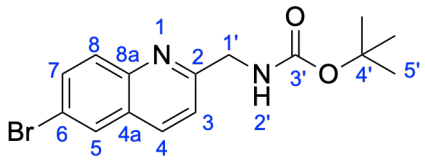


Step 1: PBr_3 (0.021 mL, 0.223 mmol, 1.0 eq.) was added dropwise to a solution of **4.30** (53 mg, 0.223 mmol, 1.0 eq.) and NEt_3 (0.031 mL, 0.222 mmol, 1.0 eq.) dissolved in CH_2Cl_2 (11 mL) at 0 °C. The solution was allowed to warm to rt and left to stir for 18 h. The solution was washed with brine, dried over Na_2SO_4, filtered and concentrated *in vacuo*.

Step 2: The crude material from step 1 was dissolved in DMF (1 mL), after which NaN_3 (27 mg, 0.415 mmol, 1.9 eq.) was added portion-wise. The resulting suspension was left to

stir at rt for 15 h. The solution was then diluted with EtOAc (20 mL), washed with $LiCl_{(aq)}$ (0.5 M, 20 mL), then washed with H_2O (20 mL). The aqueous components were washed with EtOAc (3 × 30 mL) and the combined organic components were washed with brine (40 mL), dried over Na_2SO_4, filtered and concentrated *in vacuo*. The crude was purified by flash column chromatography (0–15% EtOAc/petroleum ether) to give **4.32** as an off-white solid (32 mg, 55% over 2 steps): R_f 0.56 (20% EtOAc/Petroleum ether); m.p. 72–74 °C (from EtOAc); $\overline{\nu}_{max}$ (neat)/cm^{-1} 2110 (N=N ,s), 1490 (C-H, m), 1312 (m); ^{1}H NMR (400 MHz, $CDCl_3$) δ_H 8.11 (1H, d, *J* 8.5, H-4), 7.99 (1H, d, *J* 2.2, H-5), 7.96 (1H, d, *J* 9.0 Hz, H-8), 7.80 (1H, dd, *J* 9.0, 2.2, H-7), 7.49 (1H, d, *J* 8.5, H-3), 4.66 (2H, s, H-1'); ^{13}C NMR (151 MHz, $CDCl_3$) δ_C 156.7 (C-2), 146.5 (C-8a), 136.4 (C-4), 133.6 (C-7), 131.1 (C-8), 129.8 (C-5), 128.7 (C-4a), 120.8 (C-6), 120.7 (C-3), 56.3 (C-1'); LRMS *m/z* (ESI^+) 263 & 265 ([M^{79}+H^+] & [M^{81}+H^+], 74%); HRMS *m/z* (ESI^+) [Found: 262.9928 & 264.9907, $C_{10}H_8N_4Br^{79}$ & $C_{10}H_8N_4Br^{81}$, requires $[M+H]^+$ 262.9927 & 264.9906).

***tert*-Butyl ((6-bromoquinolin-2-yl)methyl)carbamate (4.34)**

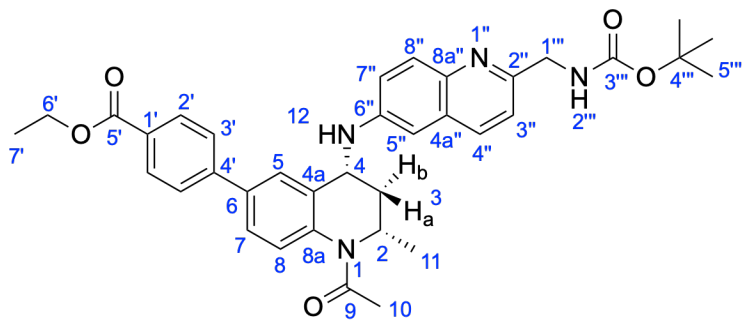


Step 1: Step 1 was carried out using a previously reported procedure.[176] PPh_3 (528 mg, 2.01 mmol, 1.1 eq.) was added to a solution of **4.32** (441 mg, 1.85 mmol, 1.0 eq.) in THF/H_2O (6.6 mL, 9:1 *v/v*). The resulting solution was stirred for 3 h. The THF was removed concentration *in vacuo* after which the solution was diluted with EtOAc (50 mL) and $HCl_{(aq)}$ (1 M, 30 mL). The aqueous and organic components were separated, and the organic components were washed with $HCl_{(aq)}$ (1 M, 2 × 50 mL). $HCl_{(aq)}$ (2 M, 50 mL) was added to the organic components and the biphasic solution was stirred vigorously for 30 min. The aqueous and organic components were separated, and the combined aqueous components were neutralised with satd. $NaHCO_{3(aq)}$. The aqueous components were then extracted with

EtOAc (3 × 70 mL) and the combined organic components from this extraction were dried over Na_2SO_4, filtered and concentrated *in vacuo*.

Step 2: The crude material from Step 1 (297 mg) was dissolved in CH_2Cl_2 (3.6 mL) and cooled to 0 °C. Di-*tert*-butyl dicarbonate (301 mg, 1.38 mmol 1.1 eq.) was added and the reaction was allowed to warm to rt and stirred for 3 h. The reaction was then concentrated *in vacuo* and purified by flash column chromatography (0–30% EtOAc/Petroleum ether) to give **4.34** as a colourless solid (206 mg, 33% over 2 steps): R_f 0.17 (20% EtOAc/Petroleum ether); m.p. 130–132 °C (from EtOAc); $\overline{\nu}_{max}$ (neat)/cm^{-1} 2977 (C-H, m), 1705 (C=O, s), 1489 (m); ^{1}H NMR (400 MHz, $CDCl_3$) δ_H 8.04 (1H, d, *J* 8.5, H-4), 7.97 (1H, d, *J* 2.2, H-5), 7.93 (1H, d, *J* 8.9, H-8), 7.77 (1H, dd, *J* 8.9, 2.2, H-7), 7.39 (1H, d, *J* 8.5, H-3), 5.91–5.80 (1H, m, H-2'), 4.61 (2H, d, *J* 5.1, H-1'), 1.50 (9H, s, H-5'); ^{13}C NMR (151 MHz, $CDCl_3$) δ_C 158.0 (C-2), 156.2 (C-3'), 146.2 (C-8a), 135.8 (C-4), 133.2 (C-7), 130.8 (C-8), 129.8 (C-5), 128.6 (C-4a), 120.8 (C-3), 120.3 (C-6), 79.8 (C-4'), 46.4 (C-1'), 28.6 (C-5'); LRMS *m/z* (ESI$^+$) 337 & 339 ([M^{79}+H$^+$] & [M^{81}+H$^+$], 75%); HRMS *m/z* (ESI$^+$)[Found: 337.0548 & 339.0528, $C_{15}H_{18}O_2N_2Br^{79}$ & $C_{15}H_{18}O_2N_2Br^{81}$, requires [M+H]$^+$ 337.0546 & 339.0526); HPLC (Method 2) Retention time = 9.48 min, 88.6%.

Ethyl 4-((2*S*,4*R*)-1-acetyl-4-((2-(((*tert*-butoxycarbonyl)amino)methyl)quinolin-6-yl)amino)-2-methyl-1,2,3,4-tetrahydroquinolin-6-yl)benzoate (4.35)

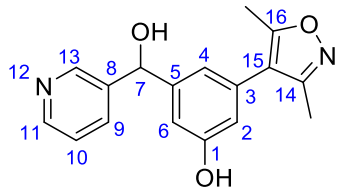


Compound **2.14** (65 mg, 0.184 mmol, 2.0 eq.), compound **4.34** (31 mg, 0.0919 mmol, 1.0 eq.), BrettPhos (16 mg, 0.0298 mmol, 0.32 eq.), BrettPhos Pd G3 (7 mg, 0.00772 mmol, 0.084 eq.) and NaO^{t}Bu (11 mg, 0.114 mmol, 1.2 eq.) were added to a dry microwave vial

which was subsequently purged with Ar. Degassed, anhydrous toluene (0.76 mL) was added and the resulting suspension was stirred at 40 °C for 24 h. The suspension was then diluted with EtOAc (10 mL) and H_2O (10 mL). The organic and aqueous components were separated, and the aqueous components were extracted with EtOAc (3 × 10 mL). The combined organic components were dried over Na_2SO_4, filtered, and concentrated *in vacuo*. The crude was purified by flash column chromatography (0–80% EtOAc/CH_2Cl_2 with 1% NEt_3) to give **4.35** as a green solid (20 mg, 36%): R_f 0.57 (60% EtOAc/CH_2Cl_2 with 1% NEt_3); $[\alpha]_D^{25}$ = +249.2 (*c* 1.0, $CHCl_3$); mp 113–117 °C (from EtOAc); $\overline{\nu}_{max}$ (thin film)/cm^{-1} 3344 (N-H, w), 1711 (C=O, s), 1627 (N-H, m); ^{1}H NMR (400 MHz, CD_3CN) δ_H 8.02–7.93 (2H, m, H-2'), 7.88 (1H, d, *J* 8.5, H-4''), 7.78 (1H, d, *J* 9.1, H-8''), 7.64–7.57 (3H, m, H-7, H-3'), 7.57–7.54 (1H, m, H-5), 7.40 (1H, d, *J* 8.1, H-8), 7.34 (1H, dd, *J* 9.1, 2.7, H-7''), 7.22 (1H, d, *J* 8.5, H-3''), 6.85 (1H, d, *J* 2.6, H-5''), 6.10–5.95 (1H, m, H-2'''), 5.22 (1H, d, *J* 8.0, H-12), 4.90–4.75 (1H, m, H-2), 4.48 (1H, ddd, *J* 12.0, 8.0, 4.1, H-4), 4.39 (1H, d, *J* 5.7, H-1'''), 4.30 (2H, q, *J* 7.1, H-6'), 2.75 (1H, ddd, *J* 12.5, 8.5, 4.1, H_a-3), 2.20 (3H, s, H-10), 1.43 (9H, s, H-5'''), 1.36–1.28 (4H, m, H_b-3, H-3'), 1.16 (3H, d, *J* 6.3, H-11); ^{13}C NMR (151 MHz, CD_3CN) δ_C 170.1 (C-9), 167.0 (C-5'), 157.0 (C-3'''), 155.2 (C-2''), 146.9 (C-6''), 145.6 (C-4'), 143.1 (C-8a''), 139.1 (C-4a), 138.3 (C-8a), 137.7 (C-6), 135.4 (C-4''), 130.8 (C-2'), 130.6 (C-8''), 130.4 (C-1'), 130.1 (C-4a''), 127.9 (C-8), 127.7 (C-3'), 126.6 (C-7), 123.2 (C-5), 122.3 (C-7''), 120.7 (C-3''), 104.8 (C-5''), 79.6 (C-4'''), 61.8 (C-6'), 50.5 (C-4), 48.7 (C-2), 46.8 (C-1'''), 41.5 (C-3), 28.6 (C-5'''), 23.4 (C-10), 21.7 (C-11), 14.6 (C-7'); LRMS *m/z* (ESI^+) 609 ($[M+H^+]^+$, 50%); HRMS *m/z* (ESI^+) [Found: 609.3063, $C_{36}H_{41}O_5N_4$, requires $[M+H]^+$ 609.3071); HPLC (Method 2) Retention time = 8.76 min, 88.9%.

6.2.4 Previously reported BET BRD ligands

3-(3,5-Dimethylisoxazol-4-yl)-5-(hydroxy(pyridin-3-yl)methyl)phenol (1.5) [31]



OXFBD04 (**1.5**) was synthesised according to the procedure described by Jennings *et al*..[31] 3-Bromopyridine (734 mg, 4.65 mmol, 5.0 eq.) was dissolved in anhydrous THF (4.2 mL) under Ar. Isopropyl-magnesium chloride lithium chloride complex (1.3 M in THF, 4.21 mL. 5.47 mmol, 6.0 eq.) was added dropwise at rt and the resulting solution was stirred for 2 h. A solution of compound **4.23** (198 mg, 0.912 mmol, 1.0 eq.) in anhydrous THF (4.2 mL) was added and the resulting solution was stirred for 2.5 h, after which the reaction was quenched with satd. $NaH_4Cl_{(aq)}$ (30 mL). The aqueous phase was extracted with EtOAc (3 × 30 mL) and the combined organic layers were washed with H_2O (20 mL) and brine (20 mL), dried over $MgSO_4$, filtered, and concentrated *in vacuo*. The crude material was purified by flash column chromatography to give OXFBD04 (**1.5**) as a yellow solid (201 mg, 74%): R_f 0.55 (10% MeOH/CH_2Cl_2); m.p. 121–125 °C (from EtOAc); ^{1}H NMR (400 MHz, DMSO) δ_H 9.59 (1H, br. s, C(1)O*H*), 8.60 (1H, d, *J* 2.2, H-13), 8.42 (1H, dd, *J* 4.8, 1.7, H-11), 7.75 (1H, dt, *J* 7.9, 2.1, H-9), 7.34 (1H, ddd, *J* 7.8, 4.8, 0.9, H-10), 6.83 – 6.79 (2H, m, H-4, H-6), 6.60 (1H, dd, *J* 2.4, 1.6, H-2), 6.07 (1H, s, C(7)O*H*), 5.74 (1H, d, *J* 4.7, H-7), 2.36 (3H, s, C(16)CH_3), 2.18 (3H, s, C(14)CH_3); LRMS *m/z* (ESI$^+$) 297 ([M+H]$^+$, 5%). HPLC (Method 1), Retention time = 5.53 min, 97.2%. These data are in agreement with the literature.[31]

6.3 General Biology Methods

6.3.1 Biological reagents and pH measurements

Biologically tested compounds 1.5, **2.1**–**2.6**, **2.13**, **2.20**–**2.23**, **2.30**–**2.33**, **3.1**, **3.41**–**3.46**, **4.2**, **4.5**, and **4.6** were synthesised according to the procedures described in **section 6.2**. Compounds **3.2**, **3.3**, **3.24**, **3.27**, **3.28**, **3.30** and **3.33** were previously synthesised by Aleksy Kwiatkowski.[139] OXFBD02 (**1.4**), OXFBD03 (**1.37**), and **1.38** were synthesised by Lily-Latimer Smith, Oliver J. Stratton, and Dr Charles Evans, respectively, using previously published procedures.[30,31] I-BET726 (**1.6**) was purchased from Cambridge Bioscience Ltd and (+)-JQ1 (**1.1**) from Stratech Scientific Ltd. All biologically tested compounds were ≥95% pure as judged by HPLC analysis.

All other biological reagents were obtained from commercial sources.

All solutions described in **section 6.3** are aqueous, unless otherwise stated.

Purified (Milli-Q) water was obtained from a Millipore Elix® Reverse Osmosis system which was further purified by a Millipore Milli-Q® Synthesis system with a 0.22 μm filter on the outlet, or from a ELGA LabWater PURELAB® Chorus 1 Complete water purification system.

pH measurements were performed using an Oakton PH 550 Benchtop pH Meter Kit, with an Oakton pH electrode with temperature sensor. Calibration was carried out between pH 4.0–7.0 and 7.0−10.0 immediately before use, with pH 4.0, pH 7.0, pH 10.0 buffer solutions from Cole-Palmer. Electrodes were stored in a 4 M aqueous potassium chloride solution.

6.3.2 Protein expression and purification

Protein concentration was estimated by measuring the absorbance at 280 nm using a NanoDrop® Lite spectrophotometer (Nanodrop® Technologies Inc.) and using the Beer-Lambert law and the following extinction coefficients: 6×His-*Sm*BRD3(2),

ε = 13410 $M^{-1}cm^{-1}$; 6xHis-*Sm*BRD3(1,2) ε = 26360 $M^{-1}cm^{-1}$; 6×His-cleaved *Sm*BRD3(1,2) ε = 24870 $M^{-1}cm^{-1}$; 6xHis-BRD4(1), ε = 28545 $M^{-1}cm^{-1}$

Protein molecular weight and molar extinction coefficient were calculated using ProtParam on the ExPASy Bioinformatics Resource Portal.

Centrifugation: Protein samples of up to 10.0 mL were centrifuged in a Beckman Allegra-X30R Centrifuge (3082 ×*g*) at 4 °C. Cell growth media and cell lysates were centrifuged in a Beckman Coulter J-25 (11,325 ×*g*: JSP F500 rotor; 9605 ×*g*: JLA-16.250 rotor and 7741 ×*g*: JA-25.50 rotor, respectively).

SDS-PAGE was carried out using NuPAGE™ 4–12%, Bis-Tris precast polyacrylamide gels (Invitrogen™) at 180 V and 1× NuPAGE™ MES SDS Running Buffer (Invitrogen™). Prior to separation by SDS-PAGE, 25 µL of protein sample was diluted with 8.3 µL of loading buffer (4× Laemelli sample buffer (Bio-Rad) and 10% (*v/v*) β-ME) and heated at 100 °C for 5 min. PageRuler™ Prestained Protein Ladder (Thermo Scientific™) (6 µL) was used as a molecular weight reference. The gels were stained using InstantBlue™ Coomassie stain (Abcam), destained using Milli-Q water and then imaged using a Bio-Rad molecular imager.

Plasmids: Plasmids for the expression of *Sm*BRD3(1,2) and *Sm*BRD3(2) were previously prepared by Dr Matthias Schiedel.

Competent bacterial cells: *Escherichia coli* (*E. coli*) strains of the following genotype was used:

- BL21 (DE3) Gold: F- ompT hsdSB (rB-mB-) gal dcm (DE3). DE3 denotes a chromosomal copy of the T7 RNA polymerase gene.

Competent bacterial cells were thawed on ice for 20 min before 5 µL of plasmid DNA (from a 80–140 ng/µL stock solution) was added to 20 µL of the competent bacterial cells. The tubes were left on ice for 30 min before incubation at 42 °C for 30 sec. The tubes were place on ice for 5 min and then 500 µL of SOC outgrowth medium (New England Biolabs Inc.)

was added gently to each tube. The tubes were incubated at 37 °C for 1 h before 100–200 µL of the transformation mixture was plated onto agar plates containing kanamycin (50 µg/mL) and incubated overnight.

6.3.2.1 Fermentation conditions for bromodomain containing proteins

The expression and purification procedures of schistosomal bromodomain-containing proteins were developed by Dr Matthias Schiedel based on a previously published procedure.[27] Under aseptic conditions, single colonies of transformed *E. coli* BL21(DE3) Gold were transferred to 100 mL of 2× TY medium containing a final concentration of 50 µg/mL kanamycin. The cultures were incubated overnight at 37 °C and 180 rpm. Under aseptic conditions, 10 mL of the overnight cultures were then added to 1 L of 2× TY medium containing a final concentration of 50 µg/mL of kanamycin. The cultures were incubated at 37 °C and 180 rpm until the OD_{600} reached a value of 0.6. OD_{600} values were measured in 1.6 mL cuvettes against a reference of 2× TY medium, using a Novaspec® II spectrometer measuring at 600 nm. The cultures were then cooled to 16 °C and IPTG was added to the culture at a final concentration of 0.1 mM. Subsequently, the cells were fermented at 16 °C, 180 rpm, overnight. Cells were harvested by centrifugation (11,325 ×*g*, 4 °C, 10 min) and the resultant pellets were combined and stored at −80 °C.

Table 6.1. Components of 2× TY media

Media	Reagent	Mass per litre (gL^{-1})
2× TY	Tryptone	16.0
	Yeast Extract	10.0
	NaCl	5.0

6.3.2.2 Purification conditions for His-tagged bromodomain containing proteins

The pellet was re-suspended in Extraction buffer (100 mL per 20 g cell mass), 250 Units (U) of Benzonase (per 100 mL of Extraction buffer) was added, then the cells were lysed by sonication (60 × 5 sec bursts, 5 sec pauses). Polyethyleneimine (PEI, 5% *v/v*) was added to a final concentration of 0.15% *v/v*, and the lysate was incubated on ice for 15 min. The

lysate was clarified by centrifugation (25,000 ×*g*, 4 °C, 15 min) and the supernatant was decanted. The supernatant was then filtered through a 0.45 µm filter and applied to a purification column. Immobilised metal affinity chromatography (IMAC) was initially used to purify the protein, at 4 °C using HisTrap™ HP (5 mL) column (GE Healthcare). The column was rinsed with 10 CV of Milli-Q water, charged with 4 CV of aqueous 100 mM $NiSO_4$ and then equilibrated with 10 CV of binding buffer (supplemented with 10 mM β-ME immediately before use). The cell lysate was diluted to a total volume of 100 mL with binding buffer and loaded at a rate of 1 mL/min. The column was washed with a step gradient of 10 CV 9% (*v/v*) elution buffer (45 mM imidazole), and 10 CV 12% (*v/v*) elution buffer (60 mM imidazole). When all residual products of bacterial fermentation were eluted, the polyhistidine-tagged protein of interest was step-eluted with 4 CV of 60% (*v/v*) elution buffer (300 mM imidazole) followed by 2 CV of 100% elution buffer (500 mM imidazole). The eluted protein was collected and fractionated. The fractions containing the highest levels of protein (as determined by SDS-PAGE gels and UV trace) were concentrated using 10k MWCO spin concentrators (Corning®) in a Beckmann Allegra™ 21R centrifuge (4,000 ×*g*, 4 °C). Strip buffer was used to remove the Ni^{2+} ions from the His-Trap™ column. Further purification was achieved using size exclusion chromatography (SEC). Concentrated fractions from the IMAC purification (approximately 1.2 mL) were loaded on a 120/300 mL Superdex 75 size exclusion chromatography column (Amersham), equilibrated with gel filtration buffer prior to loading. The eluted protein was collected and fractionated. The fractions containing the highest levels of pure protein (as determined by SDS-PAGE gels) were concentrated as described before. The protein solution was aliquoted, flash frozen in liquid nitrogen, then stored at −80 °C.

Table 6.2 Buffer type and composition for protein purification.

Buffer[a]	Reagent	Concentration
Binding buffer (pH = 7.6)	HEPES	50 mM
	NaCl	500 mM
	Imidazole	5 mM
Extraction buffer (pH = 7.6)	HEPES	50 mM
	NaCl	500 mM
	Imidazole	5 mM
	Protease Inhibitor cocktail[c]	1 Tbl/20 g pellet
Elution buffer (pH = 7.6)	HEPES	50 mM
	NaCl	500 mM
	Imidazole	500 mM
Strip buffer (pH = 7.6)	HEPES	50 mM
	NaCl	500 mM
	EDTA	100 mM
Gel filtration buffer[b] (pH = 7.6)	HEPES	50 mM
	NaCl	500 mM

[a]Filtered through a 0.22 µm filter; [b]degassed; [c]Sigma*FAST* Protease Inhibitor Cocktail Tablet, EDTA Free (Sigma-Aldrich).

6.3.2.3 Purification conditions for His-tag cleaved SmBRD3(1,2)

Fermentation and bacterial cell lysis were performed as described above for the other bromodomain containing proteins. IMAC was also performed as described above using a HisTrap™ HP (5 mL) column (GE Healthcare). Eluted protein was collected and fractionated and the fractions containing the highest levels of pure protein (as determined by SDS-PAGE gels and UV trace) were concentrated using 10k MWCO spin concentrators (Corning®) in a Beckmann Allegra™ 21R centrifuge (4,000 ×*g*, 4 °C) to approximately 5 mL. The TEV-cleavage procedure was based upon work by Dr Matthias Schiedel on the production of 6×His-cleaved *Sm*BRD3(1,2). TEV cleavage buffer (15 mL, 50 mM HEPES, 500 mM NaCl, 1 mM β-mercaptoethanol, pH 7.6) were added and the mixture was concentrated to A

volume of approximately 5 mL using 10k MWCO spin concentrators (Corning®) in a Beckmann Allegra^{TM} 21R centrifuge (4,000 ×*g*, 4 °C). After determination of the approximate concentration of 6×His-*Sm*BRD3(1,2), using TEV protease (pRK793, prepared by Dr Matthias Schiedel using a plasmid provided by the group of Prof Christopher Schofield, University of Oxford) was added in a molar ratio of 1:50 [TEV protease:6×His-*Sm*BRD3(1,2)]. The solution was diluted using TEV cleavage buffer to give a total volume of 20 mL, and the mixture was incubated overnight at 4 °C. The mixture was then concentrated to a volume of approximately 2 mL using 10k MWCO spin concentrators (Corning®) in a Beckmann Allegra^{TM} 21R centrifuge (4,000 ×*g*, 4 °C). To separate cleaved substrate protein from 6×His-tagged TEV protease, a second IMAC was performed with a HisTrap^{TM} HP (5 mL) column (GE Healthcare). The column was rinsed with 10 CV of Milli-Q water, charged with 4 CV of 100 mM $NiSO_4$ and washed with 10 CV of binding buffer (supplemented with 10 mM β-ME immediately before use). The protein solution was then loaded the at a rate of 1 mL/min. The column was washed with approximately 20 CV binding buffer. The desired *Sm*BRD3(1,2), detected in the flow-through using the UV trace, was collected and fractionated. Fractions containing the highest levels of pure protein (as determined by SDS-PAGE gels and UV trace) were concentrated 10k MWCO spin concentrators (Corning®) in a Beckmann Allegra^{TM} 21R centrifuge (4,000 ×*g*, 4 °C) to a volume of approximately 1.2 mL. Further purification was achieved using size exclusion chromatography. Concentrated fractions (approximately 1.2 mL) were loaded on a 120/300 mL Superdex 75 size exclusion chromatography column (Amersham). For the SEC purification of this protein, a modified gel filtration buffer with a reduced amount of NaCl was used (**Table 6.3**). Eluted protein was collected and fractionated; fractions containing the highest levels of pure protein (as determined by SDS-PAGE gels) were combined and the concentration was determined. For the highest purity and adequate protein for polyclonal antibody production, the lower purity fractions were combined, concentrated to approximately 1.2 mL and further purified using size exclusion chromatography. The most pure fractions, as determined by SDS-PAGE gel, were combined and the concentration was

adjusted to 0.5 mg/mL, as required for antibody production (**section 6.3.11**). The protein solution was aliquoted, flash frozen in liquid nitrogen, then stored at −80 °C.

Table 6.3. Buffer type and composition for purification of *Sm*BRD3(2).

Buffer[a]	Reagent	Concentration
Binding buffer (pH = 7.6)	HEPES	50 mM
	NaCl	500 mM
	Imidazole	5 mM
Extraction buffer (pH = 7.6)	HEPES	50 mM
	NaCl	500 mM
	Imidazole	5 mM
	Protease Inhibitor Cocktail[c]	1 Tbl/20 g pellet
Elution buffer (pH = 7.6)	HEPES	50 mM
	NaCl	500 mM
	Imidazole	500 mM
Strip buffer (pH = 7.6)	HEPES	50 mM
	NaCl	500 mM
	EDTA	100 mM
Gel filtration buffer[b] (pH = 7.6)	HEPES	50 mM
	NaCl	150 mM

[a]Filtered through a 0.22 µm filter; [b]degassed; [c]Sigma*FAST* Protease Inhibitor Cocktail Tablet, EDTA Free (Sigma-Aldrich).

6.3.3 Isothermal Titration Calorimetry

Isothermal titration calorimetry (ITC) was carried out using a procedure previously developed by Dr Matthias Schiedel and a modified procedure described by Brand *et al*.[119] ITC experiments were performed on a MicroCal PEAQ-ITC Automated or Manual (Malvern) and analysed with the MicroCal PEAQ-ITC Analysis software (Malvern 1.1.0.1262) using a single binding site model. For each experiment, the first data point was removed from the analysis. Prior to running the ITC experiments, the proteins were dialysed at 4 °C overnight in a Slide-A-LyzerR MINI Dialysis Device (2000 MWCO; Thermo Scientific Life

Technologies) into 50 mM HEPES, 150 mM NaCl containing 0.2% DMSO; pH 7.4. Proteins were centrifuged to remove aggregates (2 min, 3000 rpm, 25 °C). Protein concentrations were determined by measuring the absorbance at 280 nm using a NanoDrop Lite spectrophotometer (Nanodrop® Technologies Inc.) and adjusted using dialysis buffer (50 mM HEPES, 150 mM NaCl containing 0.2% DMSO; pH 7.4) to the required concentration. Compounds were dissolved as a DMSO stock solution and diluted to the required concentration using DMSO free dialysis buffer, and to a final DMSO concentration of 0.2%. The ITC cell was stirred at 750 rpm, reference power set to 5 µcal/s and temperature held at 25 °C. After an initial delay of 60 s, 19 × 2 µL injections (first injection 0.4 µL) were performed with a spacing of 180 s. Small molecule solutions in the calorimetric cell (250 µL for manual, 400 µL for auto, 20 to 30 µM) were titrated with the protein solutions in the syringe (40 µL for manual, 120 µL for auto, 160 to 300 µM). ITC analysis of human BRD4(1) used recombinant protein which had been previously expressed by Dr Matthias Schiedel using a previously published procedure.[27]

6.3.4 Protein X-ray crystallography

6.3.4.1 Crystallisation of SmBRD3(2)

The crystallisation of **2.1** with His-tag cleaved *Sm*BRD3(2) was based upon the crystallisation of I-BET726 (**1.6**) with *Sm*BRD3(2), conducted by Dr Matthias Schiedel and Dr Michael McDonough.

*Sm*BRD3(2)-**2.1** co-crystallization was carried out with the help of Dr Michael McDonough. *Sm*BRD3(2) (241..368aa, 6×His-tag cleaved) was co-crystallised with **2.1** by the sitting drop vapor diffusion method using high throughput (HT) crystallisation screening methods. All HT screens were performed in CrystalMation Intelli-Plate 96-3 low-profile plates (Hampton Research, HR3-119). Reservoirs and drops were dispensed using an Art Robbins Phoenix automatic liquid handler. Reservoirs contained 80 µL of sparse matrix precipitant solution and crystallisation drops (200–300 nL total volume) were placed in each of the three

subwells; subwell 1, 200 nL protein : 100 nL well solution; subwell 2, 100 nL protein : 100 nL well solution ; subwell 3, 100 nL protein : 200nL well solution. Plates were sealed using optically clear Xtra-Clear Advanced Polyolefin StarSeal (StarLab) seals and incubated at 4 °C and 19 °C. Crystallisation conditions were carried out using an optimisation screen based on the initial *Sm*BRD3(2):I-BET726 (**1.6**) complex, consisting of component ranges of 19% to 30% PEG 3350 and pH 5.5 to 6.9, 0.1 M Bis-TRIS (sitting drop, protein to-well ratio 1:2). A protein concentration of 12.31 mg/mL and a final **2.1** concentration of 2 mM was added directly to the protein prior to crystallisation from a 100 mM stock solution in DMSO. Crystals formed within 4 weeks and the resultant crystals were cryoprotected by soaking crystals in reservoir solution diluted with 25% (*v/v*) glycerol before being flash cooled in liquid nitrogen.

6.3.4.2 Data collection and processing

Data were collected and processed by Dr Michael McDonough. Data were collected using single crystals at Diamond Light Source beamline i04-1 (*Sm*BRD3(2)-**2.1**) equipped with Dectris Eiger R 4M or Pilatus 6M-F detectors, respectively. Diffraction data for *Sm*BRD3(2)-**2.1** were autoprocessed by the beamlines autoprocessing pipeline using the DIALS strategy.[177] The crystal processed in Space Group $C222_1$ with similar unit cell constants to the SmBRD3(2):I-BET726 (**1.6**) co-crystal (**Table 6.4**).

6.3.4.3 Structure solution and refinement

The co-crystal structure of **2.1** with *Sm*BRD3(2) was solved with the help of Dr Michael McDonough. This was carried out by molecular replacement (MR) using PHASER,[178] with the structure of the previously solved I-BET726 (**1.6**):*Sm*BRD3(2) co-crystal structure, developed by Dr Matthias Schiedel and Dr Michael McDonough, as the search model. The co-crystal structure of I-BET726 with *Sm*BRD3(2) was had been previously solved by Dr Michael McDonough using a structure of mouse BRD4 as the search model (PDB ID 3JVL). Two molecules were identified in the asymmetric unit. Visual inspection of initial electron

density maps indicated that each chain contained bound ligand **2.1**. The ligand **2.1** was fit to the density and iterative cycles of model fitting in COOT,[179] and refinement using PHENIX[180] were carried out until the converging R_{work} and R_{free} no longer decreased. Data collection and refinement statistics for all structures can be found in **Table 6.4**.

Table 6.4. Data collection and refinement statistic for SmBRD3(2)-I-BET726 (PDB ID: 7AMC) and *Sm*BRD3(2)-**2.1** (PDB ID: 7AMH).

Structure	*Sm*BRD3(2)-**2.1**
PDB ID	7AMH
Data Collection	
Radiation source	Synchrotron Diamond Beamline I04-1
Detector	Dectris Pilatus 6M-F
X-ray Wavelength (Å)	0.9119
Resolution Range (Å)*	63.37–1.86 (1.90–1.86)*
Space Group	$C\ 2\ 2\ 2_1$
Unit Cell Dimensions (*a* Å, *b* Å, *c* Å, α°, β°, γ°)	52.20 84.11 126.74 90.0 90.0 90.0
Total Number of Reflections Observed	276609 (10702)*
Number of Unique Reflections	23711 (1146)*
Multiplicity ⌘	11.7 (9.3)*
Completeness (%)⌘	99.9 (98.9)*
$I/\sigma(I)$	6.8 (0.5)*
R_{merge} (%)	0.227 (4.369)*
CC1/2⌘	0.995 (0.470)*
Refinement	
R_{work} (%)	0.2174
R_{free} (%)	0.2538
RMS Deviation (Bonds/Angle)	0.012/0.889
Average *B* Factor (Å^2)	37.23
Wilson B Factor (Å^2)	28.1
Number of Water Molecules	210

The R_{free}, based on 4.59% (*Sm*BRD3(2)-**2.1**) of the total reflections. The structures have been deposited by Dr Michael McDonough in the RSCB as PDB ID: 7AMH.

6.3.5 Phenotypic screening

All phenotypic screening described in **section 6.3.5** was carried out at the University of Aberystwyth. Schistosomula and adult worm compound screenings were carried out by Dr Gilda Padalino and Dr Josephine Forde-Thomas. Miracidia compound screening was conducted by Dr Gilda Padalino.

6.3.5.1 Ethics statement

All mouse procedures performed at Aberystwyth University (AU) adhered to the United Kingdom Home Office Animals (Scientific Procedures) Act of 1986 (project licenses PPL 40/3700 and P3B8C46FD) as well as the European Union Animals Directive 2010/63/EU, and were approved by AU's Animal Welfare and Ethical Review Body (AWERB).

6.3.5.2 Schistosomula drug screen

Schistosomula drug screens were carried out by Dr Gilda Padalino or Dr Josephine Forde-Thomas at the University of Aberystwyth. Schistosomula stage of *S. mansoni* were obtained by mechanical transformation from cercariae as described in literature.[181] The parasite material was seeded (120 parasites/well) in a 384-well tissue culture plate (PerkinElmer, cat. 6007460) and dosed with the selected compound as previously reported.[137,182–184] For the data in **Chapter 2**, each compound (as 10 mM DMSO stock solution) was initially tested at a single concentration point (20 μM final concentration, in duplicates) in at least three independent screens (Z′ scores above 0.35,[136]). Each screen contained the gold-containing compound auranofin (AUR) (10 μM final concentration in 0.625% DMSO) as a positive control, and a negative control of DMSO (0.625% *v/v*). For any compounds that were active in the initial single concentration point screen, a further two-fold titration (from 10 to 0.312 μM) was performed to determine the extent of their anti-schistosomal activity. For data in **Chapter 3**, each compound (as a 10 mM stock solution) was initially tested at a single concentration point (10 μM final concentration, in duplicates) with two independent screens (Z' scores above 0.35,[136]). For any compounds that were active at the initial single

concentration point, a further screen was carried out as a 7-point titration (50, 25, 10, 5, 2.5, 1.25 and 0.625 μM all in 0.625% DMSO) in duplicate (Z' scores above 0.35,[136]), with two independent screens. The screens also contained praziquantel and auranofin (AUR) (10 μM final concentration in 0.625% DMSO) as positive controls and the negative control of DMSO (0.625% *v/v*). Following 72 h schistosomula/compound co-incubation, the plate was automatically acquired and analysed by the Roboworm platform.[135] EC_{50} values were calculated from the titrated concentrations using non-linear regression, after log_{10} transformation of concentrations and data normalisation using GraphPad Prism 7.02.

6.3.5.3 Adult worm drug screen

Male and female adult *S. mansoni* worms were recovered by hepatic portal vein perfusion from female TO mice ((*Mus musculus* HsdOLa:TO - Tuck Ordinary; Envigo, UK) that were percutaneously infected seven weeks earlier with 180 cercariae.[182,185] Following perfusion, the worm material was washed and processed as previously described.[137,185] Schistosome pairs were seeded into 48 well tissue culture plates (1 worm pair/well, in duplicate) and dosed with the compounds [final concentrations of 20 μM (in 0.5% DMSO)]. DMSO (0.5%) and praziquantel (10 μM in 0.5% DMSO) were also included as negative and positive control treatments, respectively. Parasite motility was assessed using a digital image processing-based system (WormassayGP2),[137] modified after Wormassay,[138] or scored by eye using the WHO-TDR scoring metric.[145] For the data in **Chapter 2,** *in vitro* laid eggs were enumerated, and the presence or absence of paired male and female worms was noted to assess the effect of the compound on the worm fecundity as well as worm pairing.

6.3.5.4 Miracidia drug screen

S. mansoni free-living miracidium were obtained by hatching of schistosome eggs as detailed in previous works.[81] The resulting miracidial suspension was collected, washed with Chernin's balanced salt solution (CBSS)[81] and enumerated prior to being used for *in vitro* miracidia to sporocyst transformation screens, as previously reported.[81,137] Each compound was tested at 0.5, 2, 5, 10 and 25 μM (final concentration). Each treatment was

conducted in duplicate (15–25 miracidia/well) and parasites cultured in CBSS with DMSO (1% *v/v*) were set up as negative controls. After 48 h incubation at 26 °C, dead, fully transformed and partially transformed miracidia were enumerated, as previously described.[186,187]

6.3.6 Determination of compound parasite permeability

To determine compound parasite permeability, parasite material was prepared by Dr Josephine Forde-Thomas at the University of Aberystwyth. Male adult schistosomes were seeded into 24-well tissue culture plates (5 worms/well), dosed with compounds as indicated in **section 6.3.5.3** (20 µM in 0.2% DMSO *v/v*) and incubated for 24 h at 37 °C in 5% CO_2. Following the incubation period, parasites were washed three times by sequentially transferring the worms to 2 mL of fresh media lacking any compound treatment. Worms were blotted dry to remove excess media between transfers. Parasites were then snap frozen and stored at −80 °C. When ready for processing, worms were removed from the −80 °C and subject to 3 rounds of repeated snap freeze:thawing. After the final thaw step a sterile 3 mm stainless steel bead was added to each tube along with 200 µL HPLC grade MeOH and samples were homogenized with a TissueLyser (Qiagen) (3 × 3 min, 50 Hz). Finally, samples were centrifuged at 14,000 rpm for 30 min at 4 °C and the supernatant removed to a fresh tube for analysis. For the LCMS analysis of media samples, 1 µL of media was removed and lyophilised. The residue was then resuspended in 200 µL of HPLC grade MeOH and centrifuged at 14,000 rpm for 30 min at 4 °C. The supernatant was removed to a fresh tube for analysis.

LCMS analysis of parasite lysate and media samples were carried out and analysed by Dr Manfred Beckmann at the University of Aberystwyth. Samples were analysed using a Q-Exactive Plus (Thermo Scientific) with an HESI II source coupled to a Dionex Ultimate 3000 Ultra High Performance Liquid Chromatography (UHPLC) system (Thermo Scientific). Chromatographic separation was performed on a Hypersil Gold 1.9 µm, 2.1 × 200 mm column (Thermo Scientific) using water 0.1 % fomic acid (mobile phase A) and methanol

0.1% formic acid (mobile phase B) at a flow rate of 0.6 mL/min and column oven temperature at 60 °C. Each sample (5 µL) was analysed following a gradient of 0% B to 100 % B in 9 min. The flow was held at 100% B for 2.5 min and the column re-equilibrated for 1.5 min. Data were acquired in positive ESI mode. Each experiment consisted of a full scan (65-975 mass-to-charge ratio (*m/z*) at 140k resolution (AGC target 2×10^5 at 100 ms maximum injection time, IT) and MS^2 scans (*PRM multiplexed, 4* stepped, HCD normalised collision energies (nce) of 50 % and 17.5k Orbitrap mass resolution) using selected targeted mass properties for either positive or negative ionisation mode, with an AGC target of 2×10^5 and isochronous IT enabled over 13 min runtime (**Table 6.5**). The spray voltage was 3.5 kV for positive and 2.5 kV for negative ionization modes. The temperatures of the ion transfer capillary and vaporiser were 350 °C and 360 °C respectively with sheath and auxiliary gas set at 30 and 15 arbitrary units, respectively. The data were acquired using Thermo Scientific Xcalibur version 4.2.47. Mass calibration was performed regularly according to the manufacturer's recommendations. Targets were quantified using quadratic models to 1) avoid pre-concentration and 2) account for low concentrated targets within a sample outside the inherent linear range. Data were extracted as absolute area of the quantified ion using Xcalibur peak integration for the target masses of the following transitions: **2.6**: Q1 452.1969 - Q3 145.05; OXFBD02 (**1.4**): Q1 296.1282 - Q3 148.08; **2.31**: Q1 480.2282 - Q3 145.05; OXFBD03 (**1.37**): Q1 338.1387 - Q3 235.10. Concentrations and peak area of compound standard solutions for a calibration curve were $\log_{10}$-tranformed and plotted as a two-point calibration curve. This was used to estimate compound concentration from samples.

Table 6.5: Inclusion list for parallel reaction monitoring (PRM) on Q-Exactive Plus.

Mass [*m/z*]	Formula [M]	Species [*z*]	CS	Polarity	Start [min]	End [min]	(N)CE	MSX ID	Comment
452.19687	$C_{28}H_{25}N_3O_3$	+H	1	Positive	0.1	13.0	50	1	**2.6**
480.22817	$C_{30}H_{29}N_3O_3$	+H	1	Positive	0.1	13.0	50	2	**2.31**
296.12812	$C_{18}H_{17}NO_3$	+H	1	Positive	0.1	13.0	50	3	**1.4**
338.13868	$C_{20}H_{19}NO_4$	+H	1	Positive	0.1	13.0	50	4	**1.37**

CS = charge state; (N)CE = normalised collision energy

6.3.7 *In silico* molecular docking

In silico docking was carried out with the help of Patrick Brennan and Romi Aggarwal. Docking was conducted using the crystal structure of **2.1** bound to *Sm*BRD3(2) (PDB ID: 7AMH) and using GOLD version 2020.1 from the Cambridge Crystallographic Data Centre. The position of **2.1** in the template crystal structure was used to define the binding pocket for the docking of **4.4** using the 'cavity' function of GOLD. The tetrahydroquinoline and benzoic acid ring of the original **2.1** ligand were used to specify the position onto which the tetrahydroquinoline and benzoic acid rings of docked ligand **4.4** were to be superimposed, using the 'scaffold' functionality of GOLD (**Figure 6.1**). All parameters were kept as default during docking screens, except constraint weight, which was increased from the default value of 5, to 20. For the docked ligand, 50 poses were generated, and the highest ranked docking pose was visually inspected using PyMOL.

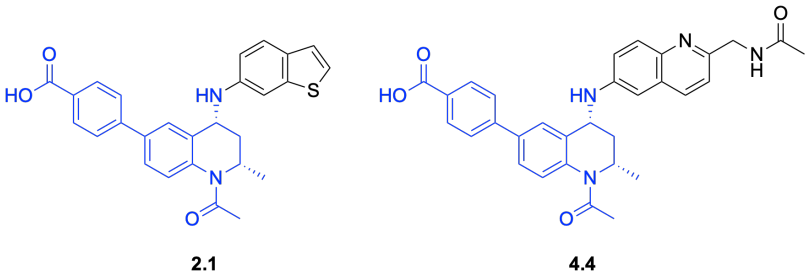


Figure 6.1 Structure of original ligand **2.1** and docked ligand **4.4**. The molecule region used to superimpose the structure of **4.5** onto the original ligand **2.1** is highlighted in blue.

6.3.8 *In vitro* diazirine probe crosslinking to recombinant protein

The diazirine probe **4.2** or **4.5** (20 or 100 μM, 0.5% DMSO) or DMSO (0.5%) were incubated with recombinant *Sm*BRD3(1,2) or *Sm*BRD3(2) (10 μM) in LCMS buffer (25 mM HEPES, 100 mM NaCl, pH 7.4) for 50 min at 4 °C in 1.5 mL Eppendorf tubes. The caps of the Eppendorf tubes were removed and the solutions were irradiated with UV light (365 nm) using an Analytik Jena 100 W, 365 nm UV lamp for 10 min at 4 °C. During this time, the 'no UV' negative controls were incubated in the dark at 4 °C. The samples were then flash frozen and stored at −80 °C until required for analysis using LCMS or in-gel fluorescence.

For analysis using LCMS, the samples were thawed prior to use and analysed using a Waters Xevo G2-XS system (Waters) fitted with a ProSwiftTM RP-2H PSDVB Reversed Phase HPLC Column (Thermofisher). Data were analysed using the MassLynx software (V4.1) and processed using the MaxEnt function. Photocrosslinking efficiencies were calculated using the intensities of the crosslinked and non-crosslinked protein deconvoluted spectra (**Equation 6.1**). Figures were made using GraphPad Prism 9.5.0.

$$Crosslinking\ yield\ (\%) = \frac{Crosslinked\ Protein\ Intensity}{Crosslinked\ Protein\ Intensity + Unmodified\ Protein\ Intensity} \times 100$$

Equation 6.1. Equation used to determine the crosslinking yields of photoaffinity probes.

For analysis by in-gel fluorescence a CuAAC reaction was carried out using a modified procedure described by Kallenmeijn *et al*.[188] The irradiated solutions were thawed and then incubated with Azide Fluor 545 (100 μM) (Sigma-Aldrich) (**4.36**), TCEP-HCl (1 mM), TBTA (100 μM) and $CuSO_4$ (1 mM) in LCMS buffer. The resulting solutions were incubated in the dark at rt for 1 h, with shaking at 700 rpm. A 20 μL sample of each reaction mixture was removed, diluted with of loading buffer [6.7 μL, 4× Laemelli buffer (Bio-Rad) and 10% (*v/v*) β-ME] and then heated at 95 °C for 5 min. The samples were separated by gel electrophoresis using NuPAGE™ 4–12%, Bis-Tris precast polyacrylamide gels (Invitrogen™) at 200 V, ensuring excess Azide Fluor 545 (**4.36**) had run off the gel. PageRuler™ Prestained Protein Ladder (Thermo Scientific™) (6 μL) was used as a

molecular weight reference. The gel was then rinsed with Milli-Q water and imaged for fluorescence using a Bio-Rad molecular imager (605/50 nm filter, UV trans illumination). The bottom of gels was cut prior to in-gel fluorescence imaging due to residual excess Azide Fluor 545 (**4.36**) diminishing the protein florescence signals. To observe non-fluorescent proteins, the gel was then stained using InstantBlue™ Coomassie stain (Abcam), destained using Milli-Q water and then imaged using a Bio-Rad molecular imager.

6.3.9 Parasite lysate preparation

Parasite lysate was prepared with the help of Dr Josephine Forde-Thomas. Mixed male and female adult worm lysate was prepared from ~200 worm pairs. Previously frozen parasite material was re-suspended with PBS containing 1× cOmplete™, Mini EDTA-free Protease Inhibitor Cocktail (Roche) and distributed between 4× 2mL, round bottomed Eppendorf tubes such that each tube contained ~500mL. A stainless 3 mm steel ball was added to each tube and the parasite material was lysed using three rounds of homogenisation with a TissueLyser (Qiagen) (3 × 3 min, 50 Hz) and snap freeze:thawing. The material was then combined and further processed using a 7mL Dounce homogeniser (100 strokes on ice), the lysate was then centrifuged at 14,000 rpm for 30 min at 4 °C. The supernatant was separated from the solid material and the total protein concentration measured by Bradford assay. If required, the concentration was increased using 10K MWCO a spin-concentrator (Amicon® Ultra-4 Centrifugal Filter Unit, Millipore). Schistosomula worm lysate was formed from approximately 1 million schistosomula using the same workflow outlined above.

UTB buffer-based lysate was prepared by Dr Josephine Forde-Thomas. Previously frozen cercariae, schistosomula and mixed male and female adult worm material were re-suspended in UTB buffer (9 M urea, 75 mM Tris-HCl, pH 7.5) and flash frozen. Using a 3 mm stainless steel ball the material was homogenized with a TissueLyser (Qiagen) (3 × 3 min, 50 Hz). Two more snap freeze:thawing and homogenization cycles were

repeated. Samples were then centrifuged at 14,000 rpm for 30 min at 4 °C and the supernatant removed to a fresh tube for analysis.

6.3.10 Parasite lysate diazirine probe engagement

Diazirine probe (1–20 μM, 0.5% DMSO) or DMSO (0.5%) was incubated with parasite lysate (1.4–1.5 mg/mL total protein concentration in PBS, with with cOmplete™, Mini EDTA-free Protease Inhibitor Cocktail, 1 tablet per 10 mL) in 0.5 mL Eppendorf tubes for 30 min at 4 °C. The caps of the Eppendorf tubes were removed, and the solutions were irradiated with UV light (365 nm) using an Analytik Jena 100 W UV lamp (10 min at 4 °C). During this time, the 'no UV' negative controls were incubated in the dark at 4 °C. The samples were then flash frozen using dry ice and stored at −80 °C until required for further analysis. For analysis using in-gel fluorescence, a CuAAC reaction was carried out using a modified procedure described by Kallenmeijn *et al*.[188] The samples were thawed and incubated with Azide Fluor 545 (**4.36**) (100 μM final concentration from a 10 mM DMSO stock solution), TCEP-HCl (1 mM final concentration from a 50 mM aqueous stock solution), TBTA (100 μM final concentration from a 10 mM DMSO stock solution) and $CuSO_4$ (1 mM final concentration from a 50 mM aqueous stock solution), which were added directly to the lysate from a pre-made 'click mix' (a solution of ratio 1:2:2:1 **4.36**: $CuSO_4$:TCEP:TBTA by volume). The resulting solutions were incubated in the dark at rt for 1 h, with shaking at 700 rpm. A 20 μL sample of each solution was taken and loading buffer [6.7 μL, NuPAGE™ 4 × LDS sample buffer and 5% (*v/v*) β-ME] was added to each sample. The samples were then heated at 95 °C for 5 min and then centrifuged for 1 min at 5,000 ×*g*. The samples (10–20 μL) were loaded onto 4–20% Mini-PROTEAN® TGX Stain-Free™ (Bio-Rad) precast polyacrylamide gel and separated by gel electrophoresis 200 V in 1× Tris/Glycine/SDS buffer (Bio-Rad). PageRuler™ Plus Prestained Protein Ladder (Thermo Scientific™) (6 μL) was used as a molecular weight standard. The gels were washed with cold distilled water before imaging in-gel fluorescence using a Bio-Rad molecular imager. The bottom of the gels was cut prior to in-gel fluorescence imaging due to residual excess Azide Fluor 545

diminishing the protein florescence signals. The gels were fixed using 50% (*v/v*) methanol + 5% (v/v) acetic acid solution, rinsed with H_2O and then stained using Colloidal Coomassie Blue (**Table 6.6**) and MeOH solution (1:4 MeOH/Colloidal Coomassie Blue stock solution), until sufficient staining of proteins was achieved, followed by destaining with 1% (v/v) acetic acid solution until sufficient contrast had been achieved. The Coomassie stained gel was then imaged using a Bio-rad molecular imager.

Table 6.6 Composition of Colloidal Coomassie Blue stock solution.

Compound	Composition	Supplier
Coomassie Brilliant Blue G250	0.1% *w/v*	Thermo-Fisher Scientific
Ortho-phosphoric acid	2% *w/v*	Merck
Ammonium sulphate	10% *w/v*	Merck

6.3.11 *Sm*BRD3 antibody production

Custom polyclonal antibody for the recognition of *Sm*BRD3(1,2) was produced by Life Sciences Solutions, Thermo Fisher Scientific, using a 0.5 mg/mL antigen of 6×His-tagged cleaved *Sm*BRD3(1,2) (expression and purification details of antigen described in **section 6.3.2.3**). The antibody was produced in 2 rabbits following a 90-day protocol, which included immunisation, serum collection and production of ELISA data. The final 50 mL bleed from the animals was affinity purified to give two antibody samples:

Animal	Volume (mL)	Concentration (mg/mL)	Total mg	Titre (ng/mL)
AB4576	10.5	1.71	17.94	< 5
AB4677	9.5	1.65	15.71	< 5

The details of the 90-day protocol followed by Thermo Fischer Scientific are detailed below:

Date	Day	Activity	Description
06/29/22	0	Injection	Initial Inoculation
06/29/22	0	Bleed	Pre-Bleed
07/05/22	6	Processed	Processed
07/13/22	14	Injection	Boost
07/27/22	28	Bleed	Production Bleed
08/01/22	33	Processed	Processed
08/10/22	42	Injection	Boost
08/24/22	56	Injection	Boost
08/24/22	56	Bleed	Production Bleed
08/29/22	61	Processed	Processed
09/07/22	70	Bleed	Production Bleed
09/09/22	72	Bleed	Production Bleed
09/12/22	75	Processed	Processed
09/14/22	77	Ship	Ship to customer

6.3.12 Western blotting

Parasite lysate samples (20 µL) were diluted with 6.7 µL of loading buffer (NuPAGE™ 4 × LDS sample buffer and 5% (*v/v*) β-ME). Recombinant 6×His-tagged cleaved *Sm*BRD3(1,2) (0.5 mg/mL, 3 µL) was diluted with H_2O (297 µL) and loading buffer (100 µL). Both lysate and recombinant protein samples were heated at 95 °C for 5 min. Parasite lysate (15 µL–20 µL) and recombinant protein samples (10 µL) were then loaded onto 4–20% Mini-PROTEAN® TGX Stain-Free™ protein gels (Bio-Rad) and subject to electrophoresis at 200 V in 1× Tris/Glycine/SDS buffer (Bio-Rad). MagicMark™ XP Western Protein Standard (Invitrogen™) (5 µL) was used as a molecular weight standard. Proteins which were separated by SDS-PAGE gel were transferred onto a PVDF membrane using a Trans-Blot Turbo Transfer System (Bio-Rad). To determine successful transfer, the membrane was stained for 2–5 min using Ponceau S (Sigma Aldrich). The membrane was then blocked using 5% milk in PBS-Tween (PBS, 0.15% Tween) overnight at 4 °C. The membrane was

washed 3 times with milk (1% in PBS-Tween) (10 min each). The primary antibodies were diluted in milk (1%in PBS-Tween) (1:250 dilution) and then the membrane was incubated with the primary antibody solution for 1 h at rt. The membranes were then washed (3 × 10 min) with 1% PBS-Tween. The secondary antibody [Anti-rabbit IgG (whole molecule)-peroxidase antibody produced in goat, Sigma-Aldrich A8275] was then diluted in 1% milk in PBS-Tween (1:5000 dilution) and the membrane was incubated with this solution for 1 h at rt. The membrane was then covered with ECL Prime Western Blotting Detection Reagent (Clarity™ Western ECL Substrate, Bio-Rad) for 1-3 min before being imaged on a Bio-Rad imager. Bio-rad Image Lab 6.1 was used to process the data.

6.3.13 Fluorescence-based parasite localisation

Fluorescence-based diazirine probe parasite localisation experiments were carried out by Dr Josephine-Forde Thomas at the University of Aberystwyth. Male adult schistosomes were seeded into 6-well tissue culture plates (5 worms/well), dosed with compounds as indicated (20 μM in 0.2% DMSO) and incubated for 24 h at 37 °C in 5% CO_2. Following the incubation period, parasites were irradiated with UV light (365 nm) using an Analytik Jena 100 W UV lamp. The following protocol for the to visualise compound localisation was adapted from a procedure reported by Collins *et al*..[158] The parasites were relaxed in a solution of 0.25% ethyl-3-aminobenzoate methanesulphonate (Sigma-Aldrich) dissolved in culture media. Relaxed parasites were then killed in a solution of $MgCl_2$ (0.6 M) and fixed for 4 h in formaldehyde (4% *v/v*) dissolved in PBSTx (PBS 1 0.3% TritonX-100). After fixation, parasites were dehydrated through sequential incubations (5 min each) with increasing concentrations of MeOH (50%, 80%, 100%) and stored at −20 °C. When ready to be processed further, samples were rehydrated by sequential incubations (5 min each) with decreasing concentrations of MeOH (100%, 80% 50%) followed by incubation in PBSTx (10 min). Rehydrated samples were bleached for 1 h in formamide bleaching solution (0.5% formamide, 0.5% SSC, and 1.2% H_2O_2), rinsed twice with PBSTx and treated with Proteinase K (5 μg/mL) for 30 min at rt. Worms were then post-fixed for 10 min in

formaldehyde (4%) in PBSTx and washed with PBS. Fluorescent labelling of compounds was achieved by incubating the worms in a solution containing $CuSO_4$ (2 mM), Alexafluor 488 conjugated azide (10 μM) and ascorbic acid (100 mM) for 30 min in the dark at room temperature before washing them twice in PBS and mounting in VECTASHIELD® Antifade Mounting Medium containing 2 μg/mL DAPI.

References

(1) Berger, S. L.; Kouzarides, T.; Shiekhattar, R.; Shilatifard, A. An Operational Definition of Epigenetics. *Genes Dev.* **2009**, *23* (7), 781–783.

(2) Maleszka, R. Epigenetic Integration of Environmental and Genomic Signals in Honey Bees. The Critical Interplay of Nutritional, Brain and Reproductive Networks. *Epigenetics.* **2008**, *3* (4), 188–192.

(3) Toranõ, E. G.; Garciá, M. G.; Fernández-Morera, J. L.; Ninõ-Garciá, P.; Fernández, A. F. The Impact of External Factors on the Epigenome: In Utero and over Lifetime. *Biomed Res Int.* **2016**, *2016* (2568635), 1–17.

(4) Mazzone, R.; Zwergel, C.; Artico, M.; Taurone, S.; Ralli, M.; Greco, A.; Mai, A. The Emerging Role of Epigenetics in Human Autoimmune Disorders. *Clin Epigenetics.* **2019**, *11* (32), 1–15.

(5) Tzika, E.; Dreker, T.; Imhof, A. Epigenitics and Metabolism in Health and Disease. *Front Genet.* **2018**, *9* (361), 1–8.

(6) Muntean, A. G.; Hess, J. L. Epigenetic Dysregulation in Cancer. *American Journal of Pathology.* **2009**, *175* (4), 1353–1361. https://doi.org/10.2353/ajpath.2009.081142.

(7) Jennings, L. E.; Measures, A. R.; Wilson, B. G.; Conway, S. J. Phenotypic Screening and Fragment-Based Approaches to the Discovery of Small-Molecule Bromodomain Ligands. *Future Medicinal Chemistry.* **2014**, *6* (2), 179–204.

(8) Zhang, P.; Torres, K.; Liu, X.; Liu, C.-G.; Pollock, R. E. An Overview of Chromatin-Regulating Proteins in Cells. *Current Protein and Peptide Science.* **2016**, *17* (5), 401–410.

(9) Jenuwein, T.; Allis, C. D. Translating the Histone Code. *Science. (1979)* **2001**, *293* (5532), 1074–1080.

(10) Bannister, A. J.; Kouzarides, T. Regulation of Chromatin by Histone Modifications. *Cell Res*. **2011**, *21* (3), 381–395.

(11) Haynes, S. R.; Dollard, C.; Winston, F.; Beck, S.; Trowsdale, J.; Dawid, I. B. The Bromodomain: A Conserved Sequence Found in Human, Drosophila and Yeast Proteins. *Nucleic Acids Res.* **1992**, *20* (10), 2603–2603.

(12) Tamkun, J. W.; Deuring, R.; Scott, M. P.; Kissinger, M.; Pattatucci, A. M.; Kaufman, T. C.; Kennison, J. A. Brahma: A Regulator of Drosophila Homeotic Genes Structurally Related to the Yeast Transcriptional Activator SNF2BWl2. *Cell.* **1992**, *68* (3), 561–572.

(13) Hewings, D. S.; Rooney, T. P. C.; Jennings, L. E.; Hay, D. A.; Schofield, C. J.; Brennan, P. E.; Knapp, S.; Conway, S. J. Progress in the Development and

Application of Small Molecule Inhibitors of Bromodomain-Acetyl-Lysine Interactions. *J Med Chem.* **2012**, *55* (22), 9393–9413.

(14) Filippakopoulos, P.; Picaud, S.; Mangos, M.; Keates, T.; Lambert, J. P.; Barsyte-Lovejoy, D.; Felletar, I.; Volkmer, R.; Müller, S.; Pawson, T.; Gingras, A. C.; Arrowsmith, C. H.; Knapp, S. Histone Recognition and Large-Scale Structural Analysis of the Human Bromodomain Family. *Cell.* **2012**, *149* (1), 214–231.

(15) Cochran, A. G.; Conery, A. R.; Sims, R. J. Bromodomains: A New Target Class for Drug Development. *Nat Rev Drug Discov*. **2019**, *18* (8), 609–628.

(16) Shortt, J.; Ott, C. J.; Johnstone, R. W.; Bradner, J. E. A Chemical Probe Toolbox for Dissecting the Cancer Epigenome. *Nat Rev Cancer*. **2017**, *17* (4), 160–183.

(17) Pfister, S. X.; Ashworth, A. Marked for Death: Targeting Epigenetic Changes in Cancer. *Nat. Rev. Drug. Discov*. **2017**, *16* (4), 241–263.

(18) Jain, A. K.; Barton, M. C. Bromodomain Histone Readers and Cancer. *J Mol Biol*. **2017**, *429* (13), 2003–2010.

(19) Tough, D. F.; Tak, P. P.; Tarakhovsky, A.; Prinjha, R. K. Epigenetic Drug Discovery: Breaking through the Immune Barrier. *Nat. Rev. Drug Discov*. **2016**, *15* (12) 835–853.

(20) Fujisawa, T.; Filippakopoulos, P. Functions of Bromodomain-Containing Proteins and Their Roles in Homeostasis and Cancer. *Nat. Rev. Mol. Cell Biol*. **2017**, *18* (4) 246–262.

(21) Xu, Y.; Vakoc, C. R. Targeting Cancer Cells with BET Bromodomain Inhibitors. *Cold Spring Harb Perspect Med* **2017**, *7* (7), 1–17.

(22) Shi, J.; Vakoc, C. R. The Mechanisms behind the Therapeutic Activity of BET Bromodomain Inhibition. *Mol. Cell*. **2014**, *54* (5), 728–736.

(23) Rahman, S.; Sowa, M. E.; Ottinger, M.; Smith, J. A.; Shi, Y.; Harper, J. W.; Howley, P. M. The Brd4 Extraterminal Domain Confers Transcription Activation Independent of PTEFb by Recruiting Multiple Proteins, Including NSD3. *Mol Cell Biol* **2011**, *31* (13), 2641–2652.

(24) Tang, P.; Zhang, J.; Liu, J.; Chiang, C. M.; Ouyang, L. Targeting Bromodomain and Extraterminal Proteins for Drug Discovery: From Current Progress to Technological Development. *J. Med. Chem*. **2021**, *64* (5), 2419–2435.

(25) Shorstova, T.; Foulkes, W. D.; Witcher, M. Achieving Clinical Success with BET Inhibitors as Anti-Cancer Agents. *British Journal of Cancer*. Springer Nature April 27, 2021, pp 1478–1490. https://doi.org/10.1038/s41416-021-01321-0.

(26) Arrowsmith, C. H.; Audia, J. E.; Austin, C.; Baell, J.; Bennett, J.; Blagg, J.; Bountra, C.; Brennan, P. E.; Brown, P. J.; Bunnage, M. E.; Buser-Doepner, C.; Campbell, R. M.; Carter, A. J.; Cohen, P.; Copeland, R. A.; Cravatt, B.; Dahlin, J. L.; Dhanak, D.;

Edwards, A. M.; Frye, S. v.; Gray, N.; Grimshaw, C. E.; Hepworth, D.; Howe, T.; Huber, K. V. M.; Jin, J.; Knapp, S.; Kotz, J. D.; Kruger, R. G.; Lowe, D.; Mader, M. M.; Marsden, B.; Mueller-Fahrnow, A.; Müller, S.; O'Hagan, R. C.; Overington, J. P.; Owen, D. R.; Rosenberg, S. H.; Roth, B.; Ross, R.; Schapira, M.; Schreiber, S. L.; Shoichet, B.; Sundström, M.; Superti-Furga, G.; Taunton, J.; Toledo-Sherman, L.; Walpole, C.; Walters, M. A.; Willson, T. M.; Workman, P.; Young, R. N.; Zuercher, W. J. The Promise and Peril of Chemical Probes. *Nat Chem Biol*. **2015**, *11* (8), 536–541.

(27) Filippakopoulos, P.; Qi, J.; Picaud, S.; Shen, Y.; Smith, W. B.; Fedorov, O.; Morse, E. M.; Keates, T.; Hickman, T. T.; Felletar, I.; Philpott, M.; Munro, S.; McKeown, M. R.; Wang, Y.; Christie, A. L.; West, N.; Cameron, M. J.; Schwartz, B.; Heightman, T. D.; La Thangue, N.; French, C. A.; Wiest, O.; Kung, A. L.; Knapp, S.; Bradner, J. E. Selective Inhibition of BET Bromodomains. *Nature.* **2010**, *468* (7327), 1067–1073.

(28) Nicodeme, E.; Jeffrey, K. L.; Schaefer, U.; Beinke, S.; Dewell, S.; Chung, C. W.; Chandwani, R.; Marazzi, I.; Wilson, P.; Coste, H.; White, J.; Kirilovsky, J.; Rice, C. M.; Lora, J. M.; Prinjha, R. K.; Lee, K.; Tarakhovsky, A. Suppression of Inflammation by a Synthetic Histone Mimic. *Nature.* **2010**, *468* (7327), 1119–1123.

(29) Dawson, M. A.; Prinjha, R. K.; Dittmann, A.; Giotopoulos, G.; Bantscheff, M.; Chan, W. I.; Robson, S. C.; Chung, C. W.; Hopf, C.; Savitski, M. M.; Huthmacher, C.; Gudgin, E.; Lugo, D.; Beinke, S.; Chapman, T. D.; Roberts, E. J.; Soden, P. E.; Auger, K. R.; Mirguet, O.; Doehner, K.; Delwel, R.; Burnett, A. K.; Jeffrey, P.; Drewes, G.; Lee, K.; Huntly, B. J. P.; Kouzarides, T. Inhibition of BET Recruitment to Chromatin as an Effective Treatment for MLL-Fusion Leukaemia. *Nature.* **2011**, *478* (7370), 529–533.

(30) Hewings, D. S.; Fedorov, O.; Filippakopoulos, P.; Martin, S.; Picaud, S.; Tumber, A.; Wells, C.; Olcina, M. M.; Freeman, K.; Gill, A.; Ritchie, A. J.; Sheppard, D. W.; Russell, A. J.; Hammond, E. M.; Knapp, S.; Brennan, P. E.; Conway, S. J. Optimization of 3,5-Dimethylisoxazole Derivatives as Potent Bromodomain Ligands. *J. Med. Chem.* **2013**, *56* (8), 3217–3227.

(31) Jennings, L. E.; Schiedel, M.; Hewings, D. S.; Picaud, S.; Laurin, C. M. C.; Bruno, P. A.; Bluck, J. P.; Scorah, A. R.; See, L.; Reynolds, J. K.; Moroglu, M.; Mistry, I. N.; Hicks, A.; Guzanov, P.; Clayton, J.; Evans, C. N. G.; Stazi, G.; Biggin, P. C.; Mapp, A. K.; Hammond, E. M.; Humphreys, P. G.; Filippakopoulos, P.; Conway, S. J. BET Bromodomain Ligands: Probing the WPF Shelf to Improve BRD4 Bromodomain Affinity and Metabolic Stability. *Bioorg. Med. Chem.* **2018**, *26* (11), 2937–2957.

(32) Gosmini, R.; Nguyen, V. L.; Toum, J.; Simon, C.; Brusq, J. M. G.; Krysa, G.; Mirguet, O.; Riou-Eymard, A. M.; Boursier, E. V.; Trottet, L.; Bamborough, P.; Clark, H.; Chung, C. W.; Cutler, L.; Demont, E. H.; Kaur, R.; Lewis, A. J.; Schilling, M. B.; Soden, P. E.;

Taylor, S.; Walker, A. L.; Walker, M. D.; Prinjha, R. K.; Nicodème, E. The Discovery of I-BET726 (GSK1324726A), a Potent Tetrahydroquinoline ApoA1 up-Regulator and Selective BET Bromodomain Inhibitor. *J Med Chem* **2014**, *57* (19), 8111–8131.

(33) Humphreys, P. G.; Atkinson, S. J.; Bamborough, P.; Bit, R. A.; Chung, C. W.; Craggs, P. D.; Cutler, L.; Davis, R.; Ferrie, A.; Gong, G.; Gordon, L. J.; Gray, M.; Harrison, L. A.; Hayhow, T. G.; Haynes, A.; Henley, N.; Hirst, D. J.; Holyer, I. D.; Lindon, M. J.; Lovatt, C.; Lugo, D.; McCleary, S.; Molnar, J.; Osmani, Q.; Patten, C.; Preston, A.; Rioja, I.; Seal, J. T.; Smithers, N.; Sun, F.; Tang, D.; Taylor, S.; Theodoulou, N. H.; Thomas, C.; Watson, R. J.; Wellaway, C. R.; Zhu, L.; Tomkinson, N. C. O.; Prinjha, R. K. Design, Synthesis, and Characterization of I-BET567, a Pan-Bromodomain and Extra Terminal (BET) Bromodomain Oral Candidate. *J. Med. Chem.* **2022**, *65* (3), 2262–2287.

(34) Steegmaier, M.; Hoffmann, M.; Baum, A.; Lénárt, P.; Petronczki, M.; Kršŝák, M.; Gürtler, U.; Garin-Chesa, P.; Lieb, S.; Quant, J.; Grauert, M.; Adolf, G. R.; Kraut, N.; Peters, J. M.; Rettig, W. J. BI 2536, a Potent and Selective Inhibitor of Polo-like Kinase 1, Inhibits Tumor Growth In Vivo. *Curr. Biol.* **2007**, *17* (4), 316–322.

(35) Ciceri, P.; Müller, S.; O'Mahony, A.; Fedorov, O.; Filippakopoulos, P.; Hunt, J. P.; Lasater, E. A.; Pallares, G.; Picaud, S.; Wells, C.; Martin, S.; Wodicka, L. M.; Shah, N. P.; Treiber, D. K.; Knapp, S. Dual Kinase-Bromodomain Inhibitors for Rationally Designed Polypharmacology. *Nat. Chem. Biol.* **2014**, *10* (4), 305–312.

(36) Wyce, A.; Ganji, G.; Smitheman, K. N.; Chung, C. wa; Korenchuk, S.; Bai, Y.; Barbash, O.; Le, B. C.; Craggs, P. D.; McCabe, M. T.; Kennedy-Wilson, K. M.; Sanchez, L. v.; Gosmini, R. L.; Parr, N.; McHugh, C. F.; Dhanak, D.; Prinjha, R. K.; Auger, K. R.; Tummino, P. J. BET Inhibition Silences Expression of MYCN and BCL2 and Induces Cytotoxicity in Neuroblastoma Tumor Models. *PLoS One* **2013**, *8* (8), e72967.

(37) McLure, K. G.; Gesner, E. M.; Tsujikawa, L.; Kharenko, O. A.; Attwell, S.; Campeau, E.; Wasiak, S.; Stein, A.; White, A.; Fontano, E.; Suto, R. K.; Wong, N. C. W.; Wagner, G. S.; Hansen, H. C.; Young, P. R. RVX-208, an Inducer of ApoA-I in Humans, Is a BET Bromodomain Antagonist. *PLoS One.* **2013**, *8* (12), e83190.

(38) Faivre, E. J.; McDaniel, K. F.; Albert, D. H.; Mantena, S. R.; Plotnik, J. P.; Wilcox, D.; Zhang, L.; Bui, M. H.; Sheppard, G. S.; Wang, L.; Sehgal, V.; Lin, X.; Huang, X.; Lu, X.; Uziel, T.; Hessler, P.; Lam, L. T.; Bellin, R. J.; Mehta, G.; Fidanze, S.; Pratt, J. K.; Liu, D.; Hasvold, L. A.; Sun, C.; Panchal, S. C.; Nicolette, J. J.; Fossey, S. L.; Park, C. H.; Longenecker, K.; Bigelow, L.; Torrent, M.; Rosenberg, S. H.; Kati, W. M.; Shen, Y. Selective Inhibition of the BD2 Bromodomain of BET Proteins in Prostate Cancer. *Nature.* **2020**, *578* (7794), 306–310.

(39) Gilan, O.; Rioja, I.; Knezevic, K.; Bell, M. J.; Yeung, M. M.; Harker, N. R.; N Lam, E. Y.; Chung, C.; Bamborough, P.; Petretich, M.; Urh, M.; Atkinson, S. J.; Bassil, A. K.; Roberts, E. J.; Vassiliadis, D.; Burr, M. L.; S Preston, A. G.; Wellaway, C.; Werner, T.; Gray, J. R.; Michon, A.-M.; Gobbetti, T.; Kumar, V.; Soden, P. E.; Haynes, A.; Vappiani, J.; Tough, D. F.; Taylor, S.; Dawson, S.-J.; Bantscheff, M.; Lindon, M.; Drewes, G.; Demont, E. H.; Daniels, D. L.; Grandi, P.; Prinjha, R. K.; Dawson, M. A. Selective Targeting of BD1 and BD2 of the BET Proteins in Cancer and Immunoinflammation. *Science.* **2020**, *368* (6489), 387–394.

(40) Steeve Provencher. *Apabetalone for Pulmonary Arterial Hypertension (APPROACH-2)*. NIH U.S National Library of Medicine. https://clinicaltrials.gov/ct2/show/NCT04915300 (accessed 2023-02-15).

(41) Slavish, P. J.; Chi, L.; Yun, M. K.; Tsurkan, L.; Martinez, N. E.; Jonchere, B.; Chai, S. C.; Connelly, M.; Brett Waddell, M.; Das, S.; Neale, G.; Li, Z.; Shadrick, W. R.; Olsen, R. R.; Freeman, K. W.; Low, J. A.; Price, J. E.; Young, B. M.; Bharatham, N.; Boyd, V. A.; Yang, J.; Lee, R. E.; Morfouace, M.; Roussel, M. F.; Chen, T.; Savic, D.; Kiplin Guy, R.; White, S. W.; Shelat, A. A.; Potter, P. M. Bromodomain-Selective BET Inhibitors Are Potent Antitumor Agents against MYC-Driven Pediatric Cancer. *Cancer. Res.* **2020**, *80* (17), 3507–3518.

(42) Law, R. P.; Atkinson, S. J.; Bamborough, P.; Chung, C. W.; Demont, E. H.; Gordon, L. J.; Lindon, M.; Prinjha, R. K.; Watson, A. J. B.; Hirst, D. J. Discovery of Tetrahydroquinoxalines as Bromodomain and Extra-Terminal Domain (BET) Inhibitors with Selectivity for the Second Bromodomain. *J. Med. Chem.* **2018**, *61* (10), 4317–4334.

(43) Shih, H. P.; Zhang, X.; Aronov, A. M. Drug Discovery Effectiveness from the Standpoint of Therapeutic Mechanisms and Indications. *Nat. Rev. Drug. Discov.* **2018**, *17* (1), 19–33.

(44) Waring, M. J.; Arrowsmith, J.; Leach, A. R.; Leeson, P. D.; Mandrell, S.; Owen, R. M.; Pairaudeau, G.; Pennie, W. D.; Pickett, S. D.; Wang, J.; Wallace, O.; Weir, A. An Analysis of the Attrition of Drug Candidates from Four Major Pharmaceutical Companies. *Nat. Rev. Drug Discov*. **2015**, *14* (7), 475–486.

(45) Fallon, D. J.; Lehmann, S.; Chung, C. wa; Phillipou, A.; Eberl, C.; Fantom, K. G. M.; Zappacosta, F.; Patel, V. K.; Bantscheff, M.; Schofield, C. J.; Tomkinson, N. C. O.; Bush, J. T. One-Step Synthesis of Photoaffinity Probes for Live-Cell MS-Based Proteomics. *Chemistry - A European Journal.* **2021**, *27* (71), 17880–17888.

(46) Comess, K. M.; McLoughlin, S. M.; Oyer, J. A.; Richardson, P. L.; Stöckmann, H.; Vasudevan, A.; Warder, S. E. Emerging Approaches for the Identification of Protein

Targets of Small Molecules-A Practitioners' Perspective. *J Med Chem* **2018**, *61* (19), 8504–8535. https://doi.org/10.1021/acs.jmedchem.7b01921.

(47) Smith, E.; Collins, I. Photoaffinity Labeling in Target-and Binding-Site Identification. *Future Med. Chem*. **2015**, *7* (2) 159–183.

(48) Preston, G. W.; Wilson, A. J. Photo-Induced Covalent Cross-Linking for the Analysis of Biomolecular Interactions. *Chem Soc Rev* **2013**, *42* (8), 3289–3301.

(49) Korovesis, D.; Beard, H. A.; Mérillat, C.; Verhelst, S. H. L. Probes for Photoaffinity Labelling of Kinases. *ChemBioChem*. **2021**, *22* (13), 2206–2218.

(50) Dubinsky, L.; Krom, B. P.; Meijler, M. M. Diazirine Based Photoaffinity Labeling. *Bioorg. Med. Chem.* **2012**, *20* (2), 554–570.

(51) Sakurai, K.; Ozawa, S.; Yamada, R.; Yasui, T.; Mizuno, S. Comparison of the Reactivity of Carbohydrate Photoaffinity Probes with Different Photoreactive Groups. *ChemBioChem* **2014**, *15* (10), 1399–1403.

(52) West, A. V.; Muncipinto, G.; Wu, H. Y.; Huang, A. C.; Labenski, M. T.; Jones, L. H.; Woo, C. M. Labeling Preferences of Diazirines with Protein Biomolecules. *J. Am. Chem. Soc.* **2021**, *143* (17), 6691–6700.

(53) West, A. v.; Amako, Y.; Woo, C. M. Design and Evaluation of a Cyclobutane Diazirine Alkyne Tag for Photoaffinity Labeling in Cells. *J. Am. Chem. Soc.* **2022**, *144* (46), 21174–21183.

(54) Nassal, M. 4-(1-Azi-2,2,2-Trifluoroethyl)Benzoic Acid, a Highly Photolabile Carbene Generating Label Readily Fixable to Biochemical Agents. *Liebigs Ann. Chem.* **1983**, *1983* (9), 1510–1523.

(55) Brunner, J.; Serin, H.; Richards, F. M. 3-Trifluoromethyl-3-Phenyldiazirine a New Carbene Generating Group for Photolabeling Reagents. *J. Biol. Chem.* **1980**, *255* (8), 3313–3318.

(56) Guo, A. Di; Wei, D.; Nie, H. J.; Hu, H.; Peng, C.; Li, S. T.; Yan, K. N.; Zhou, B. S.; Feng, L.; Fang, C.; Tan, M.; Huang, R.; Chen, X. H. Light-Induced Primary Amines and o-Nitrobenzyl Alcohols Cyclization as a Versatile Photoclick Reaction for Modular Conjugation. *Nat. Commun.* **2020**, *11* (5472), 1–13.

(57) Herner, A.; Marjanovic, J.; Lewandowski, T. M.; Marin, V.; Patterson, M.; Miesbauer, L.; Ready, D.; Williams, J.; Vasudevan, A.; Lin, Q. 2-Aryl-5-Carboxytetrazole as a New Photoaffinity Label for Drug Target Identification. *J. Am. Chem. Soc.* **2016**, *138* (44), 14609–14615.

(58) Lougee, M. G.; Pagar, V. V.; Kim, H. J.; Pancoe, S. X.; Chia, W. K.; Mach, R. H.; Garcia, B. A.; Petersson, E. J. Harnessing the Intrinsic Photochemistry of Isoxazoles for the Development of Chemoproteomic Crosslinking Methods. *Chem. Commun. (Camb.).* **2022**, *58* (65), 9116–9119.

(59) Rostovtsev, V. V.; Green, L. G.; Fokin, V. V.; Sharpless, K. B. A Stepwise Huisgen Cycloaddition Process: Copper(I)-Catalyzed Regioselective “Ligation” of Azides and Terminal Alkynes. *Angew. Chem. Int. Ed Engl.* **2002**, *41* (14), 2596–2599.

(60) Tornøe, C. W.; Christensen, C.; Meldal, M. Peptidotriazoles on Solid Phase: [1,2,3]-Triazoles by Regiospecific Copper(I)-Catalyzed 1,3-Dipolar Cycloadditions of Terminal Alkynes to Azides. *J. Org. Chem.* **2002**, *67* (9), 3057–3064.

(61) Agard, N. J.; Prescher, J. A.; Bertozzi, C. R. A Strain-Promoted [3 + 2] Azide-Alkyne Cycloaddition for Covalent Modification of Biomolecules in Living Systems. *J. Am. Chem. Soc.* **2004**, *126* (46), 15046–15047.

(62) Baskin, J. M.; Prescher, J. A.; Laughlin, S. T.; Agard, N. J.; Chang, P. V; Miller, I. A.; Lo, A.; Codelli, J. A.; Bertozzi, C. R. Copper-Free Click Chemistry for Dynamic in Vivo Imaging. *Proc. Natl. Acad. Sci. USA* **2007**, *104* (43), 16793–16797.

(63) Blackman, M. L.; Royzen, M.; Fox, J. M. Tetrazine Ligation: Fast Bioconjugation Based on Inverse-Electron-Demand Diels-Alder Reactivity. *J. Am. Chem. Soc.* **2008**, *130* (41), 13518–13519.

(64) Conway, L. P.; Jadhav, A. M.; Homan, R. A.; Li, W.; Rubiano, J. S.; Hawkins, R.; Lawrence, R. M.; Parker, C. G. Evaluation of Fully-Functionalized Diazirine Tags for Chemical Proteomic Applications. *Chem. Sci.* **2021**, *12* (22), 7839–7847.

(65) Li, Z.; Wang, D.; Li, L.; Pan, S.; Na, Z.; Tan, C. Y. J.; Yao, S. Q. “Minimalist” Cyclopropene-Containing Photo-Cross-Linkers Suitable for Live-Cell Imaging and Affinity-Based Protein Labeling. *J. Am. Chem. Soc.* **2014**, *136* (28), 9990–9998.

(66) Trowbridge, A. D.; Seath, C. P.; Rodriguez-Rivera, F. P.; Li, B. X.; Dul, B. E.; Schwaid, A. G.; Buksh, B. F.; Geri, J. B.; Oakley, J. V; Fadeyi, O. O.; Oslund, R. C.; Ryu, K. A.; White, C.; Reyes-Robles, T.; Tawa, P.; Parker, D. L.; Macmillan, D. W. C.; Dougherty, D.; Liu, D. Small Molecule Photocatalysis Enables Drug Target Identification via Energy Transfer. *Proc. Natl. Acad. Sci. USA*. **2022**, *119* (34), e2208077119.

(67) Thétiot-Laurent, S. A. L.; Boissier, J.; Robert, A.; Meunier, B. Schistosomiasis Chemotherapy. *Angew. Chem. Int. Ed. Engl*. **2013**, 52 (31), 7936–7956.

(68) Chitsulo, L.; Engels, D.; Montresor, A.; Savioli, L. The Global Status of Schistosomiasis and Its Control. *Acta. Trop.* **2000**, 77 (1), 41–51.

(69) McManus, D. P.; Dunne, D. W.; Sacko, M.; Utzinger, J.; Vennervald, B. J.; Zhou, X. N. Schistosomiasis. *Nat. Rev. Dis. Primers.* **2018**, *4* (13), 1–19.

(70) World Health Organization, *Ending the neglect to attain the Sustainable Development Goals: A road map for neglected tropical diseases 2021–2030*. https://www.who.int/publications/i/item/9789240010352 (2021). (accessed 2023-02-15).

(71) Centers for Disease Control and Prevention. *Parasites - Schistosomiasis*. https://www.cdc.gov/parasites/schistosomiasis/biology.html (accessed 2023-02-15).

(72) Colley, D. G.; Bustinduy, A. L.; Secor, W. E.; King, C. H. Human Schistosomiasis. *Lancet.* **2014**, *383* (9936), 2253–2264.

(73) Gryseels, B.; Polman, K.; Clerinx, J.; Kestens, L. *Human Schistosomiasis*. *Lancet.* **2006**, 386 (9541), 1106–1118.

(74) Cioli, D.; Pica-Mattoccia, L.; Basso, A.; Guidi, A. Schistosomiasis Control: Praziquantel Forever? *Mol. Biochem. Parasitol*. **2014**, *195* (1), 23–29.

(75) Siqueira, L. da P.; Fontes, D. A. F.; Aguilera, C. S. B.; Timóteo, T. R. R.; Ângelos, M. A.; Silva, L. C. P. B. B.; de Melo, C. G.; Rolim, L. A.; da Silva, R. M. F.; Neto, P. J. R. Schistosomiasis: Drugs Used and Treatment Strategies. *Acta Trop*. **2017**, *176*, 179–187.

(76) Cupit, P. M.; Cunningham, C. What Is the Mechanism of Action of Praziquantel and How Might Resistance Strike? *Future Med. Chem*. **2015**, *7* (6), 701–705.

(77) Vale, N.; Gouveia, M. J.; Rinaldi, G.; Brindley, P. J.; Gärtner, F.; da Costa, J. M. C. Praziquantel for Schistosomiasis: Single-Drug Metabolism Revisited, Mode of Action, and Resistance. *Antimicrob. Agents Chemother*. **2017**, *61* (5), e02582–16.

(78) da Silva, V. B. R.; Campos, B. R. K. L.; de Oliveira, J. F.; Decout, J. L.; do Carmo Alves de Lima, M. Medicinal Chemistry of Antischistosomal Drugs: Praziquantel and Oxamniquine. *Bioorg. Med. Chem*. **2017,** *25* (13), 3259–3277.

(79) Pica-Mattoccia, L.; Doenhoff, M. J.; Valle, C.; Basso, A.; Troiani, A. R.; Liberti, P.; Festucci, A.; Guidi, A.; Cioli, D. Genetic Analysis of Decreased Praziquantel Sensitivity in a Laboratory Strain of Schistosoma Mansoni. *Acta. Trop.* **2009**, *111* (1), 82–85.

(80) Anderson, L.; Pierce, R. J.; Verjovski-Almeida, S. Schistosoma Mansoni Histones: From Transcription to Chromatin Regulation; An in Silico Analysis. *Mol. Biochem. Parasitol*. **2012**, *183* (2), 105–114.

(81) Roquis, D.; Taudt, A.; Geyer, K. K.; Padalino, G.; Hoffmann, K. F.; Holroyd, N.; Berriman, M.; Aliaga, B.; Chaparro, C.; Grunau, C.; Augusto, R. de C. Histone Methylation Changes Are Required for Life Cycle Progression in the Human Parasite Schistosoma Mansoni. *PLoS. Pathog.* **2018**, *14* (5), e1007066.

(82) Roquis, D.; Lepesant, J. M. J.; Picard, M. A. L.; Freitag, M.; Parrinello, H.; Groth, M.; Emans, R.; Cosseau, C.; Grunau, C. The Epigenome of Schistosoma Mansoni Provides Insight about How Cercariae Poise Transcription until Infection. *PLoS. Negl. Trop. Dis.* **2015**, *9* (8), e0003853.

(83) Gajer, J. M.; Furdas, S. D.; Gründer, A.; Gothwal, M.; Heinicke, U.; Keller, K.; Colland, F.; Fulda, S.; Pahl, H. L.; Fichtner, I.; Sippl, W.; Jung, M. Histone Acetyltransferase Inhibitors Block Neuroblastoma Cell Growth in Vivo. *Oncogenesis.* **2015**, *4* (2), e137.

(84) Carneiro, V. C.; de Abreu da Silva, I. C.; Torres, E. J. L.; Caby, S.; Lancelot, J.; Vanderstraete, M.; Furdas, S. D.; Jung, M.; Pierce, R. J.; Fantappié, M. R. Epigenetic Changes Modulate Schistosome Egg Formation and Are a Novel Target for Reducing Transmission of Schistosomiasis. *PLoS Pathog* **2014**, *10* (5), e1004116.

(85) Yoshida, M.; Kijima, M.; Akita, M.; Beppu, T. Potent and Specific Inhibition of Mammalian Histone Deacetylase Both in Vivo and in Vitro by Trichostatin A. *J Biol Chem.* **1990**, *265* (28), 17174–17179.

(86) Richon, V. M.; Emiliani, S.; Verdin, E.; Webb, Y.; Breslow, R.; Rifkind, R. A.; Marks, P. A. A Class of Hybrid Polar Inducers of Transformed Cell Differentiation Inhibits Histone Deacetylases. *Proc Natl Acad Sc USA.* **1998**, *95* (6), 3003–3007.

(87) Göttlicher, M.; Minucci, S.; Zhu, P.; Krämer, O. H.; Schimpf, A.; Giavara, S.; Sleeman, J. P.; lo Coco, F.; Nervi, C.; Pelicci, P. G.; Heinzel, T. Valproic Acid Defines a Novel Class of HDAC Inhibitors Inducing Differentiation of Transformed Cells. *EMBO J.* **2001**, *20* (24), 6969–6978.

(88) Dubois, F.; Caby, S.; Oger, F.; Cosseau, C.; Capron, M.; Grunau, C.; Dissous, C.; Pierce, R. J. Histone Deacetylase Inhibitors Induce Apoptosis, Histone Hyperacetylation and up-Regulation of Gene Transcription in Schistosoma Mansoni. *Mol. Biochem. Parasitol.* **2009**, *168* (1), 7–15.

(89) Lancelot, J.; Caby, S.; Dubois-Abdesselem, F.; Vanderstraete, M.; Trolet, J.; Oliveira, G.; Bracher, F.; Jung, M.; Pierce, R. J. Schistosoma Mansoni Sirtuins: Characterization and Potential as Chemotherapeutic Targets. *PLoS. Negl. Trop. Dis.* **2013**, *7* (9), e2428.

(90) Grozinger, C. M.; Chao, E. D.; Blackwell, H. E.; Moazed, D.; Schreiber, S. L. Identification of a Class of Small Molecule Inhibitors of the Sirtuin Family of NAD-Dependent Deacetylases by Phenotypic Screening. *J. Biol. Chem.* **2001**, *276* (42), 38837–38843.

(91) Lara, E.; Mai, A.; Calvanese, V.; Altucci, L.; Lopez-Nieva, P.; Martinez-Chantar, M. L.; Varela-Rey, M.; Rotili, D.; Nebbioso, A.; Ropero, S.; Montoya, G.; Oyarzabal, J.; Velasco, S.; Serrano, M.; Witt, M.; Villar-Garea, A.; Inhof, A.; Mato, J. M.; Esteller, M.; Fraga, M. F. Salermide, a Sirtuin Inhibitor with a Strong Cancer-Specific Proapoptotic Effect. *Oncogene.* **2009**, *28* (6), 781–791.

(92) Uciechowska, U.; Schemies, J.; Neugebauer, R. C.; Huda, E. M.; Schmitt, M. L.; Meier, R.; Verdin, E.; Jung, M.; Sippl, W. Thiobarbiturates as Sirtuin Inhibitors: Virtual

Screening, Free-Energy Calculations, and Biological Testing. *ChemMedChem.* **2008**, *3* (12), 1965–1976.

(93) Schiedel, M.; Marek, M.; Lancelot, J.; Karaman, B.; Almlöf, I.; Schultz, J.; Sippl, W.; Pierce, R. J.; Romier, C.; Jung, M. Fluorescence-Based Screening Assays for the NAD+-Dependent Histone Deacetylase SmSirt2 from Schistosoma Mansoni. *J. Biomol. Screen.* **2015**, *20* (1), 112–121.

(94) Monaldi, D.; Rotili, D.; Lancelot, J.; Marek, M.; Wössner, N.; Lucidi, A.; Tomaselli, D.; Ramos-Morales, E.; Romier, C.; Pierce, R. J.; Mai, A.; Jung, M. Structure-Reactivity Relationships on Substrates and Inhibitors of the Lysine Deacylase Sirtuin 2 from Schistosoma Mansoni (SmSirt2). *J. Med. Chem.* **2019**, *62* (19), 8733–8759.

(95) Oger, F.; Dubois, F.; Caby, S.; Noël, C.; Cornette, J.; Bertin, B.; Capron, M.; Pierce, R. J. The Class I Histone Deacetylases of the Platyhelminth Parasite Schistosoma Mansoni. *Biochem. Biophys. Res. Commun.* **2008**, *377* (4), 1079–1084.

(96) Marek, M.; Kannan, S.; Hauser, A. T.; Moraes Mourão, M.; Caby, S.; Cura, V.; Stolfa, D. A.; Schmidtkunz, K.; Lancelot, J.; Andrade, L.; Renaud, J. P.; Oliveira, G.; Sippl, W.; Jung, M.; Cavarelli, J.; Pierce, R. J.; Romier, C. Structural Basis for the Inhibition of Histone Deacetylase 8 (HDAC8), a Key Epigenetic Player in the Blood Fluke Schistosoma Mansoni. *PLoS Pathog* **2013**, *9* (9), e1003645.

(97) Heimburg, T.; Chakrabarti, A.; Lancelot, J.; Marek, M.; Melesina, J.; Hauser, A. T.; Shaik, T. B.; Duclaud, S.; Robaa, D.; Erdmann, F.; Schmidt, M.; Romier, C.; Pierce, R. J.; Jung, M.; Sippl, W. Structure-Based Design and Synthesis of Novel Inhibitors Targeting HDAC8 from Schistosoma Mansoni for the Treatment of Schistosomiasis. *J. Med. Chem.* **2016**, *59* (6), 2423–2435.

(98) Ghazy, E.; Heimburg, T.; Lancelot, J.; Zeyen, P.; Schmidtkunz, K.; Truhn, A.; Darwish, S.; Simoben, C. V.; Shaik, T. B.; Erdmann, F.; Schmidt, M.; Robaa, D.; Romier, C.; Jung, M.; Pierce, R.; Sippl, W. Synthesis, Structure-Activity Relationships, Cocrystallization and Cellular Characterization of Novel SmHDAC8 Inhibitors for the Treatment of Schistosomiasis. *Eur. J. Med. Chem.* **2021**, *225* (2), 113745.

(99) Structural Genomics Consortium. *NVS-CECR2-1 A chemical probe for CECR2*. https://www.thesgc.org/chemical-probes/NVS-CECR2-1 (accessed 2023-03-14).

(100) Wang, J.; Paz, C.; Padalino, G.; Coghlan, A.; Lu, Z.; Gradinaru, I.; Collins, J. N. R.; Berriman, M.; Hoffmann, K. F.; Collins 3rd, J. J. Large-Scale RNAi Screening Uncovers Therapeutic Targets in the Parasite Schistosoma Mansoni. *Science.* **2020**, *369* (6511), 1649–1653.

(101) Collins, J. N. R.; Collins, J. J. Tissue Degeneration Following Loss of Schistosoma Mansoni Cbp1 Is Associated with Increased Stem Cell Proliferation and Parasite Death In Vivo. *PLoS. Pathog.* **2016**, *12* (11), e1005963.

(102) Tallant, C.; Bamborough, P.; Chung, C. W.; Gamo, F. J.; Kirkpatrick, R.; Larminie, C.; Martín, J.; Prinjha, R.; Rioja, I.; Simola, D. F.; Gabarró, R.; Calderón, F. Expanding Bromodomain Targeting into Neglected Parasitic Diseases. *ACS Infect. Dis.* **2021**, *7* (11), 2953–2958, e1005963.

(103) Maciel, R. D. M.; da Silva Dutra, D. L.; Rumjanek, F. D.; Juliano, L.; Juliano, M. A.; Fantappié, M. R. Schistosoma Mansoni Histone Acetyltransferase GCN5: Linking Histone Acetylation to Gene Activation. *Mol Biochem. Parasitol.* **2004**, *133* (1), 131–135.

(104) Bertin, B.; Oger, F.; Cornette, J.; Caby, S.; Noël, C.; Capron, M.; Fantappie, M. R.; Rumjanek, F. D.; Pierce, R. J. Schistosoma Mansoni CBP/P300 Has a Conserved Domain Structure and Interacts Functionally with the Nuclear Receptor SmFtz-F1. *Mol. Biochem. Parasitol.* **2006**, *146* (2), 180–191.

(105) Whatley, K. C. L.; Padalino, G.; Whiteland, H.; Geyer, K. K.; Hulme, B. J.; Chalmers, I. W.; Forde-Thomas, J.; Ferla, S.; Brancale, A.; Hoffmann, K. F. The Repositioning of Epigenetic Probes/Inhibitors Identifies New Anti-Schistosomal Lead Compounds and Chemotherapeutic Targets. *PLoS. Negl. Trop. Dis.* **2019**, *13* (11), e0007693.

(106) Padalino, G.; Ferla, S.; Brancale, A.; Chalmers, I. W.; Hoffmann, K. F. Combining Bioinformatics, Cheminformatics, Functional Genomics and Whole Organism Approaches for Identifying Epigenetic Drug Targets in Schistosoma Mansoni. *Int. J. Parasitol. Drugs Drug Resist.* **2018**, *8* (3), 559–570.

(107) Lu, Z.; Zhang, Y.; Berriman, M. A Web Portal for Gene Expression across All Life Stages of Schistosoma Mansoni. *bioRxiv.* **2018**.

(108) Filippakopoulos, P.; Picaud, S.; Mangos, M.; Keates, T.; Lambert, J. P.; Barsyte-Lovejoy, D.; Felletar, I.; Volkmer, R.; Müller, S.; Pawson, T.; Gingras, A. C.; Arrowsmith, C. H.; Knapp, S. Histone Recognition and Large-Scale Structural Analysis of the Human Bromodomain Family. *Cell.* **2012**, *149* (1), 214–231.

(109) Madeira, F.; Pearce, M.; Tivey, A. R. N.; Basutkar, P.; Lee, J.; Edbali, O.; Madhusoodanan, N.; Kolesnikov, A.; Lopez, R. Search and Sequence Analysis Tools Services from EMBL-EBI in 2022. *Nucleic Acids Res.* **2022**, *50* (W1), W276–W279.

(110) Robert, X.; Gouet, P. Deciphering Key Features in Protein Structures with the New ENDscript Server. *Nucleic Acids Res* **2014**, *42*, W320–W324.

(111) Jumper, J.; Evans, R.; Pritzel, A.; Green, T.; Figurnov, M.; Ronneberger, O.; Tunyasuvunakool, K.; Bates, R.; Žídek, A.; Potapenko, A.; Bridgland, A.; Meyer, C.; Kohl, S. A. A.; Ballard, A. J.; Cowie, A.; Romera-Paredes, B.; Nikolov, S.; Jain, R.; Adler, J.; Back, T.; Petersen, S.; Reiman, D.; Clancy, E.; Zielinski, M.; Steinegger, M.; Pacholska, M.; Berghammer, T.; Bodenstein, S.; Silver, D.; Vinyals, O.; Senior, A. W.;

Kavukcuoglu, K.; Kohli, P.; Hassabis, D. Highly Accurate Protein Structure Prediction with AlphaFold. *Nature.* **2021**, *596* (7873), 583–589.

(112) Niesen, F. H.; Berglund, H.; Vedadi, M. The Use of Differential Scanning Fluorimetry to Detect Ligand Interactions That Promote Protein Stability. *Nat. Protoc.* **2007**, *2* (9), 2212–2221.

(113) Hewings, D. S.; Wang, M.; Philpott, M.; Fedorov, O.; Uttarkar, S.; Filippakopoulos, P.; Picaud, S.; Vuppusetty, C.; Marsden, B.; Knapp, S.; Conway, S. J.; Heightman, T. D. 3,5-Dimethylisoxazoles Act as Acetyl-Lysine-Mimetic Bromodomain Ligands. *J. Med. Chem.* **2011**, *54* (19), 6761–6770.

(114) Hay, D.; Fedorov, O.; Filippakopoulos, P.; Martin, S.; Philpott, M.; Picaud, S.; Hewings, D. S.; Uttakar, S.; Heightman, T. D.; Conway, S. J.; Knapp, S.; Brennan, P. E. The Design and Synthesis of 5- and 6-Isoxazolylbenzimidazoles as Selective Inhibitors of the BET Bromodomains. *Medchemcomm.* **2013**, *4* (1), 140–144.

(115) Rooney, T. P. C.; Filippakopoulos, P.; Fedorov, O.; Picaud, S.; Cortopassi, W. A.; Hay, D. A.; Martin, S.; Tumber, A.; Rogers, C. M.; Philpott, M.; Wang, M.; Thompson, A. L.; Heightman, T. D.; Pryde, D. C.; Cook, A.; Paton, R. S.; Müller, S.; Knapp, S.; Brennan, P. E.; Conway, S. J. A Series of Potent Crebbp Bromodomain Ligands Reveals an Induced-Fit Pocket Stabilized by a Cation-π Interaction. *Angew. Chem Int Ed Engl.* **2014**, *53* (24), 6126–6130.

(116) Hay, D. A.; Fedorov, O.; Martin, S.; Singleton, D. C.; Tallant, C.; Wells, C.; Picaud, S.; Philpott, M.; Monteiro, O. P.; Rogers, C. M.; Conway, S. J.; Rooney, T. P. C.; Tumber, A.; Yapp, C.; Filippakopoulos, P.; Bunnage, M. E.; Müller, S.; Knapp, S.; Schofield, C. J.; Brennan, P. E. Discovery and Optimization of Small-Molecule Ligands for the CBP/P300 Bromodomains. *J. Am. Chem. Soc.* **2014**, *136* (26), 9308–9319.

(117) Sekirnik née Measures, A. R.; Hewings, D. S.; Theodoulou, N. H.; Jursins, L.; Lewendon, K. R.; Jennings, L. E.; Rooney, T. P. C.; Heightman, T. D.; Conway, S. J. Isoxazole-Derived Amino Acids Are Bromodomain-Binding Acetyl-Lysine Mimics: Incorporation into Histone H4 Peptides and Histone H3. *Angew Chem Int Ed Engl.* **2016**, *128* (29), 8493–8497.

(118) Catalano, M.; Moroglu, M.; Balbi, P.; Mazzieri, F.; Clayton, J.; Andrews, K. H.; Bigatti, M.; Scheuermann, J.; Conway, S. J.; Neri, D. Selective Fragments for the CREBBP Bromodomain Identified from an Encoded Self-Assembly Chemical Library. *ChemMedChem/* **2020**, *15* (18), 1752–1756.

(119) Brand, M.; Clayton, J.; Moroglu, M.; Schiedel, M.; Picaud, S.; Bluck, J. P.; Skwarska, A.; Bolland, H.; Chan, A. K. N.; Laurin, C. M. C.; Scorah, A. R.; See, L.; Rooney, T. P. C.; Andrews, K. H.; Fedorov, O.; Perell, G.; Kalra, P.; Vinh, K. B.; Cortopassi, W. A.; Heitel, P.; Christensen, K. E.; Cooper, R. I.; Paton, R. S.; Pomerantz, W. C. K.; Biggin,

P. C.; Hammond, E. M.; Filippakopoulos, P.; Conway, S. J. Controlling Intramolecular Interactions in the Design of Selective, High-Affinity Ligands for the CREBBP Bromodomain. *J. Med. Chem.* **2021**, *64* (14), 10102–10123.

(120) Laurin, C. M. C.; Bluck, J. P.; Chan, A. K. N.; Keller, M.; Boczek, A.; Scorah, A. R.; See, K. F. L.; Jennings, L. E.; Hewings, D. S.; Woodhouse, F.; Reynolds, J. K.; Schiedel, M.; Humphreys, P. G.; Biggin, P. C.; Conway, S. J. Fragment-Based Identification of Ligands for Bromodomain-Containing Factor 3 of Trypanosoma Cruzi. *ACS Infect. Dis.* **2021**, *7* (8), 2238–2249.

(121) ThermoFisher Scientific. *Maybridge Fragment Libraries*. https://www.thermofisher.com/uk/en/home/industrial/pharma-biopharma/drug-discovery-development/screening-compounds-libraries-hit-identification/maybridge-fragment-libraries.html (accessed 2023-03-19).

(122) University of Leeds. *PPI-Net*. https://ppi-net.org/ (accessed 2023-03-19).

(123) Shadrick, W. R.; Slavish, P. J.; Chai, S. C.; Waddell, B.; Connelly, M.; Low, J. A.; Tallant, C.; Young, B. M.; Bharatham, N.; Knapp, S.; Boyd, V. A.; Morfouace, M.; Roussel, M. F.; Chen, T.; Lee, R. E.; Kiplin Guy, R.; Shelat, A. A.; Potter, P. M. Exploiting a Water Network to Achieve Enthalpy-Driven, Bromodomain-Selective BET Inhibitors. *Bioorg. Med. Chem.* **2018**, *26* (1), 25–36.

(124) Charles, M. D.; Schultz, P.; Buchwald, S. L. Efficient Pd-Catalyzed Amination of Heteroaryl Halides. *Org. Lett.* **2005**, *7* (18), 3965–3968.

(125) Fors, B. P.; Buchwald, S. L. A Multiligand Based Pd Catalyst for C-N Cross-Coupling Reactions. *J. Am. Chem. Soc.* **2010**, *132* (45), 15914–15917.

(126) Maiti, D.; Fors, B. P.; Henderson, J. L.; Nakamura, Y.; Buchwald, S. L. Palladium-Catalyzed Coupling of Functionalized Primary and Secondary Amines with Aryl and Heteroaryl Halides: Two Ligands Suffice in Most Cases. *Chem. Sci.* **2011**, *2* (1), 57–68.

(127) Bruno, N. C.; Tudge, M. T.; Buchwald, S. L. Design and Preparation of New Palladium Precatalysts for C-C and C-N Cross-Coupling Reactions. *Chem. Sci.* **2013**, *4* (3), 916–920.

(128) Bruno, N. *Cross-Coupling Reaction Manual: Desk Reference*; Sigma-Aldrich, 2016.

(129) Harris, M. C.; Huang, X.; Buchwald, S. L. Improved Functional Group Compatibility in the Palladium-Catalyzed Synthesis of Aryl Amines. *Org Lett* **2002**, *4* (17), 2885–2888.

(130) Smith, J. A.; Jones, R. K.; Booker, G. W.; Pyke, S. M. Sequential and Selective Buchwald-Hartwig Amination Reactions for the Controlled Functionalization of 6-Bromo-2-Chloroquinoline: Synthesis of Ligands for the Tec Src Homology 3 Domain. *Journal of Organic Chemistry* **2008**, *73* (22), 8880–8892.

(131) Robinson, M. W.; Hill, A. P.; Readshaw, S. A.; Hollerton, J. C.; Upton, R. J.; Lynn, S. M.; Besley, S. C.; Boughtflower, B. J. Use of Calculated Physicochemical Properties to Enhance Quantitative Response When Using Charged Aerosol Detection. *Anal. Chem.* **2017**, *89* (3), 1772–1777.

(132) Young, R. J.; Green, D. V. S.; Luscombe, C. N.; Hill, A. P. Getting Physical in Drug Discovery II: The Impact of Chromatographic Hydrophobicity Measurements and Aromaticity. *Drug Discov. Today*. **2011**, *16* (17-18), 822–830.

(133) Bunally, S.; Young, R. J. The Role and Impact of High Throughput Biomimetic Measurements in Drug Discovery. *ADMET and DMPK*. **2018**, *6* (2), 74–84.

(134) Valkó, K.; Bevan, C.; Reynolds, D. Chromatographic Hydrophobicity Index by Fast-Gradient RP-HPLC: A High-Throughput Alternative to Log P/Log D. *Anal. Chem.* **1997**, *69* (11), 2022–2029.

(135) Paveley, R. A.; Mansour, N. R.; Hallyburton, I.; Bleicher, L. S.; Benn, A. E.; Mikic, I.; Guidi, A.; Gilbert, I. H.; Hopkins, A. L.; Bickle, Q. D. Whole Organism High-Content Screening by Label-Free, Image-Based Bayesian Classification for Parasitic Diseases. *PLoS Negl. Trop. Dis.* **2012**, *6* (7), e1762.

(136) Zhang, J.-H.; Chung, T. D. Y.; Oldenburg, K. R. A Simple Statistical Parameter for Use in Evalulation and Validation of High Throughput Screening Assays. *J Biomol Screen.* **1999**, *4* (2), 67–73.

(137) Padalino, G.; El-Sakkary, N.; Liu, L. J.; Liu, C.; Harte, D. S. G.; Barnes, R. E.; Sayers, E.; Forde-Thomas, J.; Whiteland, H.; Bassetto, M.; Ferla, S.; Johnson, G.; Jones, A. T.; Caffrey, C. R.; Chalmers, I.; Brancale, A.; Hoffmann, K. F. Anti-Schistosomal Activities of Quinoxaline-Containing Compounds: From Hit Identification to Lead Optimisation. *Eur. J. Med. Chem.* **2021**, *226*, 113823.

(138) Marcellino, C.; Gut, J.; Lim, K. C.; Singh, R.; McKerrow, J.; Sakanari, J. WormAssay: A Novel Computer Application for Whole-Plate Motion-Based Screening of Macroscopic Parasites. *PLoS. Negl. Trop. Dis.* **2012**, *6* (1), e1494.

(139) Kwiatkowski, A. Development of Ligands Selective for a Bromodomain in the Parasite Schistosoma Mansoni. MChem Dissertation, University of Oxford, Oxford, U.K., 2021.

(140) García-Rodríguez, A.; Rodríguez, A. M.; Prieto, P.; Andreu, R.; Merino, S.; Rodríguez-López, J. Swivel-Cruciform Stilbenes Based on Bithiophene. *European J. Org. Chem.* **2015**, *2015* (11), 2394–2404.

(141) ChemAxon. *Chemicalize*. https://chemicalize.com/ (accessed 2023-03-01).

(142) Amans, D.; Demont, E.; Mitchell, D. J.; Seal, J. T. Tetrahydroquinoline Derivatives as Useful Bromodomain Inhibitors, WO2012143415, 2012.

(143) ChemAxon. *Chemicalize*. https://chemicalize.com/ (accessed 2022-01-25).

(144) Serafinowska, H. T.; Ashton, R. J.; Bailey, S.; Hamden, M. R.; Jackson, S. M.; Sutton, D. Synthesis and in Vivo Evaluation of Prodrugs of 9-[2-(Phosphonomethoxy)ethoxy]adenine; *J. Med. Chem.* **1995**, *38* (8), 1372–1379.

(145) Ramirez, B.; Bickle, Q.; Yousif, F.; Fakorede, F.; Mouries, M. A.; Nwaka, S. Schistosomes: Challenges in Compound Screening. *Expert Opinion on Drug Discov*. **2007**, *2* (s1), S53–61.

(146) Brand, M. Developing Small Molecule Ligands for the Study of Bromodomain-Histone Interactions, DPhil Thesis, University of Oxford, Oxford, U.K., 2017.

(147) Giulia Stasi. Unpublished Work.

(148) Li, Z.; Hao, P.; Li, L.; Tan, C. Y. J.; Cheng, X.; Chen, G. Y. J.; Sze, S. K.; Shen, H. M.; Yao, S. Q. Design and Synthesis of Minimalist Terminal Alkyne-Containing Diazirine Photo-Crosslinkers and Their Incorporation into Kinase Inhibitors for Cell- and Tissue-Based Proteome Profiling. *Angew. Chem. Int. Ed.* **2013**, *52* (33), 8551–8556.

(149) Matthias Schiedel. Unpublished Work.

(150) Parker, C. G.; Galmozzi, A.; Wang, Y.; Correia, B. E.; Sasaki, K.; Joslyn, C. M.; Kim, A. S.; Cavallaro, C. L.; Lawrence, R. M.; Johnson, S. R.; Narvaiza, I.; Saez, E.; Cravatt, B. F. Ligand and Target Discovery by Fragment-Based Screening in Human Cells. *Cell* **2017**, *168* (3), 527-541.e29. https://doi.org/10.1016/j.cell.2016.12.029.

(151) Shneine, J. K.; Ahmad, S. M.; Zagheer, D. Sh. Recent Developments of Stetter Reaction A Brief Review. *Biomedicine and Chemical Sciences* **2022**, *1* (4), 234–240.

(152) Lennox, A. J. J.; Lloyd-Jones, G. C. Organotrifluoroborate Hydrolysis: Boronic Acid Release Mechanism and an Acid-Base Paradox in Cross-Coupling. *J. Am. Chem. Soc.* **2012**, *134* (17), 7431–7441.

(153) Wang, L.; Hou, X.; Fu, H.; Pan, X.; Xu, W.; Tang, W.; Fang, H. Design, Synthesis and Preliminary Bioactivity Evaluations of Substituted Quinoline Hydroxamic Acid Derivatives as Novel Histone Deacetylase (HDAC) Inhibitors. *Bioorg. Med. Chem.* **2015**, *23* (15), 4364–4374.

(154) *The Human Protein Atlas*. https://proteinatlas.org/ (accessed 14-02-23).

(155) Thul, P. J.; Akesson, L.; Wiking, M.; Mahdessian, D.; Geladaki, A.; Ait Blal, H.; Alm, T.; Asplund, A.; Björk, L.; Breckels, L. M.; Bäckström, A.; Danielsson, F.; Fagerberg, L.; Fall, J.; Gatto, L.; Gnann, C.; Hober, S.; Hjelmare, M.; Johansson, F.; Lee, S.; Lindskog, C.; Mulder, J.; Mulvey, C. M.; Nilsson, P.; Oksvold, P.; Rockberg, J.; Schutten, R.; Schwenk, J. M.; Sivertsson, A.; Sjöstedt, E.; Skogs, M.; Stadler, C.; Sullivan, D. P.; Tegel, H.; Winsnes, C.; Zhang, C.; Zwahlen, M.; Mardinoglu, A.; Pontén, F.; von Feilitzen, K.; Lilley, K. S.; Uhlén, M.; Lundberg, E. A Subcellular Map of the Human Proteome. *Science.* **2017**, *356* (6340), eaal3321.

(156) Brand, M.; Clayton, J.; Moroglu, M.; Schiedel, M.; Picaud, S.; Bluck, J. P.; Skwarska, A.; Bolland, H.; Chan, A. K. N.; Laurin, C. M. C.; Scorah, A. R.; See, L.; Rooney, T. P. C.; Andrews, K. H.; Fedorov, O.; Perell, G.; Kalra, P.; Vinh, K. B.; Cortopassi, W. A.; Heitel, P.; Christensen, K. E.; Cooper, R. I.; Paton, R. S.; Pomerantz, W. C. K.; Biggin, P. C.; Hammond, E. M.; Filippakopoulos, P.; Conway, S. J. Controlling Intramolecular Interactions in the Design of Selective, High-Affinity Ligands for the CREBBP Bromodomain. *J. Med. Chem.* **2021**, *64* (14), 10102–10123.

(157) Samuelson, J. C.; Caulfield, J. P. The Cercarial Glycocalyx of Schistosoma Mansoni. *J. Cel.l Biol.* **1985**, *100* (5), 1423–1434.

(158) Collins, J. J.; Wang, B.; Lambrus, B. G.; Tharp, M. E.; Iyer, H.; Newmark, P. A. Adult Somatic Stem Cells in the Human Parasite Schistosoma Mansoni. *Nature* **2013**, *494* (7438), 476–479.

(159) Buchwald, P.; Bodor, N. Quantitative Structure-Metabolism Relationships: Steric and Nonsteric Effects in the Enzymatic Hydrolysis of Noncongener Carboxylic Esters. *J. Med. Chem.* **1999**, *42* (25), 5160–5168.

(160) Fulmer, G. R.; Miller, A. J. M.; Sherden, N. H.; Gottlieb, H. E.; Nudelman, A.; Stoltz, B. M.; Bercaw, J. E.; Goldberg, K. I. NMR Chemical Shifts of Trace Impurities: Common Laboratory Solvents, Organics, and Gases in Deuterated Solvents Relevant to the Organometallic Chemist. *Organometallics* **2010**, *29* (9), 2176–2179.

(161) Inaloo, I. D.; Majnooni, S.; Esmaeilpour, M. Superparamagnetic Fe_3O_4 Nanoparticles in a Deep Eutectic Solvent: An Efficient and Recyclable Catalytic System for the Synthesis of Primary Carbamates and Monosubstituted Ureas. *European J Org Chem* **2018**, *2018* (26), 3481–3488.

(162) Valenta, V.; Bartošová, M.; Protiva, M. Carbamates and Ureas Derived from 11-Amino-6,11-Dihydrodibenzo[b,e]Thiepin; Synthesis and Pharmacological Screening. *Collect. Czechoslov. Chem.Commun.* **1980**, *45* (2), 517–528.

(163) Furuya, T.; Ritter, T. Fluorination of Boronic Acids Mediated by Silver(I) Triflate. *Org Lett* **2009**, *11* (13), 2860–2863.

(164) García-Rodríguez, A.; Rodríguez, A. M.; Prieto, P.; Andreu, R.; Merino, S.; Rodríguez-López, J. Swivel-Cruciform Stilbenes Based on Bithiophene. *European J. Org. Chem.* **2015**, *2015* (11), 2394–2404.

(165) Witten, M. R.; Wissler, L.; Snow, M.; Geschwindner, S.; Read, J. A.; Brandon, N. J.; Nairn, A. C.; Lombroso, P. J.; Käck, H.; Ellman, J. A. X-Ray Characterization and Structure-Based Optimization of Striatal-Enriched Protein Tyrosine Phosphatase Inhibitors. *J. Med. Chem.* **2017**, *60* (22), 9299–9319.

(166) Atkinson, S. J.; Soden, P. E.; Angell, D. C.; Bantscheff, M.; Chung, C. W.; Giblin, K. A.; Smithers, N.; Furze, R. C.; Gordon, L.; Drewes, G.; Rioja, I.; Witherington, J.;

Parr, N. J.; Prinjha, R. K. The Structure Based Design of Dual HDAC/BET Inhibitors as Novel Epigenetic Probes. *Medchemcomm.* **2014**, *5* (3), 342–351.

(167) Demont, E. H.; Garton, N. S.; Gosmini, R. L. M.; Hayhow, T. G. C.; Seal, J.; Wilson, D. M.; Woodrow, M. D. Tetrahydroquinoline Derivatives and Their Pharmaceutical Use, WO2011054841A1, 2011.

(168) Hayakawa, K.; Yodo, M.; Ohsuki, S.; Kanematsu, K. Novel Bicycloannulation via Tandem Vinylation and Intramolecular Diels-Alder Reaction of Five-Membered Heterocycles: A New Approach to Construction of Psoralen and Azapsoralen. *J. Am. Chem. Soc.* **1984**, *106* (22), 6735–6740.

(169) Adams, T. C.; Dupont, A. C.; Paul Carter, J.; Guzewska, M. E.; Janusz Rzeszotarski, W.; Farmer, S. G.; Noronha-Blob, L.; Kaiser, C. Aminoalkynyldithianes. A New Class of Calcium Channel Blockers, *J. Med. Chem*. **1991**, *34* (5) 1585–1593.

(170) Yan, Y.; Chen, J.; Zhang, L.; Zheng, Q.; Han, Y.; Zhang, H.; Zhang, D.; Awakawa, T.; Abe, I.; Liu, W. Multiplexing of Combinatorial Chemistry in Antimycin Biosynthesis: Expansion of Molecular Diversity and Utility. *Angew. Chem. Int. Ed. Engl.* **2013**, *52* (47), 12308–12312.

(171) Phillips, E. M.; Mesganaw, T.; Patel, A.; Duttwyler, S.; Mercado, B. Q.; Houk, K. N.; Ellman, J. A. Synthesis of Ent -Ketorfanol via a C-H Alkenylation/Torquoselective 6π Electrocyclization Cascade. *Angew Chem. Int. Ed. Engl.* **2015**, *54* (41), 12044–12048.

(172) Molander, G. A.; Canturk, B.; Kennedy, L. E. Scope of the Suzuki-Miyaura Cross-Coupling Reactions of Potassium Heteroaryltrifluoroborates. *J. Org Chem.* **2009**, *74* (3), 973–980.

(173) Oliver J. Stratton. Synthesis of a Novel PROTAC to Recruit TRIM24 as an E3 Ligase. MChem Dissertation, University of Oxford, Oxford, U.K., 2019.

(174) Dunkel, P.; Petit, M.; Dhimane, H.; Blanchard-Desce, M.; Ogden, D.; Dalko, P. I. Quinoline-Derived Two-Photon-Sensitive Octupolar Probes. *ChemistryOpen.* **2017**, *6* (5), 660–667.

(175) Picard, S.; Genin, E.; Clermont, G.; Hugues, V.; Mongin, O.; Blanchard-Desce, M. Octupolar Chimeric Compounds Built from Quinoline Caged Acetate Moieties: A Novel Approach for 2-Photon Uncaging of Biomolecules. *New J. Chem.* **2013**, *37* (12), 3899–3913.

(176) Wang, L.; Hou, X.; Fu, H.; Pan, X.; Xu, W.; Tang, W.; Fang, H. Design, Synthesis and Preliminary Bioactivity Evaluations of Substituted Quinoline Hydroxamic Acid Derivatives as Novel Histone Deacetylase (HDAC) Inhibitors. *Bioorg. Med. Chem.* **2015**, *23* (15), 4364–4374.

(177) Clabbers, M. T. B.; Gruene, T.; Parkhurst, J. M.; Abrahams, J. P.; Waterman, D. G. Electron Diffraction Data Processing with DIALS. *Acta Crystallogr. D. Struct. Biol.* **2018**, *74* (6), 506–518.

(178) McCoy, A. J.; Grosse-Kunstleve, R. W.; Adams, P. D.; Winn, M. D.; Storoni, L. C.; Read, R. J. Phaser Crystallographic Software. *J. Appl. Crystallogr.* **2007**, *40* (4), 658–674.

(179) Emsley, P.; Lohkamp, B.; Scott, W. G.; Cowtan, K. Features and Development of Coot. *Acta Crystallogr. D. Biol. Crystallogr.* **2010**, *66* (4), 486–501.

(180) Afonine, P. v.; Grosse-Kunstleve, R. W.; Echols, N.; Headd, J. J.; Moriarty, N. W.; Mustyakimov, M.; Terwilliger, T. C.; Urzhumtsev, A.; Zwart, P. H.; Adams, P. D. Towards Automated Crystallographic Structure Refinement with Phenix.Refine. *Acta Crystallogr. D. Biol. Crystallogr.* **2012**, *68* (4), 352–367.

(181) Colley, D. G.; Wikel, S. K. Schistosoma Mansoni: Simplified Method for the Production of Schistosomules. *Exp. Parasitol.* **1974**, *35* (1), 44–51.

(182) Whiteland, H. L.; Chakroborty, A.; Forde-Thomas, J. E.; Crusco, A.; Cookson, A.; Hollinshead, J.; Fenn, C. A.; Bartholomew, B.; Holdsworth, P. A.; Fisher, M.; Nash, R. J.; Hoffmann, K. F. An Abeis Procera-Derived Tetracyclic Triterpene Containing a Steroid-like Nucleus Core and a Lactone Side Chain Attenuates in Vitro Survival of Both Fasciola Hepatica and Schistosoma Mansoni. *Int. J. Parasitol. Drugs Drug Resist.* **2018**, *8* (3), 465–474.

(183) Whiteland, H.; Crusco, A.; Bloemberg, L. W.; Tibble-Howlings, J.; Forde-Thomas, J.; Coghlan, A.; Murphy, P. J.; Hoffmann, K. F. Quorum Sensing N-Acyl Homoserine Lactones Are a New Class of Anti-Schistosomal. *PLoS Negl. Trop. Dis.* **2020**, *14* (10), 1–22.

(184) Partridge, F. A.; Bataille, C. J. R.; Forman, R.; Marriott, A. E.; Forde-Thomas, J.; Häberli, C.; Dinsdale, R. L.; O'Sullivan, J. D. B.; Willis, N. J.; Wynne, G. M.; Whiteland, H.; Archer, J.; Steven, A.; Keiser, J.; Turner, J. D.; Hoffmann, K. F.; Taylor, M. J.; Else, K. J.; Russell, A. J.; Sattelle, D. B. Structural Requirements for Dihydrobenzoxazepinone Anthelmintics: Actions against Medically Important and Model Parasites: Trichuris Muris, Brugia Malayi, Heligmosomoides Polygyrus, and Schistosoma Mansoni. *ACS Infect. Dis.* **2021**, *7* (5), 1260–1274.

(185) Hulme, B. J.; Geyer, K. K.; Forde-Thomas, J. E.; Padalino, G.; Phillips, D. W.; Ittiprasert, W.; Karinshak, S. E.; Mann, V. H.; Chalmers, I. W.; Brindley, P. J.; Hokke, C. H.; Hoffmann, K. F. Schistosoma Mansoni α-N-Acetylgalactosaminidase (SmNAGAL) Regulates Coordinated Parasite Movement and Egg Production. *PLoS. Pathog.* **2022**, *18* (1), e1009828.

(186) Taft, A. S.; Norante, F. A.; Yoshino, T. P. The Identification of Inhibitors of Schistosoma Mansoni Miracidial Transformation by Incorporating a Medium-Throughput Small-Molecule Screen. *Exp Parasitol* **2010**, *125* (2), 84–94. https://doi.org/10.1016/j.exppara.2009.12.021.

(187) Azzi, A.; Cosseau, C.; Grunau, C. Schistosoma Mansoni: Developmental Arrest of Miracidia Treated with Histone Deacetylase Inhibitors. *Exp. Parasitol.* **2009**, *121* (3), 288–291.

(188) Kallemeijn, W. W.; Lanyon-Hogg, T.; Panyain, N.; Goya Grocin, A.; Ciepla, P.; Morales-Sanfrutos, J.; Tate, E. W. Proteome-Wide Analysis of Protein Lipidation Using Chemical Probes: In-Gel Fluorescence Visualization, Identification and Quantification of N-Myristoylation, N- and S-Acylation, O-Cholesterylation, S-Farnesylation and S-Geranylgeranylation. *Nat. Protoc*. **2021**, *16* (11) 5083–5122.

(189) Savitsky. P.; Bray, J.; Cooper., C. D. O; Marsden, B. D.; Mahajan, P.; Burgenn-Brown, N. A.; Gildeadi, O; High-Throughput Production of Human Proteins for Crystallization: the SJC Experimence. *J Struct Biol*. **2010,** *172* (1), 3–13.

Appendices

Appendix A: Protein expression and purification

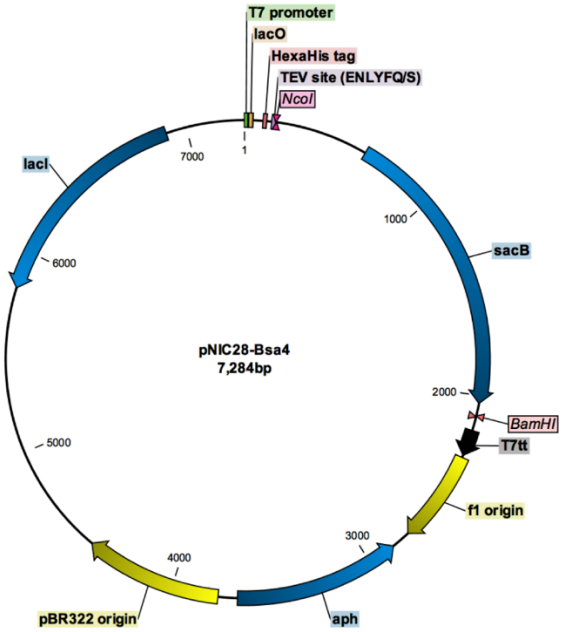


Figure S1. A visual representation of the plasmid cloning and expression vector, pNIC28-Bsa4,[189] which is drawn to scale. All expression plasmids prepared by Dr Matthias Schiedel and used in the work described in this thesis share the same vector backbone. The plasmid map was generated and annotated by using CLC Main Workbench 7.6.4 by Dr Anthony Chan.

Table S1. Primers used by Dr Matthias Schiedel to produce H6-SmBRD3(9..378aa) and H6-SmBRD3(241..368aa):

Primer	Direction	Sequence: (5' to 3')	Tm (°C)
GA_f	Forward	AGAACCTGTACTTCCAATCC	61
GA_r	Reverse	CGGAGCTCGAATTCG	60
SmBRD3(2)_f1	Forward	AGAACCTGTACTTCCAATCCCCGAAACGTGAATATGAAGAAC	61
SmBRD3(2)_r1	Reverse	CGGAGCTCGAATTCGGATCCTTATCAGCTTTCATCATCCGGC	61

Preparation of *Sm*BRD3 plasmids by Dr Matthias Schiedel:

CP2. Cloning of pSmBRD3(9..378aa):

Vector: pNIC28-Bsa4 (7,283 bp) → NcoI-HF + BamHI-HF (CutSmart) → linearized vector (5,337 bp)

Synthetic fragment: *Sm*BRD3_9_to_378aa (1,156 bp)

PCR: *Sm*BRD3_9_to_378aa (1,156 bp)+ GA_f + GA_r → p2 (1,156 bp)

Gibson assembly: Linearized vector + p2 → **p*Sm*BRD3(9..378aa)** (6,455 bp)

Sequencing primer(s): T7F or T7R

Remark: The synthetic gene (i.e. *Sm*BRD3_9_to_378aa with codons optimized for protein expression in *E. coli*) encodes the *Sm*BRD3(9..378aa) fragment (GenBank ID: CCD76183.1).

>H6-*Sm*BRD3(9..378aa)

MHHHHHHSSGVDLGTENLYFQSSEANLDSSNSIKSEPHAAKSHSSKITTNQLEYIKKEVV
GRLFKEKIVWPFTKPVDHQRLNLPDYPKIIKHPMDLGTIKQRLNLKFYHSSSECLDDLFTM
FRNCYIFNKPGDDVVAMAMKLEQIARERLKFMPTPETEICPQKTPKSIRPIGAPLQVHPPIE
PIHTAASTNHTEGLNGSAVSVDQTTLPFRPSVTSTSTKKASKKKSDSTIDELPSTPQSYDD
LSRDRRQIKKPKREYEERNVGKRLRLSEALKACSNILKDISSQRYRDLNHFFLKPVDVVAL
GLHDYYDVVKKAMDLSTIKTKLESGQYHTKYDFADDVRLMFNNCYKYNGEDSEVARVGK
QLQAIFDENFAKVPDDESDPAASPDGRP

CP24. Cloning of pSmBRD3(241..368aa):

Vector: pNIC28-Bsa4 (7,283 bp) NcoI-HF + BamHI-HF (CutSmart) → linearized vector (5,337 bp)

PCR: p*Sm*BRD3(9..378aa) (6,455 bp) + *Sm*BRD3(2)_f1 + *Sm*BRD3(2)_r1 → p24 (430 bp)

Gibson assembly: Linearized vector + p24 → **pSmBRD3(241..368aa)** (5,729 bp)

Sequencing primer(s): T7F or T7R

Remark: Native SmBRD3 (GenBank ID: CCD76183.1).

>H6-*Sm*BRD3(241..368aa)

MHHHHHHSSGVDLGTENLYFQSPKREYEERNVGKRLRLSEALKACSNILKDISSQRYRD
LNHFFLKPVDVVALGLHDYYDVVKKAMDLSTIKTKLESGQYHTKYDFADDVRLMFNNCYK
YNGEDSEVARVGKQLQAIFDENFAKVPDDES

Protein sequence of 6xHis-tag cleaved *Sm*BRD3(1,2):

SSEANLDSSNSIKSEPHAAKSHSSKITTNQLEYIKKEVVGRLFKEKIVWPFTKPVDHQRLN
LPDYPKIIKHPMDLGTIKQRLNLKFYHSSSECLDDLFTMFRNCYIFNKPGDDVVAMAMKLE
QIARERLKFMPTPETEICPQKTPKSIRPIGAPLQVHPPIEPIHTAASTNHTEGLNGSAVSVD
QTTLPFRPSVTSTSTKKASKKKSDSTIDELPSTPQSYDDLSRDRRQIKKPKREYEERNVG
KRLRLSEALKACSNILKDISSQRYRDLNHFFLKPVDVVALGLHDYYDVVKKAMDLSTIKTK
LESGQYHTKYDFADDVRLMFNNCYKYNGEDSEVARVGKQLQAIFDENFAKVPDDESDPA
ASPDGRP

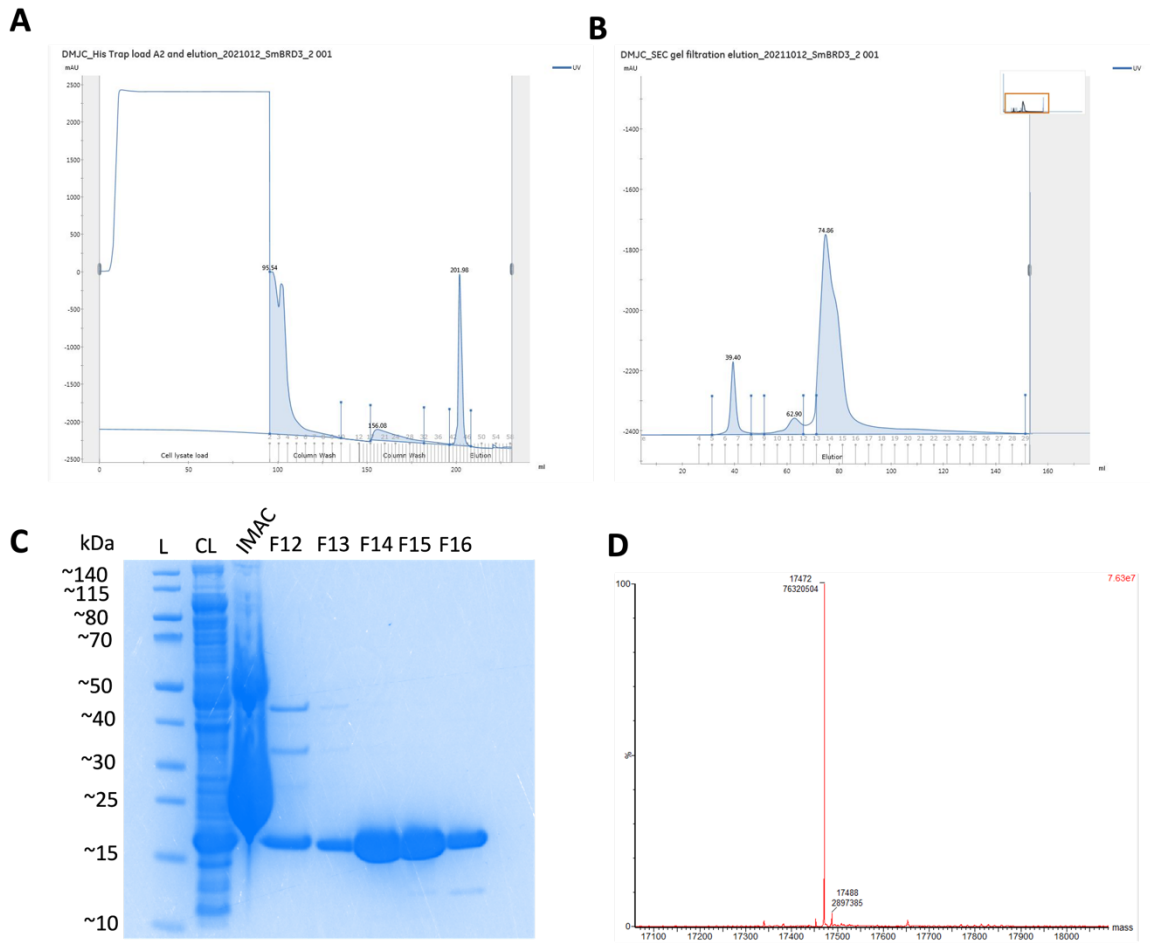


Figure S2. Purification of H6-*Sm*BRD3(241..368aa) [*Sm*BRD3(2)]. **A.** IMAC profile. **B** SEC profile. **C.** SDS-PAGE gel of SEC purification fractions, with cell lysate (CL), and combined IMAC samples as a reference. **D.** Deconvoluted protein mass spectrometry trace of H6-SmBRD3(241..368aa) (Expected = 17472 Da, Detected = 17472 Da).

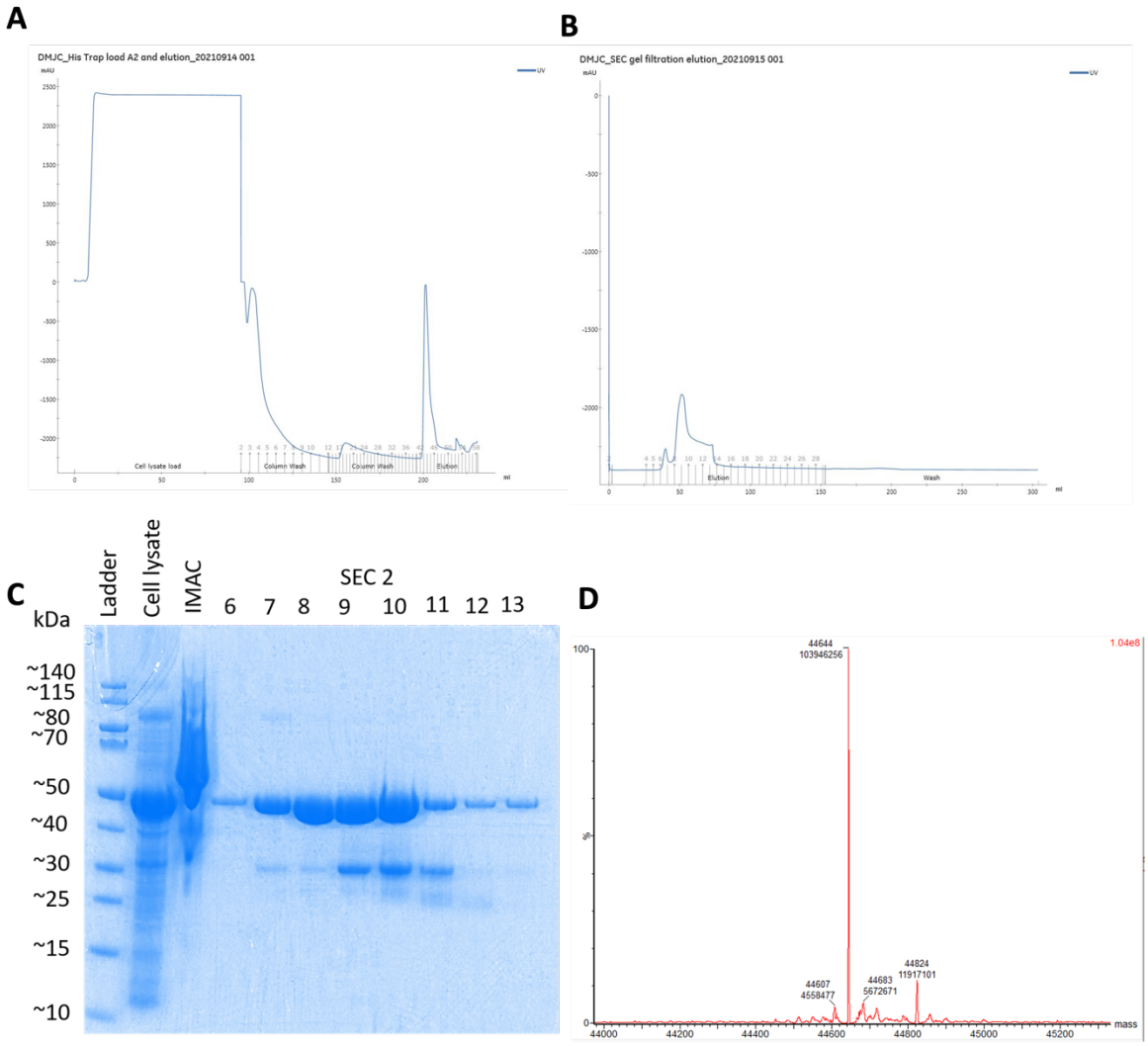


Figure S3. Purification of H6-*Sm*BRD3(9..378aa) [*Sm*BRD3(1,2)]. **A.** IMAC profile. **B** SEC profile. **C.** SDS-PAGE gel of SEC purification fractions, with cell lysate and combined IMAC samples as a reference. **D.** Deconvoluted protein mass spectrometry trace of H6-*Sm*BRD3(9..378aa) (Expected = 44644 Da, Detected = 44644 Da).

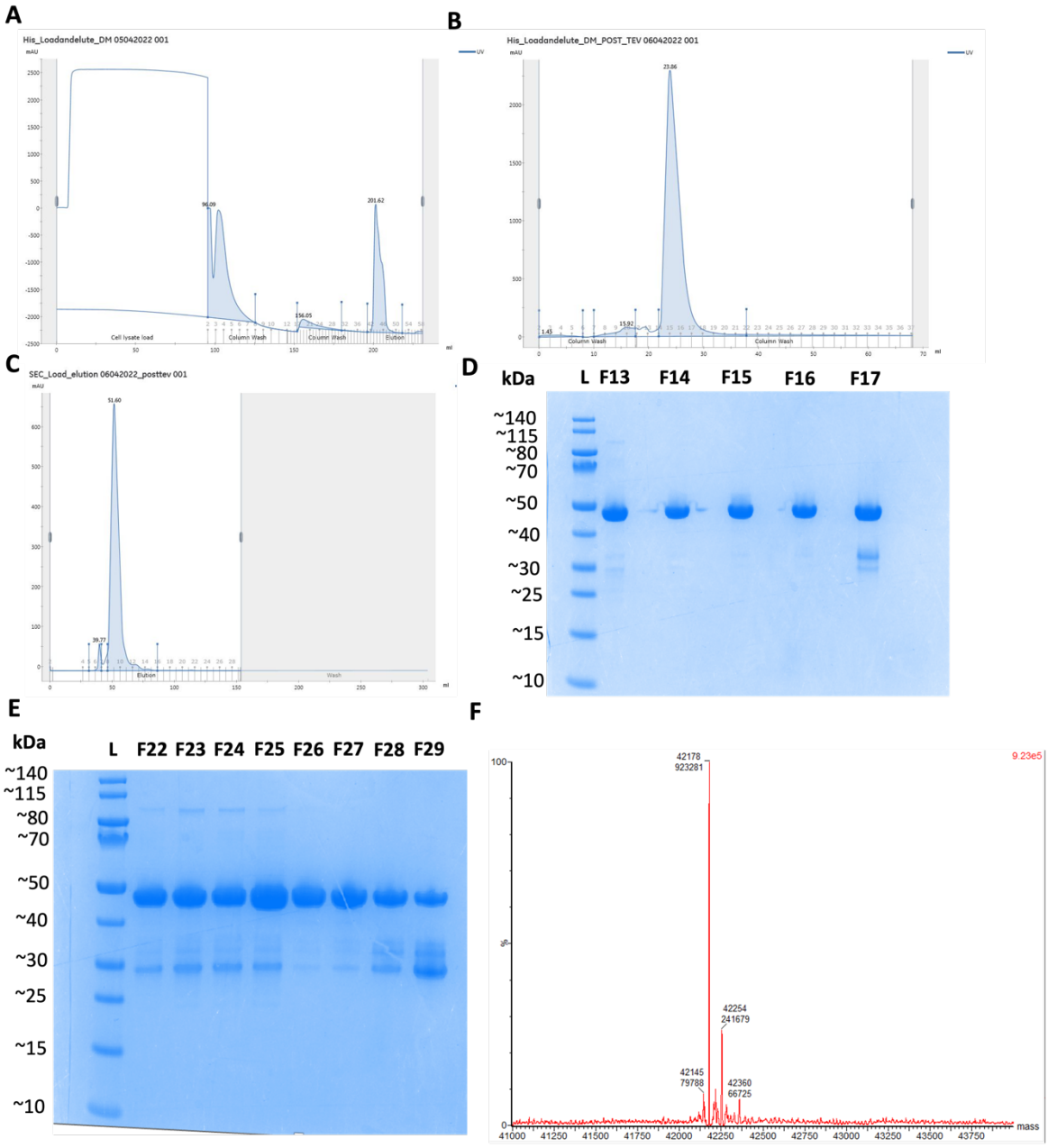


Figure S4. Purification of 6xHis-tag cleaved *Sm*BRD3(1,2). **A.** IMAC profile before TEV cleavage; **B.** SEC profile after TEV cleavage; **C.** SEC profile; **D. E.** SDS-PAGE gel of SEC purification fractions (two different SEC pufications). Fractions 14–16 from gel **D** and fraction 26 from gel **E** were combined to use as a pure antigen sample for polyclonal antibody production. **F.** Deconvoluted protein mass spectrometry trace of 6xHis-tag cleaved *Sm*BRD3(1,2) (Expected = 42178 Da, Detected = 42178 Da).

Appendix B: Isothermal Titration Calorimetry (ITC) Data

B1: Chapter 1 and 2 ITC Data

Table S2. K_d values and N numbers of compounds tested by Isothermal Titration Calorimetry (ITC) for binding to *Sm*BRD3(1,2) and *Sm*BRD3(2). SEM = Standard Error of the Mean. No binding refers to no detectable binding by ITC.

	Binding to *Sm*BRD3(1,2)									
	Repeat 1		Repeat 2		Repeat 3		Average		95% CI	
Compound	K_d (nM)	N	K_d (nM)	N	K_d (nM)	N	K_d (nM)	N	K_d	N
OXFBD03 (1.37)	675 ± 97.6	1.17 ± 1.7e-2	-	-	-	-	675 ± 97.6	1.17 ± 1.7e-2	n/a	n/a
1.38	1750 ± 301	1.05 ± 3.9e-2	-	-	-	-	1750 ± 301	1.05 ± 3.9e-2	n/a	n/a
2.33	No binding	-	-	-	-	-	No binding	n/a	n/a	n/a

	Binding to *Sm*BRD3(2)									
	Repeat 1		Repeat 2		Repeat 3		Average		95% CI	
Compound	K_d (nM)	N	K_d (nM)	N	K_d (nM)	N	K_d (nM)	N	K_d	N
OXFBD03 (1.37)	No binding	-	-	-	-	-	No binding	n/a	n/a	n/a
1.38	No binding	-	-	-	-	-	No binding	n/a	n/a	n/a
2.1	572 ± 103	1.52 ± 2.2e-2	778 ± 179	1.57 ± 3.4e-2	753 ± 176	1.64 ± 3.3e-2	701	1.58	127	6.82e-02
2.2	1060 ± 164	1.54 ± 2.5e-2	1300 ± 236	1.49 ± 3.0e-2	-	-	1180	1.52	235	4.90e-02
2.3	562 ± 79.1	1.51 ± 1.8e-2	543 ± 60.3	1.55 ± 1.4e-2	-	-	553	1.53	18.6	3.92e-02
2.4	628 ± 94.9	1.52 ± 2.0e-2	652 ± 78.5	1.71 ± 1.8e-2	672 ± 76.0	1.60 ± 1.6e-2	651	1.61	24.9	0.108
2.5	1010 ± 160	1.42 ± 2.4e-2	1270 ± 779	1.54 ± 0.101	1270 ± 349	1.49 ± 5.4e-2	1183	1.48	170	6.82e-02
2.6	320 ± 82.8	1.48 ± 2.5e-2	361 ± 70.2	1.51 ± 2.0e-2	411 ± 60.4	1.69 ± 1.8e-2	364	1.56	51.6	0.129
2.20	No binding	-	-	-	-	-	No binding	n/a	n/a	n/a
2.21	No binding	-	-	-	-	-	No binding	n/a	n/a	n/a
2.22	No binding	-	-	-	-	-	No binding	n/a	n/a	n/a
2.23	No binding	-	-	-	-	-	No binding	n/a	n/a	n/a
2.30	No binding	-	-	-	-	-	No binding	n/a	n/a	n/a
2.31	No binding	-	-	-	-	-	No binding	n/a	n/a	n/a
2.32	No binding	-	-	-	-	-	No binding	n/a	n/a	n/a
2.33	No binding	-	-	-	-	-	No binding	n/a	n/a	n/a

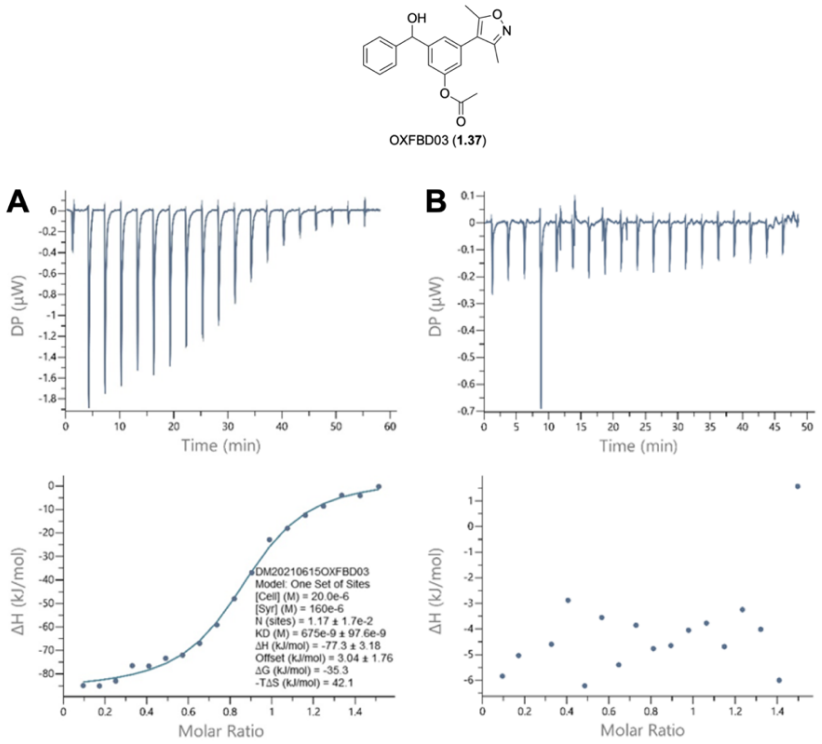


Figure S5. A) ITC trace of OXFBD03 (**1.37**) and *Sm*BRD3(1,2). **B)** ITC trace of OXFBD03 (**2**) and *Sm*BRD3(2).

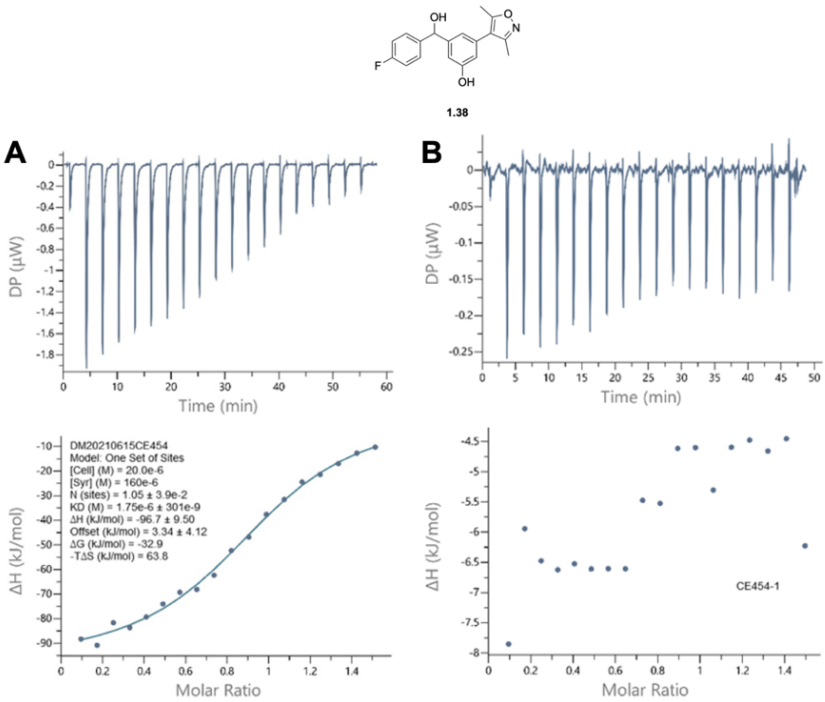


Figure S6. A) ITC trace of **1.38** and *Sm*BRD3(1,2). **B**) ITC trace of **1.37** and *Sm*BRD3(2).

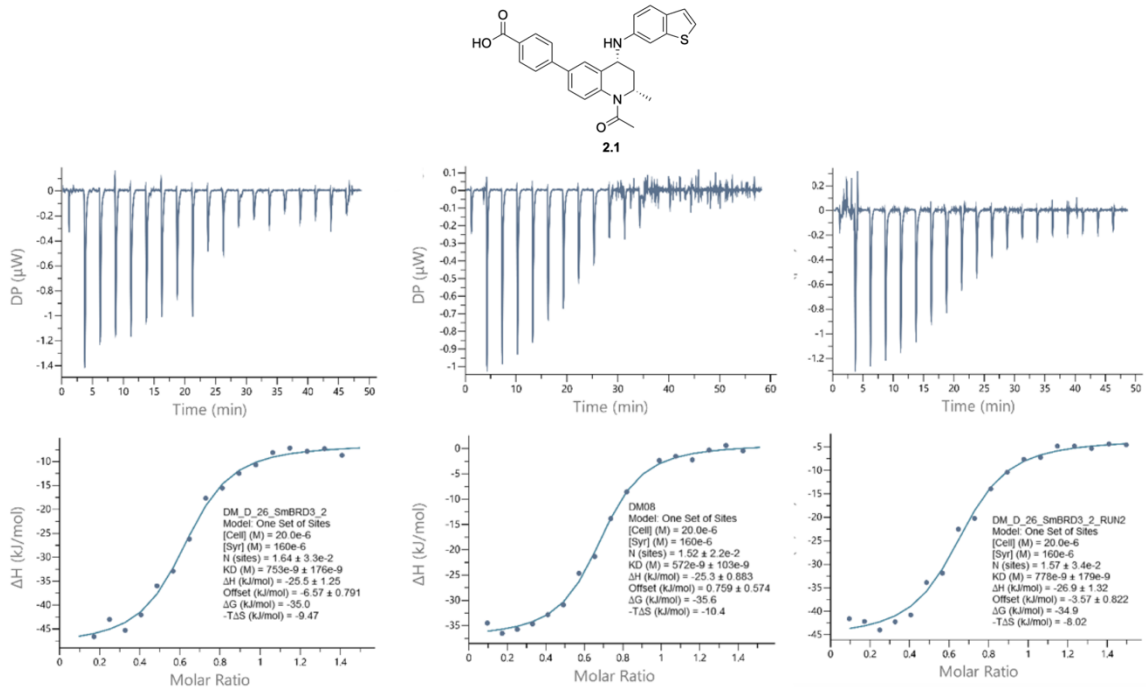


Figure S7. ITC traces of **2.1** and *Sm*BRD3(2).

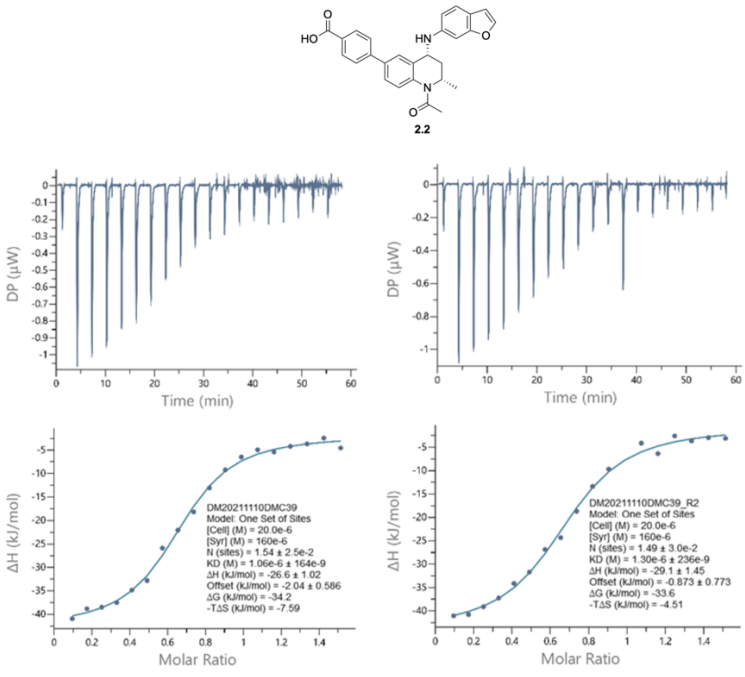


Figure S8. ITC traces of **2.2** and *Sm*BRD3(2).

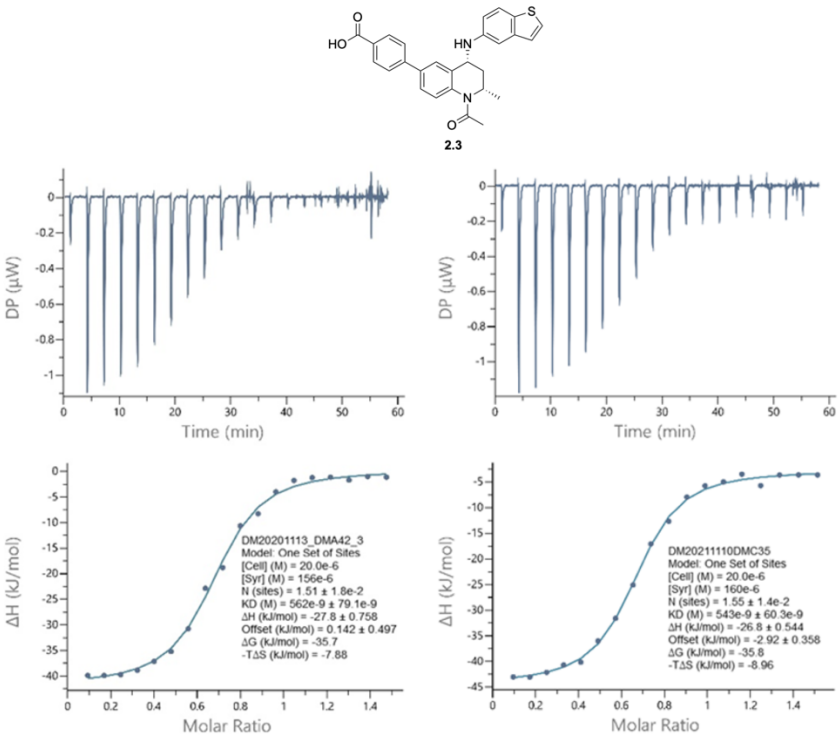


Figure S9. ITC traces of **2.3** and *Sm*BRD3(2).

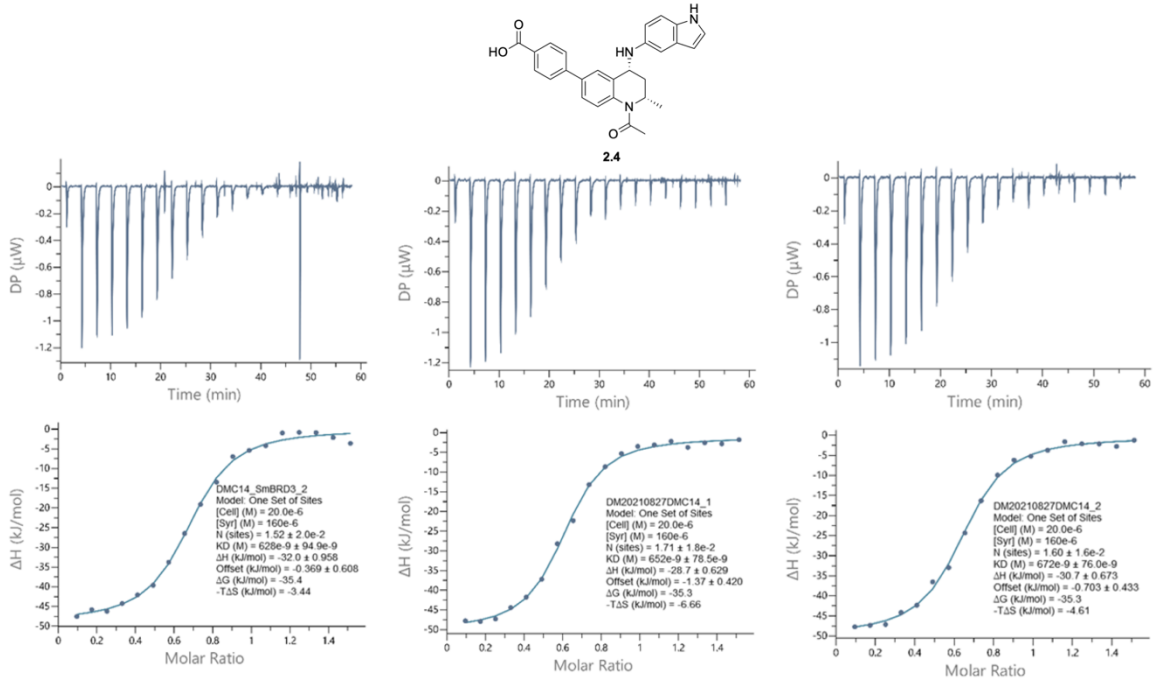


Figure S10. ITC traces of **2.4** and *Sm*BRD3(2).

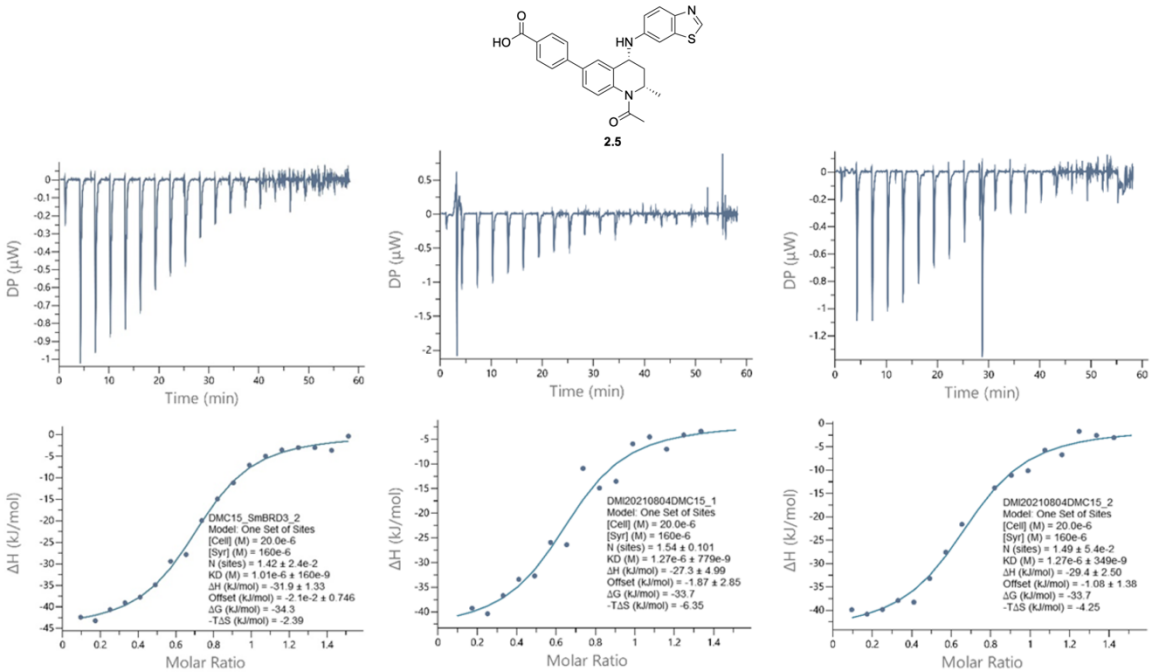


Figure S11. ITC traces of **2.5** and *Sm*BRD3(2).

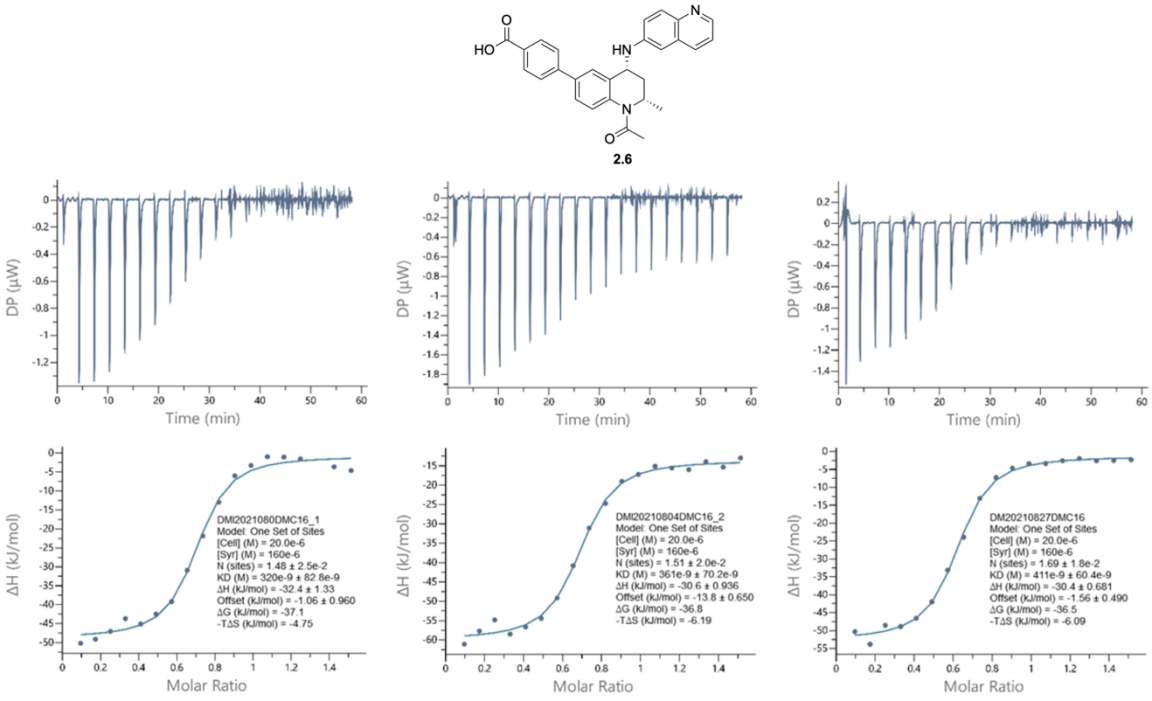


Figure S12. ITC traces of **2.5** and *Sm*BRD3(2).

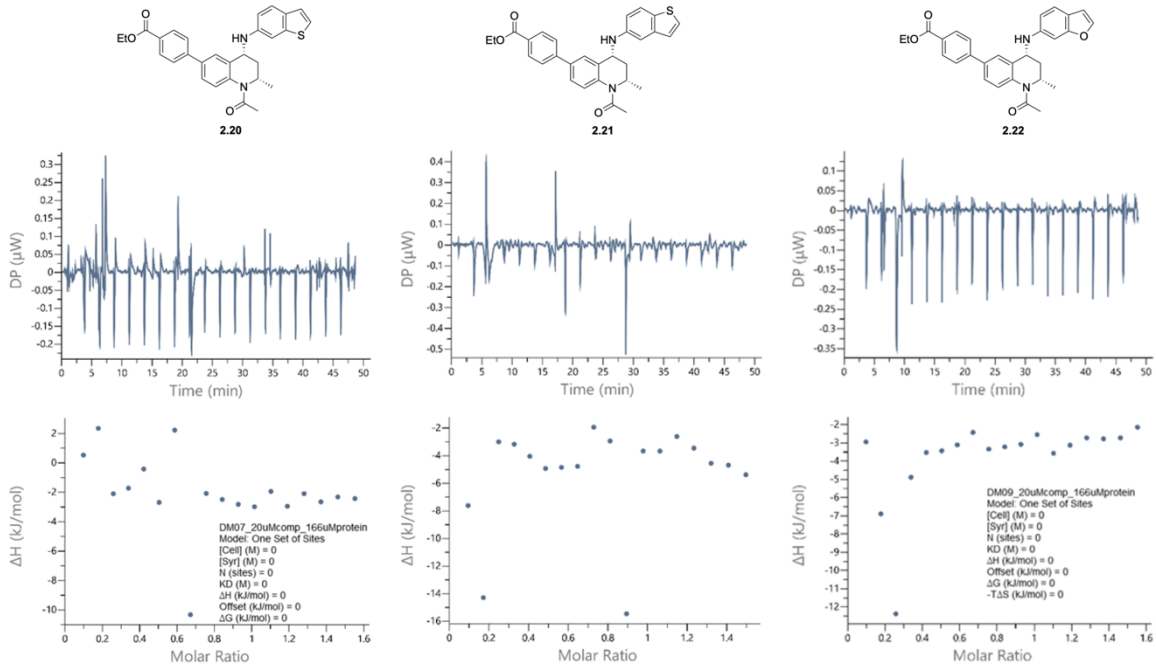


Figure S13 Isothermal Titration Calorimetry (ITC) traces of **2.20–2.22** and *Sm*BRD3(2) (No detectable binding).

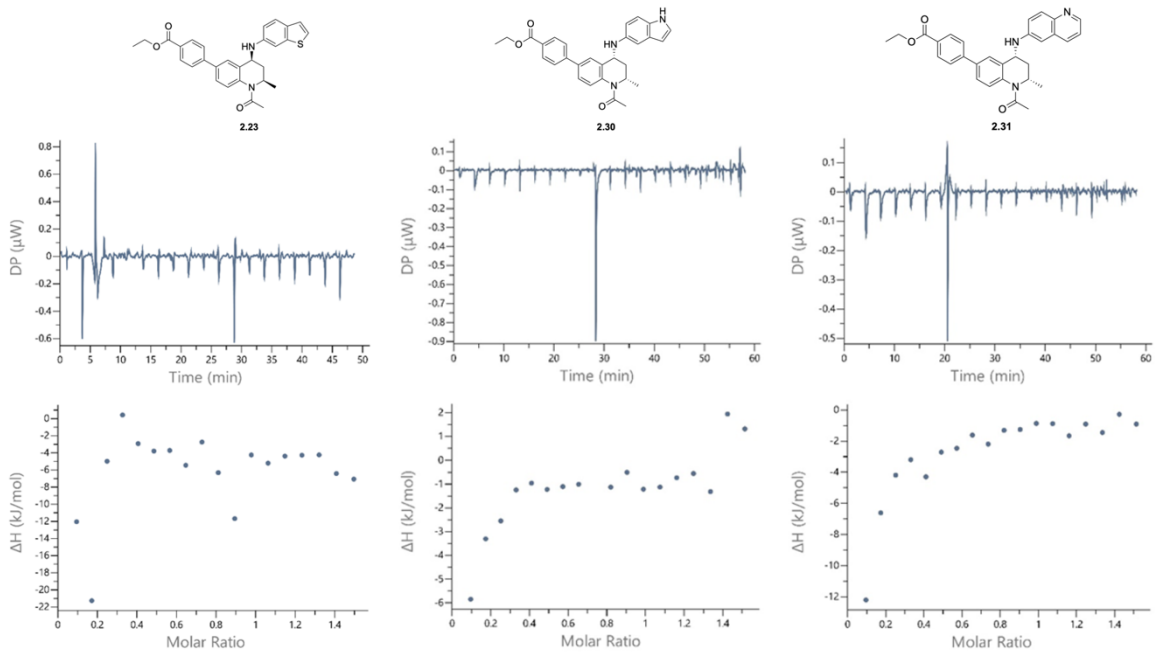


Figure S14 Isothermal Titration Calorimetry (ITC) traces of **2.20–2.22** and *Sm*BRD3(2) (No detectable binding).

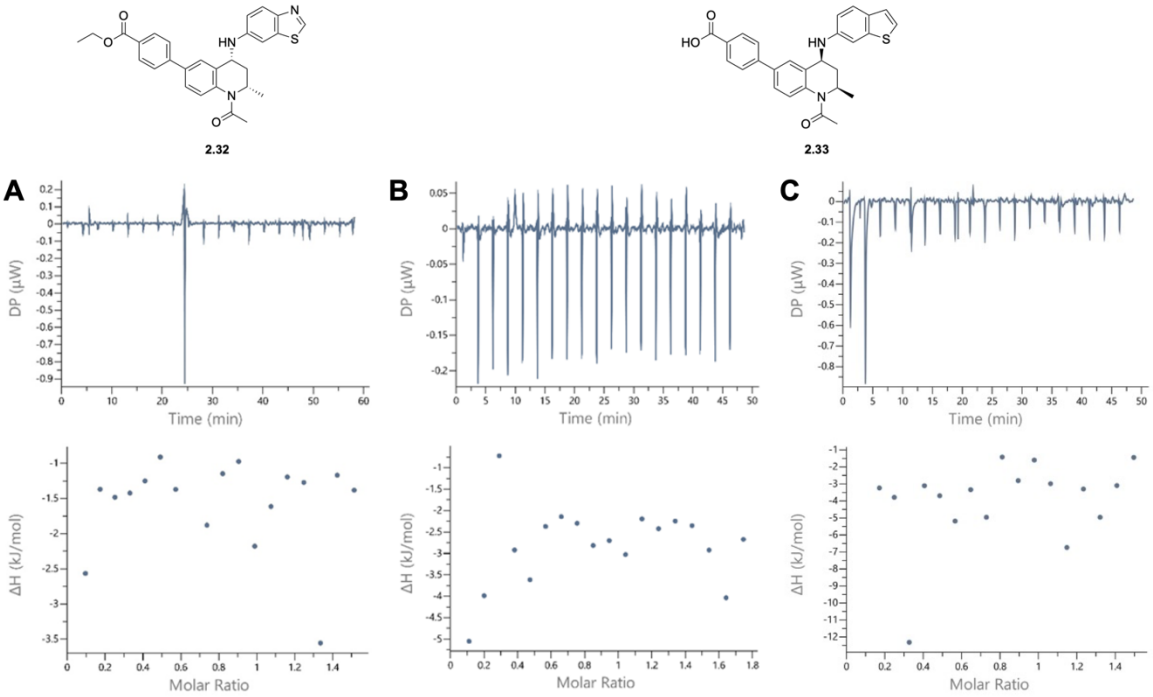


Figure S15 A) ITC trace of **2.32** and *Sm*BRD3(2) (No detectable binding). **B**) ITC trace of **2.33** and *Sm*BRD3(2) (No detectable binding). **C**) ITC trace of **2.33** and *Sm*BRD3(1,2) (No detectable binding).

B2: Chapter 3 ITC data

Table S3. K_d values and the corresponding N numbers of compounds **2.13**, **3.1**–**3.3**, **3.24**, **3.27**, **3.28**, **3.30**, **3.33** and **3.41**–**3.46** binding to *Sm*BRD3(2), and I-BET726 (**1.6**), **3.42** and **3.44** binding to *Hm*BRD4(1). SEM refers to the standard error of the mean.

Binding to *Sm*BRD3(2)

	Repeat 1		Repeat 2		Repeat 3		Average		95% CI	
Compound	K_d (μM)	N	K_d (μM)	N	K_d (μM)	N	K_d (μM)	N	K_d	N
2.13	368 ± 3630	10.0 ± 89.4	-	-	-	-	368 ± 3630	10.0 ± 89.4	n/a	n/a
3.1	6.03 ± 1.73	1.33 ± 5.80e-2	-	-	-	-	6.03 ± 1.73	1.33 ± 0.0580	n/a	n/a
3.2	5.21 ± 2.58	1.58 ± 0.111	-	-	-	-	5.21 ± 2.58	1.58 ± 0.111	n/a	n/a
3.3	26.5 ± 13.5	1.57 ± 0.150	-	-	-	-	26.5 ± 13.5	1.57 ± 0.150	n/a	n/a
3.24	No binding	-	-	-	-	-	No binding	No binding	n/a	n/a
3.27	33.7 ± 20.6	1.92 ± 0.313	-	-	-	-	33.7 ± 20.6	1.92 ± 0.313	n/a	n/a
3.28	8.12 ± 3.59	1.38 ± 9.5e-2	-	-	-	-	8.12 ± 3.59	1.38 ± 9.5e-2	n/a	n/a
3.30	12.6 ± 5.77	1.54 ± 0.112	-	-	-	-	12.6 ± 5.77	1.54 ± 0.112	n/a	n/a
3.33	7.85 ± 4.45	1.22 ± 0.111	-	-	-	-	7.85 ± 4.45	1.22 ± 0.111	n/a	n/a

Binding to *Sm*BRD3(2)

	Repeat 1		Repeat 2		Repeat 3		Average		95% CI	
Compound	K_d (nM)	N	K_d (nM)	N	K_d (nM)	N	K_d (nM)	N	K_d	N
3.41	2410 ± 355	1.68 ± 3.3e-2	-	-	-	-	2410 ± 355	1.68 ± 3.3e-2	n/a	n/a
3.42	878 ± 116	1.76 ± 2.2e-2	699 ± 75.5	1.73 ± 1.7e-2	-	-	788.5	1.75	175	2.93e-2
3.43	1620 ± 455	2.44 ± 8.1e-2	2030 ± 449	2.74 ± 7.9e-2	-	-	1825	2.59	402	0.294
3.44	714 ± 109	1.54 ± 2.0e-2	773 ± 240	1.58 ± 4.1e-2	-	-	743.5	1.56	57.8	3.92e-2
3.45	813 ± 299	1.71 ± 5.8e-2	869 ± 201	1.89 ± 4.0e-2	-	-	841	1.80	54.9	0.176
3.46	5250 ± 3260	1.95 ± 0.18	4120 ± 2210	1.55 ± 0.18	-	-	4685	1.75	1107	0.392

Binding to *Hm*BRD4(1)

	Repeat 1		Repeat 2		Repeat 3		Average		95% CI	
Compound	K_d (nM)	N	K_d (nM)	N	K_d (nM)	N	K_d (nM)	N	K_d	N
I-BET726 (1.6)	6.23 ± 1.98	1.36 ± 5.9e-3	-	-	-	-	6.23 ± 1.98	1.36 ± 5.9e-3	n/a	n/a
2.6	13.5 ± 2.47	1.59 ± 3.5e-3	-	-	-	-	13.5 ± 2.47	1.59 ± 3.5e-3	n/a	n/a
3.42	53.0 ± 4.16	1.84 ± 3.7e-3	-	-	-	-	53.0 ± 4.16	1.84 ± 3.7e-3	n/a	n/a
3.44	17.5 ± 2.82	1.63 ± 2.9e-3	-	-	-	-	17.5 ± 2.82	1.63 ± 2.9e-3	n/a	n/a

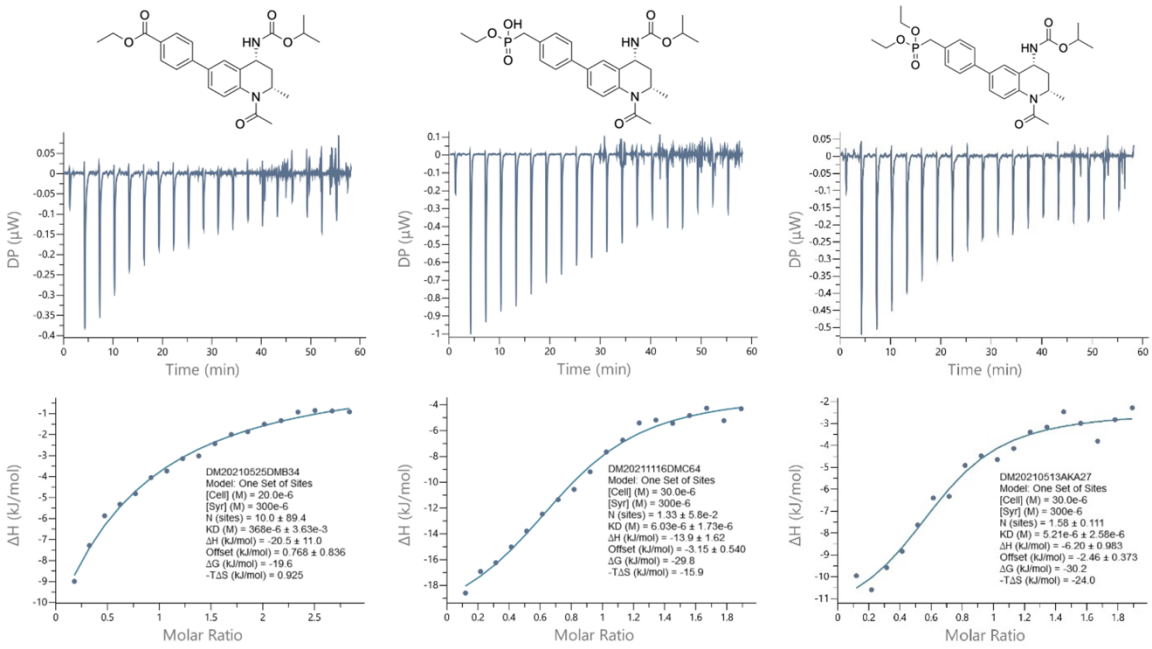


Figure S16. ITC traces of **2.13**, **3.1** and **3.2** and *Sm*BRD3(2).

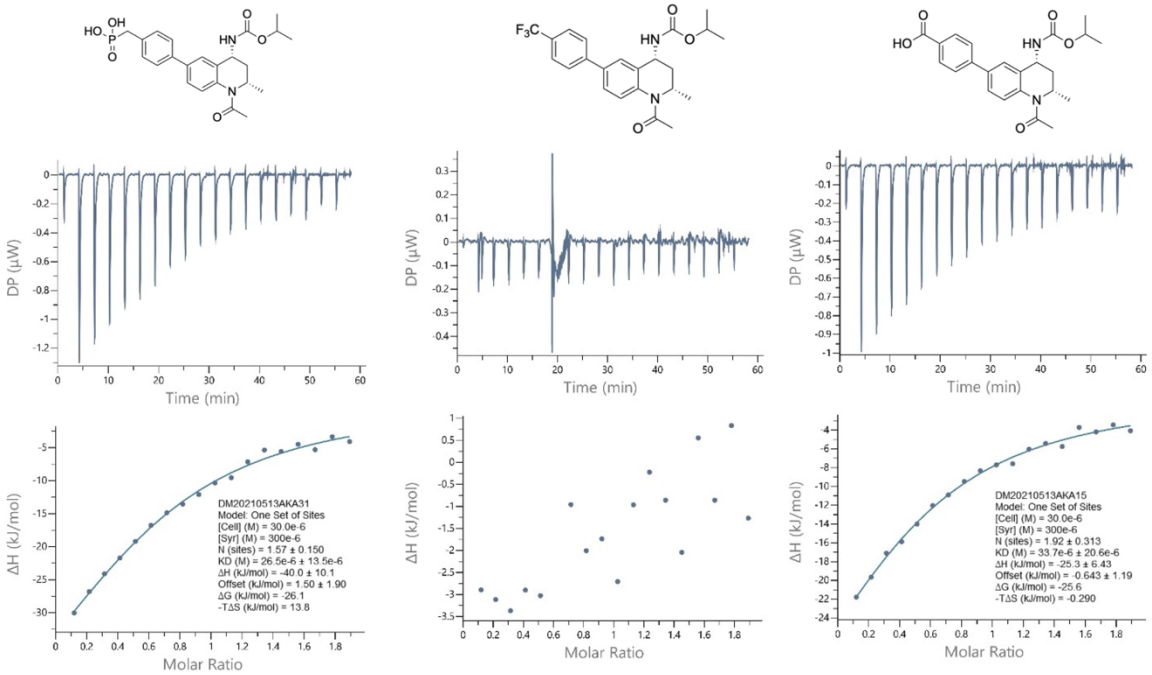


Figure S17. ITC traces of **3.3**, **3.24** and **3.27** and *Sm*BRD3(2).

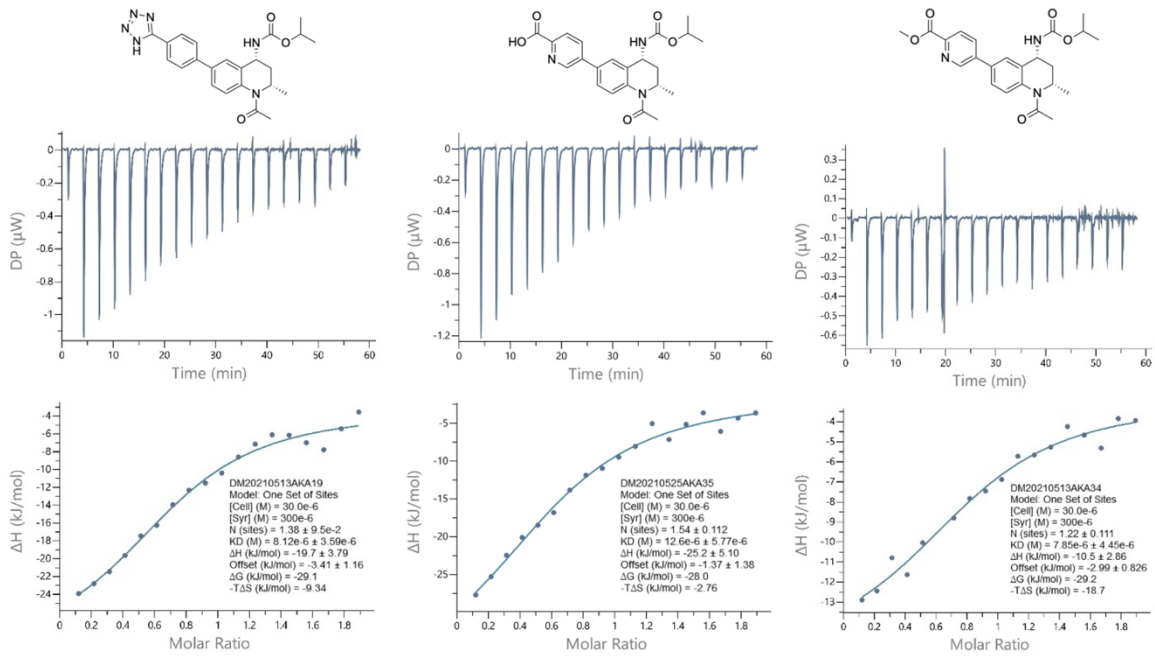


Figure S18. ITC traces of **3.28**, **3.30** and **3.33** and *Sm*BRD3(2).

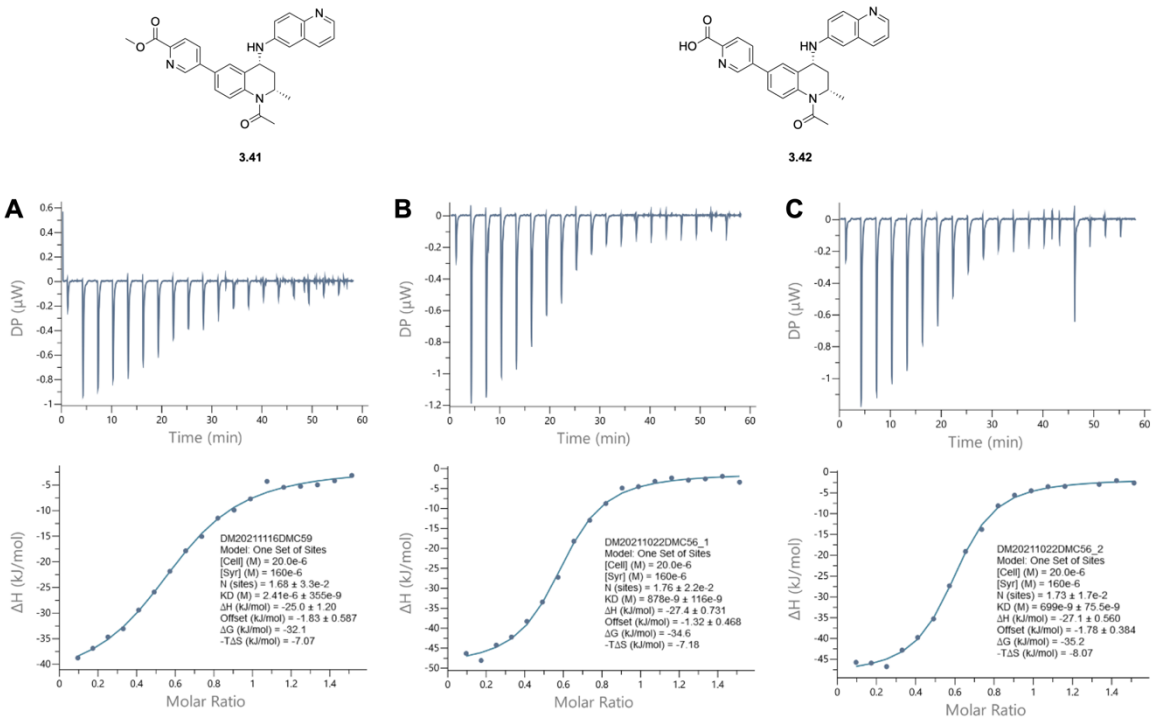


Figure S19. A) ITC trace of **3.41** and *Sm*BRD3(2). **B**) and **C**) ITC traces of **3.42** and *Sm*BRD3(2).

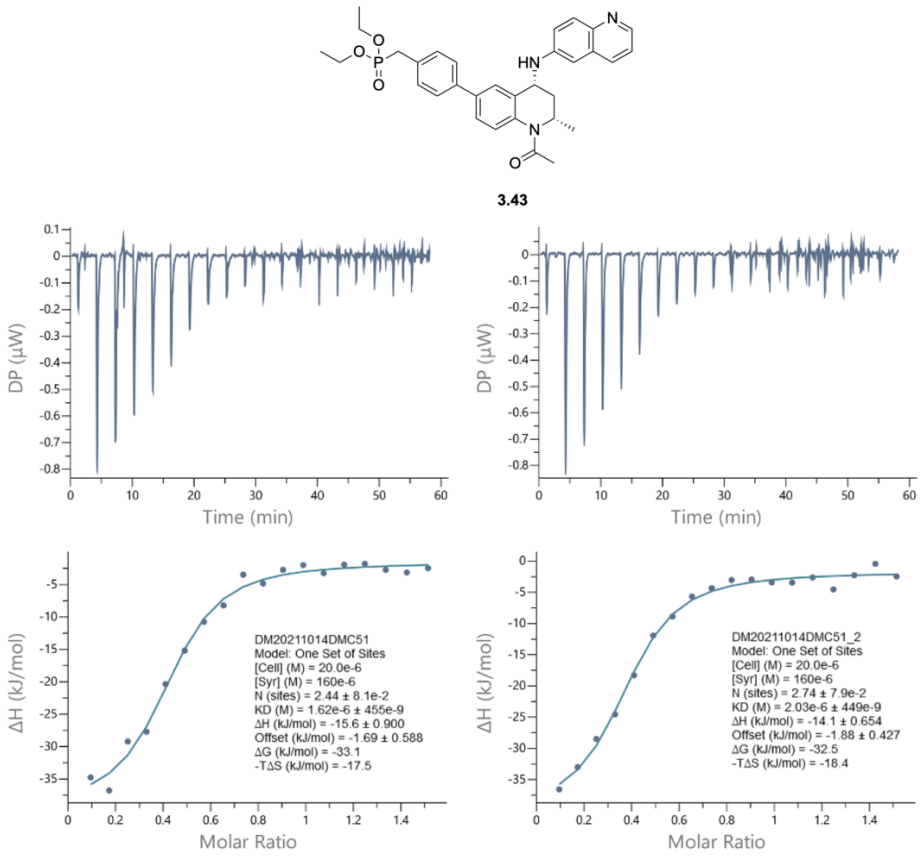


Figure S20. ITC traces of **3.43** and *Sm*BRD3(2).

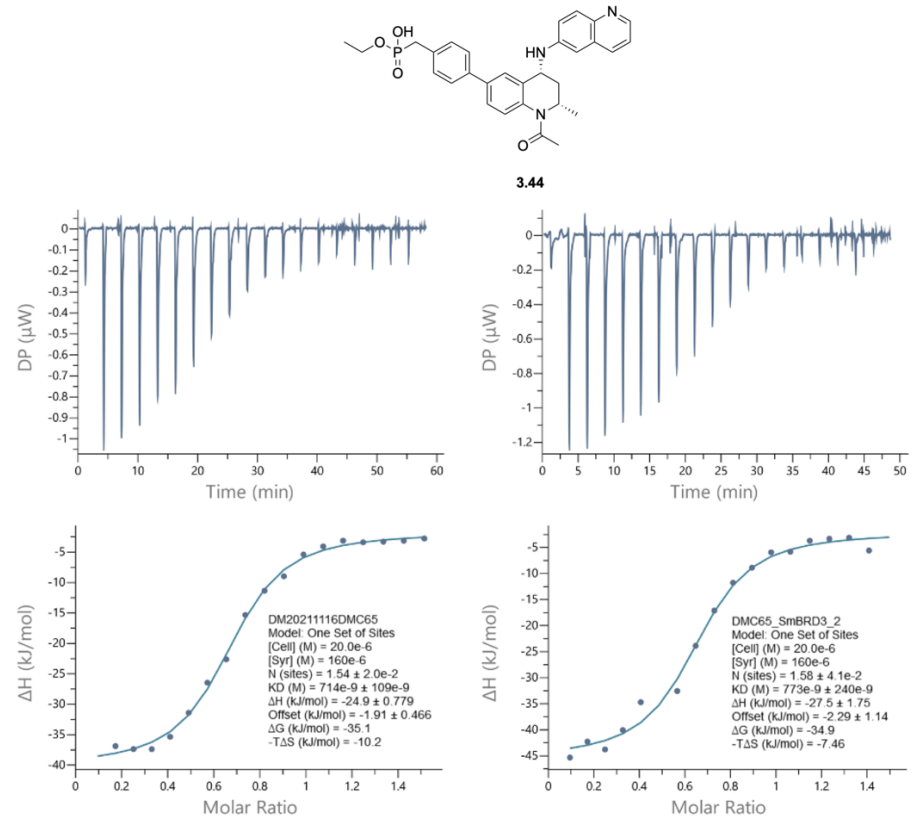


Figure S21. ITC traces of **3.44** and *Sm*BRD3(2).

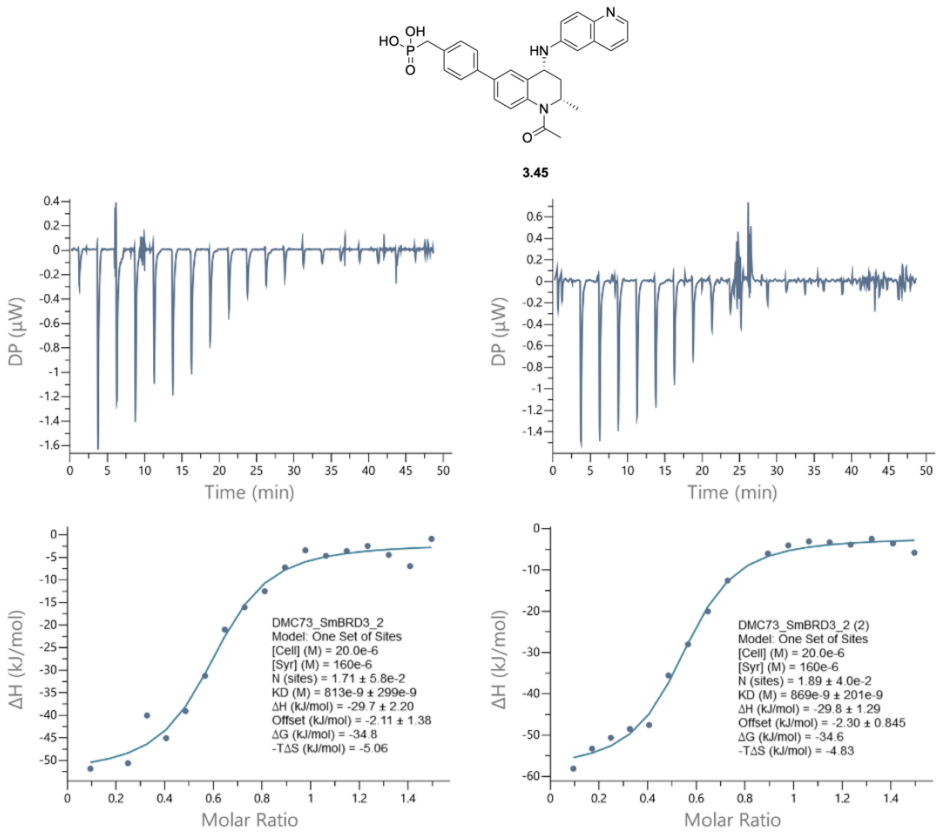


Figure S22. ITC traces of **3.45** and *Sm*BRD3(2).

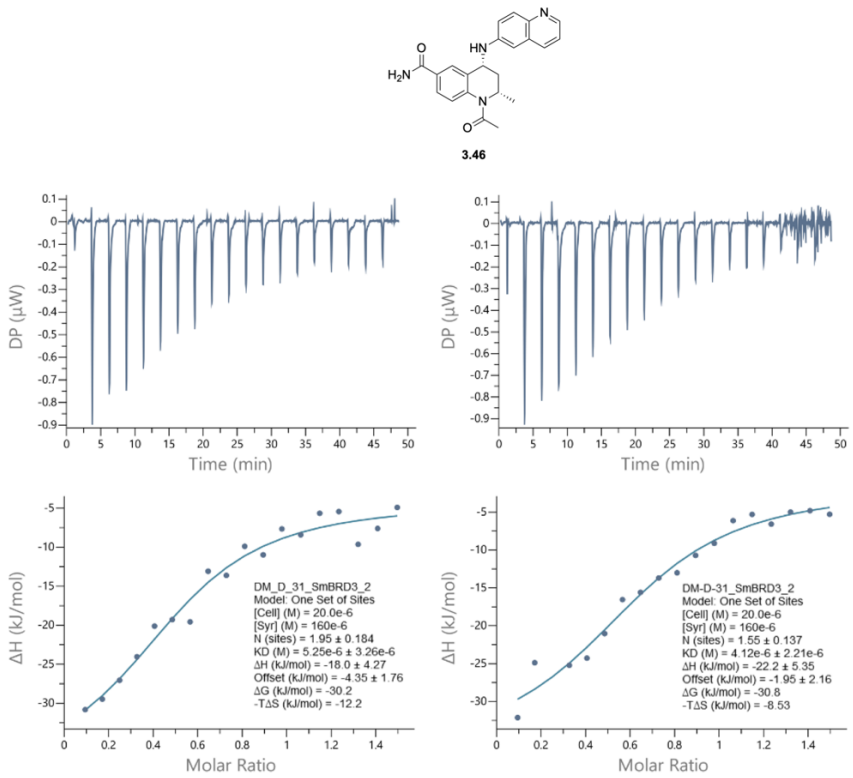


Figure S23. ITC traces of **3.46** and *Sm*BRD3(2).

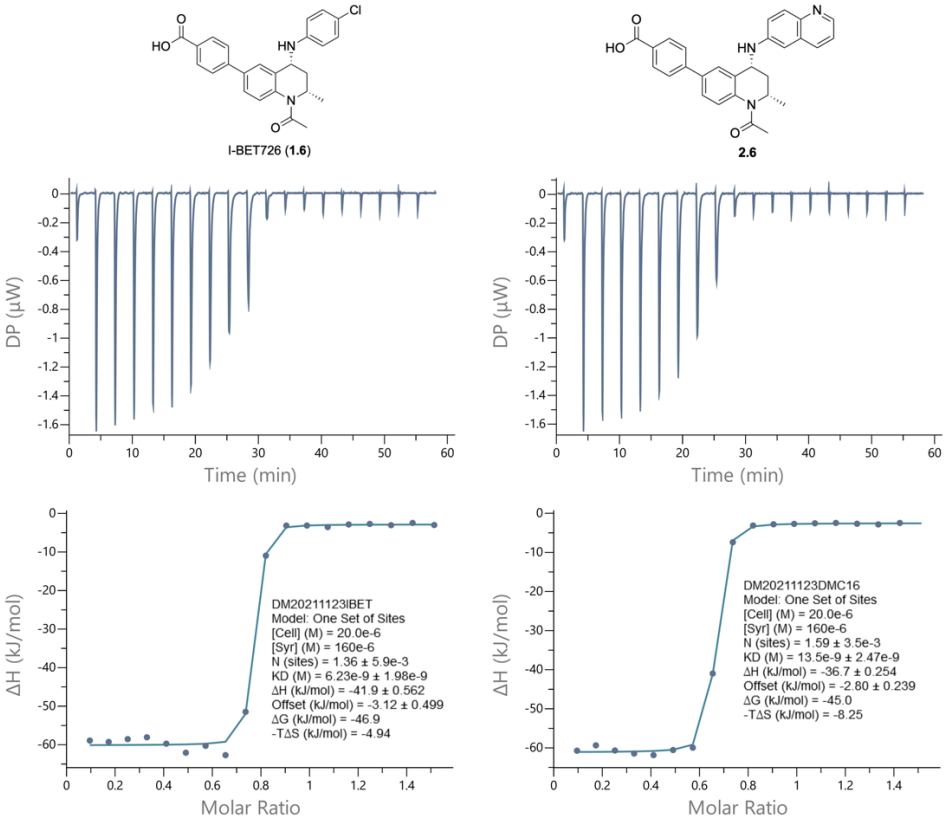


Figure S24. ITC traces of I-BET726 **(1.6)** and **2.6** binding to and *Hm*BRD4(1).

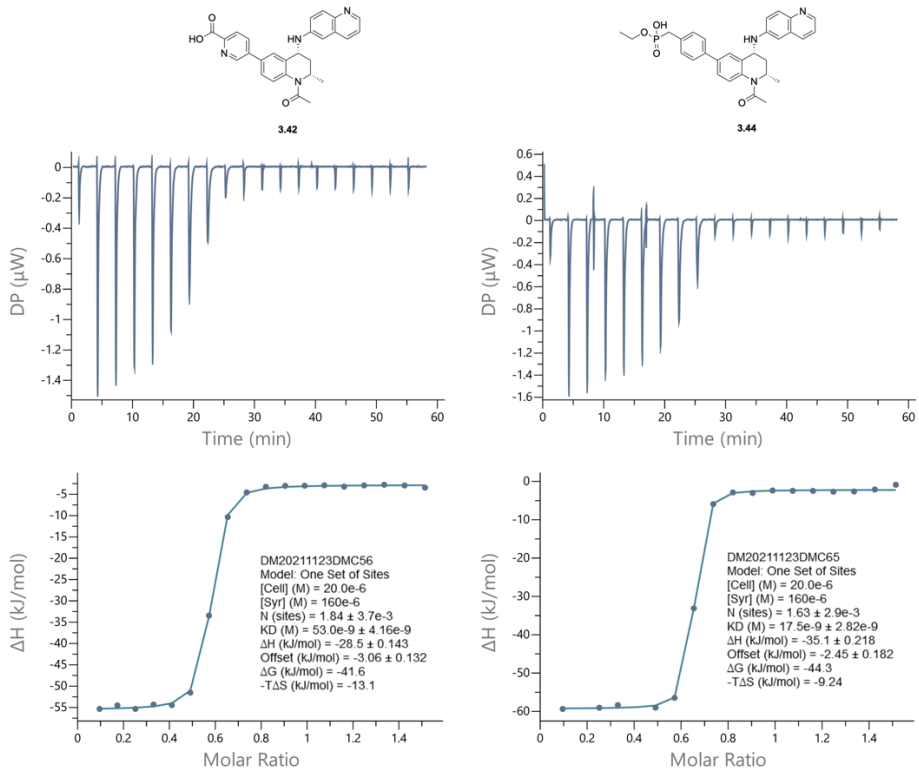


Figure S25. ITC traces of **3.42** and **3.44** binding to and *Hm*BRD4(1).

B3: Chapter 4 ITC data

Table S4. K_d values and the corresponding N numbers of compounds **4.2** binding to *Sm*BRD3(1,2) and **4.2**, **4.5** and **4.6** binding to *Sm*BRD3(2). SEM refers to the standard error of the mean.

Binding to *Sm*BRD3(1,2)

	Repeat 1		Repeat 2		Repeat 3		Average		95% CI	
Compound	K_d (nM)	N	K_d (nM)	N	K_d (nM)	N	K_d (nM)	N	K_d	N
4.2	2280 ± 345	5.97 ± 8.1e-2	3390 ± 663	5.80 ± 0.117	-	-	2835	5.89	1088	0.167

Binding to *Sm*BRD3(2)

	Repeat 1		Repeat 2		Repeat 3		Average		95% CI	
Compound	K_d (nM)	N	K_d (nM)	N	K_d (nM)	N	K_d (nM)	N	K_d	N
4.2	No binding	-	-	-	-	-	-	-	-	-
4.5	243 ± 45.1	1.24 ± 1.3e-2	282 ± 57.5	1.55 ± 1.9e-2	-	-	263	1.40	38.2	0.304
4.6	No binding	n/a	-	-	-	-	No binding	n/a	n/a	n/a

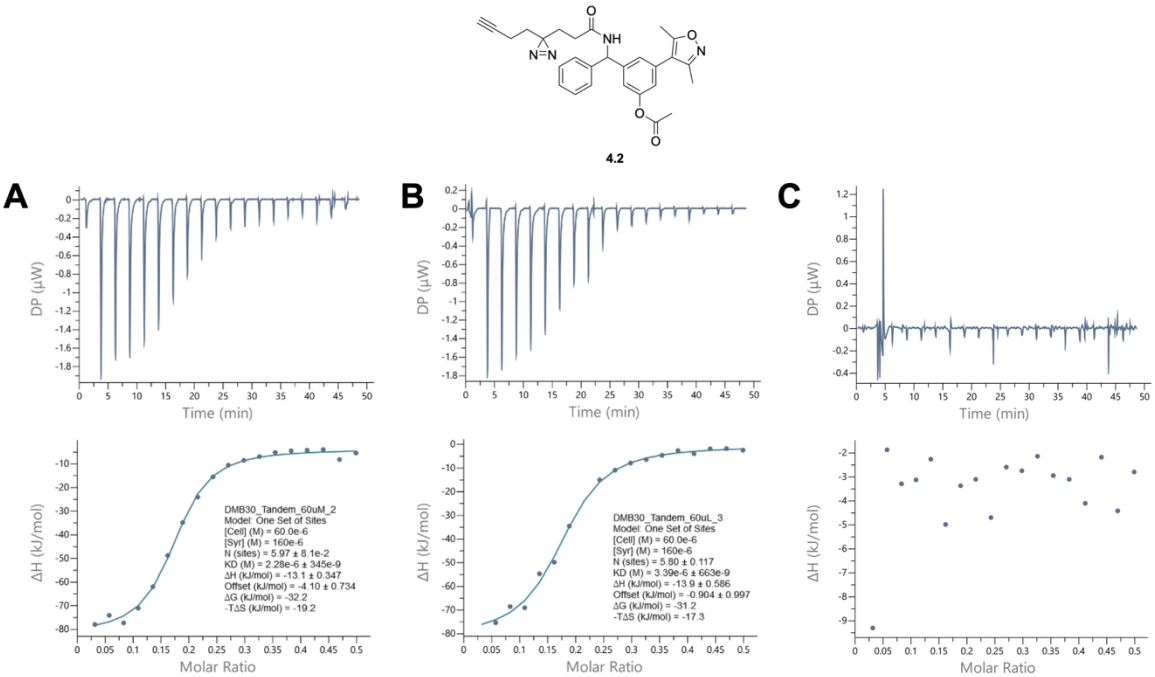


Figure S26. A) and **B)** ITC traces of **4.2** binding to *Sm*BRD3(1,2). B) ITC trace of **4.2** and *Sm*BRD3(2).

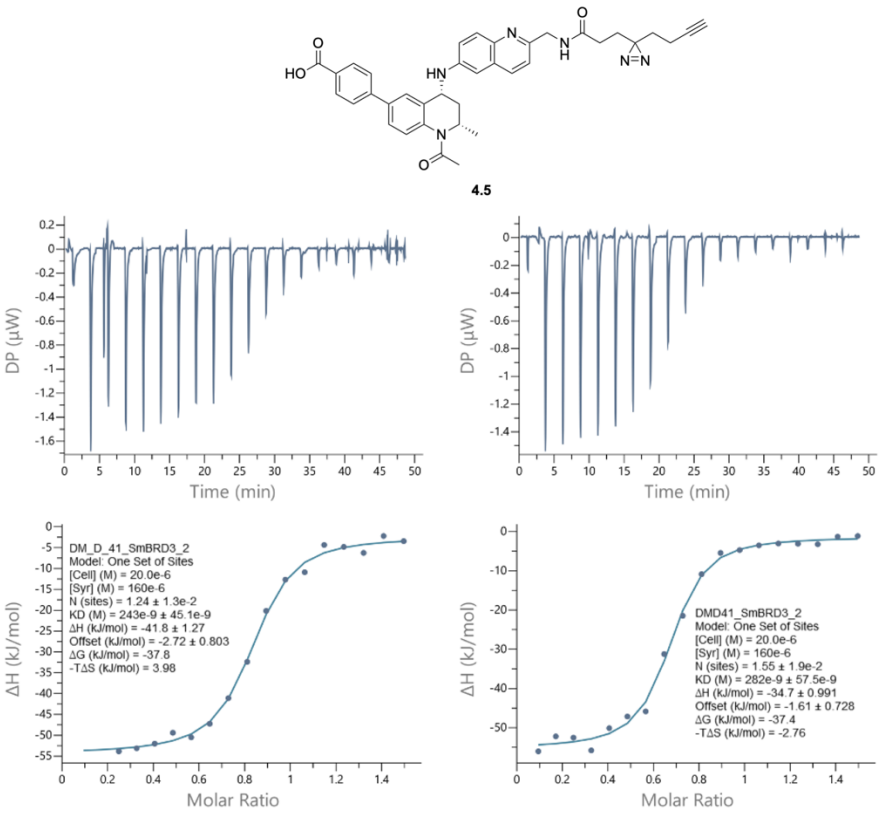


Figure S27. ITC traces of **4.5** binding to *Sm*BRD3(2).

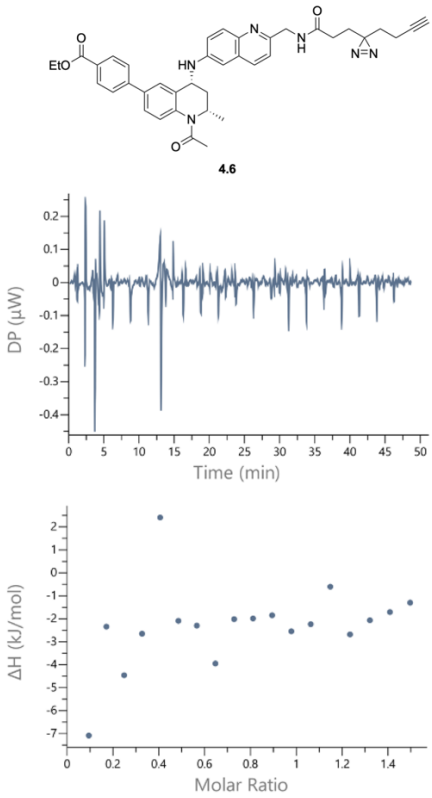


Figure S28. ITC trace of **4.6** and *Sm*BRD3(2).

Appendix C: In Vitro crosslinking to recombinant protein

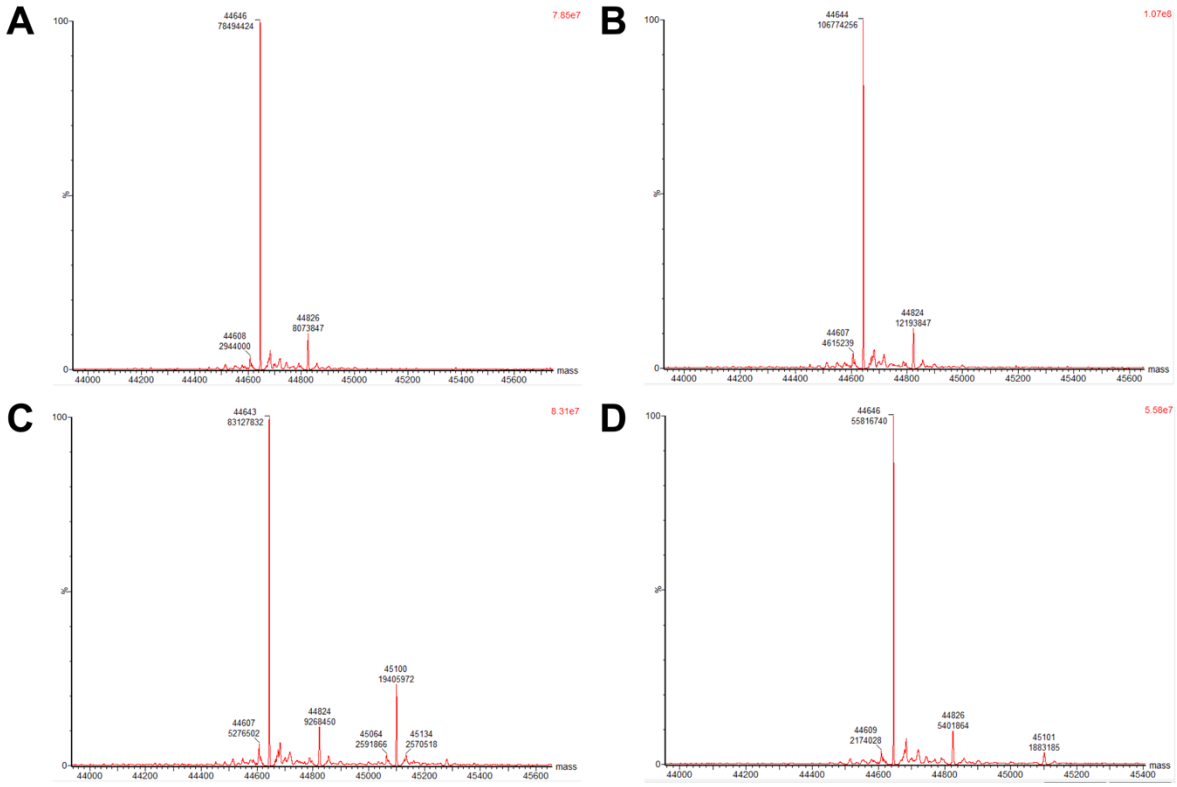


Figure S29. Deconvoluted mass spectra of *Sm*BRD3(1,2) after 50 min incubation with DMSO or **4.2** at 4 °C, followed by 10 min irradiation with UV light (where indicated) at 365 nm at 4 °C. **A**) Incubation of *Sm*BRD3(1,2) (10 μM) with DMSO (0.5% *v/v*) followed by UV irradiation. **B**) Incubation of *Sm*BRD3(1,2) (10 μM) with **4.2** (20 μM) and no UV irradiation. **C**) Incubation of *Sm*BRD3(1,2) (10 μM) with **4.2** (20 μM) and UV irradiation. **D**) Incubation of *Sm*BRD3(1,2) (10 μM) with **4.2** (20 μM) and OXFBD02 (**1.4**) (200 μM) and UV irradiation. *Sm*BRD3(1,2) (expected MW = 44644 Da), *Sm*BRD3(1,2) **4.2** adduct (expected MW = 45100 Da).

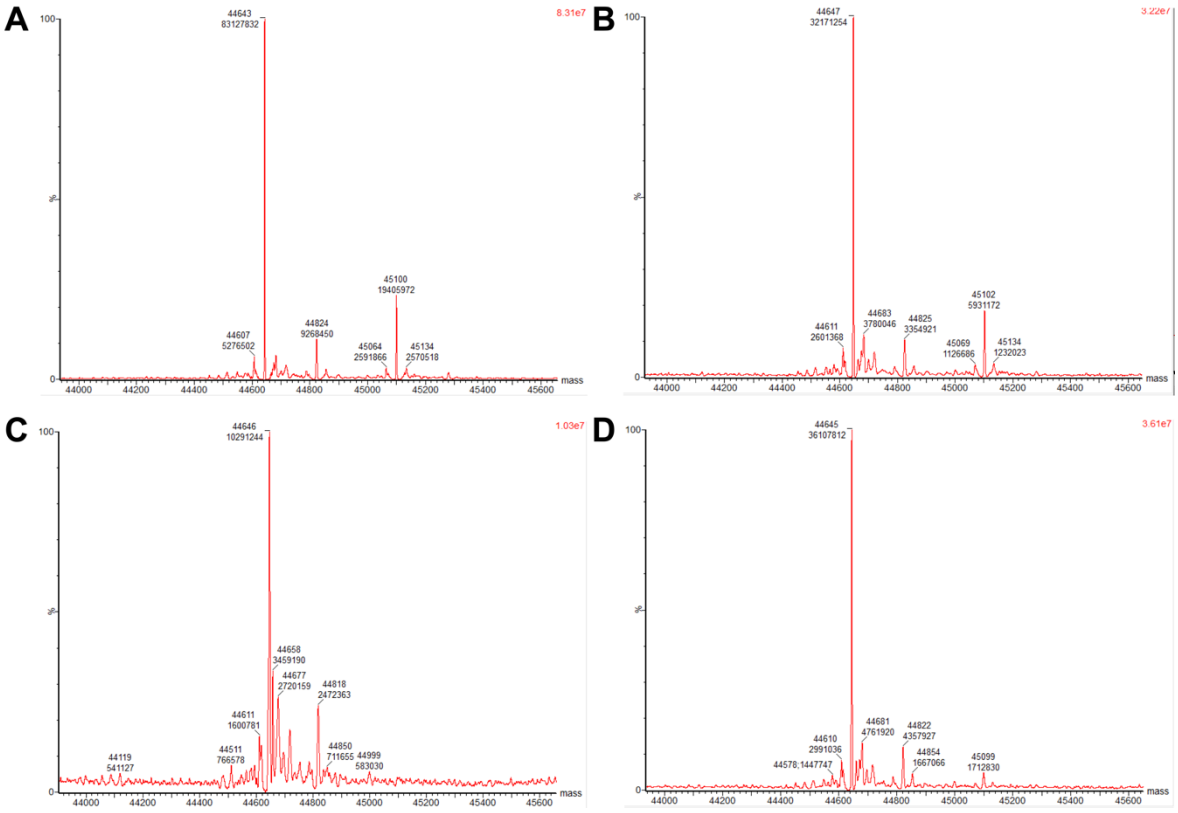


Figure S30. Deconvoluted mass spectra of *Sm*BRD3(1,2) after 50 min incubation of *Sm*BRD3(1,2) (10 μM) with **4.2** (20 μM) and **2.6** (where indicated) at 4 °C, followed by 10 min irradiation with UV light at 365 nm at 4 °C. **A**) No incubation with **2.6**; **B**) Incubation with **2.6** (10 μM); **C**) Incubation with **2.6** (20 μM). **D.** Incubation with **2.6** (40 μM). *Sm*BRD3(1,2) (expected MW = 44644 Da), *Sm*BRD3(1,2) **4.2** adduct (expected MW = 45100 Da).

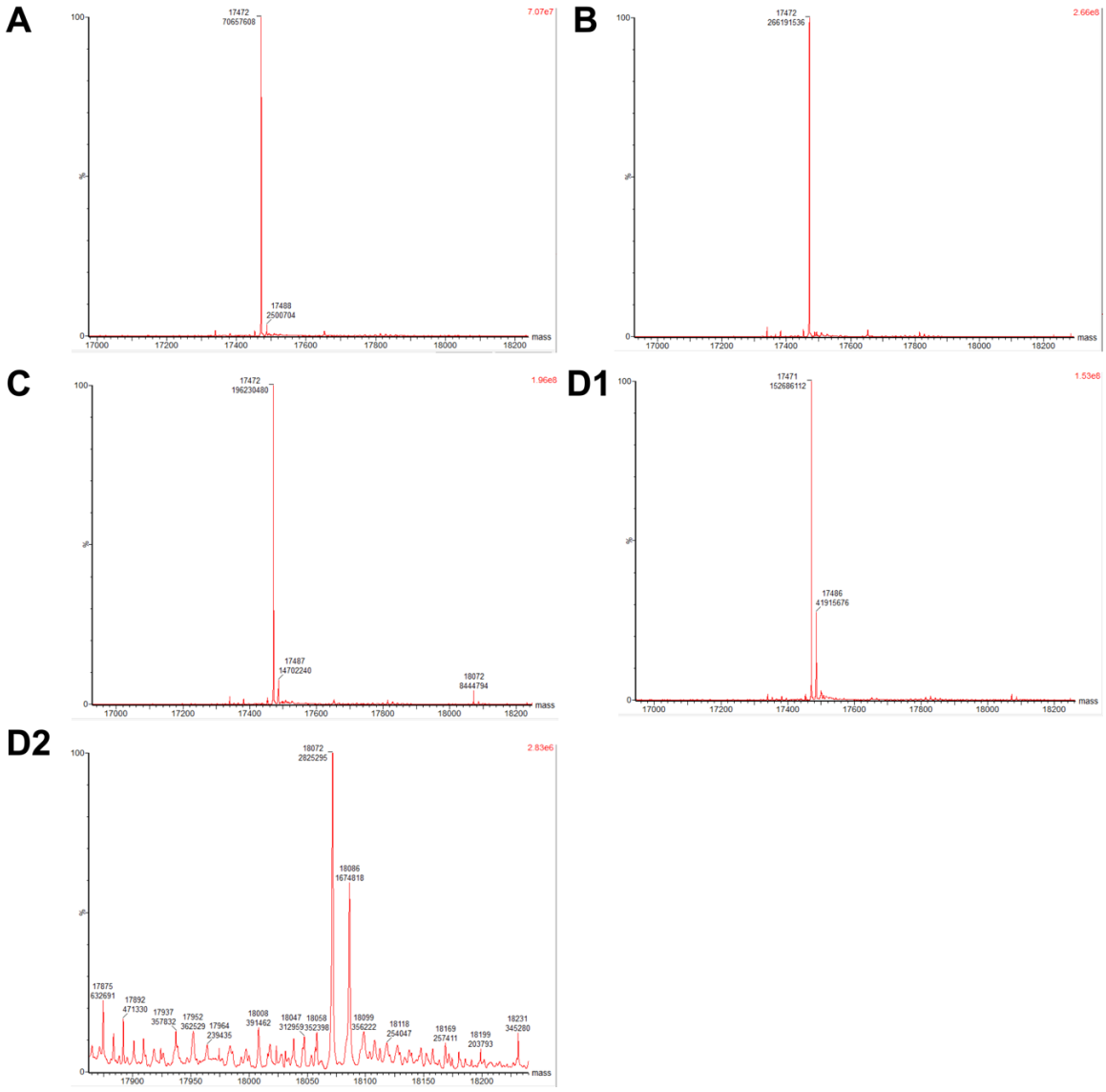


Figure S31. Deconvoluted mass spectra of *Sm*BRD3(2) after 50 min incubation at 4 °C followed by 10 min irradiation with UV light (where indicated) at 365 nm at 4 °C. **A**) Incubation of *Sm*BRD3(2) (10 μM) with DMSO (0.5% *v/v*) followed by UV irradiation. **B**) Incubation of *Sm*BRD3(2) (10 μM) with **4.5** (20 μM) and no UV irradiation. **C**) Incubation of *Sm*BRD3(2) (10 μM) with **4.5** (20 μM) and UV irradiation. **D1 and 2**) Incubation of *Sm*BRD3(2) (10 μM) with **4.5** (20 μM) and **2.6** (200 μM) and UV irradiation. The expected molecular weights of *Sm*BRD3(2) and the **4.5** *Sm*BRD3(2) adduct are 17472 Da and 18072 Da respectively.

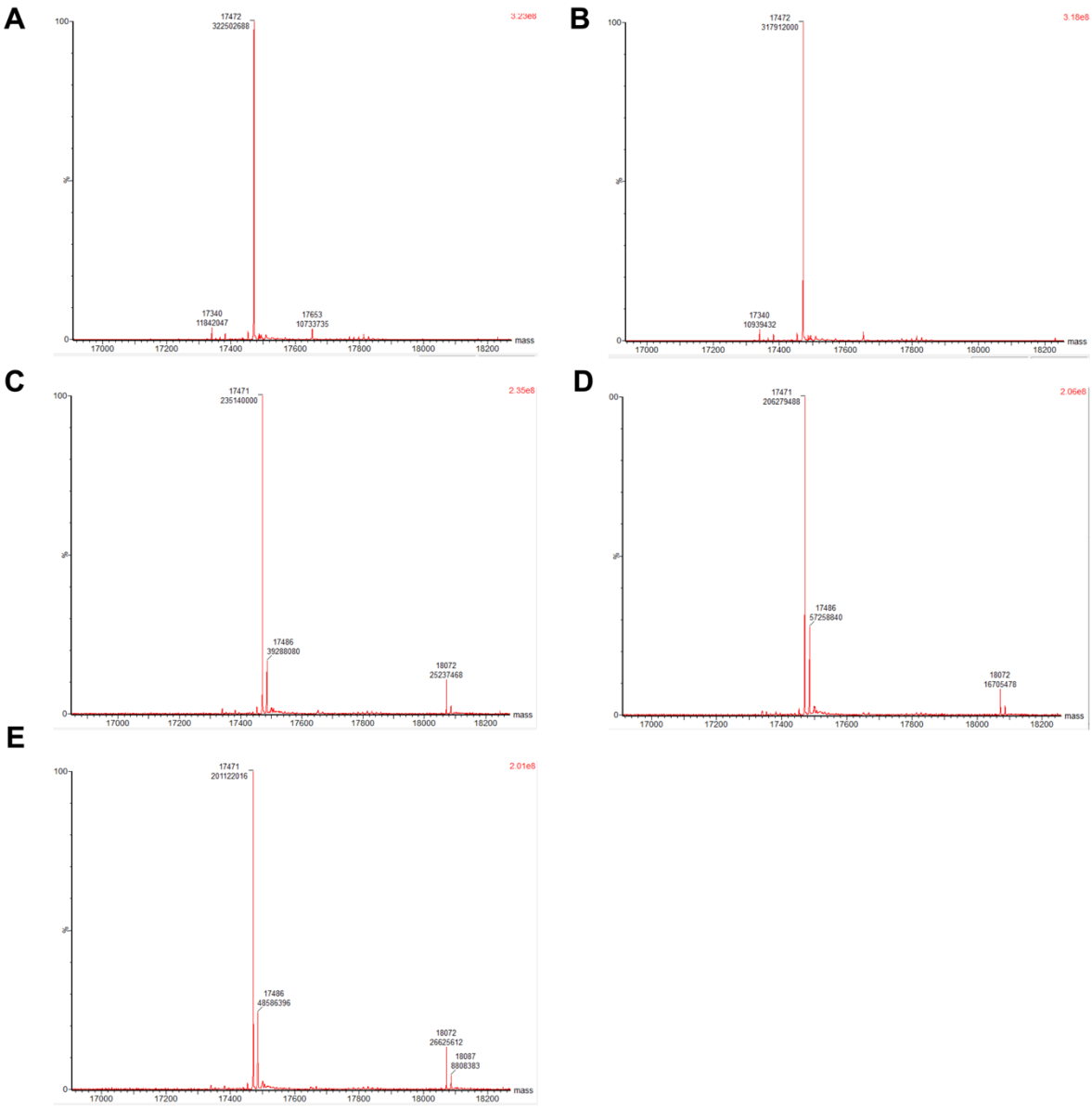


Figure S32. Deconvoluted mass spectra of *Sm*BRD3(2) after 50 min incubation at 4 °C followed by 10 min irradiation with UV light (where indicated) at 365 nm at 4 °C. **A**) Incubation of *Sm*BRD3(2) (10 μM) with DMSO (0.5% *v/v*) followed by UV irradiation; **B**) Incubation of *Sm*BRD3(2) (10 μM) with **4.5** (100 μM) and no UV irradiation; **C**) Incubation of *Sm*BRD3(2) (10 μM) with **4.5** (100 μM) and UV irradiation; **D**) Incubation of *Sm*BRD3(2) (10 μM) with **4.5** (20 μM) and **2.6** (150 μM) and UV irradiation. **E**) Incubation of *Sm*BRD3(2) (10 μM) with **4.5** (20 μM) and OXFBD02 (**1.4**) (150 μM) and UV irradiation.

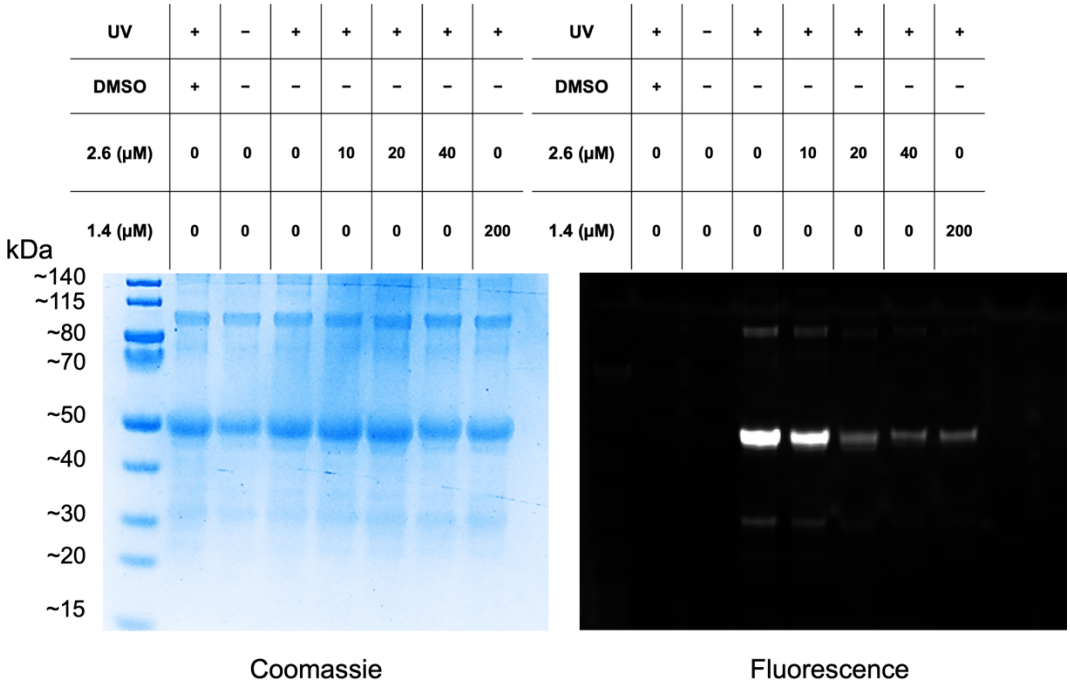


Figure S33. Coomassie and in-gel fluorescence analysis of *Sm*BRD3(1,2) separated by SDS-PAGE after 50 min incubation at 4 °C with DMSO or **4.2** (20 μM), with or without a competitor (**1.4** or **2.6**), followed by 10 min irradiation with UV light (where indicated) at 365 nm at 4 °C, and copper catalysed click reaction with Azide fluor-545 (**4.36**).

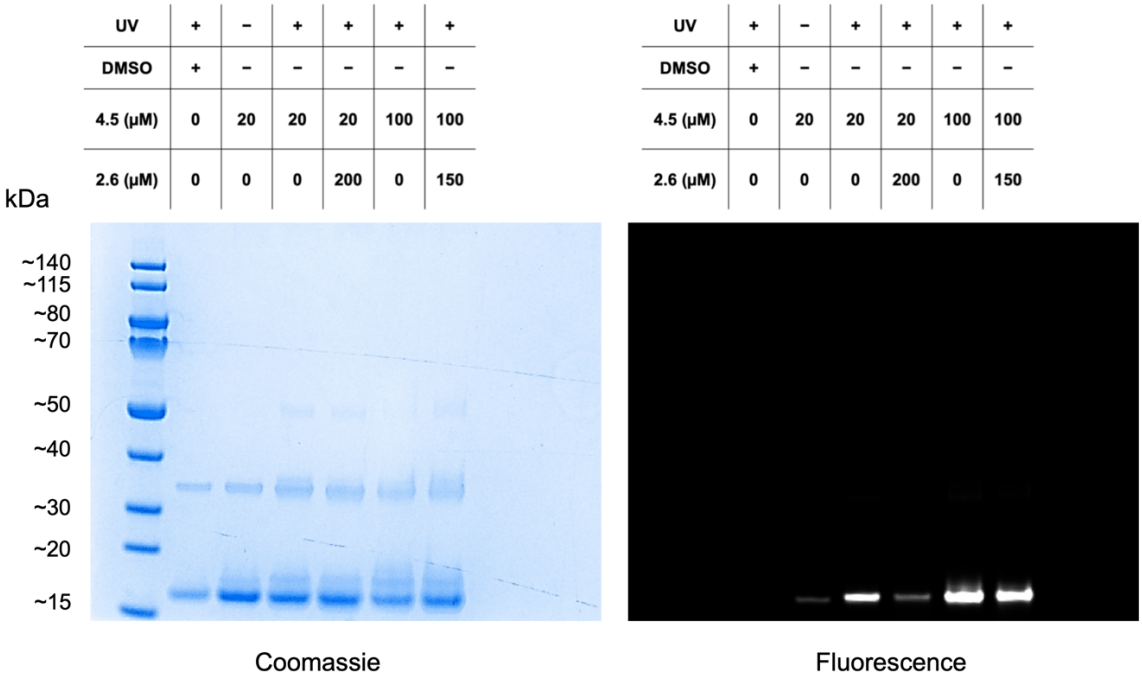


Figure S34. Coomassie and in-gel fluorescence analysis of *Sm*BRD3(2) after 50 min incubation at 4 °C with DMSO or **4.5**, with a competitor (**2.6**) where stated, followed by 10 min irradiation with UV light (where indicated) at 365 nm at 4 °C, and a CuAAC click reaction with Azide fluor-545 (**4.36**).

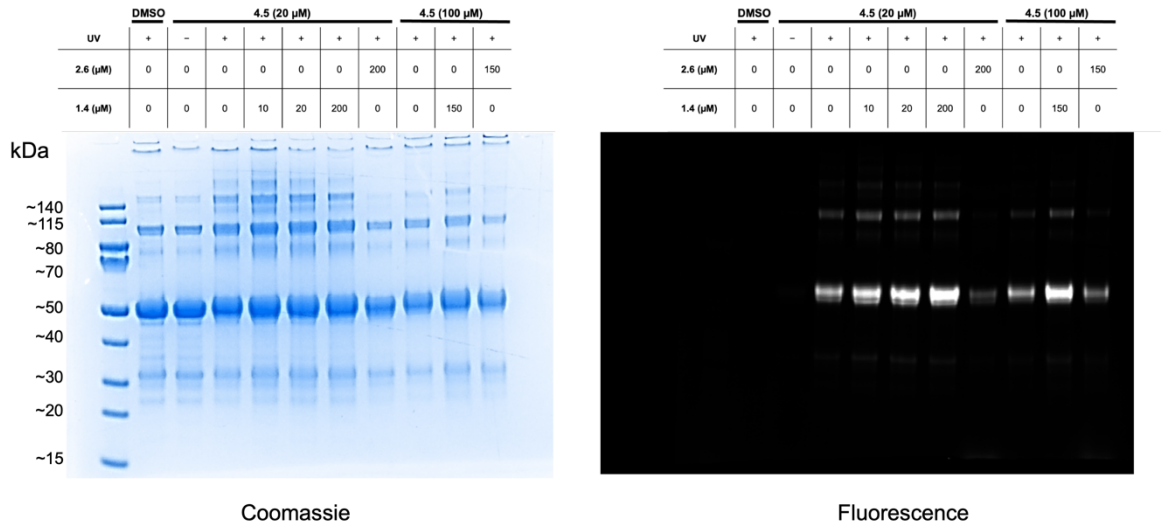


Figure S35. Coomassie and in-gel fluorescence analysis of *Sm*BRD3(1,2) after 50 min incubation at 4 °C with DMSO or **2.6**, with a competitor (**1.4** or **2.6**), followed by 10 min irradiation with UV light (where indicated) at 365 nm at 4 °C, and CuAAC reaction with Azide fluor-545 (**4.36**).

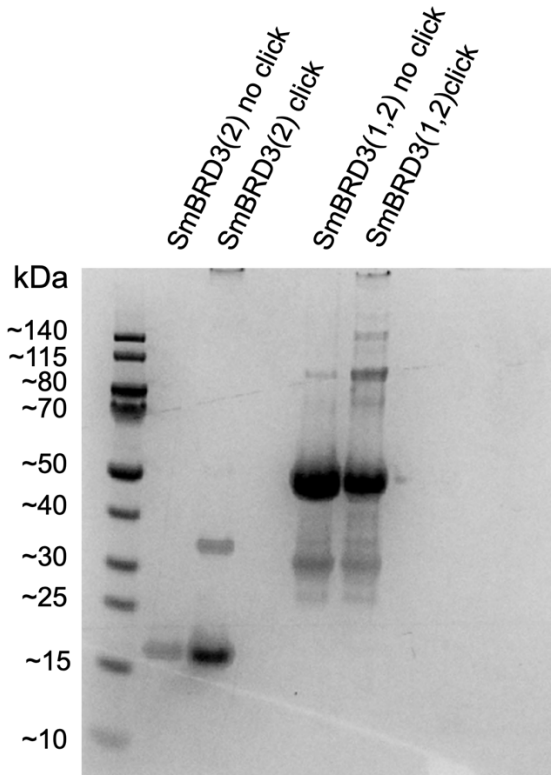


Figure S36. Control experiment to assess the stability of recombinant H6-SmBRD3(2) and H6-SmBRD3(1,2). Protein constructs (10 μM) were subject to CuAAC click conditions described in Chapter 6, section 6.3.8. These samples were separated by SDS-PAGE along with H6-SmBRD3(2) and H6-SmBRD3(1,2) which had not been subject to CuAAC conditions.

Appendix D: EC_{50} curves

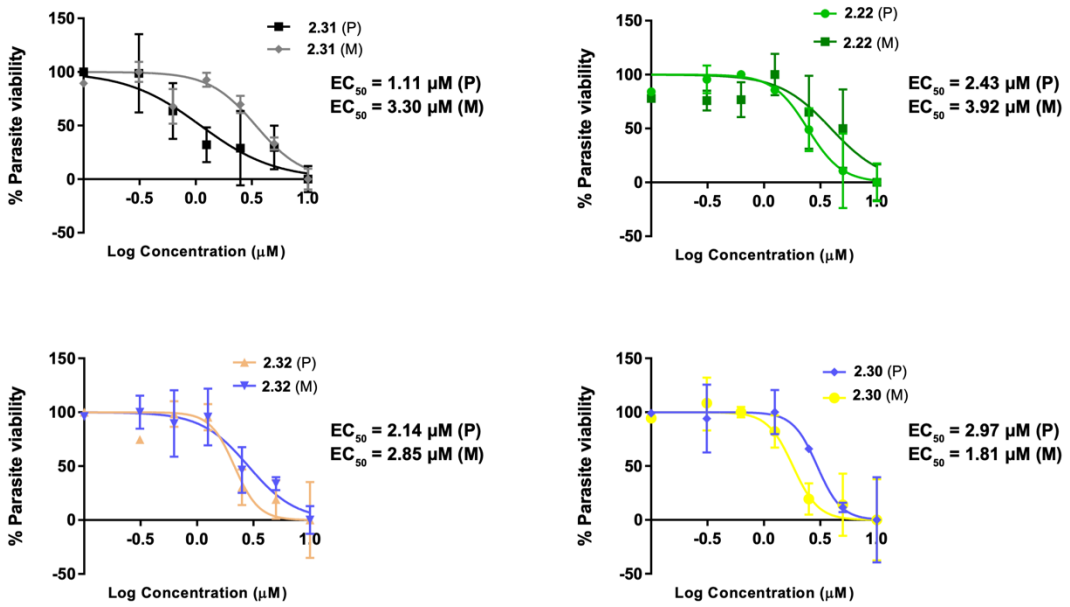


Figure S37. EC_{50} curves for the dose-dependent titration of compounds **2.22**, **2.30**, **2.31** and **2.32** on the phenotype (P) and motility (M) of schistosomula. The screening and EC50 calculations were carried out by Dr Gilda Padalino.

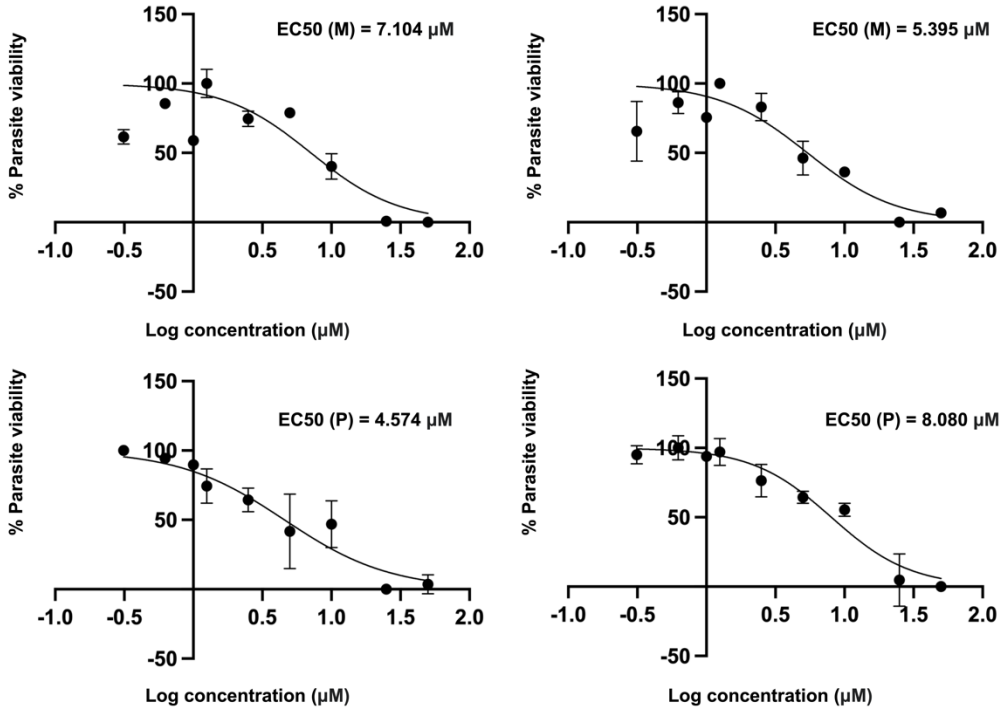


Figure S38. EC_{50} curves for the dose-dependent titration of compound **3.43** on the phenotype (P) and motility (M) of schistosomula, resulting from two independent screens. Screening was carried out by Dr Josephine Forde-Thomas.

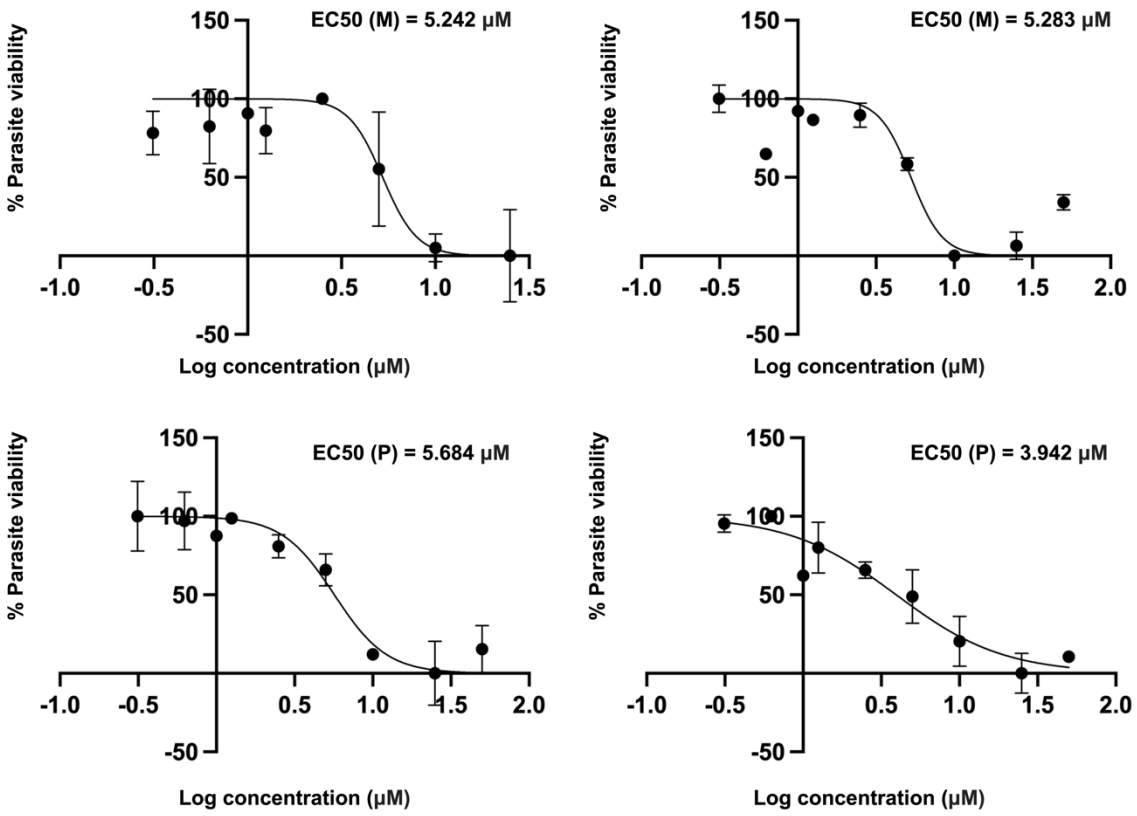
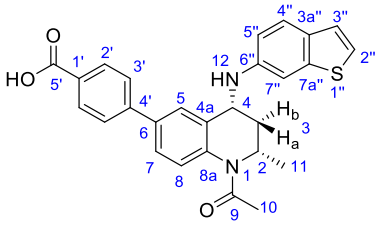
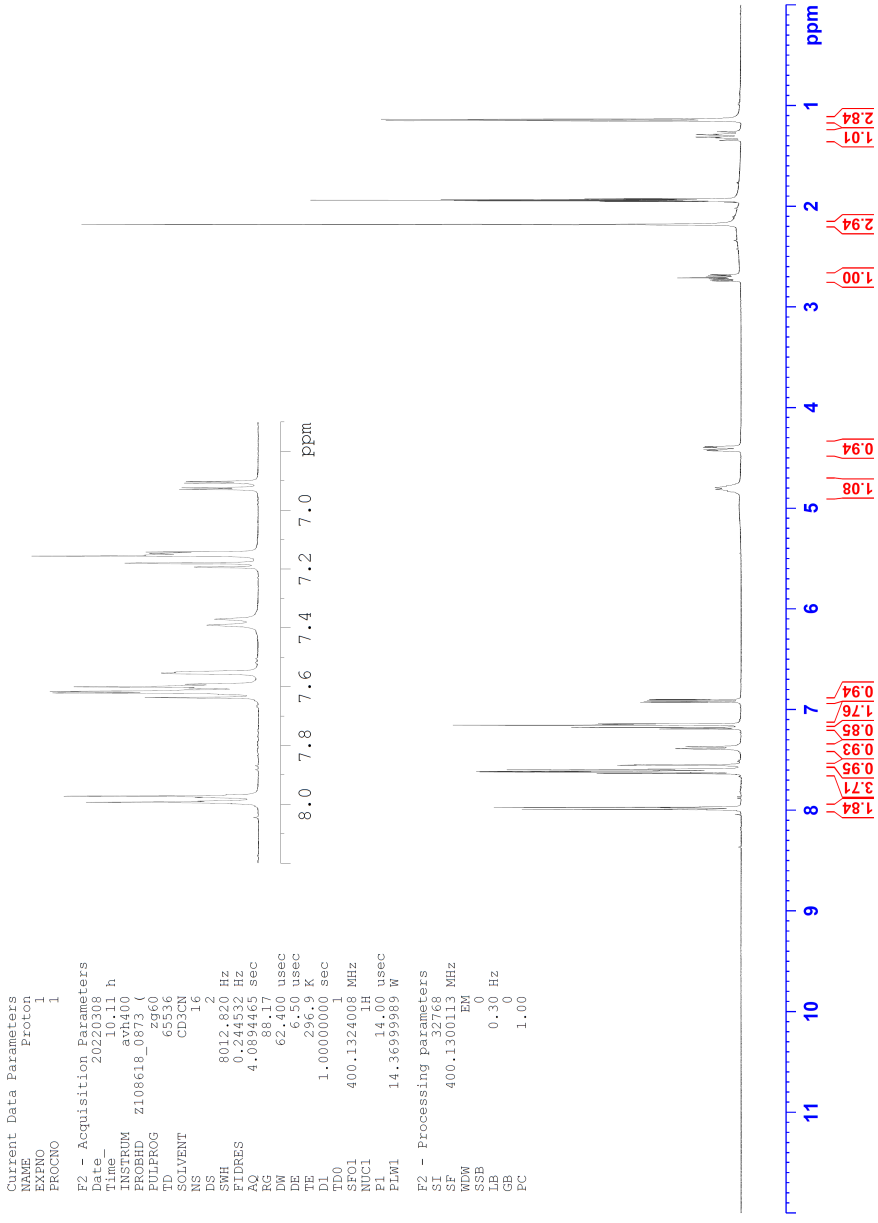


Figure S39. EC_{50} curves for the dose-dependent titration of compound **2.31** on the phenotype (P) and motility (M) of schistosomula, described in **Chapter 3**, resulting from two independent screens. Screening was carried out by Dr Josephine Forde-Thomas.

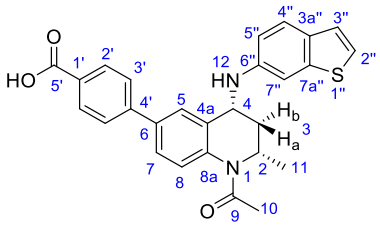
Appendix E: NMR Spectra of novel compounds

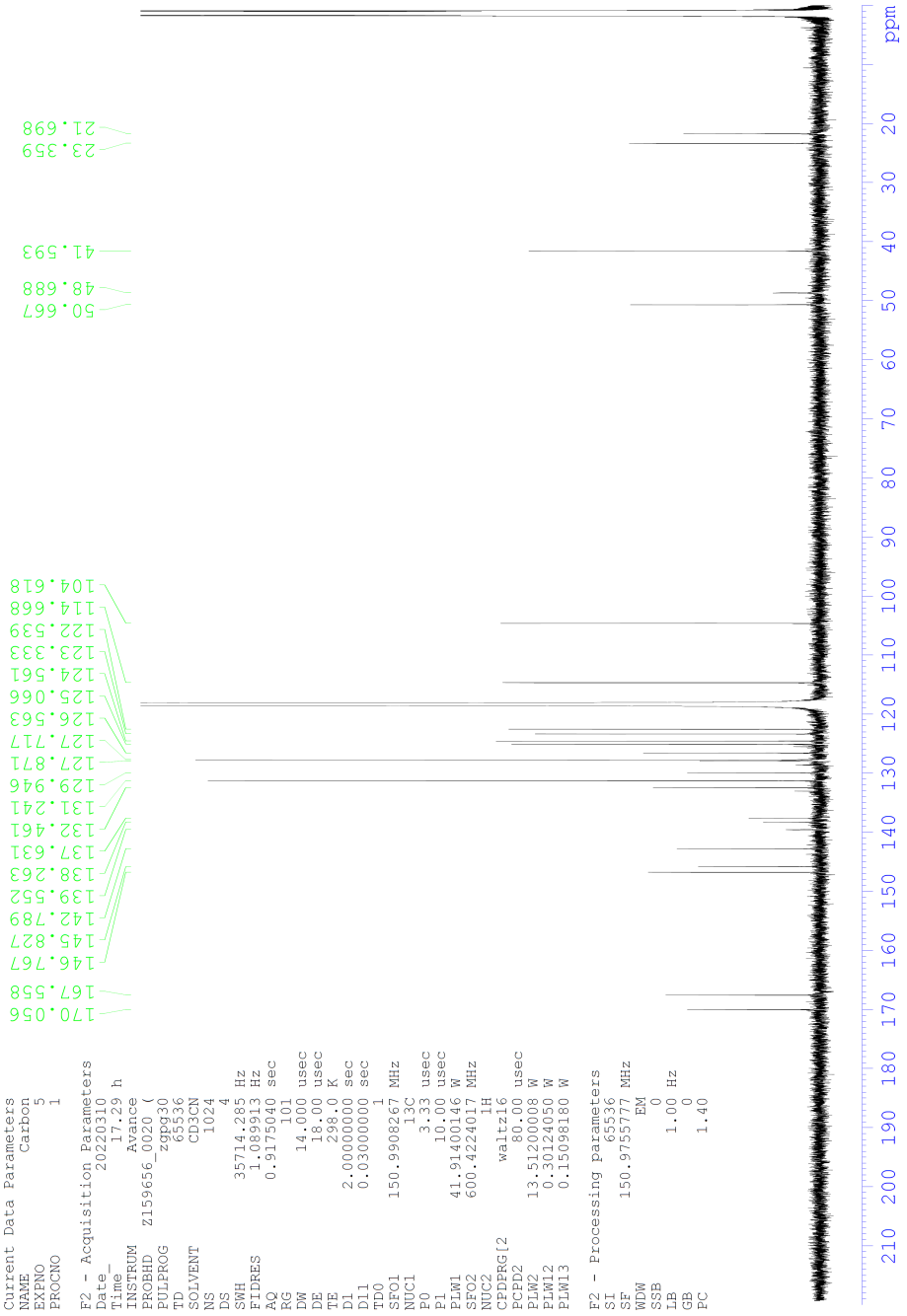
^{1}H NMR 4-{(2*S*,4*R*)-1-Acetyl-4-[(1-benzothiophen-6-yl)amino]-2-methyl-1,2,3,4-tetrahydroquinolin-6-yl}benzoic acid (2.1)



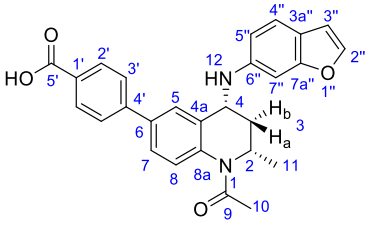


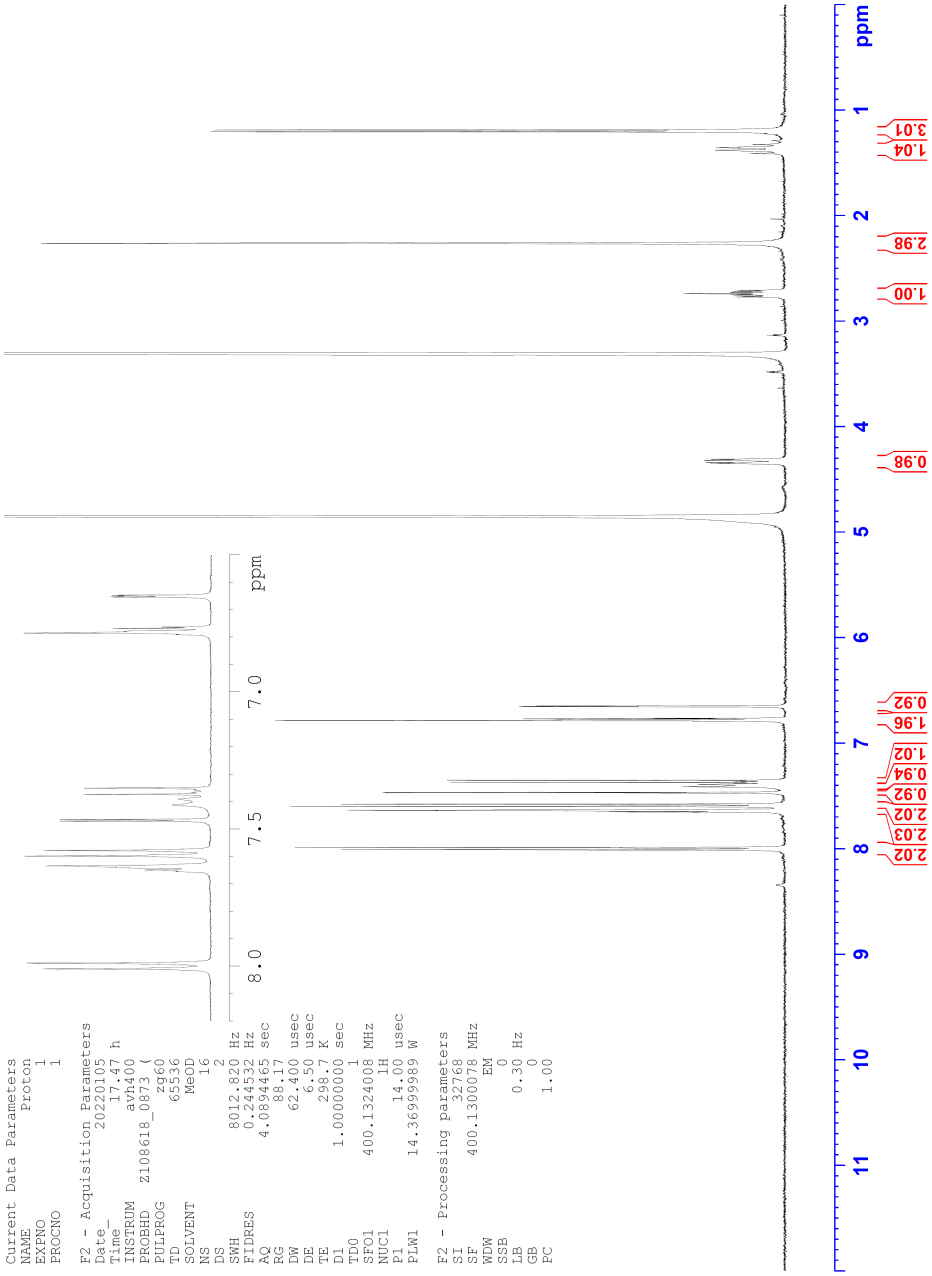
^{13}C NMR 4-{(2*S*,4*R*)-1-Acetyl-4-[(1-benzothiophen-6-yl)amino]-2-methyl-1,2,3,4-tetrahydroquinolin-6-yl}benzoic acid (2.1)



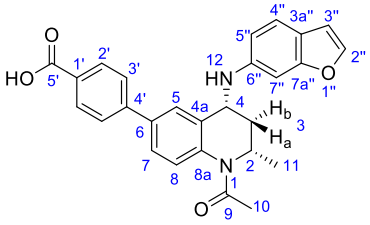


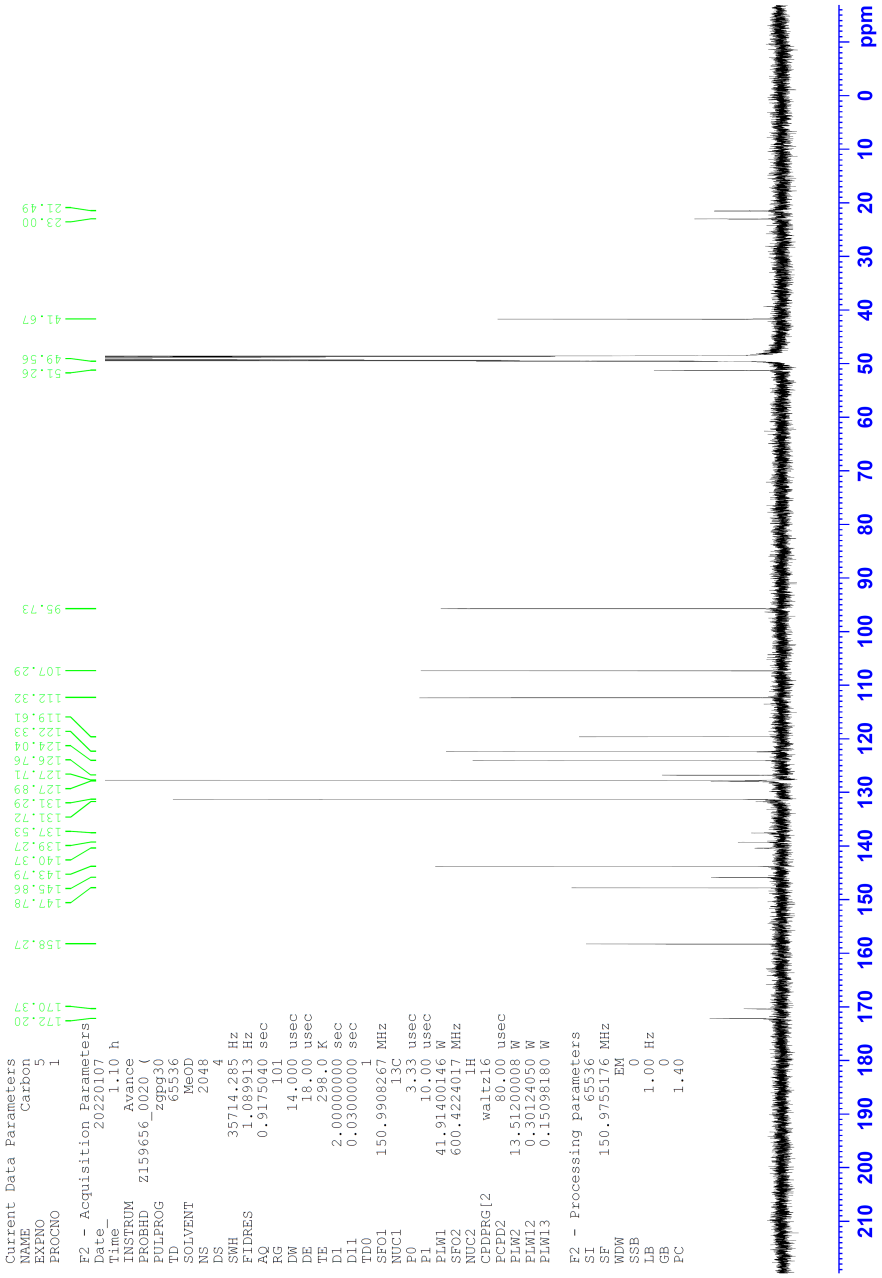
^{1}H NMR 4-((2*S*,4*R*)-1-Acetyl-4-[(1-benzofuran-6-yl)amino]-2-methyl-1,2,3,4-tetrahydroquinolin-6-yl)benzoic acid (2.2)



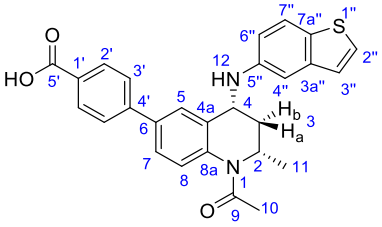


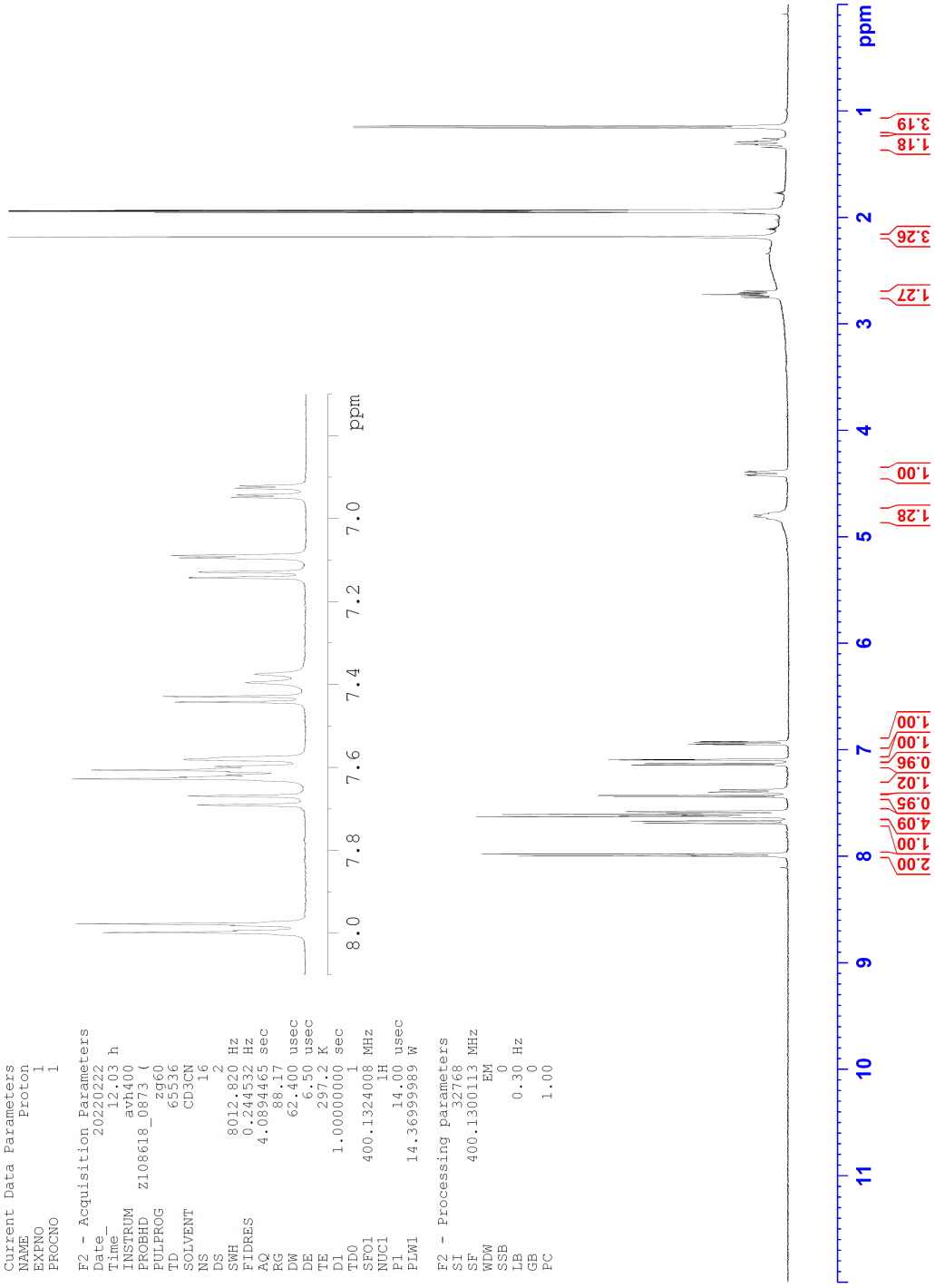
^{13}C NMR 4-((2*S*,4*R*)-1-Acetyl-4-[(1-benzofuran-6-yl)amino]-2-methyl-1,2,3,4-tetrahydroquinolin-6-yl)benzoic acid (2.2)



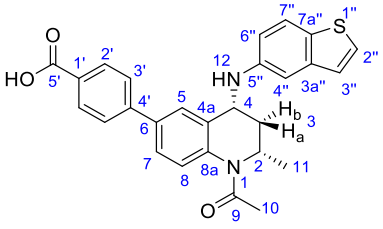


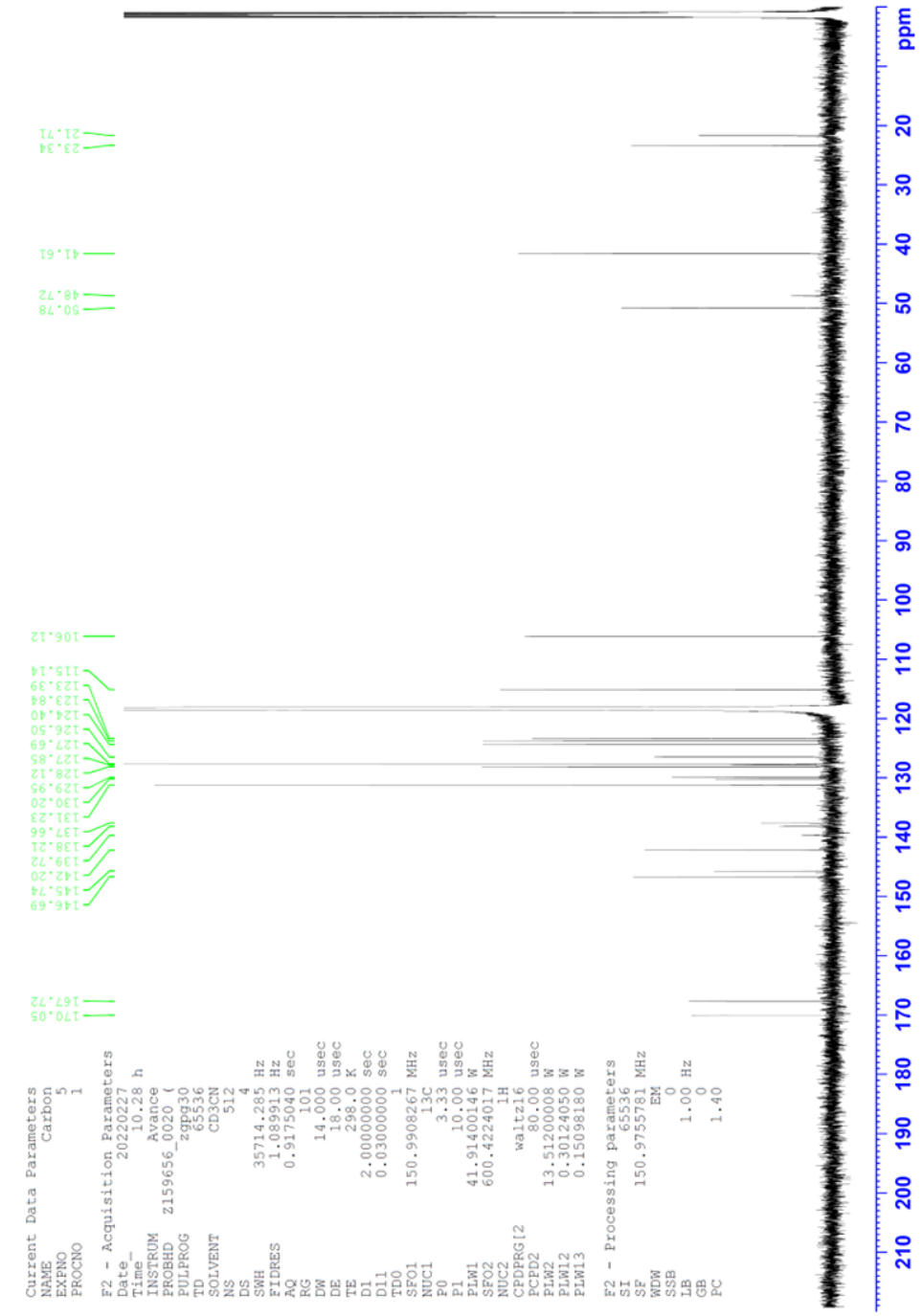
^{1}H NMR 4-((2*S*,4*R*)-1-Acetyl-4-[(1-benzothiophen-5-yl)amino]-2-methyl-1,2,3,4-tetrahydroquinolin-6-yl)benzoic acid (2.3)



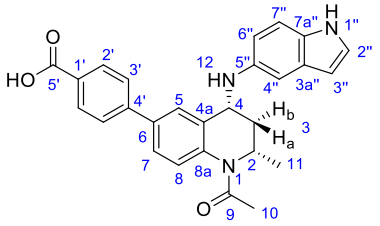


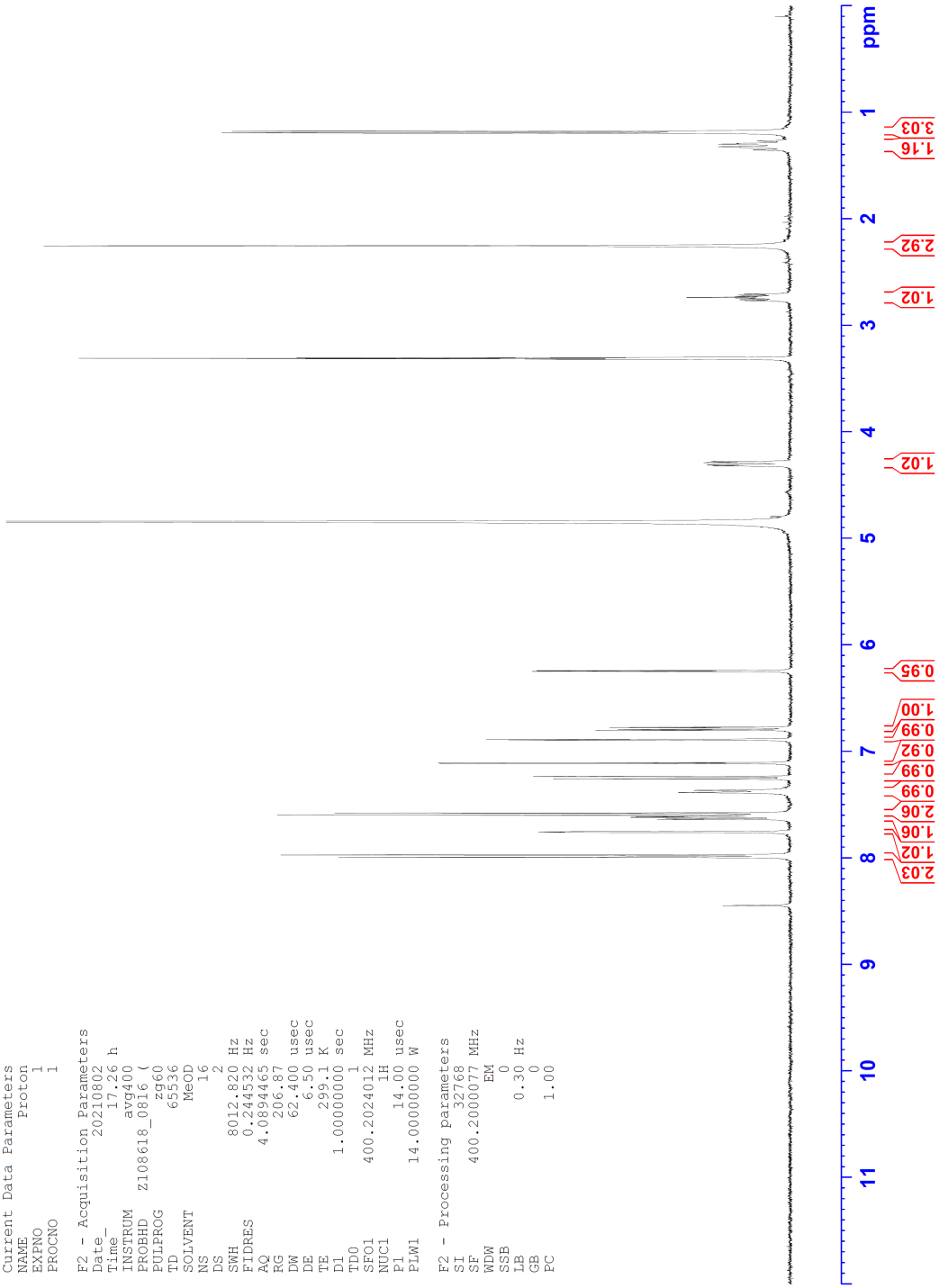
^{13}C NMR 4-((2*S*,4*R*)-1-Acetyl-4-[(1-benzothiophen-5-yl)amino]-2-methyl-1,2,3,4-tetrahydroquinolin-6-yl)benzoic acid (2.3)



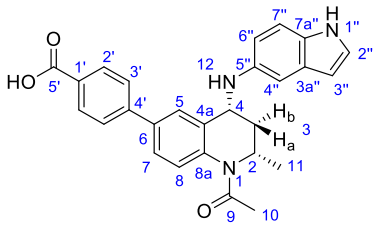


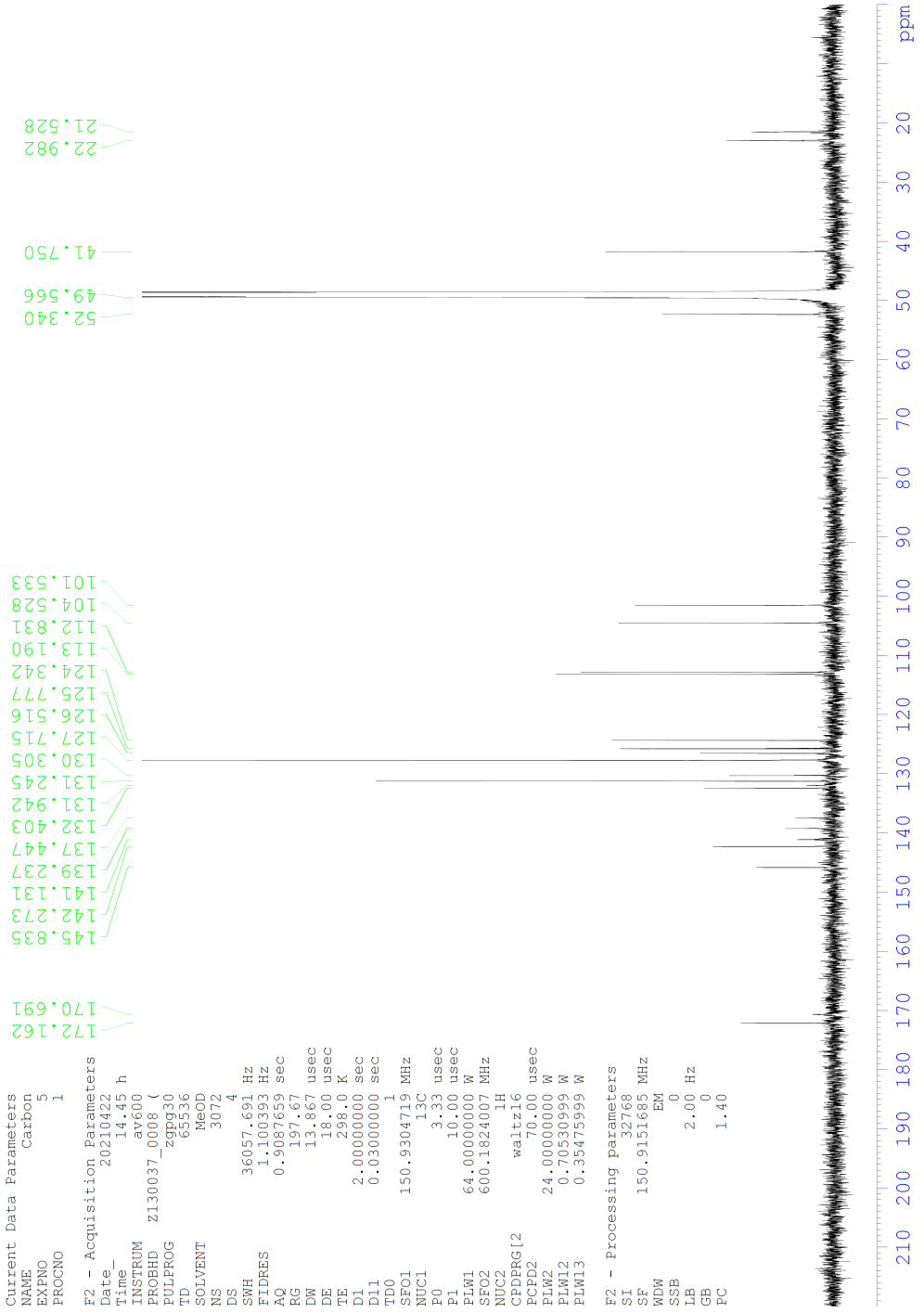
^{1}H NMR 4-{(2*S*,4*R*)-1-acetyl-4-[(1*H*-indol-5-yl)amino]-2-methyl-1,2,3,4-tetrahydroquinolin-6-yl}benzoic acid (2.4)



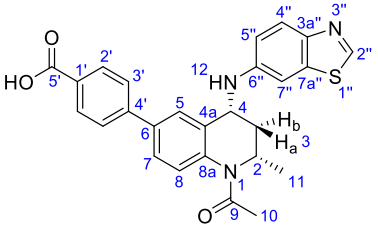


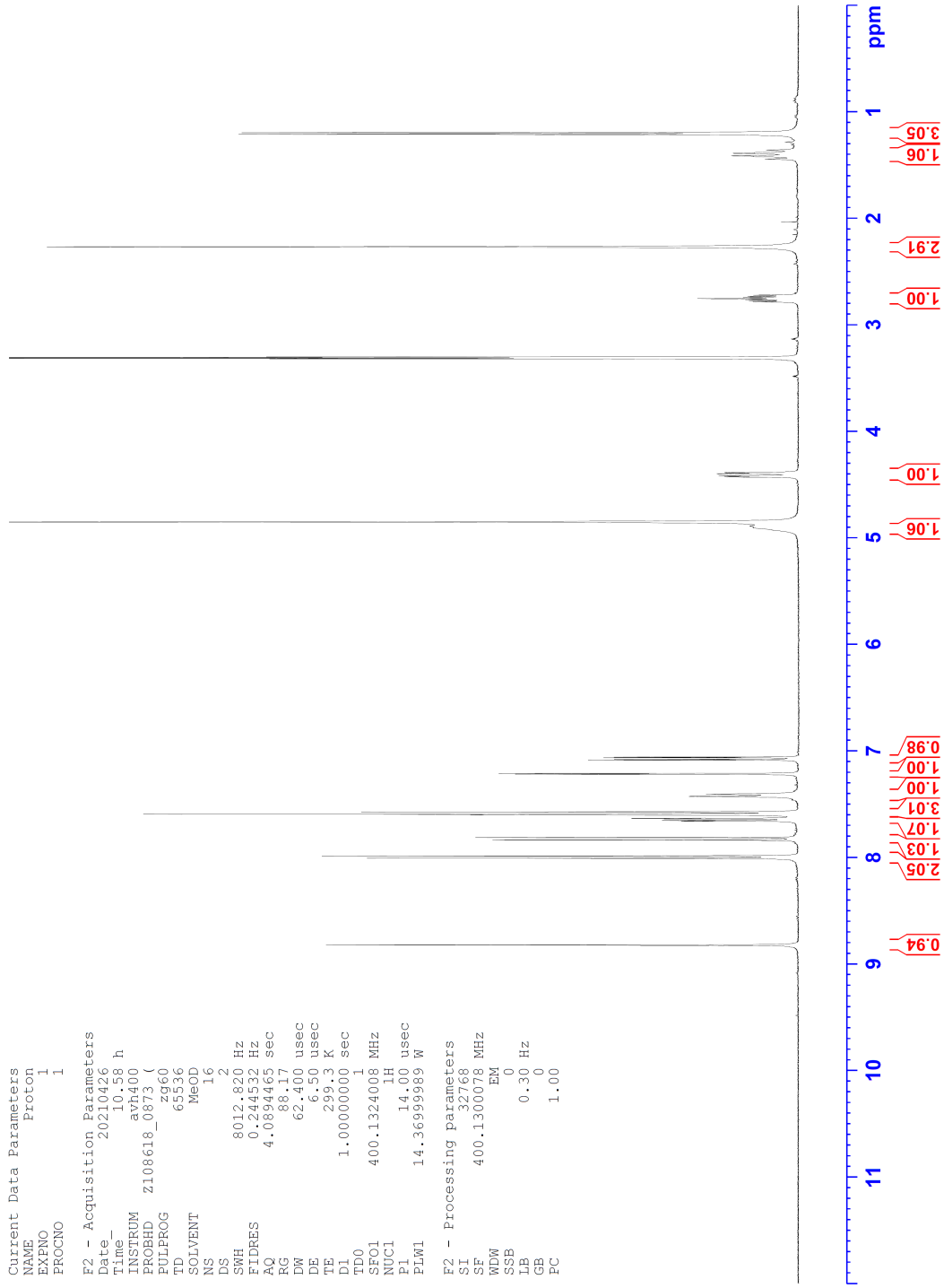
^{13}C NMR 4-{(2*S*,4*R*)-1-acetyl-4-[(1*H*-indol-5-yl)amino]-2-methyl-1,2,3,4-tetrahydroquinolin-6-yl}benzoic acid (2.4)



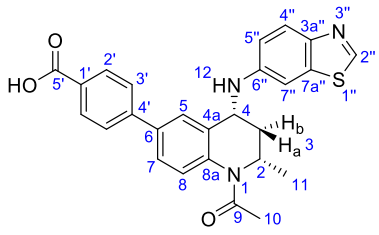


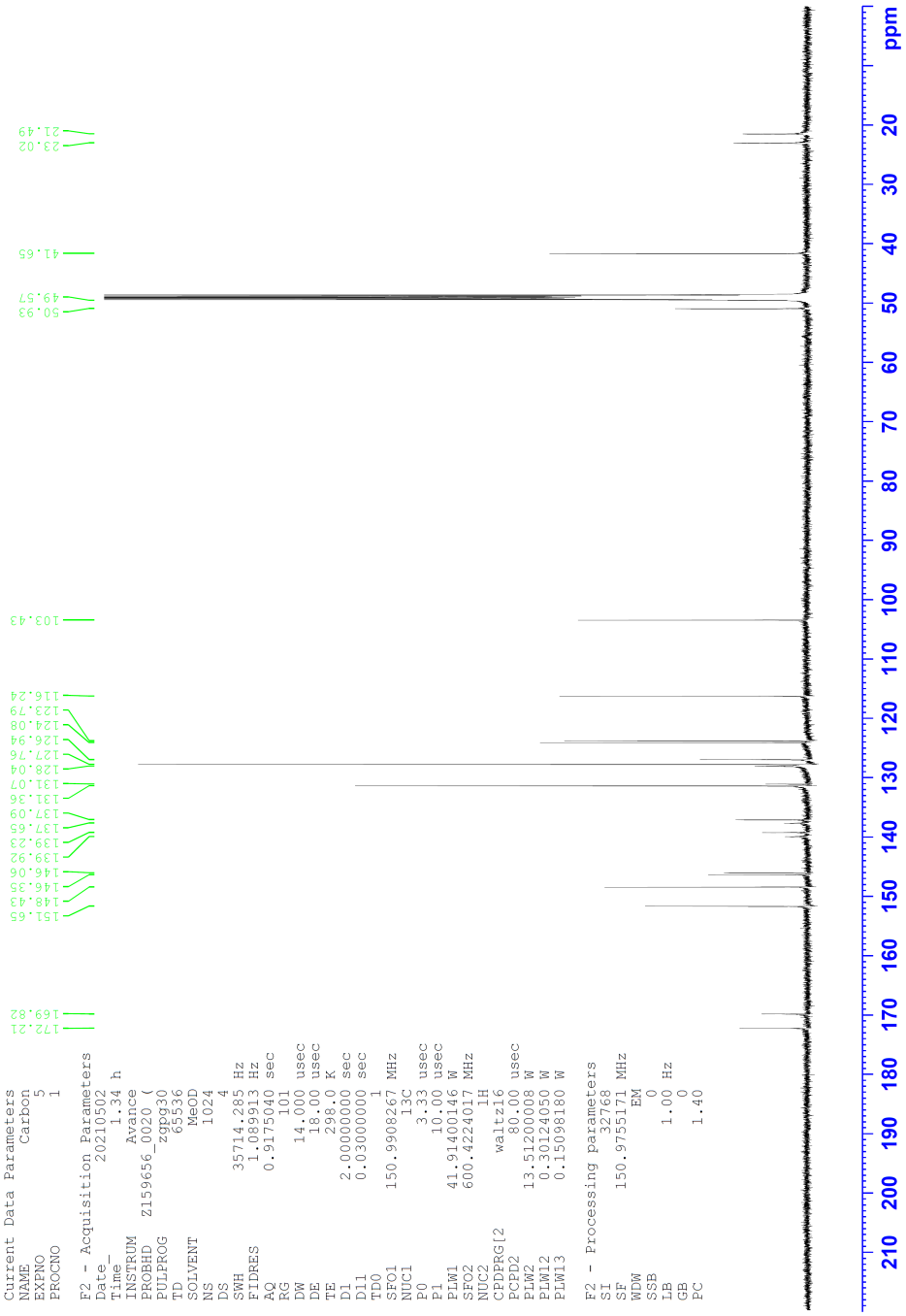
^{1}H NMR 4-{(2*S*,4*R*)1-Acetyl-4-[(1,3-benzothiazol-6-yl)amino]-2-methyl-1,2,3,4-tetrahydroquinolin-6-yl}benzoic acid (2.5)



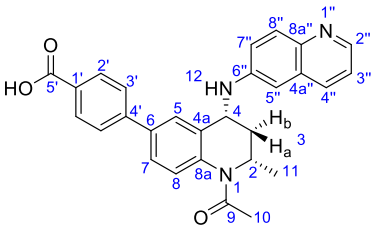


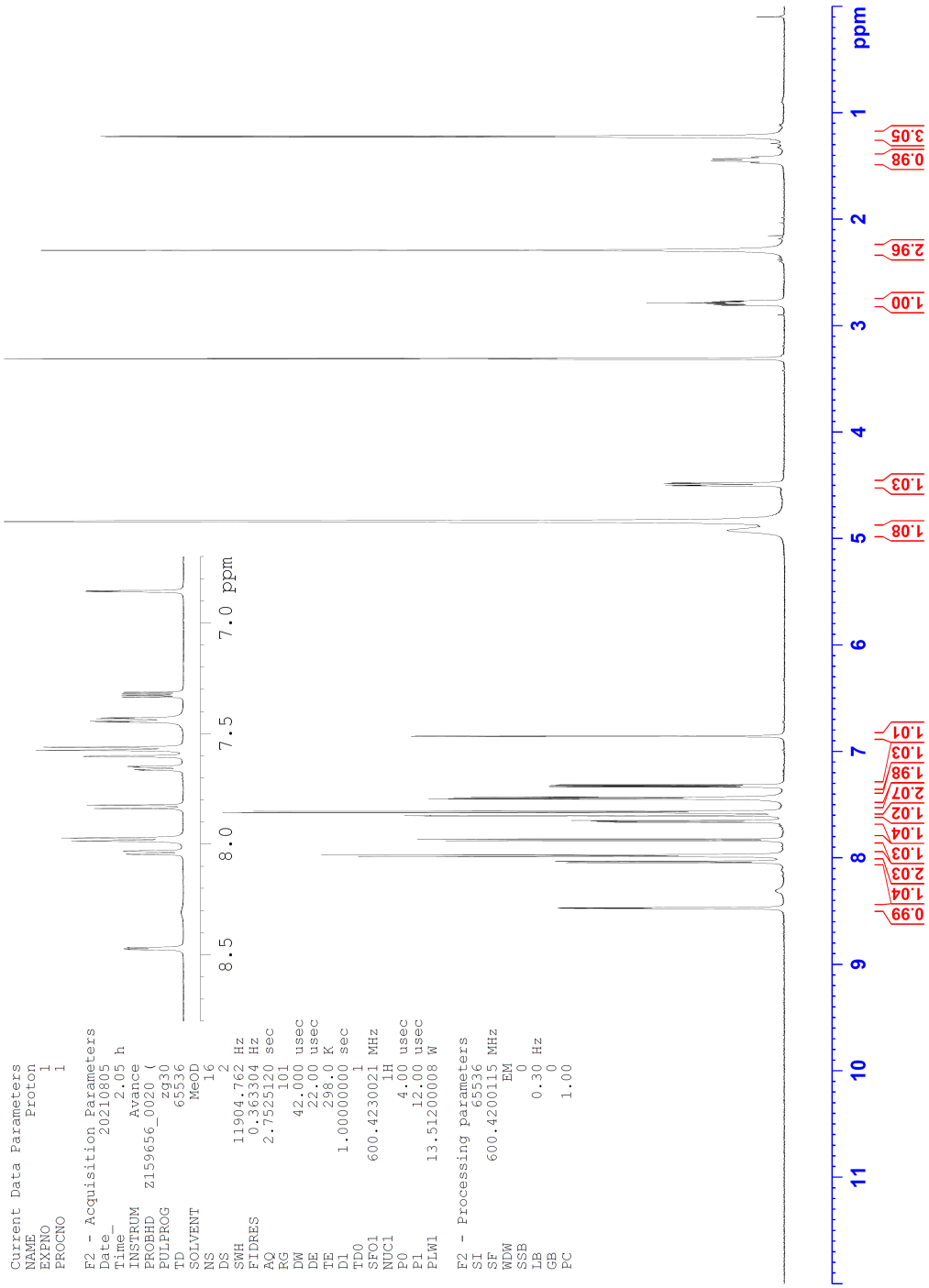
^{13}C NMR 4-{(2*S*,4*R*)1-Acetyl-4-[(1,3-benzothiazol-6-yl)amino]-2-methyl-1,2,3,4-tetrahydroquinolin-6-yl}benzoic acid (2.5)



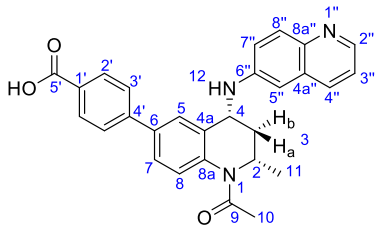


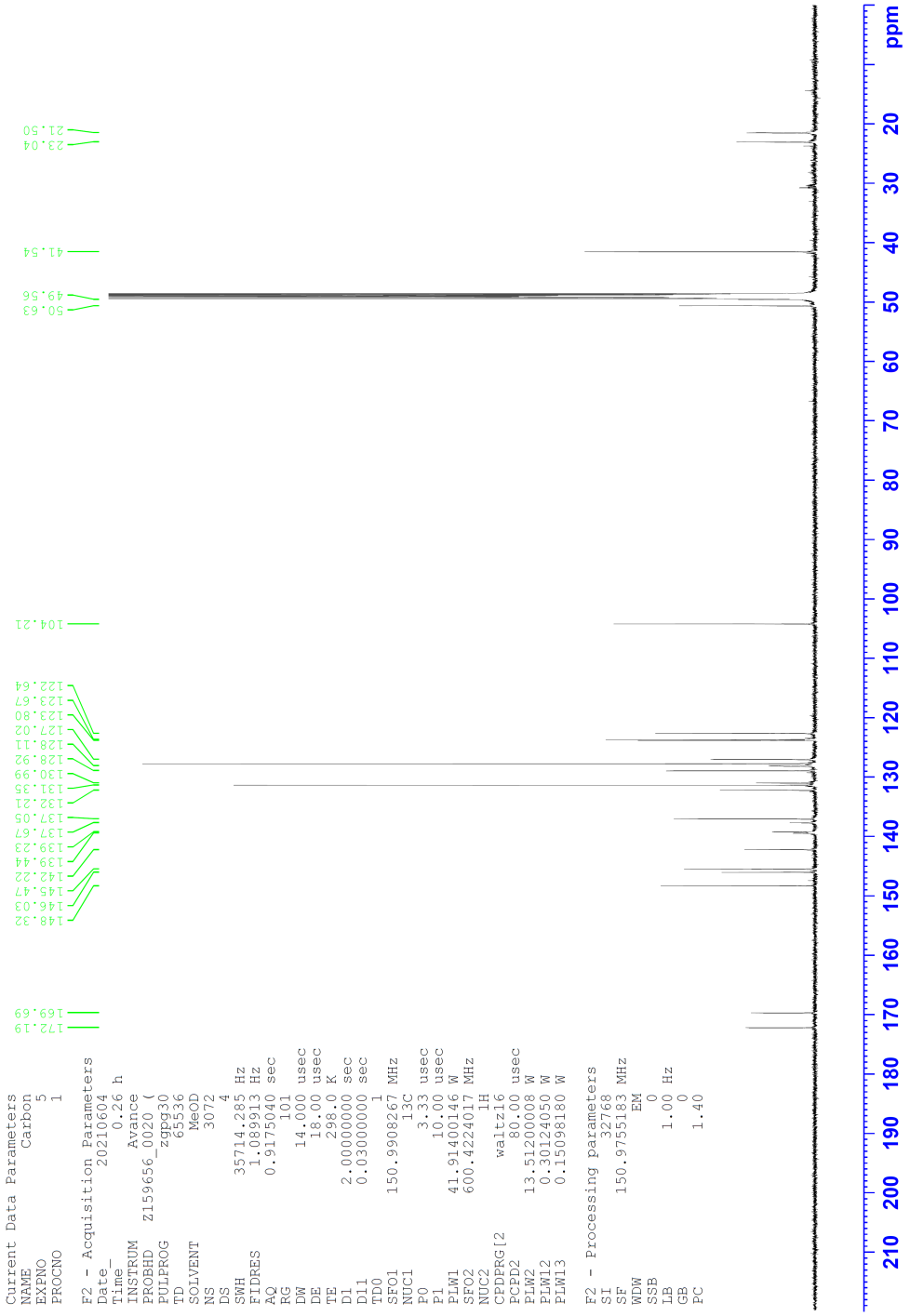
^{1}H NMR 4-{(2*S*,4*R*)-1-Acetyl-2-methyl-4-[(quinolin-6-yl)amino]-1,2,3,4-tetrahydroquinolin-6-yl}benzoic acid (2.6)



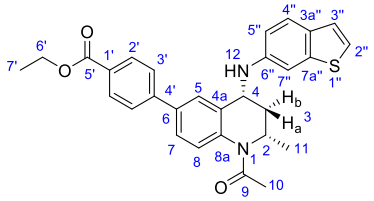


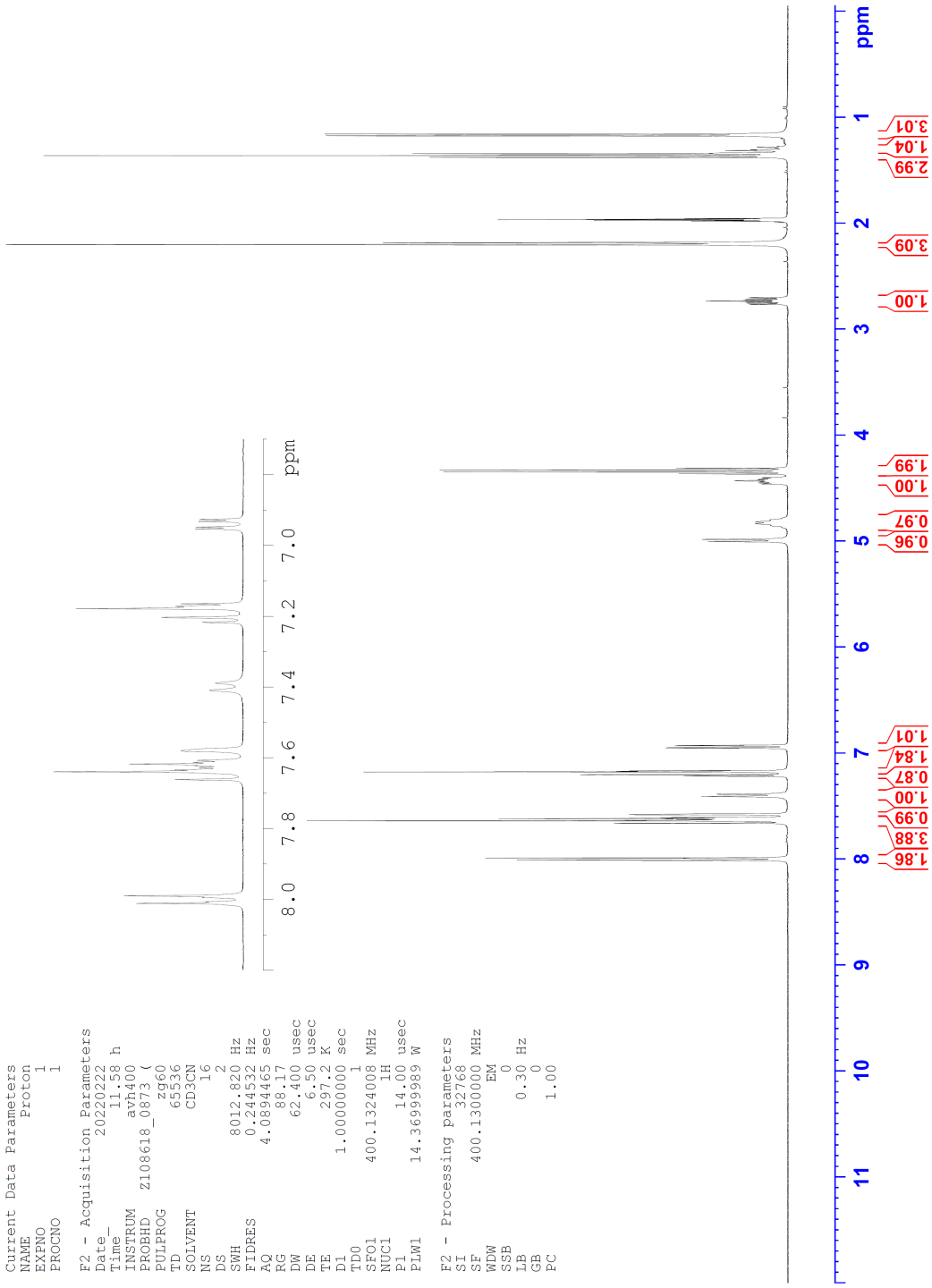
^{13}C NMR 4-{(2*S*,4*R*)-1-Acetyl-2-methyl-4-[(quinolin-6-yl)amino]-1,2,3,4-tetrahydroquinolin-6-yl}benzoic acid (2.6)



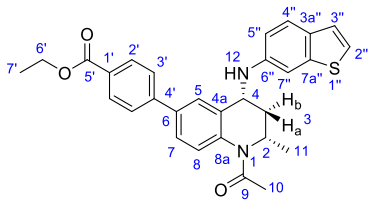


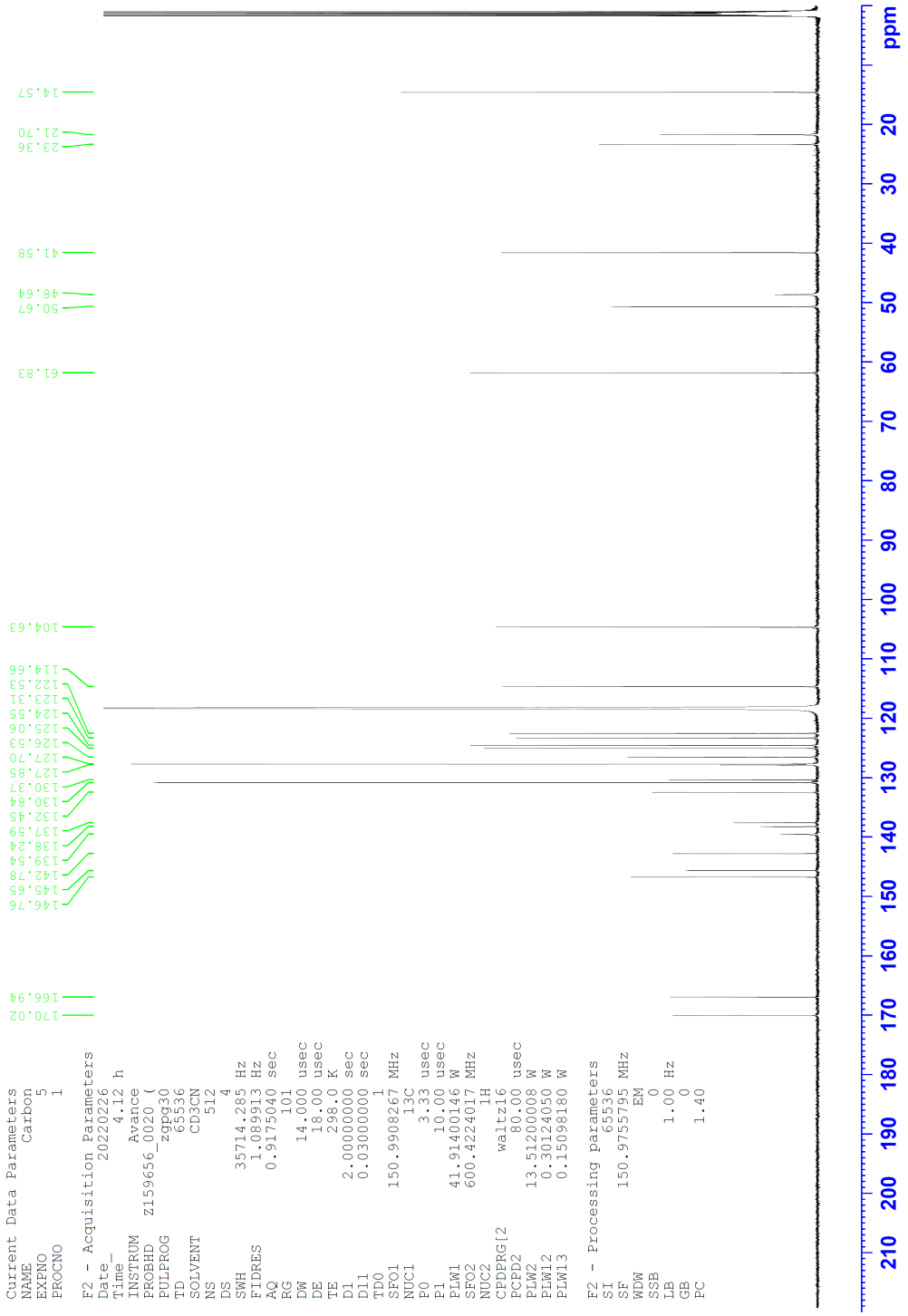
^{1}H NMR Ethyl 4-{(2*S*,4*R*)-1-acetyl-4-[(1-benzothiophen-6-yl)amino]-2-methyl-1,2,3,4-tetrahydroquinolin-6-yl}benzoate (2.20)



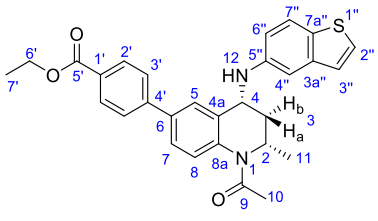


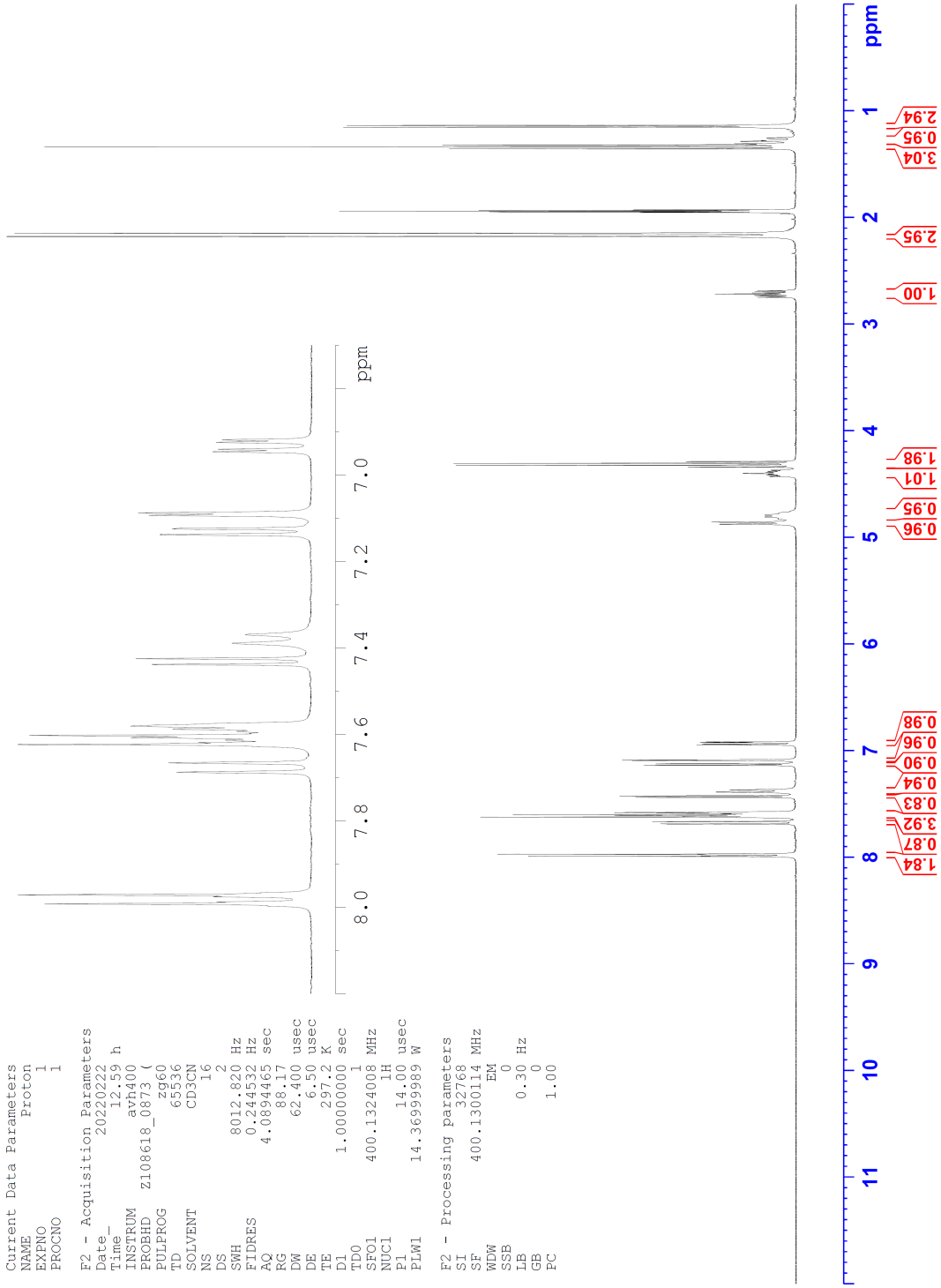
^{13}C NMR Ethyl 4-{(2*S*,4*R*)-1-acetyl-4-[(1-benzothiophen-6-yl)amino]-2-methyl-1,2,3,4-tetrahydroquinolin-6-yl}benzoate (2.20)



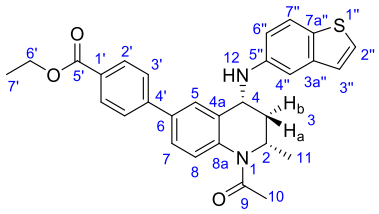


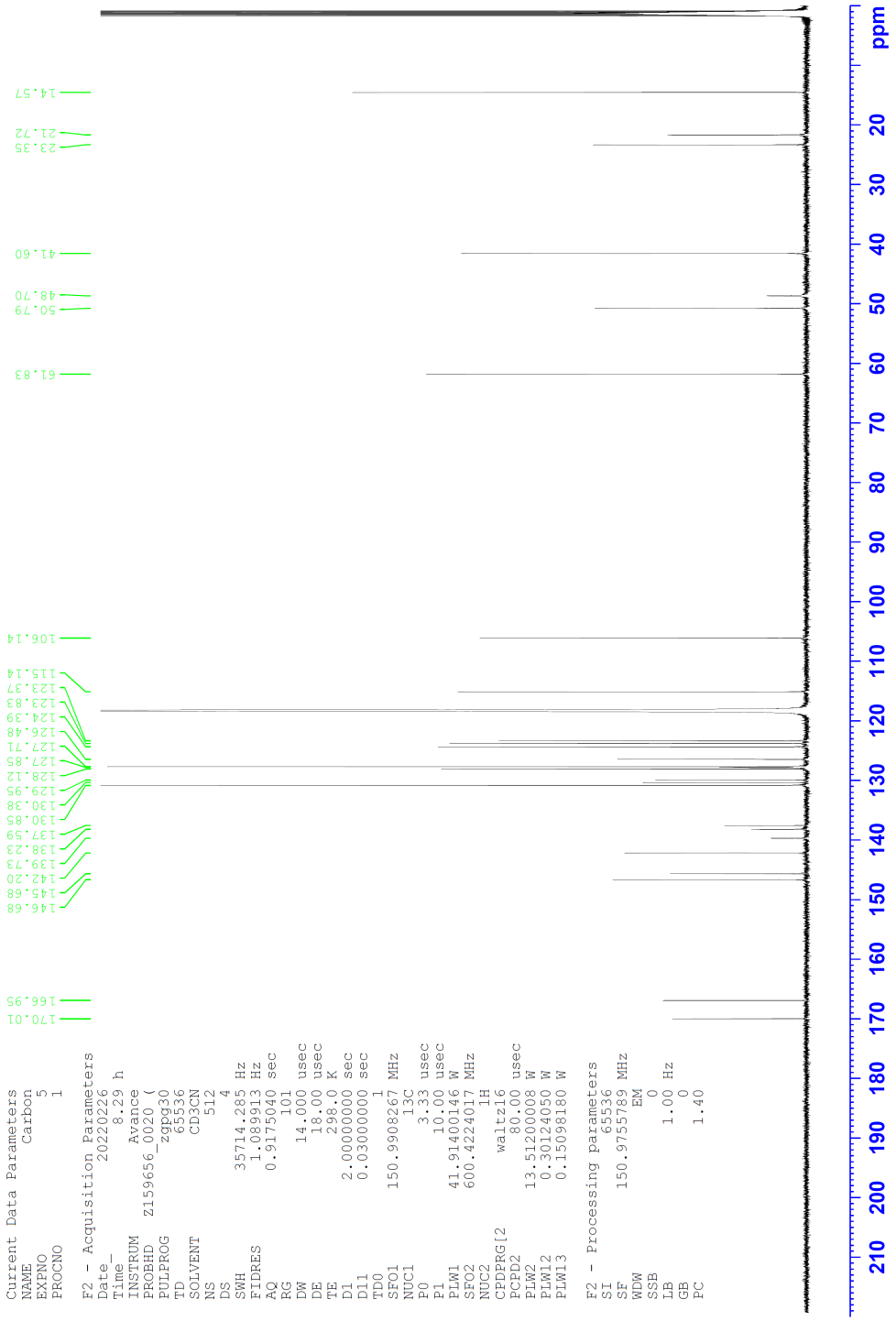
^{1}H NMR Ethyl 4-{(2*S*,4*R*)-1-acetyl-4-[(1-benzothiophen-5-ylamino]-2-methyl-1,2,3,4-tetrahydroquinolin-6-yl}benzoate (2.21)





^{13}C NMR Ethyl 4-{(2*S*,4*R*)-1-acetyl-4-[(1-benzothiophen-5-ylamino]-2-methyl-1,2,3,4-tetrahydroquinolin-6-yl}benzoate (2.21)



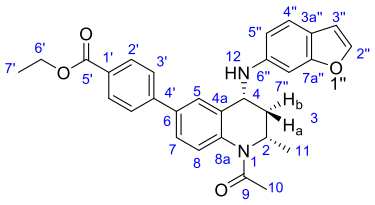


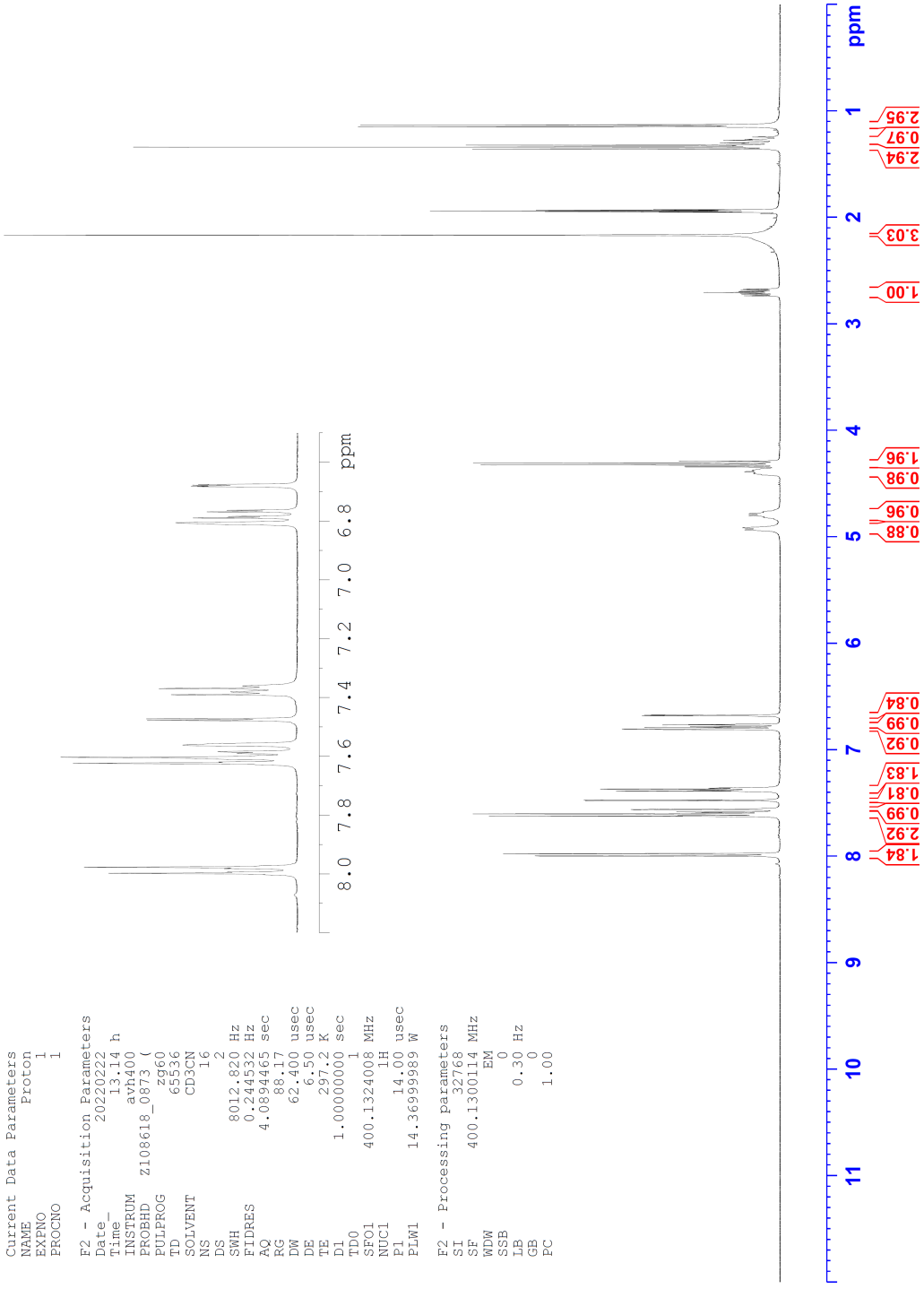
Current Data Parameters
NAME Carbon
EXPNO 5
PROCNO 1

F2 - Acquisition Parameters
Date_ 20220226
Time_ 8.29 h
INSTRUM Avance
PROBHD Z159656_0020 (
PULPROG zgpg30
TD 65536
SOLVENT CD3CN
NS 512
DS 4
SWH 35714.285 Hz
FIDRES 1.089913 Hz
AQ 0.9175040 sec
RG 101
DW 14.000 usec
DE 18.00 usec
TE 298.0 K
D1 2.00000000 sec
D11 0.03000000 sec
TD0 1
SFO1 150.9908267 MHz
NUC1 13C
P0 3.33 usec
P1 10.00 usec
PLW1 41.91400146 W
SFO2 600.4224017 MHz
NUC2 1H
CPDPRG[2 waltz16
PCPD2 80.00 usec
PLW2 13.51200008 W
PLW12 0.30124050 W
PLW13 0.15098180 W

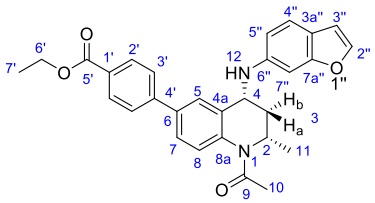
F2 - Processing parameters
SI 65536
SF 150.9755789 MHz
WDW EM
SSB 0
LB 1.00 Hz
GB 0
PC 1.40

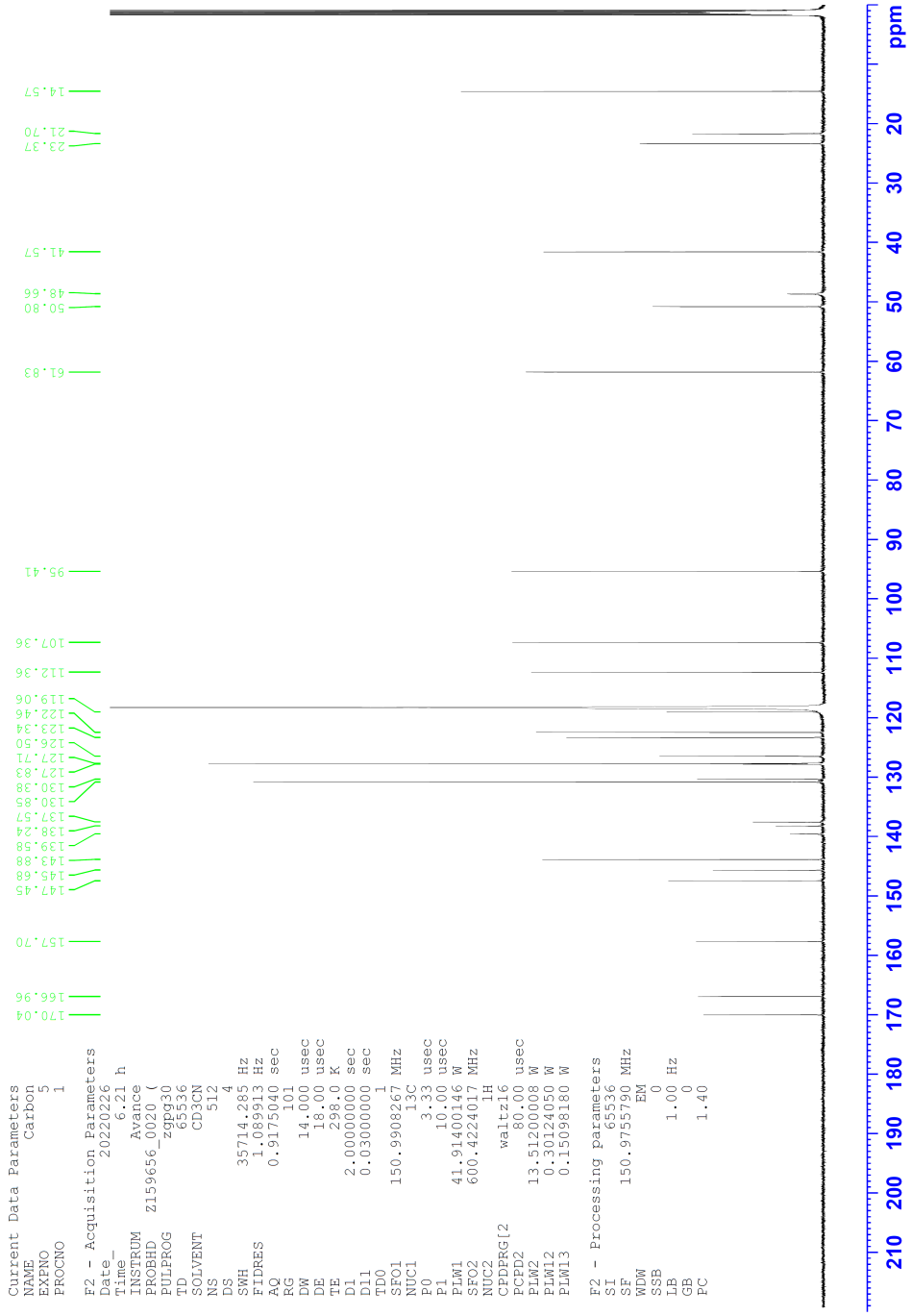
^{1}H NMR Ethyl 4-{(2*S*,4*R*)-1-acetyl-4-[(1-benzofuran-6-yl)amino]-2-methyl-1,2,3,4-tetrahydroquinolin-6-yl}benzoate (2.22)



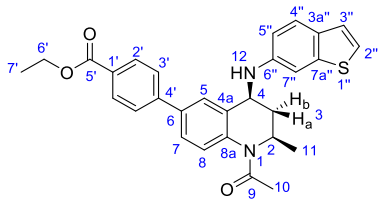


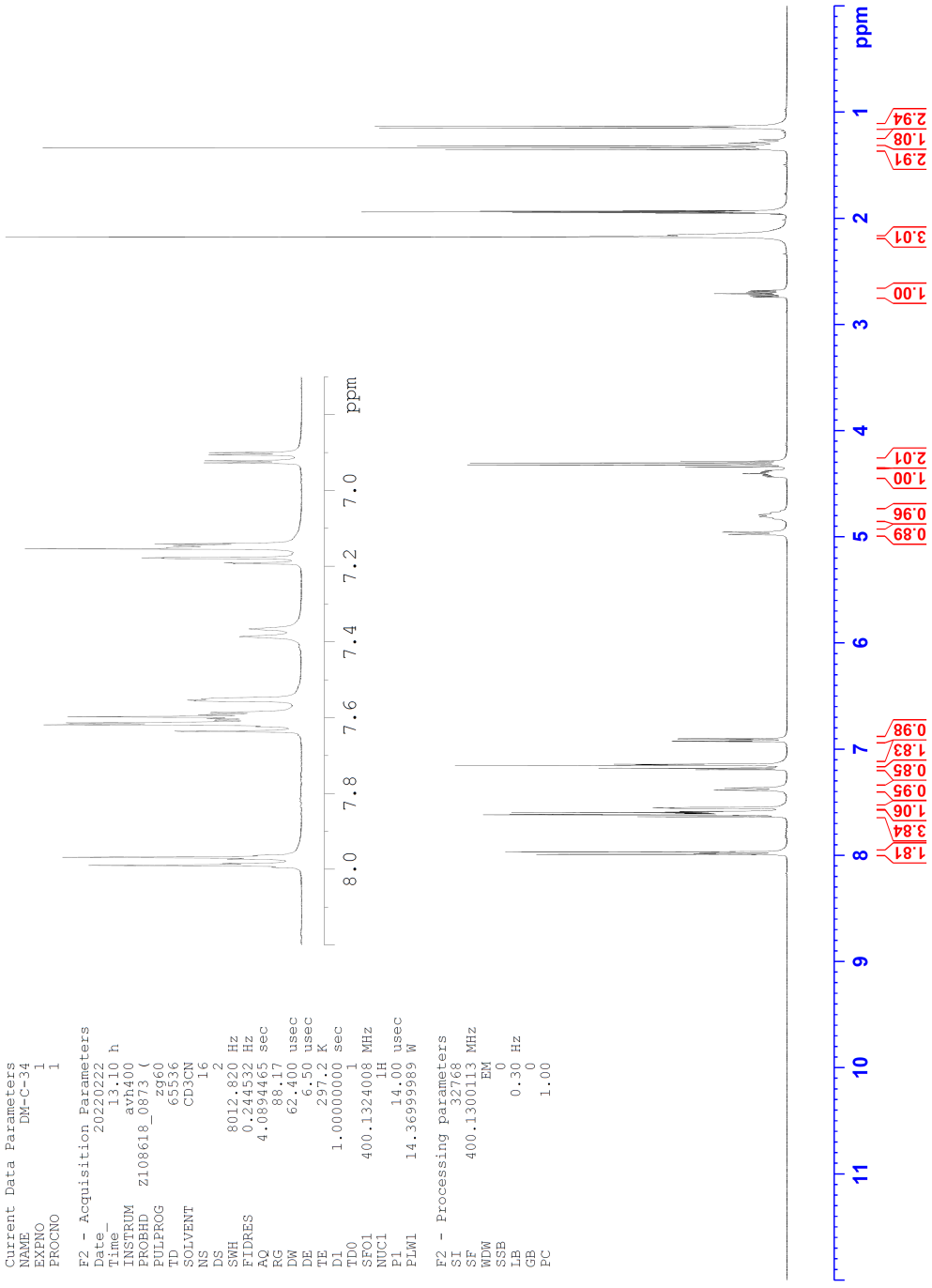
^{13}C NMR Ethyl 4-{(2*S*,4*R*)-1-acetyl-4-[(1-benzofuran-6-yl)amino]-2-methyl-1,2,3,4-tetrahydroquinolin-6-yl}benzoate (2.22)



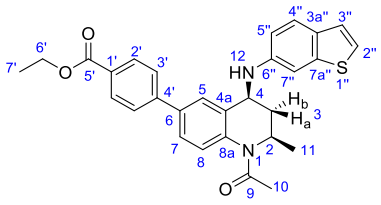


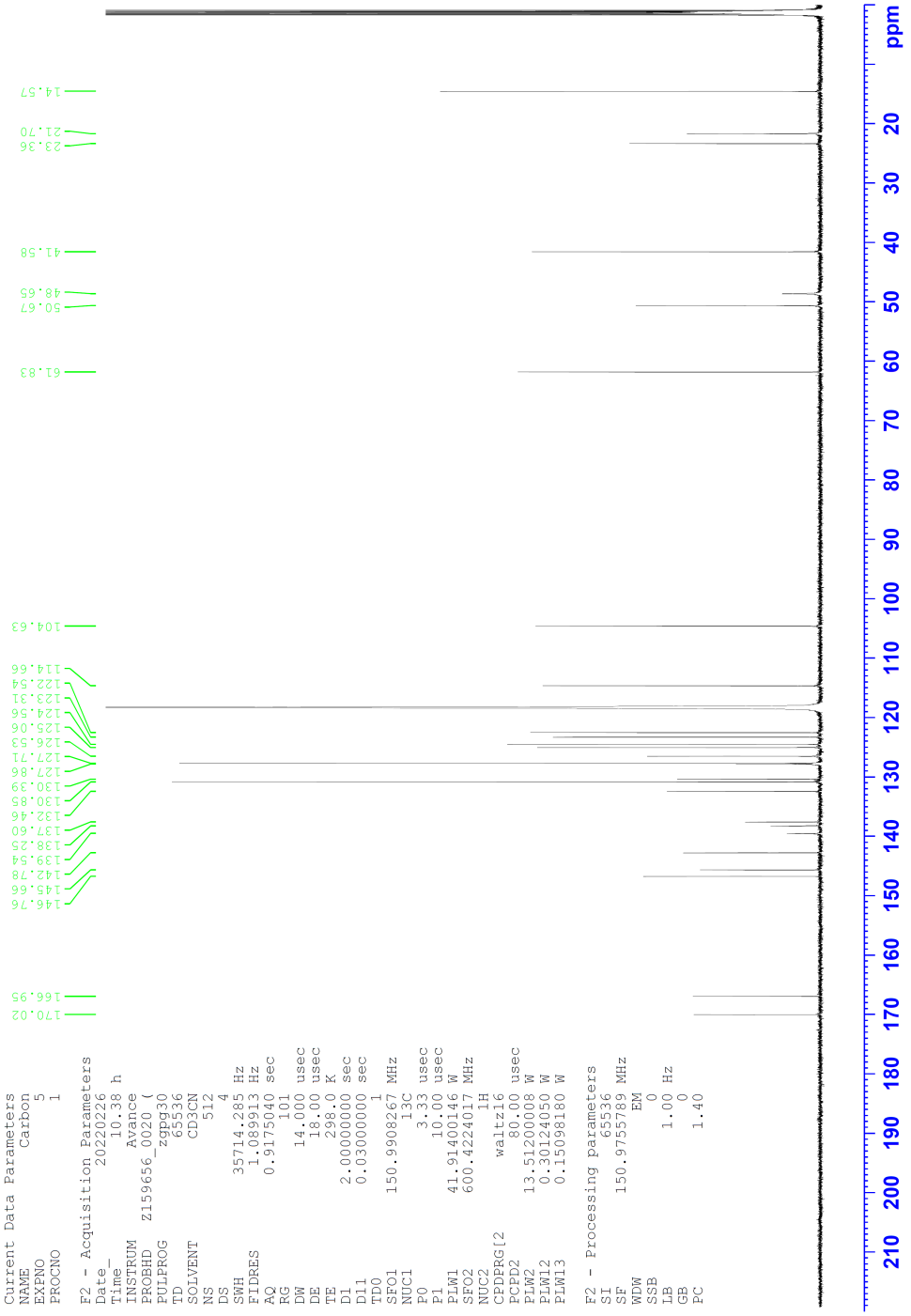
^{1}H NMR Ethyl 4-{(2*R*,4*S*)-1-acetyl-4-[(1-benzothiophen-6-yl)amino]-2-methyl-1,2,3,4-tetrahydroquinolin-6-yl}benzoate (2.23)



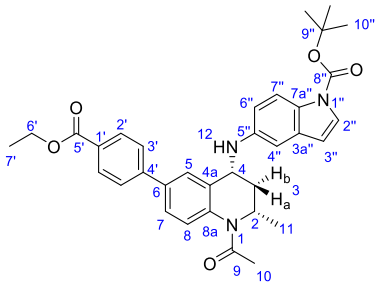


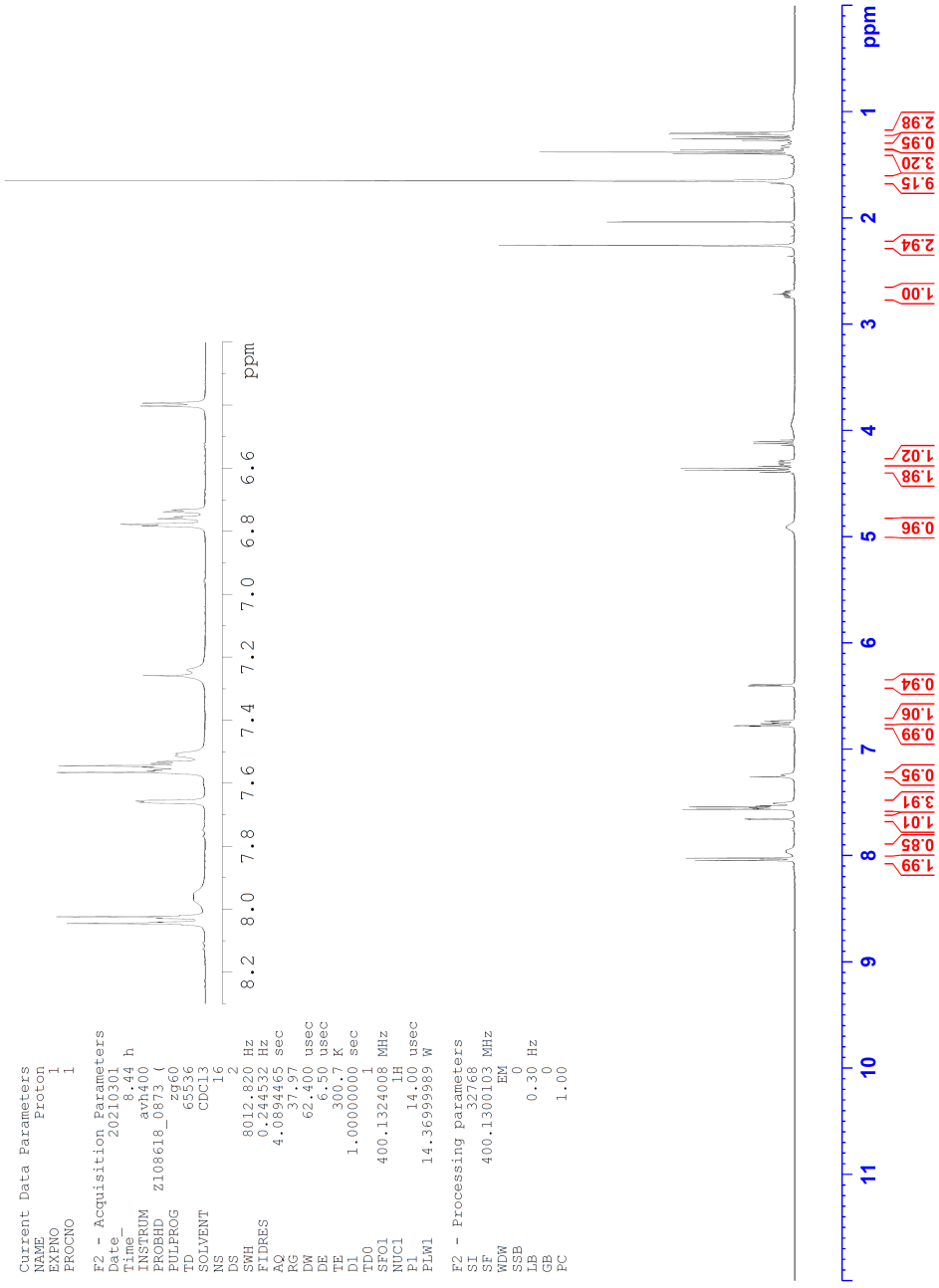
^{13}C NMR Ethyl 4-{(2*R*,4*S*)-1-acetyl-4-[(1-benzothiophen-6-yl)amino]-2-methyl-1,2,3,4-tetrahydroquinolin-6-yl}benzoate (2.23)



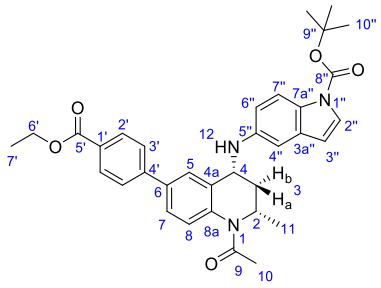


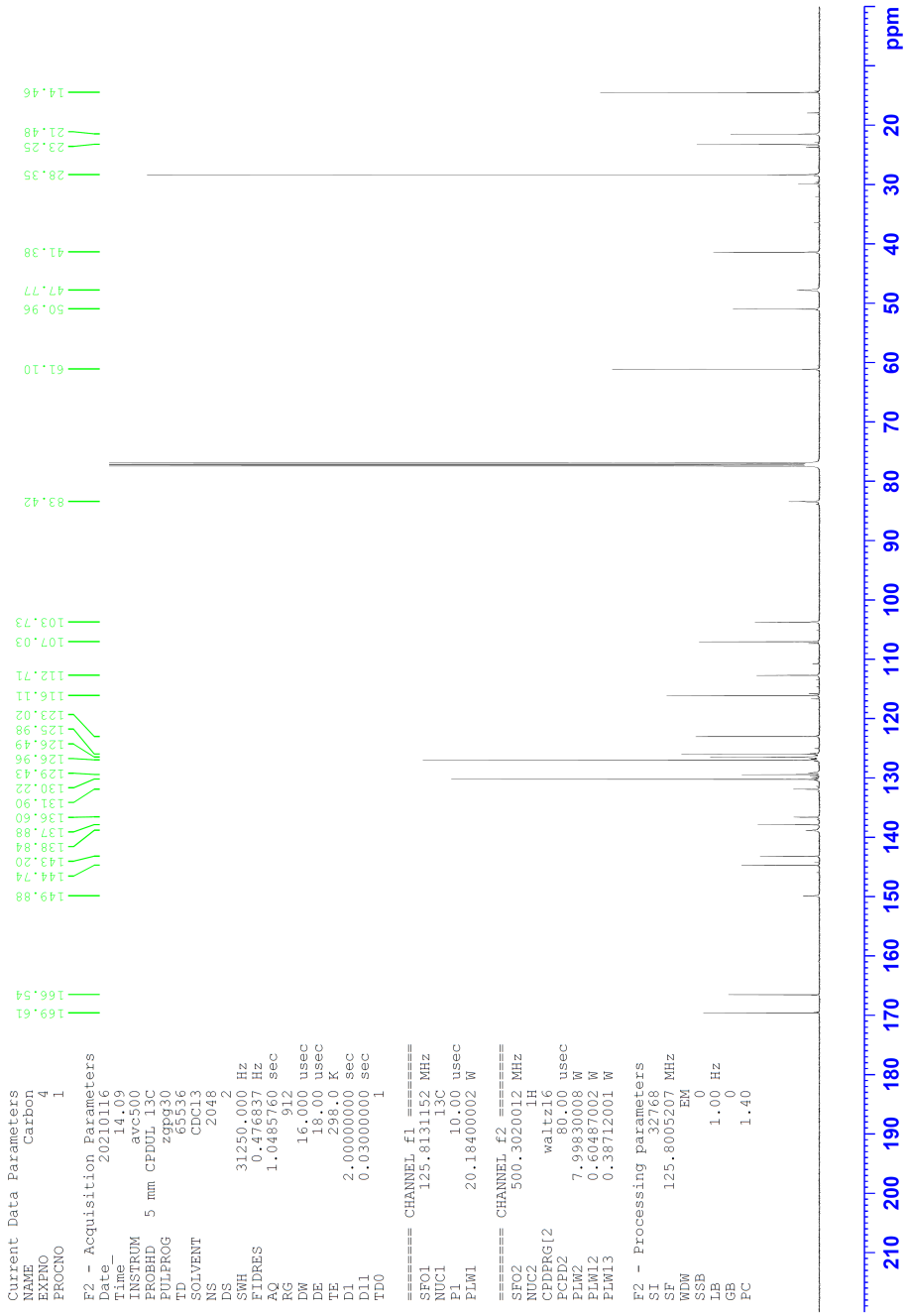
^{1}H NMR *tert*-Butyl 5-{(2*S*,4*R*)-(1-acetyl-6-[4-(ethoxycarbonyl)phenyl]-2-methyl-1,2,3,4-tetrahydroquinolin-4-yl)amino}-1*H*-indole-1-carboxylate (2.29)



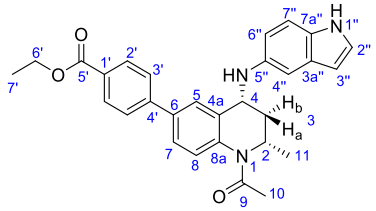


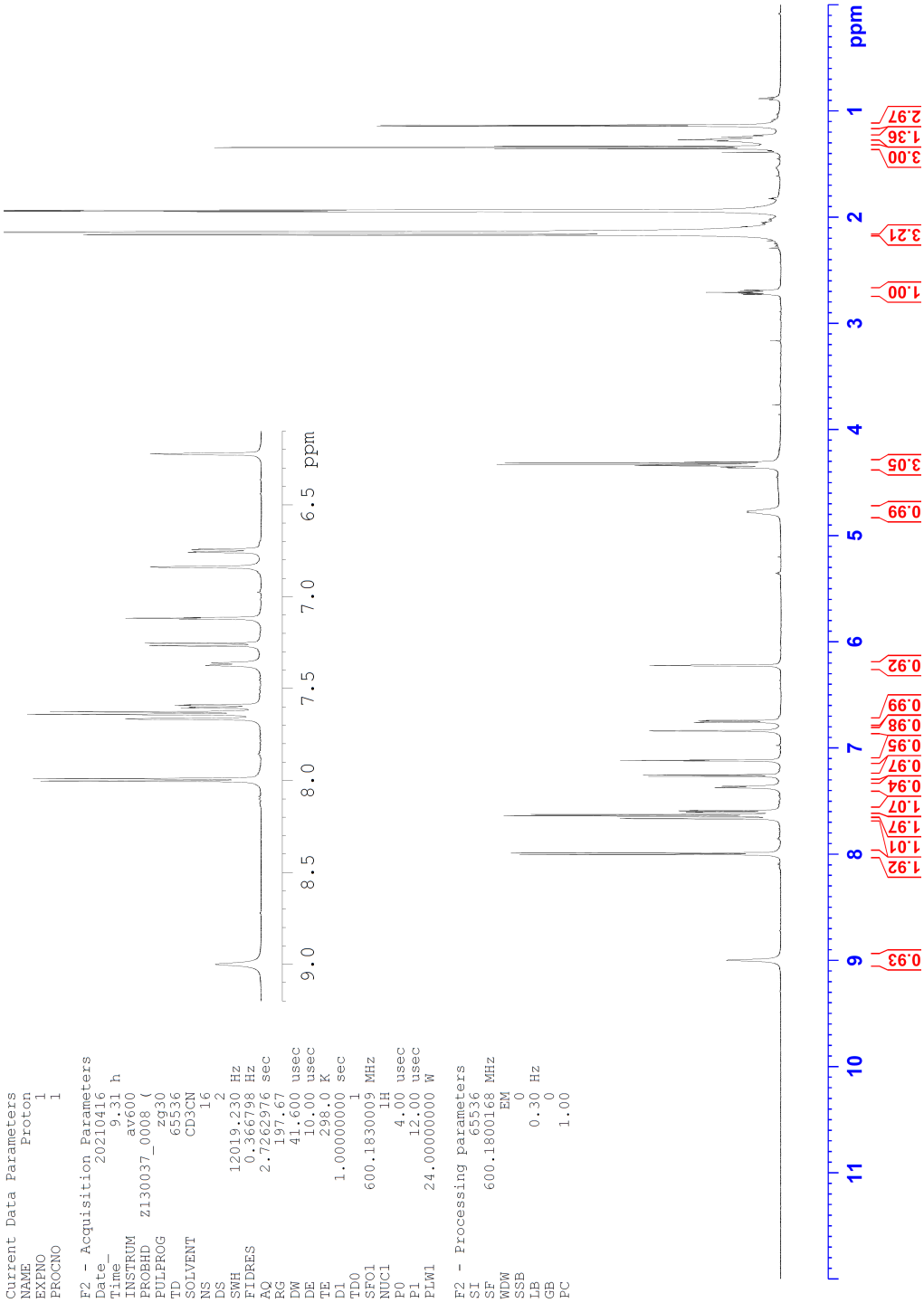
^{13}C NMR *tert*-Butyl 5-{(2*S*,4*R*)-(1-acetyl-6-[4-(ethoxycarbonyl)phenyl]-2-methyl-1,2,3,4-tetrahydroquinolin-4-yl)amino}-1*H*-indole-1-carboxylate (2.29)



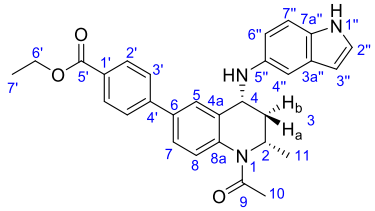


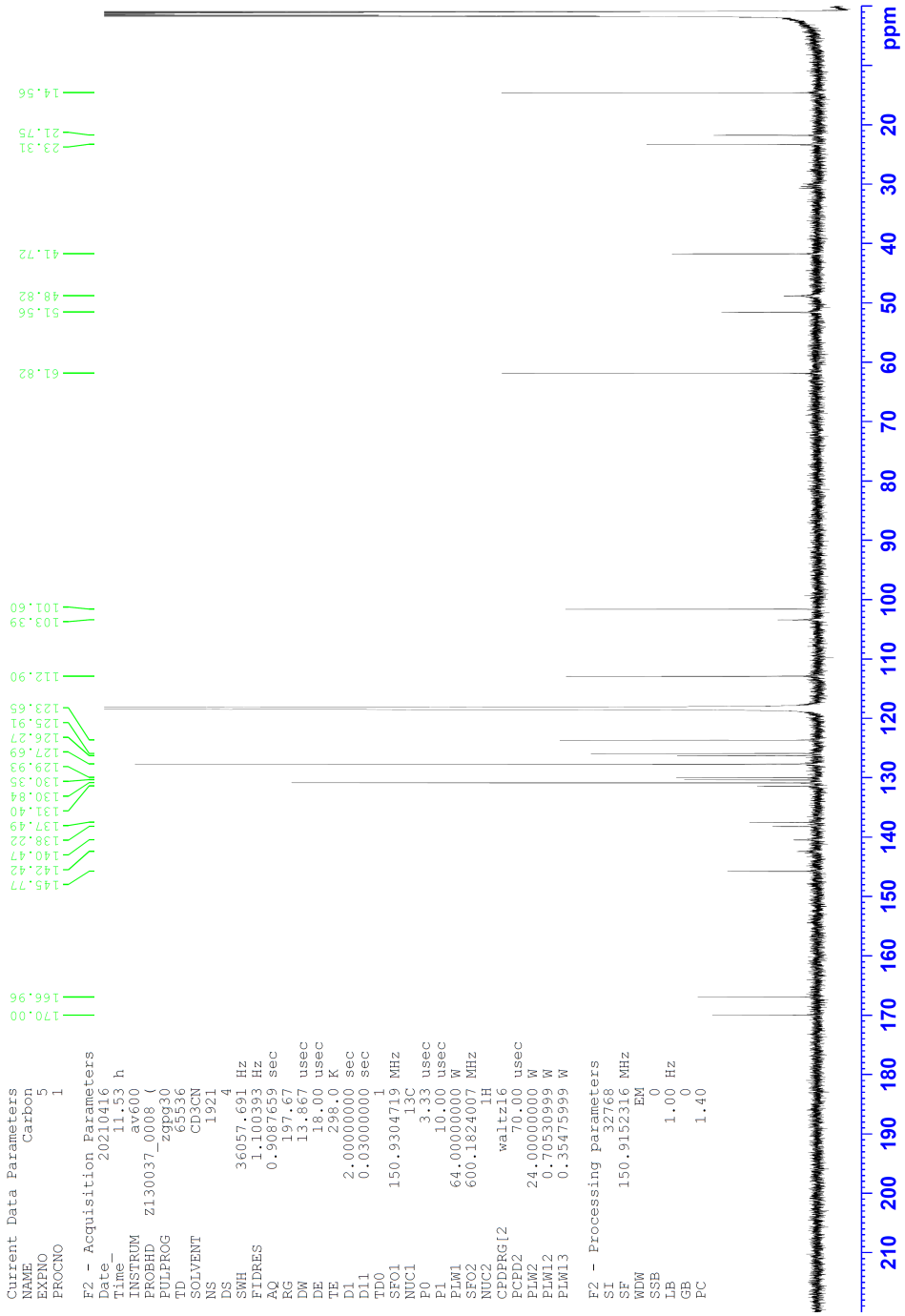
^{1}H NMR Ethyl 4-{(2*S*,4*R*)-1-acetyl-4-[(1*H*-indol-5-yl)amino]-2-methyl-1,2,3,4-tetrahydroquinolin-6-yl}benzoate (2.30)



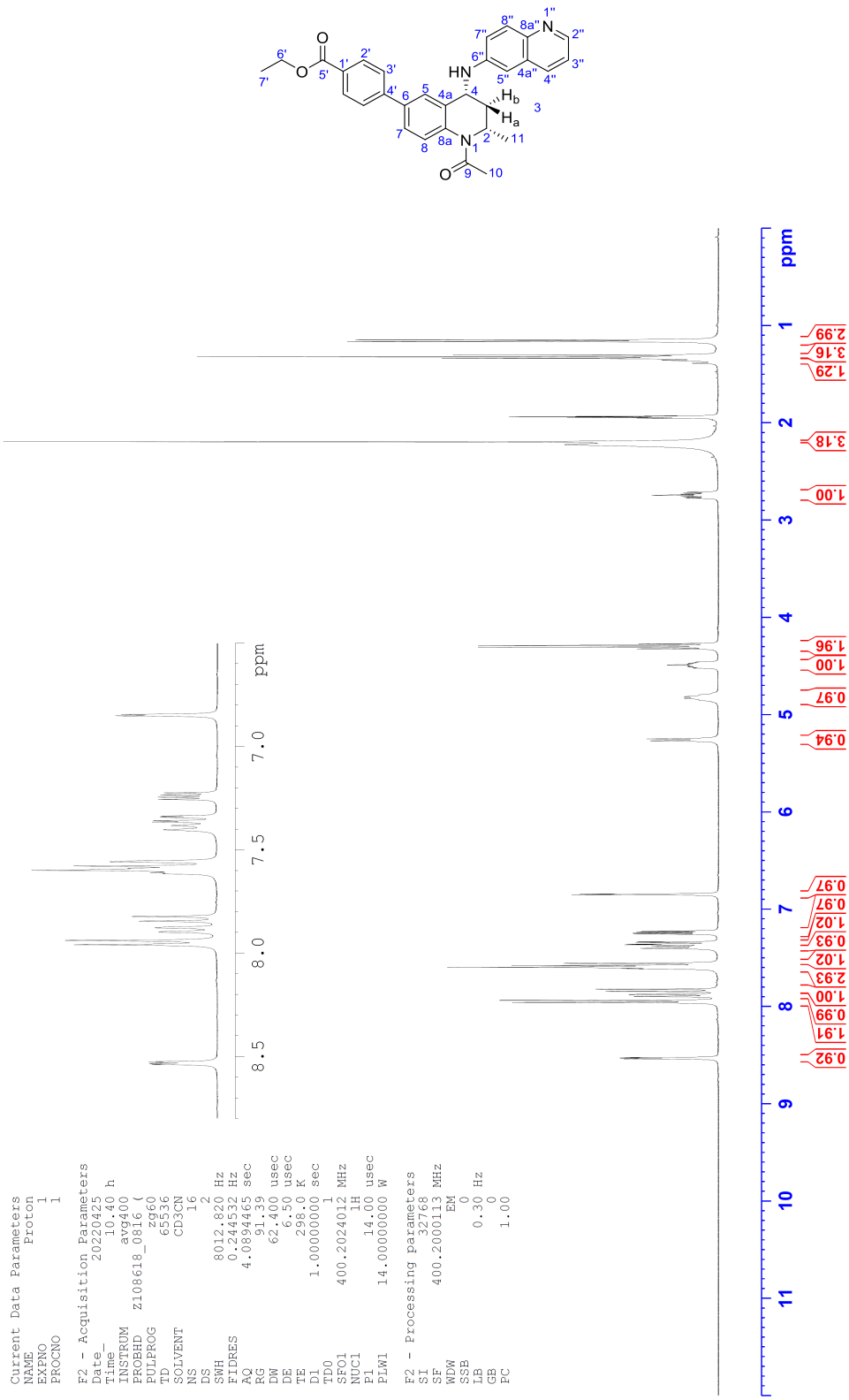


^{13}C NMR Ethyl 4-{(2*S*,4*R*)-1-acetyl-4-[(1*H*-indol-5-yl)amino]-2-methyl-1,2,3,4-tetrahydroquinolin-6-yl}benzoate (2.30)

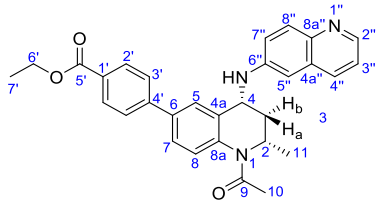


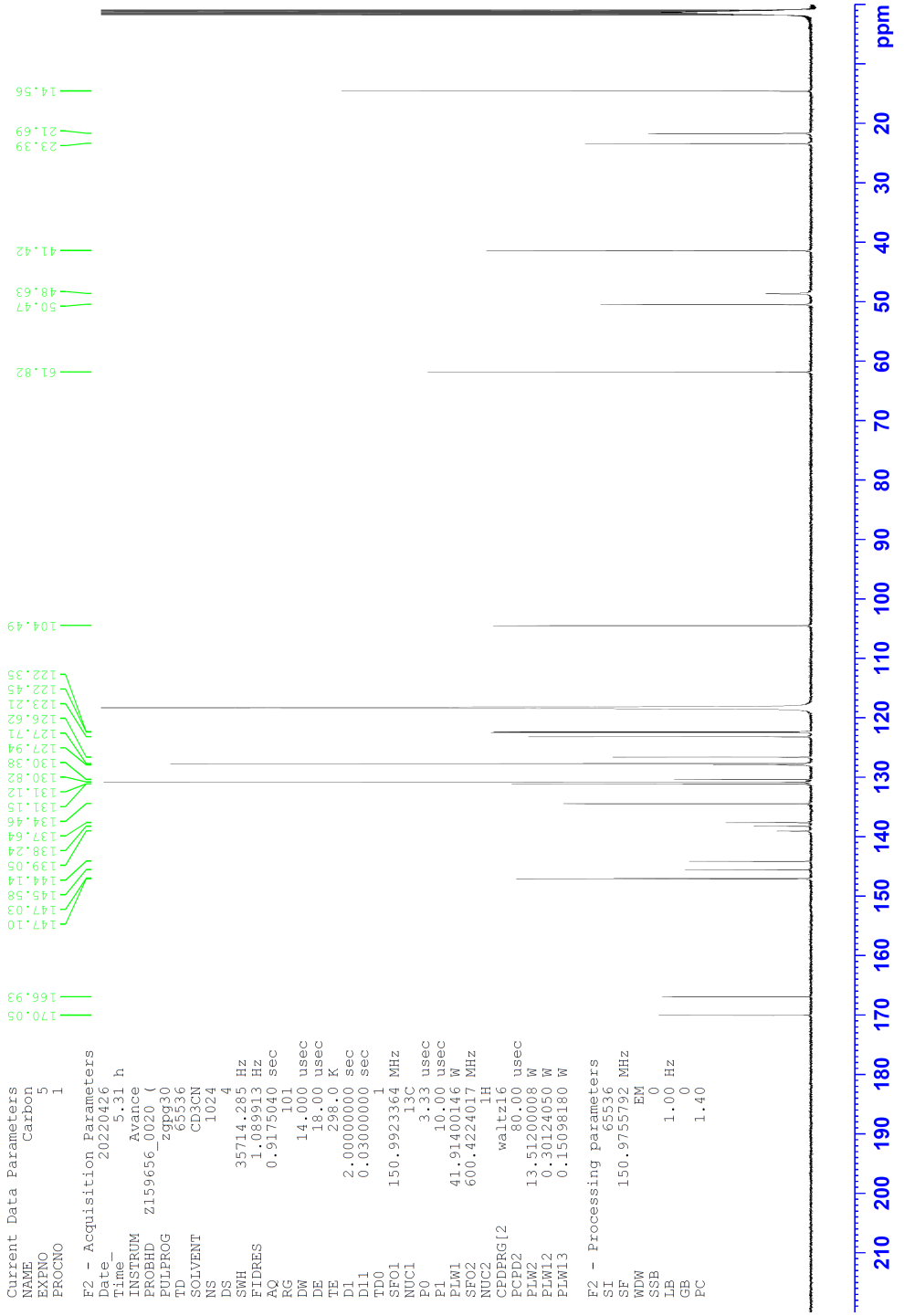


^{1}H NMR Ethyl 4-{(2*S*,4*R*)-1-acetyl-2-methyl-4-[(quinolin-6-yl)amino]-1,2,3,4-tetrahydroquinolin-6-yl}benzoate (2.31)

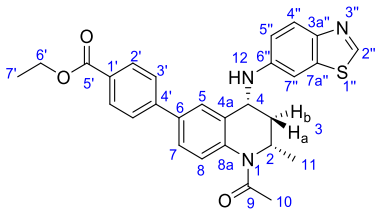


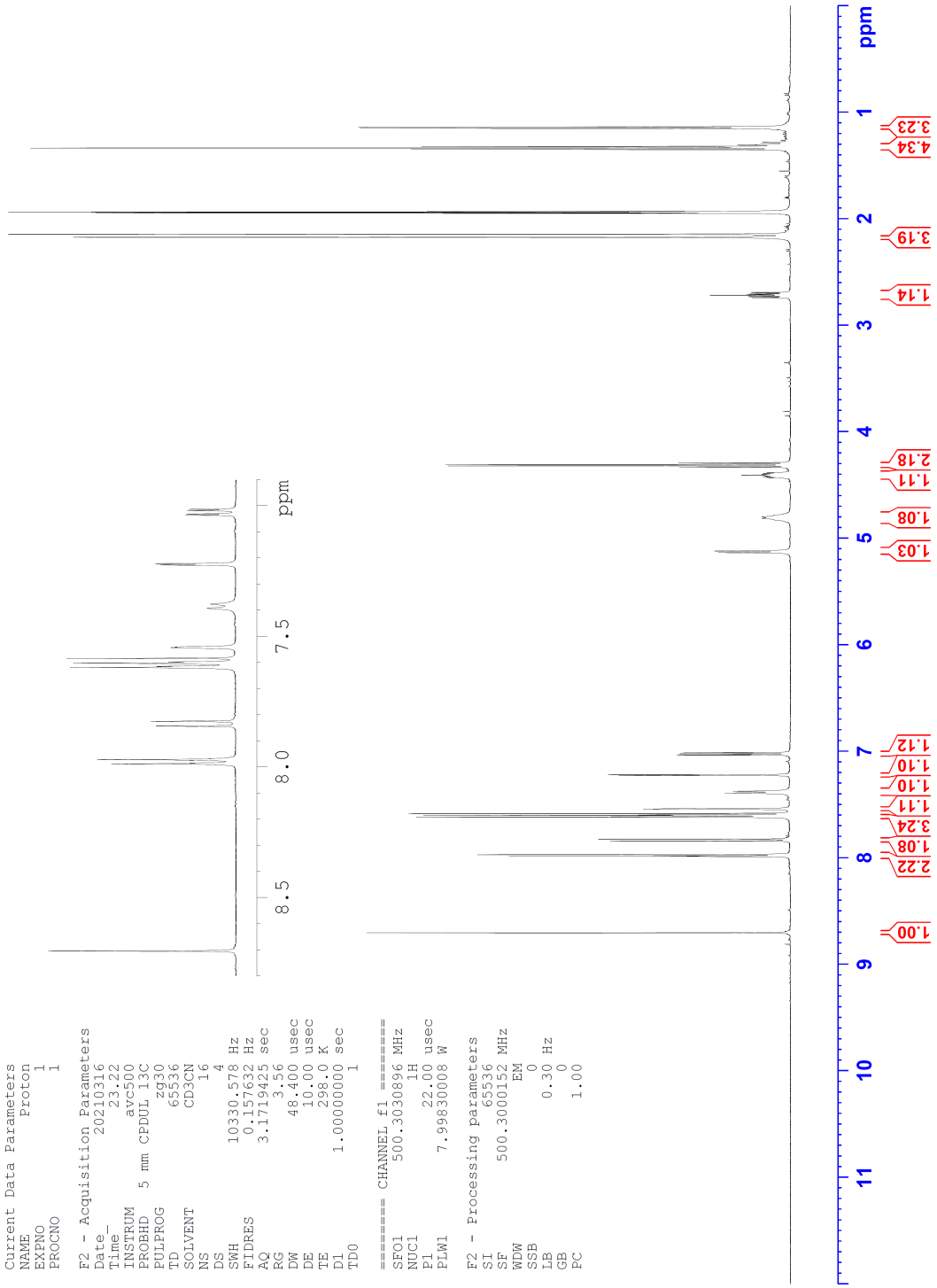
^{13}C NMR Ethyl 4-{(2*S*,4*R*)-1-acetyl-2-methyl-4-[(quinolin-6-yl)amino]-1,2,3,4-tetrahydroquinolin-6-yl}benzoate (2.31)





^{1}H NMR Ethyl 4-{(2*S*,4*R*)1-acetyl-4-[(1,3-benzothiazol-6-yl)amino]-2-methyl-1,2,3,4-tetrahydroquinolin-6-yl}benzoate (2.32)





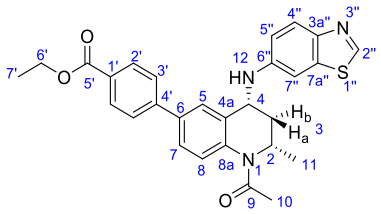

```
Current Data Parameters
NAME                  Proton
EXPNO                      1
PROCNO                     1

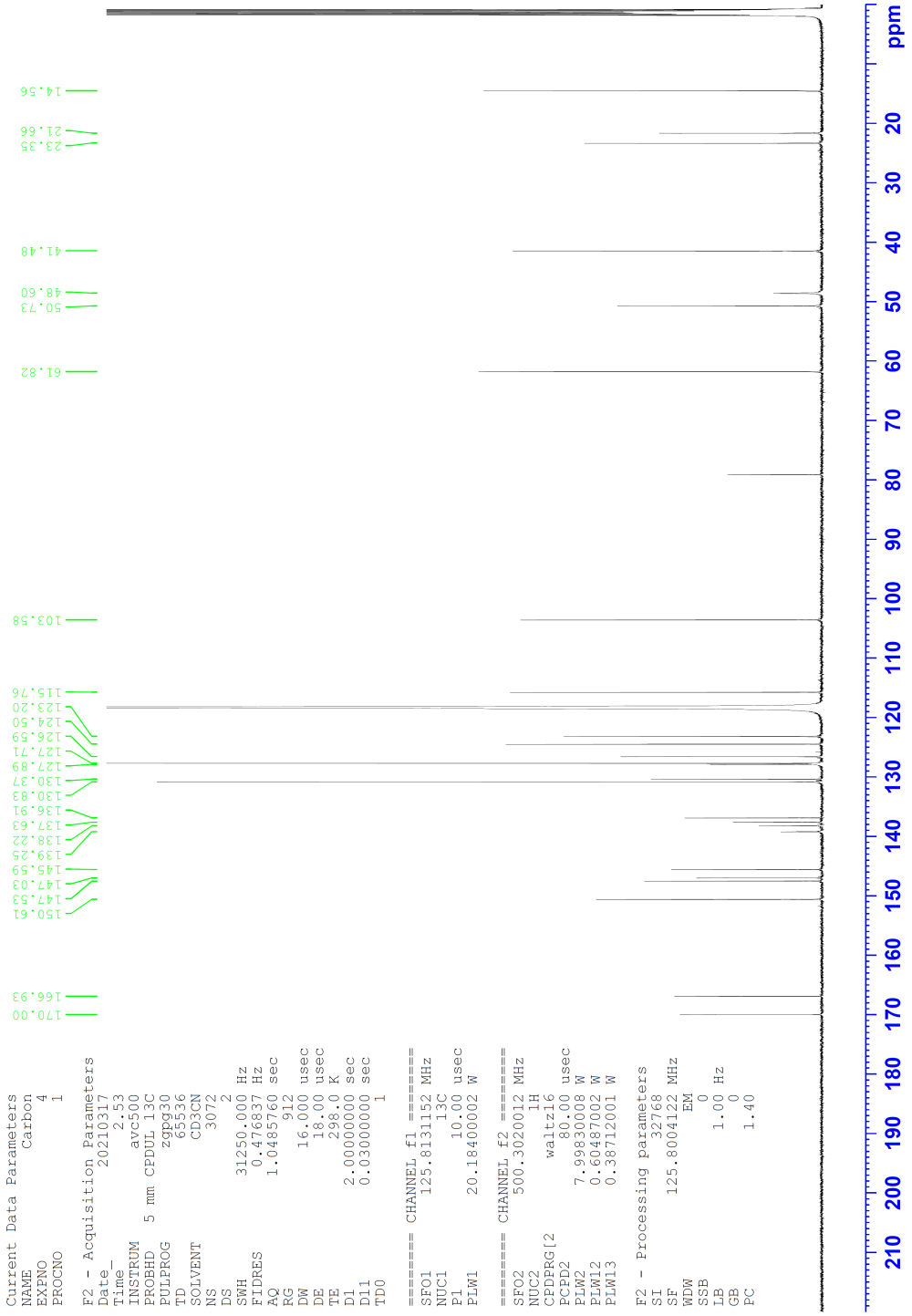
F2 - Acquisition Parameters
Date_              20210316
Time_                  23.22
INSTRUM                avc500
PROBHD   5 mm CPDUL 13C
PULPROG                zg30
TD                    65536
SOLVENT               CD3CN
NS                        16
DS                         4
SWH               10330.578 Hz
FIDRES             0.157632 Hz
AQ                 3.1719425 sec
RG                      3.56
DW                   48.400 usec
DE                   10.00 usec
TE                   298.0 K
D1                 1.00000000 sec
TD0                        1

======== CHANNEL f1 ========
SFO1              500.3030896 MHz
NUC1                      1H
P1                     22.00 usec
PLW1               7.99830008 W

F2 - Processing parameters
SI                    65536
SF                500.3000152 MHz
WDW                      EM
SSB                       0
LB                     0.30 Hz
GB                        0
PC                     1.00
```

^{13}C NMR Ethyl 4-{(2*S*,4*R*)1-acetyl-4-[(1,3-benzothiazol-6-yl)amino]-2-methyl-1,2,3,4-tetrahydroquinolin-6-yl}benzoate (2.32)






```
Current Data Parameters
NAME                  Carbon
EXPNO                      4
PROCNO                     1

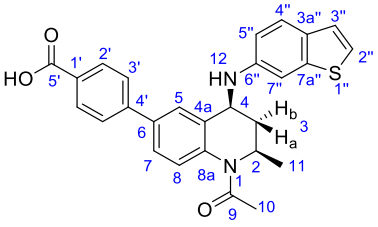
F2 - Acquisition Parameters
Date_              20210317
Time_                  2.53
INSTRUM              avc500
PROBHD   5 mm CPDUL 13C
PULPROG            zgpg30
TD                  65536
SOLVENT             CD3CN
NS                     3072
DS                        2
SWH               31250.000 Hz
FIDRES                0.476837 Hz
AQ                    1.0485760 sec
RG                       912
DW                    16.000 usec
DE                    18.00 usec
TE                    298.0 K
D1                    2.00000000 sec
D11                   0.03000000 sec
TD0                          1

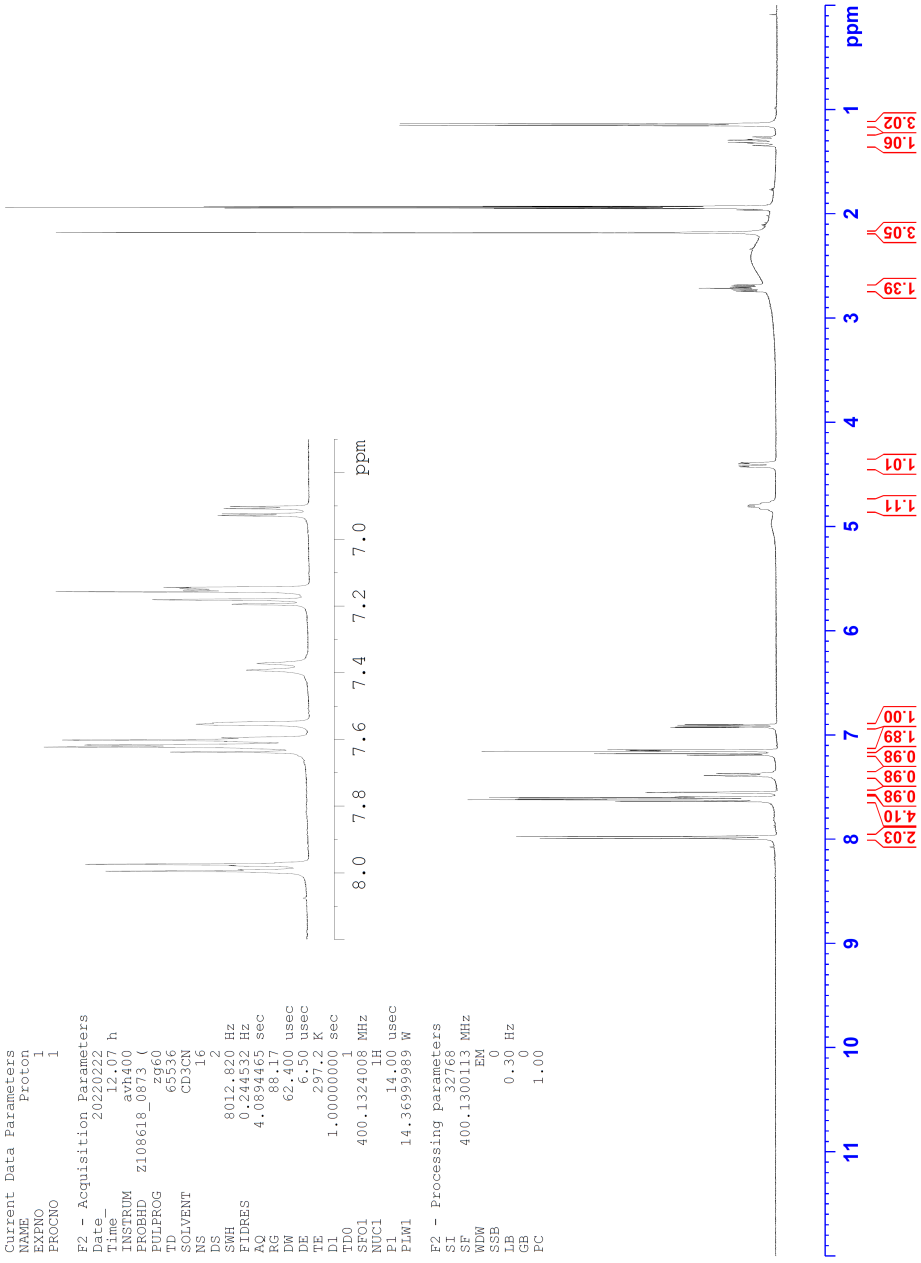
======== CHANNEL f1 ========
SFO1          125.81311152 MHz
NUC1                      13C
P1                    10.00 usec
PLW1          20.18400002 W

======== CHANNEL f2 ========
SFO2          500.3020012 MHz
NUC2                       1H
CPDPRG[2              waltz16
PCPD2                 80.00 usec
PLW2          7.99830008 W
PLW12         0.60487002 W
PLW13         0.38712001 W

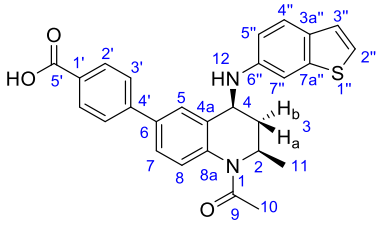
F2 - Processing parameters
SI                       32768
SF            125.8004122 MHz
WDW                        EM
SSB                         0
LB                    1.00 Hz
GB                          0
PC                    1.40
```

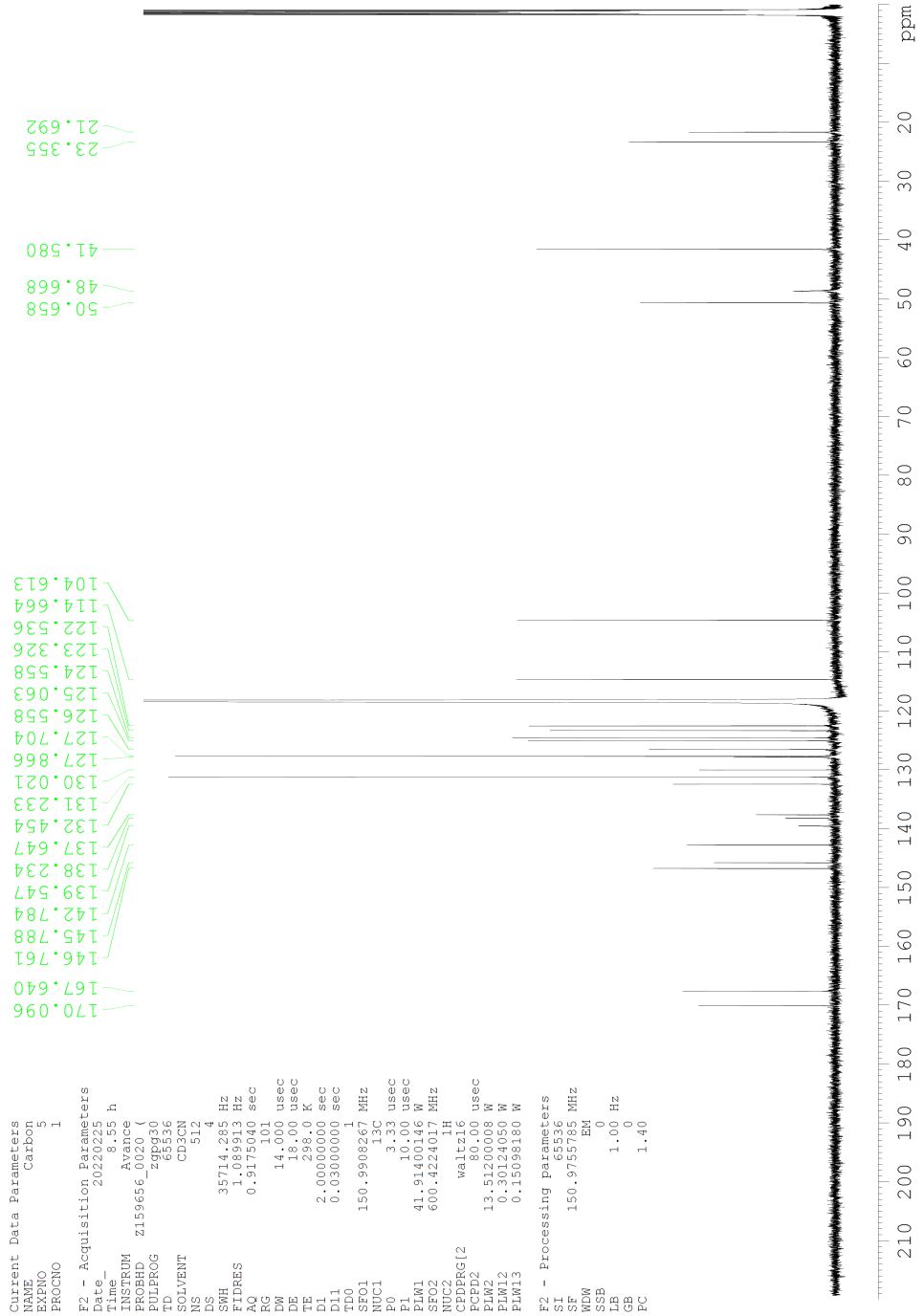
^{1}H NMR 4-{(2*R*,4*S*)-1-Acetyl-4-[(1-benzothiophen-6-yl)amino]-2-methyl-1,2,3,4-tetrahydroquinolin-6-yl}benzoic acid (2.33)



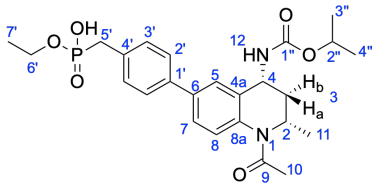


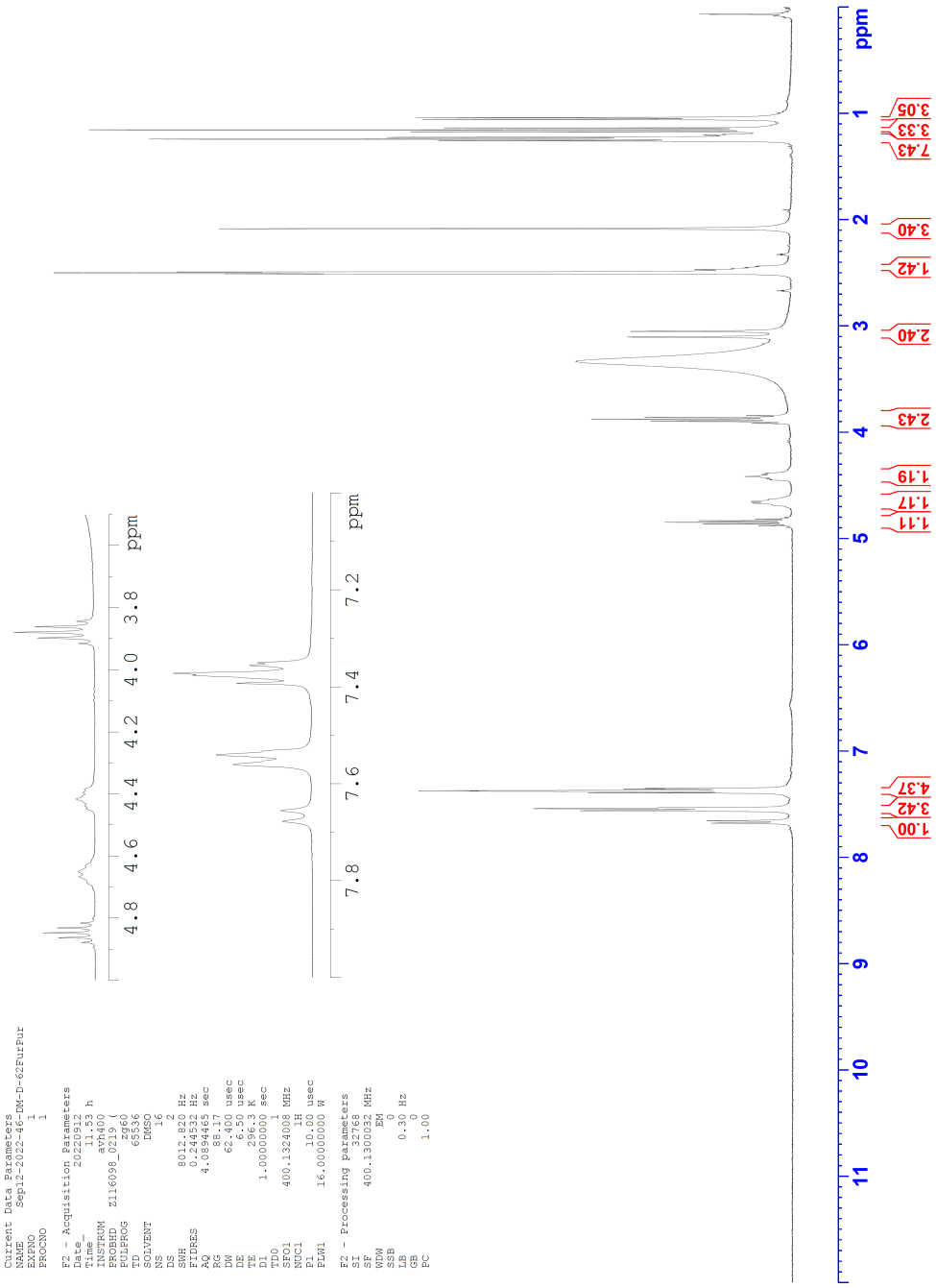
^{13}C NMR 4-{(2*R*,4*S*)-1-Acetyl-4-[(1-benzothiophen-6-yl)amino]-2-methyl-1,2,3,4-tetrahydroquinolin-6-yl}benzoic acid (2.33)



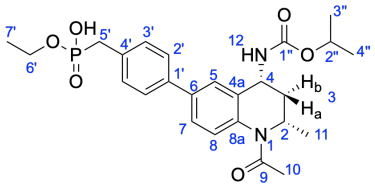


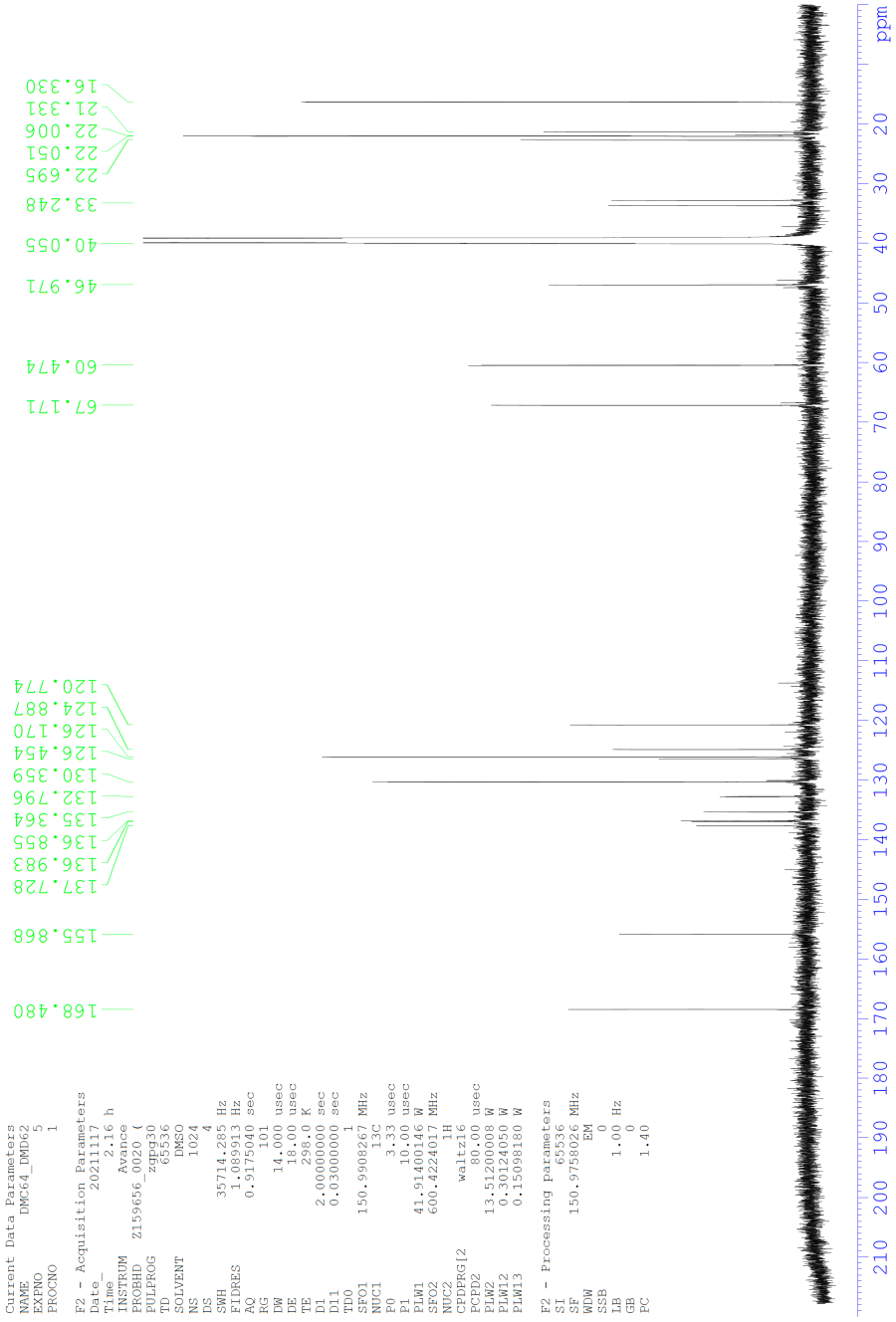
^{1}H NMR Isopropyl ((2*S*,4*R*)-1-acetyl-6-(4-((ethoxy(hydroxy)phosphoryl)methyl)phenyl)-2-methyl-1,2,3,4-tetrahydroquinolin-4-yl)carbamate (3.1)



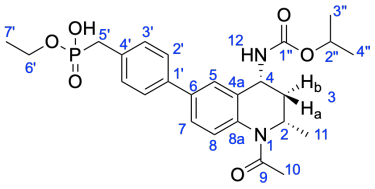


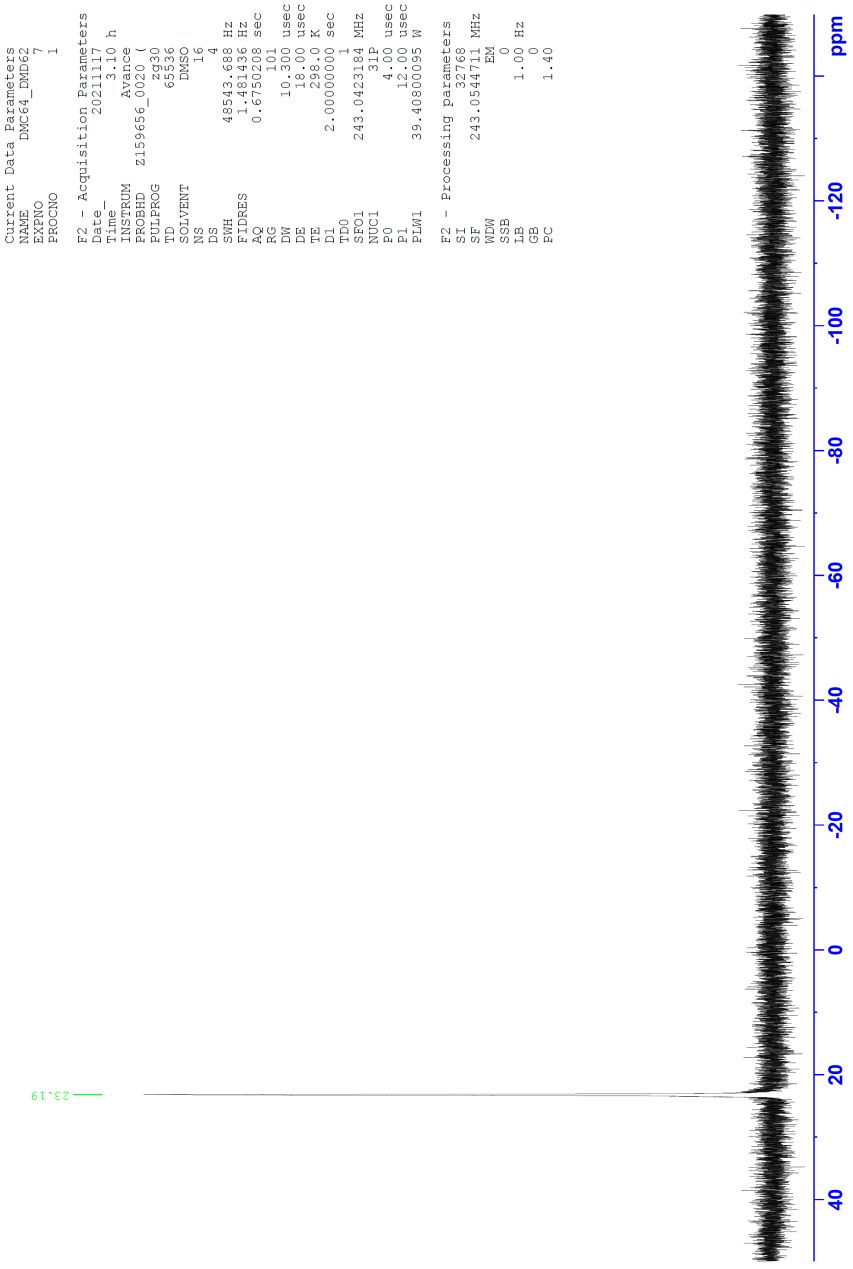
^{13}C NMR Isopropyl ((2*S*,4*R*)-1-acetyl-6-(4-((ethoxy(hydroxy)phosphoryl)methyl)phenyl)-2-methyl-1,2,3,4-tetrahydroquinolin-4-yl)carbamate (3.1)



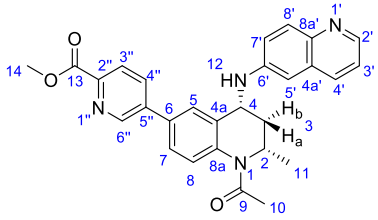


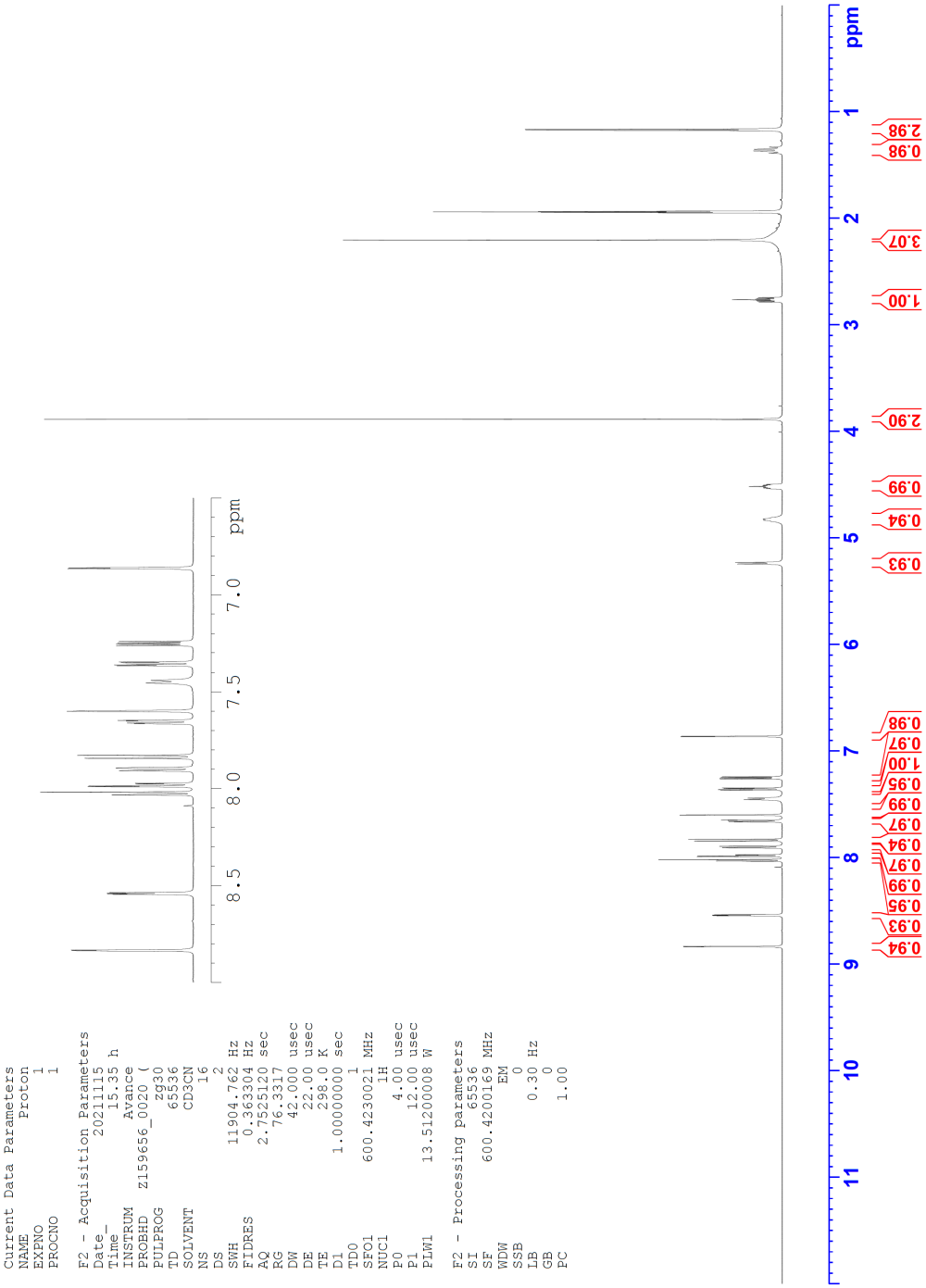
^{31}P NMR Isopropyl ((2*S*,4*R*)-1-acetyl-6-(4-((ethoxy(hydroxy)phosphoryl)methyl)phenyl)-2-methyl-1,2,3,4-tetrahydroquinolin-4-yl)carbamate (3.1)



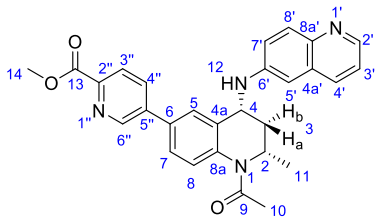


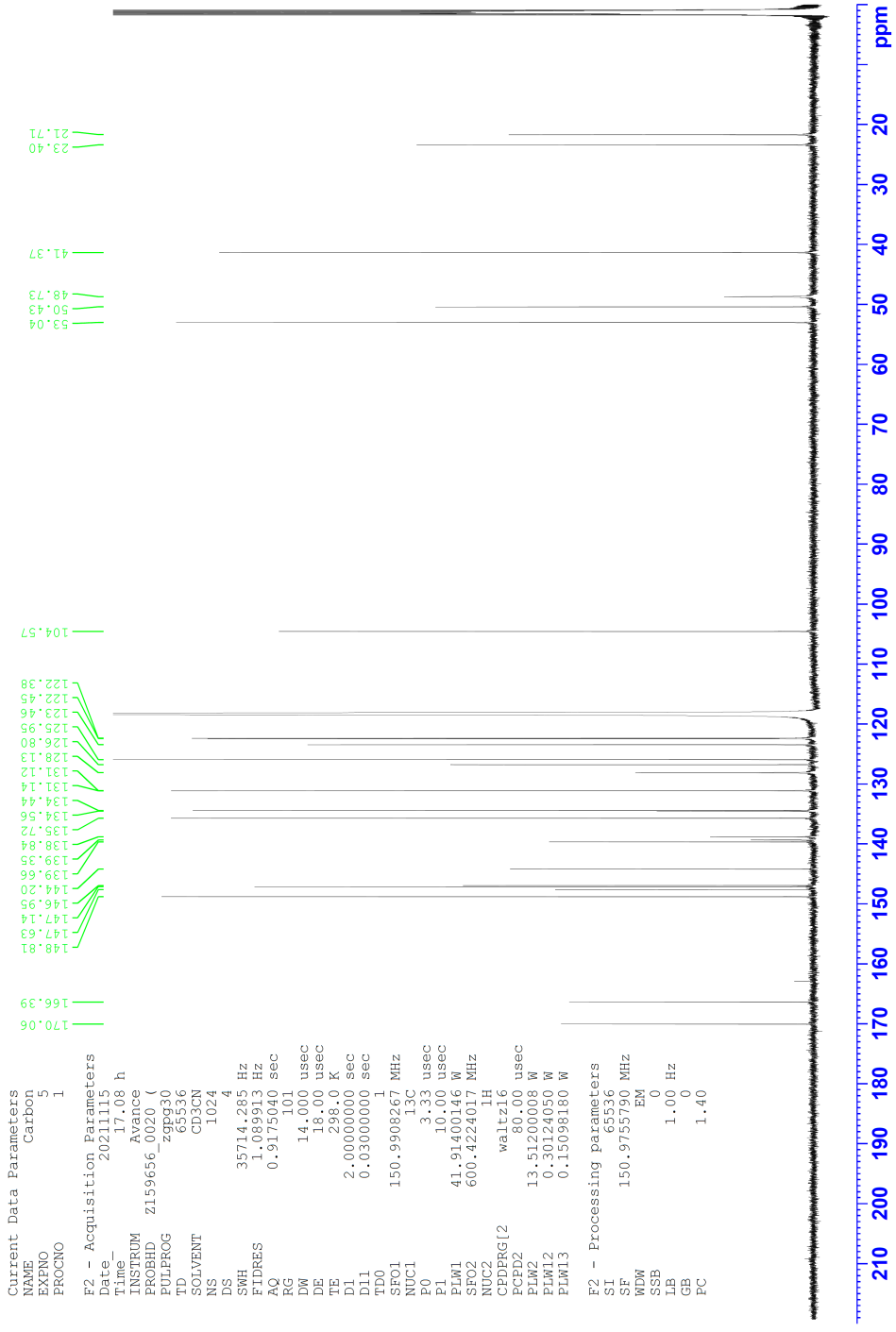
^{1}H Methyl 5-((2*S*,4*R*)-1-acetyl-2-methyl-4-(quinolin-6-ylamino)-1,2,3,4-tetrahydroquinolin-6-yl)picolinate (3.41)



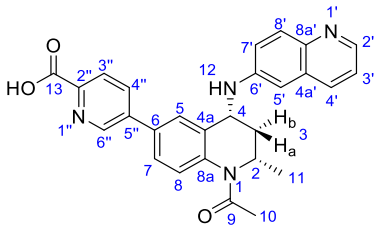


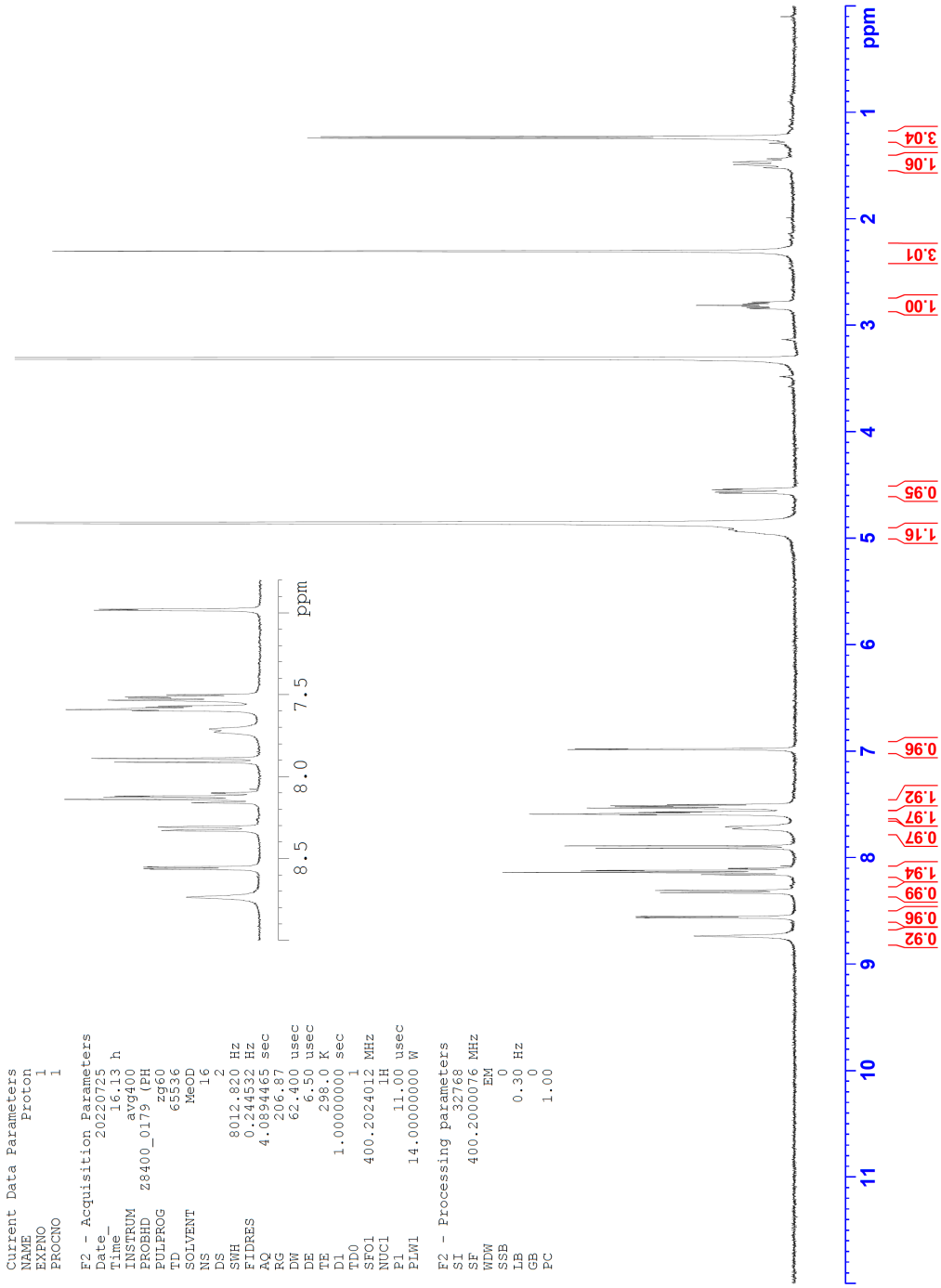
^{13}C Methyl 5-((2*S*,4*R*)-1-acetyl-2-methyl-4-(quinolin-6-ylamino)-1,2,3,4-tetrahydroquinolin-6-yl)picolinate (3.41)



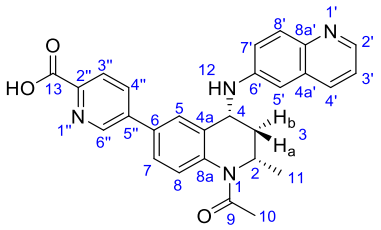


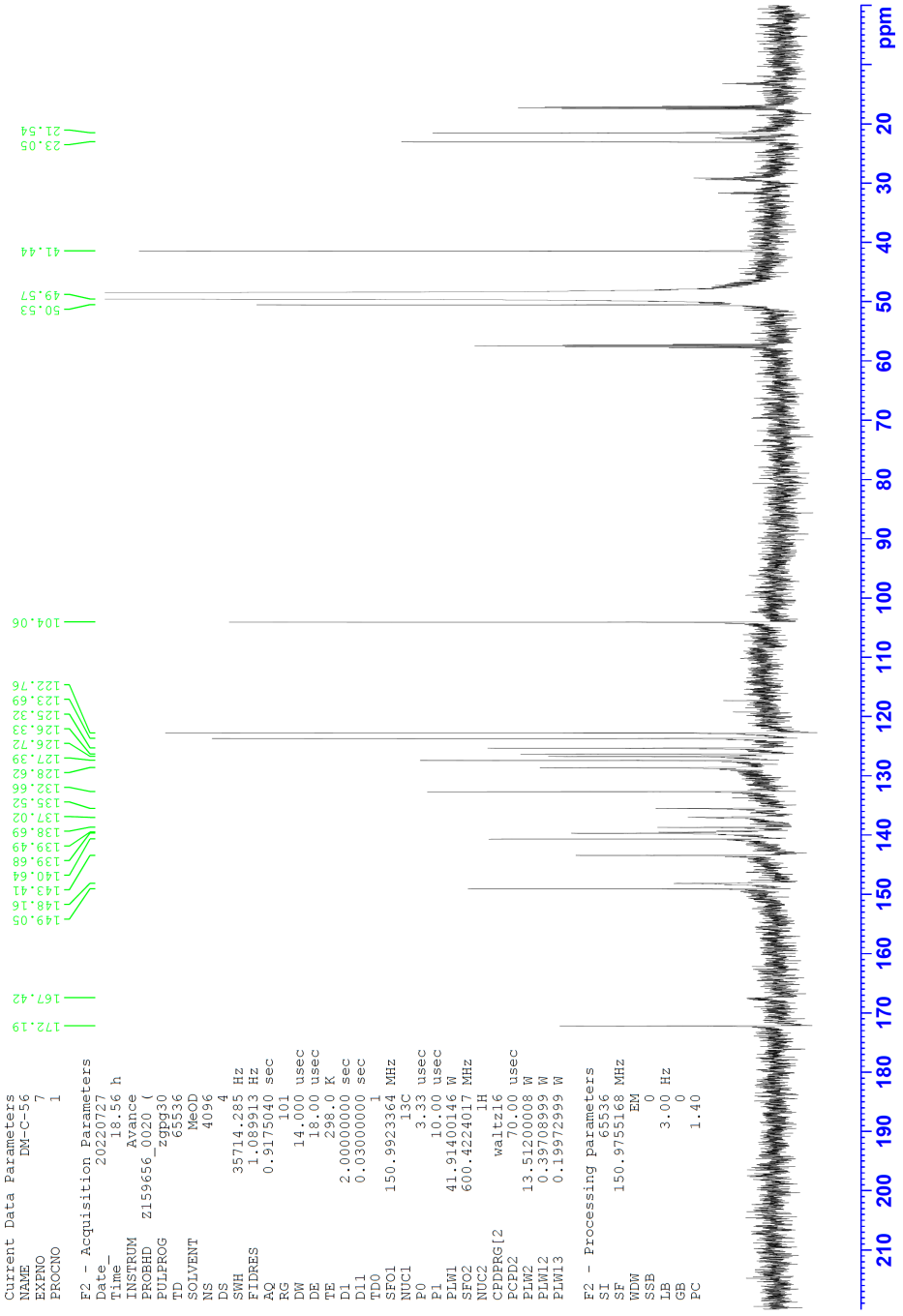
^{1}H NMR 5-((2*S*,4*R*)-1-Acetyl-2-methyl-4-(quinolin-6-ylamino)-1,2,3,4-tetrahydroquinolin-6-yl)picolinic acid (3.42)



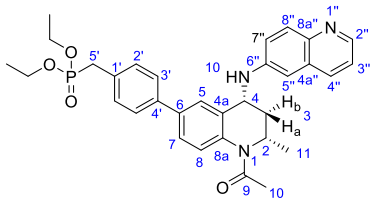


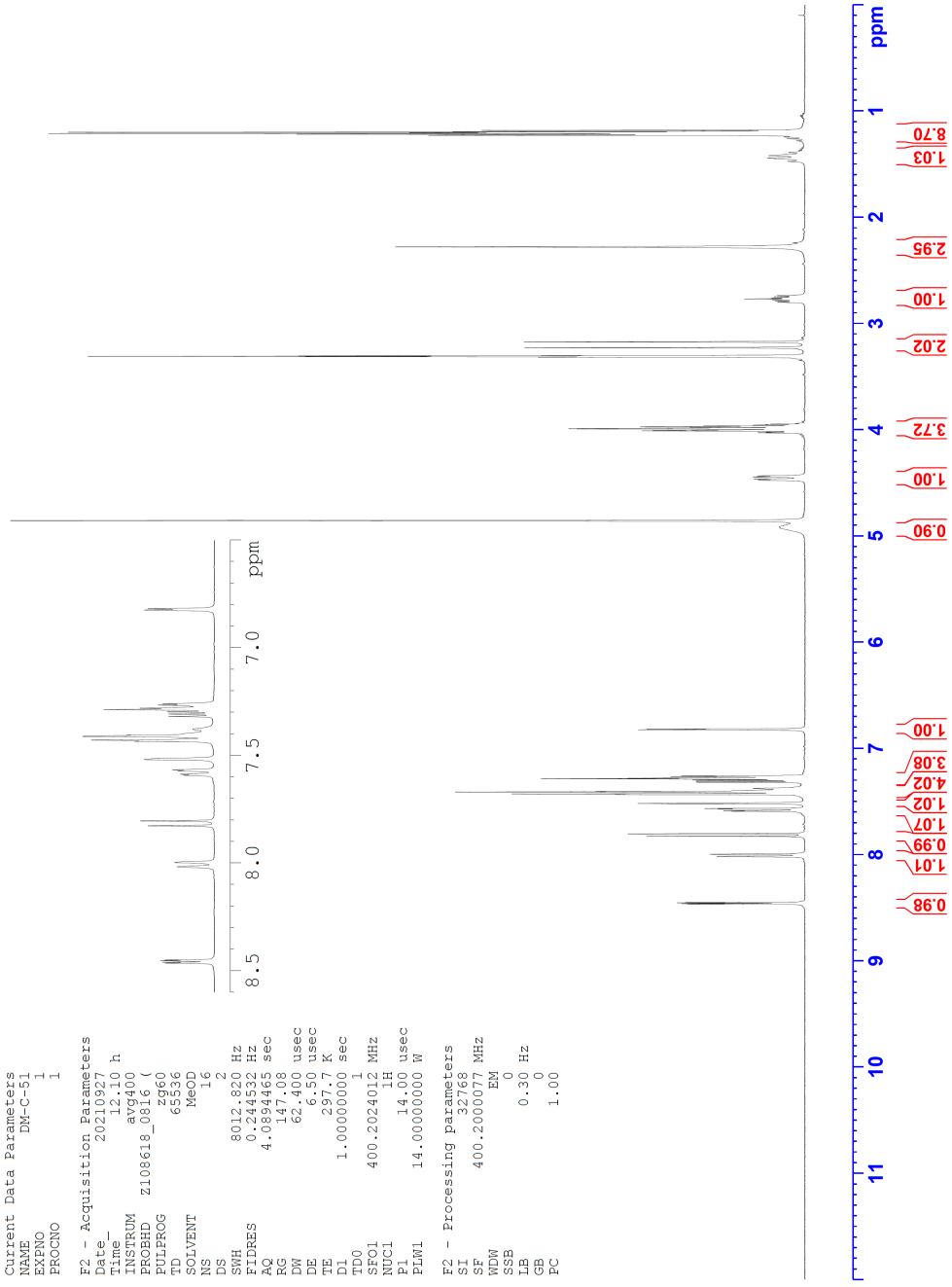
^{13}C NMR 5-((2*S*,4*R*)-1-Acetyl-2-methyl-4-(quinolin-6-ylamino)-1,2,3,4-tetrahydroquinolin-6-yl)picolinic acid (3.42)



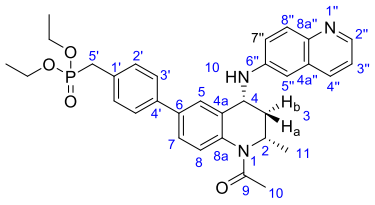


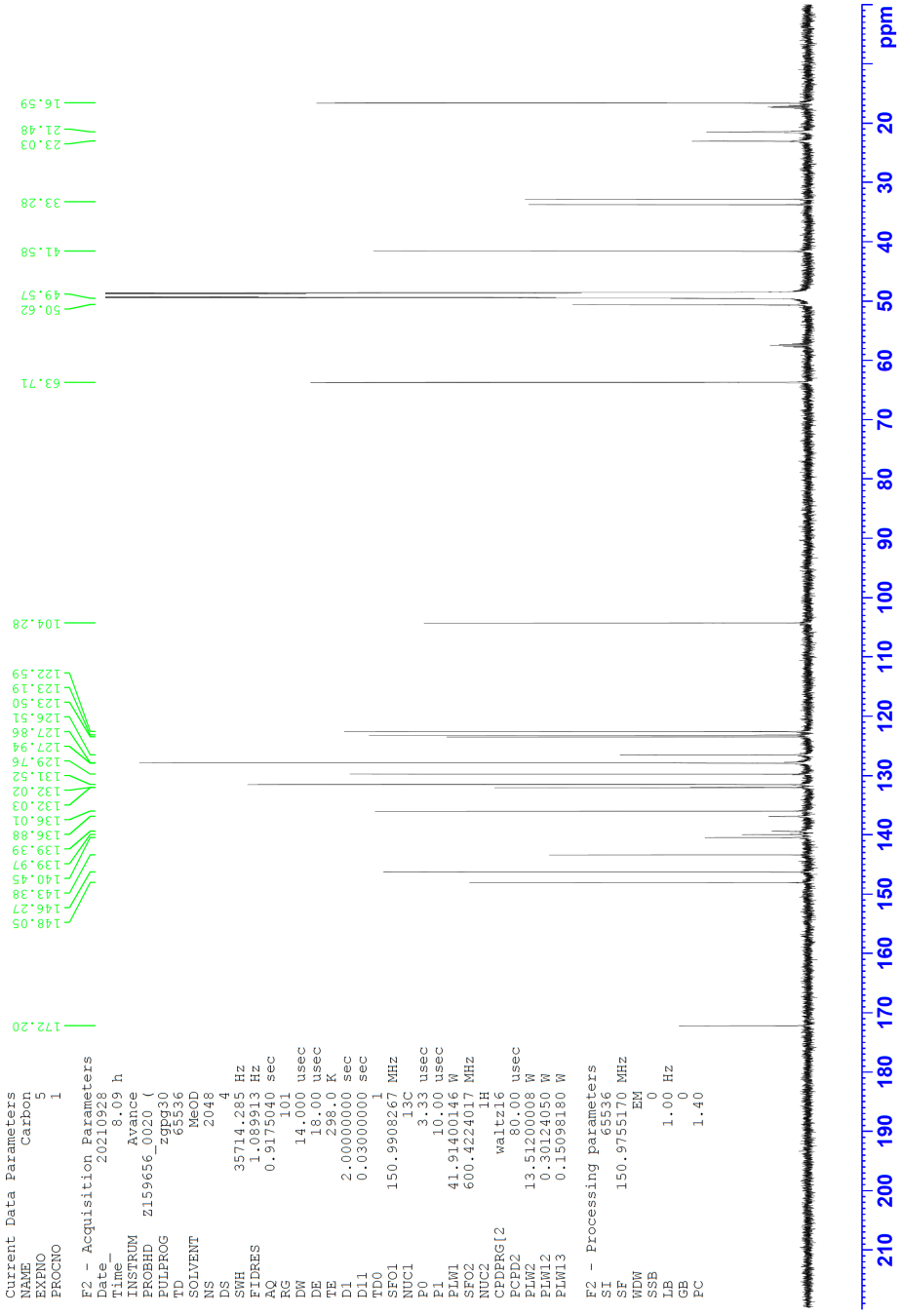
^{1}H NMR Diethyl (4'-((2*S*,4*R*)-1-acetyl-2-methyl-4-(quinolin-6''-ylamino)-1,2,3,4-tetrahydroquinolin-6-yl)benzyl)phosphonate (3.43)



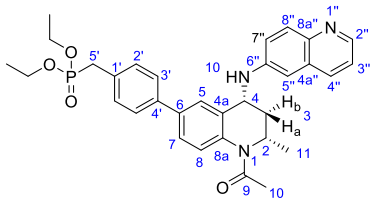


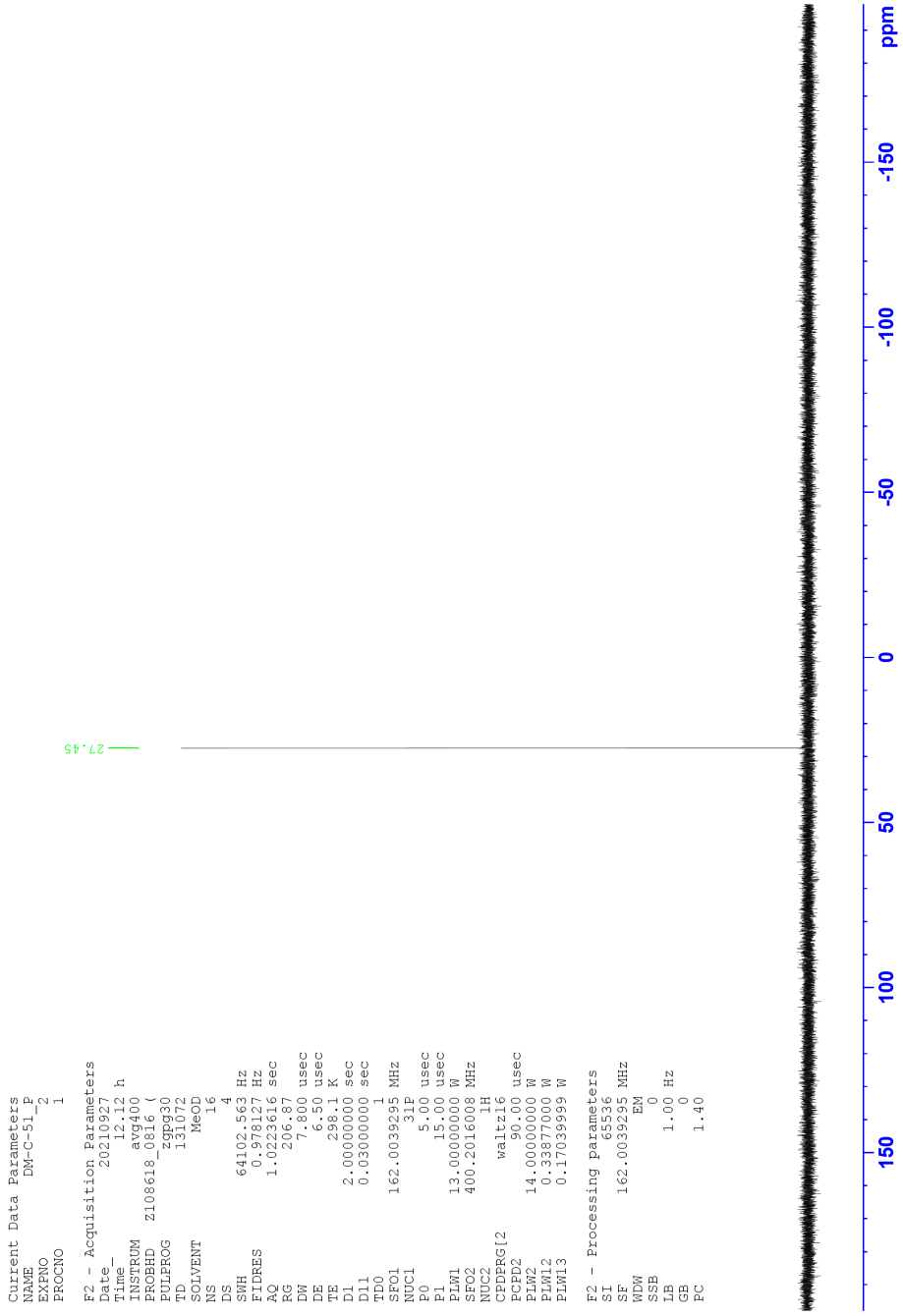
^{13}C NMR Diethyl (4'-((2*S*,4*R*)-1-acetyl-2-methyl-4-(quinolin-6''-ylamino)-1,2,3,4-tetrahydroquinolin-6-yl)benzyl)phosphonate (3.43)





^{31}P NMR Diethyl (4'-((2*S*,4*R*)-1-acetyl-2-methyl-4-(quinolin-6''-ylamino)-1,2,3,4-tetrahydroquinolin-6-yl)benzyl)phosphonate (3.43)



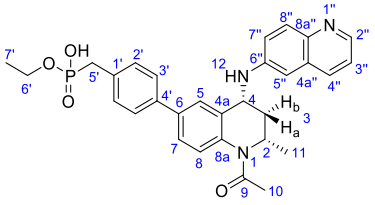


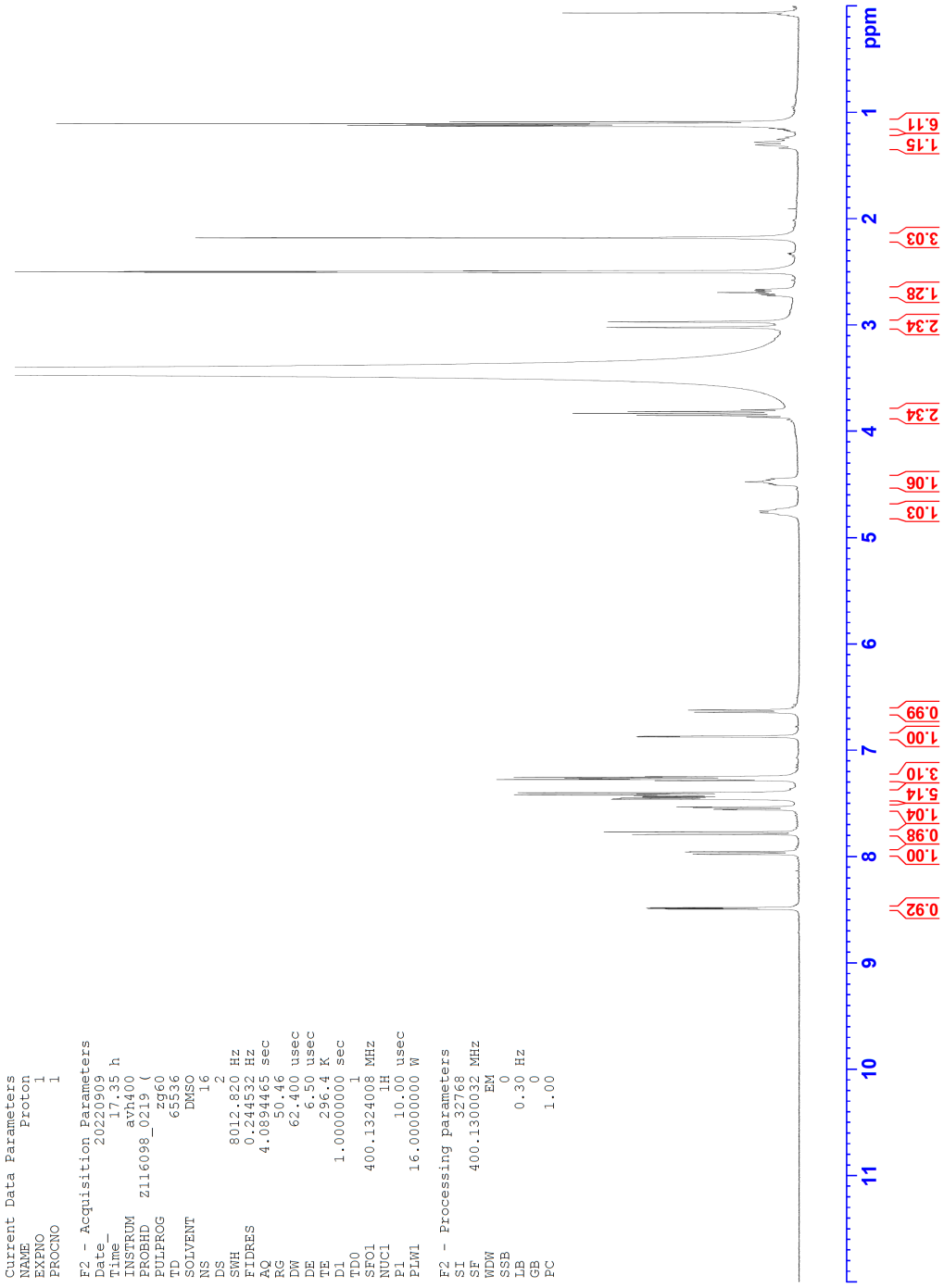

```
Current Data Parameters
NAME        DM-C-51_P
EXPNO               2
PROCNO              1

F2 - Acquisition Parameters
Date_          20210927
Time_             12.12 h
INSTRUM         avg400
PROBHD  Z108618_0816 (
PULPROG          zgpg30
TD               131072
SOLVENT             MeOD
NS                    16
DS                     4
SWH            64102.563 Hz
FIDRES         0.978127 Hz
AQ             1.0223616 sec
RG                206.87
DW                7.800 usec
DE                6.50 usec
TE                298.1 K
D1             2.00000000 sec
D11            0.03000000 sec
TD0                    1
SFO1           162.0039295 MHz
NUC1                 31P
P0                  5.00 usec
P1                 15.00 usec
PLW1           13.00000000 W
SFO2           400.2016008 MHz
NUC2                 1H
CPDPRG[2          waltz16
PCPD2              90.00 usec
PLW2           14.00000000 W
PLW12           0.33877000 W
PLW13           0.17039999 W

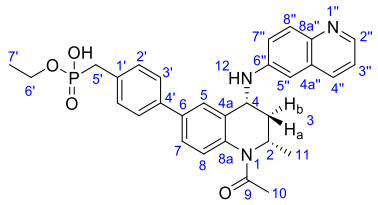
F2 - Processing parameters
SI                   65536
SF             162.0039295 MHz
WDW                     EM
SSB                      0
LB                    1.00 Hz
GB                       0
PC                    1.40
```

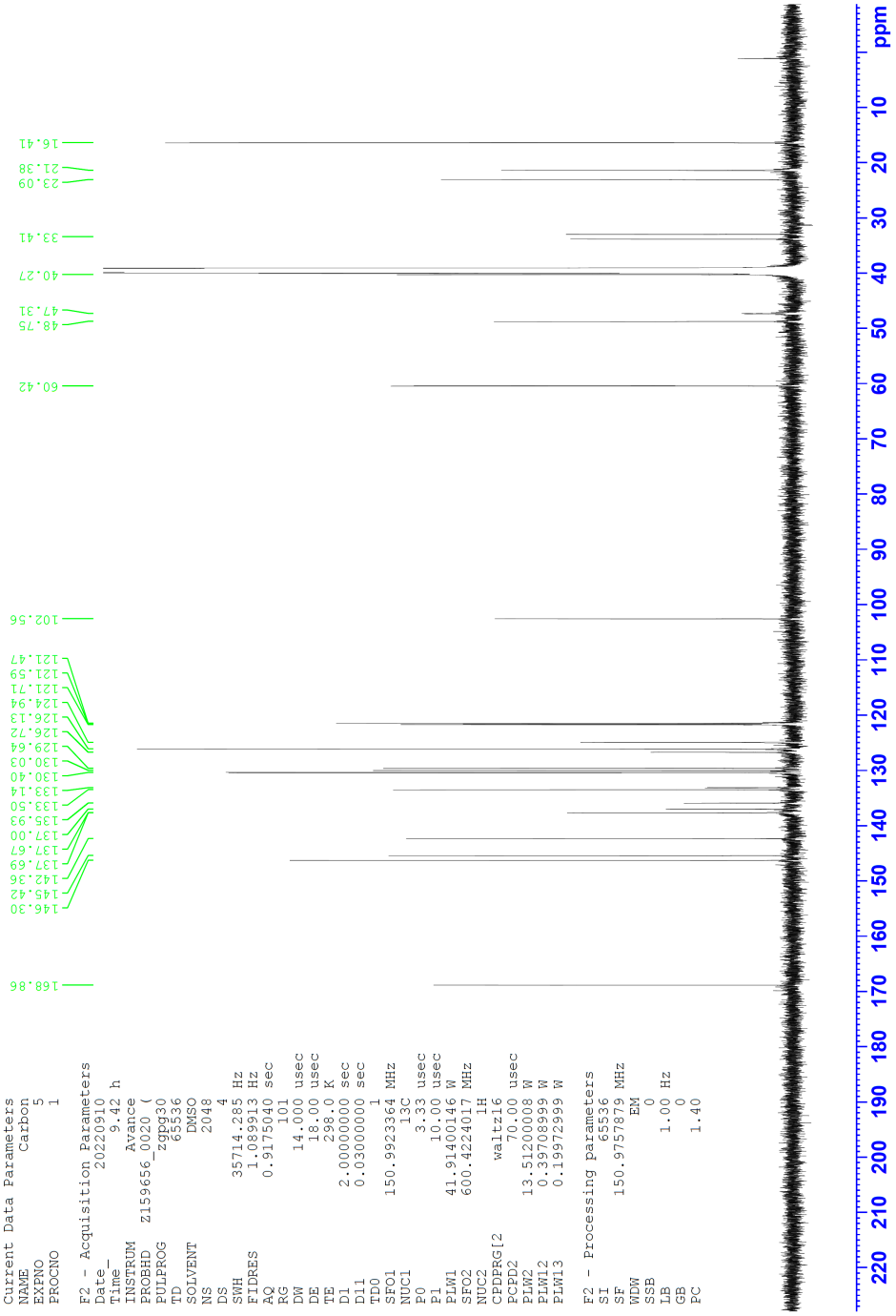
^{1}H NMR Ethyl hydrogen (4-((2*S*,4*R*)-1-acetyl-2-methyl-4-(quinolin-6-ylamino)-1,2,3,4-tetrahydroquinolin-6-yl)benzyl)phosphonate (3.44)



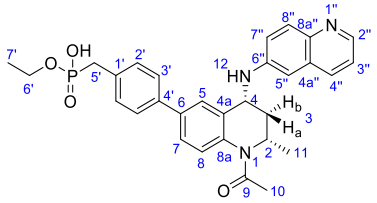


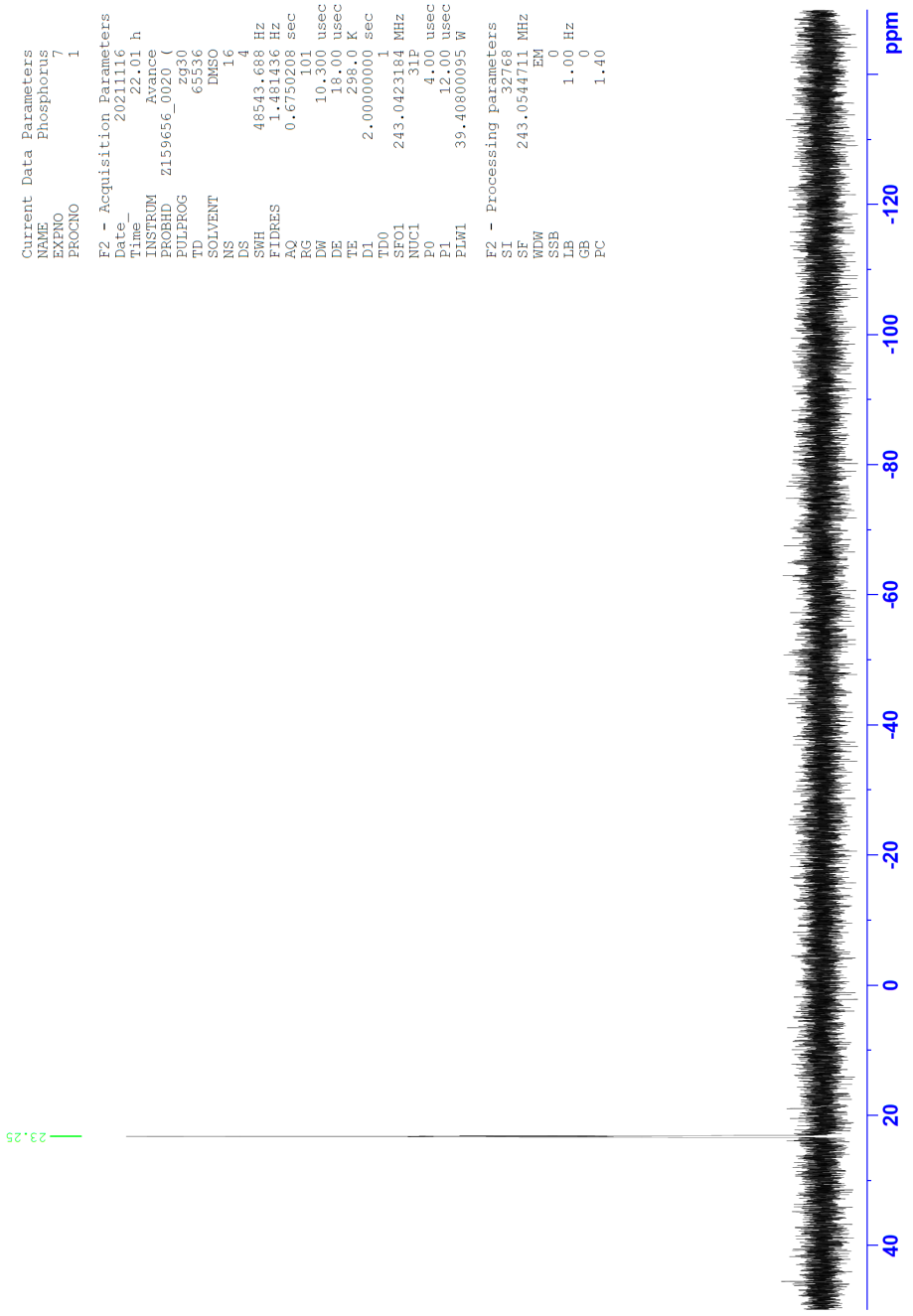
^{13}C NMR Ethyl hydrogen (4-((2*S*,4*R*)-1-acetyl-2-methyl-4-(quinolin-6-ylamino)-1,2,3,4-tetrahydroquinolin-6-yl)benzyl)phosphonate (3.44)



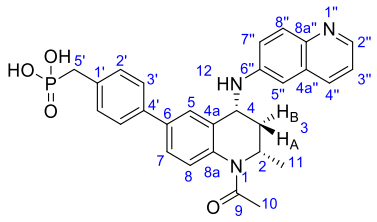


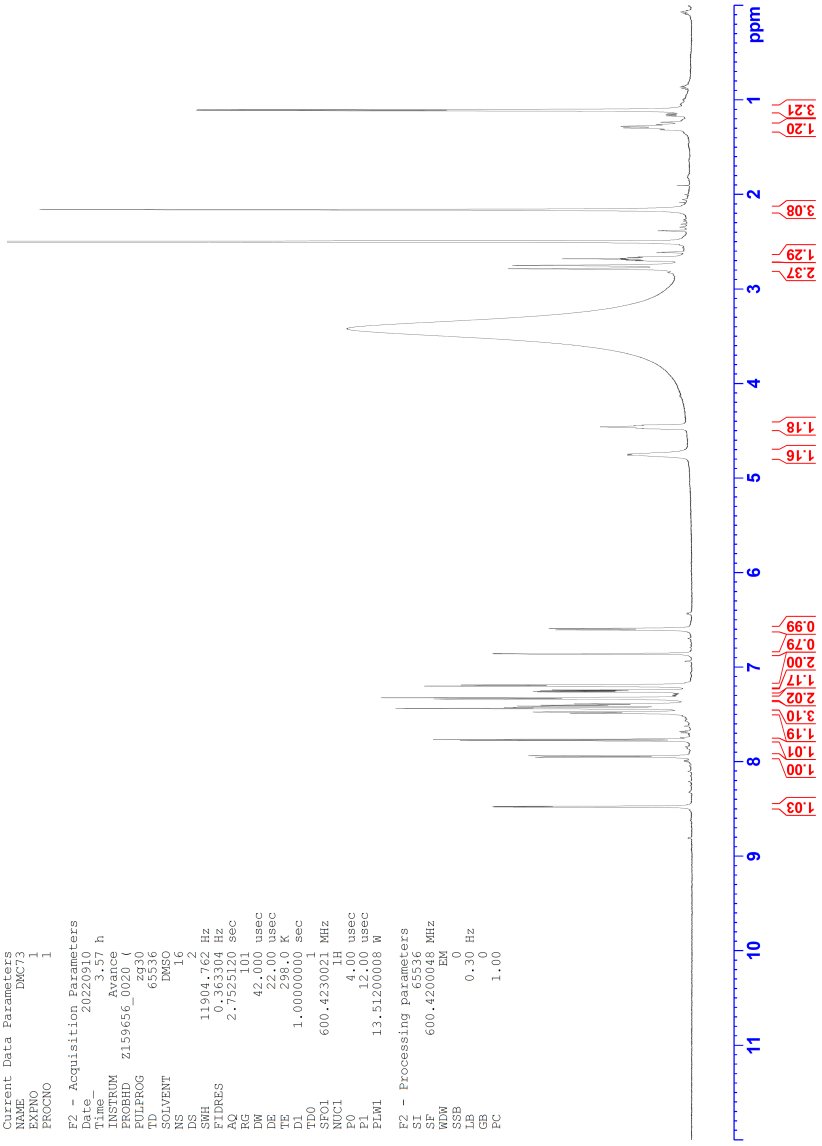
^{31}P NMR Ethyl hydrogen (4-((2*S*,4*R*)-1-acetyl-2-methyl-4-(quinolin-6-ylamino)-1,2,3,4-tetrahydroquinolin-6-yl)benzyl)phosphonate (3.44)



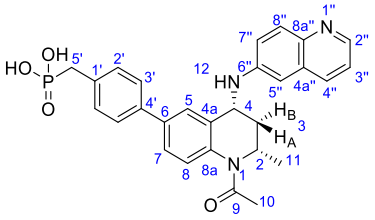


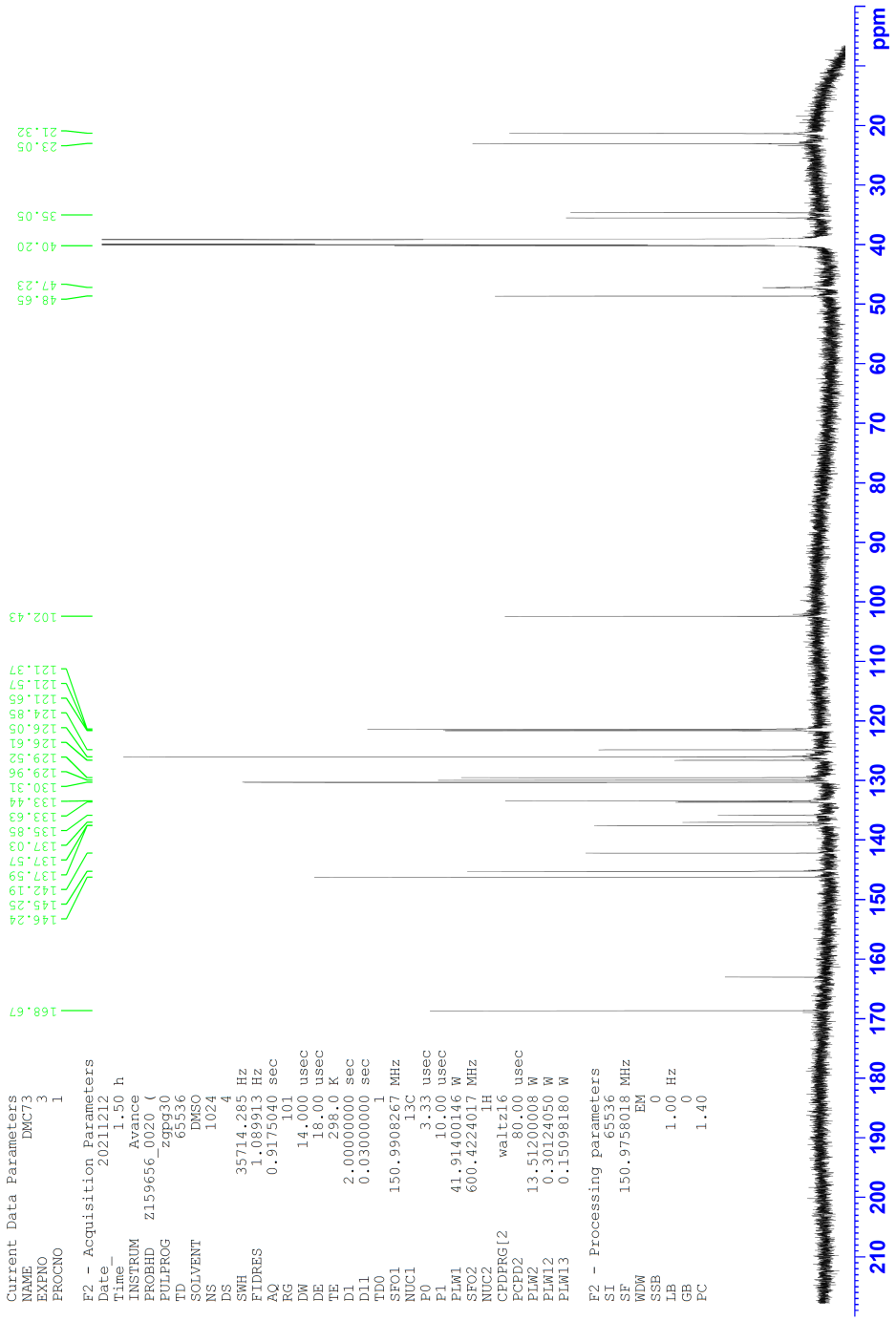
^{1}H NMR (4-((2*S*,4*R*)-1-Acetyl-2-methyl-4-(quinolin-6-ylamino)-1,2,3,4-tetrahydroquinolin-6-yl)benzyl)phosphonic acid (3.45)



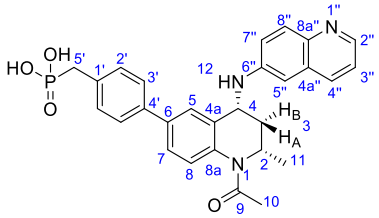


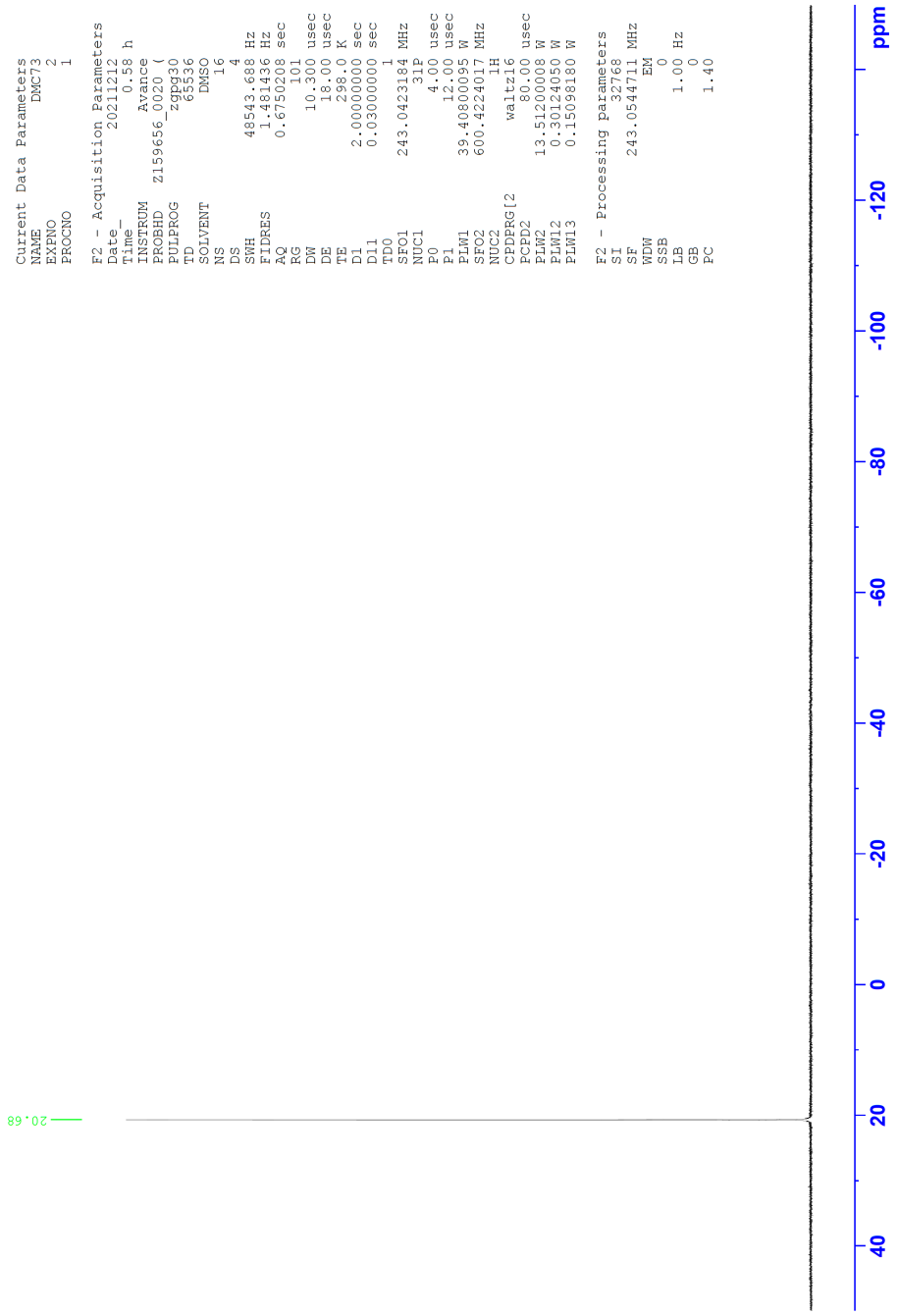
^{13}C NMR (4-((2*S*,4*R*)-1-Acetyl-2-methyl-4-(quinolin-6-ylamino)-1,2,3,4-tetrahydroquinolin-6-yl)benzyl)phosphonic acid (3.45)



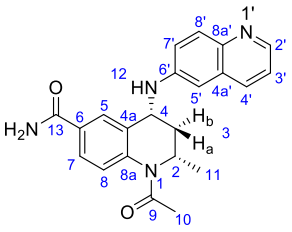


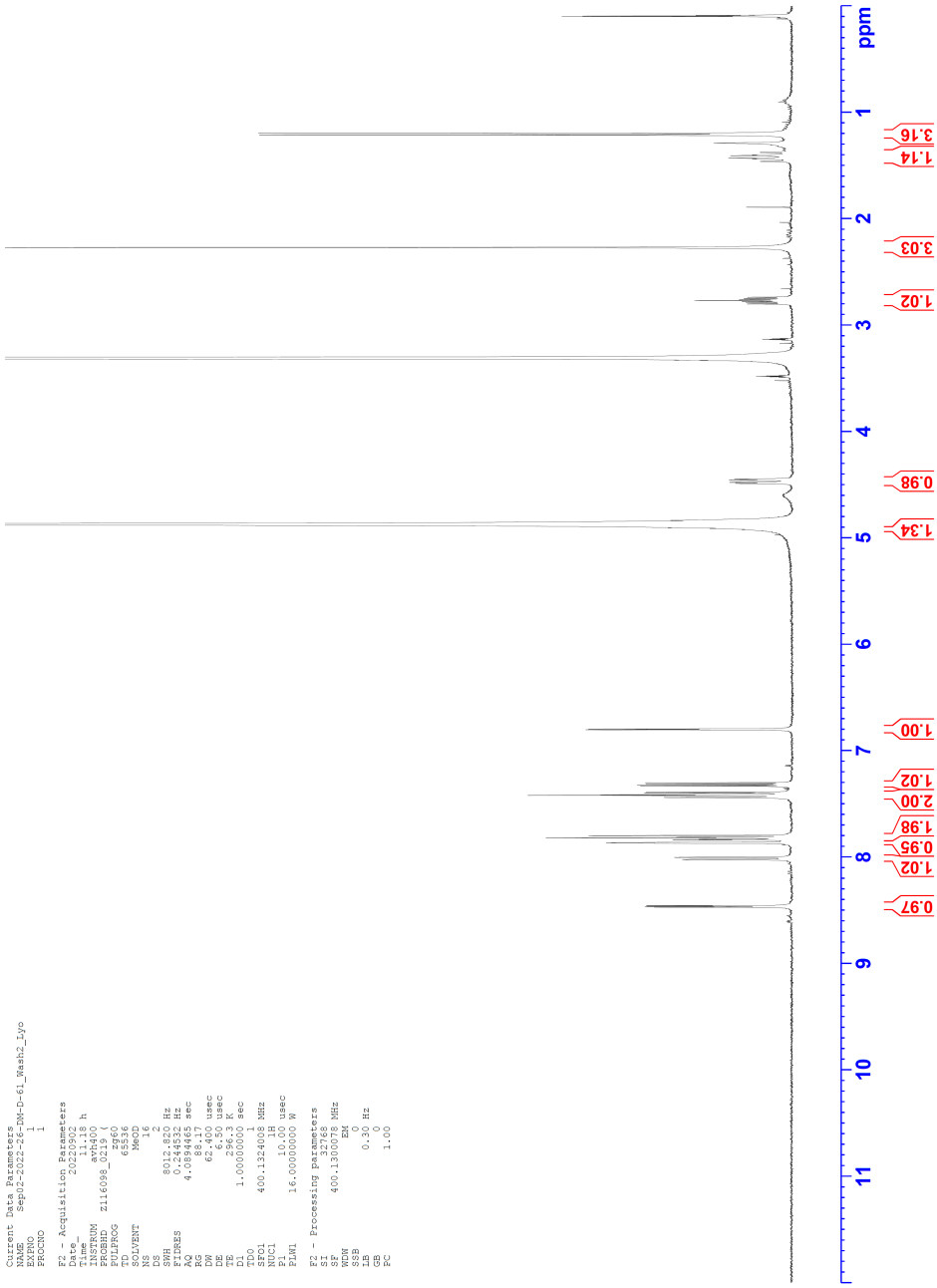
^{31}P NMR (4-((2*S*,4*R*)-1-Acetyl-2-methyl-4-(quinolin-6-ylamino)-1,2,3,4-tetrahydroquinolin-6-yl)benzyl)phosphonic acid (3.45)





^{1}H NMR (2*S*,4*R*)-1-Acetyl-2-methyl-4-(quinolin-6-ylamino)-1,2,3,4-tetrahydroquinoline-6-carboxamide (3.46)



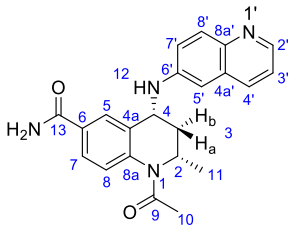


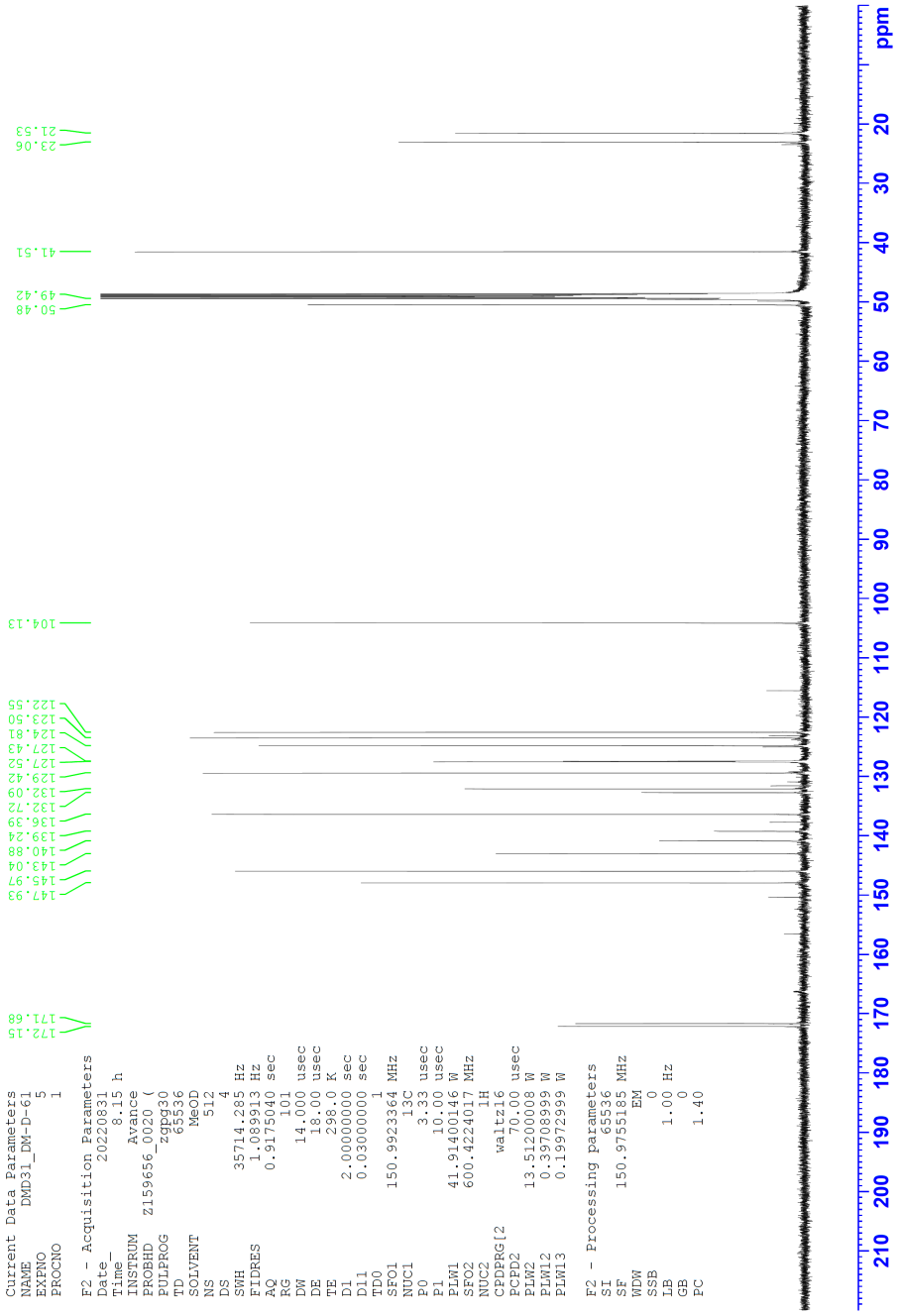
Current Data Parameters
NAME Sep02-2022-26-DM-D-61_Wash2_Iyo
EXPNO 1
PROCNO 1

F2 - Acquisition Parameters
Date_ 20220902
Time 11.18 h
INSTRUM spect
PROBHD 2116098_0219 (
PULPROG zg60
TD 65536
SOLVENT DMSO
NS 16
DS 2
SWH 8012.820 Hz
FIDRES 0.244522 Hz
AQ 4.0894465 sec
RG 88.17
DW 62.400 usec
DE 6.50 usec
TE 296.3 K
D1 1.00000000 sec
TD0 1
SFO1 400.1324008 MHz
NUC1 1H
P1 10.00 usec
PLW1 16.00000000 W

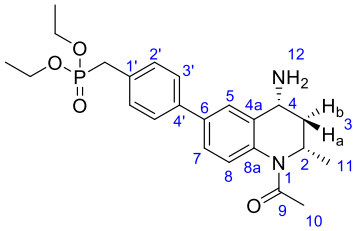
F2 - Processing parameters
SI 32768
SF 400.1300078 MHz
WDW EM
SSB 0
LB 0.30 Hz
GB 0
PC 1.00

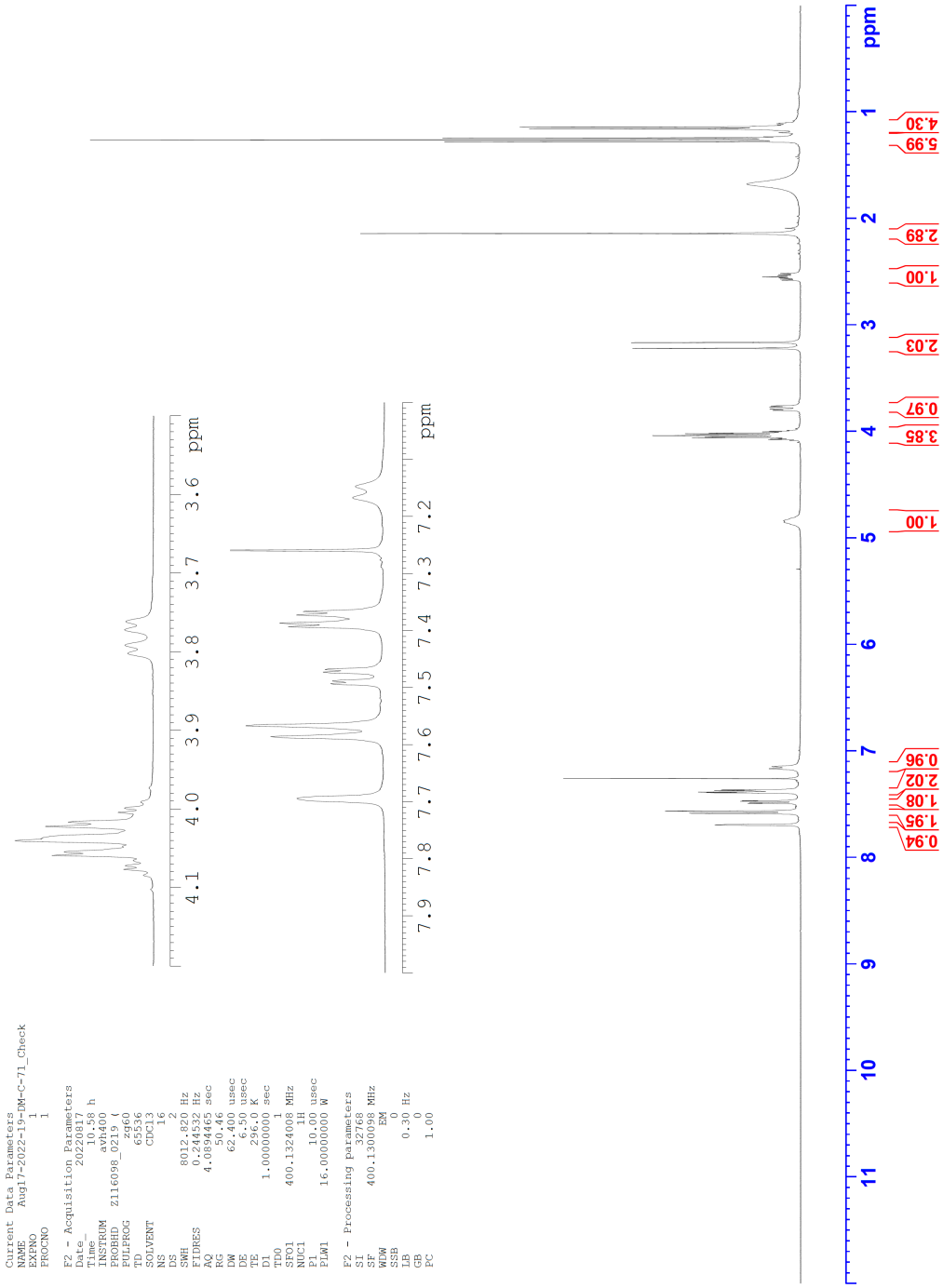
^{13}C NMR (2*S*,4*R*)-1-Acetyl-2-methyl-4-(quinolin-6-ylamino)-1,2,3,4-tetrahydroquinoline-6-carboxamide (3.46)



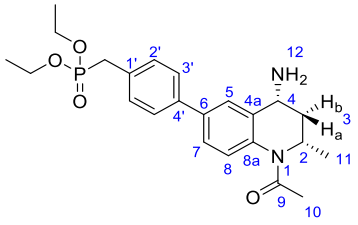


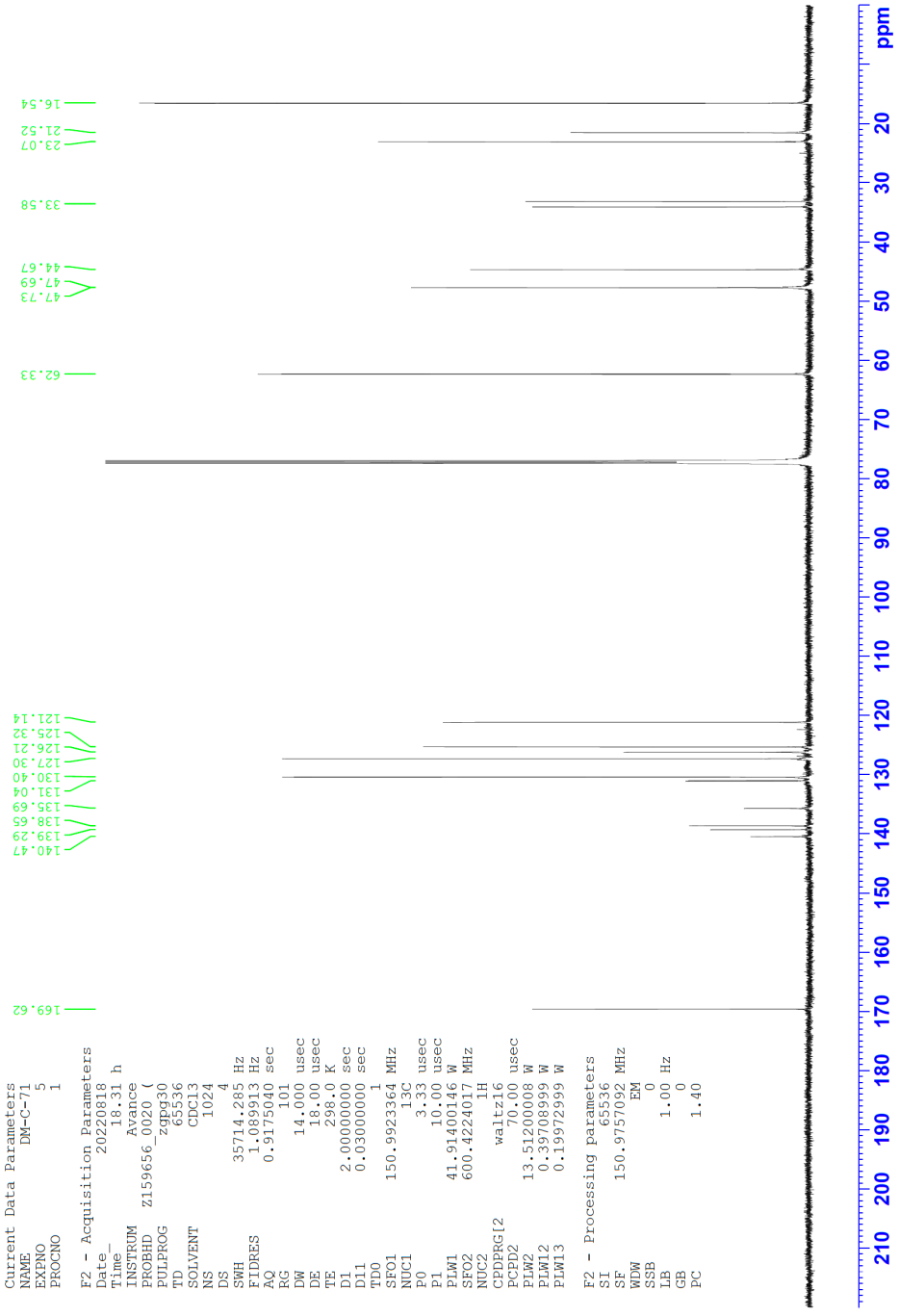
^{1}H NMR Diethyl (4'-((2*S*,4*R*)-1-acetyl-4-amino-2-methyl-1,2,3,4-tetrahydroquinolin-6-yl)benzyl)phosphonate (3.49)



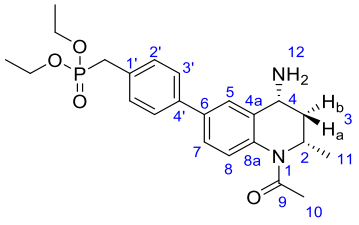


^{13}C NMR Diethyl (4'-((2*S*,4*R*)-1-acetyl-4-amino-2-methyl-1,2,3,4-tetrahydroquinolin-6-yl)benzyl)phosphonate (3.49)





^{31}P NMR Diethyl (4'-((2*S*,4*R*)-1-acetyl-4-amino-2-methyl-1,2,3,4-tetrahydroquinolin-6-yl)benzyl)phosphonate (3.49)



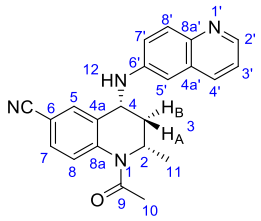


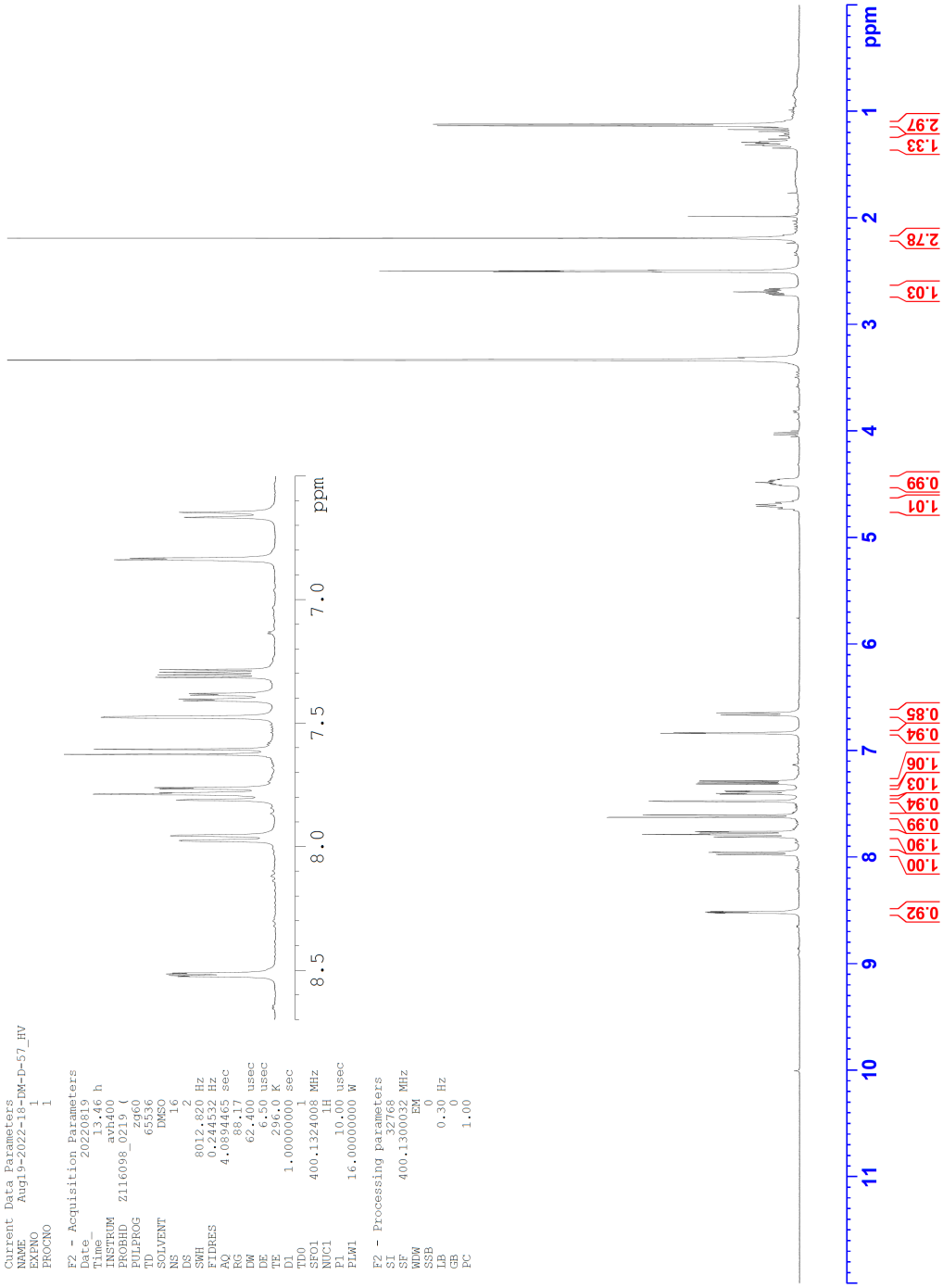

```
Current Data Parameters
NAME      Aug17-2022-19-DM-C-71_Check
EXPNO           2
PROCNO          1

F2 - Acquisition Parameters
Date_        20220817
Time            10.59 h
INSTRUM         av4n400
PROBHD  Z116098_0221 4
PULPROG         zgpg30
TD              131072
SOLVENT         CDCl3
NS                16
DS                 4
SWH         64102.563 Hz
FIDRES      0.978127 Hz
AQ          1.0223616 sec
RG             197.18
DW            7.800 usec
DE            6.50 usec
TE            296.2 K
D1          2.00000000 sec
D11         0.03000000 sec
TD0                1
SFO1    161.9755930 MHz
NUC1             31P
P0              3.73 usec
P1             11.20 usec
PLW1    59.00000000 W
SFO2    400.1316005 MHz
NUC2             1H
CPDPRG[2        waltz16
PCPD2          90.00 usec
PLW2    16.00000000 W
PLW12    0.19753000 W
PLW13    0.09935700 W

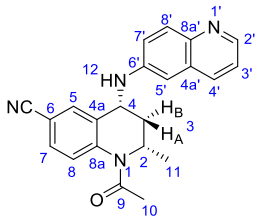
F2 - Processing parameters
SI              65536
SF      161.9755930 MHz
WDW               EM
SSB                0
LB              1.00 Hz
GB                 0
PC              1.40
```

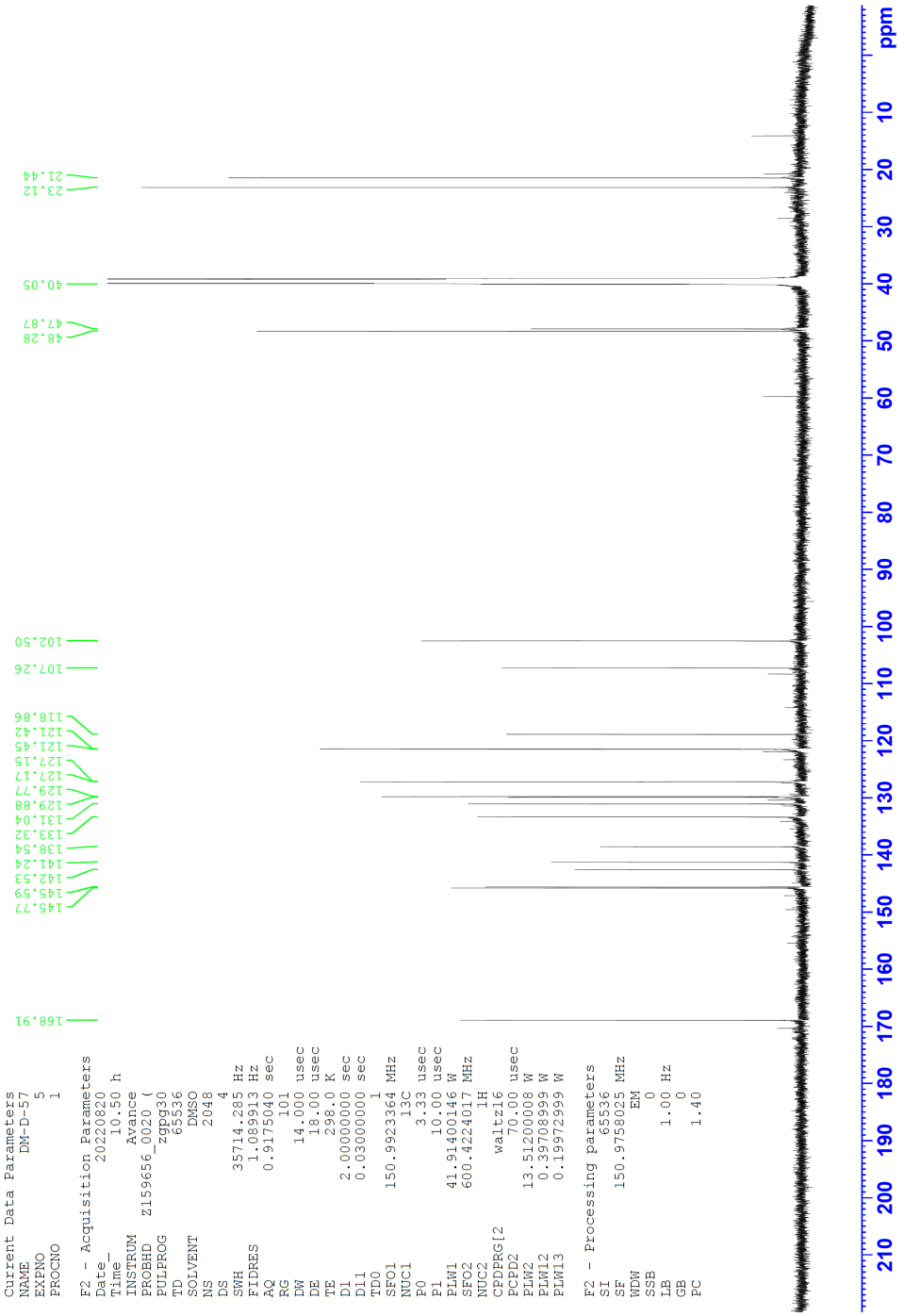
^{1}H NMR (2*S*,4*R*)-1-Acetyl-2-methyl-4-(quinolin-6-ylamino)-1,2,3,4-tetrahydroquinoline-6-carbonitrile (3.53)



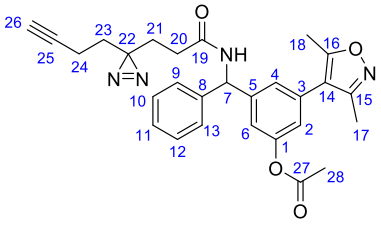


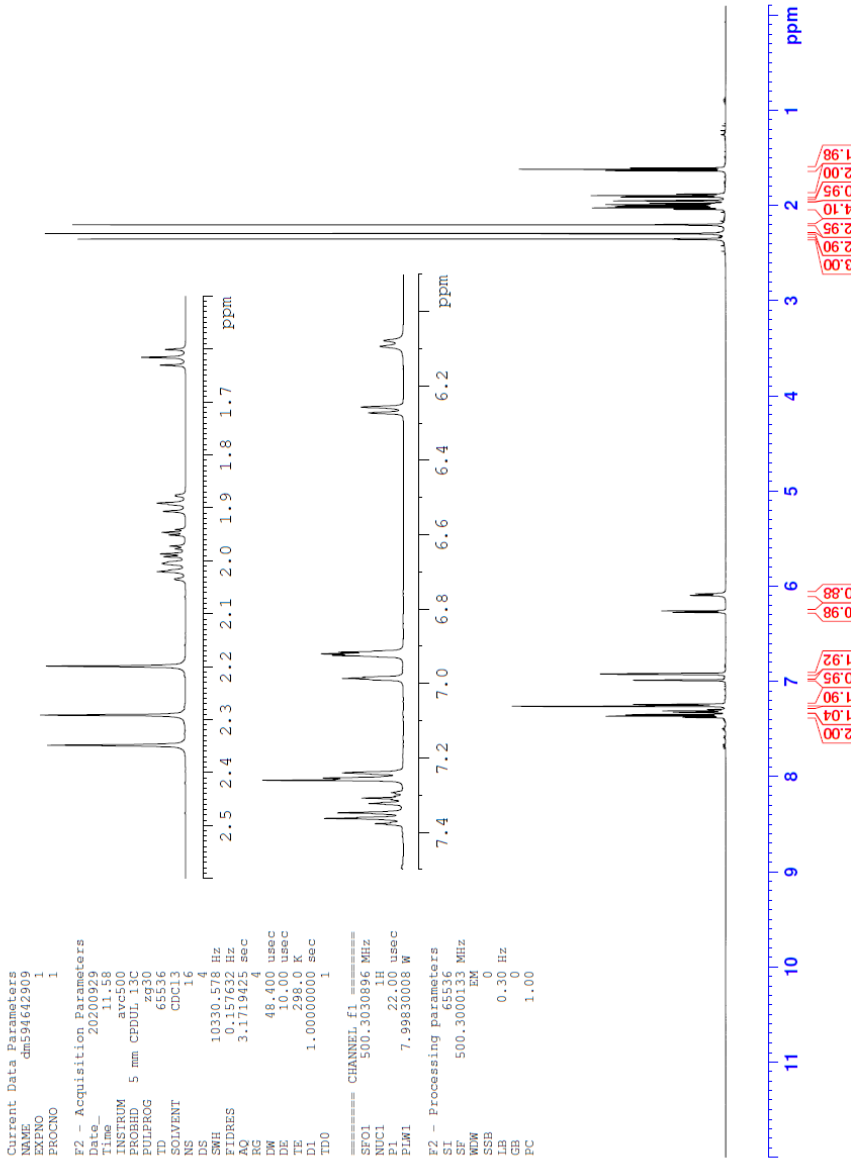
^{13}C NMR (2*S*,4*R*)-1-Acetyl-2-methyl-4-(quinolin-6-ylamino)-1,2,3,4-tetrahydroquinoline-6-carbonitrile (3.53)



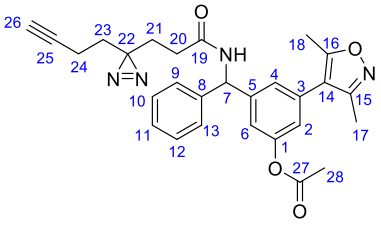


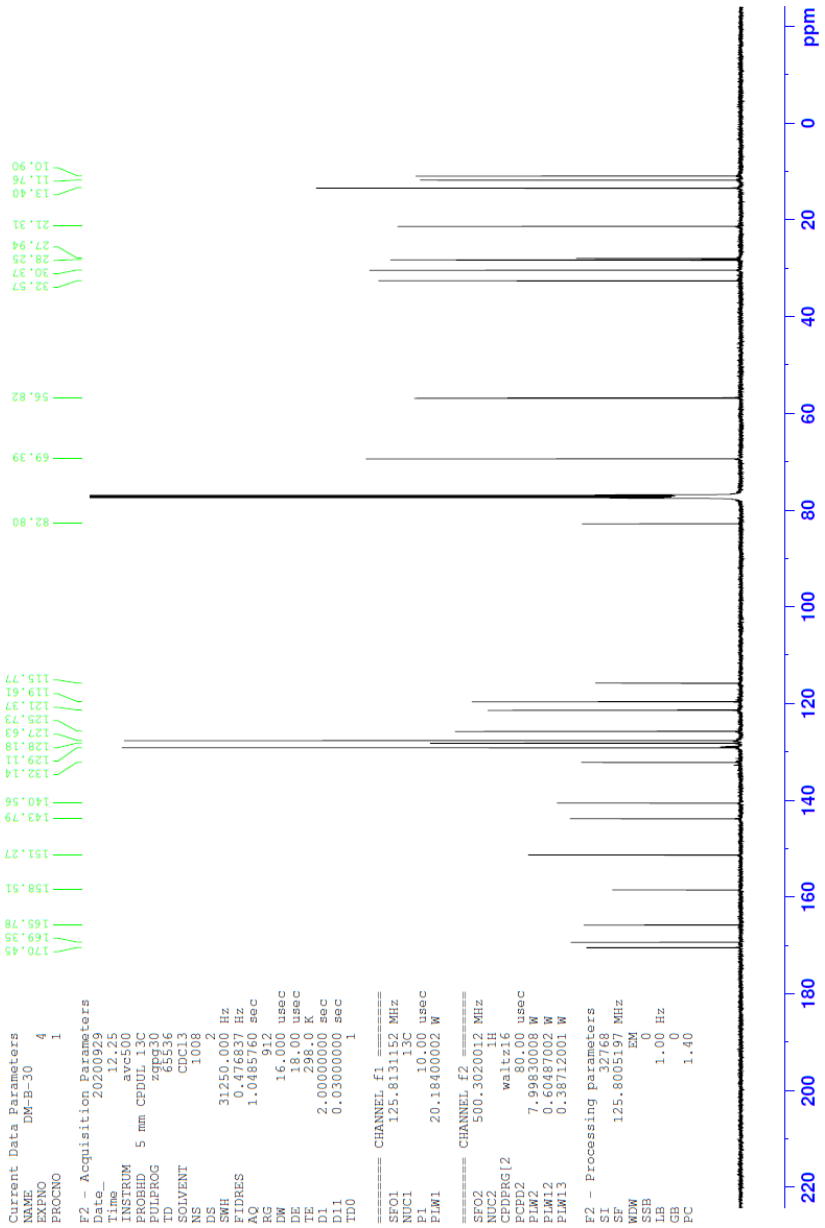
^{1}H NMR 3-((3-(3-(But-3-yn-1-yl)-3*H*-diazirin-3-yl)propanamido)(phenyl)methyl)-5-(3,5-dimethylisoxazol-4-yl)phenyl acetate (4.2)



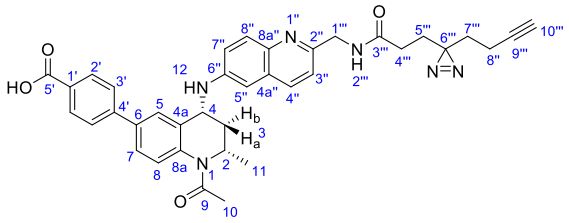


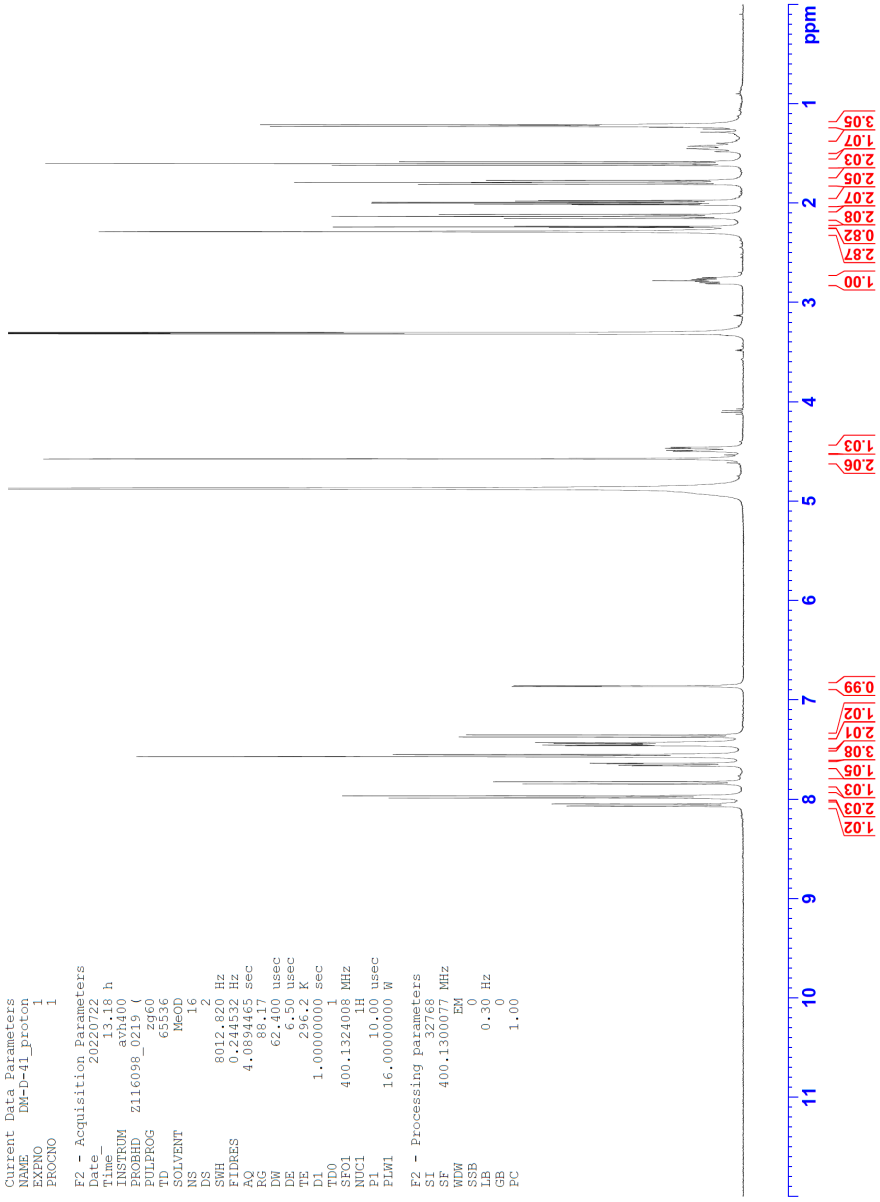
^{13}C NMR 3-((3-(3-(But-3-yn-1-yl)-3*H*-diazirin-3-yl)propanamido)(phenyl)methyl)-5-(3,5-dimethylisoxazol-4-yl)phenyl acetate (4.2)



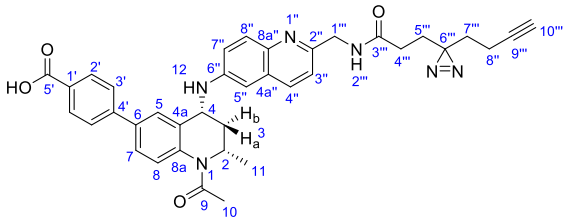


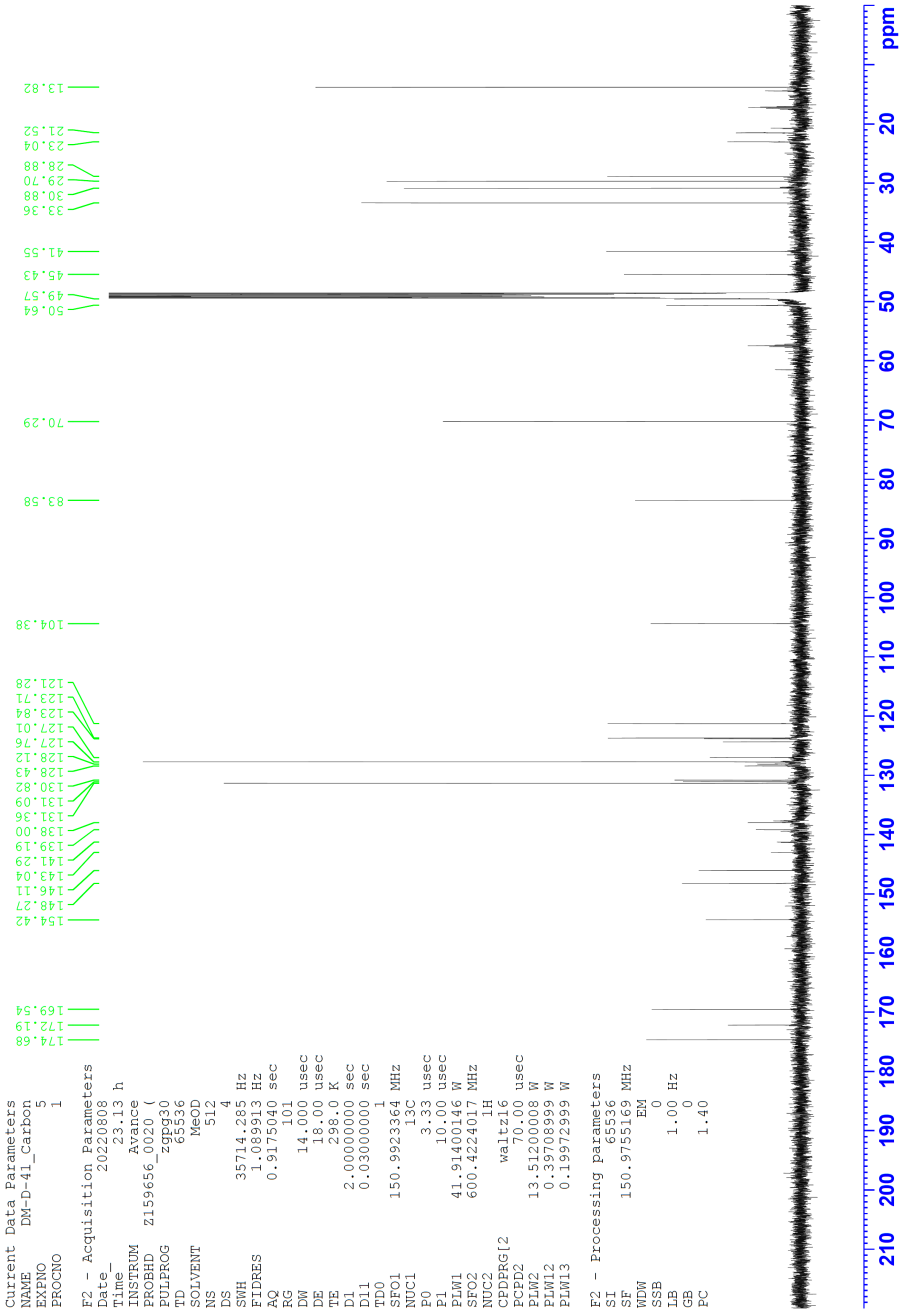
^{1}H NMR 4-((2*S*,4*R*)-1-acetyl-4-((2-((3-(3-(but-3-yn-1-yl)-3*H*-diazirin-3-yl)propanamido)methyl)quinolin-6-yl)amino)-2-methyl-1,2,3,4-tetrahydroquinolin-6-yl)benzoic acid (4.5)



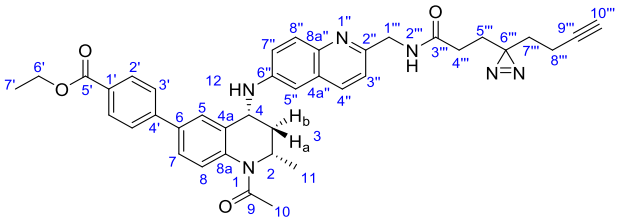


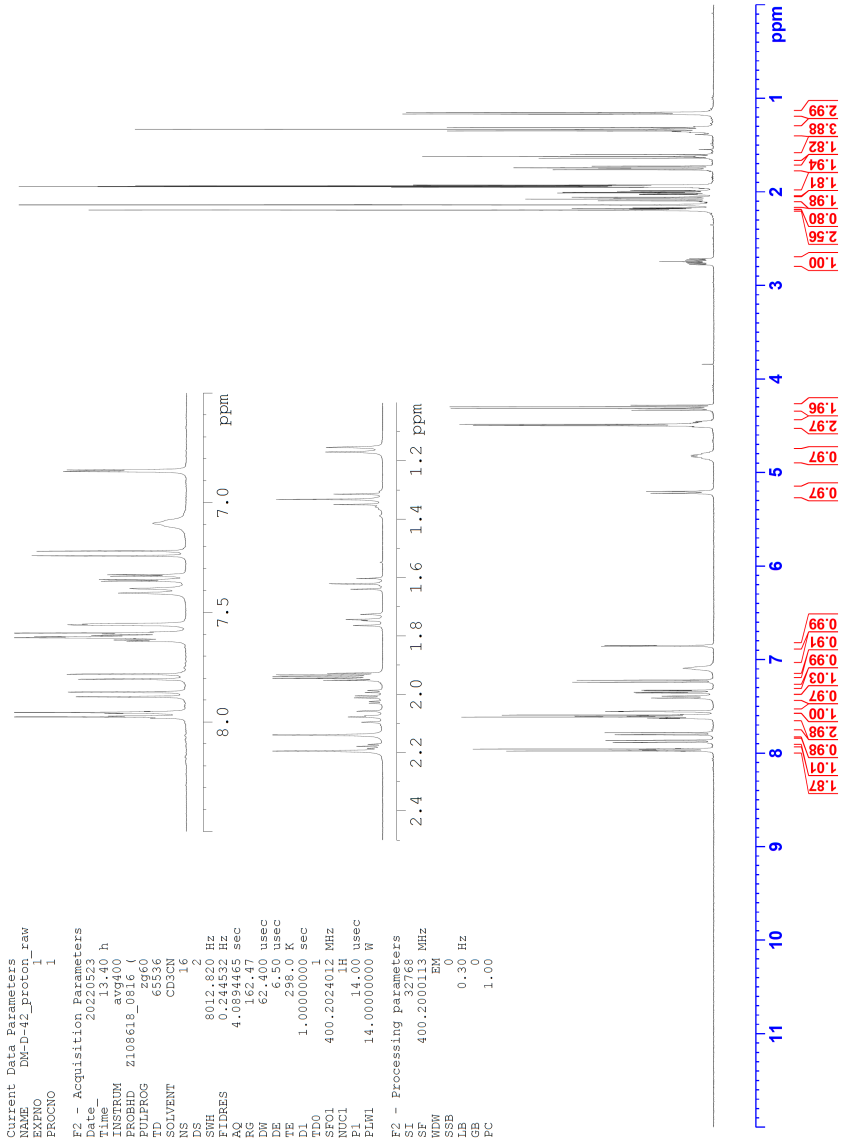
^{13}C NMR 4-((2*S*,4*R*)-1-acetyl-4-((2-((3-(3-(but-3-yn-1-yl)-3*H*-diazirin-3-yl)propanamido)methyl)quinolin-6-yl)amino)-2-methyl-1,2,3,4-tetrahydroquinolin-6-yl)benzoic acid (4.5)



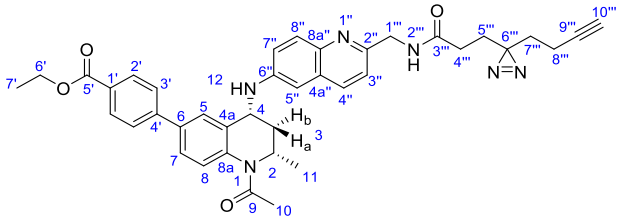


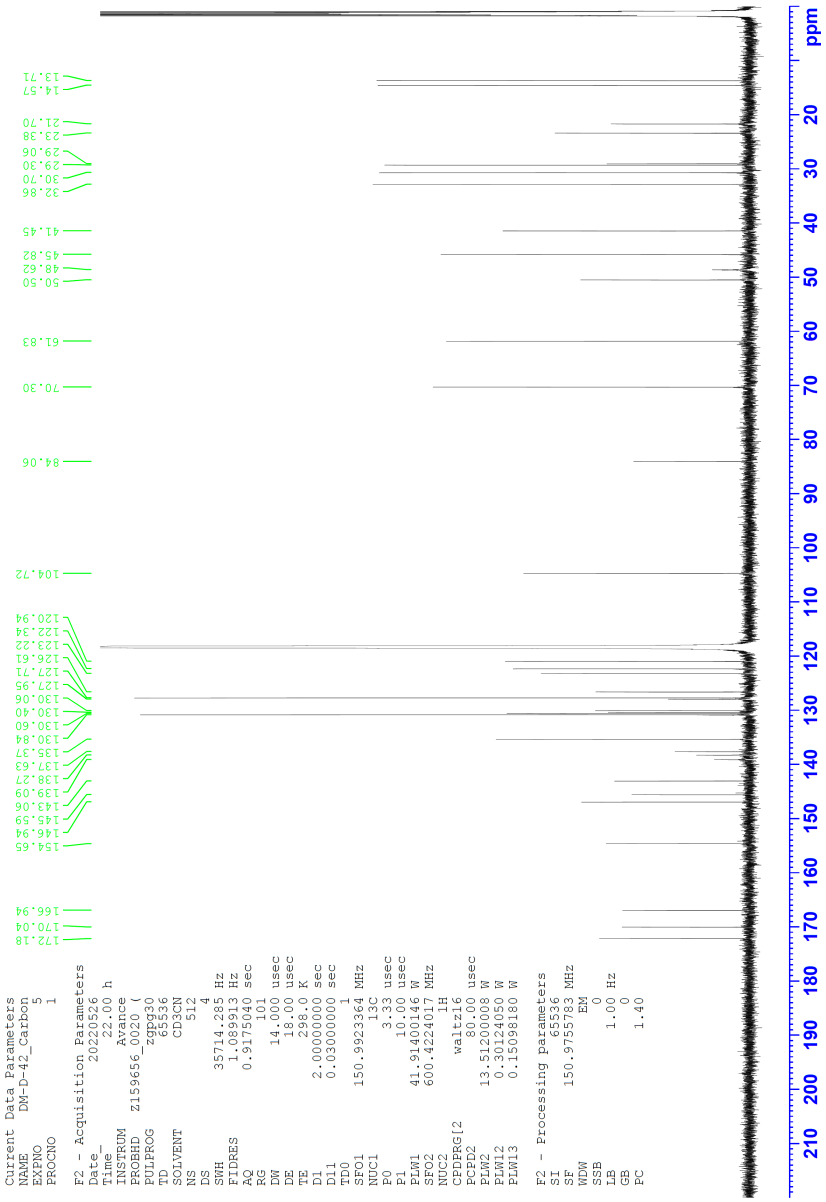
^{1}H NMR Ethyl 4-((2*S*,4*R*)-1-acetyl-4-((2-((3-(3-(but-3-yn-1-yl)-3H-diazirin-3-yl)propanamido)methyl)quinolin-6-yl)amino)-2-methyl-1,2,3,4-tetrahydroquinolin-6-yl)benzoate (4.6)



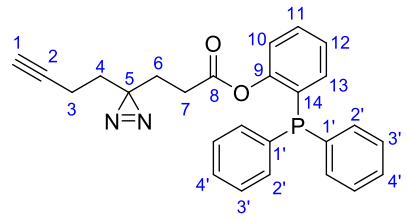


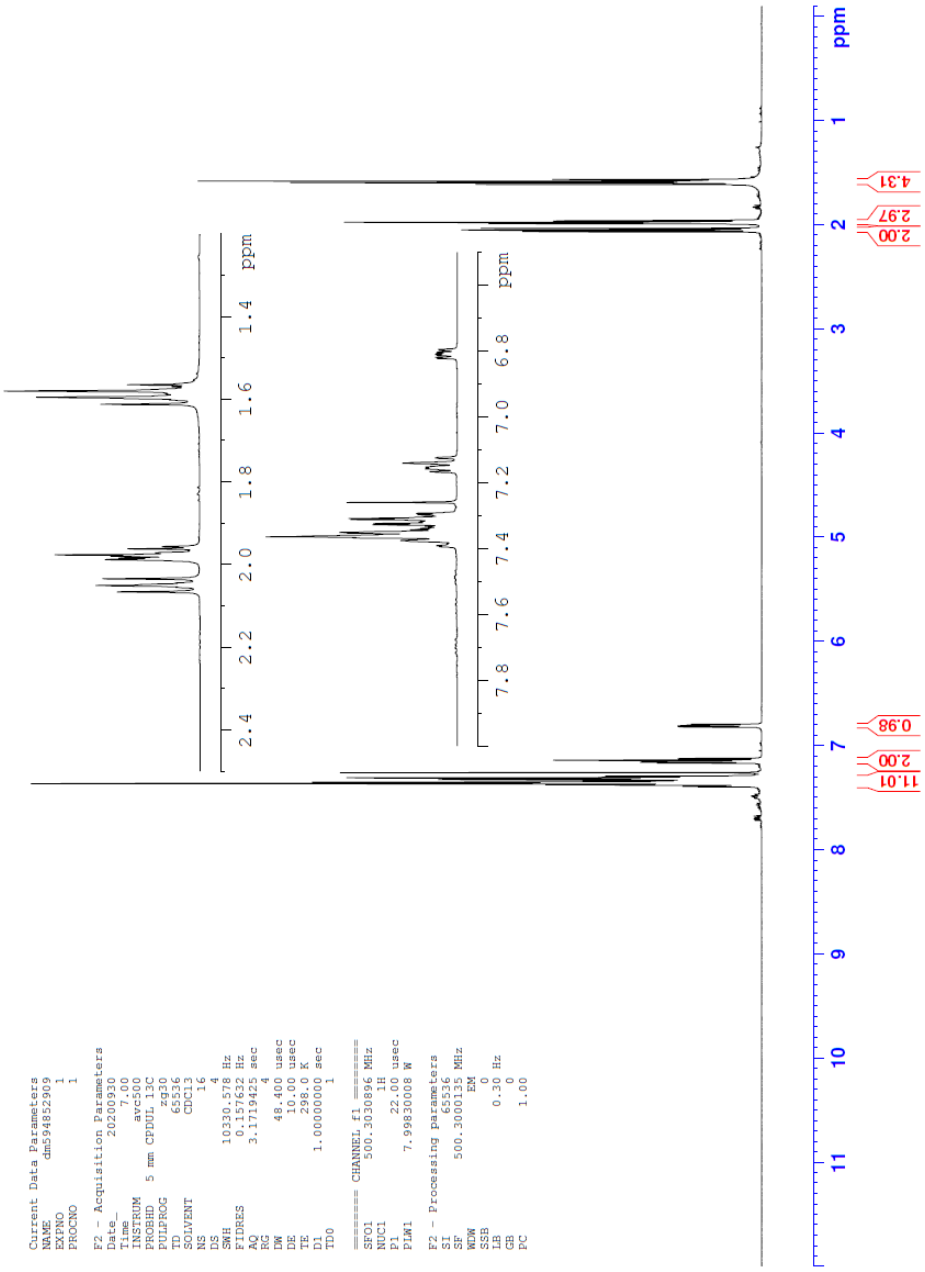
^{13}C NMR Ethyl 4-((2*S*,4*R*)-1-acetyl-4-((2-((3-(3-(but-3-yn-1-yl)-3H-diazirin-3-yl)propanamido)methyl)quinolin-6-yl)amino)-2-methyl-1,2,3,4-tetrahydroquinolin-6-yl)benzoate (4.6)



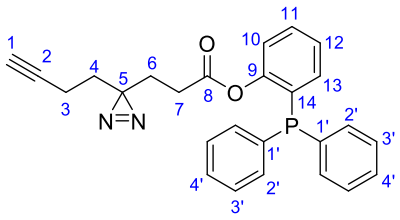


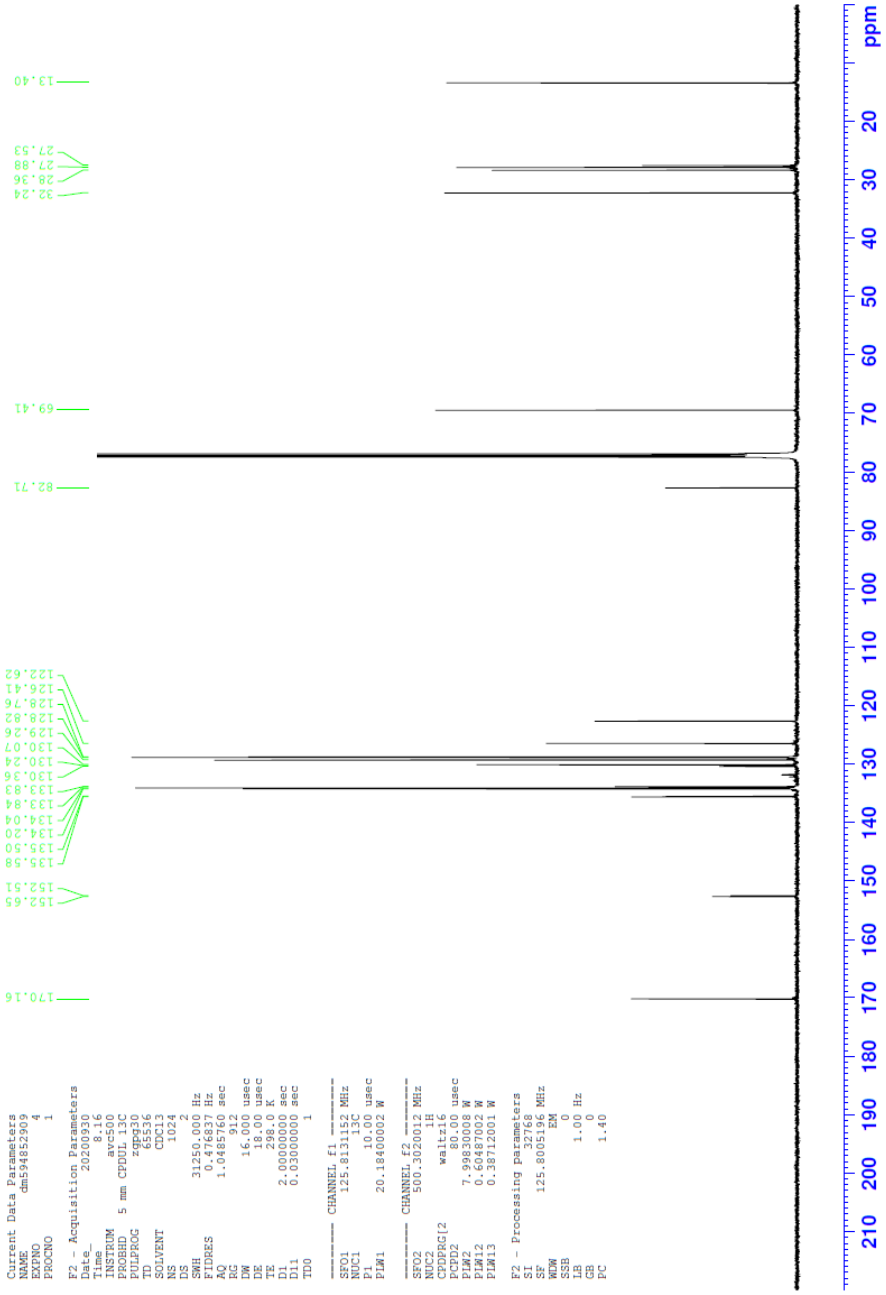
^{1}H NMR 2-(Diphenylphosphaneyl)phenyl 3-(3-(but-3-yn-1-yl)-3*H*-diazirin-3-yl)propanoate (4.27)



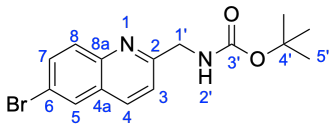


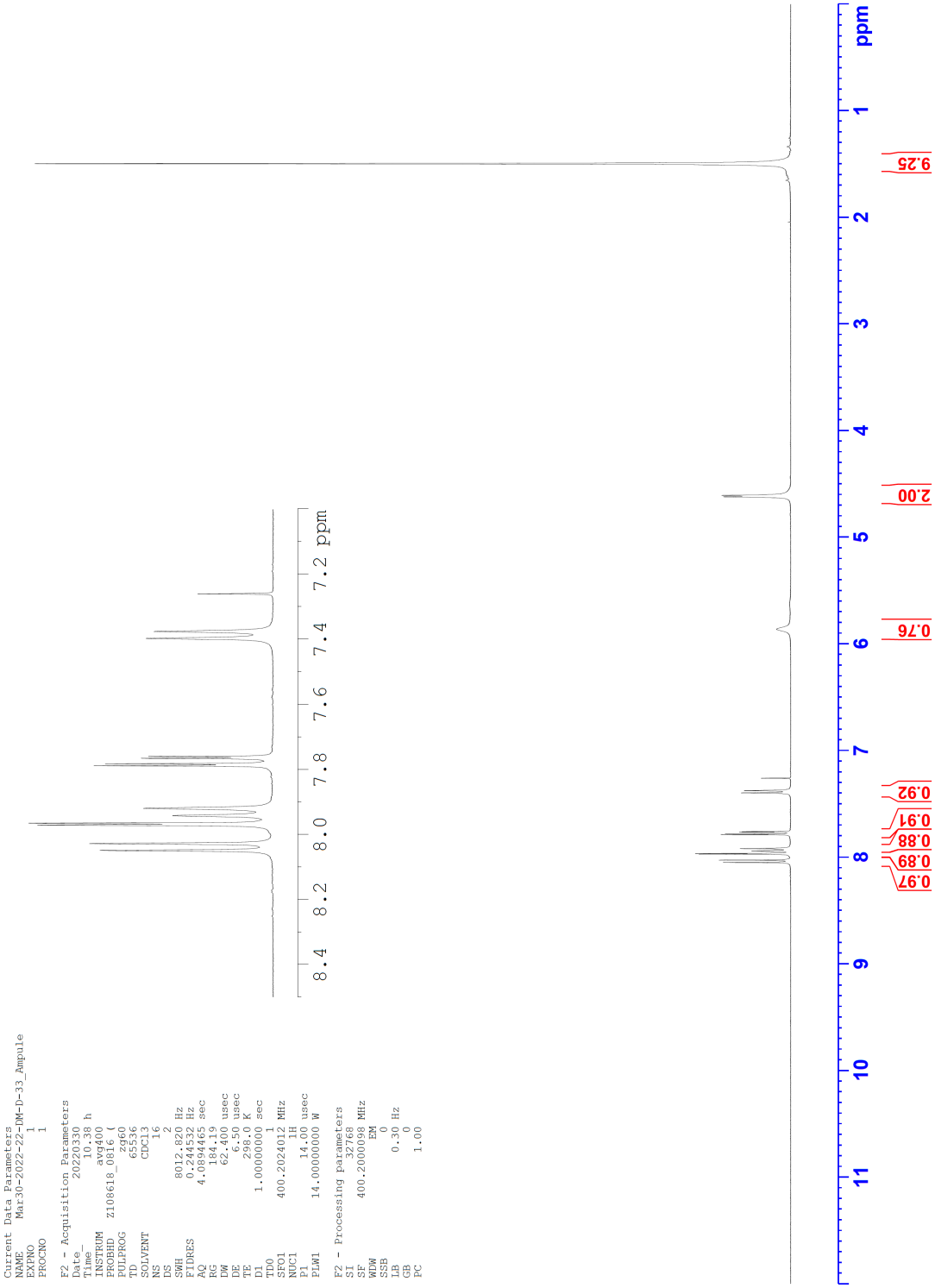
^{13}C NMR 2-(Diphenylphosphaneyl)phenyl 3-(3-(but-3-yn-1-yl)-3*H*-diazirin-3-yl)propanoate (4.27)



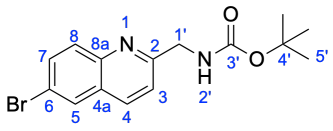


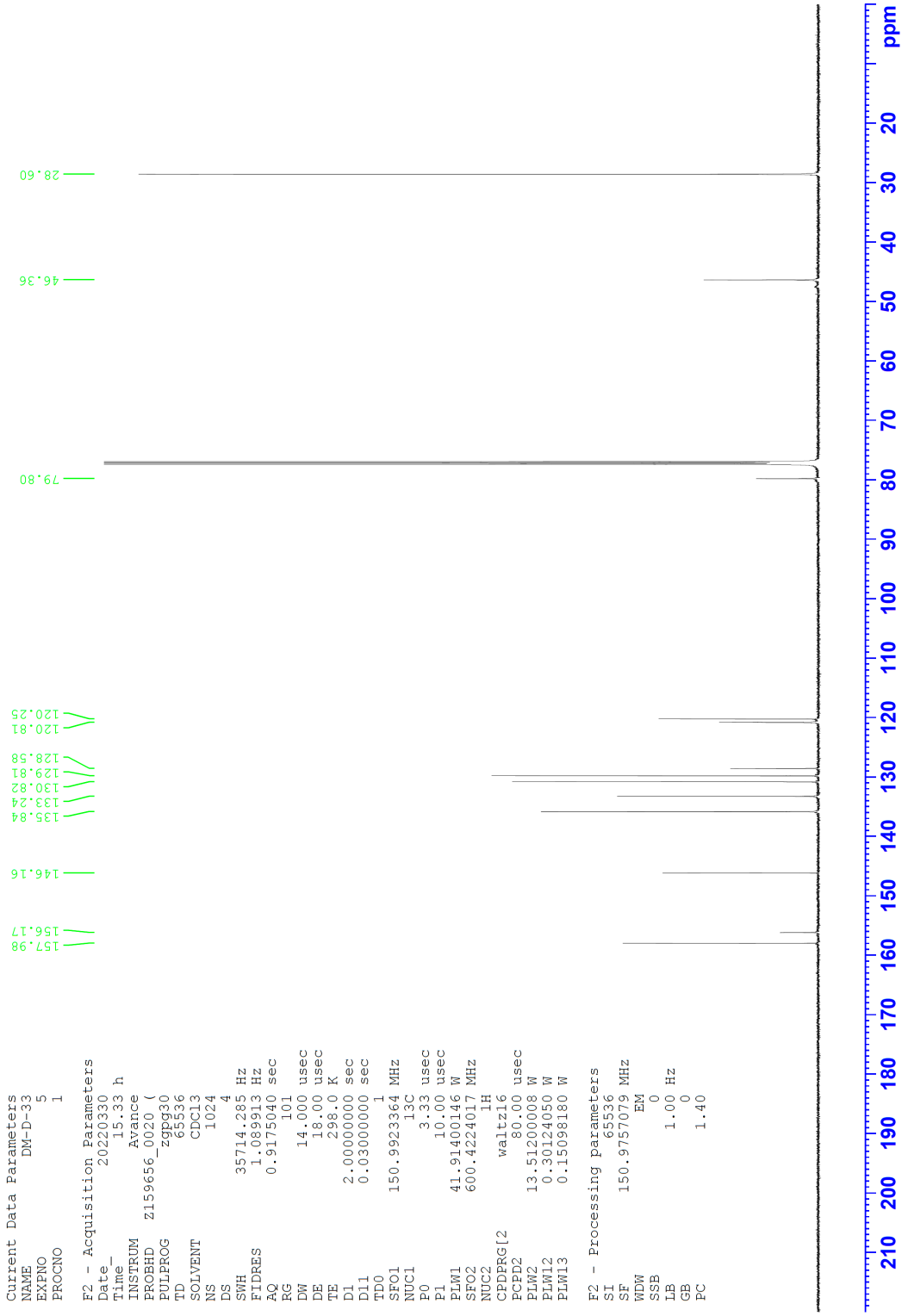
^{1}H NMR tert-Butyl ((6-bromoquinolin-2-yl)methyl)carbamate (4.34)



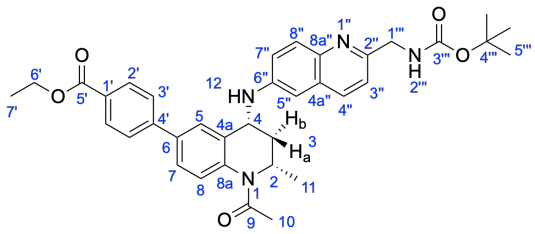


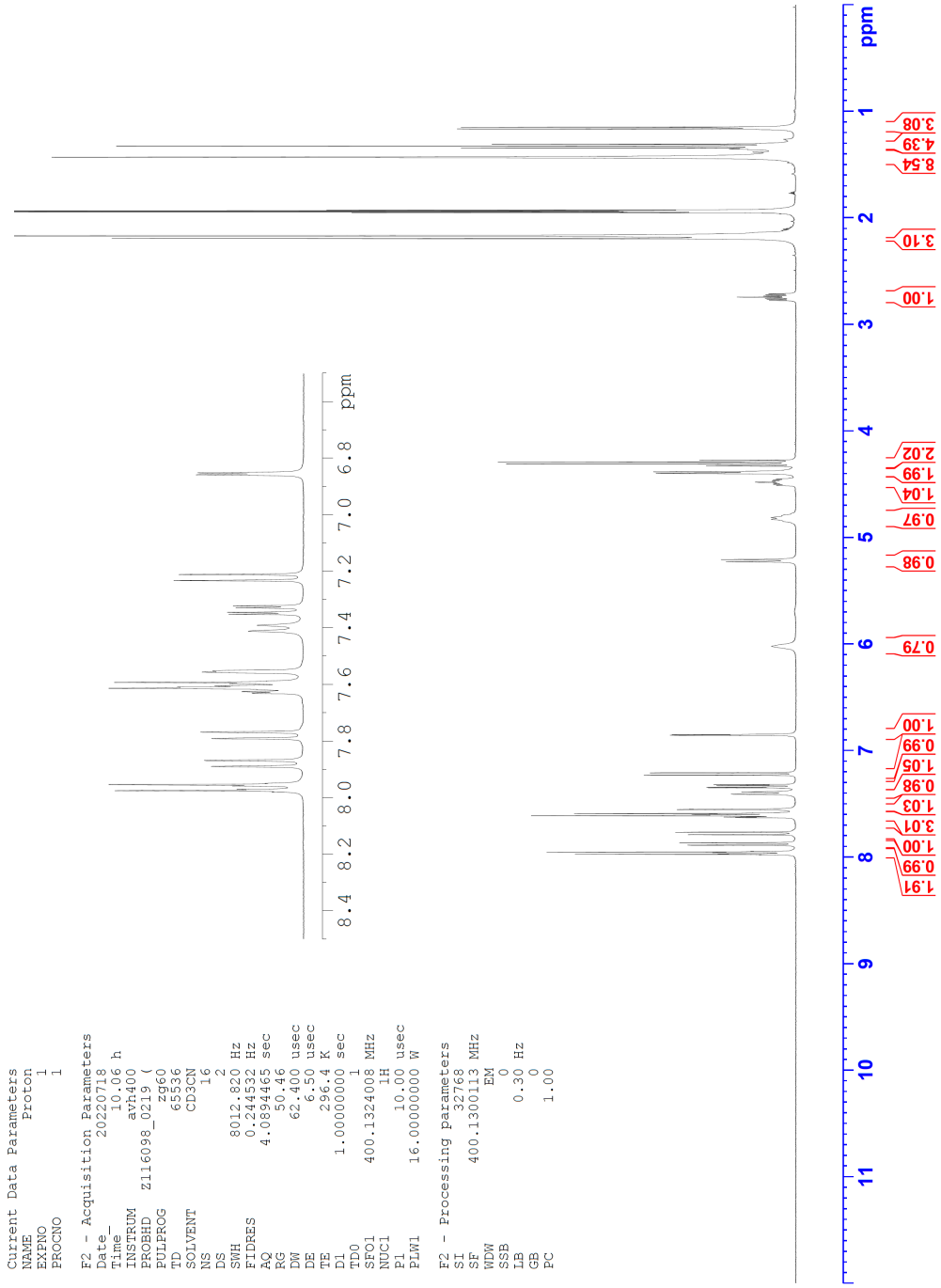
^{13}C NMR tert-Butyl ((6-bromoquinolin-2-yl)methyl)carbamate (4.34)



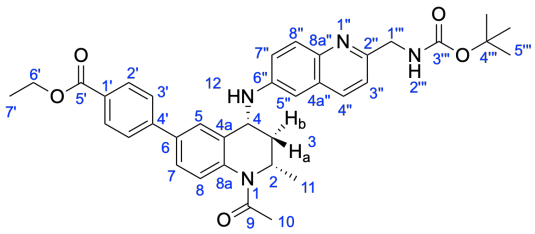


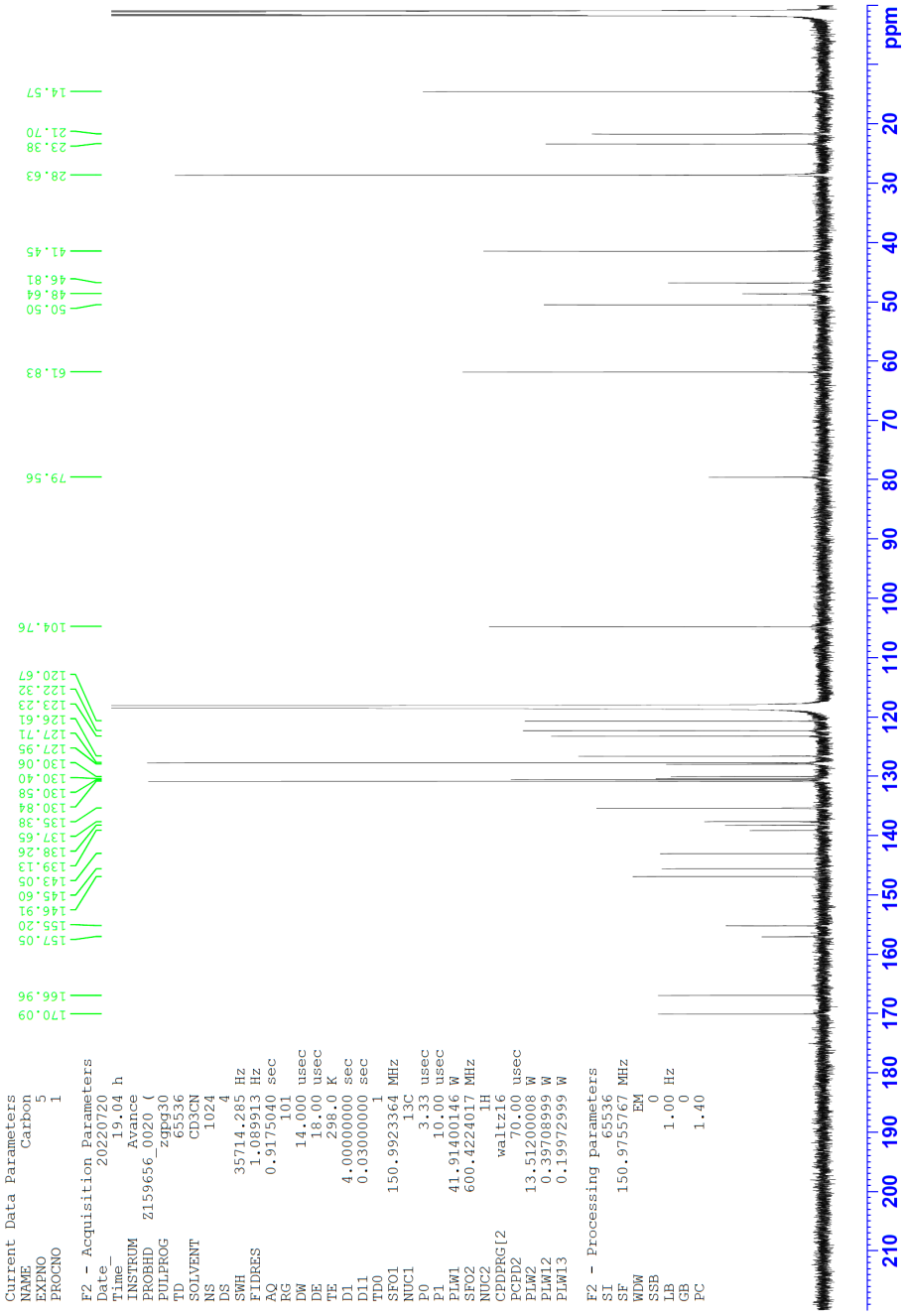
^{1}H Ethyl 4-((2*S*,4*R*)-1-acetyl-4-((2-((((*tert*-butoxycarbonyl)amino)methyl)quinolin-6-yl)amino)-2-methyl-1,2,3,4-tetrahydroquinolin-6-yl)benzoate (4.35)





^{13}C Ethyl 4-((2*S*,4*R*)-1-acetyl-4-((2-(((*tert*-butoxycarbonyl)amino)methyl)quinolin-6-yl)amino)-2-methyl-1,2,3,4-tetrahydroquinolin-6-yl)benzoate (4.35)





Appendix F: Image permissions



05/02/2023, 16:53 Rightslink® by Copyright Clearance Center

CCC RightsLink

Home | Help | Live Chat | Sign in | Create Account

ACS Publications
Most Trusted. Most Cited. Most Read.

Progress in the Development and Application of Small Molecule Inhibitors of Bromodomain–Acetyl-lysine Interactions

Author: David S. Hewings, Timothy P. C. Rooney, Laura E. Jennings, et al
Publication: Journal of Medicinal Chemistry
Publisher: American Chemical Society
Date: Nov 1, 2012

Copyright © 2012, American Chemical Society

PERMISSION/LICENSE IS GRANTED FOR YOUR ORDER AT NO CHARGE

This type of permission/license, instead of the standard Terms and Conditions, is sent to you because no fee is being charged for your order. Please note the following:

- Permission is granted for your request in both print and electronic formats, and translations.
- If figures and/or tables were requested, they may be adapted or used in part.
- Please print this page for your records and send a copy of it to your publisher/graduate school.
- Appropriate credit for the requested material should be given as follows: "Reprinted (adapted) with permission from {COMPLETE REFERENCE CITATION}. Copyright {YEAR} American Chemical Society." Insert appropriate information in place of the capitalized words.
- One-time permission is granted only for the use specified in your RightsLink request. No additional uses are granted (such as derivative works or other editions). For any uses, please submit a new request.

If credit is given to another source for the material you requested from RightsLink, permission must be obtained from that source.

BACK CLOSE WINDOW

© 2023 Copyright - All Rights Reserved | Copyright Clearance Center, Inc. | Privacy statement | Data Security and Privacy | For California Residents | Terms and ConditionsComments? We would like to hear from you. E-mail us at customercare@copyright.com